Advanced Signal Processing for MIMO-OFDM Receivers

Manchón, Carles Navarro

Publication date:
2011

Document Version
Accepted author manuscript, peer reviewed version

Advanced Signal Processing for MIMO-OFDM Receivers

Carles Navarro Manchón

Department of Electronic Systems

Aalborg University

A thesis submitted for the degree of

Doctor of Philosophy

November 2011

Abstract

This thesis deals with a wide range of topics within the research area of advanced baseband receiver design for wireless communication systems. In particular, the work focuses on signal processing algorithms for receivers in multiple-input multiple-output (MIMO) orthogonal frequency-division multiplexing (OFDM) systems, with a particular emphasis on the 3rd Generation Partnership Project (3GPP) Long Term Evolution (LTE) standard as a study case.

Signal processing in wireless receivers can be designed following different strategies. On the one hand, one can use intuitive argumentation to define the structure of the receiver with the hope that the resulting heuristic architecture will exhibit the desired behavior and performance. On the other hand, one can employ analytical frameworks to pose the problem as the optimization of a global objective function subject to certain constraints. This work includes contributions based on both types of approaches.

Our work on analytical frameworks is mainly focused on tools from variational Bayesian inference in probabilistic models and, more specifically, the mean-field (MF) and belief propagation (BP) methods. Within this context, one of our main contributions is the derivation of a novel message-passing scheme combining the MF and BP frameworks; the algorithm is derived from the stationary points of a region-based free energy approximation, and is guaranteed to converge if the underlying probabilistic model satisfies certain conditions. Moreover, we apply the combined message-passing algorithm to the probabilistic model of a MIMO-OFDM system; from the general derivation of the messages in the model, several instances of receiver structures with varying degrees of computational complexity and performance are obtained. We also explore the applicability of MF methods to the problem of estimation of sparse signals.

Among the contributions within the area of heuristic approaches, we highlight our study of iterative MIMO detection, interference cancellation and decoding for LTE systems. A detailed study of channel estimation algorithms for OFDM is also provided, including both pilot-based and data-aided schemes.

Dansk Resumé

Denne afhandling omhandler en række emner indenfor forskningsområdet for avanceret design af modtagere til trådløse kommunikationssystemer. Arbejdet fokuserer navnlig p signalbehandlingsalgoritmer til modtagere i "multiple-input multiple-output" (MIMO) "orthogonal frequency-division multiplexing" (OFDM) systemer og har særlig fokus på"3rd Generation Partnership Project" (3GPP) "Long Term Evolution" (LTE) standarden.

Signalbehandling i trådløse modtagere kan designes efter forskellige strategier. Påden ene side kan der bruges intuitive argumenter til at definere strukturen af modtageren med håbet om, at den resulterende heuristiske arkitektur vil udvise den ønskede adfærd og prstationer. Påden anden side kan der anvendes analytiske tilgange til at fremsætte problemet som optimeringen af en global funktion underlagt visse sidebetingelser. Dette arbejde omfatter bidrag baseret p begge tilgange.

Vores arbejde med den analytiske tilgang er hovedsageligt fokuseret påværktøjer til "variational Bayesian inference" i sandsynlighedsteoretiske modeller og - mere specifikt - metoderne "mean field" (MF) og "belief propagation" (BP). I denne sammenhæng er en af vores vigtigste bidrag udledningen af en ny besked-baseret algoritme, der kombinerer MF og BP. Algoritmen er udledt påbaggrund af stationære punkter i en region-baseret fri energi tilnærmelse og er garanteret at konvergere, hvis den underliggende probabilistiske model opfylder visse betingelser. Endvidere, anvender vi den kombinerede besked-baseret algoritme til den probabilistiske model af et MIMO-OFDM system. Igennem den generelle udledning af beskederne i modellen, opnås der flere eksempler påstrukturen i modtageren med varierende grader af beregningsmæssig kompleksitet og ydeevne. Vi undersøger ogsåanvendeligheden af MF metoder til problemet med estimering af signaler, som har egenskaben "sparse".

Blandt bidragene indenfor heuristiske metoder, fremhver vi vores undersøgelse af iterativ MIMO-detektion, interferens annullering og afkodning til LTE-systemer. En detaljeret undersøgelse af algoritmer til kanalestimering i OFDM systemer er ogsåfremlagt, herunder både pilot-baseret og data-støttet løsninger.

Preface

This thesis is submitted to the International Doctor School of Technology and Science at Aalborg University, Denmark, in partial fulfillment of the requirements for the degree of doctor of philosophy. The work has been carried out during the period spanning from October 2006 to November 2011 at the Department of Electronic Systems, Aalborg University. It has been partially supported by Intel Mobile Communications (IMC). Parts of this work have been performed within the ICT-216715 FP7 Network of Excellence in Wireless COMmunication (NEWCOM++) and the 4GMCT project funded by IMC, Agilent, Aalborg University and the Danish National Advanced Technology Foundation.

The main body of the thesis consists of Papers A–O, which are included as appendices and are published, submitted or under preparation for submission to peer-reviewed international conferences and journals. Chapters 1–4 set the context of the thesis and briefly describe its contribution.

I would like to express my appreciation for the guidance provided by my supervisors Professor Bernard Henri Fleury, Professor Preben Mogensen and Associate Professor Troels Bundgaard Sørensen. I would also like to express my gratitude to the members of my PhD defence committee Professor Ralf Müller, Professor Henk Wymeersch and Professor Søren Holdt Jensen for taking the time to read and assess this work. Last by not least, I would like to thank all my colleagues at the Navigation and Communication Section and the Radio Access Technology Section in the Department of Electronic Systems, Aalborg University.

Contents

1

Introduction

In this introductory chapter, we begin by succinctly discussing the rapid evolution of wireless communication systems over the last two decades. Next, we turn our attention to the influence that this evolution has in the current research challenges in the field of baseband receiver design, which is the main topic of this thesis. Finally, a brief overview of the organization of the thesis is provided.

1.1 Modern Wireless Communication Systems

Wireless communication systems have been subject to a drastic transformation during the last twenty years. From the old analog systems, focused exclusively on providing voice communication services, wireless technology has undergone a steep evolutionary path which has lead to today's wireless broadband systems, offering a wide range of multimedia services. A conceptual graph describing this evolution in terms of the data-rates and mobility degrees supported by various wireless communication standards is depicted in Figure 1.1. From the figure, it becomes apparent that a common trend has been driving the development of mobile wireless systems: a strive for higher data rates, even in high mobility scenarios. As an illustration, the International Telecommunication Union - Radiocommunication Sector (ITU-R) sets the target peak data-rate requirements for 4G systems, e.g. the Long Term Evolution-Avanced (LTE-A) system [1], at 100 Mbps for users moving at vehicular speeds and 1 Gbps for low-mobility users [2].

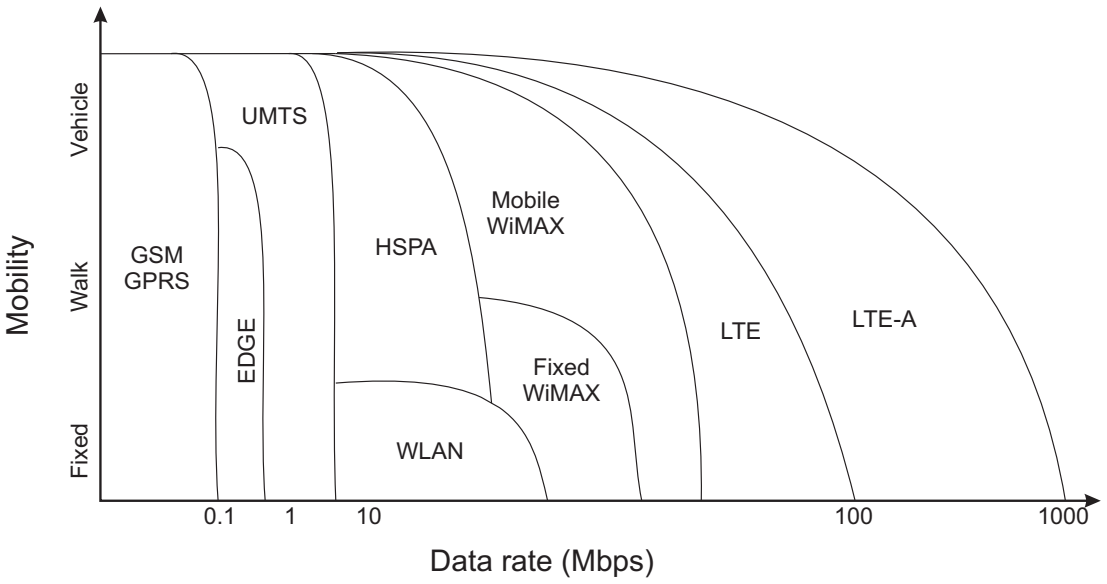

Figure 1.1: Conceptual graph of the current wireless standard landscape.

While increased data-rates have indeed been the ultimate goal in the design of wireless systems, there are other important requirements that a modern wireless standard should fulfil. In the following, we list and discuss some of them [3]:

High spectral efficiency: radio spectrum is a scarce and expensive resource that must be shared among users of a communication systems. It is therefore of crucial importance to make an efficient use of it, so that more users can be served with higher data rates for a given portion of bandwidth.

Reduced latency: the proliferation of interactive, real-time services like video-conferencing or multi-player internet gaming calls for reduced round-trip times compared to previous systems.

All-IP architecture: the transition of mobile systems to an all-IP based core network enables PC-like services and better interworking with fixed networks and other mobile standards.

Interworking: interworking with other fixed and mobile networks is required in order to advance towards network convergence, with different radio-access technologies providing access to a global, technology-transparent network.

Spectral Flexibility: besides being scarce and expensive, the radio spectrum is also highly fragmented due to the coexistence of very diverse systems and different local regulations. Thus, it is paramount for modern standards to be scalable in bandwidth, i.e. allowing deployment over wide as well as narrow bandwidth allocations.

1.2 Challenges in the Area of Baseband Receiver Design

In the previous section, we have briefly sketched some basic goals and requirements driving the progress of wireless communications during the recent years. From this general view, we now limit our scope to discuss the impact that these goals and requirements have on the design of wireless receivers.

The goal of a digital wireless receiver is, very generally, to estimate the value of a sequence of bits sent by the transmitter (or transmitters) from the digitalized baseband signal received at its antenna port(s). The quality of a receiver is commonly measured by the probability that its estimates of the bit values coincide indeed with the originally transmitted bits. Given a fixed transmission rate, a higher-quality receiver will make less bit errors than a poorer-quality receiver; or, from another point of view, a higher-quality receiver will be able to detect without error signals transmitted at a higher rate compared to a poorer-quality receiver. Thus, the design of high-performance receivers is crucial to enable systems with high spectral efficiency and, consequently, high data-rates.

Conceptually, this very basic goal in the design of wireless receivers has remained unchanged since the emergence of the first digital wireless standards. The receiver objective is to estimate the transmitted bit sequence given its received signal, regardless of the type of system in which it is operating. It is, however, the relation between the transmitted bit sequence and the received signal what is essentially different from one communication standard to another. This relation is defined by, among others, the type of transmission technology used, the type of complex modulations employed, the encoding schemes, the propagation environment, etc; in short, it is basically defined by the physical layer parameters of the system at hand. Therefore, while the conceptual

task of a receiver is independent of the type of communication system, the specific operations that are required in order to accomplish this task are very strongly determined by the system's physical layer design.

The above discussion leads us to the conclusion that, in order to understand the challenges present in the design of receivers for current wireless standards, one needs to understand the main technological advances that have been included in the physical layer design of said standards. In the following, we briefly enumerate and discuss the, in our view, most important physical-layer developments that have lead to the definition of today's mobile communication systems.

Multiple-input multiple-output (MIMO) antenna techniques: using multiple antenna elements at the transmitter, the receiver or both ends is a very effective way of increasing the reliability of a transmission, its data-rate or a combination of the two [4]. Theoretically, the capacity of a wireless link grows linearly with the minimum of the number of antenna elements at the transmitter and the receiver [5]; in practice, however, very efficient receivers, with the ability to accurately estimate the MIMO channel and work with advanced channel codes, are required in order to attain the capacity predicted by theory.

OFDM-based air interface: orthogonal frequency-division multiplexing (OFDM) and closely related techniques (like single-carrier frequency-division multiplexing or multi-carrier CDMA) have become the technology of choice for most modern wireless standards [3, 6]. Their flexibility and scalability in terms of bandwidth allocation, their ability to effectively cope with the channel temporal dispersion with simple equalization and their easy integration with MIMO techniques are some of the main reasons motivating this choice.

Advanced channel codes and high-order modulation: very important advances have been made in the field of coding theory in the last two decades with the emergence of turbo codes [7] and the popularization of low-density parity check (LDPC) codes [8]. These coding schemes allow for transmission very close to the theoretical capacity in an additive white Gaussian noise (AWGN) channel, but require iterative decoding schemes in order to do so. In addition, the use of high-order quadrature amplitude modulations, like 64-QAM or even 128-QAM, further help boosting the spectral efficiency of the system.

Given the physical layer mechanisms described above, we can already define which the main challenges present in the design of modern wireless receivers will be. First, the deployment of efficient MIMO detection techniques is required; to that end, high quality channel estimators for OFDM systems are necessary; and, moreover, these functionalities should be adequately integrated with iterative channel decoders and high-order demodulators. Additionally, all these operations must be designed under the constraint of a limited computational capability, especially for hand-held receivers.

It is clear that these challenges do not have an easy solution, and various different strategies to approach the problematic have been proposed so far. We will momentarily stop the discussion here and re-take it in Chapter 2, where we classify and summarize some of the most relevant steps made by the research community in order to answer the many open questions in the field of wireless receiver design.

1.3 Structure of the Thesis

In this chapter, we have introduced the context of this thesis. We started by concisely describing the main objectives driving the design of today's wireless communication systems and the most relevant technological advances in physical layer design enabling the achievement of said objectives. In the remainder of this work, we explore strategies for the design of advanced wireless receivers that can effectively operate in modern systems and can cope with the challenges described in Section 1.2. The rest of this thesis is organized as follows:

Chapter 2 gives an overview of the most relevant strategies for the design of wireless baseband receivers proposed in literature in the recent years. From a simple signal model of a MIMO-OFDM system, we discuss optimal and sub-optimal design strategies. Among the latter, we classify the different approaches into two different categories: heuristic designs and approaches based on analytical frameworks.

Chapter 3 summarizes the message-update equations of two well-known message-passing techniques: the sum-product algorithm and variational message passing. Additionally, the message-update equations of the message-passing approach proposed in Papers A and B are also provided.

Chapter 4 briefly classifies and describes the main contributions of this work, which are presented in the form of scientific articles published or submitted to international conferences and journals.

Papers A–O are the articles described in Chapter 4, and they contain the main scientific content of this thesis.

2

An Introduction to Baseband Receiver Design

In this chapter, we introduce the general problem of baseband receiver design and briefly summarize the main approaches that can be found in state-of-the-art research. We begin by presenting a simple OFDM signal model which is used as an illustration of the challenges found in the area of receiver design. Taking as a starting point the optimum –but computationally intractable– maximum a posteriori (MAP) design criterium, we scan the different suboptimal approaches that have been proposed in literature in the recent years. We classify the strategies into two separate categories: heuristic methods and formal inference frameworks.

2.1 A Simple Signal Model for OFDM Communications

Figure 2.1 shows the block-diagram representation of the transmitter part of a simple MIMO-OFDM system with M transmit antennas, which may belong to a single or multiple users. For the mth transmit chain, a sequence of information bits $\boldsymbol{u}_m$ is encoded and interleaved, yielding a sequence of coded bits $\boldsymbol{c}_m$. The coded bit sequence is complex modulated, producing a vector of modulated data symbols $\boldsymbol{x}_m^{(d)}$. The modulated data symbols are multiplexed with a sequence of pilot symbols $\boldsymbol{x}_m^{(d)}$. The value and allocation of the pilot symbols are known to the receiver, and they are used (mainly) to improve the accuracy of channel estimation on the receiver side. Finally, the transmitted symbol vector $\boldsymbol{x}_m$ containing both data and pilot symbols is OFDM modulated

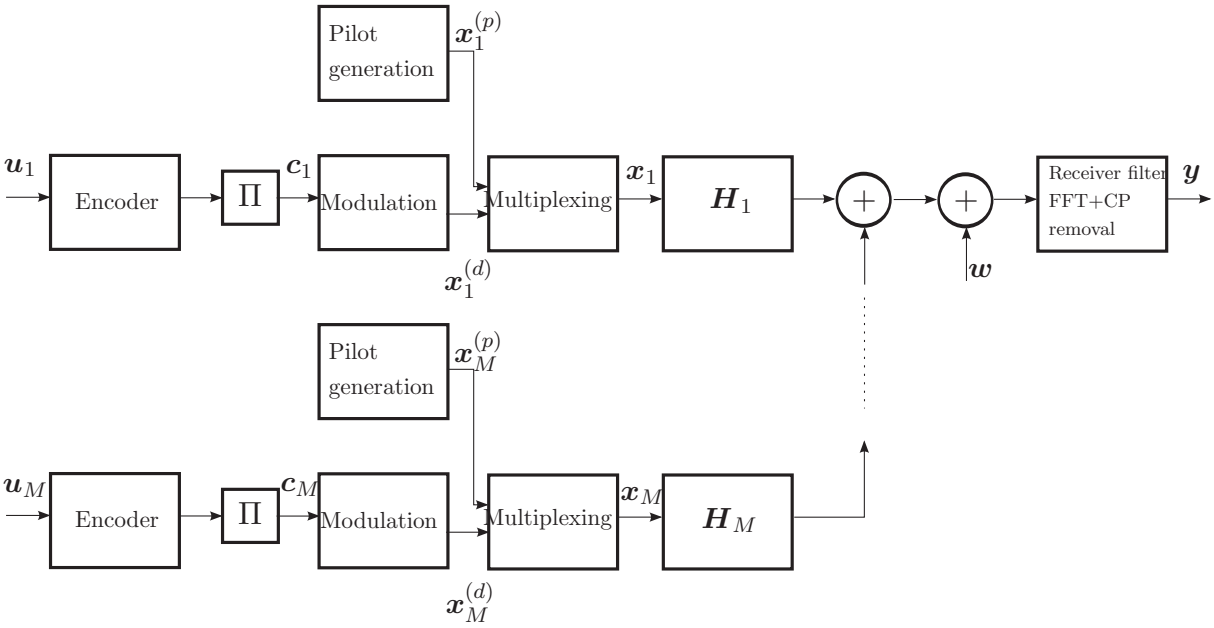

Figure 2.1: Block-diagram representation of the considered OFDM system.

and transmitted through the wireless channel. We assume that the transmission from all M different transmit antennas is perfectly synchronized in time and frequency.

Assuming that the channel response is static over the duration of an OFDM symbol and that the cyclic prefix is long enough to cope with the temporal dispersion of the channel, the signal received at the nth antenna port of a receiver with N antennas reads

$$y_n(k) = \sum_{m=1}^{M} h_{nm}(k)x_m(k) + w_n(k), \qquad k = 1, \ldots, K, n = 1, \ldots, N \tag{2.1}$$

where $h_{nm}(k)$ is the frequency-response weight of the channel between transmitter m and receiver n at subcarrier k, $w_n(k)$ denotes zero-mean complex additive white Gaussian Noise (AWGN) with variance σ_w^2 and K is the total number of subcarriers. We can re-write (2.1) for all subcarriers and all receive antennas in matrix-vector notation:

$$\boldsymbol{y} = \sum_{m=1}^{M} \boldsymbol{X}_m \boldsymbol{h}_m + \boldsymbol{w} = \sum_{m=1}^{M} \boldsymbol{H}_m \boldsymbol{x}_m + \boldsymbol{w}. \tag{2.2}$$

In (2.2), $\boldsymbol{y} = [y_1(1), \ldots, y_1(K), \ldots, y_N(1), \ldots, y_N(K)]^{\mathrm{T}}$, $\boldsymbol{X}_m = \boldsymbol{I}_N \otimes \mathrm{diag}\{\boldsymbol{x}_m\}$, $\boldsymbol{H}_m = [\mathrm{diag}\{\boldsymbol{h}_{1m}\}, \ldots, \mathrm{diag}\{\boldsymbol{h}_{Nm}\}]^{\mathrm{T}}$ and $\boldsymbol{h}_{nm} = [h_{nm}(1), \ldots, h_{nm}(K)]^{\mathrm{T}}$, with $\boldsymbol{I}_N$ and $\boldsymbol{A} \otimes \boldsymbol{B}$ denoting respectively the identity matrix of dimension N and the Kronecker product between matrices $\boldsymbol{A}$ and $\boldsymbol{B}$.

2.2 Optimum Receiver and Suboptimum Approaches

The goal of a baseband receiver is to infer the value of the information bit vectors $\boldsymbol{u}_1, \ldots, \boldsymbol{u}_M$ from the received signal in (2.2). With this goal in mind, the probability of incorrect detection is minimized by formulating a decision rule implementing the maximum a posteriori probability (MAP) criterion [9]:

$$[\hat{\boldsymbol{u}}_1^{\mathrm{T}}, \ldots, \hat{\boldsymbol{u}}_M^{\mathrm{T}}]^{\mathrm{T}} = \underset{\boldsymbol{u}_1,\ldots,\boldsymbol{u}_M}{\operatorname{argmax}}\, p(\boldsymbol{u}_1, \ldots, \boldsymbol{u}_M|\boldsymbol{y}). \tag{2.3}$$

In (2.3), $p(\boldsymbol{u}_1, \ldots, \boldsymbol{u}_M|\boldsymbol{y})$ denotes the conditional probability mass function (pmf) of the information bit vectors given the observation in (2.2), and is commonly referred to as the *a posteriori* pmf of the information bits. In the case in which all possible combinations of information bits $\boldsymbol{u}_1, \ldots, \boldsymbol{u}_M$ are equally likely to be transmitted (i.e., the prior pmf $p(\boldsymbol{u}_1, \ldots, \boldsymbol{u}_M)$ is uniform), the MAP criterion simplifies to the maximum likelihood (ML) decision criterion [9]:

$$[\hat{\boldsymbol{u}}_1^{\mathrm{T}}, \ldots, \hat{\boldsymbol{u}}_M^{\mathrm{T}}]^{\mathrm{T}} = \underset{\boldsymbol{u}_1,\ldots,\boldsymbol{u}_M}{\operatorname{argmax}}\, p(\boldsymbol{y}|\boldsymbol{u}_1, \ldots, \boldsymbol{u}_M). \tag{2.4}$$

In (2.4), $p(\boldsymbol{y}|\boldsymbol{u}_1, \ldots, \boldsymbol{u}_M)$ denotes the conditional pdf of the observation $\boldsymbol{y}$ given the information bits, and is commonly referred to as the *likelihood* function when considered as a function of $\boldsymbol{u}_1, \ldots, \boldsymbol{u}_M$, i.e for fixed $\boldsymbol{y}$.

While the MAP and ML criteria lead to a decision rule minimizing the probability of error, direct maximization of either the a posteriori pmf in (2.3) or the likelihood function in (2.4) is typically intractable or too computationally complex to be implemented in modern wireless communication systems. This is due to the presence of unknown parameters, such as the channel weight vectors $\boldsymbol{h}_1, \ldots, \boldsymbol{h}_M$ or the AWGN variance σ_w^2, together with the use of QAM complex modulation schemes and advanced channel codes. For some specific configurations, it is still possible to design a receiver following the optimum design criterion (see [10]), but in general one must resort to suboptimum approaches.

In the remainder of this chapter, we briefly discuss different strategies for the suboptimal design of baseband receivers for wireless communication systems in general and with a special focus on MIMO-OFDM systems. We classify the strategies into two main categories: heuristic approaches and formal inference frameworks. In the former,

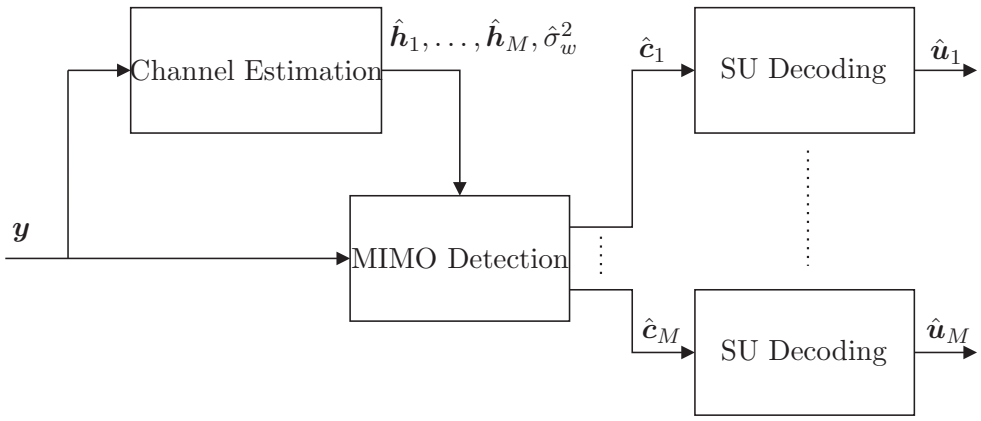

Figure 2.2: Block-diagram representation of a heuristic sequential receiver.

the receiver's operation is split into multiple smaller tasks which are then solved individually and independently from the other tasks. In the latter, on the other hand, the receiver's operation is designed in a global manner by trying to approximate the MAP/ML criteria in a structured and analytical way.

2.3 Heuristic approaches

Heuristic methods for baseband receiver design attempt to break down the general problem presented in Section 2.2 into smaller, simpler problems. Typically, they divide the receiver's operation into three main tasks: channel estimation[1], MIMO detection and single-user decoding. A conceptual block-diagram of a receiver sequentially performing these operations is shown in Figure 2.2.

By performing this division of tasks, each of the individual problems becomes simpler to solve. In fact, in many cases optimal solutions given a design criterion can be found and computed in practice. Unfortunately, locally finding the optimum solution for the individual tasks does not guarantee the computation of the globally optimum solution. In the following, we give a brief overview of state-of-art methods performing each of the tasks described in Figure 2.2, with special focus on their application to MIMO-OFDM systems.

[1]By channel estimation we refer to the estimation of all unknown channel parameters, including the complex channel weights and the AWGN variance.

For OFDM systems, one of the first problems to be tackled by the research community was the estimation of the frequency response of the wireless channel based on the information provided by pilot symbols. Amongst the methods proposed in literature, linear minimum mean-squared error (LMMSE) channel estimators exploiting the time-frequency correlation of the channel response have attracted the most attention [11]. This approach, however, has two important drawbacks: firstly, the time-frequency correlation function of the channel is, in general, not known at the receiver; secondly, LMMSE channel estimators usually involve the inversion of matrices of large dimension, which make them computationally cumbersome. In order to mitigate the first drawback, Li *et al.* give some guidelines on how to design a robust LMMSE estimator when the receiver does not have knowledge of the channel second-order statistics [12]. In order to reduce the complexity of matrix inversions, a reduced-complexity version of the estimator, based on a singular value decomposition of the channel covariance matrix, has been proposed in [13]. In a slightly different approach, some authors have proposed estimators which try to capitalize on the structure of the time-domain response in order to estimate the frequency response [14, 15]; within this context, the work by Yang *et. al* in [16], where a parametric model of the multipath wireless channel is invoked to reduce complexity of LMMSE channel estimation, is especially remarkable.

In the area of MIMO detection, most efforts have been devoted to find reduced-complexity versions of the ML MIMO detector [17], which has a computational complexity increasing exponentially with the MIMO and complex modulation orders. Among these, list-sphere decoders [18] have been shown to be a good compromise. In contraposition to ML-based detectors, which jointly detect the symbols transmitted through the MIMO channel, approaches attempting sequential detection of the symbols have also been presented. They are usually based on a linear detection step, either using zero-forcing or LMMSE filtering, followed by an interference cancellation step, in which signal components corresponding to already detected symbols are subtracted before a new detection step takes place. A first version of this sequential detection algorithm was proposed in [19], in which the interference cancellation step was based on hard decisions on the already detected symbols. A more evolved version of the algorithm was presented in [20], following the approach in [21], in which the receiver uses soft decisions on the already detected symbols and also provides soft outputs for use in channel decoders.

With regards to channel decoding, the techniques used obviously vary depending on the type of code used. For convolutional codes, the Viterbi algorithm [9] provides an ML sequence detector, i.e. minimizes the probability of an incorrect decoded sequence. An alternative is the BCJR decoder [22], which instead minimizes the probability of error of the individual bits of the transmitted sequence. Furthermore, the BCJR algorithm directly provides soft outputs, i.e. the probabilities of the bits being 1 or 0 after decoding, which makes it very attractive for use in iterative algorithms. While soft versions of the Viterbi algorithm exist (see [23]), they yield poorer performance than the BCJR method. For concatenated codes, and in particular for turbo codes, an heuristic iterative decoding scheme built upon BCJR decoding was presented in [7]; while initially derived following intuitive argumentation, the iterative decoding of turbo codes was shown later on to be an instance of the belief propagation framework [24]; similar interpretations of the BCJR algorithm within the belief propagation framework have also been proposed [25].

2.3.1 Heuristic Iterative Receivers

As we stated previously, optimum design of the individual components of the receiver depicted in Figure 2.2 does not, in general, imply global optimality of the receiver. Intuitively, it is easy to see that such a receiver does not make use of all the information available to compute its decisions. For instance, channel estimation needs to be performed as a first step based only on the receiver's knowledge of the pilot symbols, as no information about the modulated data symbols (except the type of modulation used) is available. Clearly, a better channel estimate can be obtained after MIMO detection by incorporating the receiver's knowledge on the coded bits $\boldsymbol{c}_1 \ldots, \boldsymbol{c}_M$ into the channel estimation process. Similarly, the same can be done with the knowledge acquired by the receiver after SU decoding, which can be used to refine the output of both the channel estimation and the MIMO detection modules.

Inspired by the iterative structure of the decoding of turbo codes [7], a number of iterative receiver structures based on the turbo principle have been proposed in literature. Conceptually, the receiver's operation is still subdivided into the same individual components as the sequential receiver in Figure 2.2. However, instead of performing the involved operations just once in a sequential way, the different components are interconnected and iteratively perform their operation with the output provided by

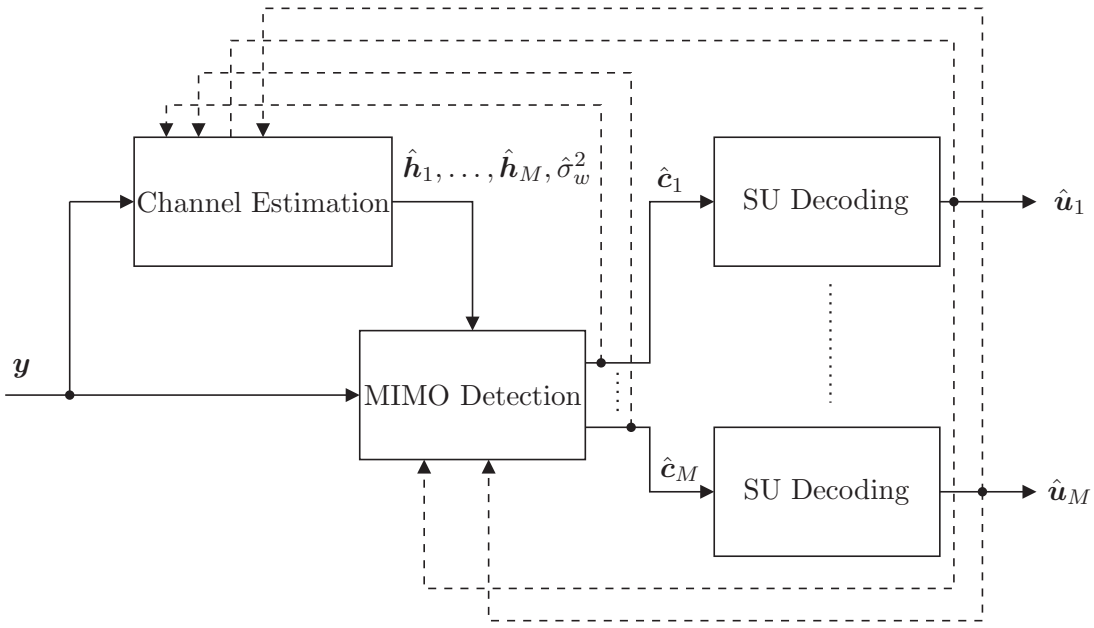

Figure 2.3: Block-diagram representation of a heuristic iterative receiver.

each module being used as an input to other receiver components. A block diagram of a heuristic iterative receiver illustrating this concept is depicted in Figure 2.3. The discontinuous lines represent all possible feedback interconnections that may be made among the individual receiver components.

Clearly, an iterative receiver following the scheme in Figure 2.3 must obtain better performance than a classical sequential receiver when designed properly, as it makes a more exhaustive use of all the information available at the receiver. However, the way in which the information provided by the different components should be combined and distributed in the receiver is unclear due to the lack of a global design criterion. As a consequence, the information flow inside this type of iterative structures is often designed using intuitive argumentation or based on the results obtained from simulation studies. As an example of this problematic, there has been a debate in the research community on whether a posteriori probabilities (APP) or extrinsic values should be fed back from the decoder to the rest of the receiver components; several authors coincide in proposing the use of extrinsic values for MIMO detection [21, 26, 27] while using APP values for channel estimation [26, 27], but no thorough justification for this choice is given apart from its superior performance shown by simulation results.

In the following, we give a very brief overview of relevant publications proposing heuristic iterative receiver architectures for wireless communication systems in general and MIMO-OFDM systems in particular. In the context of OFDM systems, a few algorithms proposing iterative channel estimation and decoding have been presented [28,29] which are mainly based on LMMSE channel estimators incorporating soft information from the decoded symbols. It is also worth mentioning the work by Hanzo *et al.*, summarized in [6]. A vast amount of work on iterative detection and decoding is available in literature; initiated by the receiver proposed in [21] and following the turbo principle used to decode turbo codes, a variety of turbo receivers performing iterative channel equalization and decoding have been proposed [30–32]. Finally, we highlight two heuristic iterative structures performing channel estimation, multi-user detection and channel decoding for CDMA systems [26] and MIMO-OFDM systems [27].

2.4 Inference Frameworks

In the previous section we dealt with heuristic methods for receiver design, in which the receiver is intuitively divided into smaller individual components iteratively exchanging information among them. In this section, we explore a different strategy. We stated in Section 2.2 that direct computation of the a posteriori pmf in (2.3) is often intractable for most practical wireless communication systems. However, one can try to find approximations to them. If a good approximation to the posterior pmf $b(\boldsymbol{u}_1, \ldots, \boldsymbol{u}_M) \approx p(\boldsymbol{u}_1, \ldots, \boldsymbol{u}_M|\boldsymbol{y})$ is found, then it is likely that a good approximation to the MAP criterion can be obtained by finding the information bit vectors maximizing $b(\boldsymbol{u}_1, \ldots, \boldsymbol{u}_M)$.

A wide range of algorithms attempting to solve approximate computation of pdf/pmfs and marginals can be found within the context of variational Bayesian inference frameworks [33,34]. Variational approximation methods are defined by two main components: a belief function $b(\boldsymbol{z})$ trying to approximate the desired pmf $p(\boldsymbol{z})$ and an objective function $F(b)$ which is optimized with respect to the approximating belief function. Typically, the objective function $F(b)$ is some type of discrepancy measure between $p(\boldsymbol{z})$ and the approximation $b(\boldsymbol{z})$. Furthermore, some constraints are usually applied to $b(\boldsymbol{z})$ to ensure that the optimization of $F(b)$ is computationally tractable. We briefly

summarize next two fundamental approaches to variational Bayesian inference: the mean-field (MF) approximation and belief propagation (BP)[1].

Assume we want to approximate the pmf

$$p(\boldsymbol{z}) = \frac{1}{Z} \prod_{a \in \mathcal{A}} f_a(\boldsymbol{z}_a) \tag{2.5}$$

where $\boldsymbol{z} = (z_i | i \in \mathcal{I})^{\mathrm{T}}$ and function $f_a(\boldsymbol{z}_a)$ has arguments $\boldsymbol{z}_a$, with the entries of $\boldsymbol{z}_a$ being a subset of the entries of $\boldsymbol{z}$ for all $a \in \mathcal{A}$. In (2.5), $Z = \int_{\boldsymbol{z}} \prod_{a \in \mathcal{A}} f_a(\boldsymbol{z}_a) d\boldsymbol{z}$ is a normalization constant. Within the MF approach, an approximation $b(\boldsymbol{z}) \approx p(\boldsymbol{z})$ is computed by minimizing the variational free energy [34]

$$F(b) = U(b) - H(b) \tag{2.6}$$

with $U(b)$ being the variational average energy

$$U(b) = \sum_{a \in \mathcal{A}} \sum_{\boldsymbol{z}} b(\boldsymbol{z}) f_a(\boldsymbol{z}_a)$$

and $H(b)$ denoting the variational entropy

$$H(b) = -\sum_{\boldsymbol{z}} b(\boldsymbol{z}) \log b(\boldsymbol{z}).$$

We can also rewrite (2.6) as

$$F(b) = -\log Z + D(b \| p)$$

where $D(b\|p) = \sum_{\boldsymbol{z}} b(\boldsymbol{z}) \log \frac{b(\boldsymbol{z})}{p(\boldsymbol{z})}$ is the Kullback-Leibler divergence between b and p [38]. Therefore, minimizing $F(b)$ is equivalent to minimizing $D(b\|p)$. The minimization of (2.6) becomes tractable by applying the following constraints to the belief function:

$$b(\boldsymbol{z}) = \prod_{i \in \mathcal{I}} b_i(z_i), \tag{2.7}$$

$$\sum_{z_i} b_i(z_i) = 1 \qquad \forall i \in \mathcal{I}. \tag{2.8}$$

[1] Some authors, e.g. Winn and Bishop [35,36], consider BP outside the variational Bayesian framework, and usually use the term *variational* only in the context of MF-like approximations. We use, however, the more general view proposed e.g. in [33,34,37], which considers BP as another algorithm for variational Bayesian inference.

We refer to (2.7) as the *factorization* constraint. It implies that the belief function factorizes with respect to each of the variables z_i. The condition in (2.8), which we name the *normalization* constraint, ensures that each of the factors is normalized. Obviously, one could consider different types of factorization, in which the belief function factorizes with respect to groups of variables; such approaches are commonly referred to as *structured* MF approaches, whereas the full factorization in (2.7) is usually named *naive* MF [33, 39].

Next, we turn to the BP approach to the problem. Instead of trying to approximate the full pmf in (2.5), BP calculates approximate marginals $b_i(z_i) \approx \sum_{\boldsymbol{z}\backslash z_i} p(\boldsymbol{z})$[1] and $b_a(\boldsymbol{z}_a) \approx \sum_{\boldsymbol{z}\backslash \boldsymbol{z}_a} p(\boldsymbol{z})$ of the desired pmf. The objective function for BP algorithms is the Bethe free energy, defined as [34]

$$F_{\text{Bethe}} = U_{\text{Bethe}} - H_{\text{Bethe}} \tag{2.9}$$

where the Bethe average energy is defined as

$$U_{\text{Bethe}} = -\sum_{a\in\mathcal{A}} \sum_{\boldsymbol{z}_a} b_a(\boldsymbol{z}_a) \log f_a(\boldsymbol{z}_a) \tag{2.10}$$

and the Bethe entropy reads

$$H_{\text{Bethe}} = \sum_{a\in\mathcal{A}} \sum_{\boldsymbol{z}_a} b_a(\boldsymbol{z}_a) \log b_a(\boldsymbol{z}_a) + \sum_{i\in\mathcal{I}} (d_i - 1) \sum_{z_i} b_i(z_i) \log b_i(z_i). \tag{2.11}$$

In (2.11), d_i denotes the degree of variable z_i, defined as the number of factors f_a, $a \in \mathcal{A}$ which have z_i as an argument. The beliefs b_i and b_a are constrained to fulfill the consistency constraints

$$\sum_{\boldsymbol{z}_a\backslash z_i} f_a(\boldsymbol{z}_a) = b_i(z_i), \qquad \forall a \in \mathcal{A}, i \in \mathcal{I} \tag{2.12}$$

and the normalization constraints

$$\sum_{z_i} b_i(z_i) = \sum_{\boldsymbol{z}_a} b_a(\boldsymbol{z}_a) = 1, \qquad \forall a \in \mathcal{A}, i \in \mathcal{I}. \tag{2.13}$$

The expression in (2.9) subject to the the constraints (2.12) and (2.13) is usually referred to as the constrained Bethe free energy, and the BP marginals b_i and b_a are calculated as its stationary points. The choice of the constrained Bethe free energy as objective

[1] The expression $\boldsymbol{z}\backslash z_i$ denotes all components of $\boldsymbol{z}$ except z_i.

functions is motivated by the fact that it is equal to the variational free energy in (2.6) when $p(\boldsymbol{z})$ can be expressed in a factor graph without cycles, i.e. a tree-structured graph [34]. When that is the case, the marginals calculated using BP are exact. For graphs with cycles, though, only approximate marginals are obtained [33, 34, 36].

Both the BP and the MF principles can be expressed as message-passing algorithms in factor graphs. Factor graphs [40] are a tool which allows for a graphical representation of a probabilistic model. The message-passing interpretation of the BP principle is known as the sum-product (SP) algorithm [40] due to the form of its message update rules, while its MF counterpart is commonly known as the variational message-passing (VMP) algorithm [35, 39]. We introduce both message-passing algorithms in Chapter 3, together with a novel algorithm proposed in [41, 42] which combines the benefits of both approaches, and which constitutes one of the important contributions of this thesis. The contributions in [41, 42] are included in the appendix of this thesis as Papers A and B.

We finalize the chapter with a brief review of relevant applications of variational Bayesian inference frameworks to the design of wireless receivers. BP was initially applied mainly to the decoding of channel codes like convolutional codes [40], turbo codes [24] or low-density parity check codes [8], and its application was later on extended to iterative detection and decoding schemes [25, 43–46]. In certain cases, the application of BP to channel estimation problems leads to algorithms which are difficult to treat numerically. In such circumstances, authors like Dauwels and Loeliger have proposed to combine BP with the expectation-maximization (EM) algorithm [47] for parameter estimation [25, 48]. An alternative approach is to find Gaussian approximations of the SP algorithm [49, 50]. Application of MF approaches to the design of wireless receivers usually involve estimation of the wireless channels, in which the MF approximation typically leads to algorithms which are computationally simpler than its BP counterpart. Among these, we wish to highlight the contributions in [51–55].

3

Message-Passing Algorithms for Bayesian Inference on Factor Graphs

As we discussed in Section 2.4, the algorithms obtained via the MF and BP inference frameworks can be expressed as message-passing algorithms in probabilistic graphs, yielding respectively the VMP [35] and the SP [40] algorithms. Since message-passing techniques are one of the central topics of this thesis, we briefly summarize the two algorithms in this chapter. Additionally, we also include the message update equations for the combined VMP-SP algorithm which is proposed in Papers A and B.

3.1 Factor Graphs for Probabilistic Models

Let $p(\boldsymbol{z})$ be the probability density function (pdf) of a vector $\boldsymbol{z}$ of random variables z_i $(i \in \mathcal{I})$ which factorizes according to

$$p(\boldsymbol{z}) = \frac{1}{Z} \prod_{a \in \mathcal{A}} f_a(\boldsymbol{z}_a) \tag{3.1}$$

where $\boldsymbol{z}_a = (z_i | i \in \mathcal{N}(a))^{\mathrm{T}}$ with $\mathcal{N}(a) \subseteq \mathcal{I}$ for all $a \in \mathcal{A}$ and $Z = \int_{\boldsymbol{z}} \prod_{a \in \mathcal{A}} f_a(\boldsymbol{z}_a) d\boldsymbol{z}$ is a normalization constant. We also define $\mathcal{N}(i) \triangleq \{a \in \mathcal{A} | i \in \mathcal{N}(a)\}$ for all $i \in \mathcal{I}$. Similarly, $\mathcal{N}(a) = \{i \in \mathcal{I} | a \in \mathcal{N}(i)\}$ for all $a \in \mathcal{A}$. The above factorization can be graphically represented by means of a factor graph [40]. A factor graph [1] is a bipartite

[1] We will use Tanner factor graphs [40] throughout this thesis

graph having a variable node i (typically represented by a circle) for each variable z_i, $i \in \mathcal{I}$ and factor node a (represented by a square) for each factor f_a, $a \in \mathcal{A}$. An edge connects a variable node i to a factor node a if, and only if, the variable z_i is an argument of the factor function f_a. The set $\mathcal{N}(i)$ contains all factor nodes connected to a variable node $i \in \mathcal{I}$ and $\mathcal{N}(a)$ is the set of all variable nodes connected to a factor node $a \in \mathcal{A}$.

Factor graphs provide a compact and intuitive representation of the statistical dependencies among the random variables in a probabilistic model. Furthermore, they enable the design of a class of iterative signal processing algorithms which are based on the nodes of the graph iteratively exchanging information (messages) with their neighbors (connected nodes). This class of algorithms has been coined *message-passing* techniques, and in the following we will describe the two instances of these techniques which have been most widely applied to signal processing for communication systems: the SP and VMP algorithms.

3.2 The Sum-Product Algorithm

The SP algorithm is a message-passing algorithm that computes the exact marginal distributions $p_i(z_i)$ of the variables z_i associated to the joint distribution $p(\boldsymbol{z})$ for tree-shaped factor graphs. When the factor graph does not have a tree structure, the outcome of the algorithm is only an approximation of the true marginal, and the approximate marginals $b_i(z_i) \approx p_i(z_i)$ are called beliefs. The message-passing algorithm is derived from the equations of the stationary points of the constrained Bethe free energy [34].

The algorithm operates iteratively by exchanging messages from variable nodes to factor nodes and vice-versa. The message computation rules for the SP algorithm read

$$
\begin{aligned}
m_{a\to i}(z_i) &= d_a \langle f_a(\boldsymbol{z}_a) \rangle_{\prod_{j\in\mathcal{N}(a)\setminus i} n_{j\to a}}, \quad \forall a \in \mathcal{A}, i \in \mathcal{N}(a) \\
n_{i\to a}(z_i) &= \prod_{c\in\mathcal{N}(i)\setminus a} m_{c\to i}(z_i), \quad \forall i \in \mathcal{I}, a \in \mathcal{N}(i)
\end{aligned}
$$

where the notation $\langle f(x) \rangle_g$ denotes the expectation of $f(x)$ taken over $g(x)$ and d_a ($a \in \mathcal{A}$) are positive constants ensuring that the beliefs are normalized. Often the constants d_a need not be calculated explicitly, and it is enough to normalize the beliefs after convergence of the algorithm (see Paper A for more details on normalization

issues). We use the notation $n_{(\cdot)\to(\cdot)}$ for output messages from a variable node to a factor node and $m_{(\cdot)\to(\cdot)}$ for input messages from a factor node to a variable node.

The variables' beliefs can be calculated at any point during the iterative algorithm as

$$b_i(z_i) = \prod_{a\in\mathcal{N}(i)} m_{a\to i}(z_i) \quad \forall i \in \mathcal{I}.$$

The SP algorithm acquired great popularity through its application to iterative decoding of, among others, turbo codes and LDPC codes, and has since then been used for the design of many iterative algorithms in a wide variety of fields [25].

3.3 The Variational Message-Passing Algorithm

The VMP algorithm is an alternative message-passing technique which is derived based on the minimization of the variational free energy subject to the mean-field approximation constraint on the beliefs. While it does not guarantee the computation of exact marginals (even for tree-shaped graphs), its convergence is guaranteed by ensuring that the variational free energy of the computed beliefs is non-increasing at each step of the algorithm [34].

The operation of the VMP algorithm is analogous to the SP algorithm; the message computation rules read

$$m_{a\to i}(z_i) = \exp\langle \log f_a(\boldsymbol{z}_a)\rangle_{\prod_{j\in\mathcal{N}(a)\setminus i} n_{j\to a}}, \quad \forall a \in \mathcal{A}, i \in \mathcal{N}(a) \tag{3.2}$$

$$n_{i\to a}(z_i) = e_i \prod_{c\in\mathcal{N}(i)} m_{c\to i}(z_i) \quad \forall i \in \mathcal{I}, a \in \mathcal{N}(i) \tag{3.3}$$

where e_i ($i \in \mathcal{I}$) are positive constants ensuring that $n_{i\to a}$ are normalized. As in the SP algorihtm, the beliefs can be obtained as

$$b_i(z_i) = e_i \prod_{c\in\mathcal{N}(i)} m_{c\to i}(z_i) = n_{i\to a}(z_i) \quad \forall i \in \mathcal{I}, a \in \mathcal{N}(i).$$

The VMP algorithm has recently attracted the attention of the wireless communication research community due to its suitability for conjugate-exponential probabilistic models [35]. The computation rule for input messages from factor to variable nodes allows for the obtention of closed-form expressions in many cases in which the SP algorithm typically requires some type of numerical approximation.

It is shown in Paper A that a message-passing interpretation of the EM algorithm can be obtained from the VMP algorithm. Assume that for a certain subset of variables z_i, $i \in \mathcal{E} \subseteq \mathcal{I}$ we want to apply an EM update while still using VMP for the rest of variables. To do so, the beliefs b_i are restricted to fulfill the constraint $b_i(z_i) = \delta(z_i - \tilde{z}_i)$ for all $i \in \mathcal{E}$ additionally to the mean-field factorization and normalization constraints. Minimizing the variational free energy subject to these conditions leads to a message passing algorithm identical to the one described in (3.2) and (3.3) except that the messages $n_{i\to a}$ for all $i \in \mathcal{E}$ and $a \in \mathcal{N}(i)$ are replaced by

$$n_{i\to a}(z_i) = \delta(z_i - \tilde{z}_i) \qquad \text{with} \quad \tilde{z}_i = \underset{\boldsymbol{z}_i}{\operatorname{argmax}} \left(\prod_{a\in\mathcal{N}(i)} m_{a\to i}(z_i) \right). \tag{3.4}$$

3.4 Combined VMP-SP Algorithm

As stated previously in this chapter, the VMP and the SP algorithms are two message-passing techniques suitable for different types of models. While SP is especially suitable in models with deterministic factor nodes, e.g. code or modulation constraints, VMP has the advantage of yielding closed-form computationally tractable expressions in conjugate-exponential models, as are found in channel weight estimation and noise variance estimation problems. Based on these facts, it seems natural to try to combine the two methods in a unified scheme capable of preserving the advantages of both.

A combined message-passing scheme based on the SP and VMP algorithms was recently proposed in Papers A and B. This hybrid technique is based on splitting the factor graph into two different parts: a VMP part and a SP part. To do this, part of the factor nodes are assigned to the VMP set ($\mathcal{A}_{\text{VMP}}$) and the rest are assigned to the SP set ($\mathcal{A}_{\text{SP}}$). Given this classification, we can express the probabilistic model in (3.1) as

$$p(\boldsymbol{z}) = \frac{1}{Z} \overbrace{\prod_{a\in\mathcal{A}_{\text{VMP}}} f_a(\boldsymbol{z}_a)}^{\text{VMPpart}} \overbrace{\prod_{c\in\mathcal{A}_{\text{SP}}} f_c(\boldsymbol{z}_c)}^{\text{SPpart}}$$

where $\mathcal{A}_{\text{VMP}} \cup \mathcal{A}_{\text{SP}} = \mathcal{A}$ and $\mathcal{A}_{\text{VMP}} \cap \mathcal{A}_{\text{SP}} = \emptyset$. By applying the Bethe approximation to the SP part and the mean-field approximation on the VMP part, a new message-passing scheme is derived from the stationary points of the region-based free energy.

The message computation rules for this algorithm read

$$m_{a\to i}^{\mathrm{VMP}}(z_i) = \exp\langle \log f_a(\boldsymbol{z}_a)\rangle_{\prod_{j\in\mathcal{N}(a)\setminus i} n_{j\to a}}, \quad \forall a \in \mathcal{A}_{\mathrm{VMP}}, i \in \mathcal{N}(a) \tag{3.5}$$

$$m_{a\to i}^{\mathrm{SP}}(z_i) = d_a \langle f_a(\boldsymbol{z}_a)\rangle_{\prod_{j\in\mathcal{N}(a)\setminus i} n_{j\to a}}, \quad \forall a \in \mathcal{A}_{\mathrm{SP}}, i \in \mathcal{N}(a) \tag{3.6}$$

$$n_{i\to a}(z_i) = e_i \prod_{c\in\mathcal{N}(i)\cap\mathcal{A}_{\mathrm{VMP}}} m_{c\to i}^{\mathrm{VMP}}(z_i) \prod_{c\in\mathcal{N}(i)\cap\mathcal{A}_{\mathrm{SP}}\setminus a} m_{c\to i}^{\mathrm{SP}}(z_i) \quad \forall i \in \mathcal{I}, a \in \mathcal{N}(i) \tag{3.7}$$

where, again, d_a and e_i are positive constants ensuring normalized beliefs. The computation rules for messages outgoing factor nodes are preserved: for factor nodes in the VMP part ($a \in \mathcal{A}_{\mathrm{VMP}}$) the messages are computed using (3.5) as in standard VMP; for factor nodes in the SP part ($a \in \mathcal{A}_{\mathrm{SP}}$) the messages are computed via (3.6), which corresponds to a standard SP message. A message from a variable node i to a factor node a is computed as a VMP message when $a \in \mathcal{A}_{\mathrm{VMP}}$ and as a SP message when $a \in \mathcal{A}_{\mathrm{SP}}$, as can be deduced from (3.7).

As with the VMP and SP algorithms, the beliefs of the variables can be retrieved at any stage of the algorithm as

$$b_i(z_i) = e_i \prod_{a\in\mathcal{N}(i)\cap\mathcal{A}_{\mathrm{VMP}}} m_{a\to i}^{\mathrm{VMP}}(z_i) \prod_{a\in\mathcal{N}(i)\cap\mathcal{A}_{\mathrm{SP}}} m_{a\to i}^{\mathrm{SP}}(z_i) \quad \forall i \in \mathcal{I}.$$

Note that we can apply the EM restriction to the belief of variables z_i which are only connected to VMP factors (i.e. $\mathcal{N}(i)\cap\mathcal{A}_{\mathrm{SP}} = \emptyset$). In that case, the message update rules remain the same except that the message $n_{i\to a}$ in (3.7) is replaced by (3.4) for the selected variables.

4

Contributions of the Thesis

In this chapter, we detail the contributions of this thesis. The main body of the thesis is composed of Papers A–O. Most of the articles propose or study one or several algorithms that deal with specific problems within the context of advanced baseband receiver design.

Following the same nomenclature made in Chapter 2, we categorize the papers according to the type of algorithm discussed in them: algorithms derived from formal inference frameworks or heuristically designed algorithms. One paragraph per article is provided which briefly introduces its content and scientific contribution.

4.1 Inference Frameworks

Papers A–H all deal with algorithms derived from variational Bayesian inference frameworks. More specifically, Papers A and B present a novel message-passing algorithm based on a combined application of the MF approximation and the BP framework; the message computation rules of this technique have already been presented in Chapter 3.4. Papers C–H, on the other hand, deal with particular applications of inference frameworks to the design of receiver structures in wireless communication systems.

Paper A In this contribution, a joint message-passing approach combining belief propagation and the mean-field approximation is presented. The algorithm is derived based on the region-based free energy approximation method in [34]. Specifically, the message-passing fixed point equations of the combined algorithm are shown

to be the stationary points of the constrained region-based free energy approximation. Moreover, some conditions on the factor-graph describing the underlying probabilistic model to ensure a convergent algorithm are given.

Paper B This article is, basically, a shortened conference version of Paper A. In it, the message-update equations of a novel message-passing algorithm combining MF and BP are derived from a constrained region-based free energy approximation. Note that, although the expressions for the message computation rules in this contribution are slightly different from the ones presented in Paper A, they are equivalent.

Paper C In this paper, we apply the combined message-passing scheme introduced in Papers A and B to the design of iterative receiver structures for a MIMO-OFDM system. From a factor graph representing the underlying probabilistic model of a MIMO-OFDM system, we derive a generic message-passing receiver iteratively performing channel weight estimation, noise variance estimation, MIMO equalization and data decoding. We show how, by applying specific scheduling schemes and different restrictions to the generic algorithm, we are able to obtain a number of particular receiver architectures which span from full-iterative, high performance receivers to simplified low-complexity implementations. Furthermore, the performance of the proposed receiver structures is demonstrated and compared to state-of-art methods by means of Monte Carlo simulations.

Paper D This paper deals with models and algorithms for estimation of sparse signals. The contribution in it is two-fold: firstly, a hierarchical Bayesian formalism for the design of sparsity-inducing priors is introduced; secondly, a variational message-passing algorithm operating in the said hierarchical Bayesian model is proposed. The general hierarchical model can be particularized for real- and complex-valued models. A Bayesian formulation of the widely-used l_1-norm constraint for sparse estimation can also be obtained as an instance of our proposed model. In addition, the model allows for the design of novel priors with better sparsity-inducing properties than the l_1-norm. Simulation results illustrate how the proposed VMP algorithm applied to the hierarchical Bayesian model outperforms state-of-the-art sparse estimation techniques, especially for low and moderate signal-to-noise ratio regimes.

Paper E This contribution presents an iterative receiver structure for multi-user OFDM systems performing channel weight and noise variance estimation, multi-user detection and single-user decoding. The receiver is derived based on the VMP algorithm (see Chapter 3.3), but uses a standard SP (equivalent to BCJR) decoder. Note that in this work VMP and SP are separately applied to different parts of the receiver, and the two algorithms are combined in an "ad-hoc" way; this is in contrast to the approach in Paper C, in which a unified VMP-SP algorithm is applied to the full probabilistic model. Nonetheless, the simulation results illustrate how the proposed scheme can significantly outperform a heuristic receiver adapted for OFDM systems from [26].

Paper F We propose an iterative receiver structure for OFDM systems with synchronous interferers. The receiver is derived based on a MF-based variational inference framework, which is referred to as the divergence minimization (DM) framework following the terminology in [52]. The proposed structure performs iterative channel estimation, interference cancellation and single-user decoding of the desired signal. The numerical results, obtained by Monte Carlo simulations, show how the proposed scheme can effectively mitigate the effect of the interferers, achieving BER values close to those of a receiver operating in an interference-free scenario. It is also worth mentioning that the receiver structure presented in this work can be seen as a specific instance of the generic receiver derived in Paper C.

Paper G In this conference contribution, we propose an iterative pilot-based channel estimator for OFDM systems with co-channel interference. The proposed estimator can be applied to systems in which the user of interest and the interferers transmit their pilot signals in the same time-frequency locations. The iterative estimator is derived following the DM framework in [52], yielding a sequential scheme in which the channel coefficients for one user are estimated after subtracting the signal contributions from all other users. As the numerical results demonstrate, the performance of the sequential estimator approaches, with a sufficient number of iterations, that of a joint LMMSE channel estimator; however, its sequential structure allows for a significantly lower computational complexity, as the cumbersome matrix inversions in the joint LMMSE estimator can be avoided with a suitable design. As in the case of Paper F, the channel estimator

proposed in this contribution can be interpreted as an instance of the generic message-passing receiver presented in Paper C.

Paper H In this work, we apply the method presented in Paper D for modeling and estimation of sparse signals to the problem of pilot-based channel estimation in OFDM systems. As a result, a channel estimator based on VMP is obtained which estimates the active components of the sparse time-domain response of the channel rather than directly estimating the channel frequency-response coefficients. Simulation results illustrate the effectiveness of the proposed approach, which outperforms commonly-used frequency-domain estimators (e.g. a robustly-designed Wiener filter) as well as other state-of-art sparse estimation techniques.

4.2 Heuristic Algorithms

Papers I–O in this thesis present contributions within the field of heuristic algorithms, mainly for OFDM systems. In particular, Papers I and J deal with schemes for iterative MIMO detection and decoding, while Papers L–O deal with issues regarding both linear and iterative channel estimation algorithms for OFDM. The specific scientific contributions made in each article are detailed in the following:

Paper I In this article, we analyze the performance of different implementations of a MIMO receiver performing sequential interference cancellation (SIC) and decoding of the transmitted signals. The different receiver structures are specifically designed for the 3GPP LTE-downlink [56] parameter settings. It is shown how SIC schemes using a "per-codeword" selection strategy clearly outperform the schemes that operate on a "per-subcarrier" basis. Furthermore, it is found that, for the evaluated schemes, providing soft-feedback from the channel decoder only improves the receiver's performance slightly compared to using hard-decision feedback.

Paper J This contribution compares two transmission technologies, namely OFDM and single-carrier frequency-domain multiplexing (SC-FDM) as potential technologies for the uplink of the 3GPP LTE-A system. The comparison is done

under the assumption that, for both transmission schemes, a turbo-receiver performing iterative interference cancellation, MIMO detection and single-user decoding, either in a sequential or a parallel fashion, is used. The numerical results presented show that, while using a turbo-receiver for SC-FDM systems can very significantly reduce the BER attained with this technology, an OFDM system with turbo receivers can attain a superior spectral efficiency than its SC-FDMA counterpart. This is especially relevant when only two receive antennas are employed; for systems with more receive than transmit antennas, both systems yield comparable performance.

Paper K The contribution of this paper is two-fold: first, a parametric channel model allowing for a more dynamical behavior of the multipath components compared to standard models is presented; next, a detailed analysis of spatial smoothing techniques [57] applied to the estimation of multipath components' delays in OFDM systems is provided. The proposed channel estimation technique uses Unitary ESPRIT [58] together with spatial smoothing techniques to obtain an estimate of the multipath components' delays; this estimate is then fed to the channel estimator proposed in [16]. From the presented simulation results, we draw two main conclusions: first, it is crucial to adequately model the dynamical behavior of multipath components in order to obtain meaningful insight from the numerical evaluation; second, spatial-smoothing techniques can, when properly designed, greatly improve the accuracy of the estimates of the multipath components' delays.

Paper L This contribution presents a heuristic iterative channel estimation algorithm for the downlink of the 3GPP LTE standard. The iterative channel estimator is based on a modified version of the robustly-designed Wiener filter [11] which incorporates the receiver information on the data symbols by means of hard-decision feedback. The effect of the number of iterations run inside the turbo decoder before and after feeding back the information to the channel estimator is analyzed via Monte Carlo simulations. The discussion of the results shows that moderate gains in terms of BER and average cell spectral efficiency can be obtained with the proposed scheme compared to a reference receiver without increasing the total number of iterations run in the turbo decoder.

Paper M In this article, several state-of-art pilot-aided channel estimation algorithms are analyzed within a downlink 3GPP LTE context. The considered estimators are defined under a unified notation that allows for a generic MSE evaluation of all of them. Two main types of estimators are considered: estimators using DFT techniques for the estimation of the channel impulse response and estimators which incorporate knowledge of the multipath components' delays. The MSE and BER analysis shows that DFT-based estimators suffer from two important degradation effects: the *leakage* effect [14] caused by the limited sampling resolution in the receiver and numerical instabilities due to the inversion of ill-conditioned matrices. On the other hand, estimators making use of the multipath components' delay information need very precise estimates of these delays to avoid severe MSE degradation.

Paper N In this work, we analyze the performance of linear pilot-aided channel estimators for OFDM systems. In particular, two DFT-based channel estimators, proposed in [15] and [59], are studied analytically and by means of Monte Carlo simulations for a system with settings similar to the downlink of the 3GPP LTE standard [56]. An MSE analysis of the estimators reveals that DFT-based estimators suffer from numerical issues due to the inversion of ill-conditioned matrices when the number of active subcarriers of the OFDM system is smaller than the DFT size. This caveat can be overcome by means of Tikhonov regularization [60], as it is done in [59]. Furthermore, a computational complexity analysis is provided which demonstrates the computational advantages of DFT-based estimators as compared to traditional Wiener filter approaches.

Paper O This contribution researches the effect of imperfections in the local oscillators of transmitters and receivers on the performance of OFDM systems. More specifically, the impact of phase noise degradation in downlink LTE systems is studied. We model the phase noise as a Wiener-Lévy process [61], and we evaluate the performance of a receiver employing LMMSE channel estimation with different pilot patterns and for several phase noise powers via Monte Carlos simulations. The numerical results show that phase noise can cause sever degradation at high SNR regimes; this effect can be mitigated by increasing the pilot-symbol density, with the associated cost of an increased transmission overhead.

References

[1] 3GPP, "Feasibility study for further advancements for E-UTRA (LTE-advanced) (release 9)," 3GPP TR 36.912, V9.3.0 (2010-06) Technical Specification, 2009. 1

[2] ITU-R, "Requirements related to technical performance for IMT-advanced radio interface(s)," Report M.2134, Nov. 2008. 1

[3] M. Ergen, *Mobile Broadband Including WiMAX and LTE*. Berkeley, CA, USA: Springer, 2009. 2, 4

[4] L. Zheng and D. N. C. Tse, "Diversity and multiplexing: a fundamental tradeoff in multiple-antenna channels." *IEEE Trans. Inform. Theory*, pp. 1073–1096, 2003. 4

[5] E. Telatar, "Capacity of multi-antenna Gaussian channels," *European Transactions on Telecommunications*, vol. 10, pp. 585–595, 1999. 4

[6] L. Hanzo, M. Munster, B. J. Choi, and T. Keller, *OFDM and MC-CDMA for Broadband Multi-User Communications, WLANs and Broadcasting*. West Sussex, England: John Wiley & Sons, 2003. 4, 14

[7] C. Berrou, A. Glavieux, and P. Thitimajshima, "Near Shannon limit error-correcting coding and decoding: Turbo codes," in *IEEE Int. Conf. Commun. (ICC)*, May 1993, pp. 1064–1070. 4, 12

[8] R. Gallager, "Low-density parity-check codes," *IEEE Trans. Inform. Theory*, vol. 8, no. 1, pp. 21–28, Jan. 1962. 4, 17

[9] J. G. Proakis and M. Salehi, *Communication Systems Engineering*, 2nd ed. Upper Saddle River, NJ, USA: Prentice-Hall, August 2001. 9, 12

[10] G. Coluccia, E. Riegler, C. Mecklenbrauker, and G. Taricco, "Optimum mimo-ofdm detection with pilot-aided channel state information," *Selected Topics in Signal Processing, IEEE Journal of*, vol. 3, no. 6, pp. 1053 –1065, dec. 2009. 9

[11] P. Hoeher, S. Kaiser, and P. Robertson, "Two-dimensional pilot-symbol-aided channel estimation by Wiener filtering," in *ICASSP-97., IEEE International Conf. on*, vol. 3, Apr. 1997, pp. 1845–1848. 11, 29

[12] Y. Li, J. Cimini, L.J., and N. Sollenberger, "Robust channel estimation for OFDM systems with rapid dispersive fading channels," *Communications, IEEE Transactions on*, vol. 46, no. 7, pp. 902–915, Jul. 1998. 11

[13] O. Edfors, M. Sandell, J.-J. van de Beek, S. Wilson, and P. Borjesson, "Ofdm channel estimation by singular value decomposition," *Communications, IEEE Transactions on*, vol. 46, no. 7, pp. 931 –939, jul 1998. 11

[14] J.-J. van de Beek, O. Edfors, M. Sandell, S. Wilson, and P. Borjesson, "On channel estimation in ofdm systems," in *Vehicular Technology Conference, 1995 IEEE 45th*, vol. 2, jul 1995, pp. 815 –819 vol.2. 11, 30

[15] L. Deneire, P. Vandenameele, L. van der Perre, B. Gyselinckx, and M. Engels, "A low-complexity ml channel estimator for ofdm," *Communications, IEEE Transactions on*, vol. 51, no. 2, pp. 135 – 140, feb 2003. 11, 30

[16] B. Yang, K. Letaief, R. Cheng, and Z. Cao, "Channel estimation for ofdm transmission in multipath fading channels based on parametric channel modeling," *Communications, IEEE Transactions on*, vol. 49, no. 3, pp. 467 –479, mar 2001. 11, 29

[17] A. van Zelst, "MIMO-OFDM for wireless LAN," Ph.D. dissertation, Department of Electrical Engineering, Eindhoven University of Technology, Apr. 2004. 11

[18] B. Hochwald and S. ten Brink, "Achieving near-capacity on a multiple-antenna channel," *Communications, IEEE Transactions on*, vol. 51, no. 3, pp. 389 – 399, march 2003. 11

[19] P. Wolniansky, G. Foschini, G. Golden, and R. Valenzuela, "V-BLAST: an architecture for realizing very high data rates over the rich-scattering wireless channel," in *Signals, Systems, and Electronics, 1998. ISSSE 98. 1998 URSI International Symposium on*, sep-2 oct 1998, pp. 295 –300. 11

[20] H. Lee, B. Lee, and I. Lee, "Iterative detection and decoding with an improved v-blast for mimo-ofdm systems," *Selected Areas in Communications, IEEE Journal on*, vol. 24, no. 3, pp. 504 –513, march 2006. 11

[21] X. Wang and H. Poor, "Iterative (turbo) soft interference cancellation and decoding for coded CDMA," *IEEE Trans. Commun.*, vol. 47, pp. 1046–1061, Jul. 1999. 11, 13, 14

[22] L. Bahl, J. Clocke, F. Jelinek, and J. Raviv, "Optimal decoding of linear codes for minimizing symbol error rate," *IEEE Trans. Inform. Theory*, vol. 20, no. 3, pp. 284–287, Mar. 1974. 12

[23] J. Hagenauer and P. Hoeher, "A viterbi algorithm with soft-decision outputs and its applications," in *Global Telecommunications Conference, 1989, and Exhibition. Communications Technology for the 1990s and Beyond. GLOBECOM '89., IEEE*, nov 1989, pp. 1680 –1686 vol.3. 12

[24] R. McEliece, D. MacKay, and J. Cheng, "Turbo decoding as an instance of Pearl's belief "propagation" algorithms," *IEEE J. Select. Areas Commun.*, vol. 16, no. 2, pp. 140–152, Feb. 1998. 12, 17

[25] H.-A. Loeliger, J. Dauwels, J. Hu, S. Korl, L. Ping, and F. Kschischang, "The factor graph approach to model-based signal processing," *Proceedings of the IEEE*, vol. 95, no. 6, pp. 1295–1322, Jun. 2007. 12, 17, 21

[26] J. Wehinger and C. Mecklenbräuker, "Iterative CDMA multiuser receiver with soft decision-directed channel estimation," *IEEE Trans. Signal Processing*, vol. 54, pp. 3922–3934, Oct. 2006. 13, 14, 27

[27] P. Rossi and R. Müller, "Joint twofold-iterative channel estimation and multiuser detection for MIMO-OFDM systems," *IEEE Trans. Wireless Commun.*, vol. 7, no. 11, pp. 4719–4729, Nov. 2008. 13, 14

[28] F. Sanzi, S. Jelting, and J. Speidel, "A comparative study of iterative channel estimators for mobile OFDM systems," *Wireless Communications, IEEE Transactions on*, vol. 2, no. 5, pp. 849 – 859, sept. 2003. 14

[29] S. Y. Park, Y. G. Kim, and C. G. Kang, "Iterative receiver for joint detection and channel estimation in OFDM systems under mobile radio channels," *IEEE Transactions on Vehicular Technology*, vol. 53, no. 2, pp. 450–460, Mar. 2004. 14

[30] R. Koetter, A. C. Singer, and M. Tücher, "Turbo equalization," *IEEE Trans. Signal Processing*, vol. 1, pp. 64–80, 2004. 14

[31] S. Haykin, M. Sellathurai, Y. de Jong, and T. Willink, "Turbo-MIMO for wireless communications," *Communications Magazine, IEEE*, vol. 42, no. 10, pp. 48 – 53, oct. 2004. 14

[32] A. Tonello, "MIMO MAP equalization and turbo decoding in interleaved space-time coded systems," *IEEE Trans. Commun.*, vol. 51, no. 2, pp. 155 – 160, feb 2003. 14

[33] M. Wainwright and M. Jordan, "Graphical models, exponential families, and variational inference," *Foundations and Trends in Machine Learning*, vol. 1, no. 1-2, pp. 1–305, Dec. 2008. 14, 15, 16, 17

[34] J. Yedidia, W. Freeman, and Y. Weiss, "Constructing free-energy approximations and generalized belief propagation algorithms," *IEEE Trans. Inform. Theory*, vol. 51, no. 7, pp. 2282–2312, July 2005. 14, 15, 16, 17, 20, 21, 25

[35] J. Winn and C. Bishop, "Variational message passing," *Journal of Machine Learning Research*, 2004. 15, 17, 19, 21

[36] C. Bishop, *Pattern Recognition and Machine Learning*. Springer, 2006. 15, 17

[37] T. Minka, "Divergence measures and message passing," Microsoft Research Ltd., Tech. Rep., 2005. 15

[38] T. Cover and J. Thomas, *Elements of Information Theory*, 2nd ed. Wiley Interscience, 2006. 15

[39] J. Dauwels, "On variational message passing on factor graphs," in *Information Theory, 2007. ISIT 2007. IEEE International Symposium on*, Jun. 2007, pp. 2546–2550. 16, 17

[40] F. Kschischang, B. Frey, and H.-A. Loeliger, "Factor graphs and the sum-product algorithm," *IEEE Trans. Inform. Theory*, vol. 47, no. 2, pp. 498–519, Feb. 2001. 17, 19

[41] E. Riegler, G. Kirkelund, C. Manchón, and B. Fleury, "Merging belief propagation and the mean field approximation: A free energy approach," in *Turbo Codes and Iterative Information Processing (ISTC), 2010 6th International Symposium on*, sept. 2010, pp. 256 –260. 17

[42] E. Riegler, G. E. Kirkelund, C. N. Manchón, and B. H. Fleury, "Merging belief propagation and the mean field approximation: A free energy approach," *IEEE Trans. Inform. Theory*, Under Preparation. 17

[43] J. Boutros and G. Caire, "Iterative multiuser joint decoding: unified framework and asymptotic analysis," *IEEE Trans. Inform. Theory*, vol. 48, no. 7, pp. 1772–1793, Jul 2002. 17

[44] G. Colavolpe and G. Germi, "On the application of factor graphs and the sum-product algorithm to ISI channels," *IEEE Trans. Commun.*, vol. 53, no. 5, pp. 818–825, 2005. 17

[45] C. Novak, G. Matz, and F. Hlawatsch, "A factor graph approach to joint iterative data detection and channel estimation in pilot-assisted IDMA transmissions," in *Acoustics, Speech and Signal Processing, 2008. ICASSP 2008. IEEE International Conference on*, 31 2008-april 4 2008, pp. 2697 –2700. 17

[46] A. P. Worthen and W. E. Stark, "Unified design of iterative receivers using factor graphs," *IEEE Trans. Inform. Theory*, vol. 47, no. 2, pp. 843–849, 2001. 17

[47] A. Dempster, N. Laird, and D. Rubin, "Maximum likelihood from incomplete data via the EM algorithm," *Journal of the Royal Statistical Society. Series B (Methodological)*, vol. 39, no. 1, pp. 1–38, 1977. 17

[48] J. Dauwels, S. Korl, and H.-A. Loeliger, "Expectation Maximization as Message Passing," in *Proceedings of the International Symposium on Information Theory*, Sep. 2005, pp. 583–586. 17

[49] C. Novak, F. Hlawatsch, and G. Matz, "Low-complexity factor graph receivers for spectrally efficient MIMO-IDMA," in *Communications, 2008. ICC '08. IEEE International Conference on*, may 2008, pp. 770 –774. 17

[50] C. Novak, G. Matz, and F. Hlawatsch, "Factor graph based design of an OFDM-IDMA receiver performing joint data detection, channel estimation, and channel length selection," in *Acoustics, Speech and Signal Processing, 2009. ICASSP 2009. IEEE International Conference on*, april 2009, pp. 2561 –2564. 17

[51] L. Christensen and J. Larsen, "On data and parameter estimation using the variational Bayesian EM-algorithm for block-fading frequency-selective MIMO channels," in *Proc. IEEE In. Conf. on Acoustics, Speech and Sign. Process.*, vol. 4, 2006, pp. 465–468. 17

[52] B. Hu, I. Land, L. Rasmussen, R. Piton, and B. Fleury, "A divergence minimization approach to joint multiuser decoding for coded CDMA," *IEEE J. Select. Areas Commun.*, vol. 26, no. 3, pp. 432–445, Apr. 2008. 17, 27

[53] D. Lin and T. Lim, "The variational inference approach to joint data detection and phase noise estimation in OFDM," *IEEE Trans. Signal Processing*, vol. 55, no. 5, pp. 1862–1874, May 2007. 17

[54] M. Nissilä, "Iterative receivers for digital communications via variational inference and estimation," Ph.D. dissertation, University of Oulu, 2008. 17

[55] X.-Y. Zhang, D.-G. Wang, and J.-B. Wei, "Joint symbol detection and channel estimation for MIMO-OFDM systems via the variational Bayesian EM algorithms," in *Wireless Commun. and Networking Conf., WCNC. IEEE*, Mar.-Apr. 2008, pp. 13–17. 17

[56] 3GPP, "General description," 3GPP TS 36.201, V8.0.0 (2007-09) Technical Specification, 2007. 28, 30

[57] H. Krim and M. Viberg, "Two decades of array signal processing research: the parametric approach," *IEEE Trans. Signal Processing*, vol. 13, no. 4, pp. 67–94, Jul. 1996. 29

[58] M. Haardt and J. Nossek, "Unitary ESPRIT: how to obtain increased estimation accuracy with a reduced computational burden," *IEEE Trans. Signal Processing*, vol. 43, no. 5, pp. 1232 –1242, May 1995. 29

[59] H. Schmidt, V. Kuhn, K. Kammeyer, R. Rueckriem, and S. Fechtel, "Channel tracking in wireless OFDM systems," in *5th World Multi-Conference on Systemics, Cybernetics and Informatics, SCI 2001*, Jul. 2001. 30

[60] A. N. Tikhonov and V. Y. Arsenin, *Solutions of Ill-Posed Problems*. V. H. Winston & Sons, Washington, D.C.: John Wiley & Sons, New York,, 1977. 30

[61] S. Wu and Y. Bar-Ness, "OFDM systems in the presence of phase noise: consequences and solutions," *IEEE Trans. Commun.*, vol. 52, no. 11, pp. 1988 – 1996, nov. 2004. 30

Paper A

Merging Belief Propagation and the Mean Field Approximation: A Free Energy Approach

Erwin Riegler, Gunvor E. Kirkelund, Carles Navarro Manchón and Bernard H. Fleury

Under preparation.

A. MERGING BELIEF PROPAGATION AND THE MEAN FIELD APPROXIMATION: A FREE ENERGY APPROACH

Merging Belief Propagation and the Mean Field Approximation: A Free Energy Approach

Erwin Riegler*, Gunvor Elisabeth Kirkelund†, Carles Navarro Manchón†, Bernard Henri Fleury†
* Vienna University of Technology (VUT), Austria
E-mail: erwin.riegler@nt.tuwien.ac.at
† Aalborg University (AAU), Denmark
E-mail: gunvor@es.aau.dk, cnm@es.aau.dk, bfl@es.aau.dk

***Abstract*—We present a joint message passing approach that combines belief propagation and the mean field approximation based on the region-based free energy approximation method proposed by Yedidia et al. We show that the message passing fixed point equations obtained by this combination correspond to stationary points of a constraint variational free energy approximation. Moreover, we present a convergent implementation of these message passing fixed point equations provided that the underlying factor graph fulfills certain technical conditions. In addition, we show how to include hard constraints in the part of the factor graph corresponding to belief propagation. As an example, we demonstrate our method for iterative channel estimation and decoding in a time-varying frequency-flat mobile channel.**

I. Introduction

Variational techniques have been used for decades in quantum and statistical physics, where they are referred to as *mean field* (MF) approximation [2]. Later, they found their way to the area of machine learning or statistical inference, see, e.g., [3]–[6]. The basic idea of variational inference is to derive the statistics of "hidden" random variables given the knowledge of "visible" random variables of a certain probability density function (pdf). This is done by approximating the pdf by some "simpler," e.g., (fully) factorized pdf and minimizing the Kullback-Leibler divergence between the approximating and the true pdf, which can be done in an iterative, i.e., message passing like way. Apart from being fully factorized, the approximating pdf typically fulfills additional constraints that allow for messages that have a simple structure and can be updated in a simple way. For example, additional exponential conjugacy constraints result in messages propagating along the edges in a Bayesian network that are described by a few parameters [5]. Variational inference methods were recently applied in [7] to the *channel state estimation/interference cancellation part* of a class of MIMO-OFDM receivers that iterate between detection, channel estimation, and decoding.

A different approach is *belief propagation* (BP) [8]. Roughly speaking, with BP one tries to find *local* approximations, which are—exactly or approximately—the marginals of a certain pdf. This can also be done in an iterative way, where messages are passed along the edges in a factor graph [9]. A typical application of BP is *decoding* of turbo or low density parity check (LDPC) codes. Based on the excellent performance of BP, a lot of variations have been derived in order to push the performance of this algorithm even further. For example, minimizing an upper bound on the log partition function of a pdf leads to the powerful tree rewighted BP algorithm [10]. An offspring of this idea is the recently developed uniformly tree rewighted BP algorithm [11]. Another example is [12], where methods from information geometry can be used to compute correction terms for the beliefs obtained by loopy BP.

The fixed point equations of both, BP and the MF approximation, can be obtained by minimizing an approximation of the Kullback-Leibler divergence, called region-based variational free energy [13]. This approach differs from other methods, see, e.g., [14][1], because the starting point for the derivation of the corresponding message passing fixed point equations is the same objective function for both, BP and the MF approximation. Since both methods have their own advantages, it is of great benefit to combine them and develop a *unified message passing algorithm*. More precisely, suppose that a probability mass function (pmf) admits an a priori factorization as a product of nonnegative real-valued functions and we want to apply BP to a certain subset of factors of this factorization and the MF approximation to the remaining factors of this factorization. The main technical result of this work is Theorem 2, where we show that the message passing fixed point equations for such a combination of BP and the MF approximation correspond to stationary points of one single constraint region-based variational free energy and state a clear rule how to couple the messages propagating in the BP and MF part. In fact, based on the factor graph corresponding to a factorization of a pmf and a choice for a separation into BP and MF factors of this factorization, Theorem 2 gives the message passing fixed point equations for the factor graph representing the whole factorization of the pmf. One example for an application of Theorem 2 is joint channel estimation, interference cancellation, and decoding. Note that typically these parts are considered as separate units and the coupling between these units is described in a heuristic way Despite having a clear rule to update the messages for the whole factor graph representing a factorization of a pmf, an additional advantage is the fact that solutions of fixed point equations for the messages are related to the stationary

[1] An information theoretical interpretation of the different objective functions used in [14] can be found in [15].

points of the corresponding constraint variational free energy approximation. This correspondence is important because it yields an interpretation of the computed beliefs for arbitrary factor graphs similar to the case of solely BP, where solutions of the message passing fixed point equations do in general not correspond to the true marginals if the factor graph has cycles but always correspond to stationary points of the constraint Bethe free energie [13]. Moreover, this observation allows us to present a systematic way of updating the messages, namely, Algorithm 2, that is guaranteed to converge provided that the factor graph representing the factorization of the pmf fulfills certain technical conditions.

The paper is organized as follows. In the remainder of this section we fix our notation. Section II is devoted to the introduction of the region-based free energy approximations proposed by [13] and to recall how BP, the MF approximation, and the EM algorithm [16] can be obtained by this method. Since the MF approximation is typically used for parameter estimation, we briefly show how it can be extended to the case of continuous random variables. Note that it is not obvious how to define the Fréchet derivative of the Kullback Leibler divergence with respect to a pdf when any point in the image of the pdf can be arbitrary close to zero. Therefore, we make use of [17, Th. 2.1] which allows to minimize the Kullback Leibler divergence without computing the Fréchet derivative in order to extend the MF approximation to the case of continuous random variables. Section III is the main part of this work. There we state our main result, namely, Theorem 2, and show how the message passing fixed point equations of a combination of BP and the MF approximation can be related to the stationary points of the corresponding constraint region-based free energy approximation. We then (i) show how to generalize Theorem 2 to the case where the factors of the pmf in the BP part are no longer restricted to be strictly positive real-valued functions and (ii) present Algorihm 2 that is a convergent implementation of the message passing update equations presented in Theorem 2 provided that the factor graph representing the factorization of the pmf fulfills certain technical conditions. As a byproduct, (i) gives insights for BP, which is a special case of the combination of BP and the MF approximation, with hard constraints, where only conjectures are formulated in [13]. In Section IV we apply Algorihm 2 to joint channel estimation and decoding of a time-varying frequency-flat mobile channel. More advanced receiver architectures together with numerical simulations and a comparison with other state of the art receivers can be found in [18]. Finally, we conclude in Section V and present an outlook for further research directions.

A. Notation

Capital calligraphic letters $\mathcal{A}, \mathcal{I}, \mathcal{N}$ denote finite sets. The cardinality of a set $\mathcal{I}$ is denoted by $|\mathcal{I}|$. If $i \in \mathcal{I}$ we write $\mathcal{I} \setminus i$ for $\mathcal{I} \setminus \{i\}$. We use the convention that $\prod_{\emptyset}(\dots) \triangleq 1$ where $\emptyset$ denotes the empty set. For any finite set $\mathcal{I}$, $I_{\mathcal{I}}$ denotes the indicatior function on $\mathcal{I}$, i.e., $\mathrm{I}_{\mathcal{I}}(i) = 1$ if $i \in \mathcal{I}$ and $\mathrm{I}_{\mathcal{I}}(i) = 0$ else. We denote by capital letters X discrete random variables with probability mass function $p(x)$ and $\sum_{x}(\dots)$ runs through all possible realizations x of X. We write $\mathbf{x} = (x_i \mid i \in \mathcal{I})^{\mathrm{T}}$ for the realization of the vector of random variables $\mathbf{X} = (X_i \mid i \in \mathcal{I})^{\mathrm{T}}$ with probability mass function $p(\mathbf{x})$. If $i \in \mathcal{I}$ then $\sum_{\mathbf{x} \setminus x_i}(\dots)$ runs through all possible realizations of $\mathbf{X}$ but X_i. For any nonnegative real valued function f with argument $\mathbf{x} = (x_i \mid i \in \mathcal{I})^{\mathrm{T}}$ and $i \in \mathcal{I}$, $f\mid_{\bar{x}_i}$ denotes f with fixed argument $x_i = \bar{x}_i$. If a function f is identically zero we write $f \equiv 0$ and $f \not\equiv 0$ means that it is not identically zero. For two real valued functions f and g with the same domain and argument x, we write $f(x) \propto g(x)$ if $f = cg$ for some real positive constant $c \in \mathbb{R}_+$. We use the convention that $0 \ln(0) = 0$, $a \ln(\frac{a}{0}) = \infty$ if $a > 0$, and $0 \ln(\frac{0}{0}) = 0$ [19, p. 31]. For $x \in \mathbb{R}$, $\delta(x) = 1$ if $x = 0$ and zero else. Matrices $\mathbf{\Lambda} \in \mathbb{C}^{m \times n}$ are denoted by capital boldface greek letters. The superscripts $^{\mathrm{T}}$ and $^{\mathrm{H}}$ stand for transposition and Hermitian transposition, respectively. For a matrix $\mathbf{\Lambda} \in \mathbb{C}^{m \times n}$, the entry in the ith row and jth column is denoted by $\lambda_{i,j}$. Finally, $\mathcal{CN}(\boldsymbol{\mu}, \mathbf{\Sigma})$ stands for the distribution of a jointly proper Gaussian random vector with mean $\boldsymbol{\mu}$ and covariance matrix $\mathbf{\Sigma}$ and $\Gamma(k, \theta)$ denotes the gamma distribution with scale parameter θ and shape parameter k.

II. Known results

A. Region-based free energy approximations [13]

Let $p(\mathbf{x})$ be a certain positive pmf of a vector $\mathbf{X}$ of random variables X_i $(i \in \mathcal{I})$ that factorizes as

$$p(\mathbf{x}) = \prod_{a \in \mathcal{A}} f_a(\mathbf{x}_a) \tag{1}$$

where $\mathbf{x} \triangleq (x_i \mid i \in \mathcal{I})^{\mathrm{T}}$ and $\mathbf{x}_a \triangleq (x_i \mid i \in \mathcal{N}(a))^{\mathrm{T}}$ with $\mathcal{N}(a) \subseteq \mathcal{I}$ for all $a \in \mathcal{A}$. We also set $\mathcal{N}(i) \triangleq \{a \in \mathcal{A} \mid i \in \mathcal{N}(a)\}$ for all $i \in \mathcal{I}$. Without loss of generality, we assume that all the factors f_a of the pmf p in (1) are real-valued positive functions. Later in Section (III), we shall show how to relax the positivity constraints for some of these factors. The factorization in (1) can be visualized in a *factor graph* [9]. In a factor graph, $\mathcal{N}(a)$ is the set of all variable nodes connected to a factor node $a \in \mathcal{A}$ and $\mathcal{N}(i)$ represents the set of all factor nodes connected to a variable node $i \in \mathcal{I}$. An example of a factor graph is depicted in Figure 1.

A *region* $R \triangleq \{\mathcal{I}_R, \mathcal{A}_R\}$ consists of subsets of indices $\mathcal{I}_R \subseteq \mathcal{I}$ and $\mathcal{A}_R \subseteq \mathcal{A}$ with the restriction that $a \in \mathcal{A}_R$ implies that $\mathcal{N}(a) \subseteq \mathcal{I}_R$. To each region R we associate a *counting number* $c_R \in \mathbb{Z}$. A set $\mathcal{R} \triangleq \{(R, c_R)\}$ of regions and associated counting numbers is called *valid* if

$$\sum_{R \in \mathcal{R}} c_R \, \mathrm{I}_{\mathcal{A}_R}(a) = \sum_{R \in \mathcal{R}} c_R \, \mathrm{I}_{\mathcal{I}_R}(i) = 1, \quad \forall a \in \mathcal{A}, i \in \mathcal{I}.$$

For an arbitrary pmf b of the vector $\mathbf{X}$ of random variables X_i $(i \in \mathcal{I})$, we define the *variational free energy* [13]

$$\begin{aligned} F(b) &\triangleq \sum_{\mathbf{x}} b(\mathbf{x}) \ln \frac{b(\mathbf{x})}{p(\mathbf{x})} \\ &= \underbrace{\sum_{\mathbf{x}} b(\mathbf{x}) \ln b(\mathbf{x})}_{\triangleq -H(b)} - \underbrace{\sum_{\mathbf{x}} b(\mathbf{x}) \ln p(\mathbf{x})}_{\triangleq -U(b)}. \end{aligned} \tag{2}$$

In (2), $H(b)$ denotes the entropy [19, p. 5] of b and $U(b)$ is called average energy of b. Note that $F(b)$ is the Kullback-Leibler divergence [19, p. 19] between b and p, i.e., $F(b) = D(b \,||\, p)$. For a set $\mathcal{R}$ of regions, the *region-based variational free energy* is defined as [13] $F_{\mathcal{R}} \triangleq U_{\mathcal{R}} - H_{\mathcal{R}}$ with

$$U_{\mathcal{R}} \triangleq - \sum_{R \in \mathcal{R}} c_R \sum_{a \in \mathcal{A}_R} \sum_{\mathbf{x}_R} b_R(\mathbf{x}_R) \ln f_a(\mathbf{x}_a),$$
$$H_{\mathcal{R}} \triangleq - \sum_{R \in \mathcal{R}} c_R \sum_{\mathbf{x}_R} b_R(\mathbf{x}_R) \ln b_R(\mathbf{x}_R).$$

Here, each b_R is defined locally on a region R. Instead of minimizing F with respect to b, we minimize $F_{\mathcal{R}}$ with respect to all b_R $((R, c_R) \in \mathcal{R})$ where the b_R have to fulfill certain constraints. The quantities b_R are called *beliefs*. We give two examples of valid sets of regions.

Example 2.1: The trivial example $\mathcal{R}_{\text{MF}} \triangleq \{(R = (\mathcal{I}, \mathcal{A}), c_R)\}$ with $c_R = 1$. It leads to the MF fixed point equations, as will be shown in subsection II-C.

Example 2.2: We define two types of regions:

1) *large regions:* $R_a \triangleq (\mathcal{N}(a), \{a\})$ with $c_{R_a} = 1 \; \forall \; a \in \mathcal{A}$;
2) *small regions:* $R_i \triangleq (\{i\}, \emptyset)$ with $c_{R_i} = 1 - |\mathcal{N}(i)| \; \forall \; i \in \mathcal{I}$.

The region-based variational free energy corresponding to the valid set of regions

$$\mathcal{R}_{\text{BP}} \triangleq \{(R_i, c_{R_i}) \mid i \in \mathcal{I}\} \cup \{(R_a, c_{R_a}) \mid a \in \mathcal{A}\}$$

is called the *Bethe free energy* [13], [20]. It leads to the BP fixed point equations, as will be shown in subsection II-B. The Bethe free energy is equal to the exact variational free energy when the factor graph has no cycles [13].

B. Belief propagation fixed point equations

The fixed point equations for BP can be obtained from the Bethe free energy by imposing additional marginalization constraints and computing the stationary points of the corresponding Lagrangian function [13], [21]. The Bethe free energy reads

$$F_{\text{BP}} = \sum_{a \in \mathcal{A}} \sum_{\mathbf{x}_a} b_a(\mathbf{x}_a) \ln \frac{b_a(\mathbf{x}_a)}{f_a(\mathbf{x}_a)} - \sum_{i \in \mathcal{I}} (|\mathcal{N}(i)| - 1) \sum_{x_i} b_i(x_i) \ln b_i(x_i) \tag{3}$$

with $b_a \triangleq b_{R_a} \; \forall \; a \in \mathcal{A}$, $b_i \triangleq b_{R_i} \; \forall \; i \in \mathcal{I}$, and $F_{\text{BP}} \triangleq F_{\mathcal{R}_{\text{BP}}}$. The normalization constraints for the beliefs b_i $(i \in \mathcal{I})$ and the marginalization constraints for the beliefs b_a $(a \in \mathcal{A})$ can be included in the Lagrangian [22, Sec. 3.1.3]

$$L_{\text{BP}} \triangleq F_{\text{BP}} - \sum_{a \in \mathcal{A}} \sum_{i \in \mathcal{N}(a)} \sum_{x_i} \lambda_{a,i}(x_i) \Big(b_i(x_i) - \sum_{\mathbf{x}_a \setminus x_i} b_a(\mathbf{x}_a) \Big) - \sum_{a \in \mathcal{A}} \gamma_a \Big(\sum_{\mathbf{x}_a} b_a(\mathbf{x}_a) - 1 \Big). \tag{4}$$

The stationary points of the Lagrangian in (4) are then related to the BP fixed point equations by the following theorem.

Theorem 1: [13, Th. 2] Stationary points of the Lagrangian in (4) must be BP fixed points with positive beliefs fulfilling (5) and vice versa.

$$\begin{cases} b_a(\mathbf{x}_a) = d_a \, f_a(\mathbf{x}_a) \prod\limits_{i \in \mathcal{N}(a)} n_{i \to a}(x_i), & \forall \; a \in \mathcal{A} \\ b_i(x_i) = \prod\limits_{a \in \mathcal{N}(i)} m_{a \to i}(x_i), & \forall \; i \in \mathcal{I} \end{cases} \tag{5}$$

with

$$\begin{cases} m_{a \to i}(x_i) = d_a \sum\limits_{\mathbf{x}_a \setminus x_i} f_a(\mathbf{x}_a) \prod\limits_{j \in \mathcal{N}(a) \setminus i} n_{j \to a}(x_j) \\ n_{i \to a}(x_i) = \prod\limits_{c \in \mathcal{N}(i) \setminus a} m_{c \to i}(x_i) \end{cases} \tag{6}$$

for all $a \in \mathcal{A}, i \in \mathcal{N}(a)$. Here, d_a $(a \in \mathcal{A})$ are positive constants that ensure that the beliefs b_a $(a \in \mathcal{A})$ are normalized to one.

Often, the following alternative system of fixed point equations is solved instead of (6).

$$\begin{cases} \widetilde{m}_{a \to i}(x_i) = \omega_{a,i} \sum\limits_{\mathbf{x}_a \setminus x_i} f_a(\mathbf{x}_a) \prod\limits_{j \in \mathcal{N}(a) \setminus i} \widetilde{n}_{j \to a}(x_j) \\ \widetilde{n}_{i \to a}(x_i) = \prod\limits_{c \in \mathcal{N}(i) \setminus a} \widetilde{m}_{c \to i}(x_i) \end{cases} \tag{7}$$

for all $a \in \mathcal{A}, i \in \mathcal{N}(a)$ where $\omega_{a,i}$ $(a \in \mathcal{A}, i \in \mathcal{N}(a))$ are arbitrary positive constants. The reason for this is that for a fixed scheduling the messages computed in (6) differ from the messages computed in (7) only by positive constants, which drop out when the beliefs are normalized. See also [13, Eq. (68) and Eq. (69)], where the " $\propto$ " symbol is used in the update equations noting that the normalization constants are irrelevant. A solution of (7) can be obtained, e.g., by updating corresponding likelihood ratios of the messages in (6) or by updating the messages according to (6) but ignoring the normalization constants d_a $(a \in \mathcal{A})$ and using as stopping criterion for the algorithm that the normalized beliefs do not change any more. In both cases, a rescaling of the messages is irrelevant and therefore a solution of (7) is obtained. However, we note that rescaling a solution of (7) has not necessarily to be a solution of (6). Hence, the beliefs obtained by solving (7) need not be stationary points of the Lagrangian in (4). To the best of our knowledge, this elementary insight is not published yet in the literature and we state a necessary and sufficient condition when a solution of (7) can be rescaled to a solution of (6) in the following lemma.

Lemma 1: Suppose that $\{\widetilde{m}_{a \to i}(x_i), \widetilde{n}_{i \to a}(x_i)\}$ $(a \in \mathcal{A}, i \in \mathcal{N}(a))$ is a solution of (7) and set

$$\tilde{d}_a \triangleq \frac{1}{\sum\limits_{\mathbf{x}_a} f_a(\mathbf{x}_a) \prod\limits_{i \in \mathcal{N}(a)} \widetilde{n}_{i \to a}(x_i)}, \quad \forall a \in \mathcal{A}. \tag{8}$$

Then this solution can be rescaled to a solution of (6) if and only if there exist positive constants e_i $(i \in \mathcal{I})$ such that

$$\omega_{a,i} = e_i \tilde{d}_a, \quad \forall \; a \in \mathcal{A}, i \in \mathcal{N}(a). \tag{9}$$

Proof: See Appendix A. ∎

Remark 2.1: Note that for factor graphs that have tree-structure the messages computed by the forward-backward algorithm [9] always fulfill (9) because we have $\omega_{a,i} = 1$ $(a \in \mathcal{A}, i \in \mathcal{N}(a))$ and $\tilde{d}_a = 1$ $(a \in \mathcal{A})$ in this case.

C. Fixed point equations for the mean field approximation

A message passing interpretation of the MF approximation was derived in [5], [23]. In this section, we briefly show how the corresponding fixed point equations can be obtained by the free energy approach. To this end we use $\mathcal{R}_{\text{MF}}$ from Example 2.1 together with the factorization constraint

$$b(\mathbf{x}) = \prod_{i \in \mathcal{I}} b_i(x_i). \tag{10}$$

Plugging (10) into the expression for the region based free energy corresponding to the trivial approximation $\mathcal{R}_{\text{MF}}$ we get

$$F_{\text{MF}} = \sum_{i \in \mathcal{I}} \sum_{x_i} b_i(x_i) \ln b_i(x_i) - \sum_{a \in \mathcal{A}} \sum_{\mathbf{x}_a} \prod_{i \in \mathcal{N}(a)} b_i(x_i) \ln f_a(\mathbf{x}_a) \tag{11}$$

with $F_{\text{MF}} \triangleq F_{\mathcal{R}_{\text{MF}}}$. Assuming that all the beliefs b_i $(i \in \mathcal{I})$ have to fulfill a normalization constraint, the stationary points of the corresponding Lagrangian for the MF approximation can easily be evaluated to be

$$b_i(x_i) = e_i \exp\left(\sum_{a \in \mathcal{N}(i)} \sum_{\mathbf{x}_a \setminus x_i} \prod_{j \in \mathcal{N}(a) \setminus i} b_j(x_j) \ln f_a(\mathbf{x}_a) \right) \tag{12}$$

for all $i \in \mathcal{I}$ where the positive constants e_i $(i \in \mathcal{I})$ are such that b_i is normalized to one for all $i \in \mathcal{I}$ [2]. The updates b_i can be obtained by iterating over $i \in \mathcal{I}$. At each step the objective function, i.e., the Lagrangian corresponding to the mean field free energy (11), cannot increase and the algorithm is guaranteed to converge. Note that in order to derive a particular update b_i $(i \in \mathcal{I})$ we need all previous updates b_j with $j \in \bigcup_{a \in \mathcal{N}(i)} \mathcal{N}(a) \setminus i$. The beliefs b_i are obtained by setting $b_i(x_i) = n_{i \to a}(x_i)$ $\forall\, i \in \mathcal{I}, a \in \mathcal{N}(i)$ and solving

$$\begin{cases} n_{i \to a}(x_i) = e_i \displaystyle\prod_{a \in \mathcal{N}(i)} m_{a \to i}(x_i) \\ m_{a \to i}(x_i) = \exp\left(\displaystyle\sum_{\mathbf{x}_a \setminus x_i} \prod_{j \in \mathcal{N}(a) \setminus i} c_j n_{j \to a}(x_j) \ln f_a(\mathbf{x}_a) \right) \end{cases} \tag{13}$$

for all $a \in \mathcal{A}, i \in \mathcal{N}(a)$. The MF approximation can be extended to the case where p is a continuous pdf, which is shown in Appendix B. Formally, each sum over states x_i with $i \in \mathcal{I}$ in (12) and (13) has to be replaced by a Lebesgue integral whenever the corresponding random variable X_i is continuous.

D. EM algorithm

Message passing interpretations of the EM algorithm [16] were derived in [24], [25]. It can be shown that the EM algorithm is a special instance of the MF approximation [26, Sec. 2.3.1], which we briefly summarize in the following. Suppose that we apply the MF approximation to p in (1) as described before. In addition, we assume that for all $i \in \mathcal{E} \subseteq \mathcal{I}$ the beliefs b_i fullfill the constraints that $b_i(x_i) = \delta(x_i - \tilde{x}_i)$. Using the fact that $0 \ln(0) = 0$, we can rewrite F_{MF} in (11) as

$$\begin{aligned} F_{\text{MF}} = &\sum_{i \in \mathcal{I} \setminus \mathcal{E}} \sum_{x_i} b_i(x_i) \ln b_i(x_i) \\ &- \sum_{a \in \mathcal{A}} \sum_{\mathbf{x}_a} \prod_{i \in \mathcal{N}(a)} b_i(x_i) \ln f_a(\mathbf{x}_a). \end{aligned} \tag{14}$$

For all $i \in \mathcal{I} \setminus \mathcal{E}$ the stationary points of F_{MF} in (14) have the same analytical expression as the one obtained in (12). For $i \in \mathcal{E}$, minimizing F_{MF} in (14) with respect to $\tilde{x}_i$ yields $b_i(x_i) = \delta(x_i - \tilde{x}_i)$ with

$$\tilde{x}_i = \operatorname*{argmax}_{x_i} \left(\prod_{a \in \mathcal{N}(i)} \exp\left(\sum_{\mathbf{x}_a \setminus x_i} \prod_{j \in \mathcal{N}(a) \setminus i} b_j(x_j) \ln f_a(\mathbf{x}_a) \right) \right). \tag{15}$$

Setting $b_i(x_i) = c_i n_{i \to a}(x_i)$ $\forall\, i \in \mathcal{I}, a \in \mathcal{N}(i)$, we get the message passing update equations defined in (13) *except* that we have to replace the messages $n_{i \to a}(x_i)$ for all $i \in \mathcal{E}$ and $a \in \mathcal{N}(i)$ by

$$n_{i \to a}(x_i) = \delta(x_i - \tilde{x}_i) \text{ with } \tilde{x}_i = \operatorname*{argmax}_{x_i} \left(\prod_{a \in \mathcal{N}(i)} m_{a \to i}(x_i) \right) \tag{16}$$

for all $i \in \mathcal{E}, a \in \mathcal{N}(a)$.

III. Combined belief propagation / mean field approximation fixed point equations

Let

$$p(\mathbf{x}) = \prod_{a \in \mathcal{A}_{\text{MF}}} f_a(\mathbf{x}_a) \prod_{a \in \mathcal{A}_{\text{BP}}} f_a(\mathbf{x}_a) \tag{17}$$

be a partially factorized pmf with $\mathcal{A}_{\text{MF}} \cap \mathcal{A}_{\text{BP}} = \emptyset$ and $\mathcal{A} \triangleq \mathcal{A}_{\text{MF}} \cup \mathcal{A}_{\text{BP}}$. As before, we have $\mathbf{x} \triangleq \{x_i \mid i \in \mathcal{I}\}$, $\mathbf{x}_a \triangleq (x_i \mid i \in \mathcal{N}(a))^{\text{T}}$ with $\mathcal{N}(a) \subseteq \mathcal{I}$ for all $a \in \mathcal{A}$, and $\mathcal{N}(i) \triangleq \{a \in \mathcal{A} \mid i \in \mathcal{N}(a)\}$ for all $i \in \mathcal{I}$. We refer to the factor graph representing the factorization $\prod_{a \in \mathcal{A}_{\text{BP}}} f_a(\mathbf{x}_a)$ in (17) as "BP part" and to the factor graph representing the factorization $\prod_{a \in \mathcal{A}_{\text{MF}}} f_a(\mathbf{x}_a)$ in (17) as "MF part". Furthermore, we set

$$\mathcal{I}_{\text{MF}} \triangleq \bigcup_{a \in \mathcal{A}_{\text{MF}}} \mathcal{N}(a) \qquad \mathcal{I}_{\text{BP}} \triangleq \bigcup_{a \in \mathcal{A}_{\text{BP}}} \mathcal{N}(a)$$

and

$$\mathcal{N}_{\text{MF}}(i) \triangleq \mathcal{A}_{\text{MF}} \cap \mathcal{N}(i) \qquad \mathcal{N}_{\text{BP}}(i) \triangleq \mathcal{A}_{\text{BP}} \cap \mathcal{N}(i).$$

Following [13], as outlined in Subsection II-A, we define the following regions and counting numbers:

1) one MF region $R_{\text{MF}} \triangleq (\mathcal{I}_{\text{MF}}, \mathcal{A}_{\text{MF}})$ with $c_{R_{\text{MF}}} = 1$;
2) small regions $R_i \triangleq (\{i\}, \emptyset)$ with $c_{R_i} = 1 - |\mathcal{N}_{\text{BP}}(i)| - \text{I}_{\mathcal{I}_{\text{MF}}}(i)$ for all $i \in \mathcal{I}_{\text{BP}}$;
3) large regions $R_a \triangleq (\mathcal{N}(a), \{a\})$ with $c_{R_a} = 1$ for all $a \in \mathcal{A}_{\text{BP}}$.

[2] The Lagrange multiplier [22, p. 283] for each belief b_i $(i \in \mathcal{I})$ corresponding to the normalization constraint can be absorbed into the positive constant e_i $(i \in \mathcal{I})$.

This yields the valid set of regions

$$\mathcal{R}_{\text{BP, MF}} \triangleq \{(R_i, c_{R_i}) \mid i \in \mathcal{I}\} \cup \{(R_a, c_{R_a}) \mid a \in \mathcal{A}_{\text{BP}}\} \cup \{(R_{\text{MF}}, c_{R_{\text{MF}}})\}. \tag{18}$$

The additional terms $\mathrm{I}_{\mathcal{I}_{\text{MF}}}(i)$ in the counting numbers of the small regions R_i $(i \in \mathcal{I})$ defined in 2) compared to the counting numbers of the small regions for the Bethe approximation (see Example 2.2) guarantee that this is indeed a valid set of regions.

The valid set of regions in (18) gives the region-based variational free energy

$$\begin{aligned} F_{\text{BP, MF}} = &\sum_{a \in \mathcal{A}_{\text{BP}}} \sum_{\mathbf{x}_a} b_a(\mathbf{x}_a) \ln \frac{b_a(\mathbf{x}_a)}{f_a(\mathbf{x}_a)} \\ &- \sum_{a \in \mathcal{A}_{\text{MF}}} \sum_{\mathbf{x}_a} \prod_{i \in \mathcal{N}(a)} b_i(x_i) \ln f_a(\mathbf{x}_a) \\ &- \sum_{i \in \mathcal{I}} (|\mathcal{N}_{\text{BP}}(i)| - 1) \sum_{x_i} b_i(x_i) \ln b_i(x_i) \end{aligned} \tag{19}$$

with $F_{\text{BP, MF}} \triangleq F_{\mathcal{R}_{\text{BP, MF}}}$. In (19), we have already plugged in the factorization constraint for the MF part, i.e., we set

$$b_{\text{MF}}(\mathbf{x}_{\text{MF}}) = \prod_{i \in \mathcal{I}_{\text{MF}}} b_i(x_i).$$

The normalization constraints for the beliefs b_i $(i \in \mathcal{I}_{\text{MF}} \setminus \mathcal{I}_{\text{BP}})$ and b_a $(a \in \mathcal{A}_{\text{BP}})$ and the marginalization constraints for the beliefs b_a $(a \in \mathcal{A}_{\text{BP}})$ can be included in the Lagrangian [22, Sec. 3.1.3]

$$\begin{aligned} L_{\text{BP, MF}} \triangleq &F_{\text{BP, MF}} \\ &- \sum_{a \in \mathcal{A}_{\text{BP}}} \sum_{i \in \mathcal{N}(a)} \sum_{x_i} \lambda_{a,i}(x_i) \Big(b_i(x_i) - \sum_{\mathbf{x}_a \setminus x_i} b_a(\mathbf{x}_a) \Big) \\ &- \sum_{i \in \mathcal{I}_{\text{MF}} \setminus \mathcal{I}_{\text{BP}}} \gamma_i \Big(\sum_{x_i} b_i(x_i) - 1 \Big) \\ &- \sum_{a \in \mathcal{A}_{\text{BP}}} \gamma_a \Big(\sum_{\mathbf{x}_a} b_a(\mathbf{x}_a) - 1 \Big). \end{aligned} \tag{20}$$

Remark 3.1: Note that there is no need to introduce normalization constraints for the beliefs b_i $(i \in \mathcal{I}_{\text{BP}})$. If $a \in \mathcal{N}_{\text{BP}}(i)$, then it follows from the marginalization and normalization constraint for the belief b_a that

$$\begin{aligned} 1 &= \sum_{\mathbf{x}_a} b_a(\mathbf{x}_a) \\ &= \sum_{x_i} \Big(\sum_{\mathbf{x}_a \setminus x_i} b_a(\mathbf{x}_a) \Big) \\ &= \sum_{x_i} b_i(x_i). \end{aligned}$$

The stationary points of the Lagrangian $L_{\text{BP, MF}}$ in (20) are then obtained by setting the derivatives of $L_{\text{BP, MF}}$ with respect to the beliefs and the Lagrange multiplier equal to zero. The following theorem relates the stationary points of the Lagrangian $L_{\text{BP, MF}}$ to solutions of fixed point equations for the beliefs.

Theorem 2: Stationary points of the Lagrangian in (20) in the combined BP/MF approach must be fixed points with positive beliefs fulfilling

$$\begin{cases} b_a(\mathbf{x}_a) = d_a \, f_a(\mathbf{x}_a) \displaystyle\prod_{i \in \mathcal{N}(a)} n_{i \to a}(x_i), \quad \forall \; a \in \mathcal{A}_{\text{BP}} \\ b_i(x_i) = e_i \displaystyle\prod_{a \in \mathcal{N}_{\text{BP}}(i)} m^{\text{BP}}_{a \to i}(x_i) \prod_{a \in \mathcal{N}_{\text{MF}}(i)} m^{\text{MF}}_{a \to i}(x_i), \quad \forall \; i \in \mathcal{I} \end{cases} \tag{21}$$

with

$$\begin{cases} n_{i \to a}(x_i) = e_i \displaystyle\prod_{c \in \mathcal{N}_{\text{BP}}(i) \setminus a} m^{\text{BP}}_{c \to i}(x_i) \prod_{c \in \mathcal{N}_{\text{MF}}(i)} m^{\text{MF}}_{c \to i}(x_i), \\ \qquad \forall \; a \in \mathcal{A}, i \in \mathcal{N}(a) \\ m^{\text{BP}}_{a \to i}(x_i) = d_a \displaystyle\sum_{\mathbf{x}_a \setminus x_i} f_a(\mathbf{x}_a) \prod_{j \in \mathcal{N}(a) \setminus i} n_{j \to a}(x_j), \\ \qquad \forall \; a \in \mathcal{A}_{\text{BP}}, i \in \mathcal{N}(a) \\ m^{\text{MF}}_{a \to i}(x_i) = \exp\Bigg(\displaystyle\sum_{\mathbf{x}_a \setminus x_i} \prod_{j \in \mathcal{N}(a) \setminus i} n_{j \to a}(x_j) \ln f_a(\mathbf{x}_a) \Bigg), \\ \qquad \forall \; a \in \mathcal{A}_{\text{MF}}, i \in \mathcal{N}(a) \end{cases} \tag{22}$$

and vice versa. Here, e_i $(i \in \mathcal{I})$ and d_a $(a \in \mathcal{A}_{\text{BP}})$ are positive constants that ensure that the beliefs b_i $(i \in \mathcal{I})$ and b_a $(a \in \mathcal{A})$ are normalized to one with $e_i = 1 \; \forall \; i \in \mathcal{I}_{\text{BP}}$.

Proof: See Appendix C. ∎

Remark 3.2: Note that for each $i \in \mathcal{I} \setminus \mathcal{I}_{\text{BP}}$ Theorem 2 can be generalized to the case where X_i is a continuous random variable following the derivation presented in Appendix B. Formally, each sum over states x_i with $i \in \mathcal{I} \setminus \mathcal{I}_{\text{BP}}$ in (21) and (22) has to be replaced by a Lebesgue integral whenever the corresponding random variable X_i is continuous.

A. Hard constraints for BP

Some conjectures on how to generalize Theorem 1 ([13, Th. 2]) to hard constraints, i.e., to the case where the factors f_a $(a \in \mathcal{A})$ of the pmf p are not restricted to be strictly positive real-valued functions, can be found in [13, Sec. VI.D]. However, the derivations in [13, Sec. VI.D] are based on the fact that we are allowed to compute the stationary points of the Lagrangian L_{BP} in (4), i.e., that we are allowed to take the corresponding derivatives, even though the factors f_a $(a \in \mathcal{A})$ of the pmf p are no longer strictly positive functions.

In the sequal, we show how to generalize Theorem 2 to the case where $f_a \geq 0 \; \forall \; a \in \mathcal{A}_{\text{BP}}$ based on the simple observation that we are interested in solutions where the variational region based free energy is not plus infinity (recall that we want to minimize this quantity). As a byproduct, this also yields an extension of Theorem 1 ([13, Th. 2]) to hard constraints by simply setting $\mathcal{A}_{\text{MF}} = \emptyset$.

To this end we analyze the first term of the free energy $F_{\text{BP, MF}}$ in (19), which is

$$F_1 \triangleq \sum_{a \in \mathcal{A}_{\text{BP}}} \sum_{\mathbf{x}_a} b_a(\mathbf{x}_a) \ln \frac{b_a(\mathbf{x}_a)}{f_a(\mathbf{x}_a)}. \tag{23}$$

Note that the remaining terms in $F_{\text{BP, MF}} - F_1$ are all finite due to the assumption that the beliefs b_i $(i \in \mathcal{I})$ are valid pmfs and,

therefore, nonnegative and bounded functions, and the factors f_a with $a \in \mathcal{A}_{\text{MF}}$ are strictly positive real-valued functions. Now let $\bar{\mathbf{x}}_a$ with $a \in \mathcal{A}_{\text{BP}}$ be a fixt state with $f_a(\bar{\mathbf{x}}_a) = 0$. Then we see from (23) that $F_1 = \infty$ unless $b_a(\bar{\mathbf{x}}_a) = 0$. Note also that, regardless of the valued of $b_a(\bar{\mathbf{x}}_a)$, we are not allowed to take the derivative of F_1 with respect to $b_a(\bar{\mathbf{x}}_a)$. Based on the fact that $F_{\text{BP, MF}} < \infty$, we set

$$b_a(\bar{\mathbf{x}}_a) = 0, \quad \forall\ \bar{\mathbf{x}}_a \text{ with } a \in \mathcal{A}_{\text{BP}}, f_a(\bar{\mathbf{x}}_a) = 0. \tag{24}$$

We distinguish between two cases:

1) Suppose that $f_a \mid_{\bar{x}_i} \equiv 0$ for some $a \in \mathcal{A}_{\text{BP}}$ and $x_i \in \mathbf{x}_a$. Then (24) implies that $b_a \mid_{\bar{x}_i} \equiv 0$. Moreover, the marginalization constraints imply that $b_i(\bar{x}_i) = 0$ and, therefore, $b_c \mid_{\bar{x}_i} = 0$ for all $c \in \mathcal{N}_{\text{BP}}(i)$. Hence, we can exclude the state $\bar{x}_i$ from the set of all possible states:

$$\text{If } f_a \mid_{\bar{x}_i} \equiv 0 \text{ with } a \in \mathcal{A}_{\text{BP}}, i \in \mathcal{N}(a) \text{ exclude } \bar{x}_i. \tag{25}$$

   Note that $f_a \mid_{\bar{x}_i} \equiv 0$ for some $a \in \mathcal{A}_{\text{BP}}$ implies that $p \mid_{\bar{x}_i} \equiv 0$. This just means that the true set of realizations of the random variable X_i is smaller.
2) Suppose that we have excluded all values $\bar{x}_i$ of x_i for all $i \in \mathcal{I}_{\text{BP}}$ from case 1) and (24) is fulfilled. The analysis for the remaining $b_a(\mathbf{x}_a)$ and $b_i(x_i)$, which are stationary points, is the same as in the proof of Theorem 2 and the resulting fixed point equations are identical to (22), because we can reintroduce the states $\bar{\mathbf{x}}_a$ from (24) in the message passing update equations, as can be seen immediately from (22). In fact, the additional terms for the states in (24) in the update of the messages $m^{\text{BP}}_{a\to i}(x_i)$ $(a \in \mathcal{A}_{\text{BP}}, i \in \mathcal{N}(a))$ do not contribute because $f_a(\bar{\mathbf{x}}_a) = 0$ for all of these states. All the beliefs b_i are still positive functions: let $i \in \mathcal{I}_{\text{BP}}$, $a \in \mathcal{N}_{\text{BP}}(i)$, and $x_i = \bar{x}_i$. Due to (25), $f_a \mid_{\bar{x}_i} \not\equiv 0$. This implies that $f_a(\bar{\mathbf{x}}_a) \neq 0$ for some state $\bar{\mathbf{x}}_a = (\bar{x}_j \mid j \in \mathcal{N}(a))^{\text{T}}$ with $i \in \mathcal{N}(a)$ and the stationary point $b_a(\bar{\mathbf{x}}_a) \neq 0$. The marginalization constraints in the BP part together with the fact that the belief b_a must be a nonnegative function then implies that $b_i(\bar{x}_i) > 0$.

B. Convergence

If the BP part has no cycles and

$$|\mathcal{N}(a) \cap \mathcal{I}_{\text{BP}}| \leq 1, \quad \forall a \in \mathcal{A}_{\text{MF}}, \tag{26}$$

then there exists a convergent implementation of the combined message passing equations in (22). In fact, we can iterate between updating the beliefs b_i with $i \in \mathcal{I}_{\text{MF}} \setminus \mathcal{I}_{\text{BP}}$ and the forward backward algorithm in the BP part, as is outlined in the following Algorithm.

Algorithm 1: If the BP part has no cycle and (26) is fulfilled, the following implementation of the fixed point equations in (22) is guaranteed to converge.

1) Initialize b_i for all $i \in \mathcal{I}_{\text{MF}} \setminus \mathcal{I}_{\text{BP}}$ and send the corresponding messages $n_{i\to a}(x_i) = b_i(x_i)$ to all factor nodes $a \in \mathcal{N}_{\text{MF}}(i)$.
2) Use all messages $m^{\text{MF}}_{a\to i}(x_i)$ with $i \in \mathcal{I}_{\text{BP}} \cap \mathcal{I}_{\text{MF}}$ and $a \in \mathcal{N}_{\text{MF}}(i)$ as fixed input for the BP part and run the forward/backward algorithm [9]. The fact that the resulting beliefs b_i with $i \in \mathcal{I}_{\text{BP}}$ can not increase the region-based variational free energy in (19) is proved in Appendix D.
3) For each $i \in \mathcal{I}_{\text{MF}} \cap \mathcal{I}_{\text{BP}}$ and $a \in \mathcal{N}_{\text{MF}}(i)$ the message $n_{i\to a}(x_i)$ is now available and can be used for further updates in the MF part.
4) For each $i \in \mathcal{I}_{\text{MF}} \setminus \mathcal{I}_{\text{BP}}$ recompute the message $n_{i\to a}(x_i)$ and send it to all $a \in \mathcal{N}_{\text{MF}}(i)$. Note that for all indices $i \in \mathcal{I}_{\text{MF}} \setminus \mathcal{I}_{\text{BP}}$ the recomputed beliefs $b_i(x_i) = n_{i\to a}(x_i)$ fulfill

$$\frac{\partial F_{\text{BP, MF}}}{b_i(x_i)} = 0 \quad \text{and} \quad \frac{\partial^2 F_{\text{BP, MF}}}{\partial b_i(x_i)^2} = \frac{1}{b_i(x_i)} > 0,$$

   which implies that the region-based free energy in (19) can not increase.
5) Proceed as described in 2).

Remark 3.3: If the factor graph representing the BP part has cycles then Algorithm 2 can be modified by running loopy BP in step 2). However, in this case the algorithm is not guaranteed to converge.

IV. Application to iterative channel estimation and decoding

In this section, we present an example where we show how to compute the updates of the messages in (22) based on Algorithm 1. We choose a simple channel model where the updates of the messages are simple enough in order to avoid overstressed notation. A class of more complicated MIMO-OFDM receiver architectures together with numerical simulations can be found in [18].

Specifically, we consider a time-varying frequency-flat channel with input-output relationship

$$\mathbf{y} = \mathbf{h} \odot \mathbf{x} + \mathbf{z}$$

where $\mathbf{z} \sim \mathcal{CN}(\mathbf{0}, \gamma^{-1}\mathbf{I}_N)$ and $\mathbf{x}, \mathbf{y} \in \mathbb{C}^n$. The symbols $x_i \in \mathbf{x}$ $(i \in [1:N])$ belong to a certain modulation alphabet. We assume that each symbol $x_i \in \mathbb{C}$ can be mapped to a unique bit vector $\mathbf{c}_i \in \{-1, 1\}^M$. We choose for the prior distributions of Γ and $\mathbf{H}$ [5]

$$p_\Gamma(\gamma) \sim \Gamma(k^{\text{p}}, 1/\beta^{\text{p}})$$
$$p_{\mathbf{H}}(\mathbf{h}) \sim \mathcal{CN}(\boldsymbol{\mu}^{\text{p}}, \boldsymbol{\Lambda}^{\text{p}-1}).$$

The pdf $p_{\mathbf{Y},\mathbf{X},\mathbf{H},\mathbf{C},\Gamma}$ with $\mathbf{C} \triangleq (\mathbf{C}_1^{\text{T}}, \ldots, \mathbf{C}_N^{\text{T}})^{\text{T}}$ admits the factorization

$$\begin{aligned} &p_{\mathbf{Y},\mathbf{X},\mathbf{H},\mathbf{C},\Gamma}(\mathbf{y}, \mathbf{x}, \mathbf{h}, \mathbf{c}, \gamma) \\ &= p_{\mathbf{Y}|\mathbf{X},\mathbf{H},\mathbf{C},\Gamma}(\mathbf{y}|\mathbf{x}, \mathbf{h}, \mathbf{c}, \gamma)\, p_{\mathbf{X}|\mathbf{C}}(\mathbf{x}|\mathbf{c})\, p_{\mathbf{C}}(\mathbf{c})\, p_{\mathbf{H}}(\mathbf{h})\, p_\Gamma(\gamma) \\ &= \prod_{i\in[1:N]} p_{Y_i|X_i,H_i,\Gamma}(y_i|x_i, h_i, \gamma) \\ &\quad \times \prod_{j\in[1:N]} p_{X_j|\mathbf{C}_j}(x_j|\mathbf{c}_j)\, p_{\mathbf{H}}(\mathbf{h})\, p_{\mathbf{C}}(\mathbf{c})\, p_\Gamma(\gamma), \end{aligned} \tag{27}$$

where we used the fact that Γ, $\mathbf{H}$, and $\mathbf{X}$ are independent. Here, the pdf $p_{\mathbf{C}}$ represents the code constraints for the bits

that typically admits an additional factorization and

$$\begin{aligned} &p_{Y_i|X_i,H_i,\Gamma}(y_i|x_i,h_i,\gamma) \\ &= \frac{\gamma}{\pi}\exp(-\gamma|y_i - h_i x_i|^2) \\ &\sim \mathcal{CN}(h_i x_i, 1/\gamma), \quad \forall i \in [1:N]. \end{aligned} \tag{28}$$

Now let

$$\begin{aligned} \mathcal{I} \triangleq &\{C_1,\ldots,C_{NM}\} \cup \{X_1,\ldots,X_N\} \\ &\cup \{H_1,\ldots,H_N\} \cup \{\Gamma\} \end{aligned} \tag{29}$$

$$\begin{aligned} \mathcal{A} \triangleq &\{p_{Y_i|X_i,H_i,\Gamma} \mid i \in [1:N]\} \cup \{p_{X_i|\mathbf{C}_i} \mid i \in [1:N]\} \\ &\cup \{p_{\mathbf{H}}(\mathbf{h})\} \cup \{p_{\mathbf{C}}, p_\Gamma\}. \end{aligned} \tag{30}$$

By a slight abuse of notation we used in (30) the names of the functions in the factorization in (27) as indices of the set $\mathcal{A}$. We shall choose the following splitting of $\mathcal{A}$ into $\mathcal{A}_{\text{BP}}$ and $\mathcal{A}_{\text{MF}}$.

$$\begin{aligned} \mathcal{A}_{\text{BP}} &\triangleq \{p_{\mathbf{C}}\} \cup \{p_{X_i|\mathbf{C}_i} \mid i \in [1:N]\} \\ \mathcal{A}_{\text{MF}} &\triangleq \{p_\Gamma\} \cup \{p_{\mathbf{H}}(\mathbf{h})\} \cup \{p_{Y_i|X_i,H_i,\Gamma} \mid i \in [1:N]\}. \end{aligned} \tag{31}$$

The splitting in (31) yields

$$\begin{aligned} \mathcal{I}_{\text{BP}} &= \{C_1,\ldots,C_{NM}\} \cup \{X_1,\ldots,X_N\} \\ \mathcal{I}_{\text{MF}} &= \{X_1,\ldots,X_N\} \cup \{H_1,\ldots,H_N\} \cup \{\Gamma\}, \end{aligned} \tag{32}$$

which implies that $\mathcal{I}_{\text{BP}} \cap \mathcal{I}_{\text{MF}} = \{X_1,\ldots,X_N\}$. The factor graph corresponding to the factorization in (27) with the splitting of $\mathcal{A}$ into $\mathcal{A}_{\text{MF}}$ and $\mathcal{A}_{\text{BP}}$ as in (31) is depicted in Figure 1.

We now show how to apply Algorithm 1 for the factor graph depicted in 1.

Algorithm 2: (Application of Algorithm 1):

1) Initialize

$$\begin{aligned} b_\Gamma(\gamma) &= \frac{\beta^k}{(k-1)!}\gamma^{k-1}\exp(-\beta\gamma) \sim \Gamma(k, 1/\beta) \\ b_{H_i}(h_i) &= \frac{1}{\pi\sigma_{H_i}^2}\exp\Big(-\frac{1}{\sigma_{H_i}^2}|h_i - \mu_{H_i}|^2\Big) \\ &\sim \mathcal{CN}(\mu_{H_i}, \sigma_{H_i}^2), \quad \forall\, i \in [1:N] \end{aligned}$$

and set

$$\begin{aligned} n_{\Gamma\to p_\Gamma}(\gamma) &= b_\Gamma(\gamma) \\ n_{\Gamma\to p_{Y_i|X_i,H_i,\Gamma}}(\gamma) &= b_\Gamma(\gamma), \quad \forall\, i \in [1:N] \\ n_{H_i\to p_{\mathbf{H}}}(h_i) &= b_{H_i}(h_i) \\ n_{H_i\to p_{Y_i|X_i,H_i,\Gamma}}(h_i) &= b_{H_i}(h_i), \quad \forall\, i \in [1:N]. \end{aligned}$$

2) Using the particular form of the distributions $p_{Y_i|X_i,H_i,\Gamma}$ $(i \in [1:N])$ in (28), we get

$$\begin{aligned} &m^{\text{MF}}_{p_{Y_i|X_i,H_i,\Gamma}\to X_i}(x_i) \\ &\propto \exp\Bigg(-\int \mathrm{d}\gamma\, n_{\Gamma\to p_{Y_i|X_i,H_i,\Gamma}}(\gamma)\gamma \\ &\quad \int \mathrm{d}h_i\, n_{H_i\to p_{Y_i|X_i,H_i,\Gamma}}(h_i)|y_i - h_i x_i|^2\Bigg) \\ &\propto \exp\Bigg(-\frac{k(\sigma_{H_i}^2 + |\mu_{H_i}|^2)}{\beta}\bigg|x_i - \frac{y_i\mu_{H_i}^*}{(\sigma_{H_i}^2 + |\mu_{H_i}|^2)}\bigg|^2\Bigg) \end{aligned}$$

for all $i \in [1:N]$.

3) Use the messages $m^{\text{MF}}_{p_{Y_i|X_i,H_i,\Gamma}\to X_i}(x_i)$ $(i \in [1:N])$ as fixed input for the BP part and run (loopy) BP.
4) After running BP in the BP part, compute the messages $n_{X_i\to p_{Y_i|X_i,H_i,\Gamma}}(x_i)$ $(i \in [1:N])$ and update the messages in the MF part. Namely, after setting

$$\begin{aligned} \mu_{X_i} &\triangleq \sum_{x_i} n_{X_i\to p_{Y_i|X_i,H_i,\Gamma}}(x_i)x_i \\ \sigma_{X_i}^2 &\triangleq \sum_{x_i} n_{X_i\to p_{Y_i|X_i,H_i,\Gamma}}(x_i)|x_i - \mu_{X_i}|^2 \end{aligned}$$

for all $i \in [1:N]$ we obtain:
(i) Update of (k,β) for b_Γ:

$$\begin{aligned} &m^{\text{MF}}_{p_{Y_i|X_i,H_i,\Gamma}\to\Gamma}(\gamma) \\ &\propto \frac{\gamma}{\pi}\exp\Bigg(-\gamma\int \mathrm{d}h_i \sum_{x_i} \\ &\quad n_{H_i\to p_{Y_i|X_i,H_i,\Gamma}}(h_i)n_{X_i\to p_{Y_i|X_i,H_i,\Gamma}}(x_i)|y_i - h_i x_i|^2\Bigg) \\ &\propto \frac{\gamma}{\pi}\exp\Big(-\gamma\big(|y_i|^2 + (\sigma_{H_i}^2 + |\mu_{H_i}|^2)(\sigma_{X_i}^2 + |\mu_{X_i}|^2) \\ &\quad - 2\Re(y_i^*\mu_{H_i}\mu_{X_i})\big)\Big) \\ &n^{\text{MF}}_{\Gamma\to p_{Y_i|X_i,H_i,\Gamma}}(\gamma) \\ &= e_\Gamma m^{\text{MF}}_{p_\Gamma\to\Gamma}(\gamma)\prod_{j\in[1:N]} m^{\text{MF}}_{p_{Y_j|X_j,H_j,\Gamma}\to\Gamma}(\gamma) \\ &= \frac{\beta^k}{(k-1)!}\gamma^{k-1}\exp(-\gamma\beta)) \end{aligned}$$

with updated shape and inverse scale parameter

$$\begin{aligned} k &= N + k_{\text{p}} \\ \beta &= \beta_{\text{p}} + \sum_{j\in[1:N]} \big(|y_j|^2 + (\sigma_{H_j}^2 + |\mu_{H_j}|^2)(\sigma_{X_j}^2 + |\mu_{X_j}|^2) \\ &\quad - 2\Re(y_j^*\mu_{H_j}\mu_{X_j})\big), \end{aligned}$$

respectively. The update for the belief b_Γ is

$$b_\Gamma(\gamma) = n^{\text{MF}}_{\Gamma\to p_{Y_i|X_i,H_i,\Gamma}}(\gamma) \sim \Gamma(k, 1/\beta). \tag{33}$$

(ii) Update of $(\mu_{H_i}, \sigma_{H_i}^2)$ for b_{H_i} $(i \in [1:N])$:

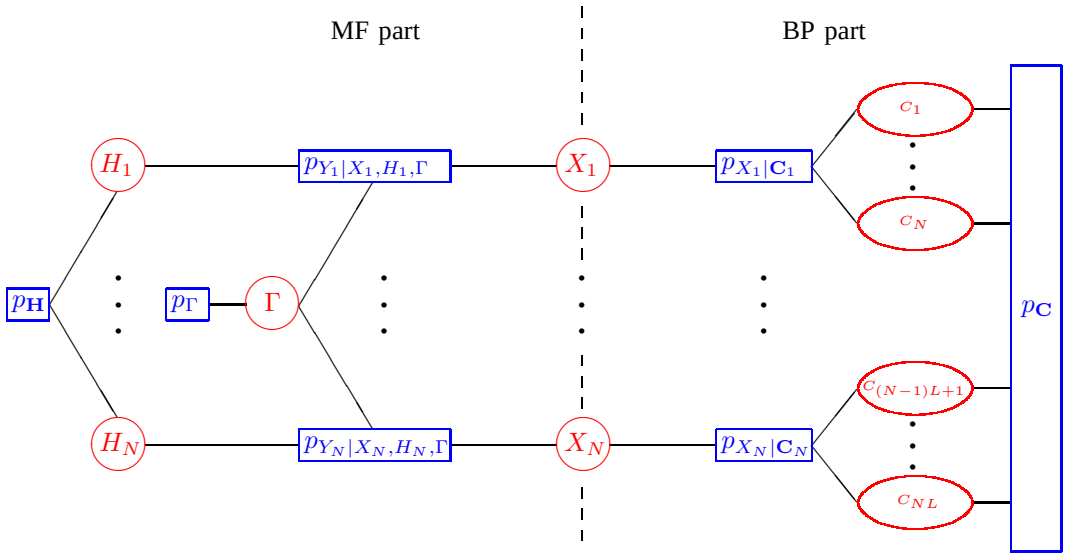

Fig. 1. Factor graph corresponding to the factorization of the pdf in (27).

$$
\begin{aligned}
&m^{\mathrm{MF}}_{p_{Y_i|X_i,H_i,\Gamma}\to H_i}(h_i)\\
&\propto \exp\Bigg(-\int \mathrm{d}\gamma n_{\Gamma\to p_{Y_i|X_i,H_i,\Gamma}}(\gamma)\gamma\\
&\quad\sum_{x_i} n_{X_i\to p_{Y_i|X_i,H_i,\Gamma}}(x_i)|y_i-h_ix_i|^2\Bigg)\\
&\propto \exp\left(-\frac{k(\sigma^2_{X_i}+|\mu_{X_i}|^2)}{\beta}\left|h_i-\frac{y_i\mu^*_{X_i}}{\sigma^2_{X_i}+|\mu_{X_i}|^2}\right|^2\right)\\
&m^{\mathrm{MF}}_{p_{\mathbf{H}}\to H_i}(h_i)\\
&\propto \exp\Bigg(-\int\prod_{j\in[1:N]\setminus i} dh_j n_{H_j\to p_{\mathbf{H}}}\\
&\quad(\mathbf{h}-\boldsymbol{\mu}^{\mathrm{p}})^{\mathrm{H}}\boldsymbol{\Lambda}^{\mathrm{p}}(\mathbf{h}-\boldsymbol{\mu}^{\mathrm{p}})\Bigg)\\
&\propto \exp\left(-\lambda^{\mathrm{p}}_{ii}\left|h_i-\frac{\sum_{j\in[1:N]\setminus i}\lambda^{\mathrm{p}}_{ij}(\mu^{\mathrm{p}}_j-\mu_{H_j})}{\lambda^{\mathrm{p}}_{ii}}-\mu^{\mathrm{p}}_i\right|^2\right)\\
&n^{\mathrm{MF}}_{H_i\to p_{Y_i|X_i,H_i,\Gamma}}(h_i)\\
&= e_{H_i} m^{\mathrm{MF}}_{p_{H_i}\to H_i}(h_i) m^{\mathrm{MF}}_{p_{Y_i|X_i,H_i,\Gamma}\to H_i}(h_i)\\
&\quad\frac{1}{\pi\sigma^2_{H_i}}\exp\left(-\frac{1}{\sigma^2_{H_i}}|h_i-\mu_{H_i}|^2\right)
\end{aligned}
$$

for all $i\in[1:N]$ where Lemma 2 yields the updated mean and variance parameters

$$
\begin{aligned}
\mu_{H_i} &= \sigma^2_{H_i}\left(\sum_{j\in[1:N]\setminus i}\lambda^{\mathrm{p}}_{ij}(\mu^{\mathrm{p}}_j-\mu_{H_j})+\lambda^{\mathrm{p}}_{ii}\mu^{\mathrm{p}}_i+\frac{ky_i\mu^*_{X_i}}{\beta}\right)\\
\sigma^2_{H_i} &= \frac{1}{\frac{k(\sigma^2_{X_i}+|\mu_{X_i}|^2)}{\beta}+\lambda^{\mathrm{p}}_{ii}}
\end{aligned}
$$

for all $i\in[1:N]$, respectively. The updates for the beliefs b_{H_i} $(i\in[1:N])$ are

$$
\begin{aligned}
b_{H_i}(h_i) &= n^{\mathrm{MF}}_{H_i\to p_{Y_i|X_i,H_i,\Gamma}}(h_i)\\
&\sim \mathcal{CN}(\mu_{H_i},\sigma^2_{H_i}),\quad \forall\, i\in[1:N].
\end{aligned}
\tag{34}
$$

5) Proceed as described in 2).

Note that there is an ambiguity in the choice of variable nodes in the MF part. For example, we could have chosen $\mathbf{H}$ to be a single variable node in the factor graph. In this case we do not make the assumption that the random variables H_i $(i\in[1:N])$ are independent in the MF approximation and the set of indices $\mathcal{I}$ in (29) has to be replaced by

$$\mathcal{I}\triangleq\{C_1,\ldots,C_{NM}\}\cup\{X_1,\ldots,X_N\}\cup\{\mathbf{H}\}\cup\{\Gamma\}.$$

Each factor node $p_{Y_i|X_i,\mathbf{H},\Gamma}$ $(i\in[1:N])$ is then connected to the same variable node $\mathbf{H}$ with

$$
\begin{aligned}
p_{Y_i|X_i,\mathbf{H},\Gamma}(y_i|x_i,\mathbf{h},\gamma) &= \frac{\gamma}{\pi}\exp(-\gamma|y_i-\mathbf{e}_i^{\mathrm{T}}\mathbf{h}x_i|^2)\\
&\sim \mathcal{CN}(\mathbf{e}_i^{\mathrm{T}}\mathbf{h}x_i,1/\gamma),\quad \forall i\in[1:N]
\end{aligned}
$$

where $\mathbf{e}_i$ denotes the i-th unit vector in $\mathbb{C}^N$.

V. Conclusion and Outlook

We showed that the message passing fixed point equations of a combination of BP and the MF approximation correspond to stationary points of one single constraint region-based variational free energy. These stationary points are in one-to-one correspondence to solutions of a coupled system of message passing fixed point equations. For an arbitrary factor graph and a choice of a splitting of the factor nodes into a set of MF and BP factor nodes, our result gives immediately the corresponding message passing fixed point equations and yields an interpretation of the computed beliefs as stationary points. Moreover, we presented an algorithm for updating the messages that is guaranteed to converge provided that the factor graph fulfills certain technical conditions. We also showed how to extend the MF part in the factor graph to

continuous random variables and to include hard constraints in the BP part of the factor graph. Finally, we showed how to compute the messages in a simple example.

An interesting extension of our result would be to generalize the functions in the factorization of the BP part to functions depending on continuous random variables. A promising approach are the results in [27], which could be used to generalize the Lagrange multiplier for the marginalization constraints to the continuous case. However, these methods are based on the assumption that the objective function is Fréchet differentiable and it seems to be not obvious how to define the Fréchet derivative of the Kullback Leibler divergence depending on pdfs. The reason for this is that in general any point in the image of a pdf can be arbitrary close to zero. Therefore, the argument of the logarithm in the Kullback Leibler divergence is not guaranteed to be nonnegative in the definition of the Fréchet derivative. An extension to continuous random variables in the BP part would allow to apply a combination of BP with the MF approximation, e.g., for sensor self-localization, where both methods are used [28], [29]. Another interesting extension could be to generalize the free energy such that the messages in the BP part are equivalent to the messages for tree rewighted BP.

APPENDIX

A. Proof of Lemma 1

Suppose that $\{\widetilde{m}_{a\to i}(x_i), \widetilde{n}_{i\to a}(x_i)\}$ $(a \in \mathcal{A}, i \in \mathcal{N}(a))$ is a solution of (7) and set

$$\begin{aligned} \widetilde{m}_{a\to i}(x_i) &= \kappa_{a,i} m_{a\to i}(x_i), \quad \forall\ a \in \mathcal{A}, i \in \mathcal{N}(a) \\ \widetilde{n}_{i\to a}(x_i) &= \tau_{a,i} n_{i\to a}(x_i), \quad \forall\ a \in \mathcal{A}, i \in \mathcal{N}(a) \end{aligned} \tag{35}$$

with $\kappa_{a,i}, \tau_{a,i} > 0$ $(a \in \mathcal{A}, i \in \mathcal{N}(a))$. Plugging (35) into (7) we obtain the following fixed point equations for the messages $\{m_{a\to i}(x_i), n_{i\to a}(x_i)\}$ $(a \in \mathcal{A}, i \in \mathcal{N}(a))$.

$$\begin{cases} \kappa_{a,i} m_{a\to i}(x_i) \\ \quad = \omega_{a,i} \Big(\prod\limits_{j \in \mathcal{N}(a)\setminus i} \tau_{a,j} \Big) \sum\limits_{\mathbf{x}_a \setminus x_i} f_a(\mathbf{x}_a) \prod\limits_{j \in \mathcal{N}(a)\setminus i} n_{j\to a}(x_j) \\ \tau_{a,i} n_{i\to a}(x_i) \\ \quad = \Big(\prod\limits_{c \in \mathcal{N}(i)\setminus a} \kappa_{c,i} \Big) \prod\limits_{c \in \mathcal{N}(i)\setminus a} m_{c\to i}(x_i) \end{cases} \tag{36}$$

for all $a \in \mathcal{A}, i \in \mathcal{N}(a)$. Now (36) is equivalent to (6) if and only if

$$\tau_{a,i} = \prod_{c \in \mathcal{N}(i)\setminus a} \kappa_{c,i}, \quad \forall\ a \in \mathcal{A}, i \in \mathcal{N}(a) \tag{37}$$

$$d_a = \frac{\omega_{a,i} \prod\limits_{j \in \mathcal{N}(a)\setminus i} \tau_{a,j}}{\kappa_{a,i}}, \quad \forall\ a \in \mathcal{A}, i \in \mathcal{N}(a) \tag{38}$$

where the positive constants d_a $(a \in \mathcal{A})$ are such that the beliefs b_a $(a \in \mathcal{A})$ in (5) are normalized to one. This normalization of the beliefs b_a $(a \in \mathcal{A})$ in (5) gives

$$\begin{aligned} \frac{1}{d_a} &= \sum_{\mathbf{x}_a} f_a(\mathbf{x}_a) \prod_{j \in \mathcal{N}(a)} n_{j\to a}(x_i) \\ &= \frac{\sum\limits_{\mathbf{x}_a} f_a(\mathbf{x}_a) \prod\limits_{j \in \mathcal{N}(a)} \widetilde{n}_{j\to a}(x_i)}{\prod\limits_{j \in \mathcal{N}(a)} \tau_{a,j}} \\ &= \frac{1}{\tilde{d}_a \prod\limits_{j \in \mathcal{N}(a)} \tau_{a,j}}, \quad \forall\ a \in \mathcal{A} \end{aligned} \tag{39}$$

where we used (35) in the second step and (8) in the last step. Combining (37), (38), and (39) we obtain

$$\begin{aligned} \frac{1}{\tilde{d}_a} &= \frac{\kappa_{a,i}\tau_{a,i}}{\omega_{a,i}} \\ &= \frac{e_i}{\omega_{a,i}}, \quad \forall\ a \in \mathcal{A}, i \in \mathcal{N}(a) \end{aligned}$$

with

$$e_i \triangleq \prod_{c \in \mathcal{N}(i)} \kappa_{c,i}, \quad \forall\ i \in \mathcal{I}.$$

Now suppose that (9) is fulfilled. Setting

$$\begin{aligned} \kappa_{a,i} &= e_i^{\frac{1}{|\mathcal{N}(i)|}}, \quad \forall\ a \in \mathcal{A}, i \in \mathcal{N}(a) \\ \tau_{a,i} &= e_i^{1-\frac{1}{|\mathcal{N}(i)|}} \quad \forall\ a \in \mathcal{A}, i \in \mathcal{N}(a) \end{aligned}$$

and reversing all the steps finishes the proof.

B. Extension of the MF approximation to continuous random variables

Suppose that $p(\mathbf{x})$ is a pdf for the vector of random variables $\mathbf{X}$. In this appendix, we assume that all integrals are Lebesgue integrals. For each $i \in \mathcal{I}$ we can rewrite F_{MF} in (11) as

$$\begin{aligned} F_{\text{MF}} &= \int b_i(x_i) \ln b_i(x_i)\, \mathrm{d}x_i - \int \ln p(\mathbf{x}) \prod_{i \in \mathcal{I}} b_i(x_i)\, \mathrm{d}x_i \\ &\quad - \sum_{j \in \mathcal{I}\setminus i} \int b_j(x_j) \ln b_j(x_j)\, \mathrm{d}x_j \\ &= D(b_i \,||\, a_i) - \sum_{j \in \mathcal{I}\setminus i} \int b_j(x_j) \ln b_j(x_j)\, \mathrm{d}x_j \end{aligned} \tag{40}$$

with

$$\begin{aligned} a_i(x_i) &\triangleq \exp\Big(\int \ln p(\mathbf{x}) \prod_{j \in \mathcal{I}\setminus i} b(x_j)\, \mathrm{d}x_j \Big) \\ &= \exp\Big(\sum_{a \in \mathcal{N}(i)} \int \ln f_a(\mathbf{x}_a) \prod_{j \in \mathcal{N}(a)\setminus i} b(x_j)\, \mathrm{d}x_j \Big), \\ &\quad \forall\ i \in \mathcal{I}. \end{aligned}$$

Suppose that a_i $(i \in \mathcal{I})$ are measurable, integrable functions. For each $i \in \mathcal{I}$, minimizing F_{MF} in (40) with respect to b_i subject to $\int b_i(x_i)\, \mathrm{d}x_i = 1$ is equivalent to minimizing

$$\begin{aligned} &D(b_i \,||\, a_i) + \lambda_i \int b_i(x_i)\, \mathrm{d}x_i \\ &= D\Big(b_i \,||\, \frac{a_i}{\int a_i(x_i)\, \mathrm{d}x_i}\Big) \\ &\quad + \Big(\lambda_i - \ln \int a_i(x_i)\, \mathrm{d}x_i\Big) \int b_i(x_i)\, \mathrm{d}x_i \end{aligned} \tag{41}$$

with Lagrange multiplier λ_i that ensures that b_i is normalized to one. Now let

$$\mu_i(E) \triangleq \int_E b_i(x_i)\,\mathrm{d}x_i$$
$$\tilde{\mu}_i(E) \triangleq \frac{\int_E a_i(x_i)\,\mathrm{d}x_i}{\int a_i(x_i)\,\mathrm{d}x_i}$$

for Lebesgue measurable sets E. If b_i is a measurable integrable function that vanishes only on sets of measure zero, we see that μ_i and $\tilde{\mu}_i$ are absolutely continuous with respect to one another. Hence, we can apply [17, Th. 2.1] with $T \equiv 0$ and find that for each $i \in \mathcal{I}$ the quantity $D(b_i \,||\, a_i)$ is minimized subject to $\int b_i(x_i)\,\mathrm{d}x_i = 1$ if and only if

$$b_i(x_i) = \frac{a_i(x_i)}{\int a_i(x_i)\,\mathrm{d}x_i}. \tag{42}$$

Formally, b_i $(i \in \mathcal{I})$ in (42) differs from b_i $(i \in \mathcal{I})$ in (12) by replacing the sum over the states x_i with the Lebesgue integral.

C. Proof of Theorem 2

The proof of Theorem 2 is based on the ideas of the proof of [13, Th. 2]. However, we will see that we get a significant simplification by augmenting it with some of the arguments originally used in [10] for Markov random fields and adopted to factor graphs in [11]. In particular, we shall make use of the following observation. Recall the expression for $F_{\text{BP, MF}}$ in (19)

$$\begin{aligned} F_{\text{BP, MF}} = &\sum_{a\in\mathcal{A}_{\text{BP}}}\sum_{\mathbf{x}_a} b_a(\mathbf{x}_a)\ln\frac{b_a(\mathbf{x}_a)}{f_a(\mathbf{x}_a)} \\ &- \sum_{a\in\mathcal{A}_{\text{MF}}}\sum_{\mathbf{x}_a}\prod_{i\in\mathcal{N}(a)} b_i(x_i)\ln f_a(\mathbf{x}_a) \\ &- \sum_{i\in\mathcal{I}}(|\mathcal{N}_{\text{BP}}(i)|-1)\sum_{x_i} b_i(x_i)\ln b_i(x_i), \end{aligned} \tag{43}$$

the marginalization constraints

$$b_i(x_i) = \sum_{\mathbf{x}_a\setminus x_i} b_a(\mathbf{x}_a), \quad \forall\ a\in\mathcal{A}_{\text{BP}}, i\in\mathcal{N}(a), \tag{44}$$

and the normalization constraints

$$\begin{aligned} &\sum_{x_i} b_i(x_i) = 1, \quad \forall\ i\in\mathcal{I}_{\text{MF}}\setminus\mathcal{I}_{\text{BP}} \\ &\sum_{\mathbf{x}_a} b_a(\mathbf{x}_a) = 1, \quad \forall\ a\in\mathcal{A}_{\text{BP}}. \end{aligned} \tag{45}$$

Using the marginalization constraints (44), we see that

$$\begin{aligned} &\sum_{a\in\mathcal{A}_{\text{BP}}}\sum_{\mathbf{x}_a} b_a(\mathbf{x}_a)\ln\prod_{i\in\mathcal{N}(a)} b_i(x_i) \\ &= \sum_{a\in\mathcal{A}_{\text{BP}}}\sum_{\mathbf{x}_a}\sum_{i\in\mathcal{N}(a)} b_a(\mathbf{x}_a)\ln b_i(x_i) \\ &= \sum_{a\in\mathcal{A}_{\text{BP}}}\sum_{i\in\mathcal{N}(a)}\sum_{x_i} b_i(x_i)\ln b_i(x_i) \\ &= \sum_{i\in\mathcal{I}_{\text{BP}}}\sum_{a\in\mathcal{N}_{\text{BP}}(i)}\sum_{x_i} b_i(x_i)\ln b_i(x_i) \\ &= \sum_{i\in\mathcal{I}_{\text{BP}}} |\mathcal{N}_{\text{BP}}(i)|\sum_{x_i} b_i(x_i)\ln b_i(x_i). \end{aligned} \tag{46}$$

Combining (46) with (43), we further get

$$\begin{aligned} F_{\text{BP, MF}} = &- \sum_{a\in\mathcal{A}_{\text{BP}}}\sum_{\mathbf{x}_a} b_a(\mathbf{x}_a)\ln f_a(\mathbf{x}_a) \\ &- \sum_{a\in\mathcal{A}_{\text{MF}}}\sum_{\mathbf{x}_a}\prod_{i\in\mathcal{N}(a)} b_i(x_i)\ln f_a(\mathbf{x}_a) \\ &+ \sum_{i\in\mathcal{I}}\sum_{x_i} b_i(x_i)\ln b_i(x_i) \\ &+ \sum_{a\in\mathcal{A}_{\text{BP}}} I_a \end{aligned} \tag{47}$$

with the mutual information [19, p. 19]

$$I_a \triangleq \sum_{\mathbf{x}_a} b_a(\mathbf{x}_a)\ln\frac{b_a(\mathbf{x}_a)}{\prod_{i\in\mathcal{N}(a)} b_i(x_i)}, \quad \forall\ a\in\mathcal{A}_{\text{BP}}. \tag{48}$$

Next, we shall compute the stationary points of the Lagrangian

$$\begin{aligned} L_{\text{BP, MF}} = &F_{\text{BP, MF}} \\ &- \sum_{a\in\mathcal{A}_{\text{BP}}}\sum_{i\in\mathcal{N}(a)}\sum_{x_i}\lambda_{a,i}(x_i)\Big(b_i(x_i) - \sum_{\mathbf{x}_a\setminus x_i} b_a(\mathbf{x}_a)\Big) \\ &- \sum_{i\in\mathcal{I}_{\text{MF}}\setminus\mathcal{I}_{\text{BP}}}\gamma_i\Big(\sum_{x_i} b_i(x_i) - 1\Big) \\ &- \sum_{a\in\mathcal{A}_{\text{BP}}}\gamma_a\Big(\sum_{\mathbf{x}_a} b_a(\mathbf{x}_a) - 1\Big) \end{aligned} \tag{49}$$

using the expression for $F_{\text{BP, MF}}$ in (47). The particular form of $F_{\text{BP, MF}}$ in (47) is convenient because the marginalization constraints in (44) imply that for all $i \in \mathcal{I}$ and $a \in \mathcal{A}_{\text{BP}}$ we have $\frac{\partial I_a}{\partial b_i(x_i)} = -\,\mathrm{I}_{\mathcal{N}_{\text{BP}}(i)}(a)$. Setting the derivative of $L_{\text{BP, MF}}$ in (49) with respect to $b_i(x_i)$ and $b_a(\mathbf{x}_a)$ equal to zero for all $i \in \mathcal{I}$ and $a \in \mathcal{A}_{\text{BP}}$, we get the following fixed point equations for the stationary points.

$$\begin{aligned} \ln b_i(x_i) = &\sum_{a\in\mathcal{N}_{\text{BP}}(i)}\lambda_{a,i}(x_i) \\ &+ \sum_{a\in\mathcal{N}_{\text{MF}}(i)}\sum_{\mathbf{x}_a\setminus x_i}\prod_{j\in\mathcal{N}(a)\setminus i} b_j(x_j)\ln f_a(\mathbf{x}_a) \\ &+ |\mathcal{N}_{\text{BP}}(i)| + \mathrm{I}_{\mathcal{I}_{\text{MF}}\setminus\mathcal{I}_{\text{BP}}}(i)\gamma_i - 1, \quad \forall\ i\in\mathcal{I} \\ \ln b_a(\mathbf{x}_a) = &\ln f_a(\mathbf{x}_a) - \sum_{i\in\mathcal{N}(a)}\lambda_{a,i}(x_i) + \ln\Big(\prod_{i\in\mathcal{N}(a)} b_i(x_i)\Big) \\ &+ \gamma_a - 1, \quad \forall\ a\in\mathcal{A}_{\text{BP}}. \end{aligned} \tag{50}$$

Setting

$$\begin{aligned} &m^{\text{BP}}_{a\to i}(x_i) \triangleq \exp\Big(\lambda_{a,i}(x_i) + 1 - \frac{1}{|\mathcal{N}_{\text{BP}}(i)|}\Big), \\ &\qquad \forall a\in\mathcal{A}_{\text{BP}}, i\in\mathcal{N}(a) \\ &m^{\text{MF}}_{a\to i}(x_i) \triangleq \exp\Bigg(\sum_{\mathbf{x}_a\setminus x_i}\prod_{j\in\mathcal{N}(a)\setminus i} b_j(x_j)\ln f_a(\mathbf{x}_a)\Bigg) \\ &\qquad \forall\ a\in\mathcal{A}_{\text{MF}}, i\in\mathcal{N}(a), \end{aligned} \tag{51}$$

we can rewrite (50) as

$$b_i(x_i) = e_i \prod_{a\in\mathcal{N}_{\text{BP}}(i)} m^{\text{BP}}_{a\to i}(x_i) \prod_{a\in\mathcal{N}_{\text{MF}}(i)} m^{\text{MF}}_{a\to i}(x_i), \quad \forall\, i\in\mathcal{I}$$
$$b_a(\mathbf{x}_a) = d_a\, f_a(\mathbf{x}_a) \prod_{i\in\mathcal{N}(a)} \frac{b_i(x_i)}{m^{\text{BP}}_{a\to i}(x_i)}, \quad \forall\, a\in\mathcal{A}_{\text{BP}} \tag{52}$$

with

$$e_i \triangleq \exp(\text{I}_{\mathcal{I}_{\text{MF}}\setminus\mathcal{I}_{\text{BP}}}(i)\gamma_i), \quad \forall\, i\in\mathcal{I} \tag{53}$$

$$d_a \triangleq \exp\left(\gamma_a - 1 + \sum_{i\in\mathcal{N}(a)}\left(1-\frac{1}{|\mathcal{N}_{\text{BP}}(i)|}\right)\right), \quad \forall\, a\in\mathcal{A}_{\text{BP}}. \tag{54}$$

Finally, we define

$$n_{i\to a}(x_i) \triangleq e_i \prod_{c\in\mathcal{N}_{\text{BP}}(i)\setminus\{a\}} m^{\text{BP}}_{c\to i}(x_i) \prod_{c\in\mathcal{N}_{\text{MF}}(i)} m^{\text{MF}}_{c\to i}(x_i), \quad \forall\, a\in\mathcal{A}, i\in\mathcal{N}(a). \tag{55}$$

Plugging the expression for $n_{i\to a}(x_i)$ in (55) into the second line in (52) , we find that

$$b_i(x_i) = e_i \prod_{a\in\mathcal{N}_{\text{BP}}(i)} m^{\text{BP}}_{a\to i}(x_i) \prod_{a\in\mathcal{N}_{\text{MF}}(i)} m^{\text{MF}}_{a\to i}(x_i), \quad \forall\, i\in\mathcal{I}$$
$$b_a(\mathbf{x}_a) = d_a\, f_a(\mathbf{x}_a) \prod_{i\in\mathcal{N}(a)} n_{i\to a}(x_i), \quad \forall\, a\in\mathcal{A}_{\text{BP}}. \tag{56}$$

Using the marginalization constraints in (44) in combination with (56) and noting that $e_i = 1$ for all $i\in\mathcal{I}_{\text{BP}}$ we further find that

$$\begin{aligned} &n_{i\to a}(x_i) m^{\text{BP}}_{a\to i}(x_i) \\ &= \prod_{a\in\mathcal{N}_{\text{BP}}(i)} m^{\text{BP}}_{a\to i}(x_i) \prod_{a\in\mathcal{N}_{\text{MF}}(i)} m^{\text{MF}}_{a\to i}(x_i) \\ &= b_i(x_i) \\ &= \sum_{\mathbf{x}_a\setminus x_i} b_a(\mathbf{x}_a) \\ &= d_a \sum_{\mathbf{x}_a\setminus x_i} f_a(\mathbf{x}_a) \prod_{j\in\mathcal{N}(a)} n_{j\to a}(x_j), \quad \forall\, a\in\mathcal{A}_{\text{BP}}, i\in\mathcal{N}(a). \end{aligned} \tag{57}$$

Dividing both sides of (57) by $n_{i\to a}(x_i)$ gives

$$m^{\text{BP}}_{a\to i}(x_i) = d_a \sum_{\mathbf{x}_a\setminus x_i} f_a(\mathbf{x}_a) \prod_{j\in\mathcal{N}(a)\setminus i} n_{j\to a}(x_j) \quad \forall\, a\in\mathcal{A}_{\text{BP}}, i\in\mathcal{N}(a). \tag{58}$$

Noting that $n_{j\to a}(x_j) = b_j(x_j)$ for all $a\in\mathcal{A}_{\text{MF}}$ and $j\in\mathcal{N}(a)$, we can write the messages $m^{\text{MF}}_{a\to i}(x_i)$ in (51) as

$$m^{\text{MF}}_{a\to i}(x_i) = \exp\left(\sum_{\mathbf{x}_a\setminus x_i} \prod_{j\in\mathcal{N}(a)\setminus i} n_{j\to a}(x_j)\ln f_a(\mathbf{x}_a)\right), \quad \forall\, a\in\mathcal{A}_{\text{MF}}, i\in\mathcal{N}(a). \tag{59}$$

Now (55), (58), and (59) is equivalent to (22) and (56) is equivalent to (21). This completes the proof that stationary points of the Lagrangian in (20) must be fixed points with positive beliefs fulfilling (21). Since all the steps are reversible, this also completes the proof of Theorem C.

D. Proof of convergence

In order to finish the proof of convergence for the algorithm presented in Subsection III-B, we need to show that running the forward/backward algorithm in the BP part in step 2) of Algorithm 1 cannot increase the free energy $F_{\text{BP, MF}}$ in (19). To this end we analyze the factorization

$$p(\mathbf{x}_{\text{BP}}) \propto \prod_{a\in\mathcal{A}_{\text{BP}}} f_a(\mathbf{x}_a) \prod_{i\in\mathcal{I}_{\text{BP}}\cap\mathcal{I}_{\text{MF}}} \prod_{b\in\mathcal{N}_{\text{MF}}(i)} m^{\text{MF}}_{b\to i}(x_i) \tag{60}$$

with $\mathbf{x}_{\text{BP}} \triangleq \{x_i \mid i\in\mathcal{I}_{\text{BP}}\}$. The factorization in (60) is the product of the factorization of the BP part in (17) and the incoming messages from the MF part and we compute the marginals of $p(\mathbf{x}_{\text{BP}})$ in (60) in step 2) of Algorithm 1. The Bethe free energy (3) corresponding to the factorization in (60) is

$$\begin{aligned} F_{\text{BP}} &= \sum_{a\in\mathcal{A}_{\text{BP}}} \sum_{\mathbf{x}_a} b_a(\mathbf{x}_a)\ln\frac{b_a(\mathbf{x}_a)}{f_a(\mathbf{x}_a)} \\ &\quad + \sum_{i\in\mathcal{I}_{\text{BP}}\cap\mathcal{I}_{\text{MF}}} \sum_{a\in\mathcal{N}_{\text{MF}}(i)} \sum_{x_i} b_i(x_i)\ln\frac{b_i(x_i)}{m^{\text{MF}}_{a\to i}(x_i)} \\ &\quad - \sum_{i\in\mathcal{I}_{\text{BP}}} (|\mathcal{N}_{\text{BP}}(i)| + |\mathcal{N}_{\text{MF}}(i)| - 1) \sum_{x_i} b_i(x_i)\ln b_i(x_i) \\ &= \sum_{a\in\mathcal{A}_{\text{BP}}} \sum_{\mathbf{x}_a} b_a(\mathbf{x}_a)\ln\frac{b_a(\mathbf{x}_a)}{f_a(\mathbf{x}_a)} \\ &\quad - \sum_{i\in\mathcal{I}_{\text{BP}}\cap\mathcal{I}_{\text{MF}}} \sum_{a\in\mathcal{N}_{\text{MF}}(i)} \sum_{x_i} b_i(x_i)\ln m^{\text{MF}}_{a\to i}(x_i) \\ &\quad - \sum_{i\in\mathcal{I}_{\text{BP}}} (|\mathcal{N}_{\text{BP}}(i)| - 1) \sum_{x_i} b_i(x_i)\ln b_i(x_i). \end{aligned} \tag{61}$$

We now show that minimizing F_{BP} in (61) is equivalent to minimizing $F_{\text{BP, MF}}$ in (19) with respect to b_a and b_i for all $a\in\mathcal{A}_{\text{BP}}$ and $i\in\mathcal{I}_{\text{BP}}$. Obvioulsy,

$$\frac{\partial F_{\text{BP, MF}}}{\partial b_i(x_i)} = \frac{\partial F_{\text{BP}}}{\partial b_i(x_i)}, \quad \forall i\in\mathcal{I}_{\text{BP}}\setminus\mathcal{I}_{\text{MF}}$$

and

$$\frac{\partial F_{\text{BP, MF}}}{\partial b_a(\mathbf{x}_a)} = \frac{\partial F_{\text{BP}}}{\partial b_a(\mathbf{x}_a)}, \quad \forall a\in\mathcal{A}_{\text{BP}}.$$

This follows from the fact that $F_{\text{BP, MF}}$ differs from F_{BP} by terms that depend only on b_i with $i\in\mathcal{I}_{\text{MF}}$.

Now suppose that $i\in\mathcal{I}_{\text{BP}}\cap\mathcal{I}_{\text{MF}}$. In this case, we find that

$$\begin{aligned} \frac{\partial F_{\text{BP, MF}}}{\partial b_i(x_i)} &= (1-|\mathcal{N}_{\text{BP}}(i)|)(\ln b_i(x_i)+1) \\ &\quad - \sum_{a\in\mathcal{N}_{\text{MF}}(i)} \sum_{\mathbf{x}_a\setminus x_i} \prod_{j\in\mathcal{N}(a)\setminus i} b_j(x_j)\ln f_a(\mathbf{x}_a) \end{aligned} \tag{62}$$

and

$$\frac{\partial F_{\text{BP}}}{\partial b_i(x_i)} = (1-|\mathcal{N}_{\text{BP}}(i)|)(\ln b_i(x_i)+1) - \sum_{a\in\mathcal{N}_{\text{MF}}(i)} \ln m^{\text{MF}}_{a\to i}(x_i). \tag{63}$$

From (22) we see that

$$m^{\text{MF}}_{a\to i}(x_i) = \exp\left(\sum_{\mathbf{x}_a\setminus x_i} \prod_{j\in\mathcal{N}(a)\setminus i} n_{j\to a}(x_j)\ln f_a(\mathbf{x}_a)\right), \quad \forall\, a\in\mathcal{N}_{\text{MF}}(i). \tag{64}$$

Note that, according to step 2) in Algorithm 1, the messages $m^{\text{MF}}_{a\to i}(x_i)$ in (64) are *fixed inputs* for the BP part. Therefore, we are not allowed to plug the expressions for the messages $m^{\text{MF}}_{a\to i}(x_i)$ in (64) into (63) in general. However, since $a \in \mathcal{A}_{\text{MF}}$ and $i \in \mathcal{I}_{\text{BP}} \cap \mathcal{I}_{\text{MF}}$, condition (26) implies that $\mathcal{N}(a)\setminus i \subseteq \mathcal{I}_{\text{MF}} \setminus \mathcal{I}_{\text{BP}}$ and guarantees that

$$n_{j\to a}(x_j) = b_j(x_j) \tag{65}$$

is constant in step 2) of Algorithm 1 for all $j \in \mathcal{N}(a) \setminus i \subseteq \mathcal{I}_{\text{MF}} \setminus \mathcal{I}_{\text{BP}}$. Therefore, we are indeed allowed to plug the expressions of the messages $m^{\text{MF}}_{a\to i}(x_i)$ in (64) into (63) and finally see that also

$$\frac{\partial F_{\text{BP, MF}}}{\partial b_i(x_i)} = \frac{\partial F_f}{\partial b_i(x_i)}, \quad \forall i \in \mathcal{I}_{\text{BP}} \cap \mathcal{I}_{\text{MF}}.$$

Hence, minimizing F_{BP} in (61) is equivalent to minimizing $F_{\text{BP, MF}}$ in (19).

By assumption, the factor graph in the BP part has tree structure. Therefore, [13, Prop. 3] implies that

1) $F_{\text{BP}} \geq 0$;
2) $F_{\text{BP}} = 0$ if and only if the beliefs $\{b_i, b_a\}$ in (61) are the marginals of the factorization in (60).

Hence, for b_j fixed with $j \in \mathcal{I}_{\text{MF}} \setminus \mathcal{I}_{\text{BP}}$, we see that $F_{\text{BP, MF}}$ in (19) is minimized by the marginals of the factorization in (60).

It remains to show that running the forward/backword algorithm in the BP part as described in step 2) in Algorithm 1 indeed computes the marginals of the factorization in (60). Applying Theorem 1 to the factorization in (60) yields the message passing fixed point equations

$$\begin{cases} n_{i\to a}(x_i) = \displaystyle\prod_{c\in\mathcal{N}_{\text{BP}}(i)\setminus a} m^{\text{BP}}_{c\to i}(x_i) \prod_{c\in\mathcal{N}_{\text{MF}}(i)} m^{\text{MF}}_{c\to i}(x_i), \\ \qquad \forall\ a \in \mathcal{A}_{\text{BP}}, i \in \mathcal{N}(a) \\ m^{\text{BP}}_{a\to i}(x_i) = d_a \displaystyle\sum_{\mathbf{x}_a\setminus x_i} f_a(\mathbf{x}_a) \prod_{j\in\mathcal{N}(a)\setminus i} n_{j\to a}(x_j), \\ \qquad \forall\ a \in \mathcal{A}_{\text{BP}}, i \in \mathcal{N}(a). \end{cases} \tag{66}$$

The message passing fixed point equations in (66) are the same as the message passing fixed point equations for the BP part in (22) with fixed input messages $m^{\text{MF}}_{a\to i}(x_i)$ for all $i \in \mathcal{I}_{\text{BP}} \cap \mathcal{I}_{\text{MF}}$ and $a \in \mathcal{N}_{\text{MF}}(i)$. Hence, running the forward/backward algorithm in the BP part indeed computes the marginals of the factorization in (60) and Algorithm 1 is guaranteed to converge.

E. Product of two Gaussian distributions

Lemma 2: Let

$$p_1(x) = \frac{1}{\pi\sigma_1}\exp\big(-\frac{1}{\sigma_1^2}|x-\mu_1|^2\big)$$
$$p_2(x) = \frac{1}{\pi\sigma_2}\exp\big(-\frac{1}{\sigma_2^2}|x-\mu_2|^2\big).$$

Then

$$p_1(x)p_2(x) \propto \frac{1}{\pi\sigma}\exp\big(-\frac{1}{\sigma^2}|x-\mu|^2\big)$$

with

$$\sigma^2 = \frac{1}{\frac{1}{\sigma_1^2}+\frac{1}{\sigma_2^2}}$$
$$\mu = \sigma^2\big(\frac{\mu_1}{\sigma_1^2}+\frac{\mu_2}{\sigma_2^2}\big).$$

Proof: Follows from direct computation. ■

REFERENCES

[1] E. Riegler, G. E. Kirkelund, C. N. Manchón, and B. H. Fleury, "Merging belief propagation and the mean field approximation: A free energy approach," in *IEEE Symp. Turbo Codes (ISTC 2010)*, Brest, France, Sep. 2010, pp. 1–5.

[2] P. Parisi, *Statistical Field Theory*. Oxford, UK: Perseus, 1988.

[3] Z. Ghahramani and M. J. Beal, *Graphical Models and Variational Methods*, D. Saad and M. Opper, Eds. Massachusetts, NY: MIT Press, 2000.

[4] M. I. Jordan, Z. Ghahramani, T. S. Jaakola, and L. K. Saul, "An introduction to variational methods for graphical models," *J. Mach. Learning*, vol. 37, no. 2, pp. 183–233, 1999.

[5] J. Winn and C. Bishop, "Variational message passing," *J. Mach. Learning*, vol. 6, no. 6, pp. 661–694, 2005.

[6] C. M. Bishop, *Pattern Recognition and Machine Learning*. New York, NY: Springer, 2006.

[7] G. E. Kirkelund, C. N. Manchón, L. P. B. Christensen, E. Riegler, and B. H. Fleury, "Variational message-passing for joint channel estimation and decoding in MIMO-OFDM," in *Proc. IEEE Globecom (GLOBECOM 2010)*, Miami, FL, Dec. 2010, pp. 1–5.

[8] J. Pearl, *Probabilistic Reasoning in Intelligent Systems: Networks of Plausible Inference*. San Francisco, CA: Morgan Kaufman, 1998.

[9] F. R. Kschischang, J. F. Brendan, and H.-A. Loeliger, "Factor graphs and the sum-product algorithm," *IEEE Trans. Inf. Th.*, vol. 47, no. 2, pp. 498–519, Feb. 2001.

[10] M. J. Wainwright, T. S. Jaakkola, and A. S. Willsky, "A new class of upper bounds on the log partition function," *IEEE Trans. Inf. Th.*, vol. 51, no. 7, pp. 2313–2335, 2005.

[11] H. Wymeersch, F. Penna, and V. Savić, "Uniformly reweighted belief propagation: A factor graph approach," in *Proc. IEEE Int. Symp. Inf. Th. (ISIT 2011)*, St. Petersburg, Russia, July–Aug. 2011, pp. 1–5.

[12] S. Ikeda, T. Tanaka, and S.-I. Amari, "Information geometry of turbo and low-density parity-check codes," *IEEE Trans. Inf. Th.*, vol. 50, no. 6, pp. 1097–1114, June 2004.

[13] J. S. Yedidia, W. T. Freeman, and Y. Weiss, "Constructing free-energy approximations and generalized belief propagation algorithms," *IEEE Trans. Inf. Th.*, vol. 51, no. 7, pp. 2282–2312, July 2005.

[14] T. Minka, "Divergence measures and message passing," *Microsoft Research, Tech. Rep. MSR-TR-2005-173*, 2005.

[15] S.-I. Amari and H. Nagaoka, *Methods of Information Geometry*. Oxford, UK: Oxford Univ. Press, 2000.

[16] A. P. Dempster, N. M. Laird, and D. B. Rubin, "Maximum-likelihood from incomplete data via the EM algorithm," *J. Roy. Statist. Soc.*, vol. 39, no. 1, pp. 1–38, 1977.

[17] S. Kullback, *Information Theory and Statistics*. New York (NY): Wiley, 1978.

[18] C. N. Manchón, G. E. Kirkelund, E. Riegler, L. Christensen, and B. H. Fleury, "Receiver architectures for MIMO-OFDM based on combined message-passing techniques," *submittet to XXX*.

[19] T. M. Cover and J. A. Thomas, *Elements of Information Theory*, 2nd ed. New York, NY: Wiley, 2006.

[20] H. A. Bethe, "Statistical theory of superlattices," in *Proc. Roy. Soc. London*, ser. A, vol. 150, no. 871, 1935, pp. 552–575.

[21] T. Heskes, "Stable fixed points of loopy belief propagation are minima of the bethe free energy," in *Adv. in Neural Inf. Process. Systems*. MIT Press, 2003, pp. 343–350.

[22] D. P. Bertsekas, *Nonlinear Programming*, 2nd ed. Belmont, MA: Athena Scientific, 2003.

[23] J. Dauwels, "On variational message passing on factor graphs," in *Proc. IEEE Int. Symp. Inf. Th. (ISIT 2007)*, Nice, France, June 2007, pp. 2546–2550.

[24] A. W. Eckford, "The factor graph EM algorithm: Applications for LDPC codes," in *Proc. IEEE SPAWC (SPAWC 2005)*, New York, NY, June 2005, pp. 910–914.

[25] J. Dauwels, S. Korl, and H.-A. Loeliger, "Expectation maximization as message passing," in *Proc. IEEE Int. Symp. Inf. Th. (ISIT 2005)*, Adelaide, Australia, Sep. 2005, pp. 1–4.
[26] B. Hu, "A variational bayesian framework divergence minimization and its application in cdma receivers," Ph.D. dissertation, July 2010.
[27] B. D. Craven, "A generalization of lagrange multipliers," *Bull. Austral. Math. Soc.*, vol. 3, pp. 353–362, 1970.
[28] H. Wymeersch, J. Lien, and M. Z. Win, "Cooperative localization in wireless networks," *Proc. IEEE*, vol. 97, no. 2, pp. 427–450, Feb. 2009.
[29] C. Pedersen, T. Pedersen, and B. H. Fleury, "A variational message passing algorithm for sensor self-localization in wireless networks," in *Proc. IEEE Int. Symp. Inf. Th. (ISIT 2011)*, St. Petersburg, Russia, Jul.–Aug. 2011, pp. 1–5.

Paper B

Merging Belief Propagation and the Mean Field Approximation: A Free Energy Approach

Erwin Riegler, Gunvor E. Kirkelund, Carles Navarro Manchón and Bernard H. Fleury

International Symposium on Turbo Codes and Iterative Information Processing, ISTC 2010. Brest, September 2010.

B. MERGING BELIEF PROPAGATION AND THE MEAN FIELD APPROXIMATION: A FREE ENERGY APPROACH

Merging Belief Propagation and the Mean Field Approximation: A Free Energy Approach

Erwin Riegler*, Gunvor Elisabeth Kirkelund†, Carles Navarro Manchón†, Bernard Henri Fleury†
* Vienna University of Technology (VUT), Austria
E-mail: erwin.riegler@nt.tuwien.ac.at
† Aalborg University (AAU), Denmark
E-mail: gunvor@es.aau.dk, cnm@es.aau.dk, bfl@es.aau.dk

***Abstract*—We present a joint message passing approach that combines belief propagation and the mean field approximation. Our analysis is based on the region-based free energy approximation method proposed by Yedidia et al., which allows to use the same objective function (Kullback-Leibler divergence) as a starting point. In this method message passing fixed point equations (which correspond to the update rules in a message passing algorithm) are then obtained by imposing different region-based approximations and constraints on the mean field and belief propagation parts of the corresponding factor graph. Our results can be applied, for example, to algorithms that perform joint channel estimation and decoding in iterative receivers. This is demonstrated in a simple example.**

I. Introduction

Variational techniques have been used for decades in quantum and statistical physics, where they are referred to as *mean field* (MF) approximation [1]. They are also applied for statistical inference, see, e.g., [2]–[5]. The basic idea of variational inference is to derive the statistics of "hidden" random variables given the knowledge of "visible" random variables of a certain probability density function (pdf). This is done by approximating the pdf by some "simpler," e.g., (fully) factorized function in an iterative (message passing like) way. Typically, such a function has to fulfill additional constraints. For example, [4] imposes additionally exponential conjugacy constraints in order to derive simple update rules for the messages that propagate along the edges in a Bayesian network. Variational inference methods were recently applied in [6] to the *channel state estimation/interference cancellation part* of a class of MIMO-OFDM receivers that iterate between detection, channel estimation, and decoding.

A different approach is *belief propagation* (BP) [7]. Roughly speaking, with BP one tries to find *local* approximations, which are—exactly or approximately—the marginals of a certain pdf. This can also be done in an iterative way, where messages are passed along the edges in a factor graph [8]. A typical application of BP is *decoding* of turbo codes.

An obvious question that arises is the following: Can we combine both approaches and develop a *unified message passing algorithm* that combines BP and the MF approach, and how do the two types of messages influence each other? The main contribution of this work is to shed light on this open problem using the free energy approach proposed in [9] and to *derive the message passing fixed point equations for a joint approach, where BP is applied to a subset of factor nodes and the MF approximation is employed to the remaining factor nodes of a factor graph.*

The paper is organized as follows. Section II is devoted to the introduction of the region-based free energy approximations proposed by [9]. We briefly summarize the main steps to derive the message passing fixed point equations for BP in Section III. In Section IV, we show how the MF approximation can be included in the free energy framework. Our main result—the combined BP/MF fixed point equations—is presented in Section V. Section VI is devoted to a discussion of a simple example and shows simulation results. Finally, we conclude in Section VII.

II. Region-based free energy approximations

In the following two sections, we follow the presentation and main results given in [9]. Let $p(\mathbf{x})$ be a certain pdf that factorizes as

$$p(\mathbf{x}) = \prod_a f_a(\mathbf{x}_a),$$

where $\mathbf{x} \triangleq \{x_i \mid i \in \mathbf{I}\}$, $\mathbf{I} \triangleq \{1, \ldots, N\}$, $\mathbf{x}_a \subseteq \mathbf{x}$, and $a \in \mathbf{A} \triangleq \{1, \ldots, M\}$. Such a factorization can be visualized in a *factor graph* [8]. We assume that $p(\mathbf{x})$ is a positive function and that $\mathbf{x}$ is a set of discrete random variables. Our analysis can be extended to continuous random variables by simply replacing sums by integrals. Now define the sets of indices

$$N(a) \triangleq \{i \mid x_i \in \mathbf{x}_a\} \quad \text{and} \quad N(i) \triangleq \{a \mid x_i \in \mathbf{x}_a\}.$$

A *region* $R \triangleq \{\mathbf{x}_R, \mathbf{A}_R\}$ consists of a subset $\mathbf{x}_R \subseteq \mathbf{x}$ of variables and a subset $\mathbf{A}_R \subseteq \mathbf{A}$ of indices with the restriction that $a \in \mathbf{A}_R$ implies that $\mathbf{x}_a \subseteq \mathbf{x}_R$. To each region R we associate a *counting number* $c_R \in \mathbb{Z}$. A set $\mathcal{R} \triangleq \{R\}$ of regions is called *valid* if

$$\sum_{R \in \mathcal{R}} c_R I_{\mathbf{A}_R}(a) = \sum_{R \in \mathcal{R}} c_R I_{\mathbf{x}_R}(x_i) = 1 \quad \forall a \in \mathbf{A}, i \in \mathbf{I},$$

where $I_{\_}(\_)$ is the indicator function.

978-1-4244-6746-4/10/$26.00 ©2010 IEEE

We define the *variational free energy* [9]

$$F(b) \triangleq \sum_{\mathbf{x}} b(\mathbf{x}) \ln \frac{b(\mathbf{x})}{p(\mathbf{x})} = \underbrace{\sum_{\mathbf{x}} b(\mathbf{x}) \ln b(\mathbf{x})}_{\triangleq -H(b)} - \underbrace{\sum_{\mathbf{x}} b(\mathbf{x}) \ln p(\mathbf{x})}_{\triangleq -U(b)}. \quad (1)$$

In (1), $H(b)$ denotes entropy and $U(b)$ is called average energy. Note that $F(b)$ is the Kullback-Leibler divergence [10, p. 19] between b and p, i.e., $F(b) = D(b \,||\, p)$. For a set $\mathcal{R}$ of regions, the *region-based variational free energy* is defined as [9] $F_{\mathcal{R}} \triangleq U_{\mathcal{R}} - H_{\mathcal{R}}$ with

$$\begin{aligned} U_{\mathcal{R}} &\triangleq \sum_{R \in \mathcal{R}} c_R U_R, \\ H_{\mathcal{R}} &\triangleq \sum_{R \in \mathcal{R}} c_R H_R, \\ U_R &\triangleq -\sum_{a \in \mathbf{A}_R} \sum_{\mathbf{x}_R} b_R(\mathbf{x}_R) \ln f_a(\mathbf{x}_a), \\ H_R &\triangleq -\sum_{\mathbf{x}_R} b_R(\mathbf{x}_R) \ln b_R(\mathbf{x}_R). \end{aligned}$$

Here, $b_R(\mathbf{x}_R)$ is defined locally on the region R. Instead of minimizing F with respect to b, we minimize $F_{\mathcal{R}}$ with respect to all b_R ($R \in \mathcal{R}$), where the b_R have to fulfill certain constraints. The quantities b_R are called *beliefs*. We give two examples of valid sets of regions.

Example II.1 The trivial example $\mathcal{R} = \{R = (\mathbf{x}, A)\}$.

Example II.2 We define two types of regions:

1) *large regions:* $R_a \triangleq (\mathbf{x}_a, \{a\})$ with $c_{R_a} = 1 \; \forall \; a \in \mathbf{A}$;
2) *small regions:* $R_i \triangleq (\{x_i\}, \emptyset)$ with $c_{R_i} = 1 - |N(i)| \; \forall \; i \in \mathbf{I}$.

Here, $|N(i)|$ denotes the cardinality of the set $N(i)$ for all $i \in \mathbf{I}$. The region-based variational free energy corresponding to the valid set of regions $\mathcal{R} = \{R_i \mid i \in \mathbf{I}\} \cup \{R_a \mid a \in \mathbf{A}\}$ is called the *Bethe free energy* [9], [11]. The exact variational free energy is equal to the Bethe free energy when the factor graph has no cycles [9].

III. Belief propagation fixed point equations

The fixed point equations for BP can be obtained from the Bethe free energy by imposing additional marginalization constraints and computing the stationary points. The Bethe free energy reads

$$F_{\mathcal{R}} = \sum_{a \in \mathbf{A}} \sum_{\mathbf{x}_a} b_a(\mathbf{x}_a) \ln \frac{b_a(\mathbf{x}_a)}{f_a(\mathbf{x}_a)} - \sum_{i \in \mathbf{I}} (|N(i)| - 1) \sum_{x_i} b_i(x_i) \ln b_i(x_i), \quad (2)$$

with $b_a(\mathbf{x}_a) \triangleq b_{R_a}(\mathbf{x}_a) \; \forall \; a \in \mathbf{A}$ and $b_i(x_i) \triangleq b_{R_i}(\{x_i\}) \; \forall \; i \in \mathbf{I}$. The summation over the index set $\mathbf{I}$ in (2) can be restricted to indices with $|N(i)| > 1$ (the dependence on beliefs $b_i(x_i)$ with $|N(i)| = 1$ drops out). In addition, we impose marginalization constraints on the beliefs

$$b_i(x_i) = \sum_{\mathbf{x}_a \setminus x_i} b_a(\mathbf{x}_a) \quad \forall i \in \mathbf{I}, a \in N(i), \quad (3)$$

which can be included in the Lagrangian

$$L \triangleq F_{\mathcal{R}} + \sum_{a \in \mathbf{A}} \sum_{i \in N(a)} \sum_{x_i} \lambda_{a,i}(x_i) \left(b_i(x_i) - \sum_{\mathbf{x}_a \setminus x_i} b_a(\mathbf{x}_a) \right), \quad (4)$$

where the $\lambda_{a,i}(x_i)$ are Lagrange multipliers [12, p. 283].

The following theorem gives a connection between the BP fixed points with *positive beliefs* and stationary points of the Lagrangian in (4).

Theorem 1 *[9, Theorem 2] Stationary points of the constrained Bethe free energy must be BP fixed points with positive beliefs and vice versa.*

Note that beliefs with tight nonnegativity constraints can only belong to critical points but not to stationary points. We summarize the main steps in the proof of Theorem 1. The stationary points of the Lagrangian in (4) can then be evaluated as

$$\begin{cases} b_a(\mathbf{x}_a) \propto f_a(\mathbf{x}_a) \exp\left(\sum_{i \in N(a)} \lambda_{a,i}(x_i)\right) & \forall \; a \in \mathbf{A} \\ b_i(x_i) \propto \exp\left(\frac{1}{|N(i)|-1} \sum_{a \in N(i)} \lambda_{a,i}(x_i)\right) & \forall \; i \in \mathbf{I}. \end{cases} \quad (5)$$

Now we apply the following lemma.

Lemma 1 *[9, p. 2292] For each $i \in \mathbf{I}$ (recall that $|N(i)| > 1$) we can reparametrize*

$$\lambda_{a,i}(x_i) = \ln \prod_{c \in N(i) \setminus a} m_{c \to i}(x_i) \quad \forall \; a \in N(i) \quad (6)$$

in an unique way with $m_{a \to i}(x_i) > 0 \; \forall a \in N(i)$. The inverse of this mapping is given by

$$m_{a \to i}(x_i) = \exp\left(\frac{2 - |N(i)|}{|N(i)| - 1} \lambda_{a,i}(x_i) + \tfrac{1}{|N(i)|-1} \sum_{b \in N(i) \setminus a} \lambda_{b,i}(x_i) \right) \quad \forall \; a \in N(i).$$

The proof of Lemma 1 is based on a simple matrix inversion. Defining

$$n_{i \to a}(x_i) \triangleq \prod_{c \in N(i) \setminus a} m_{c \to i}(x_i) \quad \forall i \in \mathbf{I}, a \in N(i), \quad (7)$$

plugging the reparametrization (6) into (5), and applying the marginalization constraints in (3) yields the following fixed point equations for BP:

$$\begin{cases} m_{a \to i}(x_i) = \sum_{\mathbf{x}_a \setminus x_i} f_a(\mathbf{x}_a) \prod_{j \in N(a) \setminus i} n_{j \to a}(x_j) \\ n_{i \to a}(x_i) = \prod_{c \in N(i) \setminus a} m_{c \to i}(x_i). \end{cases} \quad (8)$$

Remark III.1 This result can be extended to the case where the functions f_a are nonnegative under the assumption that $\sum_{\mathbf{x}_a \setminus x_i} f_a(\mathbf{x}_a) > 0$ for all $i \in N(a)$ (If this expression is zero for one $x_i = \bar{x}_i$ then $p(\mathbf{x}) = 0$ for all $\mathbf{x} \setminus x_i$ and $x_i = \bar{x}_i$ and we can remove $\bar{x}_i$). The key observation is that we must set $b_a(\bar{\mathbf{x}}_a) = 0$ whenever $f_a(\bar{\mathbf{x}}_a) = 0$ for a certain $\mathbf{x}_a = \bar{\mathbf{x}}_a$ if we assume that $F_{\mathcal{R}}$ is *finite*. The beliefs $b_i(x_i)$ are always positive.

IV. Fixed point equations for the mean field approximation

The MF approximation can be interpreted as a message passing algorithm on a factor graph [13]. In this section, we briefly show how the corresponding fixed point equations can be obtained by the free energy approach. To this end we define one region $R \triangleq (\mathbf{x}, \mathbf{A})$ with $c_R = 1$ and impose the constraint that $b(\mathbf{x})$ fully factorizes, i.e.,

$$b(\mathbf{x}) = \prod_{i \in \mathbf{I}} b_i(x_i).$$

This constraint can be directly plugged into the expression for the variational free energy in (1). Doing so we get

$$F = \sum_{i \in \mathbf{I}} \sum_{x_i} b_i(x_i) \ln b_i(x_i) - \sum_{a \in \mathbf{A}} \sum_{\mathbf{x}_a} \prod_{i \in N(a)} b_i(x_i) \ln f_a(\mathbf{x}_a).$$

The stationary points for the MF approximation can easily be evaluated:

$$b_i(x_i) \propto \exp\left(\sum_{a \in N(i)} \sum_{\mathbf{x}_a \setminus x_i} \prod_{j \in N(a) \setminus i} b_j(x_j) \ln f_a(\mathbf{x}_a) \right) \forall\, i \in \mathbf{I}.$$

The updates b_i can be evaluated by iterating over $i \in \mathbf{I}$. At each step the objective function decreases and the algorithm is guaranteed to converge. To derive a particular update b_i we need all previous updates b_j for $j \in \bigcup_{a \in N(i)} N(a) \setminus i$.

A message passing interpretation for the MF approximation can be obtained by setting $n_{i \to N(i)}(x_i) \triangleq b_i(x_i)\ \forall\ i \in \mathbf{I}$, which results in [13]

$$\begin{cases} n_{i \to N(i)}(x_i) = \prod_{a \in N(i)} m_{a \to i}(x_i) \\ m_{a \to i}(x_i) \triangleq \exp\left(\sum_{\mathbf{x}_a \setminus x_i} \prod_{j \in N(a) \setminus i} n_{j \to N(j)}(x_j) \ln f_a(\mathbf{x}_a) \right). \end{cases} \tag{9}$$

Remark IV.1 In the MF approach, we assume that the functions $f_a(\mathbf{x}_a)$ are positive.

V. Combined belief propagation / mean field fixed point equations

We are now in a position to combine BP and the MF approximation. Let

$$p(\mathbf{x}) = \prod_{a \in A_{\text{MF}}} f_a(\mathbf{x}_a) \prod_{a \in A_{\text{BP}}} f_a(\mathbf{x}_a)$$

be a partially factorized pdf. As before we have $\mathbf{x} = \{x_i \mid i \in \mathbf{I}\}$, $\mathbf{I} = \{1, \ldots, N\}$, $\mathbf{x}_a \subseteq \mathbf{x}$, and $a \in \mathbf{A} = \{1, \ldots, M\}$ with $\mathbf{A} = \mathbf{A}_{\text{MF}} \cup \mathbf{A}_{\text{BP}}$. Furthermore, we set

$$\begin{aligned} \mathbf{I}_{\text{MF}} &\triangleq \{i \in \mathbf{I} \mid \exists a \in \mathbf{A}_{\text{MF}} \text{ with } i \in N(a)\} \\ \mathbf{I}_{\text{BP}} &\triangleq \{i \in \mathbf{I} \mid \exists a \in \mathbf{A}_{\text{BP}} \text{ with } i \in N(a)\}. \end{aligned}$$

Note that $\mathbf{A}_{\text{MF}} \cap \mathbf{A}_{\text{BP}} = \emptyset$ but $\mathbf{I}_{\text{MF}} \cap \mathbf{I}_{\text{BP}} \neq \emptyset$ in general. We define the set $\mathcal{R}$ of valid regions:

1) one MF region $R_{\text{MF}} \triangleq (\mathbf{x}_{\text{MF}}, \mathbf{A}_{\text{MF}})$ with $\mathbf{x}_{\text{MF}} \triangleq \{x_i \mid i \in \mathbf{I}_{\text{MF}}\}$ and $c_{R_{\text{MF}}} = 1$;
2) small regions $R_i \triangleq (\{x_i\}, \emptyset)$ with $c_{R_i} = 1 - |N_{\text{BP}}(i)| - I_{\mathbf{I}_{\text{MF}}}(i)$ for all $i \in \mathbf{I}_{\text{BP}}$;
3) large regions $R_a \triangleq (\mathbf{x}_a, \{a\})$ with $c_{R_a} = 1$ for all $a \in \mathbf{A}_{\text{BP}}$,

with $N_{\text{BP}}(i) \triangleq \{a \in \mathbf{A}_{\text{BP}} \mid a \in N(i)\}$. This yields the region-based variational free energy

$$\begin{aligned} F_{\mathcal{R}} = &\sum_{a \in \mathbf{A}_{\text{BP}}} \sum_{\mathbf{x}_a} b_a(\mathbf{x}_a) \ln \frac{b_a(\mathbf{x}_a)}{f_a(\mathbf{x}_a)} \\ &- \sum_{a \in \mathbf{A}_{\text{MF}}} \sum_{\mathbf{x}_a} \prod_{i \in N(a)} b_i(x_i) \ln f_a(\mathbf{x}_a) \\ &- \sum_{i \in \mathbf{I}} (|N_{\text{BP}}(i)| - 1) \sum_{x_i} b_i(x_i) \ln b_i(x_i). \end{aligned} \tag{10}$$

We can restrict the summation over the index set $\mathbf{I}$ in the last term in (10) to indices $i \in \mathbf{I}$ with $|N_{\text{BP}}(i)| \neq 1$. The constraints for the BP part can be included in a Lagrangian

$$L \triangleq F_{\mathcal{R}} + \sum_{a \in \mathbf{A}_{\text{BP}}} \sum_{i \in N_{\text{BP}}(a)} \sum_{x_i} \lambda_{a,i}(x_i) \left(b_i(x_i) - \sum_{\mathbf{x}_a \setminus x_i} b_a(\mathbf{x}_a) \right).$$

We now derive the stationary points of this Lagrangian. To this end we define the set

$$\Delta \triangleq \{i \in \mathbf{I}_{\text{BP}} \cap \mathbf{I}_{\text{MF}} \mid |N_{\text{BP}}(i)| = 1\},$$

which corresponds to variable nodes that are "dead ends" in the BP part, i.e., there is a *unique* $a_i \in \mathbf{A}_{\text{BP}}$ for each $i \in \Delta$, but are connected to the MF part. The stationary points can be evaluated as

$$\begin{aligned} \lambda_{a_i,i}(x_i) &= \ln(b_i^{\text{MF}}(x_i))\ \forall\ i \in \Delta \\ b_a(\mathbf{x}_a) &\propto b_a^{\text{BP}}(\mathbf{x}_a) \prod_{i \in N(a)} b_i^{\text{MF}}(x_i)\ \ \forall\ a \in \mathbf{A}_{\text{BP}} \\ b_i(x_i) &\propto \begin{cases} b_i^{\text{MF}}(x_i) b_i^{\text{BP}}(x_i) & \forall\ i \in \mathbf{I} \setminus \Delta \\ \sum_{\mathbf{x}_{a_i} \setminus x_i} b_{a_i}(\mathbf{x}_{a_i}) & \forall\ i \in \Delta, \end{cases} \end{aligned}$$

with

$$b_a^{\text{BP}}(\mathbf{x}_a) \triangleq f_a(\mathbf{x}_a)\exp\left(\sum_{i\in N(a)\setminus\Delta}\tilde{\lambda}_{a,i}(x_i)\right) \quad \forall\, a\in\mathbf{A}_{BP}$$

$$b_i^{\text{BP}}(x_i) \triangleq \begin{cases} \exp\left(\frac{1}{|N_{\text{BP}}(i)|-1}\sum_{a\in N_{\text{BP}}(i)}\tilde{\lambda}_{a,i}(x_i)\right) & \forall\, i\in\mathbf{I}_{BP}\setminus\Delta \\ 1 & \forall\, i\in\mathbf{I}\setminus\mathbf{I}_{BP}\end{cases}$$

$$b_i^{\text{MF}}(x_i) \triangleq \begin{cases} \exp\left(\sum_{a\in N_{\text{MF}}(i)}\sum_{\mathbf{x}_a\setminus x_i}\prod_{j\in N(a)\setminus i} b_j(x_j)\ln f_a(\mathbf{x}_a)\right) & \forall\, i\in\mathbf{I}_{MF} \\ 1 & \forall\, i\in\mathbf{I}\setminus\mathbf{I}_{MF},\end{cases}$$

where we defined $N_{\text{MF}}(i)\triangleq\{a\in\mathbf{A}_{\text{MF}}\mid a\in N(i)\}$ and

$$\tilde{\lambda}_{a,i}(x_i)\triangleq\lambda_{a,i}(x_i)-\ln b_i^{\text{MF}}(x_i)\ \forall\, i\in\mathbf{I}_{\text{BP}}\setminus\Delta, a\in N_{\text{BP}}(i).$$

The messages for the BP part can now be introduced in a similar way as for solely BP. Applying Lemma 1 to $\tilde{\lambda}_{a,i}(x_i)$ for all $i\in\mathbf{I}_{\text{BP}}\setminus\Delta$ gives the reparametrization

$$\tilde{\lambda}_{a,i}(x_i)=\ln\prod_{c\in N_{\text{BP}}(i)\setminus a} m_{c\to i}^{\text{BP}}(x_i)\quad\forall\, a\in N_{\text{BP}}(i).$$

Defining the messages

$$\begin{aligned} n_{i\to N(i)}^{\text{MF}}(x_i) &\triangleq b_i^{\text{MF}}(x_i) \qquad \forall\, i\in\mathbf{I}_{\text{BP}} \\ n_{i\to a}^{\text{BP}}(x_i) &\triangleq \prod_{c\in N_{\text{BP}}(i)\setminus a} m_{c\to i}^{\text{BP}}(x_i)\ \forall\, i\in\mathbf{I}_{\text{BP}}\setminus\Delta, a\in N_{\text{BP}}(i)\end{aligned}$$

yields

$$\begin{aligned} b_a^{\text{BP}}(\mathbf{x}_a) &= f_a(\mathbf{x}_a)\prod_{i\in N(a)\setminus\Delta} n_{i\to a}^{\text{BP}}(x_i)\quad\forall\, a\in\mathbf{A}_{\text{BP}} \\ b_a(\mathbf{x}_a) &\propto b_a^{\text{BP}}(\mathbf{x}_a)\prod_{i\in N(a)} n_{i\to N(i)}^{\text{MF}}(x_i)\quad\forall\, a\in\mathbf{A}_{\text{BP}} \\ b_i(x_i) &\propto n_{i\to N(i)}^{\text{MF}}(x_i)\underbrace{\prod_{a\in N_{\text{BP}}(i)} m_{a\to i}^{\text{BP}}(x_i)}_{=b_i^{\text{BP}}(x_i)}\quad\forall\, i\in\mathbf{I}\setminus\Delta.\end{aligned}$$

Using the marginalization constraints, we end up with the fixed point equations for the BP part

$$\begin{cases} m_{a\to i}^{\text{BP}}(x_i)=\sum_{\mathbf{x}_a\setminus x_i} f_a(\mathbf{x}_a)\prod_{j\in N(a)\setminus(\{i\}\cup\Delta)} n_{j\to a}^{\text{BP}}(x_j)\prod_{j\in N(a)\setminus i} n_{j\to N(j)}^{\text{MF}}(x_j) \\ n_{i\to a}^{\text{BP}}(x_i)=\prod_{c\in N_{\text{BP}}(i)\setminus a} m_{c\to i}^{\text{BP}}(x_i)\end{cases} \tag{11}$$

for all $a\in\mathbf{A}_{\text{BP}}, i\in\mathbf{I}_{\text{BP}}\setminus\Delta$. The beliefs $b_i(x_i)$ for $i\in\Delta$ can be evaluated from the marginalization constraints, i.e.,

$$b_i(x_i)\propto n_{i\to\{a_i\}}^{\text{MF}}(x_i)\underbrace{\sum_{\mathbf{x}_{a_i}\setminus x_i} b_{a_i}^{\text{BP}}(x_{a_i})\prod_{j\in N(a_i)\setminus i} n_{j\to N(j)}^{\text{MF}}(x_j)}_{\triangleq b_i^{\text{BP}}(x_i)}$$

for all $i\in\Delta$.

It remains to introduce the remaining messages for the MF part

$$\begin{cases} n_{i\to N(i)}^{\text{MF}}(x_i) = \prod_{a\in N_{\text{MF}}(i)} m_{a\to i}^{\text{MF}}(x_i) \\ m_{a\to i}^{\text{MF}}(x_i) \triangleq \exp\left(\sum_{\mathbf{x}_a\setminus x_i}\prod_{j\in N(a)\setminus i} b_j^{\text{BP}}(x_j)\right. \\ \qquad\qquad \left. n_{j\to N(j)}^{\text{MF}}(x_j)\ln f_a(\mathbf{x}_a)\right)\end{cases} \tag{12}$$

for all $a\in\mathbf{A}_{\text{MF}}, i\in\mathbf{I}_{\text{MF}}$. All these steps are reversible. Thus, we have proved the following theorem.

Theorem 2 *Stationary points of the constrained variational free energy in the combined BP/MF approach must be fixed points with positive beliefs and vice versa. The corresponding fixed point equations are* (11) *and* (12)*.*

Remark V.1 The inclusion of hard constraints in the *BP part* can be done in the same fashion as for solely BP propagation.

VI. A SIMPLE EXAMPLE

Assume a frequency-flat time-varying channel with input-output relationship

$$\mathbf{y}=\mathbf{X}\mathbf{h}+\mathbf{z},$$

where $\mathbf{z}\in\mathcal{CN}(\mathbf{0},\gamma^{-1}\mathbf{I}), \mathbf{X}\triangleq\text{diag}(x_i\mid i=1,\ldots,n)$, and $\mathbf{y}\in\mathbb{C}^n$. The symbols $x_i\in\mathbb{C}$ belong to a certain modulation alphabet. Rewriting

$$p(\mathbf{y},\mathbf{X},\gamma,\mathbf{h}) \propto p(\mathbf{y}|\mathbf{X},\gamma,\mathbf{h})p(\gamma)p(\mathbf{h})p(\mathbf{X}),$$

where we used the fact that γ, $\mathbf{h}$, and $\mathbf{x}$ are independent, gives a factorization where we wish to apply BP for $p(\mathbf{X})$ and the MF approximation for the remaining factors. Notice that $p(\mathbf{X})$ includes modulation and the code constraints. We assume that the prior distributions of γ and $\mathbf{h}$ are of the form

$$\begin{aligned} p(\gamma) &\propto \gamma^{k^P-1}\exp(-\gamma\theta^P) \\ p(\mathbf{h}) &\propto \exp(-(\mathbf{h}-\bar{\mathbf{h}}^P)^H\mathbf{\Lambda}_{\mathbf{h}}^P(\mathbf{h}-\bar{\mathbf{h}}^P)).\end{aligned}$$

Let

$$\begin{aligned} &\bar{\mathbf{h}}\triangleq\text{E}_{b_{\mathbf{h}}}(\mathbf{h}) \qquad \mathbf{R}_{\mathbf{h}}\triangleq\text{Cov}_{b_{\mathbf{h}}}(\mathbf{h}) \qquad \bar{\gamma}\triangleq\text{E}_{b_\gamma}(\gamma) \\ &\bar{\mathbf{X}}\triangleq\text{E}_{\{b_i\}}(\mathbf{X}) \qquad \mathbf{\Sigma}\triangleq\text{Var}_{\{b_i\}}(\mathbf{X}),\end{aligned}$$

with $b_i=b_i^{\text{BP}}b_i^{\text{MF}}$ $(i=1,\ldots,n)$, $b_{\mathbf{h}}=b_{\mathbf{h}}^{\text{MF}}$, and $b_\gamma=b_\gamma^{\text{MF}}$. Then we get the following message passing update equations:
Update for γ:

$$\begin{aligned} n_{\gamma\to N(\gamma)}(\gamma) &= m_{p(\gamma)\to\gamma}^{\text{MF}}(\gamma)m_{p(\mathbf{y}|\mathbf{x},\mathbf{h},\gamma)\to\gamma}^{\text{MF}}(\gamma) \\ &= \gamma^{k^P+N-1}\exp(-\gamma(\theta^P+\underline{\theta})),\end{aligned}$$

with

$$\begin{aligned} \underline{\theta} &\triangleq \text{E}_{\{b_i\}}\text{E}_{b_{\mathbf{h}}}\|\mathbf{y}-\mathbf{X}\mathbf{h}\|^2 \\ &= \|\mathbf{y}\|^2+\text{Tr}((\mathbf{R}_{\mathbf{h}}+\bar{\mathbf{h}}\bar{\mathbf{h}}^H)(\mathbf{\Sigma}+\bar{\mathbf{X}}\bar{\mathbf{X}}^H))-2\Re(\mathbf{y}^H\bar{\mathbf{X}}\bar{\mathbf{h}}).\end{aligned}$$

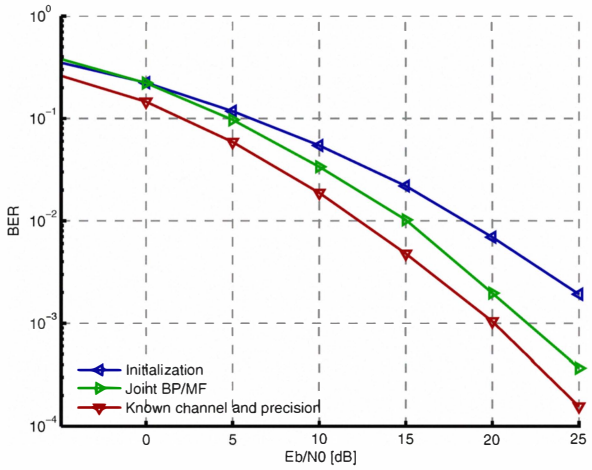

Fig. 1. Average BER versus Eb/N0 for a time-varying channel with a square Doppler spectrum. The channel code is a turbo code with polynomial $(1, 1/3)$ and codeword length of 196, the modulation scheme is 16-QAM, and the interleaver is random. A pilot based LMMSE estimate yields the initialization of $\bar{\mathbf{h}}$; two QPSK modulated pilot symbols are employed for this purpose. The channel covariance matrix is assumed to be perfectly known at the receiver.

Update for $\mathbf{h}$*:*

$$\begin{aligned} n_{\mathbf{h}\to N(\mathbf{h})}(\mathbf{h}) &= m^{\mathrm{MF}}_{p(\mathbf{h})\to\mathbf{h}}(\mathbf{h}) m^{\mathrm{MF}}_{p(\mathbf{y}|\mathbf{x},\mathbf{h},\gamma)\to\mathbf{h}}(\mathbf{h}) \\ &\propto \exp\left(-(\mathbf{h}-\bar{\mathbf{h}})^H \mathbf{R}_{\mathbf{h}}^{-1}(\mathbf{h}-\bar{\mathbf{h}})\right), \end{aligned}$$

with

$$\begin{aligned} \mathbf{R}_{\mathbf{h}}^{-1} &= (\mathbf{\Lambda}_{\mathbf{h}}^P + \underline{\mathbf{\Lambda}}) & \bar{\mathbf{h}} &= \mathbf{R}_{\mathbf{h}}(\mathbf{\Lambda}_{\mathbf{h}}^P \bar{\mathbf{h}}^P + \underline{\bar{\mathbf{h}}}) \\ \underline{\mathbf{\Lambda}} &\triangleq \bar{\gamma}(\mathbf{\Sigma} + \bar{\mathbf{X}}\bar{\mathbf{X}}^H) & \underline{\bar{\mathbf{h}}} &\triangleq \bar{\gamma}\bar{\mathbf{X}}^H \mathbf{y}. \end{aligned}$$

This follows from

$$E_{\{b_i\}} \mathrm{E}_{b_\gamma}\left(\gamma\|\mathbf{y}-\mathbf{X}\mathbf{h}\|^2 - \gamma\|\mathbf{y}\|^2\right) = \mathbf{h}^H \underline{\mathbf{\Lambda}}\mathbf{h} - 2\Re(\mathbf{h}^H \underline{\bar{\mathbf{h}}}).$$

Update for x_i $(i = 1, \ldots, n)$*:*

$$\begin{aligned} n^{\mathrm{MF}}_{i\to N(i)} &= m^{\mathrm{MF}}_{p(\mathbf{y}|\mathbf{x},\mathbf{h},\gamma)\to i} \\ &\propto \exp(E_{\{b_{j\neq i}\}} \mathrm{E}_{b_\gamma} \mathrm{E}_{b_{\mathbf{h}}}(\ln p(\mathbf{y} \mid \mathbf{x}, \mathbf{h}, \gamma))) \\ &\propto \exp(-\bar{\gamma}(|x_i|^2 [\mathbf{R}_{\mathbf{h}} + \bar{\mathbf{h}}\bar{\mathbf{h}}^H]_{ii} - 2\Re(y_i^* [\bar{\mathbf{h}}]_i x_i)). \end{aligned}$$

Fig. 1 depicts the average BER versus E_b/N_0 of three algorithms. The blue curve denotes the performance of a scheme performing separate decoding and LMMSE channel estimation based on pilot symbols, while knowing the noise precision. The green curve represents the performance of the combined BP/MF approach after convergence is reached. The former "separate" receiver is used to compute the initial values of the channel coefficients and symbol estimates. The red curve depicts the performance of a decoder having perfect knowledge of the channel coefficients and noise precision.

It can be seen that the performance of the BP/MF algorithm is close to that of the scheme having perfect channel knowledge. Moreover, the BP/MF algorithm significantly outperforms the scheme performing separate channel estimation and decoding.

VII. Conclusion

Using the region-based free energy approximation method proposed in [9], we derived message passing update equations for a factor graph where BP is applied to one part of the factor nodes and the MF approximation is implemented on the remaining factor nodes. The proposed theoretical framework provides a mean to determine the way messages computed on the same factor graph using BP and the MF approximation are to be combined.

A simple example confirmed the validity of the BP/MF method. This example shows that the method allows to combine the estimation of densities of continuous parameters with BP processing of discrete variables, unlike methods using the EM algorithm to compute point estimates of these parameters [14].

Acknowledgment

This work was supported by WWTF grant ICT08-44, FWF grant S10603-N13 within the National Research Network SISE, the 4GMCT cooperative research project funded by Infineon Technologies Denmark A/S, Agilent Technologies, Aalborg University and the Danish National Advanced Technology Foundation, by the European Commission within the FP7-ICT Network of Excellence in Wireless Communications, NEWCOM++ (Contract No.216715), the FP7-ICT STREP Wireless Hybrid Enhanced Mobile Radio Estimators, WHERE (217033), and by NOKIA Denmark.

References

[1] P. Parisi, *Statistical Field Theory.* Oxford, UK: Perseus, 1988.
[2] Z. Ghahramani and M. J. Beal, *Graphical Models and Variational Methods*, D. Saad and M. Opper, Eds. Massachusetts, NY: MIT Press, 2000.
[3] M. I. Jordan, Z. Ghahramani, T. S. Jaakola, and L. K. Saul, "An introduction to variational methods for graphical models," *J. Mach. Learning*, vol. 37, no. 2, pp. 183–233, 1999.
[4] J. Winn and C. Bishop, "Variational message passing," *J. Mach. Learning*, vol. 6, no. 6, pp. 661–694, 2005.
[5] C. M. Bishop, *Pattern Recognition and Machine Learning.* New York, NY: Springer, 2006.
[6] G. E. Kirkelund, C. N. Manchón, L. P. B. Christensen, E. Riegler, and B. H. Fleury, "Variational message-passing for joint channel estimation and decoding in MIMO-OFDM," in *Proc. IEEE Globecom (GLOBECOM 2010)*, Miami, FL, Dec. 2010, to appear.
[7] J. Pearl, *Probabilistic Reasoning in Intelligent Systems: Networks of Plausible Inference.* San Francisco, CA: Morgan Kaufman, 1998.
[8] F. R. Kschischang, J. F. Brendan, and H. A. Loeliger, "Factor graphs and the sum-product algorithm," *IEEE Trans. Inf. Th.*, vol. 47, no. 2, pp. 498–519, Feb. 2001.
[9] J. S. Yedidia, W. T. Freeman, and Y. Weiss, "Constructing free-energy approximations and generalized belief propagation algorithms," *IEEE Trans. Inf. Th.*, vol. 51, no. 7, pp. 2282–2312, July 2005.
[10] T. M. Cover and J. A. Thomas, *Elements of Information Theory*, 2nd ed. New York, NY: Wiley, 2006.
[11] H. A. Bethe, "Statistical theory of superlattices," in *Proc. Roy. Soc. London*, ser. A, vol. 150, no. 871, 1935, pp. 552–575.
[12] D. P. Bertsekas, *Nonlinear Programming*, 2nd ed. Belmont, MA: Athena Scientific, 2003.
[13] J. Dauwels, "On variational message passing on factor graphs," in *Proc. IEEE Int. Symp. Inf. Th. (ISIT 2007)*, Nice, France, June 2007, pp. 2546 – 2550.
[14] H.-A. Loeliger, J. Dauwels, J. Hu, S. Korl, L. Ping, and F. R. Kschischang, "The factor graph approach to model-based signal processing," *Proc. IEEE*, vol. 95, no. 6, pp. 1295–1322, June 2007.

Paper C

Receiver Architectures for MIMO-OFDM Based on a Combined VMP-SP Algorithm

Carles Navarro Manchón, Gunvor E. Kirkelund, Erwin Riegler, Lars P.B. Christensen and Bernard H. Fleury

Submitted to IEEE Transactions on Information Theory, November 2011.

C. RECEIVER ARCHITECTURES FOR MIMO-OFDM BASED ON A COMBINED VMP-SP ALGORITHM

Receiver Architectures for MIMO-OFDM Based on a Combined VMP-SP Algorithm

Carles Navarro Manchón, Gunvor E. Kirkelund, Erwin Riegler, Lars P. B. Christensen, Bernard H. Fleury.

Abstract

Iterative information processing, either based on heuristics or analytical frameworks, has been shown to be a very powerful tool for the design of efficient, yet feasible, wireless receiver architectures. Within this context, algorithms performing message-passing on a probabilistic graph, such as the sum-product (SP) and variational message passing (VMP) algorithms, have become increasingly popular.

In this contribution, we apply a combined VMP-SP message-passing technique to the design of receivers for MIMO-ODFM systems. The message-passing equations of the combined scheme can be obtained from the equations of the stationary points of a constrained region-based free energy approximation. When applied to a MIMO-OFDM probabilistic model, we obtain a generic receiver architecture performing iterative channel weight and noise precision estimation, equalization and data decoding. We show that this generic scheme can be particularized to a variety of different receiver structures, ranging from high-performance iterative structures to low complexity receivers. This allows for a flexible design of the signal processing specially tailored for the requirements of each specific application. The numerical assessment of our solutions, based on Monte Carlo simulations, corroborates the high performance of the proposed algorithms and their superiority to heuristic approaches.

Index Terms

MIMO, OFDM, multi-user detection, message-passing algorithms, belief propagation, mean-field approximation, sum-product, variational message-passing, iterative channel estimation, equalization and data decoding

I. Introduction

During the last two decades, wireless communication systems have undergone a rapid and steep evolution. While old analog systems mainly focused on providing voice communications, today's digital systems offer a plethora of different services such as multimedia communications, web browsing, audio and video streaming, etc. Along with the growing variety of services offered, the amount of users accessing them has also experienced a drastic increase. The combination of applications requiring large amounts of data traffic and high density of users, together with the scarceness of wireless spectrum resources, dictates high spectral efficiency to be an essential target in the design of modern wireless systems.

From a physical layer point of view, the emergence of multiple-input multiple-output (MIMO) techniques [1] together with the development of near-capacity-achieving channel codes, such as turbo [2] or low-density parity check (LDPC) [3] codes, have been the most remarkable steps towards this goal. The use of multiple antennas allows for increasing the theoretical capacity of a wireless channel linearly with the minimum of the number of antenna elements at the transmitter and at the receiver ends [4]. Depending on the specific MIMO technique employed, multiple antennas can be used to exploit the number of degrees of freedom of a wireless channel, its diversity or a mixture of both [5]. The combination with advanced channel codes enables transmission schemes with unprecedented high spectral efficiency. However, in order to realize in practice the performance predicted by theory, advanced receiver architectures combining high performance channel estimators, MIMO detectors and channel decoders are required.

Joint maximum likelihood (ML) receivers are prohibitively complex for most modern communication systems, especially systems with high MIMO order and concatenated codes. A wide-spread approach for the design of suboptimal, yet efficient receiver architectures is to separate the receiver into several individual blocks, each performing a specific task: channel weight estimation, noise estimation, interference cancellation, equalization or data decoding are some examples. Inspired by the iterative decoding scheme

of turbo codes, some structures in which the different constituent blocks exchange information in an iterative manner have been proposed [6]–[10]. In these receivers, each block is designed individually, and the way it exchanges information with the other blocks is based on heuristics. Consequently, while each block is designed to optimally perform its task, the full receiver structure does not necessarily optimize any global performance criterion. Nevertheless, these structures have shown remarkably good performance at an affordable complexity, while keeping a large degree of flexibility in their design.

Motivated by the success of heuristic iterative approaches, a set of formal frameworks for the design of algorithms performing iterative information processing have arisen in recent years. Among these, methods for variational Bayesian inference in probabilistic models [11] have attracted much attention from the communication research community in recent times. These frameworks allow for the design of iterative algorithms based on the optimization of a global cost function. Typically, they are derived from the stationary points of a discrepancy measure between the probability distribution that needs to be estimated and a postulated auxiliary distribution, the latter distribution providing an estimate of the former. The different frameworks differ on the particular discrepancy measure selected and the restrictions applied to the postulated auxiliary function. We especially highlight two main approaches suggested so far in literature: belief propagation (BP) and mean-field (MF) methods[1].

BP [16] is a Bayesian inference framework applied to graphical probabilistic models. In its message-passing form –referred to as the sum-product (SP) algorithm [17]– messages are sent from one node of the graphical model to neighboring nodes. The message computation rules for the SP algorithm are obtained from the stationary points of the Bethe free energy [14]. When the graphical model representing the system is free of cycles, the SP algorithm provides exact marginal distributions of the variables in the model. When the graph has cycles, however, the algorithm outputs only an approximation of the marginal distributions and it is, moreover, not guaranteed to converge [18]. In most cases, nonetheless, the obtained marginals are still a high quality approximation of the exact distributions. BP and the SP algorithm have found widespread application in the decoding of channel codes [17], [19], and have also been proposed for the design of iterative receiver structures in wireless communication systems [20]–[24]. However, modifications of the original algorithm are required for parameter estimation problems, such as channel estimation. This has been solved by, e.g., combining the SP algorithm with the expectation-maximization (EM) algorithm [21], [25] or approximating SP messages which are computationally untractable with Gaussian messages [26], [27].

MF approaches –proposed by Attias in [28] and formulated as the variational Bayesian expectation-maximization (VBEM) principle by Beal [29]– are based on the minimization of the Kullback-Leibler (KL) divergence [30] between a postulated auxiliary function and the distribution to be estimated. The minimization becomes especially computationally tractable under the MF approximation [31], in which the auxiliary function is assumed to completely factorize with respect to the different parameters. The obtained iterative algorithm guarantees convergence in terms of the KL divergence, but convergence to the globally optimum solution can only be guaranteed when the considered problem has a unique single optimum. However, it has proven very useful in the design of iterative receiver structures including channel estimation, e.g., channel estimation and detection for GSM systems [32], iterative multiuser channel estimation, detection and decoding [33] or channel estimation, interference cancellation and detection in OFDM systems [34], [35]. For other applications of MF methods, see [36]–[38]. Message-passing interpretations of this technique on probabilistic graphs have also been proposed in [12], [39], [40] and are commonly referred to as variational message-passing (VMP) techniques.

In this contribution, we apply a hybrid message-passing framework to the design of iterative receivers in a MIMO-OFDM setup. This hybrid framework, recently proposed in [41], [42], combines the SP and VMP algorithms in a unified message-passing technique. Message updates are obtained from the stationary points of a particular region-based free energy approximation [14] of the probabilistic system. Specifically,

[1]Some authors, e.g. Winn and Bishop [12], [13], consider BP outside the variational Bayesian framework, and usually use the term *variational* only in the context of MF-like approximations. We use, however, the more general view proposed e.g. in [11], [14], [15], which considers BP as another algorithm for variational Bayesian inference.

the combined framework allows for performing VMP in parts of the graph and SP in others, thus enabling a flexible, yet global, design.

From a MIMO-OFDM signal model, we derive a generic message-passing receiver performing channel estimation, MIMO detection and channel decoding in an iterative fashion. Channel estimation is not limited to the estimation of channel weights, but also includes estimation of the noise variance, which proves to be crucial for the operation of the receiver. The application of a unified framework to the whole receiver design unequivocally dictates the type of information that should be exchanged by the individual constituents of the receiver in the form of messages. This is in contrast to heuristic approaches which, for instance, arbitrarily select a-posteriori or extrinsic probabilities to be exchanged between the channel decoder and other modules based on intuitive argumentation or trends observed by simulation results [9], [10].

The generic messages derived can easily be particularized by applying different assumptions and restrictions to the signal model considered. Thus, our framework enables a highly scalable and flexible design of the signal processing in the receiver. For instance, applying the messages to only part of the factor graph yields simplified architectures performing just a subset of the receiver tasks; also, small modifications to the factor-graph lead to different receiver structures with different performance and computational complexity tradeoffs. These properties are illustrated in our numerical evaluation, where the performance of a few selected instances of our proposed receiver is assessed via Monte Carlo simulations. The presented results demonstrate the high accuracy of our approach, and its superiority to iterative receivers based on heuristics.

The remainder of the paper is organized as follows. The signal model of the MIMO-OFDM system considered is presented in Section II, followed by a brief review of the combined message-passing framework proposed in [41], [42] in Section III. In Section IV, the generic messages to be exchanged in the factor-graph are derived, and the performance of five different receivers obtained from the generic derivation is tested in Section V. Finally, we draw some final conclusions in Section VI.

A. Notation

Throughout the paper, lower-case boldface letters represent column vectors, while upper-case boldface letters denote matrices; $(\cdot)^{\mathrm{T}}$ and $(\cdot)^{\mathrm{H}}$ denote the transpose and conjugate-transpose of a vector or matrix respectively; $\|\cdot\|$ denotes the Euclidian norm; $\boldsymbol{A} \otimes \boldsymbol{B}$ represents the Kronecker product of matrices $\boldsymbol{A}$ and $\boldsymbol{B}$; $\boldsymbol{I}_N$ denotes the identity matrix of dimension N. Moreover, $\log$ denotes the natural logarithm; $f(x) \propto g(x)$ means that $f(x)$ is equal to $g(x)$ up to a proportionality constant; $\langle f(x) \rangle_g$ denotes the expectation of $f(x)$ over $g(x)$, i.e. $\langle f(x) \rangle_g = \int_x f(x) g(x) dx$; $\mathcal{S} \backslash s$ denotes all elements in the set $\mathcal{S}$ but s.

II. Signal Model

In this section a multi-user signal model for MIMO-OFDM is derived. The system is composed by M synchronous transmitter chains and N receiver antennas, as depicted in Fig. 1. These transmitters can represent different transmission branches of the same physical transmitter, or physically separated transmitters at different locations. For the mth transmitter, a finite sequence of information bits $\boldsymbol{u}_m$ is encoded, yielding a sequence of coded bits $\boldsymbol{c}_m$. After interleaving, the interleaved coded bits $\boldsymbol{c}_m^{\pi}$ are complex modulated, resulting in the vector $\boldsymbol{x}_m^{(d)}$ of complex-modulated data symbols. Finally, the data symbols are multiplexed with the pilot symbols $\boldsymbol{x}_m^{(p)}$, giving the transmitted symbols $\boldsymbol{x}_m = [x_m(1,1), \ldots, x_m(K,1), \ldots, x_m(1,L), \ldots, x_m(K,L)]^{\mathrm{T}}$, where $x_m(k,l)$ denotes the symbol sent by the mth transmitter on the kth subcarrier of the lth OFDM symbol of a frame. The transmitted symbols $\boldsymbol{x}_m$ are then OFDM modulated using an IFFT and the insertion of a cyclic prefix.

The signal is transmitted through a wide-sense stationary uncorrelated scattering (WSSUS) channel. The channel impulse response from transmitter m to receiver n during the transmission of the lth OFDM

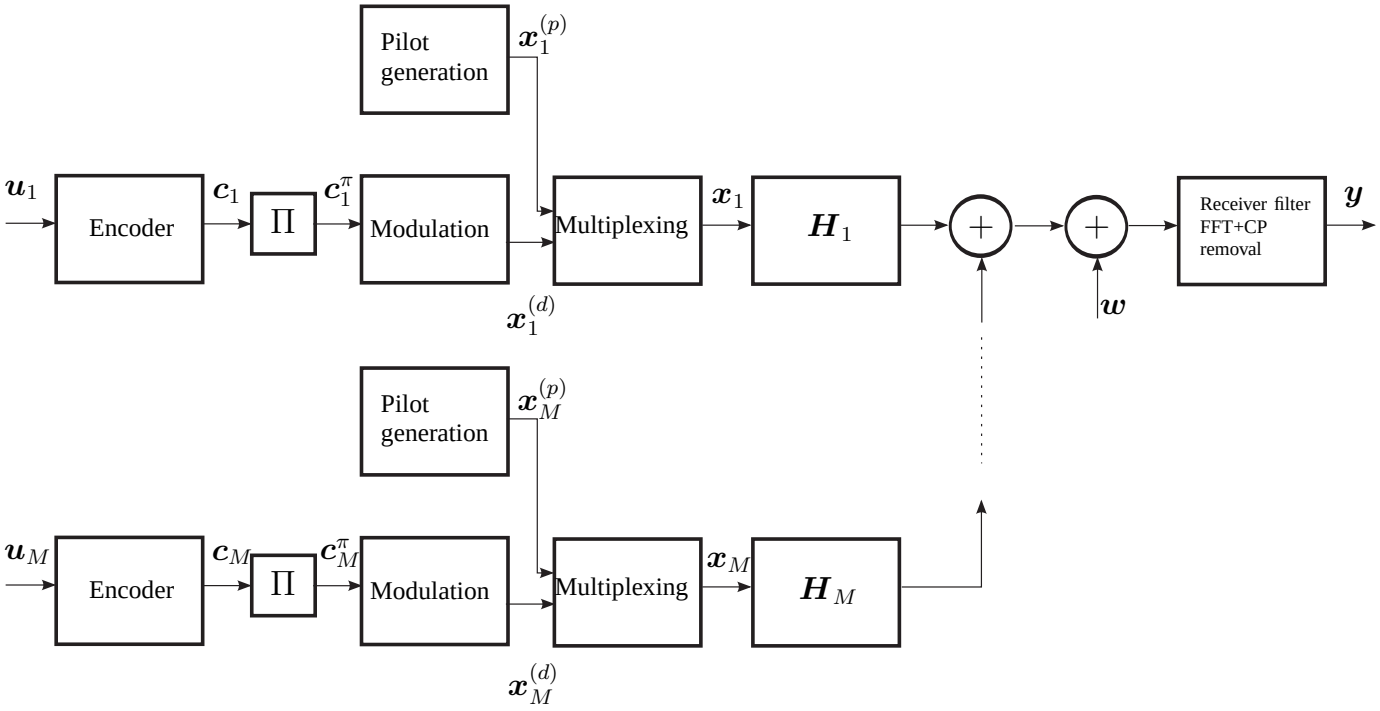

Fig. 1. Block-diagram representation of the transmission model.

symbol l can be described by

$$g_{nm}(l,\tau) = \sum_{i=1}^{I_{nm}} \alpha_{nm}^{(i)}(l)\delta(\tau - \tau_{nm}^{(i)}) \tag{1}$$

where $\alpha_{nm}^{(i)}$ and $\tau_{nm}^{(i)}$ are respectively the complex gain and delay of the i^{th} multipath component and I_{nm} is the number of multipath components. We assume that the channel response is static over the duration of an OFDM symbol, but changes from one OFDM symbol to the next. Also, the maximum delay of each wireless link $\tau_{nm}^{(I_{nm})}$ is assumed to be smaller than the duration of the OFDM cyclic prefix[2], so that no inter-symbol interference (ISI) degrades the transmission. From (1), the sample of the channel frequency response at the kth subcarrier of the lth OFDM symbol is found to be:

$$h_{nm}(k,l) = \sum_{i=1}^{I_{nm}} \alpha_{nm}^{(i)}(l)e^{-j2\pi k\Delta_f \tau_{nm}^{(i)}}.$$

In this expression, Δ_f denotes the OFDM subcarrier spacing.

At the receiver, the signal is OFDM demodulated by discarding the cyclic prefix and applying an FFT on the received samples. Under the previously stated assumptions that the channel is block fading and the maximum delays are smaller than the duration of the cyclic prefix, the signal received at the nth receive antenna on the kth subcarrier of the lth OFDM symbol reads

$$y_n(k,l) = \sum_{m=1}^{M} h_{nm}(k,l)x_m(k,l) + w_n(k,l), \qquad \begin{array}{l} n = 1,\ldots,N, \\ k = 1,\ldots,K, \\ l = 1,\ldots,L, \end{array} \tag{2}$$

with $w_n(k,l)$ denoting zero-mean additive complex white Gaussian noise (AWGN) with variance λ^{-1}. The equations in (2) can be recast in a matrix-vector notation as

$$\boldsymbol{y} = \sum_{m=1}^{M} \boldsymbol{X}_m\boldsymbol{h}_m + \boldsymbol{w} = \sum_{m=1}^{M} \boldsymbol{H}_m\boldsymbol{x}_m + \boldsymbol{w} \tag{3}$$

[2]We assume without loss of generality that the delays $\tau_{nm}^{(i)}$ are ordered in increasing order, i.e. $\tau_{nm}^{(i+1)} \geq \tau_{nm}^{(i)}$.

where $\boldsymbol{y} = [\boldsymbol{y}_1^{\mathrm{T}}, \ldots, \boldsymbol{y}_N^{\mathrm{T}}]^{\mathrm{T}}$, with $\boldsymbol{y}_n = [y_n(1,1), \ldots, y_n(K,1), \ldots, y_n(1,L), \ldots, y_n(K,L)]^T$ denoting the received signal at the nth receive antenna for a frame of K subcarriers and L OFDM symbols. Additionally, $\boldsymbol{h}_m = [\boldsymbol{h}_{1m}^{\mathrm{T}}, \ldots, \boldsymbol{h}_{Nm}^{\mathrm{T}}]^{\mathrm{T}}$, $\boldsymbol{X}_m = \boldsymbol{I}_N \otimes \mathrm{diag}\{\boldsymbol{x}_m\}$, $\boldsymbol{H}_m = [\mathrm{diag}\{\boldsymbol{h}_{1m}\}, \ldots, \mathrm{diag}\{\boldsymbol{h}_{Nm}\}]^{\mathrm{T}}$ and $\boldsymbol{h}_{nm} = [h_{nm}(1,1), \ldots, h_{nm}(K,1), \ldots, h_{n,m}(1,L), \ldots, h_{nm}(K,L)]^{\mathrm{T}}$. Equation (3) can be further compressed as

$$\boldsymbol{y} = \boldsymbol{X}\boldsymbol{h} + \boldsymbol{w} = \boldsymbol{H}\boldsymbol{x} + \boldsymbol{w}$$

where $\boldsymbol{x} = [\boldsymbol{x}_1^{\mathrm{T}}, \ldots, \boldsymbol{x}_M^{\mathrm{T}}]^{\mathrm{T}}$, $\boldsymbol{h} = [\boldsymbol{h}_1^{\mathrm{T}}, \ldots, \boldsymbol{h}_M^{\mathrm{T}}]^{\mathrm{T}}$, $\boldsymbol{X} = [\boldsymbol{X}_1, \ldots, \boldsymbol{X}_M]$ and $\boldsymbol{H} = [\boldsymbol{H}_1, \ldots, \boldsymbol{H}_M]$.

III. Message Passing Techniques

In this section, we briefly introduce message-passing techniques on factor graphs. First, we define the concept of factor graph on a probabilistic model, followed by the description of two standard message-passing schemes: the sum-product (SP) algorithm [17] and the variational message-passing (VMP) algorithm [12]. Finally, we show how to combine both algorithms to perform hybrid VMP and SP message passing in a factor graph [41].

A. Factor Graphs for Probabilistic Models

Let $p(\boldsymbol{z})$ be the probability density function (pdf) of a vector $\boldsymbol{z}$ of random variables z_i ($i \in \mathcal{I}$) which factorizes according to

$$p(\boldsymbol{z}) = \frac{1}{Z} \prod_{a \in \mathcal{A}} f_a(\boldsymbol{z}_a) \tag{4}$$

where $\boldsymbol{z}_a = (z_i | i \in \mathcal{N}(a))^{\mathrm{T}}$ with $\mathcal{N}(a) \subseteq \mathcal{I}$ for all $a \in \mathcal{A}$ and $Z = \int_{\boldsymbol{z}} \prod_{a \in \mathcal{A}} f_a(\boldsymbol{z}_a) d\boldsymbol{z}$ is a normalization constant. We also define $\mathcal{N}(i) \triangleq \{a \in \mathcal{A} | i \in \mathcal{N}(a)\}$ for all $i \in \mathcal{I}$. Similarly, $\mathcal{N}(a) = \{i \in \mathcal{I} | a \in \mathcal{N}(i)\}$ for all $a \in \mathcal{A}$. The above factorization can be graphically represented by means of a factor graph [17]. A factor graph[3] is a bipartite graph having a variable node i (typically represented by a circle) for each variable z_i, $i \in \mathcal{I}$ and a factor node a (represented by a square) for each factor f_a, $a \in \mathcal{A}$. An edge connects a variable node i to a factor node a if, and only if, the variable z_i is an argument of the factor function f_a. The set $\mathcal{N}(i)$ contains all factor nodes connected to a variable node $i \in \mathcal{I}$ and $\mathcal{N}(a)$ is the set of all variable nodes connected to a factor node $a \in \mathcal{A}$.

Factor graphs provide a compact and intuitive representation of the statistical dependencies among the random variables in a probabilistic model. Furthermore, they enable the design of a class of iterative signal processing algorithms which are based on the nodes of the graph iteratively exchanging information (messages) with their neighbors (connected nodes). This class of algorithms has been coined *message-passing* techniques, and in the following we will describe the two instances of these techniques which have been most widely applied to signal processing for communication systems: the SP and VMP algorithms.

B. The Sum-Product Algorithm

The SP algorithm is a message-passing algorithm that computes the exact marginal distributions $p_i(z_i)$ of the variables z_i associated to the joint distribution $p(\boldsymbol{z})$ for tree-shaped factor graphs. When the factor graph does not have a tree structure, the outcome of the algorithm is only an approximation of the true marginal, and the approximate marginals $b_i(z_i) \approx p_i(z_i)$ are called beliefs. The message-passing algorithm is derived from the equations of the stationary points of the constrained Bethe free energy [14].

The algorithm operates iteratively by exchanging messages from variable nodes to factor nodes and vice-versa. The message computation rules for the SP algorithm read

$$m_{a \to i}(z_i) = d_a \langle f_a(\boldsymbol{z}_a) \rangle_{\prod_{j \in \mathcal{N}(a) \setminus i} n_{j \to a}}, \quad \forall a \in \mathcal{A}, i \in \mathcal{N}(a)$$

$$n_{i \to a}(z_i) = \prod_{c \in \mathcal{N}(i) \setminus a} m_{c \to i}(z_i), \quad \forall i \in \mathcal{I}, a \in \mathcal{N}(i)$$

[3]We will use Tanner factor graphs [17] throughout this article

where d_a ($a \in \mathcal{A}$) are positive constants ensuring that the beliefs are normalized to one. Often the constants d_a need not be calculated explicitly, and it is enough to normalize the beliefs after convergence of the algorithm (see [42] for more details on normalization issues). We use the notation $n_{(\cdot)\to(\cdot)}$ for output messages from a variable node to a factor node and $m_{(\cdot)\to(\cdot)}$ for input messages from a factor node to a variable node. This convention will be kept through the rest of the paper, also for other message-passing schemes.

The variables' beliefs can be calculated at any point during the iterative algorithm as

$$b_i(z_i) = \prod_{a \in \mathcal{N}(i)} m_{a\to i}(z_i) \quad \forall i \in \mathcal{I}.$$

The SP algorithm acquired great popularity through its application to iterative decoding of, among others, turbo codes and LDPC codes, and has since then been used for the design of many iterative algorithms in a wide variety of fields [21].

C. The Variational Message-Passing Algorithm

The VMP algorithm is an alternative message-passing technique which is derived based on the minimization of the variational free energy subject to the mean-field approximation constraint on the beliefs. While it does not guarantee the computation of exact marginals (even for tree-shaped graphs), its convergence is guaranteed by ensuring that the variational free energy of the computed beliefs is non-increasing at each step of the algorithm [14].

The operation of the VMP algorithm is analogous to the SP algorithm; the message computation rules read

$$m_{a\to i}(z_i) = \exp\langle \log f_a(\boldsymbol{z}_a)\rangle_{\prod_{j\in\mathcal{N}(a)\setminus i} n_{j\to a}}, \quad \forall a \in \mathcal{A}, i \in \mathcal{N}(a) \tag{5}$$

$$n_{i\to a}(z_i) = e_i \prod_{c \in \mathcal{N}(i)} m_{c\to i}(z_i) \quad \forall i \in \mathcal{I}, a \in \mathcal{N}(i) \tag{6}$$

where e_i ($i \in \mathcal{I}$) are positive constants ensuring that $n_{i\to a}$ are normalized. As in the SP algorihtm, the beliefs can be obtained as

$$b_i(z_i) = e_i \prod_{c \in \mathcal{N}(i)} m_{c\to i}(z_i) = n_{i\to a}(z_i) \quad \forall i \in \mathcal{I}, a \in \mathcal{N}(i).$$

The VMP algorithm has recently attracted the attention of the wireless communication research community due to its suitability for conjugate-exponential probabilistic models [12]. The computation rule for input messages from factor to variable nodes allows for the obtention of closed-form expressions in many cases in which the SP algorithm typically requires some type of numerical approximation.

It is shown in [42] that a message-passing interpretation of the EM algorithm can be obtained from the VMP algorithm. Assume that for a certain subset of variables z_i, $i \in \mathcal{E} \subseteq \mathcal{I}$ we want to apply an EM update while still using VMP for the rest of variables. To do so, the beliefs b_i are restricted to fulfill the constraint $b_i(z_i) = \delta(z_i - \tilde{z}_i)$ for all $i \in \mathcal{E}$ additionally to the mean-field factorization and normalization constraints. Minimizing the variational free energy subject to these conditions leads to a message passing algorithm identical to the one described in (5) and (6) except that the messages $n_{i\to a}$ for all $i \in \mathcal{E}$ and $a \in \mathcal{N}(i)$ are replaced by

$$n_{i\to a}(z_i) = \delta(z_i - \tilde{z}_i) \qquad \text{with} \quad \tilde{z}_i = \operatorname{argmax}_{\boldsymbol{z}_i} \left(\prod_{a \in \mathcal{N}(i)} m_{a\to i}(z_i) \right). \tag{7}$$

D. Combined VMP-SP Algorithm

As stated previously in this section, the VMP and the SP algorithms are two message-passing techniques suitable for different types of models. While SP is especially suitable in models with deterministic factor nodes, e.g. code or modulation constraints, VMP has the advantage of yielding closed-form computationally tractable expressions in conjugate-exponential models, as are found in channel weight estimation and noise variance estimation problems. Based on these facts, it seems natural to try to combine the two methods in a unified scheme capable of preserving the advantages of both.

A combined message-passing scheme based on the SP and VMP algorithms was recently proposed in [41], [42]. This hybrid technique is based on splitting the factor graph into two different parts: a VMP part and a SP part. To do this, part of the factor nodes are assigned to the VMP set ($\mathcal{A}_{\rm VMP}$) and the rest are assigned to the SP set ($\mathcal{A}_{\rm SP}$). Given this classification, we can express the probabilistic model in (4) as

$$p(\boldsymbol{z}) = \frac{1}{Z} \overbrace{\prod_{a\in\mathcal{A}_{\rm VMP}} f_a(\boldsymbol{z}_a)}^{\rm VMPpart} \overbrace{\prod_{c\in\mathcal{A}_{\rm SP}} f_c(\boldsymbol{z}_c)}^{\rm SPpart}$$

where $\mathcal{A}_{\rm VMP}\cup\mathcal{A}_{\rm SP} = \mathcal{A}$ and $\mathcal{A}_{\rm VMP}\cap\mathcal{A}_{\rm SP} = \emptyset$. By applying the Bethe approximation to the SP part and the mean-field approximation on the VMP part, a new message-passing scheme is derived from the stationary points of the region-based free energy [41], [42]. The message computation rules for this algorithm read

$$m^{\rm VMP}_{a\to i}(z_i) = \exp\langle \log f_a(\boldsymbol{z}_a)\rangle_{\prod_{j\in\mathcal{N}(a)\setminus i} n_{j\to a}}, \quad \forall a\in\mathcal{A}_{\rm VMP}, i\in\mathcal{N}(a) \tag{8}$$

$$m^{\rm SP}_{a\to i}(z_i) = d_a \langle f_a(\boldsymbol{z}_a)\rangle_{\prod_{j\in\mathcal{N}(a)\setminus i} n_{j\to a}}, \quad \forall a\in\mathcal{A}_{\rm SP}, i\in\mathcal{N}(a) \tag{9}$$

$$n_{i\to a}(z_i) = e_i \prod_{c\in\mathcal{N}(i)\cap\mathcal{A}_{\rm VMP}} m^{\rm VMP}_{c\to i}(z_i) \prod_{c\in\mathcal{N}(i)\cap\mathcal{A}_{\rm SP}\setminus a} m^{\rm SP}_{c\to i}(z_i) \quad \forall i\in\mathcal{I}, a\in\mathcal{N}(i) \tag{10}$$

where, again, d_a and e_i are positive constants ensuring normalized beliefs. The computation rules for messages outgoing factor nodes are preserved: for factor nodes in the VMP part ($a\in\mathcal{A}_{\rm VMP}$) the messages are computed using (8) as in standard VMP; for factor nodes in the SP part ($a\in\mathcal{A}_{\rm SP}$) the messages are computed via (9), which corresponds to a standard SP message. A message from a variable node i to a factor node a is computed as a VMP message when $a\in\mathcal{A}_{\rm VMP}$ and as a SP message when $a\in\mathcal{A}_{\rm SP}$, as can be deduced from (10).

As with the VMP and SP algorithms, the beliefs of the variables can be retrieved at any stage of the algorithm as

$$b_i(z_i) = e_i \prod_{a\in\mathcal{N}(i)\cap\mathcal{A}_{\rm VMP}} m^{\rm VMP}_{a\to i}(z_i) \prod_{a\in\mathcal{N}(i)\cap\mathcal{A}_{\rm SP}} m^{\rm SP}_{a\to i}(z_i) \quad \forall i\in\mathcal{I}.$$

Note that we can apply the EM restriction to the belief of variables z_i which are only connected to VMP factors (i.e. $\mathcal{N}(i)\cap\mathcal{A}_{\rm SP} = \emptyset$). In that case, the message update rules remain the same except that the message $n_{i\to a}$ in (10) is replaced by (7) for the selected variables.

IV. MIMO-OFDM Receiver Based on Combined VMP-SPA

In this section, we present a generic iterative receiver for MIMO-OFDM systems based on the mixed VMP and SP message-passing strategy outlined in Section III-D. Recalling the signal model presented in Section II, we can now postulate the probabilistic model to which we will apply the combined VMP-SP technique. In our case, we identify the observation to be the received signal vector $\boldsymbol{y}$. As unknown parameters, we include the vector of information bits $\boldsymbol{u} = [\boldsymbol{u}_1^{\rm T},\ldots,\boldsymbol{u}_M^{\rm T}]^{\rm T}$, the vector of coded bits $\boldsymbol{c} = [\boldsymbol{c}_1^{\rm T},\ldots,\boldsymbol{c}_M^{\rm T}]^{\rm T}$, the vector of modulated symbols $\boldsymbol{x} = [\boldsymbol{x}_1,\ldots,\boldsymbol{x}_M]^{\rm T}$, the vector of complex channel weights $\boldsymbol{h} = [\boldsymbol{h}_1,\ldots,\boldsymbol{h}_M]^{\rm T}$ and the AWGN precision λ. The system function of our model is the joint pdf of all parameters, which can be factorized as

$$p(\boldsymbol{u},\boldsymbol{c},\boldsymbol{x},\boldsymbol{h},\lambda,\boldsymbol{y}) = \underbrace{p(\boldsymbol{y}|\boldsymbol{h},\boldsymbol{x},\lambda)}_{f_{\rm O}} \underbrace{p(\boldsymbol{h})}_{f_{\rm C}} \underbrace{p(\lambda)}_{f_{\rm N}} \underbrace{p(\boldsymbol{x},\boldsymbol{c},\boldsymbol{u})}_{f_{\rm M}} \tag{11}$$

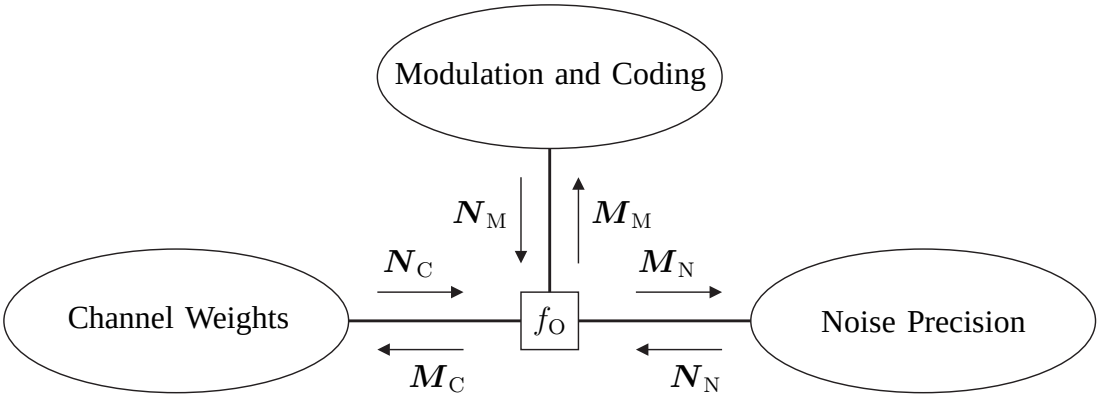

Fig. 2. Generic factor graph of the receiver.

where we have chosen to group the factors on the right-hand side into four functions. Factor $f_{\mathrm{O}}(\boldsymbol{y}, \boldsymbol{h}, \boldsymbol{x}, \lambda) \triangleq p(\boldsymbol{y}|\boldsymbol{h}, \boldsymbol{x}, \lambda)$ denotes the likelihood of the channel weights $\boldsymbol{h}$, the noise precision λ and the transmitted symbols $\boldsymbol{x}$ given the observation $\boldsymbol{y}$. Factor $f_{\mathrm{C}}(\boldsymbol{h}) \triangleq p(\boldsymbol{h})$ contains the assumed prior model of the channel weights, which is relevant for channel weight estimation. Function $f_{\mathrm{N}}(\lambda) \triangleq p(\lambda)$, likewise, contains the assumed prior model for the noise precision parameter λ which defines how estimation of the noise precision is done. Finally, function $f_{\mathrm{M}}(\boldsymbol{x}, \boldsymbol{c}, \boldsymbol{u}) \triangleq p(\boldsymbol{x}, \boldsymbol{c}, \boldsymbol{u})$ denotes the modulation and code constraints. Note that further factorization of the factors in (11) is possible and will, in fact, be used later in this section.

A schematic factor-graph-like representation of the model in (11) is depicted in Fig. 2. The observation factor node f_{O} is connected to three ovals: channel weights, noise precision and modulation and coding. Each of the ovals represents a subgraph corresponding to factors f_{C}, f_{N} and f_{M} in (11). The three subgraphs are connected to f_{O}, which reads

$$f_{\mathrm{O}}(\boldsymbol{y}, \boldsymbol{x}, \boldsymbol{h}, \lambda) \propto \lambda^{KNL} \exp\left\{-\lambda \|\boldsymbol{y} - \boldsymbol{X}\boldsymbol{h}\|^2\right\} = \lambda^{KNL} \exp\left\{-\lambda \|\boldsymbol{y} - \boldsymbol{H}\boldsymbol{x}\|^2\right\}.$$

Each of the subgraphs in Fig. 2 will be detailed in the remainder of this section. For now, we define the sets $\mathcal{A}_{\mathrm{C}}$, $\mathcal{A}_{\mathrm{N}}$ and $\mathcal{A}_{\mathrm{M}}$ as the set of factor nodes inside the channel weights, noise precision and modulation and coding subgraphs respectively. Likewise, we define the sets $\mathcal{I}_{\mathrm{C}}$, $\mathcal{I}_{\mathrm{N}}$ and $\mathcal{I}_{\mathrm{M}}$ as the set of variable nodes inside the channel weights, noise precision and modulation and coding subgraphs respectively. With these definitions, the set of all factor nodes in the graph is given by[4]

$$\mathcal{A} = \{f_{\mathrm{O}}\} \cup \mathcal{A}_{\mathrm{C}} \cup \mathcal{A}_{\mathrm{N}} \cup \mathcal{A}_{\mathrm{M}},$$

and the set of all variable nodes reads

$$\mathcal{I} = \mathcal{I}_{\mathrm{C}} \cup \mathcal{I}_{\mathrm{N}} \cup \mathcal{I}_{\mathrm{M}}.$$

From the observation factor node f_{O}, sets of messages $\boldsymbol{M}_{\mathrm{C}}$, $\boldsymbol{M}_{\mathrm{N}}$ and $\boldsymbol{M}_{\mathrm{M}}$ are sent to the respective subgraphs. These sets are composed of individual messages $m_{f_{\mathrm{O}} \to z}$, $z \in \mathcal{I}$. The specific composition of the sets of messages depends on the exact configuration of variable and factor nodes of the corresponding subgraph, which will be described later in the section. After processing is completed at each subgraph, sets of messages $\boldsymbol{N}_{\mathrm{C}}$, $\boldsymbol{N}_{\mathrm{N}}$ and $\boldsymbol{N}_{\mathrm{M}}$, which correspond to the updated estimates of the channel weights, the noise precision and the transmitted symbols respectively, are send back to f_{O}.

In order to apply the combined VMP-SP algorithm, we need to define which factor nodes are assigned to the VMP set $\mathcal{A}_{\mathrm{VMP}}$ and which are assigned to the SP set $\mathcal{A}_{\mathrm{SP}}$. We select the following splitting:

$$\begin{aligned} \mathcal{A}_{\mathrm{VMP}} &\triangleq \{f_{\mathrm{O}}\} \cup \mathcal{A}_{\mathrm{C}} \cup \mathcal{A}_{\mathrm{N}} \\ \mathcal{A}_{\mathrm{SP}} &\triangleq \mathcal{A}_{\mathrm{M}} \end{aligned}$$

[4]With a slight abuse of notation, from this point on we use the names of functions and variables as indices of the sets $\mathcal{A}$ and $\mathcal{I}$ respectively.

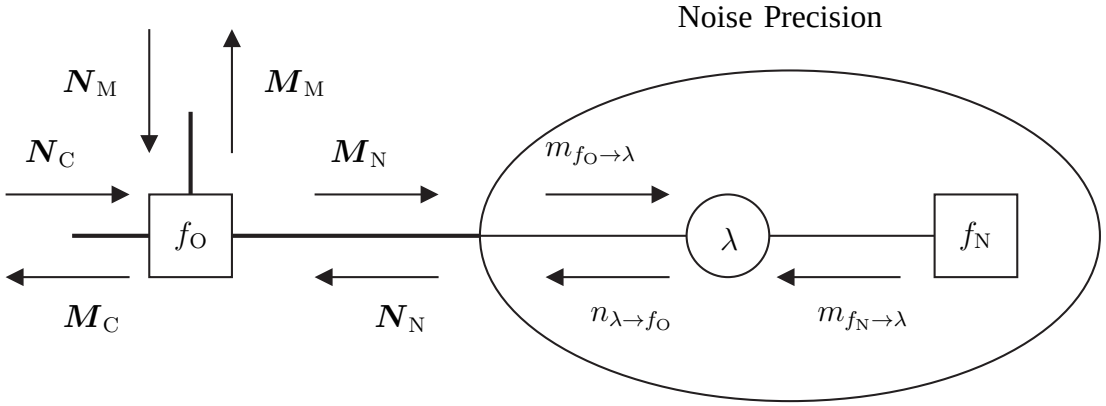

Fig. 3. Subgraph corresponding to the noise precision prior model.

i.e. the observation factor node and all factors in the channel weight and noise precision subgraphs are assigned to the VMP set, and all factor nodes in the modulation and coding subgraph are assigned to the SP set.

In the remainder of this section, we will present the details of each of the subgraphs, with several alternative factor-graph representations yielding different message-passing configurations. The performance of the individual receiver structures obtained will be evaluated and compared in Section V.

A. Noise Precision Subgraph

The noise precision subgraph is the graphical representation of f_{N} in (11), which we specify now as

$$f_{\mathrm{N}}(\lambda) \triangleq p(\lambda)$$

where $p(\lambda)$ denotes the prior distribution of λ. With this, we can now specify the sets

$$\begin{aligned}\mathcal{A}_{\mathrm{N}} &= \{f_{\mathrm{N}}\}\\ \mathcal{I}_{\mathrm{N}} &= \{\lambda\}.\end{aligned}$$

The factor graph representation of the subgraph is depicted in Fig. 3. It only consists of the variable node λ and the factor node f_{N}. Since there is only one variable node connected to f_{O}, the set of messages $\boldsymbol{M}_{\mathrm{N}}$ reduces to $\boldsymbol{M}_{\mathrm{N}} = \{m_{f_{\mathrm{O}}\to\lambda}\}$. Analogously, $\boldsymbol{N}_{\mathrm{N}} = \{n_{\lambda\to f_{\mathrm{O}}}\}$.

According to the message-computation rules given in Section III, the message transmitted from f_{O} to λ is calculated as

$$m_{f_{\mathrm{O}}\to\lambda}(\lambda) = \exp\left\{\langle \log f_{\mathrm{O}}(\boldsymbol{y},\boldsymbol{x},\boldsymbol{h},\lambda)\rangle_{\boldsymbol{N}_{\mathrm{C}}\boldsymbol{N}_{\mathrm{M}}}\right\} = \lambda^{KLN}\exp\{-\lambda A\} \tag{12}$$

with

$$A = \|\boldsymbol{y} - \hat{\boldsymbol{X}}\hat{\boldsymbol{h}}\|^2 + \mathrm{Tr}\left\{\hat{\boldsymbol{B}}^{\mathrm{H}}\hat{\boldsymbol{C}}\hat{\boldsymbol{B}} + \hat{\boldsymbol{B}}^{\mathrm{H}}\hat{\boldsymbol{H}}^{\mathrm{H}}\hat{\boldsymbol{H}}\hat{\boldsymbol{B}}\right\} + \mathrm{Tr}\left\{\hat{\boldsymbol{X}}\hat{\boldsymbol{\Sigma}}_{\boldsymbol{h}}\hat{\boldsymbol{X}}^{\mathrm{H}}\right\}.$$

In the above expression, $\hat{\boldsymbol{h}} = \langle \boldsymbol{h}\rangle_{\boldsymbol{N}_{\mathrm{C}}}$, $\hat{\boldsymbol{H}} = \langle \boldsymbol{H}\rangle_{\boldsymbol{N}_{\mathrm{C}}}$, $\hat{\boldsymbol{x}} = \langle \boldsymbol{x}\rangle_{\boldsymbol{N}_{\mathrm{M}}}$, $\hat{\boldsymbol{X}} = \langle \boldsymbol{X}\rangle_{\boldsymbol{N}_{\mathrm{M}}}$ are the means of $\boldsymbol{h}$, $\boldsymbol{H}$, $\boldsymbol{x}$ and $\boldsymbol{X}$ respectively taken with respect to the channel weights and modulation and coding output messages. Moreover, $\hat{\boldsymbol{\Sigma}}_{\boldsymbol{h}} = \langle \boldsymbol{h}\boldsymbol{h}^{\mathrm{H}}\rangle_{\boldsymbol{N}_{\mathrm{C}}} - \hat{\boldsymbol{h}}\hat{\boldsymbol{h}}^{\mathrm{H}}$, and $\hat{\boldsymbol{C}} = \langle \boldsymbol{H}^{\mathrm{H}}\boldsymbol{H}\rangle_{\boldsymbol{N}_{\mathrm{M}}} - \hat{\boldsymbol{H}}^{\mathrm{H}}\hat{\boldsymbol{H}}$. Finally, $\hat{\boldsymbol{B}} = \boldsymbol{U}\boldsymbol{\Lambda}^{1/2}$ where $\boldsymbol{\Lambda}$ is the diagonal matrix of eigenvalues and $\boldsymbol{U}$ is the matrix containing the eigenvectors of $\hat{\boldsymbol{\Sigma}}_{\boldsymbol{x}} = \langle \boldsymbol{x}\boldsymbol{x}^{\mathrm{H}}\rangle_{\boldsymbol{N}_{\mathrm{M}}} - \hat{\boldsymbol{x}}\hat{\boldsymbol{x}}^{\mathrm{H}}$, i.e. $\hat{\boldsymbol{\Sigma}}_{\boldsymbol{x}} = \boldsymbol{U}\boldsymbol{\Lambda}\boldsymbol{U}^{\mathrm{H}}$.

The message in (12) is proportional to the pdf of a complex central Wishart distribution of dimension 1, $KLN+1$ degrees of freedom and associated covariance A^{-1} [43]. We select the prior pdf $p(\lambda)$ to be conjugate, i.e., a complex Wishart. This yields the message

$$m_{f_{\mathrm{N}}\to\lambda}(\lambda) = p(\lambda) \propto \lambda^{a-1}\exp\{-\lambda A_{\text{prior}}\}.$$

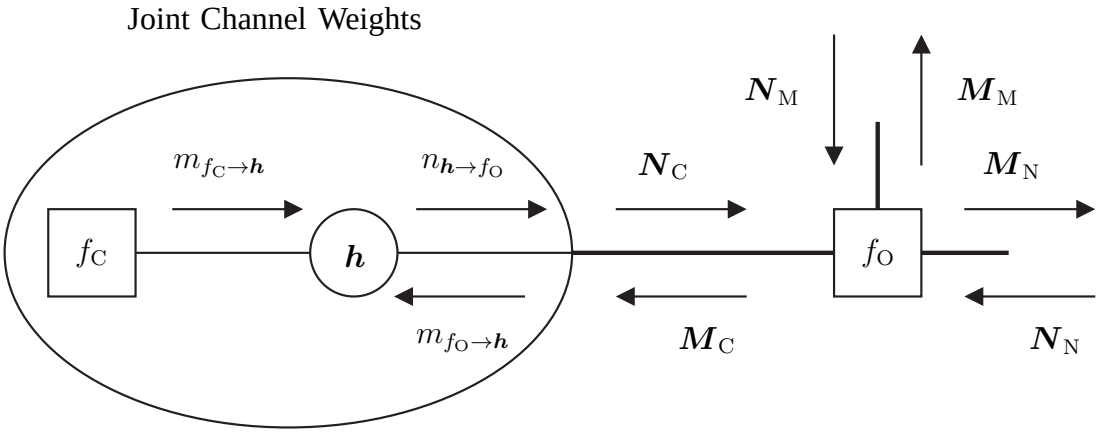

Fig. 4. Subgraph corresponding to the prior model of the joint channel weights.

Given the two incoming messages $m_{f_{\rm N}\to\lambda}$ and $m_{f_{\rm O}\to\lambda}$, the outgoing message from λ is also proportional to a complex Wishart pdf

$$n_{\lambda\to f_{\rm O}}(\lambda) \propto m_{f_{\rm N}\to\lambda}(\lambda) m_{f_{\rm O}\to\lambda}(\lambda) \propto \lambda^{KLN+a-1} \exp\{-\lambda(A + A_{\text{prior}})\}.$$

Since usually no prior information on the noise precision is available at the receiver, we select $p(\lambda)$ non-informative with parameters $a = 0$ and $A_{\text{prior}} = 0$. With this choice, the mean of λ with respect to $\boldsymbol{N}_{\rm N}$ reads

$$\hat{\lambda} = \langle \lambda \rangle_{\boldsymbol{N}_{\rm N}} = \frac{KLN}{A}. \tag{13}$$

Note that the above update for $\hat{\lambda}$ coincides with the ML estimate of the noise precision. Since, as we will see later in the section, only the first moment of λ is needed to compute other messages, it is sufficient to pass just this value to the rest of the graph.

B. Channel Weights Subgraph

The channel weights subgraph includes the graphical description of the factor $f_{\rm C}$ in (11). We will present in the following two alternative subgraphs representing two possible definitions of $f_{\rm C}$: in the first one, coined *joint* channel weights subgraph, all channel weights for all transmit antennas are grouped together in a single variable node $\boldsymbol{h}$; in the second one, which we refer to as *disjoint* channel weights subgraph, the weights are split into M variable nodes $\boldsymbol{h}_1, \ldots, \boldsymbol{h}_M$ each of them containing the channel weights associated with an individual transmit antenna.

1) Joint Channel Weights Model: The joint channel weights subgraph is obtained from the following definition:

$$f_{\rm C}(\boldsymbol{h}) \triangleq p(\boldsymbol{h})$$

with $p(\boldsymbol{h})$ denoting the prior pdf of the vector of channel weights $\boldsymbol{h}$. Using this model for $f_{\rm C}$ leads to defining the factor and variable node sets as

$$\begin{aligned} \mathcal{A}_{\rm C} &= \{f_{\rm C}\} \\ \mathcal{I}_{\rm C} &= \{\boldsymbol{h}\}. \end{aligned}$$

The factor graph describing the joint channel weight option is presented in Fig. 4. As there is only one variable node connected to the factor node $f_{\rm O}$, the set of input messages to the channel weights subgraph is simply $\boldsymbol{M}_{\rm C} = \{m_{f_{\rm O}\to\boldsymbol{h}}\}$ and the set of output messages is the singleton $\boldsymbol{N}_{\rm C} = \{n_{\boldsymbol{h}\to f_{\rm O}}\}$.

The message from $f_{\rm O}$ to $\boldsymbol{h}$ is given by

$$m_{f_{\rm O}\to\boldsymbol{h}}(\boldsymbol{h}) = \exp\{\langle \log f_{\rm O}(\boldsymbol{y}, \boldsymbol{x}, \boldsymbol{h}, \lambda) \rangle_{\boldsymbol{N}_{\rm M}\boldsymbol{N}_{\rm N}}\} \propto \exp\left\{-\hat{\lambda}\left(\|\boldsymbol{y} - \hat{\boldsymbol{X}}\boldsymbol{h}\|^2 + \boldsymbol{h}^{\rm H}\hat{\boldsymbol{D}}\boldsymbol{h}\right)\right\}$$

with $\hat{\boldsymbol{D}} = \langle \boldsymbol{X}^{\mathrm{H}}\boldsymbol{X}\rangle_{\boldsymbol{N}_{\mathrm{M}}} - \hat{\boldsymbol{X}}^{\mathrm{H}}\hat{\boldsymbol{X}}$. Hence, $m_{f_{\mathrm{O}}\to\boldsymbol{h}}(\boldsymbol{h})$ is proportional to a Gaussian pdf. We also impose the prior $p(\boldsymbol{h})$ to be Gaussian, which yields the message

$$m_{f_{\mathrm{C}}\to\boldsymbol{h}}(\boldsymbol{h}) = p(\boldsymbol{h}) \propto \exp\left\{-(\boldsymbol{h}-\boldsymbol{h}_{\text{prior}})^{\mathrm{H}}\boldsymbol{\Sigma}^{-1}_{\boldsymbol{h}_{\text{prior}}}(\boldsymbol{h}-\boldsymbol{h}_{\text{prior}})\right\}.$$

For most practical channels it is reasonable to assume that $\boldsymbol{h}_{\text{prior}} = 0$. The receiver needs an estimate of the prior covariance of the channel $\boldsymbol{\Sigma}_{\boldsymbol{h}_{\text{prior}}}$. In order to obtain the outgoing message $n_{\boldsymbol{h}\to f_{\mathrm{O}}}(\boldsymbol{h})$, the two incoming messages are combined, leading to

$$n_{\boldsymbol{h}\to f_{\mathrm{O}}}(\boldsymbol{h}) \propto m_{f_{\mathrm{O}}\to\boldsymbol{h}}(\boldsymbol{h}) m_{f_{\mathrm{C}}\to\boldsymbol{h}}(\boldsymbol{h}) \propto \exp\left\{-(\boldsymbol{h}-\hat{\boldsymbol{h}})^{\mathrm{H}}\hat{\boldsymbol{\Sigma}}^{-1}_{\boldsymbol{h}}(\boldsymbol{h}-\hat{\boldsymbol{h}}).\right\}$$

Thus, $n_{\boldsymbol{h}\to f_{\mathrm{O}}}$ is proportional to a Gaussian pdf with covariance matrix

$$\hat{\boldsymbol{\Sigma}}_{\boldsymbol{h}} = \left(\hat{\lambda}\hat{\boldsymbol{X}}^{\mathrm{H}}\hat{\boldsymbol{X}} + \hat{\lambda}\hat{\boldsymbol{D}} + \boldsymbol{\Sigma}^{-1}_{\boldsymbol{h}_{\text{prior}}}\right)^{-1}$$

and mean value

$$\hat{\boldsymbol{h}} = \hat{\boldsymbol{\Sigma}}_{\boldsymbol{h}}\left(\hat{\lambda}\hat{\boldsymbol{X}}^{\mathrm{H}}\boldsymbol{y} + \boldsymbol{\Sigma}^{-1}_{\boldsymbol{h}_{\text{prior}}}\boldsymbol{h}_{\text{prior}}\right).$$

2) Disjoint Channel Weights Model: The disjoint channel weights subgraph is obtained by factorizing f_{C} with respect to each transmitter. More specifically, we define

$$f_{\mathrm{C}}(\boldsymbol{h}) = \prod_{m=1}^{M} f_{\mathrm{C}_m}(\boldsymbol{h}_m)$$

with $f_{\mathrm{C}_m}(\boldsymbol{h}_m) \triangleq p(\boldsymbol{h}_m)$, $m = 1,\ldots,M$ denoting the prior pdf of the channel weights for the mth transmit antenna. We also specify the sets

$$\begin{aligned}\mathcal{A}_{\mathrm{C}} &= \{f_{\mathrm{C}_m} | m = 1,\ldots,M\}\\ \mathcal{I}_{\mathrm{C}} &= \{\boldsymbol{h}_m | m = 1,\ldots,M\}.\end{aligned}$$

Fig. 5 shows the factor graph of the disjoint channel weights model with the above definitions. With this configuration, the channel weight vector $\boldsymbol{h}$ is split into M variable nodes $\boldsymbol{h}_1,\ldots,\boldsymbol{h}_M$, each of them containing the weights associated with one transmit antenna. Each of these variable nodes is furthermore connected to a factor node f_{C_m}. Due to this separation, the set of incoming messages reads $\boldsymbol{M}_{\mathrm{C}} = \{m_{f_{\mathrm{O}}\to\boldsymbol{h}_m} | m = 1,\ldots,M\}$, while the set of outgoing messages is $\boldsymbol{N}_{\mathrm{C}} = \{n_{\boldsymbol{h}_m\to f_{\mathrm{O}}} | m = 1,\ldots,M\}$. With this structure, the channel weight vectors are estimated sequentially by iterating through the transmit antenna index m.

For the mth transmit antenna, the incoming message reads

$$\begin{aligned}m_{f_{\mathrm{O}}\to\boldsymbol{h}_m}(\boldsymbol{h}_m) &= \exp\left\{\langle \log f_{\mathrm{O}}(\boldsymbol{y},\boldsymbol{x},\boldsymbol{h},\lambda)\rangle_{\boldsymbol{N}_{\mathrm{M}}\boldsymbol{N}_{\mathrm{N}}\boldsymbol{N}_{\mathrm{C}}^{(m)}}\right\}\\ &\propto \exp\left\{-\hat{\lambda}\left(\left\|\boldsymbol{y} - \sum_{m'\neq m}\hat{\boldsymbol{X}}_{m'}\hat{\boldsymbol{h}}_{m'} - \hat{\boldsymbol{X}}_m\boldsymbol{h}_m\right\|^2 + \boldsymbol{h}_m^{\mathrm{H}}\hat{\boldsymbol{D}}_m\boldsymbol{h}_m\right)\right\}\end{aligned}$$

where $\boldsymbol{N}_{\mathrm{C}}^{(m)} = \left\{n_{\boldsymbol{h}_{m'}\to f_{\mathrm{O}}}\right\}_{\substack{\forall m'=1,\ldots,M\\ m'\neq m}}$ denotes the set of all output channel weight messages except the mth one. Furthermore, $\hat{\boldsymbol{h}}_{m'} = \langle \boldsymbol{h}_{m'}\rangle_{\boldsymbol{N}_{\mathrm{C}}^{(m)}}$, $\hat{\boldsymbol{X}}_m = \langle \boldsymbol{X}_m\rangle_{\boldsymbol{N}_{\mathrm{M}}}$ and $\hat{\boldsymbol{D}}_m = \langle \boldsymbol{X}_m^{\mathrm{H}}\boldsymbol{X}_m\rangle_{\boldsymbol{N}_{\mathrm{M}}} - \hat{\boldsymbol{X}}_m^{\mathrm{H}}\hat{\boldsymbol{X}}_m$. Again, $m_{f_{\mathrm{O}}\to\boldsymbol{h}_m}$ is observed to be proportional to a Gaussian pdf. Analogously to the joint channel weights case, we need to specify the prior of each individual channel vector $\boldsymbol{h}_m$. Defining them as Gaussians leads to the message

$$m_{f_{\mathrm{C}_m}\to\boldsymbol{h}_m}(\boldsymbol{h}_m) = p(\boldsymbol{h}_m) \propto \exp\left\{-(\boldsymbol{h}_m-\boldsymbol{h}_{m,\text{prior}})^{\mathrm{H}}\boldsymbol{\Sigma}^{-1}_{\boldsymbol{h}_{m,\text{prior}}}(\boldsymbol{h}_m-\boldsymbol{h}_{m,\text{prior}})\right\}$$

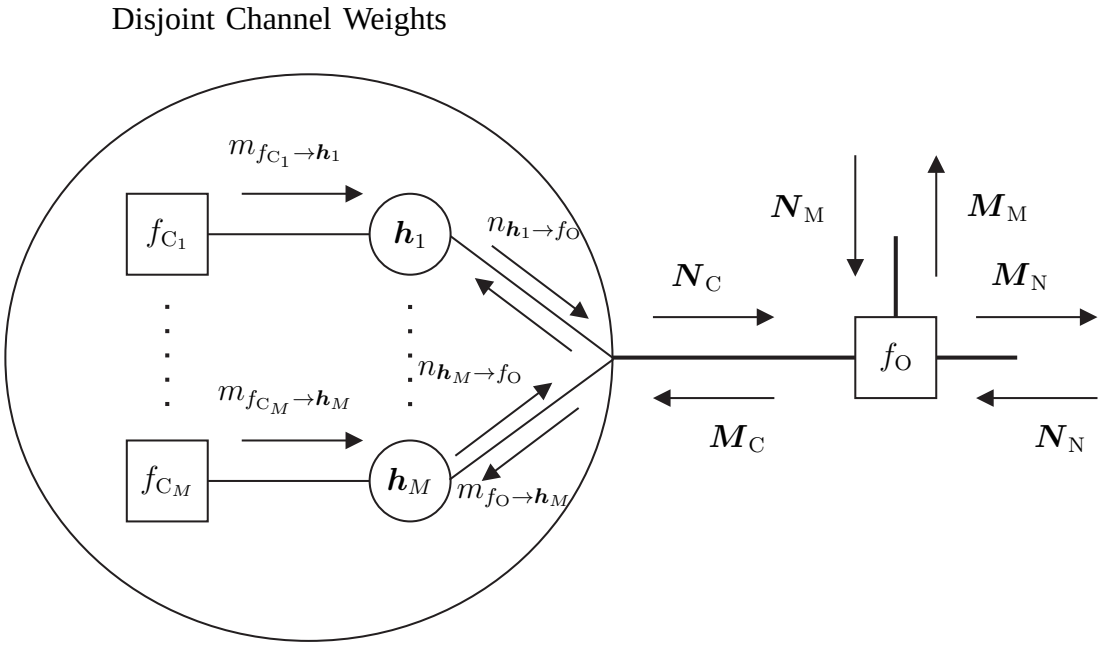

Fig. 5. Subgraph corresponding to the prior model of the disjoint channel weights.

where, once more, the receiver requires estimates of the prior parameters of the channel for each transmitter. The outgoing message from variable node $\boldsymbol{h}_m$ is obtained by multiplying both incoming messages, leading to

$$n_{\boldsymbol{h}_m\to f_{\mathrm{O}}}(\boldsymbol{h}_m) \propto m_{f_{\mathrm{O}}\to\boldsymbol{h}_m}(\boldsymbol{h}_m) m_{f_{\mathrm{C}_m}\to\boldsymbol{h}_m}(\boldsymbol{h}_m) \propto \exp\left\{-(\boldsymbol{h}_m-\hat{\boldsymbol{h}}_m)^{\mathrm{H}}\hat{\boldsymbol{\Sigma}}_{\boldsymbol{h}_m}^{-1}(\boldsymbol{h}_m-\hat{\boldsymbol{h}}_m)\right\},$$

which equals, up to a proportionality constant, a Gaussian pdf with covariance matrix

$$\hat{\boldsymbol{\Sigma}}_{\boldsymbol{h}_m} = \left(\hat{\lambda}\hat{\boldsymbol{X}}_m^{\mathrm{H}}\hat{\boldsymbol{X}}_m + \hat{\lambda}\hat{\boldsymbol{D}}_m + \boldsymbol{\Sigma}_{\boldsymbol{h}_{m,\mathrm{prior}}}^{-1}\right)^{-1}$$

and mean value

$$\hat{\boldsymbol{h}}_m = \hat{\boldsymbol{\Sigma}}_{\boldsymbol{h}_m}\left(\hat{\lambda}\hat{\boldsymbol{X}}_m^{\mathrm{H}}\left(\boldsymbol{y}-\sum_{m'\neq m}\hat{\boldsymbol{X}}_{m'}\hat{\boldsymbol{h}}_{m'}\right)+\boldsymbol{\Sigma}_{\boldsymbol{h}_{m,\mathrm{prior}}}^{-1}\boldsymbol{h}_{m,\mathrm{prior}}\right).$$

It is important to note that every time a new message $n_{\boldsymbol{h}_m\to f_{\mathrm{O}}}$ is computed, the set of messages $\boldsymbol{M}_{\mathrm{C}}$ needs to be recomputed again, as all $m_{f_{\mathrm{O}}\to\boldsymbol{h}_{m'}}, m'\neq m$ depend on the updated messages $n_{\boldsymbol{h}_m\to f_{\mathrm{O}}}$.

C. Modulation and Coding Subgraph

The modulation and coding subgraph describes the factor f_{M} in (11). We choose to factorize this factor according to

$$f_{\mathrm{M}}(\boldsymbol{x},\boldsymbol{c},\boldsymbol{u}) = \prod_{m=1}^{M} f_{\mathcal{P}_m}(\boldsymbol{x}_m^{(p)}) f_{\mathcal{M}_m}(\boldsymbol{x}_m^{(d)},c_{m,1},\ldots,c_{m,C_m}) f_{\mathcal{C}_m}(c_{m,1},\ldots,c_{m,C_m},u_{m,1},\ldots,u_{m,U_m}) \prod_{i=1}^{U_m} f_{u_{m,i}}(u_{m,i})$$

where $f_{\mathcal{P}_m}(\boldsymbol{x}_m^{(p)}) \triangleq p(\boldsymbol{x}_m^{(p)})$ denotes the prior pdf of the pilot symbols transmitted from the mth transmitter, $f_{\mathcal{M}_m}(\boldsymbol{x}_m^{(d)},c_{m,1},\ldots,c_{m,C_m}) \triangleq p(\boldsymbol{x}_m^{(d)}|c_{m,1},\ldots,c_{m,C_m})$ denotes the modulation constraints on the data symbols of the mth transmitter, $f_{\mathcal{C}_m}(c_{m,1},\ldots,c_{m,C_m},u_{m,1},\ldots,u_{m,U_m}) \triangleq p(c_{m,1},\ldots,c_{m,C_m}|u_{m,1},\ldots,u_{m,U_m})$ represents the code constraints for the mth codeword and $f_{u_{m,i}}(u_{m,i}) \triangleq p(u_{m,i})$ is the prior pdf of the ith information bit transmitted by the mth antenna. In addition, the vectors $\boldsymbol{x}_m^{(p)}$ and $\boldsymbol{x}_m^{(d)}$ contain, respectively,

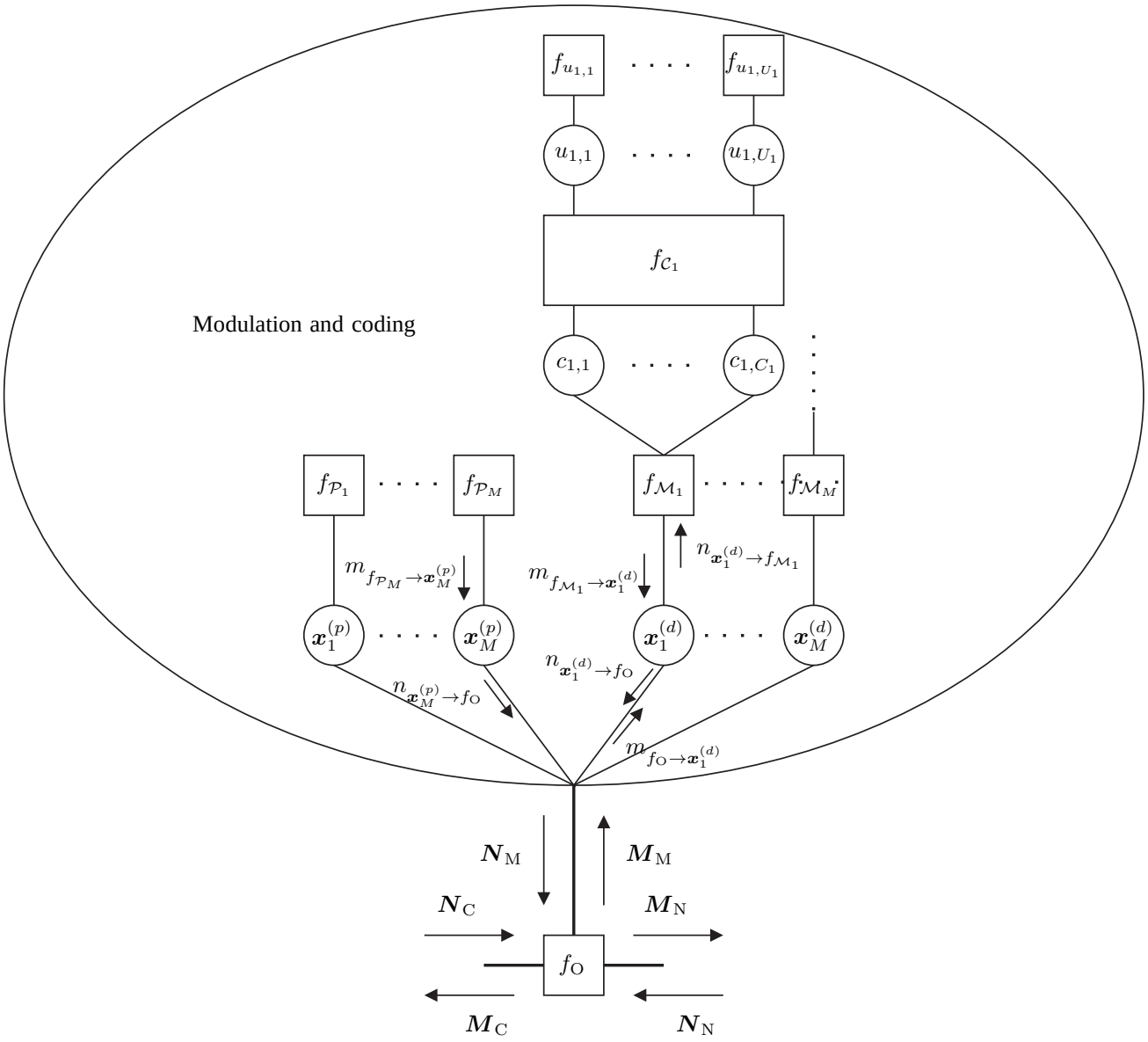

Fig. 6. Subgraph corresponding to the modulation and coding constraints.

the modulated pilot and data symbols transmitted from the mth antenna. Finally, C_m and U_m denote the number of coded and information bits respectively transmitted in a codeword from the mth antenna. Using this factorization of f_{M}, we define the sets $\mathcal{A}_{\mathrm{M}}$ and $\mathcal{I}_{\mathrm{M}}$ as

$$\begin{aligned}\mathcal{A}_{\mathrm{M}} =&\{f_{\mathcal{P}_m}|m=1,\dots,M\}\cup\{f_{\mathcal{M}_m}|m=1,\dots,M\}\cup\{f_{\mathcal{C}_m}|m=1,\dots,M\}\\ &\cup\{f_{u_{m,i}}|m=1,\dots,M,i=1\dots U_m\}\\ \mathcal{I}_{\mathrm{M}} =&\{\boldsymbol{x}_m^{(p)}|m=1\dots,M\}\cup\{\boldsymbol{x}_m^{(d)}|m=1\dots,M\}\cup\{c_{m,i}|m=1,\dots,M,i=1\dots C_m\}\\ &\cup\{u_{m,i}|m=1,\dots,M,i=1\dots U_m\}.\end{aligned}$$

The factor graph with the modulation and coding constraints is shown in Fig. 6. As it can be observed, the modulated symbols have been separated into different variable nodes according to the transmit antenna index m from which they are sent. The symbols corresponding to each transmit antenna port have been further subdivided into two different variable nodes $\boldsymbol{x}_m^{(p)}$ and $\boldsymbol{x}_m^{(d)}$, the first containing the pilot symbols and the second containing the modulated data symbols. The modulated data symbols $\boldsymbol{x}_m^{(d)}$ are connected to the encoded bits $c_{m,1},\dots,c_{m,C_m}$ via the modulation factor node $f_{\mathcal{M}_m}$, which describes the mapping of bits

onto a complex constellation. The coded bits are, in turn, related to the information bits $u_{m,1},\ldots,u_{m,U_m}$ through the specific channel code and interleaving scheme utilized, which is represented in a simplified manner by the factor $f_{\mathcal{C}_m}$ in Fig. 6. Finally, every information bit $u_{m,i}$ has an associated prior probability represented by the factor node $f_{u_{m,i}}$. For the vast majority of applications, however, the values of the bits will be assumed to be equiprobable. With the proposed structure, the set of incoming messages is defined as $\boldsymbol{M}_{\mathrm{M}}=\left\{m_{f_{\mathrm{O}}\to\boldsymbol{x}_m^{(p)}}|m=1,\ldots,M\right\}\cup\left\{m_{f_{\mathrm{O}}\to\boldsymbol{x}_m^{(d)}}|m=1,\ldots,M\right\}$, while the set of outgoing messages becomes $\boldsymbol{N}_{\mathrm{M}}=\left\{n_{\boldsymbol{x}_m^{(p)}\to f_{\mathrm{O}}}|m=1,\ldots,M\right\}\cup\left\{n_{\boldsymbol{x}_m^{(d)}\to f_{\mathrm{O}}}|m=1,\ldots,M\right\}$.

In order to ease the derivation of the messages for this subgraph, we can re-write $f_{\mathrm{O}}(\boldsymbol{y},\boldsymbol{x},\boldsymbol{h},\lambda)$ as

$$f_{\mathrm{O}}(\boldsymbol{y},\boldsymbol{x},\boldsymbol{h},\lambda)\propto\lambda^{KNL}\exp\left\{-\lambda\left\|\boldsymbol{y}^{(d)}-\sum_{m=1}^{M}\boldsymbol{H}_m^{(d)}\boldsymbol{x}_m^{(d)}\right\|^2-\lambda\left\|\boldsymbol{y}^{(p)}-\sum_{m=1}^{M}\boldsymbol{H}_m^{(p)}\boldsymbol{x}_m^{(p)}\right\|^2\right\}$$

where the contribution of pilot and data symbols has been split into two separate terms. We start by computing the message that factor node f_{O} sends to $\boldsymbol{x}_m^{(d)}$:

$$\begin{aligned}m_{f_{\mathrm{O}}\to\boldsymbol{x}_m^{(d)}}(\boldsymbol{x}_m^{(d)})&=\exp\left\{\langle\log f_{\mathrm{O}}(\boldsymbol{y},\boldsymbol{x},\boldsymbol{h},\lambda)\rangle_{\boldsymbol{N}_{\mathrm{N}}\boldsymbol{N}_{\mathrm{C}}\boldsymbol{N}_{\mathrm{M}}^{(m)}}\right\}\\&\propto\exp\left\{-\hat{\lambda}\left(\left\|\boldsymbol{y}^{(d)}-\sum_{m'\neq m}\hat{\boldsymbol{H}}_{m'}^{(d)}\hat{\boldsymbol{x}}_{m'}^{(d)}-\hat{\boldsymbol{H}}_m^{(d)}\boldsymbol{x}_m^{(d)}\right\|^2+(\boldsymbol{x}_m^{(d)})^{\mathrm{H}}\hat{\boldsymbol{C}}_m^{(d)}\boldsymbol{x}_m^{(d)}\right.\right.\\&\quad\left.\left.+\sum_{m'\neq m}\left((\boldsymbol{x}_m^{(d)})^{\mathrm{H}}\hat{\boldsymbol{C}}_{mm'}^{(d)}\hat{\boldsymbol{x}}_{m'}^{(d)}+(\hat{\boldsymbol{x}}_{m'}^{(d)})^{\mathrm{H}}(\hat{\boldsymbol{C}}_{mm'}^{(d)})^{\mathrm{H}}\boldsymbol{x}_m^{(d)}\right)\right)\right\}.\end{aligned}\tag{14}$$

In the above expression, and similarly to previous definitions, $\hat{\boldsymbol{x}}_{m'}^{(d)}=\langle\boldsymbol{x}_{m'}^{(d)}\rangle_{\boldsymbol{N}_{\mathrm{M}}}$, $\hat{\boldsymbol{H}}_{m'}^{(d)}=\langle\boldsymbol{H}_{m'}^{(d)}\rangle_{\boldsymbol{N}_{\mathrm{C}}}$, $\hat{\boldsymbol{C}}_m^{(d)}=\langle(\boldsymbol{H}_m^{(d)})^{\mathrm{H}}\boldsymbol{H}_m^{(d)}\rangle_{\boldsymbol{N}_{\mathrm{C}}}-(\hat{\boldsymbol{H}}_m^{(d)})^{\mathrm{H}}\hat{\boldsymbol{H}}_m^{(d)}$ and $\hat{\boldsymbol{C}}_{mm'}^{(d)}=\langle(\boldsymbol{H}_m^{(d)})^{\mathrm{H}}\boldsymbol{H}_{m'}^{(d)}\rangle_{\boldsymbol{N}_{\mathrm{C}}}-(\hat{\boldsymbol{H}}_m^{(d)})^{\mathrm{H}}\hat{\boldsymbol{H}}_{m'}^{(d)}$. Additionally, $\boldsymbol{N}_{\mathrm{M}}^{(m)}=\{n_{\boldsymbol{x}_i^{(p)}\to f_{\mathrm{O}}}|i=1,\ldots,M\}\cup\{n_{\boldsymbol{x}_i^{(d)}\to f_{\mathrm{O}}}|i=1,\ldots,M,i\neq m\}$ denotes the set of all outgoing detection messages except $n_{\boldsymbol{x}_m^{(d)}\to f_{\mathrm{O}}}$. The message in (14) is proportional to a Gaussian pdf with covariance matrix

$$\hat{\boldsymbol{\Sigma}}_{\boldsymbol{x}_{m,\mathrm{VMP}}^{(d)}}=\hat{\lambda}^{-1}\left((\hat{\boldsymbol{H}}_m^{(d)})^{\mathrm{H}}\hat{\boldsymbol{H}}_m^{(d)}+\hat{\boldsymbol{C}}_m^{(d)}\right)^{-1}$$

and mean

$$\hat{\boldsymbol{x}}_{m,\mathrm{VMP}}^{(d)}=\hat{\lambda}\hat{\boldsymbol{\Sigma}}_{\boldsymbol{x}_{m,\mathrm{VMP}}^{(d)}}\left((\hat{\boldsymbol{H}}_m^{(d)})^{\mathrm{H}}\left(\boldsymbol{y}^{(d)}-\sum_{m'\neq m}\hat{\boldsymbol{H}}_{m'}^{(d)}\hat{\boldsymbol{x}}_{m'}^{(d)}\right)-\sum_{m'\neq m}\hat{\boldsymbol{C}}_{mm'}^{(d)}\hat{\boldsymbol{x}}_{m'}^{(d)}\right).$$

The outgoing message $n_{\boldsymbol{x}_m^{(d)}\to f_{\mathrm{O}}}(\boldsymbol{x}_m^{(d)})$ is obtained by multiplying the messages $m_{f_{\mathrm{O}}\to\boldsymbol{x}_m^{(d)}}(\boldsymbol{x}_m^{(d)})$ and $m_{f_{\mathcal{M}_m}\to x_m^{(d)}}$. In this case, $m_{f_{\mathcal{M}_m}\to x_m^{(d)}}$ is a SP message reading

$$m_{f_{\mathcal{M}_m}\to x_m^{(d)}}\propto\prod_{i=1}^{N_d}\left(\sum_{s\in\mathcal{S}_m}\beta_{x_m^{(d)}(i)}(s)\delta(x_m^{(d)}(i)-s)\right)\tag{15}$$

where $\mathcal{S}_m$ is the modulation set for user m and $\beta_{x_m^{(d)}(i)}(s)$ represents the extrinsic values of $x_m^{(d)}(i)$ for each constellation point $s\in\mathcal{S}_m$, obtained from the SP demodulator and decoder. The combined message fed back to the observation factor node reads

$$\begin{aligned}n_{\boldsymbol{x}_m^{(d)}\to f_{\mathrm{O}}}(\boldsymbol{x}_m^{(d)})&\propto m_{f_{\mathrm{O}}\to\boldsymbol{x}_m^{(d)}}(\boldsymbol{x}_m^{(d)})m_{f_{\mathcal{M}_m}\to x_m^{(d)}}(\boldsymbol{x}_m^{(d)})\\&\propto\prod_{i=1}^{N_d}\left(\sum_{s\in\mathcal{S}_m}\beta_{x_m^{(d)}(i)}(s)\exp\left\{\frac{-|s-\hat{x}_{m,\mathrm{VMP}}^{(d)}(i)|^2}{\sigma^2_{x_m^{(d)}}(i)}\right\}\delta(x_m^{(d)}(i)-s)\right),\end{aligned}\tag{16}$$

where $\sigma^2_{x_m^{(d)}}(i)$ is the ith entry in the main diagonal of $\hat{\boldsymbol{\Sigma}}_{\boldsymbol{x}_{m,\text{VMP}}^{(d)}}$. It can be observed that the message factorizes with respect to the individual modulated symbols $x_m^{(d)}(i)$, so the mean and variance of each data symbol can be computed independently and used to build the mean vector $\hat{\boldsymbol{x}}$ and the covariance matrix $\hat{\boldsymbol{\Sigma}}_{\boldsymbol{x}}$ by inserting the updated mean and variances in their corresponding positions.

It is important to note that, because the factor node $f_{\mathcal{M}_m}$ is a SP factor node, the message $n_{\boldsymbol{x}_m^{(d)} \to f_{\mathcal{M}_m}}$ is obtained by multiplying all messages received at variable node $\boldsymbol{x}_m^{(d)}$ except the message coming from $f_{\mathcal{M}_m}$, which in this particular setup reduces to

$$n_{\boldsymbol{x}_m^{(d)} \to f_{\mathcal{M}_m}}(\boldsymbol{x}_m^{(d)}) = m_{f_{\text{O}} \to \boldsymbol{x}_m^{(d)}}(\boldsymbol{x}_m^{(d)}).$$

All message-passing among the modulation factor nodes, coded bits and information bits is completed by using the standard SP algorithm, and will therefore not be described here.

It remains to describe the income and outcome messages involving pilot symbols. As pilot symbols are known by the receiver, their prior distribution is $p(x_m^{(p)}(i)) = \delta(x_m^{(p)}(i) - p_m(i))$ with $p_m(i)$ denoting the ith pilot symbol sent from transmit antenna m. This imposes that the outgoing message $n_{\boldsymbol{x}_m^{(p)} \to f_{\text{O}}}$ is also a Dirac delta, which can also be described as a degenerate Gaussian message with mean $\hat{\boldsymbol{x}}_m^{(p)} = \boldsymbol{p}_m$ and covariance $\hat{\boldsymbol{\Sigma}}_{\boldsymbol{x}_m^{(p)}} = \mathbf{0}$.

V. Simulation Results

In this section, we propose a number of receiver structures based on the derivations made in Section IV and evaluate their performance by means of Monte-Carlo simulations. First, we present the parameters of the MIMO-OFDM system considered, followed by a description of the specific receiver structures that will be evaluated. Finally, the BER performance results obtained are presented and discussed.

A. Description of the MIMO-OFDM System

We begin by describing the MIMO-OFDM system used for obtaining the numerical results. Its main parameters are summarized in Table I. We consider an OFDM system with $M = N = 2$ antennas at both transmitter and receiver ends. Two streams of random bits are independently encoded using a convolutional code with rate 1/3 and generating polynomials 133, 171 and 165 (octal). After channel interleaving, the coded bits are mapped onto symbols of a QPSK or 16QAM constellation (with Gray mapping) which are then inserted into an OFDM frame consisting of $L = 7$ OFDM symbols with $K = 75$ subcarriers and with a subcarrier spacing of 15kHz. Part of the time-frequency elements are reserved for the transmission of pilot symbols. We specify the following pilot patterns: pilot symbols are transmitted in the first and fifth OFDM symbol of the frame, with a frequency spacing of 12 subcarriers, resulting in a total of 13 pilot symbols per frame. Note that both transmit antennas share the same time-frequency elements for the simultaneous transmission of pilot symbols. Pilot symbols are randomly chosen from a QPSK constellation.

Realizations of the channel time-frequency response are randomly generated using the extended typical urban (ETU) model from the 3GPP LTE standard [44] with 9 Rayleigh-fading taps. The channel responses corresponding to two different transmitters are uncorrelated and remain static over the duration of an OFDM frame. A new channel response is generated for each OFDM frame, with the responses of two different frames being also uncorrelated.

B. Receiver Structures

We introduce now the specific receiver architectures that will be evaluated in this section. All receivers are based on the generic message-passing receiver presented in Section IV. The messages exchanged can be obtained by particularizing the generic messages according to the specific receiver configuration, as it will be detailed in the following. We evaluate three main types of VMP-SP receiver, which are described next.

TABLE I
PARAMETERS OF THE OFDM SYSTEM SIMULATED

Parameter	Value
Tx antennas (M)	2
Rx antennas (N)	2
Subcarriers (K)	75
OFDM symbols (L)	7
Subcarrier spacing (Δf)	15 kHz
Channel coding	1/3 Convolutional
Symbol mapping	16QAM
Pilot symbols	13
Channel model	3GPP ETU

1) I-DJC-DD and I-DSC-DD Receivers: First, we introduce a full iterative receiver using exactly the messages derived in Section IV. The receiver operates by iteratively updating the beliefs of the channel weight vector, the data symbols and information bits and, finally, the noise precision parameter.

Initialization of the beliefs of the channel weights and the transmitted symbols is required. The initialization of the channel weights is obtained from a pilot-based joint linear minimum mean-squared-error (LMMSE) channel estimator. For the initialization of the transmitted symbols, maximum-likelihood detection (MLD) is used, followed by soft-in soft-out (SISO) BCJR decoding. The belief of the transmitted data symbols is set to a Gaussian pdf with mean and covariance values obtained from soft modulation of the a-posteriori probabilities (APP) of the coded bits obtained from the SISO BCJR decoder. An initial estimate of the noise precision is obtained as in Section IV-A. After the initialization, a full iteration of the receiver consists of updating the beliefs of the channel weight vectors (using either the joint channel weight model in Fig. 4 or the disjoint channel weight model in Fig. 5), a message-passing run on the modulation and coding subgraph (updating the beliefs of transmitted symbols, coded bits and information bits) and, finally, an update of the noise precision parameter. Note that the message-passing operations done through the channel code factor node can be replaced by SISO BCJR decoding. In this case, the SP messages $n_{c_{m,k}\to f_{\mathcal{M}_m}}$ can be identified to be the extrinsic values of the coded bits output by the BCJR decoder.

We refer to the described architectures as Iterative - Data-aided Joint Channel estimation - Data Decoding (I-DJC-DD) for the receiver using the joint channel weights model and Iterative - Data-aided Sequential Channel estimation - Data Decoding (I-DSC-DD) for the receiver obtained using the disjoint channel weights model.

2) DJC-DD and DSC-DD Receivers: We introduce now a class of receivers which perform iterative data-aided channel weights and noise precision estimation together with equalization and demodulation of the transmitted symbols. Compared to the receivers presented before, channel decoding is left outside of the iterative process, and is performed only once at the end after convergence of the algorithm. The receiver capitalizes on just the knowledge of the complex modulation structure of the transmitted signal to refine its channel estimates, and not on the code structure. This receiver architecture is obtained by applying a special scheduling to the message computation and exchange between the subgraphs. Specifically, no messages are passed from variable nodes $\boldsymbol{x}_m^{(d)}$ to factor nodes $f_{\mathcal{M}_m}$ until the last iteration of the algorithm. Instead, after the messages $m_{f_{\mathrm{O}}\to\boldsymbol{x}_m^{(d)}}$ are computed, the updated message $n_{\boldsymbol{x}_m^{(d)}\to f_{\mathrm{O}}}$ is directly computed using (16). To this end, an initial value of the messages $m_{f_{\mathcal{M}_m}\to x_m^{(d)}}$ is needed. This can be obtained by setting

$$\beta_{x_m^{(d)}(i)}(s) = \frac{1}{|\mathcal{S}_m|} \quad \forall m = 1,\ldots,M, i = 1,\ldots,N_d, s \in \mathcal{S}_m$$

in (15). In the expression above, $|\mathcal{S}_m|$ denotes the cardinality of the set $\mathcal{S}_m$. Note that this initialization corresponds to assuming that all modulated symbols in the constellation are equally likely, which is a valid assumption when the information bits are equiprobable and the channel code is regular.

As for the previous receivers, an initialization of the beliefs of the channel weight vector, noise precision and transmitted symbols is required. The channel weight vectors are initialized as a Gaussian pdf, with mean obtained from a pilot-based LMSSE channel estimator and null covariance. Similarly, the beliefs of the transmitted symbols are also set to a Gaussian pdf with mean and covariance values obtained from a MIMO MLD (no BCJR decoding is done, as opposed to the I-DJC-DD and I-DSC-DD receivers). An initial estimate of the noise precision is then obtained following the procedure in Section IV-A. After the initialization, the receiver operates by iteratively updating the beliefs of the channel weights (either jointly as in Fig. 4, or sequentially as in Fig. 5), the transmitted symbols and noise precision parameter. After convergence of the algorithm (or maximum number of iterations attained), the messages $n_{\boldsymbol{x}_m^{(d)} \to f_{\mathcal{M}_m}}$ are computed, and a round of decoding based on the SP algorithm is performed, yielding the beliefs of the information bits.

We refer to these receivers as Data-aided Joint Channel estimation - Data Decoding (DJC-DD) for the receiver using the joint channel weight prior model (Section IV-B1) and Data-aided Sequential Channel estimation - Data Decoding (DSC-DD) for the receiver using the disjoint channel weight prior model (Section IV-B2).

3) PSC-DD Receiver: Finally we present a simple receiver consisting of a pilot-aided channel estimator, a MIMO maximum likelihood detector (MLD) and data decoding. The channel estimation module is based on the VMP-SP generic receiver described in Section IV. It updates iteratively the beliefs of the channel weight vectors corresponding to each transmit antenna and the noise precision. To this end, the channel estimator only exploits the pilot signals transmitted from each transmit antenna and does not capitalize on data symbols to refine its estimates.

In order to obtain this pilot-aided channel estimator from the generic receiver architecture in Section IV, the messages $n_{\boldsymbol{x}_m^{(d)} \to f_{\mathrm{O}}}$ must be set to

$$n_{\boldsymbol{x}_m^{(d)} \to f_{\mathrm{O}}}(\boldsymbol{x}_m^{(d)}) = \prod_i \delta(x_m^{(d)}(i)).$$

This enforces that data symbols are not employed for channel weight estimation. In addition, the disjoint channel weights setup (see Fig. 5) is selected. With this configuration, the output messages $\boldsymbol{N}_{\mathrm{M}}$ are constant, reflecting the receiver's knowledge on the value of the pilot symbols. Hence, expectations taken over $\boldsymbol{N}_{\mathrm{M}}$ in the channel weights and noise precision subgraphs reduce to the value of the pilot symbols (or zero for data symbols), with all second-order terms vanishing. Note that, for this channel estimator, no update of the beliefs of the data symbols is performed. Equalization and decoding are done outside the VMP-SP framework.

Additionally, a small modification in the processing corresponding to the noise precision subgraph is required. Note that, for the computation of the message $m_{f_{\mathrm{O}} \to \lambda}$, the signal received at all –pilot and data– subcarriers is used, while only the signals received at pilot positions are utilized for channel weight estimation. This can be avoided by restricting this message to include only the observation at pilot positions, i.e. calculating $m_{f_{\mathrm{O}^{(p)}} \to \lambda}$ instead, where

$$f_{\mathrm{O}^{(p)}}(\boldsymbol{y}^{(p)}, \boldsymbol{x}^{(p)}, \boldsymbol{h}^{(p)}, \lambda) \triangleq p(\boldsymbol{y}^{(p)} | \boldsymbol{x}^{(p)}, \boldsymbol{h}^{(p)}, \lambda) \propto \lambda^{N^{(p)}} \exp\left\{ -\lambda \left\| \boldsymbol{y}^{(p)} - \boldsymbol{X}^{(p)} \boldsymbol{h}^{(p)} \right\|^2 \right\},$$

with $N^{(p)}$ denoting the total number of pilots in a frame.

The initialization for this estimator is simpler compared to that of the other receivers. It consists of setting the beliefs of the channel weight vector corresponding to each transmit antenna to a Gaussian prior with zero mean and zero covariance, while an initial value for the noise precision can be obtained from the signal received at pilot subcarriers. The receiver operates by sequentially updating the channel weight vectors corresponding to each transmitter $\boldsymbol{h}_1, \ldots, \boldsymbol{h}_M$ following the procedure described in Section IV-B2. This is followed by an update of the noise precision parameter. The channel responses belonging to each transmit antenna obtained after convergence of the iterative estimator are fed to a MIMO maximum

TABLE II
SUMMARY OF RECEIVER STRUCTURES

	Initialization		Operation	
Receiver	Channel Weights	Transmitted Symbols	Channel Weight Model	Demodulation & Decoding
PSC-DD	Null mean and covariance	–	Disjoint	–
DJC-DD	LMMSE estimator	ML detector	Joint	Demodulation only
DSC-DD	LMMSE estimator	ML detector	Disjoint	Demodulation only
I-DJC-DD	LMMSE estimator	MLD + BCJR	Joint	Demodulation and decoding
I-DSC-DD	LMMSE estimator	MLD + BCJR	Disjoint	Demodulation and decoding

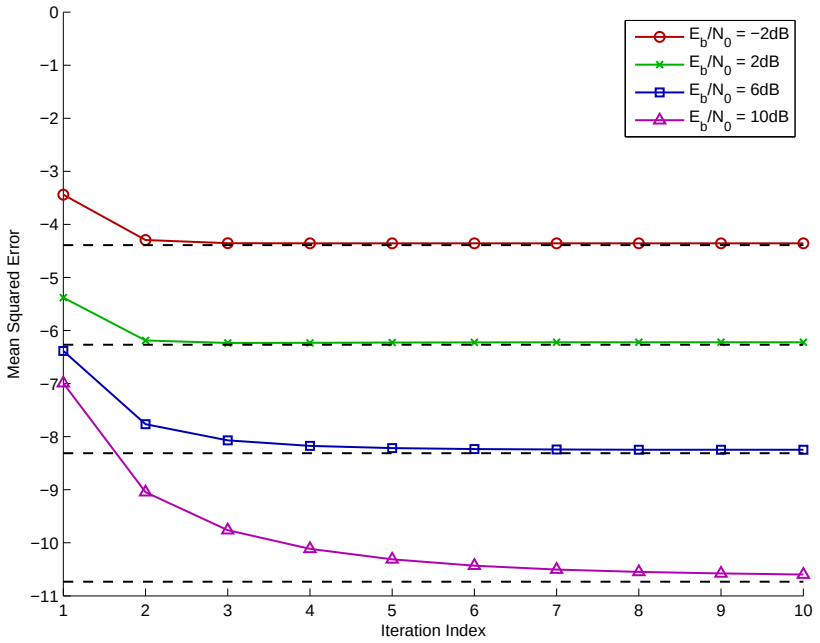

Fig. 7. MSE of the estimates of the channel weights for the PSC-DD receiver versus the iteration index. 13 pilot symbols are inserted per OFDM frame. The dashed black lines represent the MSE obtained with pilot-based LMMSE joint channel estimation.

likelihood detector (MLD), followed by BCJR decoding. Thus, we can obtain BER performance results and benchmark them with analogous receiver structures using a different channel estimator.

As we will see in the performance evaluation, this iterative estimator approximates the performance of a pilot-based joint LMMSE channel estimator with perfect knowledge of the noise variance. The iterative estimator, however, presents the advantage of avoiding cumbersome matrix inversions depending on the specific values of the pilot-symbols. This estimator was presented (outside the context of message-passing techniques) in [34]. A more detailed discussion of the computational advantages of this estimator over the LMMSE estimator is provided in this contribution.

In the following, we refer to this receiver as Pilot-aided Sequential Channel estimation - Data Decoding (PSC-DD) receiver.

The main characteristics of all the receivers presented above are summarized in Table II.

C. Numerical Results

We evaluate separately the performance of the three architectures described in Section V-B, beginning with the simplest scheme, the PSC-DD receiver; we follow with the DJC-DD and DSC-DD receivers and conclude with the most advanced structures: the I-DJC-DD and I-DSC-DD receivers.

In Fig. 7, the mean squared error (MSE) of the estimates of the channel weights obtained with the PSC-DD receiver is depicted. The MSE is plotted for three different E_b/N_0 values as a function of the number of iterations performed. It is observed that the performance of the sequential pilot-based

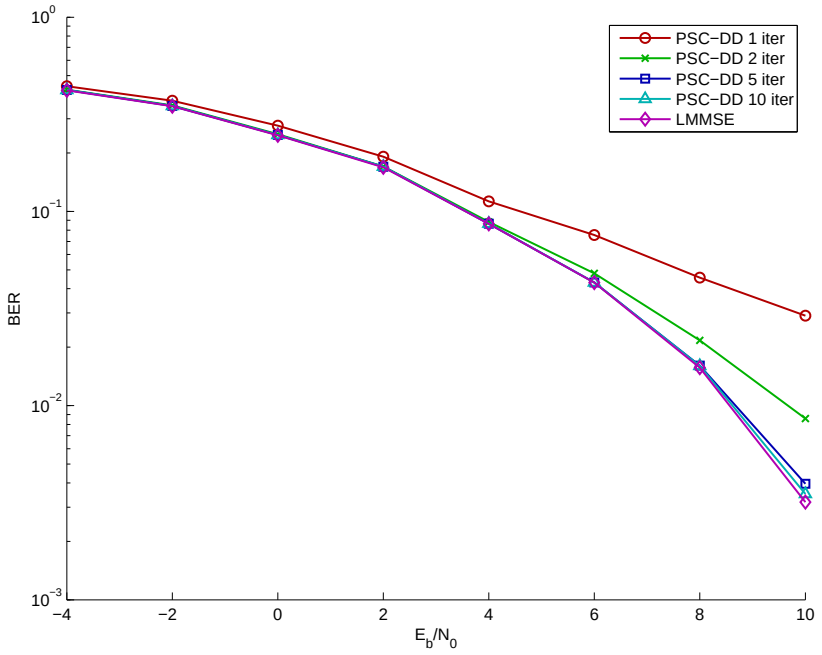

Fig. 8. BER as a function of E_b/N_0 for the PSC-DD receiver with QPSK modulation. 13 pilot symbols are inserted per OFDM frame. The BER performance of a similar receiver using LMMSE channel estimation with knowledge of the noise variance is included as a reference.

estimator approaches the performance of a joint LMMSE estimator with sufficient number of iterations. It is especially interesting to note the dependency of the number of iterations required for convergence on the E_b/N_0 value. For $E_b/N_0 = -2$dB and $E_b/N_0 = 2$dB, between 2 and 3 iterations are sufficient to achieve an MSE virtually equal to the LMMSE bound. When increasing E_b/N_0 to 6dB, however, a minimum number of 5 iterations is needed, and about 10 iterations are required for $E_b/N_0 = 10$dB. Similar observations can be made when evaluating the BER of the receiver with QPSK modulation, as shown in Fig. 8. Again, the performance of the PSC-DD receiver equals that of the receiver with the LMMSE estimator when enough iterations for the receiver to converge have been run, and fewer iterations are needed the smaller E_b/N_0 is. These results suggest that the iterative channel estimator in the PSC-DD receiver would be a good choice to obtain an initial channel estimate for the more complex iterative structures that we will discuss next. Furthermore, this channel estimator has the additional benefit of outputting soft estimates (the beliefs) of both the channel weights and the noise precision. Classical channel estimators, on the other hand, typically require separate noise estimation prior to the estimation of the channel weights, and only provide hard (point) estimates.

BER results for the DJC-DD and DSC-DD receivers are portrayed in Fig. 9. The results have been obtained using a QPSK constellation for the modulation of data symbols. They indicate that a significant performance gain can be obtained by iteratively updating the channel weights, transmitted data symbols and noise precision parameter after the initialization, even though the receiver does not capitalize on the code structure within the iterative process. For both receivers (with joint and sequential channel estimation), most of the improvement with respect to the initialization is obtained in the first three iterations, with only marginal gains obtained after further processing. Regarding the channel estimation approach, DJC-DD leads to a slightly better performance than DSC-DD in the whole simulated E_b/N_0 range; the improved accuracy of the joint estimation approach comes at the expense of a larger computational complexity, as it operates with vectors and matrices of dimensions M times as large as in the sequential estimation approach, which can be a problem when calculating the necessary matrix inversions.

Note that the receivers evaluated in Fig. 9 operate by capitalizing on the structure of the constellation used for the modulation of data symbols. Hence, their performance strongly depends on the type of modulation used. Low-order modulations, such as BPSK or QPSK, favor this receiver, as there is a relatively large

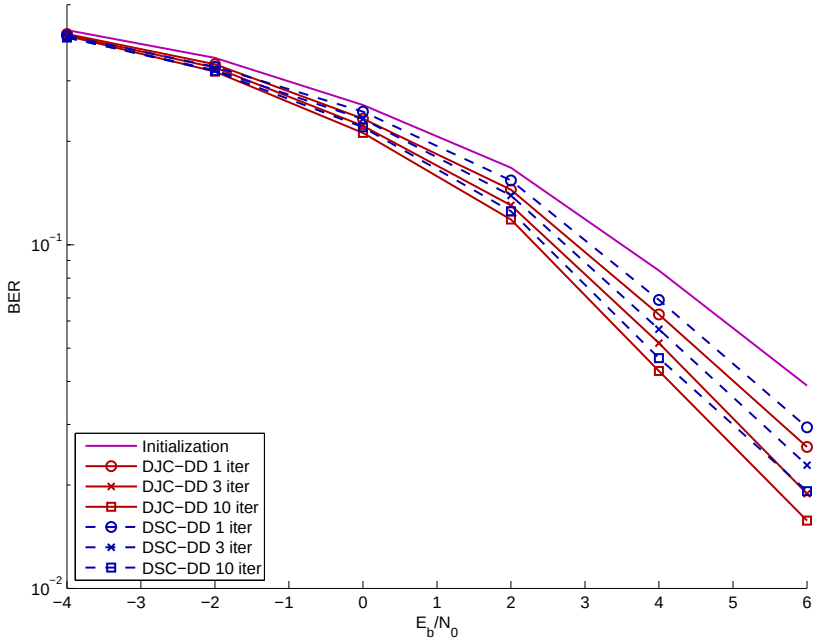

Fig. 9. BER as a function of E_b/N_0 for the DJC-DD and DSC-DD receivers with QPSK modulation. 13 pilot symbols are inserted per OFDM frame.

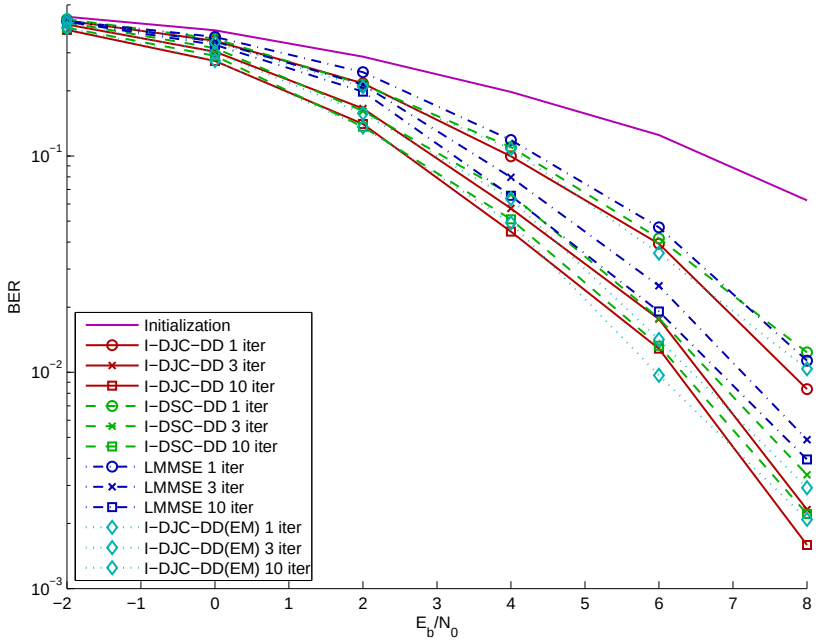

Fig. 10. BER as a function of E_b/N_0 for the I-DJC-DD and I-DSC-DD receivers with 16-QAM modulation. 13 pilot symbols are inserted per OFDM frame.

distance between the points in the constellation, allowing better refining (through SP message-passing) of the VMP estimates of the transmitted symbols. When using higher order modulations, however, the receiver's performance suffers from the relatively small distance between adjacent constellation points. Specifically for the system investigated in this work, we found that the DJC-DD and DSC-DD receivers for 16-QAM or higher order modulations do not improve the performance with respect to the initialization.

The aforementioned problem with high-order modulations can be circumvented with the inclusion of the channel code structure in the iterative processing, as done in the I-DJC-DD and I-DSC-DD receivers.

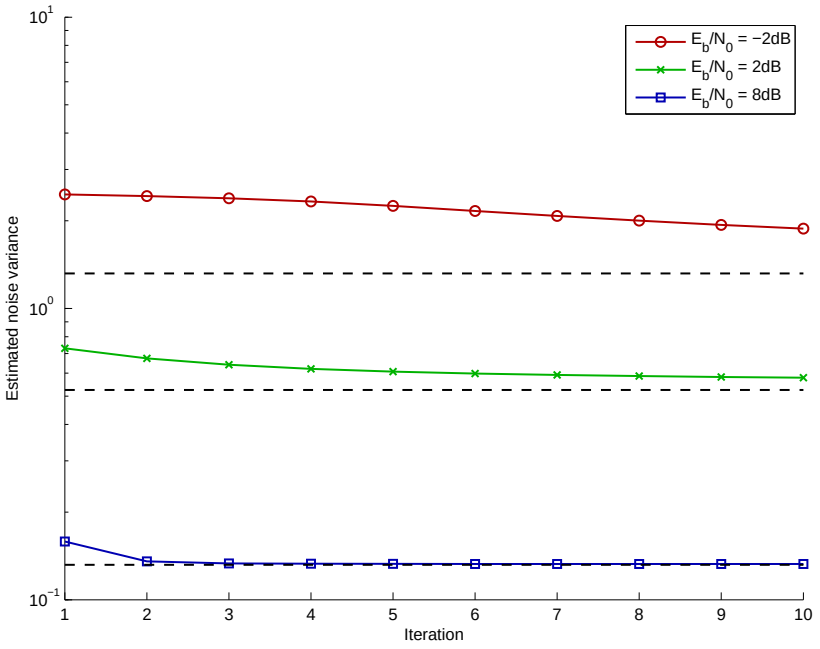

Fig. 11. Average noise variance estimated by the I-DJC-DD receiver as a function of the iteration index. 13 pilot symbols are inserted per OFDM frame. The dashed black lines represent the true noise variance for each E_b/N_0 value.

The BER performance of both receivers with 16-QAM modulated data symbols is depicted in Fig. 10. For benchmarking purposes, the BER performance of a heuristically designed iterative receiver with analogous features to the I-DJC-DD receiver is also plotted. We refer to this receiver as LMMSE receiver, as the channel estimation and MIMO detection modules are separately designed after the LMMSE principle. The LMMSE receiver is based on the design proposed in [9] for a multiuser CDMA receiver, and was adapted to MIMO-OFDM in [40], where a detailed description of its operational principles can be found. In addition, the BER performance of a modified version of the I-DJC-DD receiver has also been included. This receiver, which we denote as I-DJC-DD(EM) receiver, results from applying the EM restriction to the beliefs of the channel weights $\boldsymbol{h}$ and the noise precision parameter λ. Thus, this receiver is identical to the I-DJC-DD receiver except that the messages $n_{\boldsymbol{h}\to f_{\mathrm{O}}}$ and $n_{\lambda\to f_{\mathrm{O}}}$ are computed according to (7). This modified messages imply that all terms depending on the second order moments of $b_{\boldsymbol{h}} = n_{\boldsymbol{h}\to f_{\mathrm{O}}}$ vanish.

The results show that vast improvements in BER of the I-DJC-DD and I-DSC-DD receivers with respect to the initialization are obtained, even for very low E_b/N_0 values. As in the case of the DJC-DD and DSC-DD receivers, joint estimation of the channel weights performs marginally better than sequential estimation. Both message-passing receivers clearly outperform the heuristic LMMSE receiver, with E_b/N_0 gains close to 1dB at a BER of 1%. We explain these gains by the fact that, contrary to the separate design of the different modules in the LMMSE receiver, our VMP-SP receivers are analytically derived based on a global objective function, namely the region-based free energy. This global design ensures that the information shared by the different receiver components is treated correctly, and resolves the choice of the appropriate type of information to be passed from the channel decoder to the other component parts of the receiver. It is also remarkable that the EM-constrained version of the I-DJC-DD receiver achieves roughly the same performance as the non-constrained version. This result seems to indicate that there is no significant gain to be achieved by computing soft channel estimates as compared to just point estimates, at least for the system considered.

Another key feature of the I-DJC-DD and I-DSC-DD receivers is the estimation of the noise precision. This functionality does not only account for the AWGN, but also includes inaccuracies in the estimates of the channel weights and data symbols. Fig. 11 depicts the averaged noise variance estimate (inverse of the noise precision estimate λ) provided by the I-DJC-DD receiver as a function of the iteration index

for three different E_b/N_0 levels. The true AWGN variances are also depicted as dashed black lines. It is apparent from the results that the behavior of the noise variance estimates (with respect to the true value) depends heavily on the regime in which the receiver is operating. For the very low E_b/N_0 regime, the receiver significantly overestimates the noise variance; this is due to the low accuracy of the channel weights estimates and the large amount of errors in the estimates of the data symbols obtained. At the other extreme, for high E_b/N_0 values, the estimates of the channel weights and data symbols become so accurate (as it can be observed from the low BER values) that the noise variance estimate rapidly converges to the true AWGN variance, as the contribution of the estimates' inaccuracies becomes negligible. In the medium E_b/N_0 range, the noise variance estimate slowly converges to a value larger than the true variance, the difference between both values depending again on the accuracy of the other parameters' estimates.

Conceptually, the estimate of the noise precision represents the amount of 'trust' that the algorithm has on the beliefs of the channel weights and data symbols. With high noise precision values, the receiver has high confidence on these beliefs, leading to a rapid convergence towards a stable solution. On the contrary, low noise precision values will yield slower changes on the beliefs from one iteration to the next, resulting in a slower convergence rate.

VI. Conclusion

In this article we have used a hybrid VMP-SP message passing framework [41], [42] for the design of iterative receivers for wireless communication. The framework has been applied to the factor graph of a generic MIMO-OFDM system. The messages obtained from the generic derivation have been used to obtain a set of receiver architectures ranging from computationally simple solutions to full-scale iterative architectures performing channel weight estimation, noise precision estimation, MIMO equalization and channel decoding. The performance of the proposed receivers has been assessed and compared to state-of-the-art solutions via Monte Carlo simulations.

A fundamental contribution of this work is the application of a unified framework that jointly optimizes the receiver architecture based on a global cost function, namely the region-based variational free energy. The message-passing scheme used in this work can be obtained from the equations of the stationary points of a particular region-based free energy approximation. The resulting algorithm applies the VMP and SP algorithms to different parts of the graph and unequivocally defines how the messages of the two respective frameworks are to be combined. As a result, the hybrid technique allows for a convenient design of wireless receivers in which the SP algorithm is used for demodulation and channel decoding and the VMP algorithm is applied for channel weight estimation, noise covariance estimation and MIMO equalization. The connection between the specific receiver component parts is defined by the message-computation rules, in contrast to other approaches in which the selection of information to be exchanged among the specific receiver components is done based on numerical results and/or intuitive argumentation.

We illustrate the application of the framework by applying it to the design of receivers in a MIMO-OFDM communications system. From the factor-graph representing the underlying probabilistic model, a set of generic messages exchanged between different parts of the model, represented by sub-graphs, is derived. We choose to split the factor graph in three main subgraphs corresponding to the channel weights prior model, the noise precision model and the modulation and coding constraints. The advantage of this modular approach is that it enables a scalable, flexible design of the receiver in which the modification of a specific sub-graph does not modify the processing performed in other parts of the graph. Thus, a collection of different receiver architectures can be obtained by applying different initialization and scheduling strategies.

In order to assess the performance of the receivers derived with the proposed framework, we define five specific instances of the generic message-passing receiver. The particular architectures selected span from to full-scale iterative schemes, in which the output of the channel decoder is used to refine the estimates of the channel parameters and the transmitted symbols, to low-complexity solutions, in which only pilot symbols are used for channel weight and noise variance estimation. This particular selection

of receiver architectures serves as an illustration of how the tradeoff between computational complexity and receiver performance can be adjusted, with the generic message-passing receiver as a starting point. The numerical results, obtained via Monte Carlo simulations in a realistic MIMO-OFDM setup, confirm the effectiveness of the receivers derived following the hybrid VMP-SP framework. In particular, the convergence behavior of the receivers tested is especially remarkable. All receiver instances yield an improved or equal performance with increasing number of iterations, both in terms of BER and MSE of the channel weight estimates. We explain these favorable convergence properties by the use of the unique, global cost function from which the algorithm is derived. The estimation of the noise precision parameter, accounting for the uncertainty on the estimates of the channel weights and transmitted symbols in addition to the AWGN variance, is another key feature of the proposed architecture.

REFERENCES

[1] D. Gesbert, M. Shafi, D. shan Shiu, P. Smith, and A. Naguib, "From theory to practice: an overview of MIMO space-time coded wireless systems," *Selected Areas in Communications, IEEE Journal on*, vol. 21, no. 3, pp. 281 – 302, apr 2003.

[2] C. Berrou, A. Glavieux, and P. Thitimajshima, "Near Shannon limit error-correcting coding and decoding: Turbo codes," in *IEEE Int. Conf. Commun. (ICC)*, May 1993, pp. 1064–1070.

[3] R. Gallager, "Low-density parity-check codes," *IEEE Trans. Inform. Theory*, vol. 8, no. 1, pp. 21–28, Jan. 1962.

[4] E. Telatar, "Capacity of multi-antenna Gaussian channels," *European Transactions on Telecommunications*, vol. 10, pp. 585–595, 1999.

[5] L. Zheng and D. N. C. Tse, "Diversity and multiplexing: a fundamental tradeoff in multiple-antenna channels." *IEEE Transactions on Information Theory*, pp. 1073–1096, 2003.

[6] X. Wang and H. Poor, "Iterative (turbo) soft interference cancellation and decoding for coded CDMA," *IEEE Trans. Commun.*, vol. 47, pp. 1046–1061, Jul. 1999.

[7] R. Koetter, A. C. Singer, and M. Tücher, "Turbo equalization," *IEEE Trans. Signal Processing*, vol. 1, pp. 64–80, 2004.

[8] M. Lončar, R. Müller, J. Wehinger, C. Mecklenbräuker, and T. Abe, "Iterative channel estimation and data detection in frequency-selective fading MIMO channels," *Euro. Trans. Telecomms*, vol. 15, pp. 459–470, 2004.

[9] J. Wehinger and C. Mecklenbräuker, "Iterative CDMA multiuser receiver with soft decision-directed channel estimation," *IEEE Trans. Signal Processing*, vol. 54, pp. 3922–3934, Oct. 2006.

[10] P. Rossi and R. Müller, "Joint twofold-iterative channel estimation and multiuser detection for MIMO-OFDM systems," *IEEE Trans. Wireless Commun.*, vol. 7, no. 11, pp. 4719–4729, Nov. 2008.

[11] M. Wainwright and M. Jordan, "Graphical models, exponential families, and variational inference," *Foundations and Trends in Machine Learning*, vol. 1, no. 1-2, pp. 1–305, Dec. 2008.

[12] J. Winn and C. Bishop, "Variational message passing," *Journal of Machine Learning Research*, 2004.

[13] C. Bishop, *Pattern Recognition and Machine Learning*. Springer, 2006.

[14] J. Yedidia, W. Freeman, and Y. Weiss, "Constructing free-energy approximations and generalized belief propagation algorithms," *IEEE Trans. Inform. Theory*, vol. 51, no. 7, pp. 2282–2312, July 2005.

[15] T. Minka, "Divergence measures and message passing," Microsoft Research Ltd., Tech. Rep., 2005.

[16] J. Pearl, *Probabilistic reasoning in intelligent systems: networks of plausible inference*. Morgan Kaufmann, 1988.

[17] F. Kschischang, B. Frey, and H.-A. Loeliger, "Factor graphs and the sum-product algorithm," *IEEE Trans. Inform. Theory*, vol. 47, no. 2, pp. 498–519, Feb. 2001.

[18] K. P. Murphy, Y. Weiss, and M. I. Jordan, "Loopy belief propagation for approximate inference: an empirical study," in *Proceedings of uncertainty in artificial intelligence*, 1999, pp. 467–475.

[19] R. McEliece, D. MacKay, and J. Cheng, "Turbo decoding as an instance of Pearl's belief "propagation" algorithms," *IEEE J. Select. Areas Commun.*, vol. 16, no. 2, pp. 140–152, Feb. 1998.

[20] J. Boutros and G. Caire, "Iterative multiuser joint decoding: unified framework and asymptotic analysis," *IEEE Trans. Inform. Theory*, vol. 48, no. 7, pp. 1772–1793, Jul 2002.

[21] H.-A. Loeliger, J. Dauwels, J. Hu, S. Korl, L. Ping, and F. Kschischang, "The factor graph approach to model-based signal processing," *Proceedings of the IEEE*, vol. 95, no. 6, pp. 1295–1322, Jun. 2007.

[22] G. Colavolpe and G. Germi, "On the application of factor graphs and the sum-product algorithm to ISI channels," *IEEE Trans. Commun.*, vol. 53, no. 5, pp. 818–825, 2005.

[23] C. Novak, G. Matz, and F. Hlawatsch, "A factor graph approach to joint iterative data detection and channel estimation in pilot-assisted IDMA transmissions," in *Acoustics, Speech and Signal Processing, 2008. ICASSP 2008. IEEE International Conference on*, 31 2008-april 4 2008, pp. 2697 –2700.

[24] A. P. Worthen and W. E. Stark, "Unified design of iterative receivers using factor graphs," *IEEE Trans. Inform. Theory*, vol. 47, no. 2, pp. 843–849, 2001.

[25] T. Moon, "The expectation maximization algorithm," *IEEE Signal Processing Mag.*, pp. 47–60, 2004.

[26] C. Novak, F. Hlawatsch, and G. Matz, "Low-complexity factor graph receivers for spectrally efficient MIMO-IDMA," in *Communications, 2008. ICC '08. IEEE International Conference on*, may 2008, pp. 770 –774.

[27] C. Novak, G. Matz, and F. Hlawatsch, "Factor graph based design of an OFDM-IDMA receiver performing joint data detection, channel estimation, and channel length selection," in *Acoustics, Speech and Signal Processing, 2009. ICASSP 2009. IEEE International Conference on*, april 2009, pp. 2561 –2564.

[28] H. Attias, "Inferring parameters and structure of latent variable models by variational Bayes," in *Proceedings of the Fifteenth Conf. on Uncertainty in Artificial Intelligence*, 1999, pp. 21–30.

[29] M. Beal, "Variational algorithms for approximate inference," Ph.D. dissertation, University of Cambridge, May 2003.
[30] T. Cover and J. Thomas, *Elements of Information Theory*, 2nd ed. Wiley Interscience, 2006.
[31] G. Parisi, *Statistical Field Theory*. Perseus Books, 1988.
[32] L. Christensen and J. Larsen, "On data and parameter estimation using the variational Bayesian EM-algorithm for block-fading frequency-selective MIMO channels," in *Proc. IEEE In. Conf. on Acoustics, Speech and Sign. Process.*, vol. 4, 2006, pp. 465–468.
[33] B. Hu, I. Land, L. Rasmussen, R. Piton, and B. Fleury, "A divergence minimization approach to joint multiuser decoding for coded CDMA," *IEEE J. Select. Areas Commun.*, vol. 26, no. 3, pp. 432–445, Apr. 2008.
[34] C. N. Manchon, B. Fleury, G. Kirkelund, P. Mogensen, L. Deneire, T. Sorensen, and C. Rom, "Channel estimation based on divergence minimization for OFDM sytems with co-channel interference," in *IEEE Int. Conf. Commun. (ICC'09)*, 2009.
[35] C. N. Manchon, G. E. Kirkelund, B. H. Fleury, P. Mogensen, L. Deneire, T. B. Sorensen, and C. Rom, "Interference cancellation based on divergence minimization for mimo-ofdm receivers," in *Global Telecommunications Conference, 2009. GLOBECOM 2009. IEEE*, 30 2009-dec. 4 2009, pp. 1 –6.
[36] D. Lin and T. Lim, "The variational inference approach to joint data detection and phase noise estimation in OFDM," *IEEE Trans. Signal Processing*, vol. 55, no. 5, pp. 1862–1874, May 2007.
[37] M. Nissilä, "Iterative receivers for digital communications via variational inference and estimation," Ph.D. dissertation, University of Oulu, 2008.
[38] X.-Y. Zhang, D.-G. Wang, and J.-B. Wei, "Joint symbol detection and channel estimation for MIMO-OFDM systems via the variational Bayesian EM algorithms," in *Wireless Commun. and Networking Conf., WCNC. IEEE*, Mar.-Apr. 2008, pp. 13–17.
[39] J. Dauwels, "On variational message passing on factor graphs," in *Information Theory, 2007. ISIT 2007. IEEE International Symposium on*, Jun. 2007, pp. 2546–2550.
[40] G. Kirkelund, C. Manchon, L. Christensen, E. Riegler, and B. Fleury, "Variational message-passing for joint channel estimation and decoding in MIMO-OFDM," in *GLOBECOM 2010, 2010 IEEE Global Telecommunications Conference*, Dec. 2010, pp. 1 –6.
[41] E. Riegler, G. Kirkelund, C. Manchón, and B. Fleury, "Merging belief propagation and the mean field approximation: A free energy approach," in *Turbo Codes and Iterative Information Processing (ISTC), 2010 6th International Symposium on*, sept. 2010, pp. 256 –260.
[42] E. Riegler, G. E. Kirkelund, C. N. Manchón, and B. H. Fleury, "Merging belief propagation and the mean field approximation: A free energy approach," *IEEE Trans. Inform. Theory*, submitted for publication.
[43] J. Tauge and C. Caldwell, "Expectations of useful complex Wishart forms," *Multidimensional Systems and Signal Processing archive*, vol. 5, pp. 263–278, 1994.
[44] 3GPP, "Base station (BS) radio transmission and reception," 3GPP TS 36.212, V8.12.0 (2011-06) Technical Specification, 2011.

Paper D

Sparse Estimation using Bayesian Hierarchical Prior Modeling for Real and Complex Models

Niels L. Pedersen, Dimitriy Shutin, Carles Navarro Manchón and Bernard H. Fleury

Under revision for re-submission to IEEE Transactions on Signal Processing, November 2011.

Sparse Estimation using Bayesian Hierarchical Prior Modeling for Real and Complex Models

Niels Lovmand Pedersen*, Dmitriy Shutin†, Carles Navarro Manchón*, Bernard Henri Fleury*

*Department of Electronic Systems, Aalborg University

Niels Jernes Vej 12, DK-9220 Aalborg, Denmark, Email: {nlp,cnm,bfl}@es.aau.dk

†Department of Electrical Engineering, Princeton University

E-QUAD B311, Olden Street, Princeton, 08544 NJ, USA, Email: dshutin@princeton.edu

Abstract

Sparse modeling and estimation of complex signals is not uncommon in practice. However, historically, much attention has been drawn to real-valued system models, lacking the research of sparse signal modeling and estimation for complex-valued models. This paper introduces a unifying sparse Bayesian formalism that generalizes to complex- as well as real-valued systems. The methodology relies on hierarchical Bayesian sparsity-inducing prior modeling of the parameter of interest. This approach allows for the Bayesian modeling of ℓ_1-norm constraint for complex-valued as well as real-valued models. In addition, the proposed two-layer hierarchical model allows for the design of novel priors for sparse estimation that outperform the Bayesian formulation of the ℓ_1-norm constraint and lead to estimators approximating a soft-thresholding rule. An extension of the two-layer model to a three-layer model is also presented. Varying the free parameters of the three-layer model leads to estimators that approximate a hard-thresholding rule. Finally, a variational message-passing (VMP) implementation of the proposed Bayesian method that effectively exploits the hierarchical structure of the inference problem is presented. The simulation results show that the VMP algorithm outperforms existing sparse methods both in terms of the sparsity of the estimation results and achieved mean squared error in low and moderate SNR regimes.

This work was supported in part by the 4GMCT cooperative research project funded by Intel Mobile Communications, Agilent Technologies, Aalborg University and the Danish National Advanced Technology Foundation. This research was also supported in part by the project ICT- 248894 Wireless Hybrid Enhanced Mobile Radio Estimators (WHERE2) and by Erwin Schrödinger Postdoctoral Fellowship, Austrian Science Fund (FWF) Project J2909-N23.

I. INTRODUCTION

During the last decade the research on compressive techniques and sparse signal representations has received considerable attention (see e.g., [1]–[4]). With a few minor variations, the general goal of sparse reconstruction is to estimate the parameter vector $\boldsymbol{\alpha}$ of the following canonical model:

$$\boldsymbol{y} = \boldsymbol{H}\boldsymbol{\alpha} + \boldsymbol{w}. \tag{1}$$

In this expression $\boldsymbol{y}$ is a $M \times 1$ vector of measurement samples, $\boldsymbol{H} = [\boldsymbol{h}_1, \ldots, \boldsymbol{h}_L]$ is an $M \times L$ measurement matrix with L column vectors $\boldsymbol{h}_l$. The additive term $\boldsymbol{w}$ is an $M \times 1$ perturbation vector, which is assumed to be a white Gaussian random vector with zero-mean and covariance matrix $\boldsymbol{\Sigma} = \lambda^{-1}\boldsymbol{I}$ with $\lambda > 0$ being the noise precision parameter. The unknown $L \times 1$ parameter vector $\boldsymbol{\alpha} = [\alpha_1, \ldots, \alpha_L]^T$ has only K non-zero entries, i.e., $\boldsymbol{\alpha}$ is assumed to be K-sparse. System model (1) can be either real-valued, when $\boldsymbol{H}$ and $\boldsymbol{w}$ are real and $\boldsymbol{\alpha}$ is real [1], [2], or complex-valued, when $\boldsymbol{H}$ or $\boldsymbol{w}$ is complex and $\boldsymbol{\alpha}$ is complex as well.

Historically, a real-valued system model has dominated the research in sparse signal reconstruction and compressive sampling techniques. However, complex systems are not so uncommon in practice in which sparse parameter estimation is sought as well. An example is the estimation of the dominant multipath components in the response of wireless channels [4], [5]. Motivated by the lack of formal tools for sparse learning in complex-valued system models and inspired by the recent developments of sparse Bayesian methods [3], [6]–[11] we propose a unifying sparse Bayesian formalism that applies to both real- and complex-valued system models. The formalism enables to generalize and improve the sparse Bayesian methods proposed nowadays.

Sparse Bayesian learning (SBL) [3], [12], [13] applied to model (1) aims at finding a sparse *maximum a posteriori* (MAP) estimate of $\boldsymbol{\alpha}$

$$\widehat{\boldsymbol{\alpha}}_{\mathrm{MAP}} = \underset{\boldsymbol{\alpha}}{\operatorname{argmin}} \left\{ \rho \|\boldsymbol{y} - \boldsymbol{H}\boldsymbol{\alpha}\|_2^2 + \lambda^{-1} Q(\boldsymbol{\alpha}) \right\}, \tag{2}$$

with $\rho = 1/2$ (real model) or $\rho = 1$ (complex model), the Euclidean norm $\|\cdot\|_2$, and the penalty term $Q(\boldsymbol{\alpha}) \propto^e -\log p(\boldsymbol{\alpha})$,[1] by modeling the prior $p(\boldsymbol{\alpha})$ using a hierarchical structure, which involves a conditional prior $p(\boldsymbol{\alpha}|\boldsymbol{\gamma})$ and a hyperprior $p(\boldsymbol{\gamma})$. The hierarchical approach to the representation of sparsity-inducing prior has several important advantages. First of all, one is free to choose the prior pdfs in the formulation of the hierarchical structure, which is advantageous for the generalization of

[1] $x \propto^e y$ denotes $\exp(x) = \exp(\beta)\exp(y)$ and thus $x = \beta + y$ for some arbitrary constant β.

SBL for complex- and real-valued system models. When carefully chosen, the resulting hierarchical structure also allows for the construction of efficient inference algorithms, in terms of sparsity enhancing capability, and an analytical derivation of the inference expressions. Second, the two-layer hierarchy can be naturally extended with an additional hierarchy tier by treating the parameters of the hyperprior – the hyperparameters – as random variables specified by a hyper-hyperprior distribution. This yields additional degrees of freedom in controlling the sparsity properties of the resulting inference scheme, as will be demonstrated later in this work.

The SBL methodology has developed following two distinct approaches that differ in the way the hierarchical prior model is constructed. The first approach is exemplified by the relevance vector machines (RVMs) [12]. In RVM, each component of $\boldsymbol{\alpha}$ is independently constrained using a two-layer hierarchical prior $p(\alpha_l|\gamma_l)p(\gamma_l)$, where $p(\alpha_l|\gamma_l)$ is a Gaussian probability density function (pdf) with zero-mean and variance γ_l, and $p(\gamma_l) \equiv p(\gamma_l; a_l, b_l) = b_l^{a_l}\gamma_l^{-a_l-1}\exp(-b_l/\gamma_l)/\Gamma(a_l)$ is an inverse gamma hyperprior pdf with parameters a_l and b_l.[2] Further in the text we refer to this formulation of the hierarchical prior pdf as a Gaussian-Inverse gamma (G-IGa) prior model. Notice that the G-IGa prior model applies equally well to the modeling of complex-valued as well as real-valued α_l. Using the G-IGa prior model an RVM algorithm is then formulated to estimate the hyperparameters $\boldsymbol{\gamma} = [\gamma_1, \ldots, \gamma_L]^T$ by maximizing its posterior pdf $p(\boldsymbol{\gamma}|\boldsymbol{y}, \lambda) \propto p(\boldsymbol{\gamma}) \int p(\boldsymbol{y}|\boldsymbol{\alpha}, \lambda)p(\boldsymbol{\alpha}|\boldsymbol{\gamma})\mathrm{d}\boldsymbol{\alpha}$; as γ_l decreases it drives the corresponding weight α_l towards zero, thus encouraging a solution with only a few non-zero coefficients in $\boldsymbol{\alpha}$. It is known [12] that the prior $p(\boldsymbol{\alpha}) = \int p(\boldsymbol{\alpha}, \boldsymbol{\gamma})\mathrm{d}\boldsymbol{\gamma}$ is the product of pdfs of Student-t distributions over α_l. Under such a prior most of the probability mass is concentrated along the coordinate axes in the parameter space, thus encouraging a posterior distribution with a mode lying close to these axes in the $\boldsymbol{\alpha}$-space [13]. The analytical tractability of the resulting inference problem allows for a further analysis of SBL with these hierarchical priors, especially in case of a non-informative hyperprior $p(\boldsymbol{\gamma}) \propto \prod_{l=1}^{L}\gamma_l^{-1}$, which is also termed automatic relevance determination (ARD) [11], [12]. In the latter case the prior $p(\boldsymbol{\alpha})$ is improper: $p(\boldsymbol{\alpha}) \propto \prod_{l=1}^{L} 1/|\alpha_l|$. It leads to the log-sum penalization term $Q(\boldsymbol{\alpha}) = \sum_{l=1}^{L}\log|\alpha_l|$ in (2), which is known to strongly promote sparsity [7], [8].[3] Furthermore, ARD leads to very efficient and fast inference schemes [6], [14], [15].

The second approach to SBL was proposed in [16] for real-valued models to realize a popular ℓ_1-

[2]In the original formulation of the RVM algorithm the parameter γ_l models the precision (inverse variance) of the conditional Gaussian prior $p(\alpha_l|\gamma_l)$ and the hyperprior $p(\gamma_l; a_l, b_l)$ is a gamma pdf. The model has been reformulated here to match the framework adopted in this sequel of the paper.

[3]Note, however, that the hierarchical formulation realizes this log-sum penalty term indirectly through the product of two pdfs that form a conjugate family.

norm regularization for each component of $\boldsymbol{\alpha}$. This approach consists in independently constraining each element of $\boldsymbol{\alpha}$ using a two-layer hierarchical prior $p(\alpha_l|\gamma_l)p(\gamma_l)$. Similarly to the G-IGa model $p(\alpha_l|\gamma_l)$ is a Gaussian pdf with zero-mean and variance γ_l; however, the hyperprior $p(\gamma_l) \equiv p(\gamma_l;\eta)$ is selected as an exponential pdf with rate parameter η. We refer to this formulation of the hierarchical prior pdf as a Gaussian-exponential (G-E) prior model. It can be shown [16] that in this case the prior pdf $p(\boldsymbol{\alpha};\eta) = \int p(\boldsymbol{\alpha}|\boldsymbol{\gamma})p(\boldsymbol{\gamma};\eta)\mathrm{d}\boldsymbol{\gamma} \propto \prod_{l=1}^{L} \exp\left(-\sqrt{2\eta}|\alpha_l|\right)$ is the product of Laplace pdfs with zero-mean and scale parameter $\sqrt{2\eta}$. In this case the penalty term in (2) reads $Q(\boldsymbol{\alpha}) = \sqrt{2\eta}\|\boldsymbol{\alpha}\|_1$ with $\|\cdot\|_1$ denoting the ℓ_1-norm. The MAP estimate with this selection of $Q(\boldsymbol{\alpha})$ is called Least Absolute Shrinkage and Selection Operator (LASSO) [17]. The popularity of the LASSO regression is mainly attributed to the convexity of the ℓ_1 penalty term $Q(\boldsymbol{\alpha}) = \sqrt{2\eta}\|\boldsymbol{\alpha}\|_1$ as well as to its provable sparsity-inducing properties (see, e.g., [2], [18]).

The sparsity properties of the LASSO estimator depend heavily on the value of the regularization parameter $\kappa = \lambda^{-1}\sqrt{2\eta}$. If κ is selected too large, the resulting estimator produces overly sparse estimates, i.e., relevant information will be discarded; in contrast, small values of κ lead to non-sparse solutions, especially in low signal-to-noise ratio (SNR) regime. While techniques exist for empirically choosing the regularization parameters [8], the Bayesian methodology provides all the tools necessary for finding an optimal regularization term. In other words, by modeling η and λ as random variables and incorporating them into the inference framework, an optimal value of κ can be found. This requires extending the two-layer prior modeling of $p(\boldsymbol{\alpha})$ with a third layer — the "hyper-hyperprior" pdf for η. Naturally, the "hyper-hyperprior" again depends on some parameters that have to be specified. However, it is reasonable to assume that the performance of the resulting estimator is less sensitive to the exact choice of these "hyper-hyperparameters": the tiers of such hierarchical priors can be seen as different layers of abstraction from the actual model parameter vector $\boldsymbol{\alpha}$. Thus, on the highest layer such a "hyper-hyperprior" gives a very abstract description of the representation of $\boldsymbol{\alpha}$. In this work we propose several extensions and generalizations of this hierarchical modeling approach.

Our goal in this work is threefold. First, we extend the G-E prior model to complex domain, effectively generalizing the hierarchical prior formulation for real as well as complex models. We do so by using a gamma hyperprior $p(\gamma_l;\epsilon,\eta_l)$ instead of an exponential prior; furthermore, L individual parameters η_l are used instead of a single regularization parameter. We will refer to this new hierarchical prior formulation as Gaussian-gamma (G-Ga) prior model. The obtained results naturally generalize those obtained in [16] for real $\boldsymbol{\alpha}$. We demonstrate that by varying the shape parameter ϵ of the gamma hyperprior $p(\gamma_l;\epsilon,\eta_l)$ a family of solutions for $\boldsymbol{\alpha}$ that approximate a soft-thresholding rule with different degrees of sparseness

is obtained. Second, instead of a two-layer prior we propose a three-layer hierarchical prior for both real and complex parameters. This is realized by modeling the hyperprior parameters η_l as random variables with the gamma pdf $p(\eta_l) \equiv p(\eta_l; a_l, b_l) = b_l^{a_l} \eta_l^{a_l - 1} \exp(-b_l \eta_l)/\Gamma(a_l)$. This leads to a model with $2L+1$ free parameters, i.e., ϵ and a_l, b_l, $l = 1, \ldots, L$, to control the degree of sparseness of the resulting solution. We show that, in contrast to the G-Ga model, varying the parameter ϵ with fixed a_l and b_l leads in this case to a family of solutions for $\boldsymbol{\alpha}$ that approximate a hard-thresholding rule. Moreover, a weakly informative prior can be constructed that induces an equivalent weighted log-sum penalization of the parameter likelihood function [8], [10]. This three-layer prior model we term Gaussian-gamma-gamma (G-Ga-Ga) prior model. Furthermore, we show that for both two-layer and three-layer prior models, choosing non-informative hyperpriors yields a log-sum penalization of the parameter likelihood, which is identical to the ARD formulation of the RVM-type of hierarchical prior. Finally, we propose a variational Bayesian message passing algorithm that exploits the hierarchical structure of the inference problem. Due to the adopted choice of the pdfs in the hierarchical prior model it is possible to compute the messages in closed form. Thus, inference can be implemented very efficiently. We should mention that a three-layer prior model has been also independently proposed in [7] for hierarchical adaptive LASSO (HAL). In [7] the authors use a three-layer hierarchical prior to motivate the adaptive version of the LASSO estimator. There are, however, several important distinctions between their approach and the one advocated in our work. First of all, although a three-layer hierarchy is used, the prior pdfs used in the hierarchy prohibit an application of this structure to models with complex parameters; specifically, one does not obtain a LASSO-type of objective function when this hierarchical modeling is applied to models with complex parameters. Second, the inference algorithm does not really exploit the three-layer hierarchy. Instead, it works with a two-layer structure, where the first layer is a Laplace pdf and the second layer is a gamma pdf. Such a two-layer structure has been explicitly used earlier for sparse estimation of multipath wireless channels in [5]. More on this will be discussed later in the text.

Throughout this paper we shall make use of the following notation. For vectors $\boldsymbol{x}$ and matrices $\boldsymbol{X}$, $(\cdot)^T$ and $(\cdot)^H$ denote respectively the transpose and the Hermitian transpose. The expression $\langle f(\boldsymbol{x}) \rangle_{q(\boldsymbol{x})}$ denotes the expectation of a function $f(\boldsymbol{x})$ with respect to a density $q(\boldsymbol{x})$. For a random vector $\boldsymbol{x}$, $\mathrm{N}(\boldsymbol{x}|\boldsymbol{a}, \boldsymbol{B})$ and $\mathrm{CN}(\boldsymbol{x}|\boldsymbol{a}, \boldsymbol{B})$ denote respectively a multivariate real and a multivariate complex Gaussian pdf with a mean $\boldsymbol{a}$ and a covariance matrix $\boldsymbol{B}$; similarly, $\mathrm{Ga}(x|a, b) = \frac{b^a}{\Gamma(a)} x^{a-1} \exp(-bx)$ denotes a Gamma pdf with shape parameter a and rate parameter b. The range of integration of integrals will not be explicitly given when it is obvious.

II. BAYESIAN FRAMEWORK FOR SPARSE ESTIMATION

We begin with the specification of the probabilistic structure of the SBL problem for model (1). Two types of hierarchical prior models for $\boldsymbol{\alpha}$ are considered: a two-layer and a three-layer hierarchical model. Later we will see that these models lead to priors for $\boldsymbol{\alpha}$ with distinct sparsity-inducing properties.

The joint pdf of system model (1) with a two-layer prior model for $\boldsymbol{\alpha}$ reads

$$p(\boldsymbol{y}, \boldsymbol{\alpha}, \boldsymbol{\gamma}, \lambda) = p(\boldsymbol{y}|\boldsymbol{\alpha}, \lambda)p(\lambda)p(\boldsymbol{\alpha}|\boldsymbol{\gamma})p(\boldsymbol{\gamma}). \tag{3}$$

The joint pdf of system model (1) with a three-layer prior model for $\boldsymbol{\alpha}$ is obtained by assuming that the parameters $\boldsymbol{\eta}$ of the $p(\boldsymbol{\gamma})$ in (3) are random. The resulting joint pdf is then specified as

$$p(\boldsymbol{y}, \boldsymbol{\alpha}, \boldsymbol{\gamma}, \boldsymbol{\eta}, \lambda) = p(\boldsymbol{y}|\boldsymbol{\alpha}, \lambda)p(\lambda)p(\boldsymbol{\alpha}|\boldsymbol{\gamma})p(\boldsymbol{\gamma}|\boldsymbol{\eta})p(\boldsymbol{\eta}). \tag{4}$$

Both the two-layer formulation (3) and the three-layer formulation (4) share the same likelihood function $p(\boldsymbol{y}|\boldsymbol{\alpha}, \lambda)$ and the prior pdf of the noise precision parameter $p(\lambda)$. Due to (1) the likelihood function is Gaussian: $p(\boldsymbol{y}|\boldsymbol{\alpha}, \lambda) = \mathrm{N}(\boldsymbol{y}|\boldsymbol{H}\boldsymbol{\alpha}, \lambda^{-1}\boldsymbol{I})$ for the real-valued system model and $p(\boldsymbol{y}|\boldsymbol{\alpha}, \lambda) = \mathrm{CN}(\boldsymbol{y}|\boldsymbol{H}\boldsymbol{\alpha}, \lambda^{-1}\boldsymbol{I})$ for the complex-valued model. The prior $p(\lambda)$ is selected as a gamma prior, i.e., $p(\lambda) = p(\lambda; c, d) \triangleq \mathrm{Ga}(\lambda|c, d)$. This choice is convenient since the gamma distribution is a conjugate prior for the precision of a Gaussian likelihood function. Additionally, selecting $c = d = 0$ makes this prior non-informative.

Let us specify the structure of the hierarchical priors of $\boldsymbol{\alpha}$ in (3) and (4). Motivated by [12], [16] we select the conditional prior $p(\boldsymbol{\alpha}|\boldsymbol{\gamma}) = \prod_{l=1}^{L} p(\alpha_l|\gamma_l)$ to be the product of Gaussian pdfs. While in [12], [16] real-valued $\boldsymbol{\alpha}$ was considered, here we consider both real- and complex-valued $\boldsymbol{\alpha}$. To this end we define

$$p(\alpha_l|\gamma_l) = \left(\frac{\rho}{\pi\gamma_l}\right)^{\rho} \exp\left(-\rho\frac{|\alpha_l|^2}{\gamma_l}\right) \tag{5}$$

with the parameter $\rho \in \{\frac{1}{2}, 1\}$. The conditional prior $p(\alpha_l|\gamma_l)$ for real-valued α_l is realized by selecting $\rho = 1/2$, while $\rho = 1$ entails the prior for complex-valued α_l. In the next section we compute the prior for $\boldsymbol{\alpha}$ that results from the two-layer prior model and analyze its sparsity-inducing property. We redo the same exercise in the following section with the three-layer prior model.

A. Two-Layer Hierarchical Prior Model

As we have already mentioned, the original G-E prior model in [16] assumes that $p(\boldsymbol{\gamma})$ is a product of exponential pdfs with a common rate parameter η. We can easily generalize this model by considering $p(\boldsymbol{\gamma})$ as a product of gamma pdfs with individual rate parameters. Specifically, we assume that $p(\boldsymbol{\gamma}) = \prod_{l=1}^{L} p(\gamma_l)$ with $p(\gamma_l) = p(\gamma_l; \epsilon, \eta_l) \triangleq \mathrm{Ga}(\gamma_l|\epsilon, \eta_l)$. The G-E prior model is then the special case with the settings $\epsilon = 1$ and $\eta_1 = \ldots = \eta_L = \eta$. We define now $\boldsymbol{\eta} = [\eta_1, \ldots, \eta_L]^T$ and compute the prior of $\boldsymbol{\alpha}$ to be

$$p(\boldsymbol{\alpha}; \epsilon, \boldsymbol{\eta}) = \int_0^\infty p(\boldsymbol{\alpha}|\boldsymbol{\gamma}) p(\boldsymbol{\gamma}; \epsilon, \boldsymbol{\eta}) \mathrm{d}\boldsymbol{\gamma} = \prod_{l=1}^{L} p(\alpha_l; \epsilon, \eta_l) \tag{6}$$

with

$$p(\alpha_l; \epsilon, \eta_l) = \frac{2\rho^{\frac{(\epsilon+\rho)}{2}}}{\pi^\rho \Gamma(\epsilon)} \eta_l^{\frac{(\epsilon+\rho)}{2}} |\alpha_l|^{\epsilon-\rho} K_{\epsilon-\rho}(2\sqrt{\rho\eta_l}|\alpha_l|). \tag{7}$$

In this expression, $K_\nu(\cdot)$ is the modified Bessel function of the second kind and order $\nu \in \mathbb{R}$. Further in the text we refer to this formulation of the hierarchical prior pdf as Gaussian-gamma (G-Ga) prior model. The prior (7) is valid for real-valued ($\rho = 1/2$) as well as for complex-valued ($\rho = 1$) α_l.

By selecting $\epsilon = 1$, $\rho = 1/2$, and using the identity $K_{\frac{1}{2}}(z) = \sqrt{\frac{\pi}{2z}} \exp(-z)$ [19], (7) yields the Laplace prior for real α_l:

$$p(\alpha_l; \epsilon = 1, \eta_l) = \sqrt{\frac{\eta_l}{2}} \exp(-\sqrt{2\eta_l}|\alpha_l|), \quad \alpha_l \in \mathbb{R}. \tag{8}$$

In the complex case, when $\rho = 1$, it is easy to see that selecting $\epsilon = 3/2$ leads to the same order of the Bessel function in (7) as in the real case. Making use of the same identity for the Bessel function we find the corresponding prior for complex α_l:

$$p(\alpha_l; \epsilon = 3/2, \eta_l) = \frac{2\eta_l}{\pi} \exp(-2\sqrt{\eta_l}|\alpha_l|), \quad \alpha_l \in \mathbb{C}. \tag{9}$$

Hence, the G-Ga prior model realizes the ℓ_1 penalty term $Q(\boldsymbol{\alpha}; \boldsymbol{\eta}) = 2\sum_{l=1}^{L} \sqrt{\rho\eta_l}|\alpha_l|$ with $\epsilon = 1$ for real $\boldsymbol{\alpha}$ and with $\epsilon = 3/2$ for complex $\boldsymbol{\alpha}$.

The G-Ga prior model can be used with arbitrary values of ϵ, leading to the general optimization problem (2) with

$$Q(\boldsymbol{\alpha}; \epsilon, \boldsymbol{\eta}) = \sum_{l=1}^{L} \log\left(|\alpha_l|^{\epsilon-\rho} K_{\epsilon-\rho}\left(2\sqrt{\rho\eta_l}|\alpha_l|\right)\right). \tag{10}$$

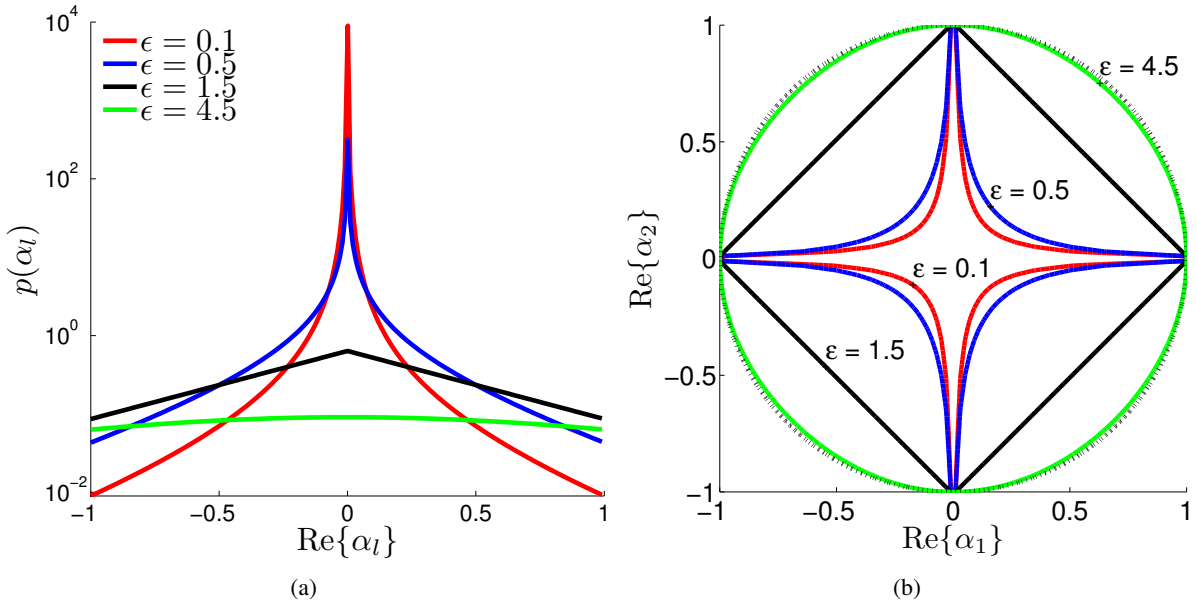

Fig. 1. Two-layer hierarchical prior pdf for the complex system model with the setting $\eta = 1$: (a) The restriction to $\mathbb{R}$ ($\mathrm{Im}\{\alpha_l\} = 0$) of $p(\alpha_l; \epsilon, \eta)$ (7) for different values of ϵ. (b) Contour plot of the restriction to the $\mathrm{Im}\{\alpha_1\} = \mathrm{Im}\{\alpha_2\} = 0$ – plane of $Q(\alpha_1, \alpha_2; \epsilon, \eta) \propto^e -\log p(\alpha_1; \epsilon, \eta) p(\alpha_2; \epsilon, \eta)$. In (b) the black dashed line indicates the penalty term resulting when the prior pdf is a circular symmetric Gaussian pdf.

One important observation is that decreasing ϵ beyond $3/2$ in the complex case (or equivalently beyond 1 in the real case) leads to a non-convex penalty term that resembles the ℓ_p-norm penalty for $0 < p < 1$.[4] Unfortunately, in this case the optimization problem (2) with penalty term (10) is no longer convex. Note, however, that the hierarchical approach advocated in this work does not involve a direct optimization of the objective function in (2). Instead, the non-convex penalty term (10) is realized indirectly as a product of Gaussian and gamma pdfs. Moreover, since in the G-Ga model formulation the prior $p(\boldsymbol{\alpha}|\boldsymbol{\gamma})$ is Gaussian, the resulting MAP objective function for $\boldsymbol{\alpha}$ is necessarily convex with respect to $\boldsymbol{\alpha}$ irrespective of the value of ϵ.[5]

Let us stress that (6) represents a family of prior pdfs for $\boldsymbol{\alpha}$ parameterized by ϵ and $\boldsymbol{\eta}$. While the entries in $\boldsymbol{\eta}$ can be recognized as multiple regularization parameters, the impact of ϵ is less straightforward. To better understand its influence on the shape of (6) we visualize in Fig. 1(a) the restriction[6] to $\mathbb{R}$ of the prior $p(\alpha_l, \epsilon, \eta_l)$ in (7) with $\rho = 1$ for various values of ϵ. Observe the change of the shape of $p(\alpha_l; \epsilon, \eta_l)$

[4]The norm ℓ_p, $0 < p < 1$, better approximates the pseudo-norm ℓ_0 — the number of non-zero entries in the vector — as compared to ℓ_p with $p \geq 1$.

[5]The same is true for G-E and G-IGa models.

[6]Let f denote a function defined on a set A. The restriction of f to a subset $B \subset A$ is the function defined on B that coincides with f on this subset.

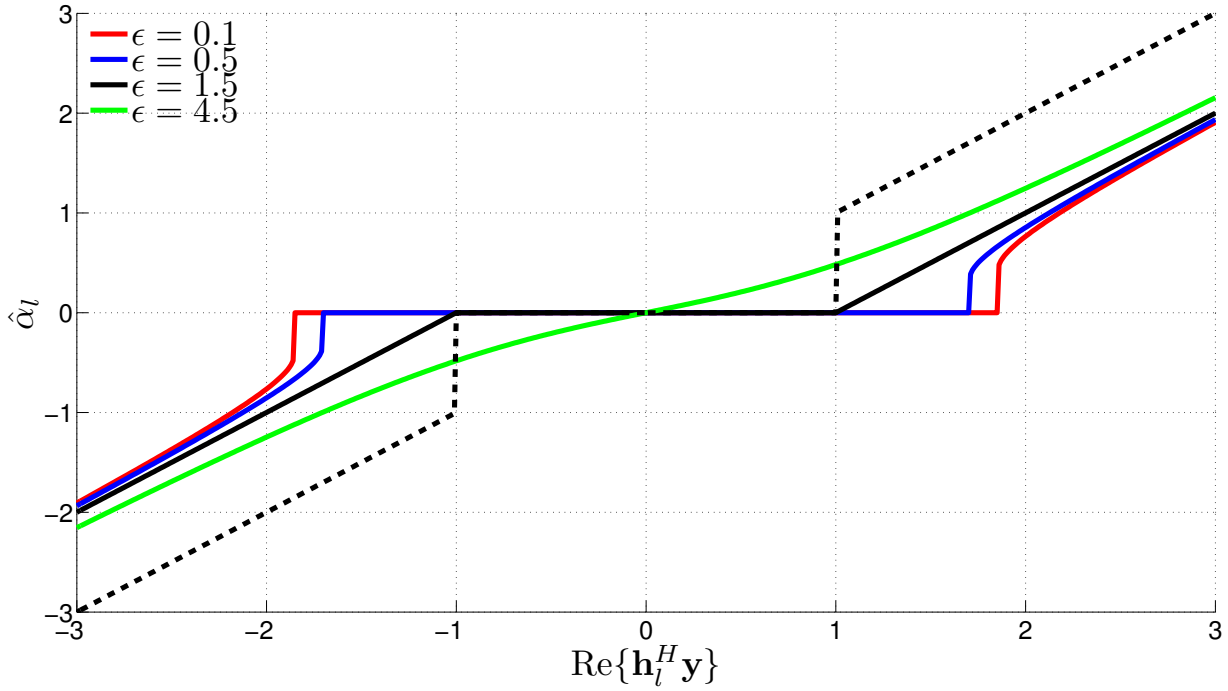

Fig. 2. Two-layer hierarchical prior for the complex system model: Restriction to $\mathrm{Im}\{\boldsymbol{h}_l^H\boldsymbol{y}\} = 0$ of the resulting MAP estimation rule (2) with ϵ as a parameter in the case when $\boldsymbol{H}$ is orthonormal. The black dashed line indicates the hard-threshold rule [20].

with ϵ: the smaller the value of ϵ the more rapidly $p(\alpha_l, \epsilon, \eta_l)$ decays around the origin. In Fig. 1(b) we show the contour lines of the restriction to $\mathbb{R}$ of $Q(\alpha_1, \alpha_2; \epsilon, \eta) \propto^e -\log p(\alpha_1; \epsilon, \eta)p(\alpha_2; \epsilon, \eta)$; each contour line is computed for a specific choice of ϵ. It can be seen from the plots that as ϵ decreases towards 0 more probability mass concentrates along the $\boldsymbol{\alpha}$-axes; as a consequence, the mode of the resulting posterior is more likely to be found close to the axes, thus indicating a sparse solution. The behavior of the classical ℓ_1 penalty term obtained for $\epsilon = 3/2$ can also be clearly recognized.

In order to get further insight into the impact of ϵ on the MAP estimate $\widehat{\boldsymbol{\alpha}}$ with penalty term (10), we consider the case when $\boldsymbol{H}$ is orthonormal, i.e., when $\boldsymbol{h}_l^H\boldsymbol{h}_k = \delta_{k,l}$, where $\delta_{k,l}$ is the Kronecker delta. In this case the solution $\widehat{\boldsymbol{\alpha}}$ can be easily computed since the optimization (2) decouples into L independent scalar optimization problems. Furthermore, when the G-Ga prior model realizes an ℓ_1-norm constraint, i.e., the prior pdfs (8) (real case) or (9) (complex case) is selected, the MAP solution can even be computed analytically as follows:

$$\hat{\alpha}_l = \mathrm{sign}(\boldsymbol{h}_l^H\boldsymbol{y})\max\left\{0, |\boldsymbol{h}_l^H\boldsymbol{y}| - \lambda^{-1}\sqrt{\frac{\eta_l}{\rho}}\right\}, \quad l = 1, \ldots, L, \tag{11}$$

where $\mathrm{sign}(x) = x/|x|$. The interpretation of this result is quite intuitive: for complex α_l the region where the estimate $\hat{\alpha}_l$ is exactly zero is the closed disc with radius $\lambda^{-1}\sqrt{\eta_l}$ centered at origin; for real α_l it is given by the closed interval $\left[-\lambda^{-1}\sqrt{2\eta_l}, \lambda^{-1}\sqrt{2\eta_l}\right]$. Correspondingly, the solution (11) is a soft-thresholding rule for each entry in $\widehat{\boldsymbol{\alpha}}$ with threshold $\lambda^{-1}\sqrt{\frac{\eta_l}{\rho}}$. In Fig. 2 we visualize the estimation rules produced by the MAP solver for different values of ϵ. Note their typical soft-threshold-like behavior. As $\epsilon \to 0$, more components of $\widehat{\boldsymbol{\alpha}}$ are pulled towards zero since the threshold value increases, thus encouraging a sparser solution.

B. Three-Layer Hierarchical Prior Model

We now turn to the SBL problem with a three-layer prior model for $\boldsymbol{\alpha}$ represented by the joint pdf in (4). Specifically, we extend the G-Ga prior model to a three-layer model by considering the hyperparameters in $\boldsymbol{\eta}$ as random. We assume that $p(\boldsymbol{\eta}) = \prod_l^L p(\eta_l)$, where $p(\eta_l) = p(\eta_l; a_l, b_l) \triangleq \mathrm{Ga}(\eta_l|a_l, b_l)$. The resulting three-layer model we term Gaussian-gamma-gamma (G-Ga-Ga) prior model.

Let us now compute the prior $p(\boldsymbol{\alpha})$ that corresponds to the G-Ga-Ga model. First, we note that $p(\boldsymbol{\alpha}, \boldsymbol{\gamma}, \boldsymbol{\eta}) = p(\boldsymbol{\alpha}|\boldsymbol{\gamma})p(\boldsymbol{\gamma}|\boldsymbol{\eta})p(\boldsymbol{\eta}) = \prod_{l=1}^L p(\alpha_l|\gamma_l)p(\gamma_l|\eta_l)p(\eta_l)$ and marginalize $p(\boldsymbol{\alpha}, \boldsymbol{\gamma}, \boldsymbol{\eta})$ over $\boldsymbol{\eta}$. This requires computing $p(\boldsymbol{\alpha}|\boldsymbol{\gamma})p(\boldsymbol{\gamma}) = p(\boldsymbol{\alpha}|\boldsymbol{\gamma}) \int p(\boldsymbol{\gamma}|\boldsymbol{\eta})p(\boldsymbol{\eta})\mathrm{d}\boldsymbol{\eta}$. Defining $\boldsymbol{a} \triangleq [a_1, \ldots, a_l]^T$ and $\boldsymbol{b} \triangleq [b_1, \ldots, b_L]^T$ we obtain

$$p(\boldsymbol{\gamma}; \epsilon, \boldsymbol{a}, \boldsymbol{b}) = \prod_l^L \int_0^\infty p(\gamma_l|\eta_l; \epsilon)p(\eta_l; a_l, b_l)\mathrm{d}\eta_l = \prod_l^L p(\gamma_l; \epsilon, a_l, b_l), \tag{12}$$

where

$$p(\gamma_l; \epsilon, a_l, b_l) = \frac{b_l^{a_l}\Gamma(\epsilon + a_l)}{\Gamma(\epsilon)\Gamma\left(a_l\right)}\gamma_l^{\epsilon-1}(\gamma_l + b_l)^{-(\epsilon+a_l)}. \tag{13}$$

Finally, marginalizing $p(\boldsymbol{\alpha}|\boldsymbol{\gamma})p(\boldsymbol{\gamma}; \epsilon, \boldsymbol{a}, \boldsymbol{b})$ over $\boldsymbol{\gamma}$ yields

$$p(\boldsymbol{\alpha}; \epsilon, \boldsymbol{a}, \boldsymbol{b}) = \prod_l^L p(\alpha_l; \epsilon, a_l, b_l) \tag{14}$$

with

$$\begin{aligned} p(\alpha_l; \epsilon, a_l, b_l) &= \int_0^\infty p(\alpha_l|\gamma_l)p(\gamma_l)\mathrm{d}\gamma_l \\ &= \left(\frac{\rho}{\pi b_l}\right)^\rho \frac{\Gamma(\epsilon + a_l)\Gamma(a_l + \rho)}{\Gamma(\epsilon)\Gamma(a_l)} \left(\rho\frac{|\alpha_l|^2}{b_l}\right)^{\epsilon-\rho} U\left(\epsilon + a_l; \epsilon - \rho + 1; \rho\frac{|\alpha_l|^2}{b_l}\right). \end{aligned} \tag{15}$$

In this expression, $U(\cdot;\cdot;\cdot)$ is the confluent hypergeometric function [19]. Unfortunately, this function

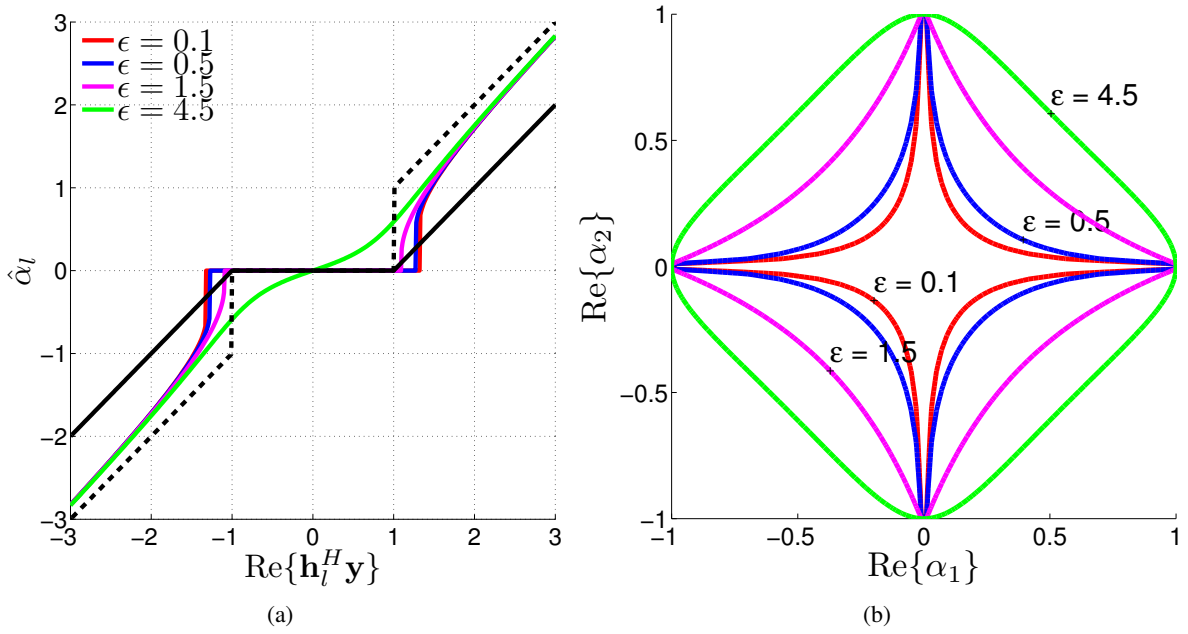

(a) (b)

Fig. 3. Three-layer hierarchical prior pdf for the complex system model with the setting $a = 1$, $b = 0.1$: (a) Restriction to $\mathrm{Im}\{\boldsymbol{h}_l^H\boldsymbol{y}\} = 0$ of the resulting MAP estimation rule (2) with ϵ as a parameter in the case when $\boldsymbol{H}$ is orthonormal. The black dashed line indicates the hard-threshold rule and the black solid line the soft-threshold rule (11). (b) Contour plot of the restriction to the $\mathrm{Im}\{\alpha_1\} = \mathrm{Im}\{\alpha_2\} = 0$ – plane of the penalty term $Q(\alpha_1, \alpha_2; \epsilon, a, b) \propto^e -\log p(\alpha_1; \epsilon, a, b)p(\alpha_2; \epsilon, a, b)$.

makes a further analytical investigation of (15) rather difficult. Nonetheless, we can study its behavior numerically. Following the same approach as for the G-Ga prior model, we show the estimation rules produced by the MAP solver for different values of ϵ and fixed parameters a_l and b_l when $\boldsymbol{H}$ is orthonormal in Fig. 3(a). Notice, the estimation rules obtained with the G-Ga-Ga prior model approximate the hard-thresholding rule. In Fig. 3(b), we depict the contour of the penalty term $Q(\alpha_1, \alpha_2; \epsilon, a, b) \propto^e -\log p(\alpha_1; \epsilon, a, b)p(\alpha_2; \epsilon, a, b)$. Observe that although the contours are qualitatively similar to those shown in Fig. 1(b) for the G-Ga model, the corresponding estimation rules in Fig. 3(a) are not.

C. Weighted log-sum Penalization

The use of the additional third layer in the G-Ga-Ga prior model leads to the introduction of the additional free parameter vectors $\boldsymbol{a}$ and $\boldsymbol{b}$ which must be selected in addition to the prior parameter ϵ. In this section we discuss a selection of these parameters that leads to a "weakly" informative prior for $\boldsymbol{\alpha}$ with good sparsity-inducing properties.

Recall that the entries in $\boldsymbol{\eta}$ in the G-Ga prior model represent regularization parameters. The range of appropriate values for $\boldsymbol{\eta}$ is primarily determined by the particular SNR, measurement signal $\boldsymbol{y}$, and dictionary $\boldsymbol{H}$ (see (11)); this range can be quite large in general. Thus, it makes sense to employ a

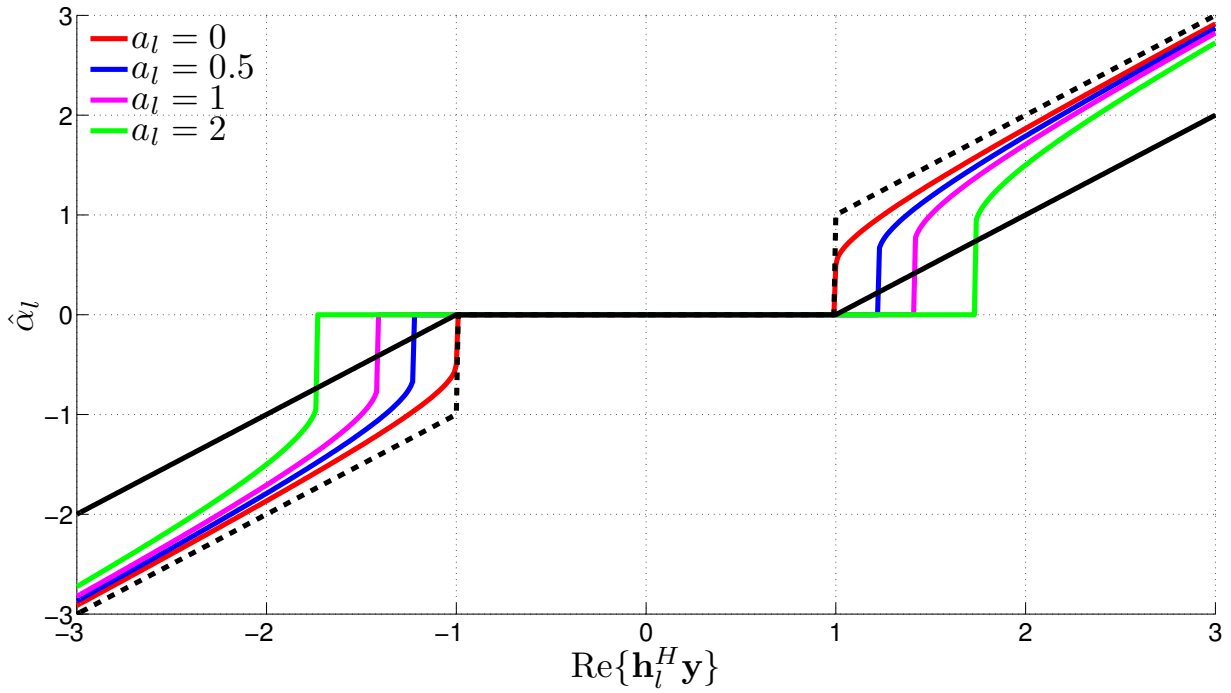

Fig. 4. Three-layer hierarchical prior for the complex system model with small b ($b = 10^{-6}$): Restriction to $\mathrm{Im}\{\boldsymbol{h}_l^H \boldsymbol{y}\} = 0$ of the resulting MAP estimation rule (2) with a_l as a parameter in the case when $\boldsymbol{H}$ is orthonormal. The black dashed line indicates the hard-threshold rule and the black solid line the soft-threshold rule (11).

diffuse prior over $\boldsymbol{\eta}$. This can be achieved by selecting the entries in $\boldsymbol{b}$ to be small; practically, we set $b_l = 10^{-6}$, $l = 1, \ldots, L$. For small b_l the prior (13) can be approximated as

$$p(\gamma_l; \epsilon, a_l, b_l) \approx \frac{b_l^{a_l} \Gamma(\epsilon + a_l)}{\Gamma(\epsilon)\Gamma(a_l)} \gamma_l^{-(a_l+1)}. \tag{16}$$

If in addition we select $\epsilon = 0$ we obtain the improper prior for γ_l

$$p(\gamma_l; a_l) \propto \gamma_l^{-(a_l+1)}. \tag{17}$$

The prior $p(\alpha_l; a_l)$ obtained by marginalizing $p(\alpha_l|\gamma_l)p(\gamma_l; a_l)$ over γ_l is also improper in this case:

$$p(\alpha_l; a_l) \propto |\alpha_l|^{-2(a_l+\rho)}. \tag{18}$$

The prior (18) leads to a weighted log-sum penalty term $Q(\boldsymbol{\alpha}; \boldsymbol{a}) = 2\sum_{l=1}^{L}(a_l + \rho)\log|\alpha_l|$ parametrized by $\boldsymbol{a}$ in the MAP objective function. Observe that selecting $\boldsymbol{a} = \boldsymbol{0}$ in (18) the log-sum penalty term is automatically obtained. Such form of penalty appears in the ARD formulation of the G-IGa prior model [12], [21], as well as in the re-weighted ℓ_1 optimization [8].

The dependency of (18) on a_l gives some extra degree of freedom to further adjust the sparsity property of this prior. To demonstrate this, let us again consider the special case of an orthogonal measurement matrix $\boldsymbol{H}$. In Fig. 4 we depict the corresponding MAP estimation rules for α_l with penalty term $Q(\alpha_l; a_l) = 2(a_l + \rho)\log|\alpha_l|$. Observe that increasing the value of a_l also increases the values of the effective threshold, thus resulting in sparser solutions of $\boldsymbol{\alpha}$.

III. Related Approaches and Methods

In this section we establish the relationship between the sparse Bayesian modeling approach with hierarchical priors developed in Sec. II and other state-of-the-art sparse estimation techniques proposed in the literature.

The iterative re-weighted ℓ_1 minimization method studied by [8], [10], [21] solves the weighted optimization problem for the real system model ($\rho = 1/2$) in (2) with penalty term

$$Q(\boldsymbol{\alpha}; \boldsymbol{\beta}) = \sum_{l=1}^{L} \beta_l |\alpha_l|, \tag{19}$$

where β_l, $l = 1, \ldots, L$, are some fixed weights. In [8] it is proposed to update the weights as

$$\beta_l = (|\hat{\alpha}_l| + \varsigma)^{-1}, \tag{20}$$

where ς is some small constant and $\hat{\alpha}_l$ is the current estimate of α_l; such an algorithm leads to a sequence of re-weighted ℓ_1 minimization problems.

We show that our proposed G-Ga prior model also implements the same objective function, albeit for real as well as complex system models. Indeed, the MAP estimate of $\boldsymbol{\alpha}$ computed using the G-Ga hierarchal prior model with the setting $\epsilon = \rho + 1/2$ yields the penalty term

$$Q(\boldsymbol{\alpha}; \boldsymbol{\eta}) = 2\sum_{l=1}^{L} \sqrt{\rho\eta_l}|\alpha_l|. \tag{21}$$

Hence, (21) is equivalent to (19) with the weighting factors $\beta_l = 2\sqrt{\rho\eta_l}$, $l = 1, \ldots, L$. Quite naturally this relationship can be exploited by selecting the hyperparameters $\eta_l = 1/(4\rho(|\hat{\alpha}_l| + \varsigma)^2)$ as proposed in [8]. Moreover, in contrast to [8] and as already mentioned in Sec. II, the Bayesian hierarchical approach is not constrained to the ℓ_1-type of penalty term obtained with $\epsilon = \rho + 1/2$, but can be used for arbitrary values of ϵ, leading to the general re-weighted constrained optimization problem by updating η_l in (10). We will demonstrate that due to the strong sparsity-inducing nature of the prior (7) for $\epsilon < \rho + 1/2$, (10) leads to a sparser estimate as compared to that obtained using (21).

Similarly to the G-Ga prior model, the two-layer G-IGa prior model proposed in [12] also requires specifying the hyperprior parameters. In [12] the variance γ_l follows an inverse gamma distribution. The corresponding marginal distribution of α_l can be shown to follow a Student-t distribution. This result can be easily generalized for complex variables, leading to the prior for α_l

$$p(\alpha_l; a_l, b_l) = \left(\frac{\rho}{\pi}\right)^{\rho} \frac{b_l^{a_l}\Gamma(a_l+\rho)}{\Gamma(a_l)} \left(b_l + \rho|\alpha_l|^2\right)^{-(a_l+\rho)}. \tag{22}$$

Setting a_l and b_l to zero leads to a special case of non-informative hyperpriors and ARD, with an improper prior $p(\boldsymbol{\alpha}) \propto \prod_{l=1}^{L} |\alpha_l|^{-2\rho}$ that leads to the log-sum penalty term $Q(\boldsymbol{\alpha}) = 2\rho \sum_{l=1}^{L} \log|\alpha_l|$. We should also add that the ℓ_1 re-weighting scheme in [8] has also been motivated using the log-sum penalty term (see [8] for more details). Moreover, it has been demonstrated [10], [21] that the ARD approach to SBL based on the G-IGa prior model can also be interpreted as a series of re-weighted ℓ_1 minimization problems; the computation of the weighting factors, however, differs from that used in [8].

Similarly, in [16] the author also suggests to make use of Jeffreys' prior for the variance γ_l in the G-E prior model. It can be shown that this choice of hyperprior in fact again leads to the same improper ARD prior $p(\alpha_l) \propto |\alpha_l|^{-2\rho}$. Hence, the G-IGa model proposed by Tipping in [12] and the G-E model proposed by Figueiredo in [16] are equivalent when the hyperpriors are chosen to be non-informative. Note that since the G-Ga prior model endorses the G-E model as a special case, the same is true when $\epsilon = \eta_l = 0$, $l = 1, \ldots, L$, in (7). Furthermore, for the three-layer prior model it is easily seen that letting $a_l = b_l = \epsilon = 0$ in (13) also entails the non-informative Jeffreys' prior for γ_l. Thus, the equivalent marginalized prior $p(\alpha_l)$ coincides with that obtained in [12] and [16] when non-informative hyperpriors are assumed. In other words, when second or third layer priors are chosen to be non-informative, an instance of ARD is obtained regardless of the hierarchal prior model used.

While two-layer models in general require specifying the regularization parameters, three-layer prior models effectively lead to an alternative automatic procedure for selecting the parameters η_l. The three-layer structure has been implicitly exploited in [5] for sparse variational Bayesian extension of the SAGE algorithm for parameter estimation in sparse wireless channels and explicitly in [7] for hierarchical adaptive LASSO. In [5] the authors exploit the two-layer prior structure, where the first layer is the ℓ_1 prior, i.e., $p(\boldsymbol{\alpha}|\tilde{\boldsymbol{\eta}}) \propto \prod_{l=1}^{L} \exp(-2\tilde{\eta}_l|\alpha_l|)$ and the second layer is the gamma hyperprior $p(\tilde{\boldsymbol{\eta}}) = \prod_{l=1}^{L} \mathrm{Ga}(\tilde{\eta}_l|a_l, b_l)$. Obviously, the prior $p(\boldsymbol{\alpha}|\tilde{\boldsymbol{\eta}})$ can be constructed via the G-Ga model as we showed in Sec. II-A with $\tilde{\eta}_l = \sqrt{\eta_l}$; thus, the two-layer ℓ_1-gamma prior model used in [5] is equivalent to the three-layer structure discussed in Sec. II-B with the selected hyper-hyperprior $p(\boldsymbol{\eta}) = \prod_{l=1}^{L} \mathrm{Ga}(\sqrt{\eta_l}|a_l, b_l)$.

Thus, $\tilde{\eta}_l = \sqrt{\eta_l}$ following a generalized gamma distribution [22]. The resulting update expressions for $\tilde{\eta}_l$ can then be computed as [5], [7]

$$\tilde{\eta}_l = \frac{a_l + \rho^{-1}}{b_l + \rho^{-1}|\hat{\alpha}_l|}. \tag{23}$$

Notice the similarity between the update expression (23) and the one proposed in [8] for the weights β_l in (19). Let us stress that although the authors in [7] discuss the three-layer structure, they do not exploit the hierarchy for constructing the inference algorithm; instead, the first two layers are combined together to give the Laplace prior. This leads to the desired LASSO-type objective function for estimating $\boldsymbol{\alpha}$ and makes their approach numerically equivalent to that proposed in [5]. Nonetheless, despite formal similarities between the update expressions for the ℓ_1 weighting parameters obtained with the three-layer hierarchical prior and those proposed in [8], a substantial difference between these schemes lies in the order in which the parameters are updated. Specifically, in [8] the weights are updated once a single weighted ℓ_1 optimization problem has been solved with fixed weights η_l, $l = 1, \ldots, L$; similarly, the ARD approach estimates the corresponding weighting parameters once the vector $\boldsymbol{\alpha}$ that optimizes the ARD objective function are computed [21]. In contrast, in [5] and [7] the update expressions for the weights of the weighted ℓ_1 optimization are evaluated concurrently with the update expressions for the model parameter vector $\boldsymbol{\alpha}$; in other words, a weight η_l is updated each time the corresponding parameter α_l is updated.

IV. Variational Message Passing

In this section we present a variational message passing (VMP) algorithm for estimating $\boldsymbol{\alpha}$ given the observation $\boldsymbol{y}$. First, we derive the VMP inference expressions for the SBL problem with the two- and the three-layer prior models. Then, a procedure for removing a basis function from the measurement matrix $\boldsymbol{H}$ is described.

A. The VMP algorithm

Let $\boldsymbol{\Phi} = \{\boldsymbol{\alpha}, \boldsymbol{\gamma}, \boldsymbol{\eta}, \lambda\}$ be the set of unknown parameters to be estimated and let $p(\boldsymbol{y}, \boldsymbol{\Phi})$ be the joint pdf specified in (4). The factor graph [23] that encodes the factorization of $p(\boldsymbol{y}, \boldsymbol{\Phi})$ in (4) is shown in Fig. 5. Consider an auxiliary pdf $q(\boldsymbol{\Phi})$ for the unknown parameters that factorizes according to $q(\boldsymbol{\Phi}) = q(\boldsymbol{\alpha})q(\boldsymbol{\gamma})q(\boldsymbol{\eta})q(\lambda)$. The VMP algorithm is an iterative scheme that attempts to compute the auxiliary pdf $q(\boldsymbol{\Phi})$ by minimizing the Kullback-Leibler (KL) divergence $\mathrm{KL}(q(\boldsymbol{\Phi})\|p(\boldsymbol{\Phi}|\boldsymbol{y}))$. In the following we summarize its key steps; the reader is referred to [24] for more information on VMP.

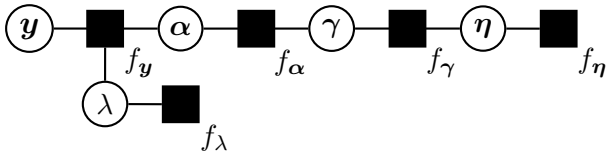

Fig. 5. A factor graph [23] that represents the joint pdf (4). In this figure $f_{\boldsymbol{y}} \equiv p(\boldsymbol{y}|\boldsymbol{\alpha}, \lambda)$, $f_{\boldsymbol{\alpha}} \equiv p(\boldsymbol{\alpha}|\boldsymbol{\gamma})$, $f_{\boldsymbol{\gamma}} \equiv p(\boldsymbol{\gamma})$, $f_{\boldsymbol{\eta}} \equiv p(\boldsymbol{\eta})$, and $f_\lambda \equiv p(\lambda)$.

From [24] the auxiliary function $q(\phi_i)$, $\phi_i \in \boldsymbol{\phi}$ is updated as the product of incoming messages from the neighboring factor nodes f_n to the variable node ϕ_i:

$$q(\phi_i) \propto \prod_{f_n \in \mathcal{N}_{\phi_i}} m_{f_n \to \phi_i}. \tag{24}$$

In (24) $\mathcal{N}_{\phi_i}$ is the set of factor nodes neighboring the variable node ϕ_i and $m_{f_n \to \phi_i}$ denotes the message from factor node f_n to variable node ϕ_i. This message is computed as

$$m_{f_n \to \phi_i} = \exp\left(\langle \ln f_n \rangle_{\prod_j q(\phi_j),\, \phi_j \in \mathcal{N}_{f_n} \setminus \{\phi_i\}} \right), \tag{25}$$

where $\mathcal{N}_{f_n}$ is the set of variable nodes neighboring the factor node f_n. After an initialization procedure, the individual factors of $q(\boldsymbol{\Phi})$ are then updated iteratively in a round-robin fashion using (24) and (25).

In the following we derive two versions of the VMP algorithm: one applied to the two-layer G-Ga prior model (referred to as VMP-2L), and another one applied to the three-layer G-Ga-Ga model (VMP-3L). The messages corresponding to VMP-2L are easily obtained as a special case of the messages computed for VMP-3L by assuming $q(\eta_l) = \delta(\eta_l - \hat{\eta}_l)$, where $\delta(\cdot)$ is a Dirac delta function and $\hat{\eta}_l$ is some fixed number. We compute the messages for both real-valued ($\rho = 1/2$) and complex-valued ($\rho = 1$) signal models (1).

1) Update of $q(\boldsymbol{\alpha})$: According to (24) the computation of $q(\boldsymbol{\alpha})$ requires evaluating the product of messages $m_{p_{\boldsymbol{y} \to \boldsymbol{\alpha}}}$ and $m_{p_{\boldsymbol{\alpha} \to \boldsymbol{\alpha}}}$. These are obtained as

$$\begin{aligned} m_{p_{\boldsymbol{y} \to \boldsymbol{\alpha}}} &= \exp(\langle \ln p(\boldsymbol{y}|\boldsymbol{\alpha}, \lambda) \rangle_{q(\lambda)}) \\ &\propto \exp\left(-\rho \langle \lambda \rangle_{q(\lambda)} \|\boldsymbol{y} - \boldsymbol{H}\boldsymbol{\alpha}\|_2^2 \right), \end{aligned} \tag{26}$$

$$\begin{aligned} m_{p_{\boldsymbol{\alpha} \to \boldsymbol{\alpha}}} &= \exp(\langle \ln p(\boldsymbol{\alpha}|\boldsymbol{\gamma}) \rangle_{q(\boldsymbol{\gamma})}) \\ &\propto \exp\left(-\rho \boldsymbol{\alpha}^H \boldsymbol{V}(\boldsymbol{\gamma}) \boldsymbol{\alpha} \right), \end{aligned} \tag{27}$$

where we define $\boldsymbol{V}(\boldsymbol{\gamma}) = \mathrm{diag}\{\langle\gamma_1^{-1}\rangle_{q(\boldsymbol{\gamma})}, \ldots, \langle\gamma_L^{-1}\rangle_{q(\boldsymbol{\gamma})}\}$. Multiplying (26) and (27) yields the Gaussian auxiliary pdf $q(\boldsymbol{\alpha}) = \mathrm{CN}\left(\boldsymbol{\alpha}|\hat{\boldsymbol{\alpha}}, \hat{\boldsymbol{\Sigma}}_{\boldsymbol{\alpha}}\right)$ when $\rho = 1$ and $q(\boldsymbol{\alpha}) = \mathrm{N}\left(\boldsymbol{\alpha}|\hat{\boldsymbol{\alpha}}, \hat{\boldsymbol{\Sigma}}_{\boldsymbol{\alpha}}\right)$ when $\rho = 1/2$ with corresponding mean and covariance given by

$$\hat{\boldsymbol{\Sigma}}_{\boldsymbol{\alpha}} = (\langle\lambda\rangle_{q(\lambda)}\boldsymbol{H}^H\boldsymbol{H} + \boldsymbol{V}(\boldsymbol{\gamma}))^{-1}, \tag{28}$$

$$\hat{\boldsymbol{\alpha}} = \langle\boldsymbol{\alpha}\rangle_{q(\boldsymbol{\alpha})} = \langle\lambda\rangle_{q(\lambda)}\hat{\boldsymbol{\Sigma}}_{\boldsymbol{\alpha}}\boldsymbol{H}^H\boldsymbol{y}. \tag{29}$$

2) Update of $q(\boldsymbol{\gamma})$: The computation of $q(\boldsymbol{\gamma})$ requires evaluating the messages $m_{p_{\boldsymbol{\alpha}}\to\boldsymbol{\gamma}}$ and $m_{p_{\boldsymbol{\gamma}}\to\boldsymbol{\gamma}}$:

$$\begin{aligned} m_{p_{\boldsymbol{\alpha}}\to\boldsymbol{\gamma}} &= \exp(\langle\ln p(\boldsymbol{\alpha}|\boldsymbol{\gamma})\rangle_{q(\boldsymbol{\alpha})}) \\ &\propto \prod_{l=1}^{L}\gamma_l^{-\rho}\exp\left(-\rho\gamma_l^{-1}\langle|\alpha_l|^2\rangle_{q(\boldsymbol{\alpha})}\right), \end{aligned} \tag{30}$$

$$m_{p_{\boldsymbol{\gamma}}\to\boldsymbol{\gamma}} \propto \prod_{l=1}^{L}\gamma_l^{\epsilon-1}\exp(-\gamma_l\langle\eta_l\rangle_{q(\boldsymbol{\eta})}). \tag{31}$$

Notice that $\langle|\alpha_l|^2\rangle_{q(\boldsymbol{\alpha})}$ in (30) is the lth diagonal element of $\langle\boldsymbol{\alpha}\boldsymbol{\alpha}^H\rangle_{q(\boldsymbol{\alpha})} = \hat{\boldsymbol{\Sigma}}_{\boldsymbol{\alpha}} + \hat{\boldsymbol{\alpha}}\hat{\boldsymbol{\alpha}}^H$. Multiplying (30) and (31) yields

$$q(\boldsymbol{\gamma}) \propto \prod_{l=1}^{L}\gamma_l^{\epsilon-\rho-1}\exp\left(-\gamma_l^{-1}\rho\langle|\alpha_l|^2\rangle_{q(\boldsymbol{\alpha})} - \gamma_l\langle\eta_l\rangle_{q(\boldsymbol{\eta})}\right). \tag{32}$$

The right-hand side expression in (32) is recognized as the product of Generalized Inverse Gaussian (GIG) pdfs [25], i.e., $q(\boldsymbol{\gamma}) = \prod_{l=1}^{L} q(\gamma_l; p, u_l, v_l)$ where $q(\gamma_l; p, u_l, v_l) = \frac{(u_l/v_l)^{\frac{p}{2}}}{2K_p(\sqrt{u_l v_l})}\gamma_l^{p-1}\exp\left(-\frac{u_l}{2}\gamma_l - \frac{v_l}{2}\gamma_l^{-1}\right)$ with order $p = \epsilon - \rho$ and parameters $u_l = 2\langle\eta_l\rangle_{q(\boldsymbol{\eta})}$ and $v_l = 2\rho\langle|\alpha_l|^2\rangle_{q(\boldsymbol{\alpha})}$.

Observe that the computation of $\boldsymbol{V}(\boldsymbol{\gamma})$ in (28) requires evaluating $\langle\gamma_l^{-1}\rangle_{q(\boldsymbol{\gamma})}$ for all $l = 1, \ldots, L$. Luckily, the moments of the GIG distribution are given in closed form for any $n \in \mathbb{R}$ [25]:

$$\langle\gamma_l^n\rangle_{q(\boldsymbol{\gamma})} = \left(\frac{\rho\langle|\alpha_l|^2\rangle_{q(\boldsymbol{\alpha})}}{\langle\eta_l\rangle_{q(\boldsymbol{\eta})}}\right)^{\frac{n}{2}}\frac{K_{p+n}\left(2\sqrt{\rho\langle\eta_l\rangle_{q(\boldsymbol{\eta})}\langle|\alpha_l|^2\rangle_{q(\boldsymbol{\alpha})}}\right)}{K_p\left(2\sqrt{\rho\langle\eta_l\rangle_{q(\boldsymbol{\eta})}\langle|\alpha_l|^2\rangle_{q(\boldsymbol{\alpha})}}\right)}. \tag{33}$$

In the special case of ℓ_1-norm priors, i.e., when $p = \epsilon - \rho = 1/2$, using the identity $K_\nu(\cdot) = K_{-\nu}(\cdot)$ [19], (33) simplifies to

$$\langle\gamma_l^{-1}\rangle_{q(\boldsymbol{\gamma})} = \left(\frac{\langle\eta_l\rangle_{q(\boldsymbol{\eta})}}{\rho\langle|\alpha_l|^2\rangle_{q(\boldsymbol{\alpha})}}\right)^{\frac{1}{2}}. \tag{34}$$

3) Update of $q(\boldsymbol{\eta})$: The update of $q(\boldsymbol{\eta})$ is the product of messages $m_{p_{\boldsymbol{\eta}}\to\boldsymbol{\eta}}$ and $m_{p_{\boldsymbol{\gamma}}\to\boldsymbol{\eta}}$:

$$q(\boldsymbol{\eta}) \propto \prod_{l=1}^{L} \eta_l^{\epsilon+a_l-1} \exp\left(-(\langle\gamma_l\rangle_{q(\boldsymbol{\gamma})} + b_l)\eta_l\right), \tag{35}$$

which is identified as a gamma pdf. The first moment of η_l used in (33) is easily computed as

$$\langle\eta_l\rangle_{q(\boldsymbol{\eta})} = \frac{\epsilon + a_l}{\langle\gamma_l\rangle_{q(\boldsymbol{\gamma})} + b_l}. \tag{36}$$

Naturally, $q(\boldsymbol{\eta})$ is only computed for VMP-3L.

4) Update of $q(\lambda)$: The update of $q(\lambda)$ can be shown to be $q(\lambda) = \mathrm{Ga}(\lambda|\rho M + c, \rho\langle\|\boldsymbol{y} - \boldsymbol{H}\boldsymbol{\alpha}\|_2^2\rangle_{q(\boldsymbol{\alpha})} + d)$. The first moment of λ used in (28) and (29) is therefore computed as

$$\langle\lambda\rangle_{q(\lambda)} = \frac{\rho M + c}{\rho\langle\|\boldsymbol{y} - \boldsymbol{H}\boldsymbol{\alpha}\|_2^2\rangle_{q(\boldsymbol{\alpha})} + d}. \tag{37}$$

B. Pruning a basis function

When the estimation algorithm produces a sparse parameter vector $\widehat{\boldsymbol{\alpha}}$ with $\widehat{K}$ non-zero components, the remaining $L - \widehat{K}$ basis function in the measurement matrix $\boldsymbol{H}$ can be removed from the model. This basis function pruning drastically lowers the computational complexity of the VMP algorithm. Specifically, it reduces the computational complexity of the inversion of the covariance matrix in (28) from $O(L^3)$ to $O(\widehat{K}^3)$.

A closer inspection of (28) reveals that the parameters $\langle\gamma_l^{-1}\rangle_{q(\boldsymbol{\gamma})}$ are in fact classical regularization terms for estimating the weights $\boldsymbol{\alpha}$. Quite naturally, the larger the value of $\langle\gamma_l^{-1}\rangle_{q(\boldsymbol{\gamma})}$, i.e., the larger the regularization for the lth basis function $\boldsymbol{h}_l$, the smaller the estimate of the corresponding α_l. Thus, it makes sense to remove $\boldsymbol{h}_l$ in $\boldsymbol{H}$ when $\langle\gamma_l^{-1}\rangle_{q(\boldsymbol{\gamma})}$ exceeds a certain large threshold. The same method was used in [12] for the G-IGa prior model to obtain a sparse solution.

V. Numerical Results

We perform Monte Carlo simulations to evaluate the performance of the two versions of the derived VMP algorithm in Sec. IV. A complex-valued signal model (1) is considered in all experiments, where for each Monte Carlo run a random $M \times L$ matrix $\boldsymbol{H}$, a K-sparse vector $\boldsymbol{\alpha}$, and a random perturbation vector $\boldsymbol{w}$ are generated. In order to test the methods on a realistic benchmark we use a random dictionary $\boldsymbol{H}$ whose entries are independent and identically distributed (iid) zero-mean complex symmetric Gaussian random variables with unit variance. The indices of the K non-zero components of $\boldsymbol{\alpha}$ are uniformly drawn from the set $\{1, 2, \ldots, L\}$. The K non-zero components of $\boldsymbol{\alpha}$ are iid and drawn from a zero-mean

Legend	Model	Parameters
VMP-2L($\epsilon = 3/2$)	G-Ga	$\epsilon = 3/2$
VMP-2L($\epsilon = 0$)	G-Ga	$\epsilon = 0$
VMP-3L($\epsilon = 3/2$)	G-Ga-Ga	$\epsilon = 3/2$, $\boldsymbol{a} = \mathbf{1}$, $\boldsymbol{b} = 10^{-6}\mathbf{1}$
VMP-3L($\epsilon = 0$)	G-Ga-Ga	$\epsilon = 0$, $\boldsymbol{a} = \mathbf{1}$, $\boldsymbol{b} = 10^{-6}\mathbf{1}$

TABLE I
THE SELECTED PARAMETERS FOR THE PROPOSED PRIOR MODELS PRESENTED IN SEC. II. HERE, $\mathbf{1} := [1, \ldots, 1]^T$.

complex circular symmetric Gaussian distribution with unit variance. All reported curves are computed based on a total of 200 Monte Carlo runs.

Table I summarizes the choice of the free parameters for the G-Ga and G-Ga-Ga prior models discussed in Sec. II. As indicated in the table, the selected value of ϵ used in the different versions of the VMP algorithm is appended to their acronyms.

To initialize the VMP algorithm we set $\langle\lambda\rangle_{q(\lambda)}$ equal to $(\mathbb{V}\text{ar}\{\boldsymbol{y}\})^{-1}$ and $\langle\gamma_l^{-1}\rangle_{q(\boldsymbol{\gamma})}$ equal to the inverse number of columns L. Furthermore, we let $c = d = 0$ in (37), which corresponds to a non-informative prior for λ. Once the initialization is completed, the algorithm sequentially updates the auxiliary pdfs $q(\boldsymbol{\alpha})$, $q(\boldsymbol{\gamma})$, $q(\lambda)$, and $q(\boldsymbol{\eta})$ until convergence is achieved. As stated in Sec. IV, $q(\boldsymbol{\eta})$ is only updated for VMP-3L, whereas for VMP-2L the entries in $\boldsymbol{\eta}$ are free parameters that must be determined. Therefore, we propose to use the re-weighting scheme of [8] to update η_l once the VMP-2L algorithm has converged and a solution $\hat{\alpha}_l$ is produced. The parameters η_l, $l = 1, \ldots, L$, are then updated based on the corresponding estimates $\hat{\alpha}_l$ and the VMP-2L algorithm is iterated once more with the updated parameters. Specifically, η_l is updated as [8]

$$\eta_l = (|\hat{\alpha}_l| + \varsigma)^{-2} \tag{38}$$

with the parameter ς set to $\varsigma = 10^{-3}$. Empirically we have observed that only a few (roughly $3 - 4$) re-weighting updates are needed. Initially, we choose $\boldsymbol{\eta} = [1, \ldots, 1]^T$ the first time the VMP-2L algorithm solves the optimization problem.

In the sequel we perform the following investigations: first, the performance of the VMP-2L and VMP-3L is analyzed; then, the VMP algorithm is compared with several state-of-the-art sparse estimation schemes. The performance of the compared algorithms is evaluated based on the mean-squared error (MSE) of $\widehat{\boldsymbol{\alpha}}$ and the number of non-zero elements $\widehat{K}$ in $\widehat{\boldsymbol{\alpha}}$. Note that the estimate $\hat{\alpha}_l$ is set to zero when $\langle\gamma_l^{-1}\rangle_{q(\boldsymbol{\gamma})}$ exceeds a fixed threshold set at 10^6.

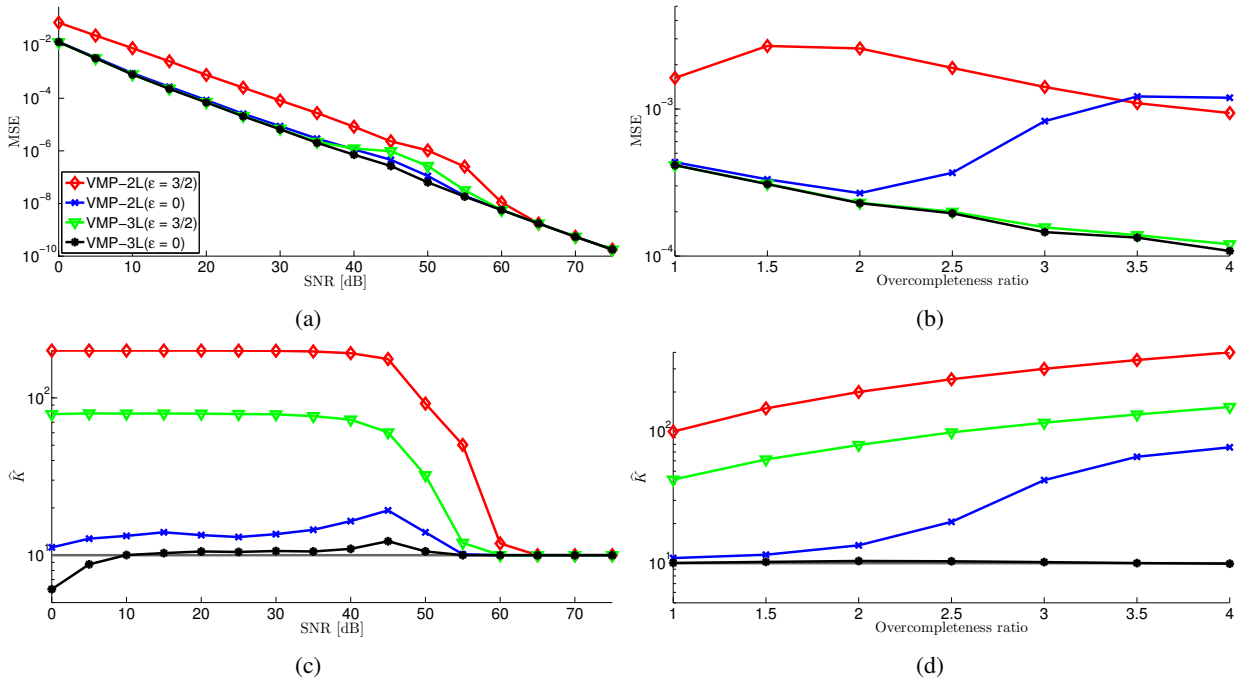

Fig. 6. Performance of the VMP algorithm: (a,b) MSE versus (a) SNR and (b) overcompleteness ratio L/M with $M = 100$. (c,d) Estimated number of non-zero components $\widehat{K}$ versus (c) SNR and (d) overcompleteness ratio L/M (M=100) at 15 dB SNR. The gray horizontal line indicates the true number of non-zero components in $\boldsymbol{\alpha}$.

A. Performance of the VMP algorithm

Here we evaluate the performance of the VMP algorithm versus (i) the SNR per received signal component and (ii) the overcompleteness ratio L/M. The results illustrate the sensitivity of the algorithm to measurement noise and its performance in classical compressive sampling test setting, where the number of basis functions L exceeds the number of measurements samples M. In these investigations the true number of non-zero components in $\boldsymbol{\alpha}$ is set to $K = 10$.

In Figs. 6(a) and 6(c) the performance of the algorithm is evaluated versus the SNR with $M = 100$ and $L = 200$, which yields an overcompleteness ratio of $L/M = 2$. Notice that in a very high SNR regime, i.e., when the observation is practically noise free, the performance of the compared schemes is almost indistinguishable. However, when the noise cannot be neglected, VMP-3L($\epsilon = 0$) clearly outperforms the other three schemes in terms of the estimate $\widehat{K}$, followed closely by VMP-2L($\epsilon = 0$); VMP-2L($\epsilon = 3/2$) clearly performs worse than the other schemes both in terms of the achieved sparseness and MSE. Observe that when $\epsilon = 3/2$, which is equivalent to the ℓ_1-norm parameter constraint, both G-Ga and G-Ga-Ga models induce a heavily overestimation of K; in contrast, setting $\epsilon = 0$ leads to much sparser solutions. Also, notice that for a fixed ϵ, the G-Ga-Ga model generally leads to an estimator that produces sparser

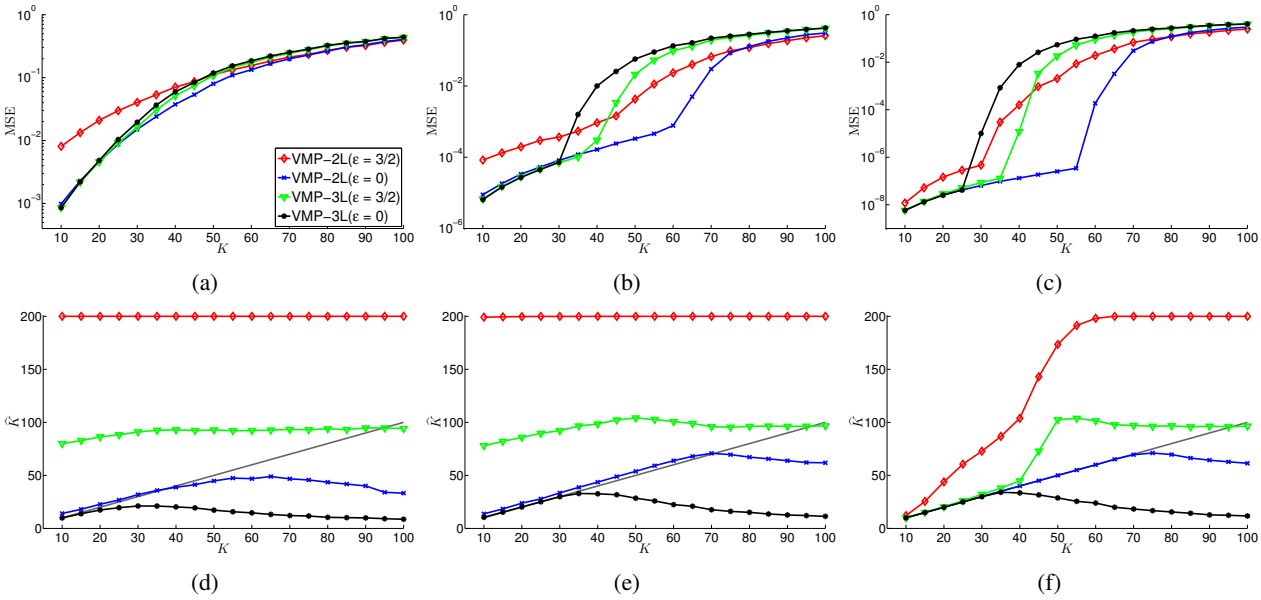

Fig. 7. Performance of the VMP algorithm: (a)-(c) MSE performance and (d)-(f) estimated number of non-zero components $\widehat{K}$ versus the true number of non-zero components K. The SNR is set to 10 dB in (a) and (d), 30 dB in (b) and (e), and 60 dB in (c) and (f).

results as compared to that of the G-Ga model.

In Figs. 6(b) and 6(d) the performance of the algorithm is compared as a function of the overcompleteness ratio L/M for an SNR level fixed at 15 dB. Here again VMP-3L($\epsilon = 0$) is a clear winner. We also notice that for a fixed ϵ the G-Ga-Ga model induces better performance over the G-Ga model, and the case $\epsilon = 0$ outperforms the schemes realizing the ℓ_1-norm parameter constraints with $\epsilon = 3/2$.

Next we evaluate the performance of the schemes as a function of the number of non-zero components K in $\boldsymbol{\alpha}$. To this end we set $M = 100$, $L = 200$ and vary K from 10 to M. The MSE and the estimate $\widehat{K}$ are compared for SNR fixed at 10 dB, 30 dB, and 60 dB. The corresponding results are shown in Fig. 7. In low SNR regime ($\sim$ 10 dB) VMP-2L($\epsilon = 0$), VMP-3L($\epsilon = 3/2$), and VMP-3L($\epsilon = 0$) exhibit an almost identical MSE performance, with VMP-2L($\epsilon = 3/2$) performing worse only for low K values. However, $\widehat{K}$ does vary for these schemes. For $\epsilon = 3/2$ the estimate $\widehat{K}$ is almost independent of the true number of non-zero components K. However, when $\epsilon = 0$, VMP-3L($\epsilon = 0$) underestimates K, performing best only if $K < 20$; in contrast VMP-2L($\epsilon = 0$) exhibits acceptable performance for $K < 40$. As the SNR increases, the performance of all schemes improves, yet the MSE curves begin to exhibit an interesting thresholding effect, which gives the highest K value for which the algorithm is still able to recover the true number of non-zero components. Here, VMP-2L($\epsilon = 0$) performs the best, exhibiting the thresholding behavior at $K \approx 60$ or even $K \approx 70$ as the SNR grows to 60 dB. It

is followed by VMP-3L($\epsilon = 0$), exhibiting the thresholding effect already at $K \approx 30$ for both 30 dB and 60 dB SNR. However, the performance of both schemes with $\epsilon = 0$ significantly degrades when K increases beyond the corresponding sparsity threshold levels, i.e., when the signal becomes less sparse. Specifically, the number of non-zero components in $\boldsymbol{\alpha}$ is underestimated, leading to an abrupt increase in the MSE of the estimates. The VMP schemes with $\epsilon = 3/2$ become effective only when the SNR level becomes very high, with VMP-3L($\epsilon = 3/2$) inducing superior performance than VMP-2L($\epsilon = 3/2$).

In what follows we compare the performance of VMP-2L($\epsilon = 0$) and VMP-3L($\epsilon = 0$) with several other sparse estimation algorithms.

B. Comparison with Existing Sparse Methods

In the following, we compare VMP-2L($\epsilon = 0$) and VMP-3L($\epsilon = 0$) to the ARD formulation of the RVM [12], [13], the *sparse reconstruction by separable approximation* (SpaRSA) algorithm [26],[7] and a re-weighted version of SpaRSA. The SpaRSA algorithm is a proximal gradient method for solving the LASSO cost function. We can easily extend the framework of [26] to solve the weighted LASSO cost function:

$$\widehat{\boldsymbol{z}} = \underset{\boldsymbol{z}\in\mathbb{C}^L}{\operatorname{argmin}} \left\{ \frac{1}{2}\|\boldsymbol{y} - \boldsymbol{H}\boldsymbol{B}^{-1}\boldsymbol{z}\|_2^2 + \kappa\|\boldsymbol{z}\|_1 \right\}, \tag{39}$$

where $\boldsymbol{\alpha} = \boldsymbol{B}^{-1}\boldsymbol{z}$ and $\boldsymbol{B} \triangleq \operatorname{diag}\{\boldsymbol{\beta}\}$. The components of $\boldsymbol{\beta} \triangleq [\beta_1, \ldots, \beta_L]^T$ are updated according to (20) with $\varsigma = 10^{-3}$ a total of 3 times. Further in the text we will refer to this algorithm as Reweighted SpaRSA. Note that the choice of κ has a crucial impact on the performance of the resulting inference. For large κ the algorithm produces very sparse estimates; however, the MSE performance in this case might significantly degrade. In our implementation of this estimation scheme we select $\kappa = 0.2$ for SpaRSA and $\kappa = 0.05$ for Reweighted SpaRSA. The latter values were empirically found to balance well the achieved signal sparsity with the MSE. As already mentioned, VMP-3L, in contrast, provides the necessary mechanism to set this regularization parameter automatically.

In Fig. 8 the performance of the compared schemes is depicted for $K = 10$. In Figs. 8(a), 8(c) the dependency of the estimates' MSE on the SNR for the overcompleteness ratio $L/M = 2$ with $M = 100$ is visualized. Observe that VMP-2L($\epsilon = 0$) and VMP-3L($\epsilon = 0$) achieve lower MSE in the SNR range up to 60 dB as compared to the other schemes. Furthermore, in this SNR range they also produce sparser estimates. However, Reweighted SpaRSA "catches" the VMP curves already at 30 dB, slightly

[7]The software is available on-line at http://www.lx.it.pt/~mtf/SpaRSA/

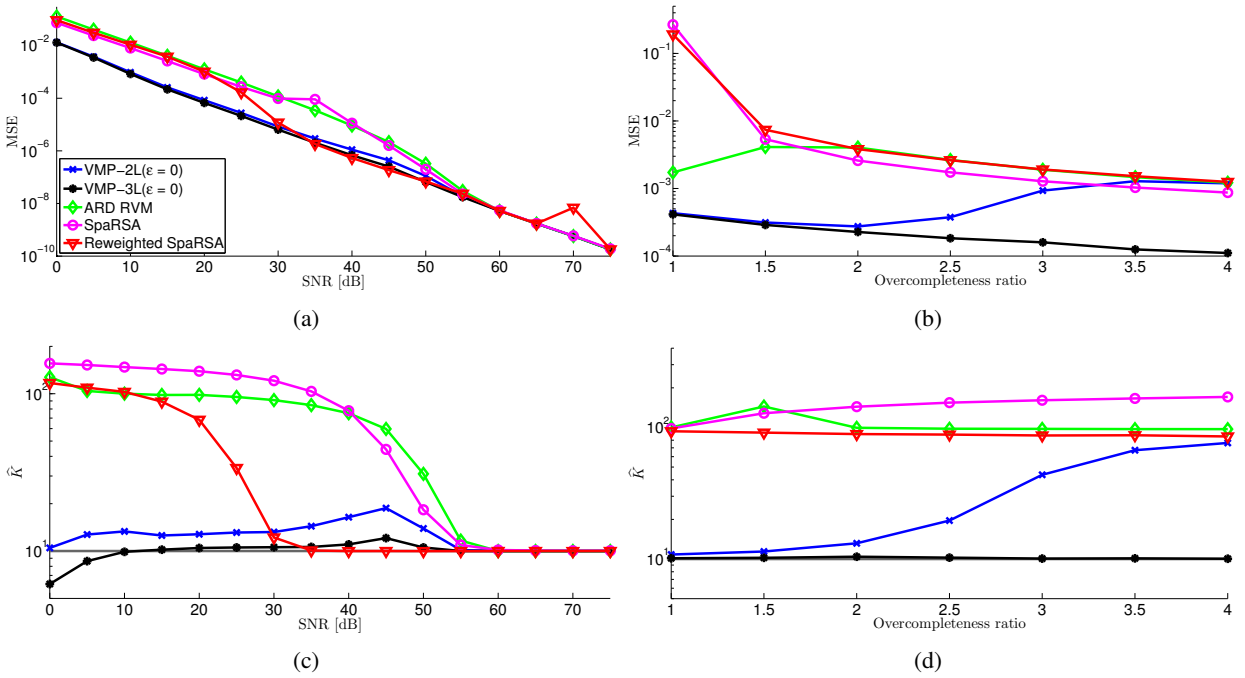

Fig. 8. Performance comparisons of VMP-2L($\epsilon = 0$) and VMP-3L($\epsilon = 0$) with ARD RVM, SparseRSA and Reweighted SparseRSA algorithms: (a,b) MSE versus (a) SNR and (b) overcompleteness ratio L/M with $M = 100$. (c,d) Estimated number of non-zero components $\widehat{K}$ versus (c) SNR and (d) overcompleteness ratio L/M (M=100) at 15 dB SNR. The gray horizontal line indicates the true number of non-zero components in $\boldsymbol{\alpha}$.

outperforming VMP-2L($\epsilon = 0$) in terms of the estimated number of non-zero components. A similar trend is observed when the algorithm performance is compared as a function of the overcompleteness ratio L/M in Figs. 8(b) and 8(d). Although the G-Ga and G-Ga-Ga models with $\epsilon = 0$ lead to estimators with better performance than the other schemes, the performance of VMP-2L($\epsilon = 0$) degrades as the ratio L/M increases, while VMP-3L($\epsilon = 0$) performs well almost independently of the actual overcompleteness ratio.

Now we test the performance of the algorithms versus K with $L/M = 2$ and $M = 100$. The corresponding results are shown in Fig. 9 for the SNR level fixed at 10 dB, 30 dB, and 60 dB. Interestingly, a similar thresholding behavior is observed here also for ARD RVM and both SparseRSA schemes. The VMP schemes perform better in low ($\sim$ 10 dB) and moderate ($\sim$ 30 dB) SNR regimes. In high SNR regime ARD RVM performs almost as well as VMP-2L($\epsilon = 0$), yet it significantly overestimates K for $K > 70$. Reweighted SparseRSA also performs quite well in the high SNR regime, for $K < 50$, overestimating K as K grows.

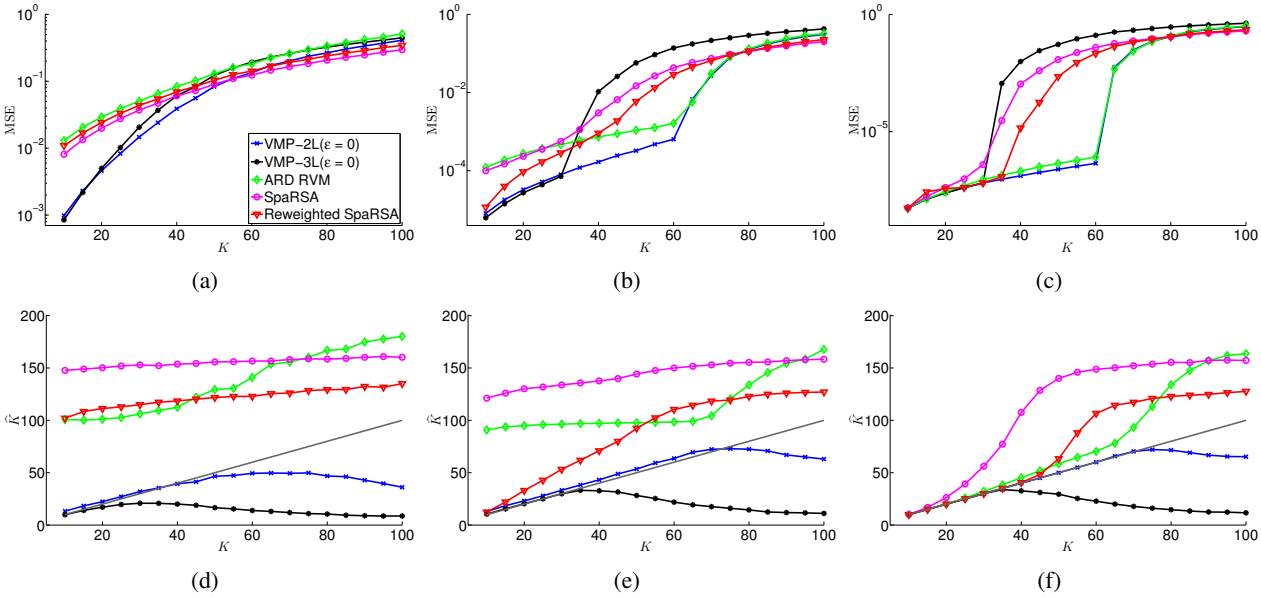

Fig. 9. Performance comparisons of VMP-2L($\epsilon = 0$) and VMP-3L($\epsilon = 0$) with ARD RVM, SparseRSA and Reweighted SparseRSA algorithms: (a)-(c) MSE performance and (d)-(f) estimated number of non-zero components $\widehat{K}$ versus the true number of non-zero components K. The SNR is set to 10 dB in (a) and (d), 30 dB in (b) and (e), and 60 dB in (c) and (f).

VI. Conclusion

In this paper a unifying sparse Bayesian formalism with hierarchical sparsity prior modeling was proposed. The presented methodology generalizes the sparse modeling of complex- as well as real-valued systems. Taking as a starting point the hierarchical structure for modeling the ℓ_1 parameter constraint, originally proposed by M. Figueredo, we extend this model to the complex domain, which leads to a parametric family of sparsity-inducing hierarchical priors.

The new approach uses a product of zero-mean Gaussian priors defined for each element of the parameter vector $\boldsymbol{\alpha}$, with the variance of each prior following a gamma distribution characterized by a shape parameter ϵ and a component specific scale parameter η_l. This model we termed the Gaussian-gamma prior model. The choice $\epsilon = 3/2$ in case of complex-valued models and $\epsilon = 1$ in case of real-valued models corresponds to the Bayesian hierarchical modeling of the ℓ_1-norm constraint in the objective function. Naturally, other values of $\epsilon \geq 0$ can be utilized. This additional degree of freedom in controlling the sparsity properties with ϵ leads to priors with strong sparsity properties. More specifically, it was shown that the case $\epsilon = 0$ encourages a sparser solution than the ℓ_1-norm constraint. Furthermore, varying the parameter ϵ of the Gaussian-gamma model leads to estimators of $\boldsymbol{\alpha}$ that approximate a well-known soft-thresholding rule.

We also considered a further extension of the Gaussian-gamma prior model by modeling the hyperparameters η_l as random variables with a gamma prior pdf. The new model – the Gaussian-gamma-gamma prior model – also generalizes complex- as well as real-valued scenarios and allows for an automatic selection of the parameter η_l. Similarly to the Gaussian-gamma model, the three-layer Gaussian-gamma-gamma prior also leads to a family of parametric priors with different sparsity-inducing properties. However, varying the free parameters of the Gaussian-gamma-gamma model leads to estimators of $\boldsymbol{\alpha}$ that approximate a hard-thresholding rule.

Finally, we proposed a variational message passing (VMP) algorithm for the estimation of the model parameters. The proposed VMP algorithm effectively exploits the probabilistic structure of the inference problem. It was shown that in general the case $\epsilon = 0$ outperforms the ℓ_1-norm constraint both in terms of the sparsity as well as in the achieved MSE. The proposed extension of the Bayesian hierarchical model for sparsity constraint is a very powerful, yet analytically tractable and simple mechanism for implementing sparse estimators. Our numerical results show that we obtained a very significant performance improvement over existing sparse methods when testing in low and moderate SNR regimes, in which state-of-art estimators failed to produce sparse solutions.

REFERENCES

[1] R. Baraniuk, "Compressive sensing," *IEEE Signal Processing Magazine*, vol. 24, no. 4, pp. 118–121, July 2007.

[2] M. Wakin, "An introduction to compressive sampling," *IEEE Signal Process. Mag.*, vol. 25, no. 2, pp. 21–30, Mar. 2008.

[3] D. G. Tzikas, A. C. Likas, and N. P. Galatsanos, "The variational approximation for Bayesian inference," *IEEE Signal Process. Mag.*, vol. 25, no. 6, pp. 131–146, November 2008.

[4] W. Bajwa, J. Haupt, A. Sayeed, and R. Nowak, "Compressed channel sensing: A new approach to estimating sparse multipath channels," *Proceedings of the IEEE*, vol. 98, no. 6, pp. 1058–1076, June 2010.

[5] D. Shutin and B. H. Fleury, "Sparse variational Bayesian SAGE algorithm with application to the estimation of multipath wireless channels," *IEEE Trans. on Sig. Proc.*, vol. 59, pp. 3609–3623, 2011.

[6] D. Shutin, T. Buchgraber, S. R. Kulkarni, and H. V. Poor, "Fast variational sparse Bayesian learning with automatic relevance determination for superimposed signals," *submitted to IEEE Transactions on Signal Processing*.

[7] A. Lee, F. Caron, A. Doucet, and C. Holmes, "A hierarchical bayesian framework for constructing sparsity-inducing priors," Sep. 2010. [Online]. Available: arXiv:1009.1914

[8] E. J. Candes, M. B. Wakin, and S. P. Boyd, "Enhancing sparsity by reweighted ℓ_1 minimization," *Journal of Fourier Analysis and Applications*, vol. 14, pp. 877–905, 2008.

[9] M. Seeger and D. Wipf, "Variational bayesian inference techniques," *Signal Processing Magazine, IEEE*, vol. 27, no. 6, pp. 81 –91, 2010.

[10] D. Wipf and S. Nagarajan, "Iterative reweighted ℓ_1 and ℓ_2 methods for finding sparse solutions," *IEEE Journal of Selected Topics in Signal Processing*, vol. 4, no. 2, pp. 317–329, 2010.

[11] ——, "A new view of automatic relevance determination," in *Proc. 21 Annual Conf. on Neural Inform. Process. Systems*. Vancouver, British Columbia, Canada: MIT Press, Dec. 2007.

[12] M. Tipping, "Sparse Bayesian Learning and The Relevance Vector Machine," *J. of Machine Learning Res.*, vol. 1, pp. 211–244, June 2001.

[13] D. Wipf and B. Rao, "Sparse Bayesian learning for basis selection," *IEEE Trans. on Sig. Proc.*, vol. 52, no. 8, pp. 2153 – 2164, aug. 2004.

[14] M. E. Tipping and A. C. Faul, "Fast marginal likelihood maximisation for sparse Bayesian models," in *Proc. 9th International Workshop on Artificial Intelligence and Statistics*, Key West, FL, January 2003.

[15] D. Shutin, T. Buchgraber, S. R. Kulkarni, and H. V. Poor, "Fast adaptive variational sparse Bayesian learning with automatic relevance determination," in *Proc. IEEE Int. Conf. Acoustics, Speech, and Signal Processing (ICASSP)*, Prague, Czech Republic, 2011, to appear.

[16] M. Figueiredo, "Adaptive sparseness for supervised learning," *IEEE Trans. on Pattern Analysis and Machine Intel.*, vol. 25, no. 9, pp. 1150–1159, 2003.

[17] R. Tibshirani, "Regression shrinkage and selection via the LASSO," *J. R. Statist. Soc.*, vol. 58, pp. 267–288, 1994.

[18] A. Fletcher, S. Rangan, and V. Goyal, "Necessary and sufficient conditions for sparsity pattern recovery," *IEEE Transactions on Information Theory*, vol. 55, no. 12, pp. 5758 –5772, 2009.

[19] M. Abramowitz and I. A. Stegun, *Handbook of Mathematical Functions with Formulas, Graphs, and Mathematical Tables*. Dover, 1972.

[20] P. Moulin and J. Liu, "Analysis of multiresolution image denoising schemes using generalized Gaussian and complexity priors," *IEEE Transactions on Information Theory*, vol. 45, no. 3, pp. 909–919, 1999.

[21] D. P. Wipf and S. Nagarajan, "A new view of automatic relevance determination," *Proc. Neural Information Processing Systems (NIPS)*, vol. 20, 2008.

[22] E. W. Stacy, "A generalization of the gamma distribution," *The Annals of Mathematical Statistics*, vol. Vol. 33, no. 3, pp. 1187–1192, Sep. 1962.

[23] F. R. Kschischang, B. J. Frey, and H. A. Loeliger, "Factor graphs and the sum-product algorithm," *IEEE Transactions on Information Theory*, vol. 47, no. 2, pp. 498–519, Feb 2001.

[24] J. Winn and C. M. Bishop, "Variational Message Passing," *J. Mach. Learn. Res.*, vol. 6, pp. 661–694, 2005.

[25] B. Jorgensen, *Statistical Properties of the Generalized Inverse Gaussian Distribution (Lecture Notes in Statistics 9)*. Springer-Verlag New York Inc, 1982.

[26] S. J. Wright, R. D. Nowak, and M. A. T. Figueiredo, "Sparse reconstruction by separable approximation," *IEEE Trans. on Sig. Proc.*, vol. 57, no. 7, pp. 2479–2493, 2009.

Paper E

Variational Message-Passing for Joint Channel Estimation and Decoding in MIMO-OFDM

Gunvor E. Kirkelund, Carles Navarro Manchón, Lars P.B. Christensen, Erwin Riegler and Bernard H. Fleury

IEEE Global Communications Conference, GLOBECOM 2010. Miami, December 2010.

E. VARIATIONAL MESSAGE-PASSING FOR JOINT CHANNEL ESTIMATION AND DECODING IN MIMO-OFDM

This full text paper was peer reviewed at the direction of IEEE Communications Society subject matter experts for publication in the IEEE Globecom 2010 proceedings.

Variational Message-Passing for Joint Channel Estimation and Decoding in MIMO-OFDM

Gunvor Elisabeth Kirkelund*, Carles Navarro Manchón*, Lars P. B. Christensen†, Erwin Riegler§ and Bernard Henri Fleury*
*Department of Electronic Systems, Aalborg University, Denmark
†Modem Algorithm Design, NOKIA, Denmark
§Vienna University of Technology (VUT)
Email: {gunvor, cnm}@es.aau.dk, lars.christensen@nokia.com, erwin.riegler@nt.tuwien.ac.at, bfl@es.aau.dk

***Abstract*—In this contribution, a multi-user receiver for M-QAM MIMO-OFDM operating in time-varying and frequency-selective channels is derived. The proposed architecture jointly performs semi-blind estimation of the channel weights and noise inverse variance, serial interference cancellation and decoding in an iterative manner. The scheme relies on a variational message-passing approach, which enables a joint design of all these functionalities or blocks but the last one. Decoding is performed using the sum-product algorithm. This is in contrast to nowadays proposed approaches in which all these blocks are designed and optimized individually. Simulation results show that the proposed receiver outperforms in coded bit-error-rate a state-of-the-art iterative receiver of same complexity, in which all blocks are designed independently. Joint block design and, as a result, the fact that the uncertainty in the channel estimation is accounted for in the proposed receiver explain this better performance.**

I. INTRODUCTION

During recent years, algorithms based on iterative information processing or "turbo" techniques have become widespread in wireless receiver design [1]–[3]. The success of these algorithms can be explained by their remarkable properties: high performance at tractable complexity and flexibility in their design. An emblematic example is turbo-codes, which, when associated with turbo-decoding, allow for transmission close to capacity at tractable complexity [1].

In this paper, we focus on a specific application of iterative information processing, namely to design efficient, feasible algorithms for channel estimation (i.e. estimation of both the channel transfer function and the channel inverse noise variance), interference cancellation, and decoding in MIMO-OFDM systems. Some related work is already available in the literature. Worth noticing is the iterative algorithm for detection and interference cancellation [4] applied to multiuser CDMA. This algorithm is extended for various transmission schemes in [5]–[7] to include estimation of the channel response into the iterative process. We coin this receiver the LMMSE-based receiver, according to the dominant structure implemented in its constituent blocks. An essential feature of this receiver is that its constituent blocks are designed and optimized individually. These blocks are connected afterwards to form the iterative structure.

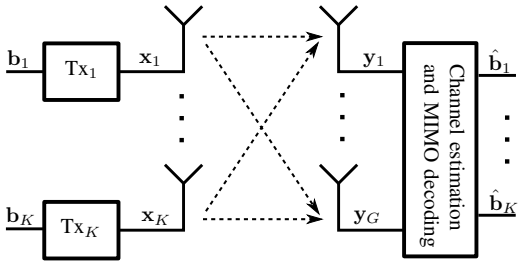

Fig. 1. Baseband signal model of the considered MIMO-OFDM system.

In this contribution, we apply variational Bayesian (VB) inference [8] and one of its applications, namely the variational Bayesian expectation maximization (VBEM) algorithm [9] to perform channel weight and noise inverse variance estimation as well as serial interference cancellation in an M-QAM MIMO-OFDM system operating in time-variant frequency-selective channels. Decoding is performed using the sum-product (SP) algorithm [3]. The VBEM algorithm has already been applied in [10] for GSM channel estimation and detection. In [11] it is combined with the sum-product algorithm for the design of a multiuser CDMA receiver. Further related work is found in [12]–[15]. In our paper, we apply the VBEM scheme in [11] to MIMO-OFDM and reformulate it as a variational message-passing (VMP) algorithm on factor graphs [16].

The proposed VMP receiver and the LMMSE-based receiver from [5]–[7] share similar features in their respective structures. Thus, we find it useful to also include a comparison of the two schemes. A crucial difference is that the estimation of the noise and residual interference power in the VMP receiver accounts for the uncertainty in the channel coefficient estimates, an effect not considered in the LMMSE-based receiver. This, combined with the joint design of all receiver blocks but decoding, yields a superior performance of the VMP receiver, as our simulation results demonstrate.

The notational convention for the rest of the paper is as follows: the superscripts $(\cdot)^{\mathrm{T}}$ and $(\cdot)^{\mathrm{H}}$ denote transposition and Hermitian transposition respectively. The symbol $\cdot \propto \cdot$ denotes proportionality. The trace operator is designated as $\mathrm{tr}(\cdot)$. The expectation operation with respect to a function $q(x)$ is represented by $\langle\cdot\rangle_{q(x)}$. The newest estimate of the mean or covariance of a variable is denoted by $\hat{\cdot}$. The operators $\mathrm{diag}(\cdot)$ and $\mathrm{Diag}(\cdot)$ denote the vectorized diagonal of a matrix and the diagonalized matrix of a vector respectively. For matrices $\mathbf{A}$ and $\mathbf{B}$, the Kronecker and Hadamard products are represented

978-1-4244-5638-3/10/$26.00 ©2010 IEEE

by $\mathbf{A}\otimes\mathbf{B}$ and $\mathbf{A}\odot\mathbf{B}$ respectively (for the Hadamard product $\mathbf{A}$ and $\mathbf{B}$ are assumed to have the same dimension). The identity matrix of dimension K is designated as $\mathbf{I}_K$ and $\mathbf{1}_G$ represents the all-one matrix of dimension $G \times G$. We employ $\mathbf{0}_K$ and $[1 \dots 1]_K$ to designate respectively the all-zero column-vector and the all-one row-vector of length K.

II. Signal Model

We consider the LTE-like MIMO-OFDM system depicted in Fig. 1 in which we have K transmitters, indexed by k, and G receivers, indexed by g. In the kth transmitter, denoted by Tx_k, the bit-stream $\mathbf{b}_k$ is encoded, interleaved and modulated into data symbols, which are then multiplexed with pilot symbols to allow for channel estimation in the receiver. Pilot and data symbols are arranged in an OFDM frame of L OFDM symbols consisting of N subcarriers each. The OFDM frame of Tx_k is represented by $\mathbf{x}_k \triangleq [x_{k11} \dots x_{knl} \dots x_{kNL}]^{\mathrm{T}} \in \mathcal{X}_k$, where l indexes the OFDM symbols and n indexes the subcarrier number. The set $\mathcal{X}_k$ of legal M-ary sequences of Tx_k is determined by the coding and modulation scheme and the multiplexing scheme of data and pilot symbols.

The OFDM frames are transmitted across a time-variant frequency-selective channel. The samples of the time-frequency response of the sub-channel from transmit antenna k to receive antenna g are concatenated in the channel weight vector $\mathbf{a}_{gk} \triangleq [a_{gk11} \dots a_{gk1L} \dots a_{gknl} \dots a_{gkNL}]^{\mathrm{T}}$. Assuming that inter-symbol and inter-subcarrier interferences are negligible, the received signals at all G antenna ports are given in vector notation by

$$\mathbf{y} = \sum_{k=1}^{K} \mathbf{A}_k \mathbf{x}_k + \mathbf{w} \tag{1}$$

$$= \mathbf{X}\mathbf{a} + \mathbf{w} \tag{2}$$

$$= \mathbf{A}\mathbf{x} + \mathbf{w}. \tag{3}$$

The vector $\mathbf{y}$ is the concatenation of the output vectors of all receive antennas, $\mathbf{y} \triangleq [\mathbf{y}_1^{\mathrm{T}} \dots \mathbf{y}_g^{\mathrm{T}} \dots \mathbf{y}_G^{\mathrm{T}}]^{\mathrm{T}}$ with $\mathbf{y}_g \triangleq [y_{g11} \dots y_{gnl} \dots y_{gNL}]^{\mathrm{T}}$ denoting the output of receive antenna g. The channel matrix for transmitter k is defined as $\mathbf{A}_k \triangleq \mathrm{Diag}(\mathbf{a}_k)([1 \dots 1]_G^{\mathrm{T}} \otimes \mathbf{I}_N)$. The noise vector $\mathbf{w}$ is white and circularly symmetric complex Gaussian: $\mathbf{w} \sim \mathcal{CN}(\mathbf{0}_{GNL}, \sigma_w^2 \mathbf{I}_{GNL})$, with σ_w^2 denoting the noise variance. We define the precision parameter $\lambda \triangleq \sigma_w^{-2}$. The matrix $\mathbf{X}$ is defined as $\mathbf{X} \triangleq \mathbf{I}_G \otimes (([1 \dots 1]_K \otimes \mathbf{I}_N)\mathrm{Diag}(\mathbf{x}))$ and $\mathbf{a} \triangleq [\mathbf{a}_{11}^{\mathrm{T}} \dots \mathbf{a}_{gk}^{\mathrm{T}} \dots \mathbf{a}_{GK}^{\mathrm{T}}]^{\mathrm{T}}$. The matrix $\mathbf{A} \triangleq (\mathbf{I}_G \otimes ([1 \dots 1]_K \otimes \mathbf{I}_N))\mathrm{Diag}(\mathbf{a})(([1 \dots 1]_G^{\mathrm{T}} \otimes \mathbf{I}_K) \otimes \mathbf{I}_N)$ is the MIMO channel matrix. The vector $\mathbf{x} \triangleq [\mathbf{x}_1^{\mathrm{T}} \dots \mathbf{x}_k^{\mathrm{T}} \dots \mathbf{x}_K^{\mathrm{T}}]^{\mathrm{T}}$ contains the concatenated OFDM codewords from all transmit antennas. The receiver outputs an estimate $\hat{\mathbf{b}}_k$ of the bit-stream for any k.

III. Graphical Representation

In this section, we present a graphical representation of the signal model introduced in the previous section. This graphical representation will be used to derive the message-passing algorithm in Section IV. Let

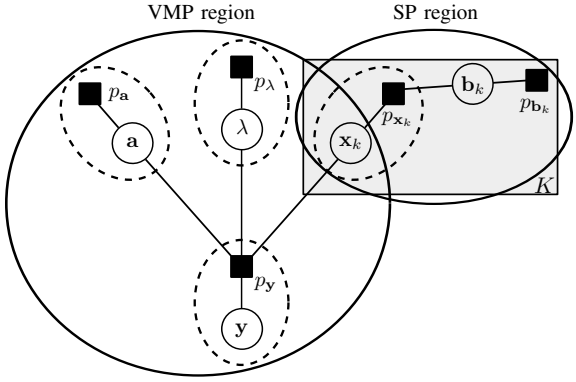

Fig. 2. Factor-graph [3] of the signal model in Section II. The parameter K indicates that the corresponding block is repeated K times, one for each transmitter. Notice that the left region is equivalent to the Bayesian network representation from [17].

$$\mathbf{\Phi} \triangleq \{\mathbf{y}, \mathbf{a}, \lambda, \mathbf{x}_1, \dots \mathbf{x}_K, \mathbf{b}_1, \dots \mathbf{b}_K\} \tag{4}$$

denote the set of all (observed and unobserved) variables in (1). Based on the assumptions made in Section II, the joint probability density function (pdf) of $\mathbf{\Phi}$ factorizes as

$$p_{\mathbf{\Phi}}(\mathbf{\Phi}) = p_{\mathbf{y}}(\mathbf{y}|\mathbf{a}, \lambda, \mathbf{x}_1, \dots \mathbf{x}_K) p_{\mathbf{a}}(\mathbf{a}) p_\lambda(\lambda) \prod_k p_{\mathbf{x}_k}(\mathbf{x}_k|\mathbf{b}_k) p_{\mathbf{b}_k}(\mathbf{b}_k). \tag{5}$$

The constraints imposed by coding, modulation and multiplexing of the deterministic pilot symbols are included in the factor $p_{\mathbf{x}_k}$ for transmitter k. A straightforward graphical representation of this factorization is the Tanner factor-graph [3] depicted in Fig. 2. Factors are represented as squares, variables as circles. An edge between a variable node and a factor node indicates that the variable is an argument of the factor.

Based on this graphical representation of the signal model, we employ iterative algorithms to estimate the joint pdf $p_{\mathbf{\Phi}}$. We split the graph into two regions as depicted in Fig. 2. In the right-hand region, we apply the SP algorithm [3] to compute the marginals $p_{\mathbf{x}_k}$ and $p_{\mathbf{b}_k}$. In the left-hand region, we apply the VMP algorithm [16] to estimate $p_{\mathbf{a}}$ and p_λ. The VMP algorithm is used to reformulate the VB inference method proposed in [11] in terms of messages.

The motivation for splitting the Tanner graph in this way and applying two different message-passing methods is as follows. The SP algorithm is a well-established algorithm for computing the marginal probability mass functions $p_{\mathbf{x}_k}$ and $p_{\mathbf{b}_k}$ in known channel conditions. Direct computation of the channel marginals $p_{\mathbf{a}}$ and p_λ by means of the SP algorithm is, however, computationally infeasible. In this case, one has to rely on techniques for approximating these marginals, e.g. particle filters or the EM algorithm [18]. Here, we propose another avenue and compute these marginals with the VMP algorithm. We define the set of unknown variables in the VMP region as $\mathbf{\Phi}_{\mathrm{VMP}} \triangleq \{\mathbf{a}, \lambda, \mathbf{x}_1, \dots \mathbf{x}_K\} \subseteq \mathbf{\Phi}$.

978-1-4244-5638-3/10/$26.00 ©2010 IEEE

Variational Message-Passing (VMP)

We consider an arbitrary factor-graph. The message from factor node f to a variable node ϕ in the set $\mathcal{N}_f$ of neighbouring nodes of f is

$$m_{f\to\phi} \triangleq \exp\langle \ln f\rangle_{m_{\phi'\to f}\forall\phi'\in\mathcal{N}_f\setminus\phi}. \quad (6)$$

The message from variable node ϕ to any factor node f in the set $\mathcal{N}_\phi$ of factor nodes neighbouring ϕ is

$$m_{\phi\to f} \triangleq \prod_{f'\in\mathcal{N}_\phi} m_{f'\to\phi}. \quad (7)$$

The estimated auxiliary function of ϕ is

$$b_\phi \propto m_{\phi\to f}. \quad (8)$$

IV. Variational Message-Passing

In this section, we apply the VMP algorithm [11], [17] to the left-hand region in the factor-graph in Fig. 2, see [16] and references therein for variational inference on factor-graphs. The message-passing rules are summarized in (6)-(8). Their derivations are sketched in App. A.

The VMP algorithm approximates the joint pdf $p_{\mathbf{\Phi}_{\mathrm{VMP}},\mathbf{y}}(\mathbf{\Phi}_{\mathrm{VMP}},\mathbf{y}) = p_{\mathbf{y}}(\mathbf{y}|\mathbf{a},\lambda,\mathbf{x}_1,\dots\mathbf{x}_K)p_{\mathbf{a}}(\mathbf{a})p_\lambda(\lambda)\prod_k p_{\mathbf{x}_k}(\mathbf{x}_k)$ with an auxiliary function $b_{\mathbf{\Phi}_{\mathrm{VMP}}}(\mathbf{\Phi}_{\mathrm{VMP}})$ in such a way that the KL divergence from $b_{\mathbf{\Phi}_{\mathrm{VMP}}}(\mathbf{\Phi}_{\mathrm{VMP}})$ to $p_{\mathbf{\Phi}_{\mathrm{VMP}},\mathbf{y}}(\mathbf{\Phi}_{\mathrm{VMP}},\mathbf{y})$ is minimized [17]. We constrain the auxiliary function to factorize according to $b_{\mathbf{\Phi}_{\mathrm{VMP}}}(\mathbf{\Phi}_{\mathrm{VMP}}) = b_{\mathbf{a}}(\mathbf{a})b_\lambda(\lambda)b_{\mathbf{x}_1}(\mathbf{x}_1)\dots b_{\mathbf{x}_K}(\mathbf{x}_K)$.

The VMP algorithm implements sequential message updates to update the factors in $b_{\mathbf{\Phi}_{\mathrm{VMP}}}(\mathbf{\Phi}_{\mathrm{VMP}})$. Updating $b_{\mathbf{a}}(\mathbf{a})$, $b_\lambda(\lambda)$, and $b_{\mathbf{x}_k}(\mathbf{x}_k)$ corresponds to estimating the channel weights, estimating the precision parameter, i.e. the channel inverse noise variance, and interference cancellation, respectively.

A. Estimation of the Channel Weights

In this subsection, we derive the messages to and from the variable node $\mathbf{a}$. These messages are used to update $b_{\mathbf{a}}$ by means of (8). The message to node $\mathbf{a}$ from $p_{\mathbf{y}}$ is obtained from (6):

$$m_{p_{\mathbf{y}}\to\mathbf{a}} = \exp\left(\langle \ln\, p_{\mathbf{y}}(\mathbf{y}|\mathbf{a},\lambda,\mathbf{x})\rangle_{m_{\lambda\to p_{\mathbf{y}}}\prod_k m_{\mathbf{x}_k\to p_{\mathbf{y}}}}\right). \quad (16)$$

Solving the expectation yields

$$m_{p_{\mathbf{y}}\to\mathbf{a}} \propto p_{\mathcal{CN}}(\hat{\lambda}_{\mathrm{VMP}}\hat{\mathbf{C}}_{p_{\mathbf{y}}\to\mathbf{a}}\hat{\mathbf{X}}^{\mathrm{H}}\mathbf{y}, \hat{\mathbf{C}}_{p_{\mathbf{y}}\to\mathbf{a}}). \quad (17)$$

Here, $p_{\mathcal{CN}}(\boldsymbol{\mu},\mathbf{C})$ is a multivariate complex Gaussian pdf with mean vector $\boldsymbol{\mu}$ and covariance matrix $\mathbf{C}$, and $\hat{\mathbf{C}}_{p_{\mathbf{y}}\to\mathbf{a}} \triangleq (\hat{\lambda}_{\mathrm{VMP}}\hat{\mathbf{X}}^{\mathrm{H}}\hat{\mathbf{X}} + \hat{\lambda}_{\mathrm{VMP}}(\mathbf{I}_G\otimes\hat{\mathbf{C}}_{\mathbf{x}}))^{-1}$. The matrix $\hat{\mathbf{C}}_{\mathbf{x}}$ is the block-diagonal concatenation of the estimates $\hat{\mathbf{C}}_{\mathbf{x}_k}$ of the covariance matrices of $\mathbf{x}_k$, $k = 1\dots K$. Both $\hat{\mathbf{C}}_{\mathbf{x}_k}$ and the estimate $\hat{\lambda}_{\mathrm{VMP}}$ of the precision parameter are defined later in this section. We impose the prior $p_{\mathbf{a}}$ to belong to the family of conjugate pdfs of $\mathbf{a}$ for $p_{\mathbf{y}}$. This choice guarantees that the auxiliary pdf $b_{\mathbf{a}}$ is also in this family. From (16) the conjugate family of pdfs of $\mathbf{a}$ for $p_{\mathbf{y}}$ is the Gaussian family. Thus, from (6)

$$m_{p_{\mathbf{a}}\to\mathbf{a}} = p_{\mathcal{CN}}(\mathbf{0}_{GKNL}, \mathbf{C}_{\mathbf{a}}), \quad (18)$$

where $\mathbf{C}_{\mathbf{a}}$ is the prior channel covariance matrix. Inserting (17) and (18) in (7) yields

$$m_{\mathbf{a}\to p_{\mathbf{y}}} \propto p_{\mathcal{CN}}(\hat{\mathbf{a}}, \hat{\mathbf{C}}_{\mathbf{a}}) = b_{\mathbf{a}} \quad (19)$$

with $\hat{\mathbf{a}} = \hat{\lambda}_{\mathrm{VMP}}\hat{\mathbf{C}}_{\mathbf{a}}\hat{\mathbf{X}}^{\mathrm{H}}\mathbf{y}$ and $\hat{\mathbf{C}}_{\mathbf{a}} = (\mathbf{C}_{\mathbf{a}}^{-1} + \hat{\mathbf{C}}_{p_{\mathbf{y}}\to\mathbf{a}}^{-1})^{-1}$. As the Gaussian pdf is fully defined by these two moments – its natural statistics – it is enough to pass them to $p_{\mathbf{y}}$.

B. Estimation of the Precision Parameter

In this subsection, we define the messages to and from variable node λ. The auxiliary function b_λ is then updated by plugging these messages in (8). The message from $p_{\mathbf{y}}$ to λ reads from (6)

$$m_{p_{\mathbf{y}}\to\lambda} = \exp\left(\langle \ln\, p_{\mathbf{y}}(\mathbf{y}|\mathbf{a},\lambda,\mathbf{x})\rangle_{m_{\mathbf{a}\to p_{\mathbf{y}}}\prod_k m_{\mathbf{x}_k\to p_{\mathbf{y}}}}\right). \quad (20)$$

Evaluating the expectation under the assumption that the messages $m_{\mathbf{a}\to p_{\mathbf{y}}}$ and $m_{\mathbf{x}_k\to p_{\mathbf{y}}}$, $k = 1\dots K$, are Gaussian densities [11] yields

$$m_{p_{\mathbf{y}}\to\lambda} \propto p_{\mathcal{CW}_1}\left(\hat{W}^{-1}, GNL+1\right). \quad (21)$$

In this expression, $p_{\mathcal{CW}_F}(\mathbf{M}^{-1},d)$ is a complex Wishart pdf defined by three parameters: the dimension F, the degree of freedom d, and a matrix $\mathbf{M}$ of dimension $F\times F$ [19]. Here, $F=1$, $d = GNL+1$, and $\mathbf{M}$ is a scalar given as $\hat{W} \triangleq \mathrm{tr}((\mathbf{y}-\hat{\mathbf{A}}\hat{\mathbf{x}})(\mathbf{y}-\hat{\mathbf{A}}\hat{\mathbf{x}})^{\mathrm{H}} + \hat{\mathbf{X}}\hat{\mathbf{C}}_{\mathbf{a}}\hat{\mathbf{X}}^{\mathrm{H}} + \sum_k \hat{\mathbf{A}}_k\hat{\mathbf{C}}_{\mathbf{x}_k}\hat{\mathbf{A}}_k^{\mathrm{H}} + \sum_k(\mathbf{1}_G\otimes\hat{\mathbf{C}}_{\mathbf{x}_k})\odot\mathrm{Diag}(\mathrm{diag}(\hat{\mathbf{C}}_{\mathbf{a}_k})))$. The estimate $\hat{\mathbf{C}}_{\mathbf{a}_k}$ of the auto-covariance matrix of $\mathbf{a}_k$ can be obtained from $\hat{\mathbf{C}}_{\mathbf{a}}$. The estimate $\hat{\mathbf{C}}_{\mathbf{x}_k}$ of the covariance matrix of $\mathbf{x}_k$ is defined later in this section.

We select p_λ to be a conjugate pdf of λ, which is a complex Wishart pdf of dimension one [20, Sec. IVb]. From (6)

$$m_{p_\lambda\to\lambda} = p_{\mathcal{CW}_1}\left(M_{\mathrm{pr}}^{-1}, d_{\mathrm{pr}}\right) \quad (22)$$

with given parameters M_{pr} and d_{pr}. By inserting (21) and (22) into the message-passing rule (7), we obtain the complex Wishart pdf

$$m_{\lambda\to p_{\mathbf{y}}} \propto p_{\mathcal{CW}_1}\left((\hat{W}+M_{\mathrm{pr}})^{-1}, d_{\mathrm{pr}}+GNL\right) = b_\lambda. \quad (23)$$

It is enough to pass the first moment $\hat{\lambda}_{\mathrm{VMP}} = (d_{\mathrm{pr}}+GNL)(\hat{W}+M_{\mathrm{pr}})^{-1}$ [20, Eq. (22)] of this pdf, since the other message updates only depend on this value. As we have no prior information on λ, we select p_λ to be uniform over the range of λ. For this improper prior, we have $M_{\mathrm{pr}}=0$ and $d_{\mathrm{pr}}=0$ [20].

C. MIMO Decoding

To update $b_{\mathbf{x}_k}$, we compute the messages to and from the variable node $\mathbf{x}_k$. From (6), the message from node $p_{\mathbf{y}}$ to variable node $\mathbf{x}_k$ is

$$m_{p_{\mathbf{y}}\to\mathbf{x}_k} = \exp\left(\langle \ln\, p_{\mathbf{y}}(\mathbf{y}|\mathbf{a},\lambda,\mathbf{x})\rangle_{m_{\mathbf{a}\to p_{\mathbf{y}}}m_{\lambda\to p_{\mathbf{y}}}\prod_{k'\neq k} m_{\mathbf{x}_{k'}\to p_{\mathbf{y}}}}\right). \quad (24)$$

Channel Estimation

VMP receiver:

$$\hat{\mathbf{a}} = \left(\mathbf{C}_{\mathbf{a}}^{-1} + \hat{\lambda}_{\mathrm{VMP}}\hat{\mathbf{X}}^{\mathrm{H}}\hat{\mathbf{X}} + \hat{\lambda}_{\mathrm{VMP}}(\mathbf{I}_G \otimes \hat{\mathbf{C}}_{\mathbf{x}})\right)^{-1} \hat{\lambda}_{\mathrm{VMP}}\hat{\mathbf{X}}^{\mathrm{H}}\mathbf{y} \tag{9}$$

LMMSE-based receiver:

$$\hat{\mathbf{a}} = \left(\mathbf{C}_{\mathbf{a}}^{-1} + \hat{\mathbf{X}}^{\mathrm{H}}\hat{\mathbf{\Lambda}}^{\mathrm{chan}}_{\mathrm{LMMSE}}\hat{\mathbf{X}}\right)^{-1} \hat{\mathbf{X}}^{\mathrm{H}}\hat{\mathbf{\Lambda}}^{\mathrm{chan}}_{\mathrm{LMMSE}}\mathbf{y} \tag{10}$$

MIMO Detection/Interference Cancellation

VMP receiver:

$$\hat{\mathbf{x}}_k = \left(\hat{\lambda}_{\mathrm{VMP}}\hat{\mathbf{A}}_k^{\mathrm{H}}\hat{\mathbf{A}}_k + \hat{\lambda}_{\mathrm{VMP}}\sum_{g'}\sum_{g}\mathrm{Diag}(\mathrm{diag}(\hat{\mathbf{C}}_{\mathbf{a}_{kg}\mathbf{a}_{kg'}}))\right)^{-1} \hat{\lambda}_{\mathrm{VMP}}\hat{\mathbf{A}}_k^{\mathrm{H}}\left(\mathbf{y} - \sum_{k'\neq k}\hat{\mathbf{A}}_{k'}\hat{\mathbf{x}}_{k'}\right) \tag{11}$$

LMMSE-based receiver:

$$\hat{\mathbf{x}}_k = \left(\mathbf{C}_{\mathbf{x}_k}^{-1} + \hat{\mathbf{A}}_k^{\mathrm{H}}\hat{\mathbf{\Lambda}}^{\mathrm{det}}_{\mathrm{LMMSE}}\hat{\mathbf{A}}_k\right)^{-1} \hat{\mathbf{A}}_k^{\mathrm{H}}\hat{\mathbf{\Lambda}}^{\mathrm{det}}_{\mathrm{LMMSE}}\left(\mathbf{y} - \sum_{k'\neq k}\hat{\mathbf{A}}_{k'}\hat{\mathbf{x}}_{k'}\right) \tag{12}$$

Estimation of the Precision Matrix

VMP receiver: $\hat{\mathbf{\Lambda}}_{\mathrm{VMP}} = \hat{\lambda}_{\mathrm{VMP}}\mathbf{I}_{GNL}$ with

$$\hat{\lambda}_{\mathrm{VMP}} = \left(\frac{\mathrm{tr}\left((\mathbf{y}-\hat{\mathbf{A}}\hat{\mathbf{x}})(\mathbf{y}-\hat{\mathbf{A}}\hat{\mathbf{x}})^{\mathrm{H}} + \hat{\mathbf{X}}\hat{\mathbf{C}}_{\mathbf{a}}\hat{\mathbf{X}}^{\mathrm{H}} + \sum_k \hat{\mathbf{A}}_k\hat{\mathbf{C}}_{\mathbf{x}_k}\hat{\mathbf{A}}_k^{\mathrm{H}} + \sum_k(\mathbf{1}_G \otimes \hat{\mathbf{C}}_{\mathbf{x}_k}) \odot \mathrm{Diag}(\mathrm{diag}(\hat{\mathbf{C}}_{\mathbf{a}_k}))\right)}{GNL}\right)^{-1} \tag{13}$$

LMMSE-based receiver: σ_a^2 is the average power of the channel

$$\hat{\mathbf{\Lambda}}^{\mathrm{chan}}_{\mathrm{LMMSE}} = \left(\left(\frac{\mathrm{tr}\left(\left(\mathbf{y}-\hat{\mathbf{A}}\hat{\mathbf{x}}\right)\left(\mathbf{y}-\hat{\mathbf{A}}\hat{\mathbf{x}}\right)^{\mathrm{H}}\right)}{GNL}\right)\mathbf{I}_{GNL} + \sigma_a^2\mathbf{I}_G \otimes \sum_k \hat{\mathbf{C}}_{\mathbf{x}_k}\right)^{-1} \tag{14}$$

$$\hat{\mathbf{\Lambda}}^{\mathrm{det}}_{\mathrm{LMMSE}} = \left(\left(\frac{\mathrm{tr}\left(\left(\mathbf{y}-\hat{\mathbf{A}}\hat{\mathbf{x}}\right)\left(\mathbf{y}-\hat{\mathbf{A}}\hat{\mathbf{x}}\right)^{\mathrm{H}}\right)}{GNL}\right)\mathbf{I}_{GNL} + \sum_{k'\neq k}\hat{\mathbf{A}}_{k'}\hat{\mathbf{C}}_{\mathbf{x}_{k'}}\hat{\mathbf{A}}_{k'}^{\mathrm{H}}\right)^{-1} \tag{15}$$

Fig. 3. Channel estimation, MIMO detection/interference cancellation and the precision matrix estimation in the VMP and LMMSE-based receiver.

Solving the expectation, yields

$$m_{p_{\mathbf{y}}\to\mathbf{x}_k} \propto p_{\mathcal{CN}}(\hat{\mathbf{x}}_k, \hat{\mathbf{C}}_{\mathbf{x}_k}) \tag{25}$$

with mean vector $\hat{\mathbf{x}}_k = \hat{\lambda}_{\mathrm{VMP}}\hat{\mathbf{C}}_{\mathbf{x}_k}\hat{\mathbf{A}}_k^{\mathrm{H}}\big(\mathbf{y} - \sum_{k'\neq k}\hat{\mathbf{A}}_{k'}\hat{\mathbf{x}}_{k'}\big)$ and covariance matrix $\hat{\mathbf{C}}_{\mathbf{x}_k} = (\hat{\lambda}_{\mathrm{VMP}}\hat{\mathbf{A}}_k^{\mathrm{H}}\hat{\mathbf{A}}_k + \hat{\lambda}_{\mathrm{VMP}}\sum_{g'}\sum_{g}\mathrm{diag}(\hat{\mathbf{C}}_{\mathbf{a}_{kg}\mathbf{a}_{kg'}}))^{-1}$. The estimate $\hat{\mathbf{C}}_{\mathbf{a}_{kg}\mathbf{a}_{kg'}}$ of the cross-covariance matrix of the channel vectors $\mathbf{a}_{kg}$ and $\mathbf{a}_{kg'}$ can be obtained from $\hat{\mathbf{C}}_{\mathbf{a}}$.

Demodulation and decoding are performed in the right region of the graph in Fig. 2 using the SP algorithm. The estimated mean of a symbol x_{knl} in $\mathbf{x}_k$ is computed to be $\hat{x}_{knl} = \sum_{x\in\mathcal{M}} xP(x_{knl} = x|\hat{\mathbf{x}}_k)$, where $P(x_{knl} = x|\hat{\mathbf{x}}_k) = \sum_{\mathbf{x}_k\in\mathcal{X}_k, x_{knl}=x} m_{p_{\mathbf{y}}\to\mathbf{x}_k}(\mathbf{x}_k)$ with $\mathcal{M}$ denoting the set of constellation points of the selected M-QAM modulation. For convolutional codes, these marginals can be obtained with the BCJR algorithm. Likewise, the estimated variance of x_{knl} is $\hat{\sigma}^2_{x_{knl}} = \sum_{x\in\mathcal{M}} x^2P(x_{knl} = x|\hat{\mathbf{x}}_k) - \hat{x}^2_{knl}$. Any two distinct symbols are assumed to be uncorrelated. As a result, the estimate of the covariance matrix of $\mathbf{x}_k$ after decoding reads $\hat{\mathbf{C}}_{\mathbf{x}_k} = \mathrm{Diag}(\hat{\sigma}^2_{x_{k11}}, \ldots \hat{\sigma}^2_{x_{knL}})$.

We approximate the message from $\mathbf{x}_k$ to $p_{\mathbf{y}}$ by a Gaussian pdf. Notice that the Gaussian family is the conjugate family of $\mathbf{x}_k$ for $p_{\mathbf{y}}$. With this approximation and from (25) we obtain

$$m_{\mathbf{x}_k\to p_{\mathbf{y}}} \propto p_{\mathcal{CN}}(\hat{\mathbf{x}}_k, \hat{\mathbf{C}}_{\mathbf{x}_k}) = b_{\mathbf{x}_k}. \tag{26}$$

We only pass the natural statistics $\hat{\mathbf{x}}_k$, $\hat{\mathbf{C}}_{\mathbf{x}_k}$ to $p_{\mathbf{y}}$. From (8), the message (26) represents the estimated posterior pdf of $\mathbf{x}_k$.

V. Comparison with the LMMSE-based receiver

In this section, we compare the VMP receiver derived in the previous section to a state-of-the-art iterative receiver proposed in [5], further developed for detection in multiuser CDMA [6], and applied to MIMO-OFDM systems in [7]. We refer to this receiver as the LMMSE-based receiver. Due to lack of space, the derivation of the LMMSE-based receiver is not included in this work, but the expressions of the different component blocks are summarized in Fig. 3 together with the corresponding expressions obtained for the VMP receiver.

The conceptual difference between the two schemes is that in the LMMSE-based receiver the different constituent blocks are designed independently, while in the VMP receiver the blocks corresponding to factors in the VMP region are designed jointly, by minimizing a global cost function, i.e. a KL divergence, in this region.

By inspecting the expressions in Fig. 3 we observe that the LMMSE-based receiver and the VMP receiver share some structural properties. For instance, from (9) and (10) it is clear that both algorithms use an LMMSE-like channel estimator, which mainly depends on the channel prior covariance, estimates of the transmitted symbols and an estimate of the precision matrix, namely $\hat{\lambda}_{\mathrm{VMP}}\mathbf{I}$ in the VMP receiver and $\hat{\mathbf{\Lambda}}^{\mathrm{chan}}_{\mathrm{LMMSE}}$ in the LMMSE-based receiver. Similarly, the detection part of both receivers consists of interference cancellation followed by LMMSE filtering of the residual interference. However, we can highlight two critical differences between

978-1-4244-5638-3/10/$26.00 ©2010 IEEE

TABLE I
PARAMETER SETTINGS FOR THE SIMULATIONS

Cyclic prefix length	4.7 μs
Symbol duration	66.7 μs
Subcarrier spacing	15 kHz
Pilot overhead	4.8% pilots
Pilot pattern	Regular spacing/diamond, QPSK
Modulation alphabet	16-QAM
Number of information bits	660
Number of subcarriers N	75
Number of OFDM symbols L	7
Number of transmitters K	2
Number of receivers G	2
Channel interleaver	block
Convolutional code	$(155, 117, 127)_8$

the two algorithms: firstly, only one scalar estimate of the precision parameter is needed in the VMP receiver, while the LMMSE-based receiver calculates two different precision matrices, one for channel estimation ($\hat{\mathbf{\Lambda}}^{\text{chan}}_{\text{LMMSE}}$) and one for detection ($\hat{\mathbf{\Lambda}}^{\text{det}}_{\text{LMMSE}}$); secondly, the LMMSE-based receiver does not deal with the uncertainty in the channel weight estimates and considers them as the true values in the detection part, while the VMP receiver accounts for channel estimation errors via the term $\hat{\mathbf{C}}_{\mathbf{a}}$ in (11) and (13).

VI. Simulation Results

To verify the performance of the VMP receiver, we perform Monte-Carlo simulations for an LTE-like 2×2 system with the settings reported in Table I. We consider a pilot scheme where all transmitters transmit pilots in the same time-frequency resources. Realizations of the channel time-frequency response are generated using the extended typical urban (ETU) channel model from the 3GPP LTE standard [21], with Rayleigh-fading channel taps, and assuming no correlation over transmit or receive antennas. Note that the channel is wide-sense-stationary and uncorrelated-scattering (WSSUS) [22]. We compute the prior covariance matrix $\mathbf{C}_{\mathbf{a}}$ from the channel time-frequency correlation function.

We test the OFDM-MIMO system with the two receivers described in Fig. 3. Both receivers use the same initialization, consisting of MMSE pilot-based channel estimation and joint soft-decision maximum likelihood (ML) detection, followed by soft-in soft-out sequential decoding. In both receivers an iteration consists of estimation of the channel weights, followed by sequential detection and decoding of all K transmitted frames, and ending with estimation of the precision parameter or matrices.

The bit-error-rate (BER) performance of both receivers versus the signal-to-noise ratio (E_b/N_0) is illustrated in Fig. 4. For the sake of comparison, the initialization is also depicted (denoted by the 'Linear Receiver' tag). Both receivers perform 10 iterations. The results show that both iterative structures significantly improve the performance of the linear receiver, especially for E_b/N_0 larger than 0 dB. Moreover, the VMP receiver outperforms the LMMSE-based receiver in the considered signal-to-noise range. The gain is about 0.5 dB in the operation range of the MIMO-OFDM system. The convergence behaviour of both iterative structures is described

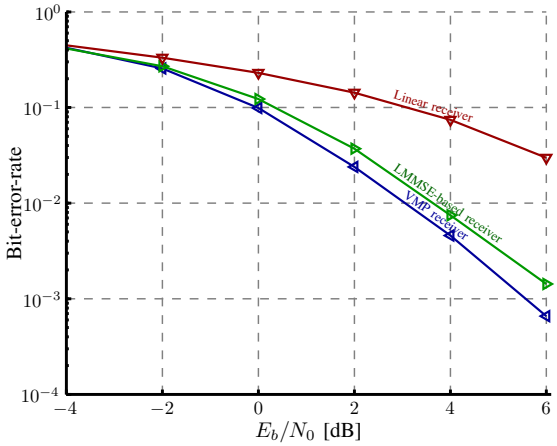

Fig. 4. Coded bit-error-rate.

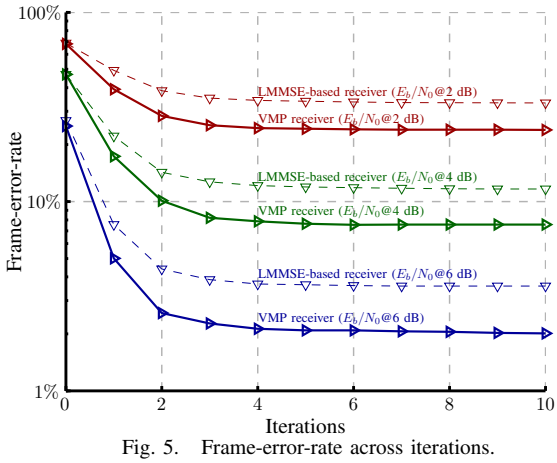

Fig. 5. Frame-error-rate across iterations.

in Fig. 5, which depicts the frame-error-rate versus the number of iterations at the receiver for three different E_b/N_0 values. Both receivers converge after approximately 5 iterations for all operation points. Again, the VMP receiver outperforms the LMMSE-based receiver regardless of the number of iterations.

VII. Conclusion

We derive a novel iterative receiver structure for M-QAM MIMO-OFDM operating in frequency-selective time-variant channels. The scheme performs jointly semi-blind estimation of the channel weights and of the noise inverse variance based on both data and pilot symbols, serial interference cancellation, and decoding. The scheme was already proposed for CDMA in [11]. A variational message-passing (VMP) interpretation of it is provided here.

The VMP receiver is compared with the LMMSE-based iterative receiver derived in [5]–[7]. Both iterative architectures are made of the same blocks and exhibit similar complexity. However, in the VMP receiver all blocks but decoding are jointly optimized according to a global cost function, the KL divergence, while in the LMMSE-based receiver all blocks are designed independently. Furthermore, the VMP framework yields a structure that takes into account the inaccuracy of the channel weight estimates. This inaccuracy is neglected in the LMMSE-based receiver.

In order to assess the effect of these structural differences,

978-1-4244-5638-3/10/$26.00 ©2010 IEEE

we evaluate the performance of both receivers in an LTE-like scenario. The simulation results show that the VMP receiver outperforms the LMMSE-based receiver with a signal-to-noise ratio gain of 0.5 dB at relevant BER values.

An issue not addressed in the paper is how to combine efficiently the VMP algorithm – used for channel weight and noise inverse variance estimation as well as serial interference cancellation – and the sum-product algorithm – employed for decoding – in the receiver. A solution has been recently proposed in [23].

VIII. Acknowledgements

The authors would like to thank NOKIA Denmark for the financial support which made this work possible. This work has also been supported in part by the 4GMCT cooperative research project funded by Infineon Technologies Denmark A/S, Agilent Technologies, Aalborg University and the Danish National Advanced Technology Foundation, by the European Commission within the FP7-ICT Network of Excellence in Wireless Communications, NEWCOM++ (Contract No. 216715) and by WWTF grant ICT08-44, FWF grant S10603-N13 within the National Research Network SISE.

Appendix A
The Variational Message-Passing Algorithm

In VB inference [11] we consider as the cost function the KL divergence $\mathcal{D}_{\mathrm{KL}}(b_{\mathbf{\Phi}} \| f_{\mathbf{\Phi}}) \triangleq \int \mathrm{d}\mathbf{\Phi}\; b_{\mathbf{\Phi}} \log \frac{b_{\mathbf{\Phi}}}{f_{\mathbf{\Phi}}}$, where $f_{\mathbf{\Phi}}$ is a pdf of a set of variables $\mathbf{\Phi}$ and $b_{\mathbf{\Phi}}$ is an auxiliary function, which approximates $f_{\mathbf{\Phi}}$. We seek an auxiliary function that minimizes the cost function.

We reformulate the VB inference problem to message-passing on a factor-graph [16]. We assume that $f_{\mathbf{\Phi}}$ factorizes according to $f_{\mathbf{\Phi}} = \prod_a f_a(\mathcal{N}_{f_a})$, where $\mathcal{N}_{f_a} \subseteq \mathbf{\Phi}$ is the set of neighbouring variables of f_a. We select an auxiliary function $b_{\mathbf{\Phi}}$, which factorizes according to $b_{\mathbf{\Phi}} = \prod_{\phi \in \mathbf{\Phi}} b_\phi$. As shown in [11], the factor b_ϕ of $b_{\mathbf{\Phi}}$ which minimizes $\mathcal{D}_{\mathrm{KL}}(b_{\mathbf{\Phi}} \| f_{\mathbf{\Phi}})$ with all other factors $b_{\phi'}$, $\forall \phi' \in \mathbf{\Phi} \backslash \phi$ fixed is

$$b_\phi \propto \exp\langle \sum_{f_a \in \mathcal{N}_\phi} \ln f_a \rangle_{b_{\phi'} \forall \phi' \in \mathcal{N}_{f_a} \backslash \phi} \tag{27}$$

$$\propto \prod_{f_a \in \mathcal{N}_\phi} \exp\langle \ln f_a \rangle_{b_{\phi'} \forall \phi' \in \mathcal{N}_{f_a} \backslash \phi}, \tag{28}$$

where $\mathcal{N}_\phi$ is the set of neighbouring factors of ϕ. With the definitions in (6) and (7) we can recast (28) as

$$b_\phi \propto \prod_{f'_a \in \mathcal{N}_\phi} m_{f'_a \to \phi} = m_{\phi \to f_a} \tag{29}$$

for any $f_a \in \mathcal{N}_\phi$, and we have

$$b_{\mathbf{\Phi}} = \prod_{\phi \in \mathbf{\Phi}} b_\phi \propto \prod_{\phi \in \mathbf{\Phi}} \prod_{f'_a \in \mathcal{N}_\phi} m_{f'_a \to \phi}. \tag{30}$$

Identity (28) can be used to design an iterative algorithm which at each iteration updates a given factor b_ϕ of $b_{\mathbf{\Phi}}$ while keeping the other factors fixed. The iterative algorithm converges in the sense of the KL divergence, since $\mathcal{D}_{\mathrm{KL}}(b_{\mathbf{\Phi}} \| f_{\mathbf{\Phi}})$ is minimized at each iteration. The identities in (29) provide a message-passing interpretation of the updating steps.

References

[1] C. Berrou, A. Glavieux, and P. Thitimajshima, "Near Shannon limit error-correcting coding and decoding: Turbo codes," in *Proc. IEEE Int. Conf. Commun. (ICC'93)*, May 1993, pp. 1064–1070.

[2] R. Koetter, A. C. Singer, and M. Tücher, "Turbo equalization," *IEEE Trans. Signal Processing*, vol. 1, pp. 64–80, 2004.

[3] F. Kschischang, B. Frey, and H.-A. Loeliger, "Factor graphs and the sum-product algorithms," *IEEE Trans. Inform. Theory*, vol. 47, no. 2, pp. 498–519, Feb. 2001.

[4] X. Wang and H. Poor, "Iterative (turbo) soft interference cancellation and decoding for coded CDMA," *IEEE Trans. Commun.*, vol. 47, pp. 1046–1061, Jul. 1999.

[5] M. Lončar, R. Müller, J. Wehinger, C. Mecklenbräuker, and T. Abe, "Iterative channel estimation and data detection in frequency-selective fading MIMO channels," *Euro. T. Telecom.*, vol. 15, pp. 459–470, 2004.

[6] J. Wehinger and C. Mecklenbräuker, "Iterative CDMA multiuser receiver with soft decision-directed channel estimation," *IEEE Trans. Signal Processing*, vol. 54, pp. 3922–3934, Oct. 2006.

[7] P. Rossi and R. Müller, "Joint twofold-iterative channel estimation and multiuser detection for MIMO-OFDM systems," *IEEE Trans. Wireless Commun.*, vol. 7, no. 11, pp. 4719–4729, Nov. 2008.

[8] H. Attias, "A variational Bayesian framework for graphical models," *Advances in Neural Information Processing Systems*, pp. 209–215, 2000.

[9] M. Beal, "Variational algorithms for approximate inference," Ph.D. dissertation, University of Cambridge, May 2003.

[10] L. Christensen and J. Larsen, "On data and parameter estimation using the variational Bayesian EM-algorithm for block-fading frequency-selective MIMO channels," in *Proc. IEEE Int. Conf. on Acoustics, Speech and Sign. Process. (ICASSP'06)*, vol. 4, 2006, pp. 465–468.

[11] B. Hu, I. Land, L. Rasmussen, R. Piton, and B. Fleury, "A divergence minimization approach to joint multiuser decoding for coded CDMA," *IEEE J. Select. Areas Commun.*, vol. 26, no. 3, pp. 432–445, Apr. 2008.

[12] D. Lin and T. Lim, "The variational inference approach to joint data detection and phase noise estimation in OFDM," *IEEE Trans. Signal Processing*, vol. 55, no. 5, pp. 1862–1874, May 2007.

[13] M. Nissilä, "Iterative receivers for digital communications via variational inference and estimation," Ph.D. dissertation, Oulu University, 2008.

[14] X.-Y. Zhang, D.-G. Wang, and J.-B. Weiss, "Joint symbol detection and channel estimation for MIMO-OFDM systems via the variational Bayesian EM algorithms," in *Proc. IEEE Wireless Commun. and Networking Conf. (WCNC'08)*, Mar.-Apr. 2008, pp. 13–17.

[15] C. N. Manchon, G. Kirkelund, B. Fleury, P. Mogensen, L. Deneire, T. Sorensen, and C. Rom, "Interference cancellation based on divergence minimization for MIMO-OFDM receivers," in *Proc. IEEE Global Telecom. Conf. (GLOBECOM'09)*, Dec. 2009.

[16] J. Dauwels, "On variational message passing on factor graphs," in *IEEE Int. Symp. on Inform. Theory (ISIT'07)*, Jun. 2007, pp. 2546–2550.

[17] J. Winn and C. Bishop, "Variational message passing," *Journal of Machine Learning Research*, 2004.

[18] H.-A. Loeliger, J. Dauwels, J. Hu, S. Korl, L. Ping, and F. Kschischang, "The factor graph approach to model-based signal processing," *Proceedings of the IEEE*, vol. 95, no. 6, pp. 1295–1322, Jun. 2007.

[19] J. Tauge and C. Caldwell, "Expectations of useful complex Wishart forms," *Multidimensional Systems and Signal Processing Archive*, vol. 5, pp. 263–278, 1994.

[20] L. Svensson and M. Lundberg, "On posterior distributions for signals in Gaussian noise with unknown covariance matrix," *IEEE Trans. Signal Processing*, vol. 53, no. 9, pp. 3554–3571, Sept. 2005.

[21] 3GPP, "Evolved Universal Terrestrial Radio Access (E-UTRA); LTE Physical Layer - base station (BS) radion transmission and reception (release 8)," 3GPP, Tech. Rep. TS 36.104, V8.8.0, Dec. 2009.

[22] P. Bello, "Characterization of randomly time-variant linear channels," *IEEE Trans. Commun.*, vol. 11, no. 4, pp. 360–393, Dec. 1963.

[23] E. Riegler, G. E. Kirkelund, C. N. Manchón, and B. H. Fleury, "Merging belief propagation and the mean field approximation: a free energy approach," in *Proc. 6th Int. Symp. on Turbo Codes & Iterative Information Processing, (ISTC'10)*, accepted for publication.

Paper F

Interference Cancellation Based on Divergence Minimization for MIMO-OFDM Receivers

Carles Navarro Manchón, Gunvor E. Kirkelund, Bernard H. Fleury, Preben Mogensen, Luc Deneire, Troels B. Sørensen and Christian Rom

IEEE Global Communications Conference, GLOBECOM 2009. Honolulu, December 2009.

F. INTERFERENCE CANCELLATION BASED ON DIVERGENCE MINIMIZATION FOR MIMO-OFDM RECEIVERS

Interference Cancellation Based on Divergence Minimization for MIMO-OFDM Receivers

Carles Navarro Manchón*, Gunvor E. Kirkelund*, Bernard Fleury*†, Preben Mogensen*,
Luc Deneire*‡, Troels B. Sørensen* and Christian Rom§
*Department of Electronic Systems, Aalborg University
Niels Jernes Vej 12, 9220 Aalborg East
†Forschungszentrum Telekommunikation Wien (FTW), Vienna, Austria
‡Université de Nice, Sophia Antipolis
Centre National de la Recherche Scientifique
I3S, UMR 6070, France
§Infineon Technologies Denmark A/S
Alfred Nobels Vej 25, DK-9220 Aalborg, Denmark

***Abstract*—In this paper, we present a novel iterative receiver for MIMO-OFDM systems with synchronous interferers. The receiver is derived based on the Kullback-Leibler divergence minimization framework, and combines channel estimation, interference cancellation and residual noise estimation in an iterative manner. By using both the pilot and data symbols, the channel estimator improves the accuracy of the estimates in each iteration, which leads to a more effective interference cancellation and data detection process. A performance evaluation based on Monte-Carlo simulations shows that the proposed scheme can effectively mitigate the effect of interferers, and operates very close to the single-user performance even in severe interference scenarios.**

I. Introduction

Orthogonal Frequency Division Multiplexing (OFDM) has become the selected transmission technique for several recent wireless standards, such as the IEEE standard for local and metropolitan area networks (better known as WiMAX) [1], or the 3GPP UTRA Long Term Evolution (LTE) [2]. Its ability to cope with time-dispersive channels while allowing for receivers with low complexity, its ability to easily integrate multiple antenna techniques and its flexibility in terms of bandwidth usage and resource allocation are some of the advantages that have motivated its selection.

In OFDM, the transmission bandwidth is divided into multiple narrowband subcarriers. By the addition of a proper cyclic prefix (CP), these subcarriers become fully orthogonal and experience frequency flat fading conditions in time-invariant channels [3]. This allows for simple equalization of the signal at the receiver, while keeping a high spectral efficiency due to the use of orthogonal overlapping subcarriers. In OFDM systems with frequency re-use, however, the signal transmitted from other cells may create co-channel interference which, if not correctly treated, can induce a severe degradation of the receiver performance, especially at the cell edge.

Much work has been done in interference cancellation techniques for OFDM, as in [4]–[6]. These methods, however, assume perfect knowledge of the channel at the receiver. In [7], a minimum mean-squared error interference rejection combiner (MMSE-IRC) for OFDM receivers with multiple antennas is proposed. The combiner parameters are estimated using a discrete-Fourier-transform-based robust MMSE instantaneous correlation estimator, which is therefore sensitive to the *leakage* effect [8] when the channel delays are not perfectly aligned with the receiver sampling grid.

In our latest work, we proposed an iterative pilot-based channel estimator for OFDM systems with synchronous interferers and super-imposed pilots [9]. In this work, we propose an iterative receiver performing channel estimation, interference cancellation and residual noise variance estimation. Our receiver is derived by applying the Kullback-Leibler (KL) divergence minimization (DM) principle, which was presented in [10] for multiuser detection in a code-division multiple access scenario. The channel estimator combines the information available from the pilot symbols with information from soft-decisions on the data symbols, thus outperforming typical schemes using only the pilot symbols. Furthermore, the channel estimation error is taken into account in the interference cancellation and detection process by estimating the covariance of the channel estimates and the residual noise covariance.

The remainder of the paper is organized as follows. The signal model for our considered scenario is presented in Section II. In Section III, the DM framework is briefly introduced, and the proposed iterative receiver is derived. Its performance is assessed by means of Monte-Carlo simulations in Section IV and finally some concluding remarks are provided in Section V.

The following notation will be used throughout the paper. Vectors are represented by boldface lowercase letters, while matrices are denoted as boldface uppercase letters; $(\cdot)^T$ and $(\cdot)^H$ denote respectively the transpose and conjugate transpose of a vector; $\mathrm{tr}\{\cdot\}$ denotes the trace operation, and $\mathrm{diag}\{\mathbf{x}\}$ represents a diagonal matrix with the elements of vector $\mathbf{x}$; $\mathbf{A} \otimes \mathbf{B}$ denotes the Kronecker product of matrices $\mathbf{A}$ and $\mathbf{B}$; $\mathbf{I}_N$ represents the $N \times N$ identity matrix; $x \propto y$ denotes direct proportionality, i.e., $x = \alpha y$, and $x \propto^e y$ denotes

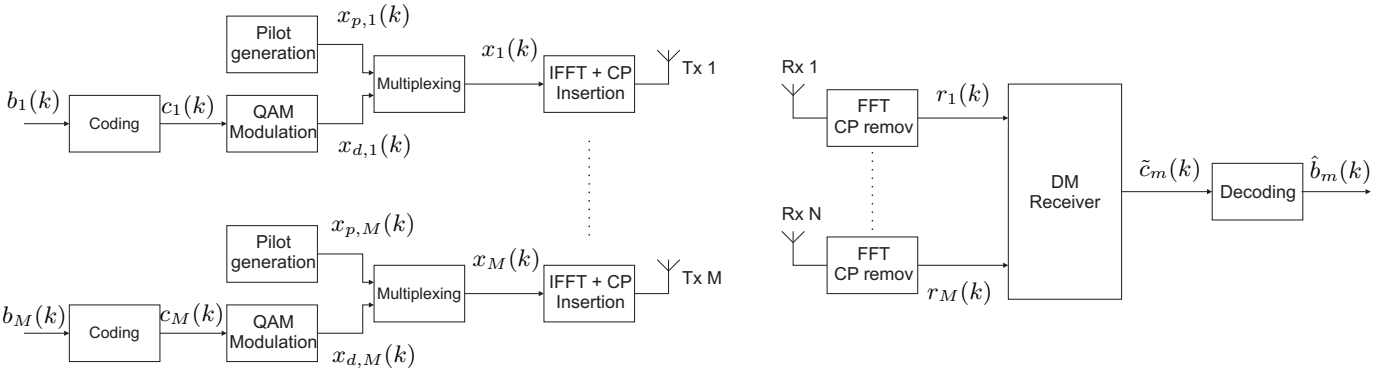

Fig. 1. Block diagram of the considered system.

exponential proportionality, i.e., $\exp[x] = \exp[\beta + y]$, for arbitrary constants α and β; finally, $\mathrm{E}_{q_x}\{f(\mathbf{x})\}$ represents the expectation of the function $f(\mathbf{x})$ with respect to the probability distribution $q_x(\mathbf{x})$ of $\mathbf{x}$.

II. Signal Model

We consider a MIMO-OFDM system with M transmit antennas and a receiver with N receive antennas, as depicted in Fig. 1. Transmit antennas $1, \ldots, M_d$ transmit the signal of interest, while antennas $M_d + 1, \ldots, M$ are regarded as interferers. We assume that all transmitters in the system are perfectly synchronized in time and use the same frequency resources. For the m^{th} transmitter, the information bits $b_m(k)$, $k = 1, \ldots, K_{b,m}$ are encoded, yielding a stream of coded bits $c_m(k)$, $k = 1, \ldots, K_{c,m}$, which is modulated onto a set of QAM/QPSK symbols denoted by $x_{d,m}(k)$, $k = 1, \ldots, K_d$. The data symbols are then multiplexed with a sequence of pilot symbols $x_{p,m}(k)$, $k = 1, \ldots, K_p$, resulting in the transmitted symbols sequence $x_m(k)$, $k = 1, \ldots, K$. The transmitted symbols are then OFDM modulated by means of an inverse fast Fourier transform (IFFT) and the insertion of a cyclic prefix. We assume that the sets of pilot subcarriers $\mathcal{P} = \{p_1, \ldots, p_{K_p}\}$ and data subcarriers $\mathcal{D} = \{d_1, \ldots, d_{K_d}\}$ are the same for all transmitters, and hence

$$x_m(k) = \begin{cases} x_{p,m}(i), & k = p_i \\ x_{d,m}(i), & k = d_i \end{cases} . \tag{1}$$

Note that $\mathcal{P} \cup \mathcal{D} = \{1, \ldots, K\}$ and $\mathcal{P} \cap \mathcal{D} = \emptyset$. K denotes the total number of subcarriers in the system, while K_p and K_d denote the number of pilot and data subcarriers respectively.

The signal received at each of the antenna ports is OFDM demodulated by removing the cyclic prefix and performing a fast Fourier transform (FFT). Assuming that the channel is static during one OFDM symbol and that the cyclic prefix is longer than the maximum excess delay of the channel, the signal received at the k^{th} subcarrier of receive antenna n reads

$$r_n(k) = \sum_{m=1}^{M} h_{nm}(k) x_m(k) + w_n(k) \tag{2}$$

where $h_{nm}(k)$ denotes the channel frequency response from transmitter m to receive antenna n at subcarrier k and $w_n(k)$ is additive white Gaussian noise (AWGN) with variance σ_w^2. The received signal at all subcarriers in all receive antenna ports can be expressed in vector-matrix notation as

$$\mathbf{r} = \sum_{m=1}^{M} \mathbf{H}_m \mathbf{x}_m + \mathbf{w}. \tag{3}$$

In the above expression, $\mathbf{r} = [\mathbf{r}_1^T, \ldots, \mathbf{r}_N^T]^T$, $\mathbf{H}_m = [\mathrm{diag}\{\mathbf{h}_{1m}\}, \ldots, \mathrm{diag}\{\mathbf{h}_{Nm}\}]^T$, $\mathbf{x}_m = [x_m(1), \ldots, x_m(K)]^T$ and $\mathbf{w} = [w_1(1), \ldots, w_1(K), \ldots, w_N(1) \ldots, w_N(K)]^T$. Furthermore, $\mathbf{r}_n = [r_n(1), \ldots, r_n(K)]^T$, $\mathbf{h}_{nm} = [h_{nm}(1), \ldots, h_{nm}(K)]^T$ and we also define $\mathbf{h}_m = [\mathbf{h}_{1m}^T, \ldots, \mathbf{h}_{Nm}^T]^T$.

III. Proposed Receiver

In this section, our proposed iterative receiver with channel estimation and interference cancellation is presented. First, the general DM principle is briefly explained, followed by the application to our specific scenario. Finally, some remarks on implementation issues are given.

A. The Divergence Minimization principle

Let $\mathbf{\Phi}$ denote a vector including as components all the unknown parameters to be estimated and $p(\mathbf{\Phi}|\mathbf{r})$ be the posterior probability density function (pdf) of $\mathbf{\Phi}$ given an observation $\mathbf{r}$. The DM framework approximates $p(\mathbf{\Phi}|\mathbf{r})$ by an auxiliary pdf $q(\mathbf{\Phi})$ minimizing the KL divergence [11]

$$D\Big(q(\mathbf{\Phi})\Big\|p(\mathbf{\Phi}|\mathbf{r})\Big) \triangleq \int d\mathbf{\Phi} q(\mathbf{\Phi}) \log \frac{q(\mathbf{\Phi})}{p(\mathbf{\Phi}|\mathbf{r})}. \tag{4}$$

In our application, we are interested in estimating the desired transmitted signals $\mathbf{x}_1, \ldots, \mathbf{x}_{M_d}$. To achieve this reliably, we need estimates of the channel transfer functions $\mathbf{h}_1, \ldots, \mathbf{h}_M$, the interfering signals $\mathbf{x}_{M_d+1}, \ldots, \mathbf{x}_M$ and the inverse of the noise covariance matrix $\mathbf{\Sigma}_w^{-1}$, with $\mathbf{\Sigma}_w = \mathrm{E}\{\mathbf{w}\mathbf{w}^H\}$. Therefore, the set of parameters to be estimated is $\mathbf{\Phi} = \{\mathbf{\Sigma}_w^{-1}, \mathbf{h}_1, \ldots, \mathbf{h}_M, \mathbf{x}_1, \ldots, \mathbf{x}_M\}$, while the observation vector $\mathbf{r}$ is given by (3). In order to obtain a solution that can be computed with tractable complexity, we define an auxiliary function $q(\mathbf{\Phi})$ that factorizes according to

$$q(\mathbf{\Phi}) = q_{\Sigma_w^{-1}}(\mathbf{\Sigma}_w^{-1}) \prod_{m=1}^{M} q_{h_m}(\mathbf{h}_m) q_{x_m}(\mathbf{x}_m). \tag{5}$$

The auxiliary function is iteratively updated by minimizing the KL divergence in (4) with respect to one of the factors in (5) while keeping the rest fixed. By alternatively updating the different factors, the KL divergence is minimized and the auxiliary distribution $q(\mathbf{\Phi})$ approximates the true posterior pdf $p(\mathbf{\Phi}|\mathbf{r})$. More details about the formal principles of the DM framework can be found in [10].

In the following, the updating steps of $q(\mathbf{\Phi})$ with respect to the different parameters are described. The algorithm assumes initial distributions $q^{[0]}_{\Sigma_w^{-1}}(\mathbf{\Sigma}_w^{-1})$, $q^{[0]}_{h_m}(\mathbf{h}_m)$ and $q^{[0]}_{x_m}(\mathbf{x}_m)$, where the superindex $(\cdot)^{[i]}$ indicates the i^{th} updating step.

B. Update of the channel gain distributions

When updating the channel distribution $q_{h_m}(\mathbf{h}_m)$ in the $(i+1)^{th}$ updating step, the distributions $q^{[i]}_{\Sigma_w^{-1}}(\mathbf{\Sigma}_w^{-1})$, $q^{[i]}_x(\mathbf{x}) = \prod_{j=1}^M q^{[i]}_{x_j}(\mathbf{x}_j)$ and $q^{[i]}_{\tilde{h}_m}(\mathbf{h}) = \prod_{j\neq m} q^{[i]}_{h_j}(\mathbf{h}_j)$ are treated as constants. The updated distribution $q^{[i+1]}_{h_m}(\mathbf{h}_m)$ is obtained by solving the minimization problem:

$$\begin{array}{ll}\text{minimize} & D\Big(q_{h_m}(\mathbf{h}_m)q^{[i]}_{\tilde{h}_m}(\mathbf{h})q^{[i]}_x(\mathbf{x})q^{[i]}_{\Sigma_w^{-1}}(\mathbf{\Sigma}_w^{-1})\Big|\Big|p(\mathbf{\Phi}|\mathbf{r})\Big)\\ \text{subject to} & \int q_{h_m}(\mathbf{h}_m)d\mathbf{h}_m = 1\\ & q_{h_m}(\mathbf{h}_m)\geq 0,\end{array} \tag{6}$$

which leads to the solution

$$q^{[i+1]}_{h_m}(\mathbf{h}_m)\propto p(\mathbf{h}_m) \cdot \exp\Big[\mathrm{E}_{q^{[i]}_x}\big\{\mathrm{E}_{q^{[i]}_{\tilde{h}}}\big\{\mathrm{E}_{q^{[i]}_{\Sigma_w^{-1}}}\big\{\log p(\mathbf{r}|\mathbf{\Phi})\big\}\big\}\big\}\Big] \tag{7}$$

where $p(\mathbf{h}_m)$ denotes the prior distribution of $\mathbf{h}_m$. The log-likelihood function in (7) reads

$$\log p(\mathbf{r}|\mathbf{\Phi}) \propto^e \log|\mathbf{\Sigma}_w^{-1}| - (\mathbf{r}-\sum_{m=1}^M \mathbf{H}_m\mathbf{x}_m)^H\mathbf{\Sigma}_w^{-1}(\mathbf{r}-\sum_{m=1}^M \mathbf{H}_m\mathbf{x}_m). \tag{8}$$

By assuming that the prior distribution of $\mathbf{h}_m$ is Gaussian with zero mean and covariance matrix $\mathbf{\Sigma}_{h_m} = \mathrm{E}\{\mathbf{h}_m\mathbf{h}_m^H\}$, the marginalizations in (7) lead to an updated distribution which is also Gaussian, with pdf

$$q^{[i+1]}_{h_m}(\mathbf{h}_m) \propto \exp\Big[-(\mathbf{h}_m-\mathbf{h}_m^{[i+1]})^H{\mathbf{\Sigma}^{[i+1]}_{h_m}}^{-1}(\mathbf{h}_m-\mathbf{h}_m^{[i+1]})\Big]. \tag{9}$$

The mean value is given by

$$\mathbf{h}_m^{[i+1]} = \big(\mathbf{\Sigma}_{h_m}^{-1} + {\tilde{\mathbf{X}}_m^{[i]}}^H(\mathbf{\Omega}_w^{-1})^{[i]}\tilde{\mathbf{X}}_m^{[i]} + {\mathbf{B}_m^{[i]}}^H(\mathbf{\Omega}_w^{-1})^{[i]}\mathbf{B}_m^{[i]}\big)^{-1} \cdot {\tilde{\mathbf{X}}_m^{[i]}}^H(\mathbf{\Omega}_w^{-1})^{[i]}(\mathbf{r}-\sum_{j\neq m}\mathbf{H}_j^{[i]}\tilde{\mathbf{x}}_j^{[i]}) \tag{10}$$

and the covariance is

$$\mathbf{\Sigma}^{[i+1]}_{h_m} = \big(\mathbf{\Sigma}_{h_m}^{-1} + {\tilde{\mathbf{X}}_m^{[i]}}^H(\mathbf{\Omega}_w^{-1})^{[i]}\tilde{\mathbf{X}}_m^{[i]} + {\mathbf{B}_m^{[i]}}^H(\mathbf{\Omega}_w^{-1})^{[i]}\mathbf{B}_m^{[i]}\big)^{-1}. \tag{11}$$

In the above equations, $\tilde{\mathbf{x}}_j^{[i]} = \mathrm{E}_{q^{[i]}_{x_j}}\{\mathbf{x}_j\}$, $\tilde{\mathbf{X}}_j^{[i]} = \mathbf{I}_M \otimes \mathrm{diag}\{\tilde{\mathbf{x}}_j^{[i]}\}$, and $\mathbf{B}_j^{[i]} = \mathbf{I}_M \otimes \mathrm{diag}\{\sigma^{[i]}_{x_j(1)},\ldots,\sigma^{[i]}_{x_j(K)}\}$ with ${\sigma^{[i]}_{x_j(k)}}^2 = \mathrm{E}_{q^{[i]}_{x_j}}\{|x_j(k)|^2\} - |\tilde{x}_j^{[i]}(k)|^2$. Details on $(\mathbf{\Omega}_w^{-1})^{[i]}$ will be given in the following subsection.

C. Update of the inverse noise covariance distribution

For the update of the inverse noise covariance distribution $q_{\Sigma_w^{-1}}(\mathbf{\Sigma}_w^{-1})$, the distributions $q^{[i]}_x(\mathbf{x})$ and $q^{[i]}_h(\mathbf{h}) = \prod_{j=1}^M q^{[i]}_{h_j}(\mathbf{h}_j)$ are kept fixed, leading to the following minimization problem:

$$\begin{array}{ll}\text{minimize} & D\Big(q_{\Sigma_w^{-1}}(\mathbf{\Sigma}_w^{-1})q^{[i]}_h(\mathbf{h})q^{[i]}_x(\mathbf{x})\Big|\Big|p(\mathbf{\Phi}|\mathbf{r})\Big)\\ \text{subject to} & \int q_{\Sigma_w^{-1}}(\mathbf{\Sigma}_w^{-1})d\mathbf{\Sigma}_w^{-1} = 1\\ & q_{\Sigma_w^{-1}}(\mathbf{\Sigma}_w^{-1})\geq 0.\end{array} \tag{12}$$

Analogously to the channel gain update, the solution of the minimization reads

$$q^{[i+1]}_{\Sigma_w^{-1}}(\mathbf{\Sigma}_w^{-1}) \propto p(\mathbf{\Sigma}_w^{-1})\exp\Big[\mathrm{E}_{q^{[i]}_h}\big\{\mathrm{E}_{q^{[i]}_x}\big\{\log p(\mathbf{r}|\mathbf{\Phi})\big\}\big\}\Big]. \tag{13}$$

After performing the marginalizations with respect to the channel distribution and the transmitted symbols distribution, and assuming $p(\mathbf{\Sigma}_w^{-1})$ is a uniform distribution, we obtain an updated distribution given by

$$q^{[i+1]}_{\Sigma_w^{-1}}(\mathbf{\Sigma}_w^{-1}) \propto |\mathbf{\Sigma}_w^{-1}|\exp\big[\mathrm{tr}\{-\mathbf{\Sigma}_w^{-1}\mathbf{C}^{[i]}\}\big] \tag{14}$$

with

$$\mathbf{C}^{[i]} = (\mathbf{r}-\sum_{j=1}^M\tilde{\mathbf{X}}_j^{[i]}\mathbf{h}_j^{[i]})(\mathbf{r}-\sum_{j=1}^M\tilde{\mathbf{X}}_j^{[i]}\mathbf{h}_j^{[i]})^H + \sum_{j=1}^M\mathbf{B}_j^{[i]}\mathbf{\Sigma}_{h_j}^{[i]}{\mathbf{B}_j^{[i]}}^H + \sum_{j=1}^M\mathbf{B}_j^{[i]}\mathbf{h}_j^{[i]}{\mathbf{h}_j^{[i]}}^H{\mathbf{B}_j^{[i]}}^H + \sum_{j=1}^M\tilde{\mathbf{X}}_j^{[i]}\mathbf{\Sigma}_{h_j}^{[i]}{\tilde{\mathbf{X}}_j^{[i]}}^H. \tag{15}$$

The above expression has the form of a complex Wishart distribution [12]. Specifically, the matrix $\mathbf{\Sigma}_w^{-1}$ is Wishart distributed as $\mathbf{\Sigma}_w^{-1} \sim W_{NK}(NK+2, {\mathbf{C}^{[i]}}^{-1})$, and has mean value

$$(\mathbf{\Omega}_w^{[i+1]})^{-1} \triangleq \mathrm{E}_{q^{[i+1]}_{\Sigma_w^{-1}}}\Big\{\mathbf{\Sigma}_w^{-1}\Big\} = \left(\frac{\mathbf{C}^{[i]}}{NK+2}\right)^{-1}. \tag{16}$$

In order to obtain simpler expressions, it can be further assumed that $\mathbf{\Sigma}_w^{-1}$ represents the covariance matrix of a white Gaussian process with $\mathbf{\Sigma}_w^{-1} = \sigma_w^{-2}\mathbf{I}_{NK}$. Under these conditions, the corresponding distribution of the reciprocal variance becomes

$$q_{\sigma_w^{-2}}(\sigma_w^{-2}) = (\sigma_w^{-2})^{NK}\exp\big[-\sigma_w^{-2}\mathrm{tr}\{\mathbf{C}^{[i]}\}\big] \tag{17}$$

which is chi-square distributed [12], with mean value

$$(\sigma_w^{-2})^{[i+1]} \triangleq \mathrm{E}_{q_{\sigma_w^{-2}[i+1]}}\Big\{\sigma_w^{-2}\Big\} = \left(\frac{\mathrm{tr}\{\mathbf{C}^{[i]}\}}{NK+2}\right)^{-1}. \tag{18}$$

D. Update of the transmitted symbol distributions

Analogously to the other updates, when updating the distribution $q_{x_m}(\mathbf{x}_m)$, the distributions $q^{[i]}_{\tilde{x}_m}(\mathbf{x}) = \prod_{j\neq m} q^{[i]}_{x_j}(\mathbf{x}_j)$, $q^{[i]}_h(\mathbf{h}) = \prod_{j=1}^{M} q^{[i]}_{h_j}(\mathbf{h}_j)$ and $q^{[i]}_{\Sigma_w^{-1}}(\mathbf{\Sigma}_w^{-1})$ are kept fixed, and the update is achieved by solving

$$\begin{aligned} \text{minimize} \quad & D\Big(q_{x_m}(\mathbf{x}_m) q^{[i]}_{\tilde{x}_m}(\mathbf{x}) q^{[i]}_h(\mathbf{h}) q^{[i]}_{\Sigma_w^{-1}}(\mathbf{\Sigma}_w^{-1}) \Big|\Big| p(\mathbf{\Phi}|\mathbf{r})\Big) \\ \text{subject to} \quad & \sum_{\forall \mathbf{x}_m} q_{x_m}(\mathbf{x}_m) = 1 \\ & q_{x_m}(\mathbf{x}_m) \geq 0. \end{aligned} \tag{19}$$

The solution to (19) reads

$$\begin{aligned} q^{[i+1]}_{x_m}(\mathbf{x}_m) \propto & p(\mathbf{x}_m) \\ & \cdot \exp\Big[\mathrm{E}_{q^{[i]}_h}\big\{\mathrm{E}_{q^{[i]}_{\tilde{x}}}\big\{\mathrm{E}_{q^{[i]}_{\Sigma_w^{-1}}}\big\{\log p(\mathbf{r}|\mathbf{\Phi})\big\}\big\}\big\}\Big] \end{aligned} \tag{20}$$

Since no prior information on the transmitted data symbols is available (we assume that the receiver has perfect information on the pilot symbols), a uniform prior distribution is assumed, and $p(\mathbf{x}_m)$ can be removed from (20). After marginalizing with respect to the fixed distributions, the updating step is given by

$$q^{[i+1]}_{x_m}(\mathbf{x}_m) \propto \exp\Big[2\sigma_w^{-2^{[i]}} \sum_{k=1}^{K} \mathrm{Re}\big\{x_m^*(k) \sum_{n=1}^{N} h^{[i]^*}_{nm} \gamma_{nm}(k)^{[i]}\big\}\Big] \tag{21}$$

with

$$\begin{aligned} \gamma_{nm}(k)^{[i]} = & r_{nm}(k) - \sum_{j\neq m} h^{[i]}_{nj}(k) \tilde{x}^{[i]}_j(k) \\ & - \frac{1}{2}\left(h^{[i]}_{nm}(k) x_m(k) + \frac{x_m(k)}{h^{[i]^*}_{nm}(k)} \mathbf{\Sigma}^{[i]}_{h_{nm}}[k,k]\right), \end{aligned} \tag{22}$$

where we have assumed that $\mathbf{\Sigma}_w^{-1} = \sigma_w^{-2}\mathbf{I}_{NK}$, as in (18). As it can be observed in the above expressions, the updated distribution is obtained by cancelling the signal contribution from other transmitters. Also, the covariance of the channel estimates, $\mathbf{\Sigma}^{[i]}_{h_{nm}}$, is taken into account. From the updated distribution, the values of $\tilde{\mathbf{x}}_m^{[i+1]}$ and $\mathbf{B}_m^{[i+1]}$ are calculated to be used in the updates of the inverse noise covariance and the channel gain distributions. When the last iteration of the algorithm is reached, the distributions $q_{x_m}(\mathbf{x}_m)$, $m = 1,\ldots,M_d$ are used to obtain soft estimates of the coded symbols, which are fed to the channel decoder in order to detect the information bits.

E. Implementation Issues

1) Order of the updates: While the DM framework allows to obtain the update rules for each of the distributions minimizing the KL divergence with respect to the true posterior distribution, there is so far no formal way of determining the optimal updating sequence. Therefore, this has to be determined by performing a performance evaluation of the different possible updating orderings by, e.g., Monte-Carlo simulations. In this work, we opt to evaluate the following scheme:

1) Update $q_{h_m}(\mathbf{h}_m)$, $m = 1,\ldots,M$.
2) Update $q_{x_m}(\mathbf{x}_m)$, $m = 1,\ldots,M$.
3) Update $q_{\Sigma_w^{-1}}(\mathbf{\Sigma}_w^{-1})$.

The above sequence of updates represents a full iteration of the receiver. Although there is no evidence of this scheme being optimal, simulation results shown in the next section confirm the good performance of a receiver using this design.

2) Initialization: Although the convergence of the DM receiver is ensured due to the minimization performed at each update step, the receiver might converge to different stationary points depending on the initial values used in the algorithm. It is therefore of crucial importance to initialize the iterative receiver properly. In this work, we choose to initialize the channel estimates with a linear minimum mean-squared error (LMMSE) channel estimator using only the signal received at pilot subcarriers. The expression of the LMMSE channel estimates for channel $\mathbf{h}_m$ reads

$$\mathbf{h}_m^{[0]} = \mathbf{\Sigma}_{h_m h_{p,m}} \mathbf{X}_{p,m}^H \big(\sum_{j=1}^{M} \mathbf{X}_{p,j} \mathbf{\Sigma}_{h_{p,j}} \mathbf{X}_{p,j}^H + \mathbf{\Sigma}_{w_p}\big)^{-1} \mathbf{r}_p \tag{23}$$

where $\mathbf{\Sigma}_{w_p} = \mathrm{E}\{\mathbf{w}_p \mathbf{w}_p^H\}$, $\mathbf{\Sigma}_{h_m h_{p,m}} = \mathrm{E}\{\mathbf{h}_m \mathbf{h}_{p,m}^H\}$ and $\mathbf{\Sigma}_{h_{p,j}} = \mathrm{E}\{\mathbf{h}_{p,j}\mathbf{h}_{p,j}^H\}$. The subindex p in matrices and vectors indicates that only elements corresponding to the pilot subcarriers are taken. The initial values for the covariance of the channel estimates are taken from the prior channel covariance, i.e., $\mathbf{\Sigma}^{[0]}_{h_m h_m} = \mathbf{\Sigma}_{h_m h_m}$.

Once an initial value for the channel estimates is available, estimates of the transmitted symbols can be obtained. In our proposed implementation, these are obtained using a soft-output maximum-likelihood detector (MLD) [13]. From the soft output detector, the initial values $\tilde{\mathbf{x}}_m^{[0]}$ and $\mathbf{B}_m^{[0]}$ are obtained for $m = 1\ldots,M$. With these initial values, the initial estimate of the inverse noise covariance $(\mathbf{\Omega}_w^{[0]})^{-1}$ is obtained by using either (16) or (18).

IV. Performance Evaluation

In this section, we evaluate the performance of the proposed channel estimator by means of Monte-Carlo simulations. In order to do so, we define an OFDM system with parameters inspired by the 3GPP Long Term Evolution (LTE) 5 MHz downlink physical layer parameters [2]. The system operates with an FFT size of 512, with 300 active subcarriers, and a frequency spacing of 15 KHz between them. Pilot subcarriers are transmitted in every OFDM symbol, with a frequency spacing of 12 subcarriers (i.e. 600 KHz) between them. The desired and interfering signals have their pilots in the same subcarriers, and perfect synchronization between the transmitters is assumed. Hence, pilots of all transmitted signals overlap in frequency. The pilot sequences are made of random independent and uniformly distributed QPSK symbols. A convolutional code is used for channel coding, with BCJR [14]

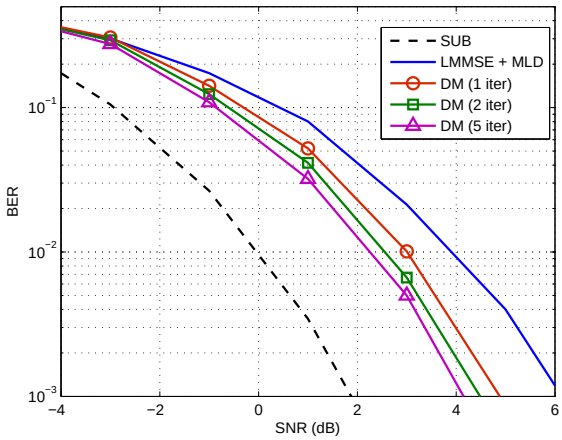

Fig. 2. BER performance of the DM receiver

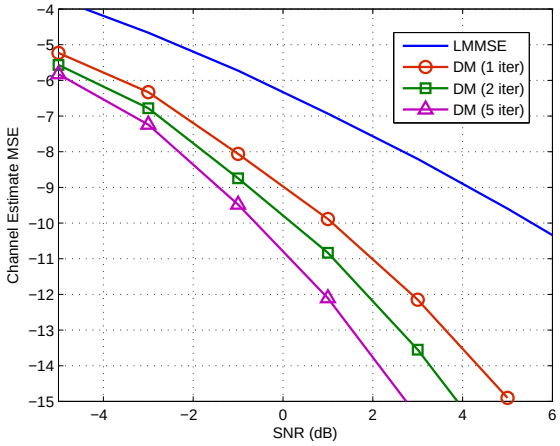

Fig. 3. MSE performance of the DM receiver's channel estimator.

decoding at the receiver, and QPSK modulation is employed for the data symbols.

We consider a scenario with two single-antenna transmitters, one transmitting the desired signal and the other being an interferer. The receiver has two receive antennas, and the signal-to-interference level per receive antenna branch is 0 dB (i.e., both the desired and interfering signal are received with the same power). The channel responses are generated according to the extended Typical Urban channel model [15], which consists of 9 taps and has a maximum excess delay of 5 μs. Block fading is used, i.e., the channel response is static over the duration of an OFDM symbol, and we assume that the cyclic prefix is long enough to cope with the inter-symbol interference due to multipath propagation.

In Fig. 2, the bit error rate performance of our proposed receiver in the considered scenario is depicted. For comparison's sake, the performance of a receiver using LMMSE channel estimation and MLD detection (also used as initialization for the DM receiver) is shown, as well as the single-user bound (SUB). As it can be seen, the iterative process greatly improves the performance of the receiver with a few iterations. After the first iteration of the algorithm, the receiver shows a gain of 0.9 dB at 1% BER with respect to the initialization, which is further improved up to a 1.7 dB gain with five iterations. After the first few iterations the receiver converges, achieving a performance which is only slightly more than 2 dB away from the SUB, even in such a strong interference environment.

In Fig. 3, the performances of the DM receiver's channel estimator and the pilot-based LMMSE channel estimator are compared. As the plot shows, a great improvement in the channel estimates' accuracy is obtained after just the first iteration. This is due to the increase of information used in the channel estimator: while the LMMSE only makes use of the observations at pilot subcarriers, the DM channel estimator combines those with the estimates at the data subcarriers and the partial information available on the data symbols. In subsequent iterations, the reliability of the information on the data symbols is increased due to the interference cancellation at the detector and the estimate of the noise covariance, leading to an improvement in the channel estimates.

V. Conclusion

In this work we have presented a novel iterative receiver for MIMO-OFDM systems with synchronized interferers. The receiver, derived under the DM framework, combines channel estimation, interference cancellation and residual noise estimation in an iterative fashion, and is guaranteed to converge due to the formal principle under which it has been derived. The performance has been assessed by means of Monte-Carlo simulations, showing that our proposed scheme performs very closely to the single-user bound, even with an interference level as high as 0 dB. This is due, in large proportion, to the channel estimator, which combines the information available from the pilot symbols with the information obtained from soft-decisions on the data symbols, allowing to drastically reduce the channel estimates' error.

Acknowledgment

This work has been partly funded by the FP7-ICT Network of Excellence in Wireless Communications, NEWCOM++ (Contract No. 216715). The authors would also like to thank Infineon Technologies Denmark A/S and Nokia Denmark A/S for the financial support which made this work possible.

References

[1] *IEEE Standard for Local and metropolitan area networks Part 16: Air Interface for Fixed and Mobile Broadband Wireless Access Systems Amendment 2: Physical and Medium Access Control Layers for Combined Fixed and Mobile Operation in Licensed Bands and Corrigendum 1*, IEEE Std. 802.16e-2005, 2006.

[2] "Evolved Universal Terrestrial Radio Access (E-UTRA); LTE Physical Layer - General Description (release 8)," 3rd Generation Partnership Project, Tech. Rep. TS 36.211, V8.1.0, Nov. 2007.

[3] L. Hanzo, M. Munster, B. J. Choi, and T. Keller, *OFDM and MC-CDMA for Broadband Multi-User Communications, WLANs and Broadcasting*. West Sussex, England: John Wiley & Sons, 2003.

[4] M. Munster, T. Keller, and L. Hanzo, "Co-channel interference suppression assisted adaptive OFDM in interference limited environments," *Vehicular Technology Conference, 1999. VTC 1999 - Fall. IEEE VTS 50th*, vol. 1, pp. 284–288 vol.1, 1999.

[5] J. Li, K. Ben Letaief, and Z. Cao, "Co-channel interference cancellation for space-time coded OFDM systems," *Wireless Communications, IEEE Transactions on*, vol. 2, no. 1, pp. 41–49, Jan. 2003.

[6] C.-S. Ni and K.-C. Chen, "Cochannel interference suppression for coded OFDM systems over frequency-selective slowly fading channels," *Vehicular Technology Conference, 2004. VTC2004-Fall. 2004 IEEE 60th*, vol. 1, pp. 679–683 Vol. 1, Sept. 2004.

[7] Y. Li and N. Sollenberger, "Adaptive antenna arrays for OFDM systems with cochannel interference," *Communications, IEEE Transactions on*, vol. 47, no. 2, pp. 217–229, Feb 1999.

[8] J.-J. van de Beek, O. Edfors, M. Sandell, S. Wilson, and P. Borjesson, "On channel estimation in ofdm systems," *Vehicular Technology Conference, 1995 IEEE 45th*, vol. 2, pp. 815–819 vol.2, Jul 1995.

[9] C. Navarro, B. Fleury, G. Kirkelund, P. Mogensen, L. Deneire, T. Sø rensen, and C. Rom, "Channel estimation based on divergence minimization for OFDM systems with co-channel interference," *Communications, 2009. ICC '09. IEEE International Conference on*, Accepted for Publication.

[10] B. Hu, I. Land, L. Rasmussen, R. Piton, and B. Fleury, "A divergence minimization approach to joint multiuser decoding for coded CDMA," *Selected Areas in Communications, IEEE Journal on*, vol. 26, no. 3, pp. 432–445, April 2008.

[11] T. Cover and J. Thomas, *Elements of information theory*. John Wiley & Sons, 1991.

[12] A. Gupta and D. Nagar, *Matrix Variate Distributions*. Chapman & Hall/CRC, 2000.

[13] A. van Zelst, "MIMO for OFDM wireless LAN," Ph.D. dissertation, Eindhoven Univ. of Technology, Den Doelch 2, 5612 AZ Eindoven, Apr. 2004.

[14] L. Bahl, J. Cocke, F. Jelinek, and J. Raviv, "Optimal decoding of linear codes for minimizing symbol error rate," *Information Theory, IEEE Transactions on*, vol. 20, no. 2, pp. 284–287, Mar 1974.

[15] "Evolved Universal Terrestrial Radio Access (E-UTRA); LTE Physical Layer - base station (BS) radion transmission and reception (release 8)," 3rd Generation Partnership Project, Tech. Rep. TS 36.104, V8.0.0, Dec. 2007.

Paper G

Channel Estimation Based on Divergence Minimization for OFDM Systems with Co-Channel Interference

Carles Navarro Manchón, Bernard H. Fleury, Gunvor E. Kirkelund, Preben Mogensen, Luc Deneire, Troels B. Sørensen and Christian Rom

IEEE International Conference on Communications, ICC 2009. Dresden, June 2009.

G. CHANNEL ESTIMATION BASED ON DIVERGENCE MINIMIZATION FOR OFDM SYSTEMS WITH CO-CHANNEL INTERFERENCE

Channel Estimation Based on Divergence Minimization for OFDM Sytems with Co-Channel Interference

Carles Navarro Manchón*, Bernard Fleury*†, Gunvor E. Kirkelund*, Preben Mogensen*,
Luc Deneire*‡, Troels B. Sørensen* and Christian Rom§
*Department of Electronic Systems, Aalborg University
Niels Jernes Vej 12, 9220 Aalborg East
†Forschungszentrum Telekommunikation Wien (FTW), Vienna, Austria
‡Université de Nice, Sophia Antipolis
Centre National de la Recherche Scientifique
I3S, UMR 6070, France
§Infineon Technologies Denmark A/S
Alfred Nobels Vej 25, DK-9220 Aalborg, Denmark

***Abstract*—In this paper, we present a novel approach for pilot-aided channel estimation in OFDM systems with synchronous co-channel interference. The estimator is derived based on the Kullback-Leibler divergence minimization framework. The obtained solution iteratively updates both the desired user's and the interferer's channels, using a combination of minimum mean squared-error filtering and interference cancellation, avoiding the complex matrix inversions involved in pure MMSE channel estimation approaches. Estimation of the noise variance is also included in the iterative algorithm, accounting for the Gaussian noise and residual interference after each iteration. The estimates of both channels are used at the equalizer to reject the interfering signal, thus mitigating the degradation due to co-channel interference. Simulation results show that a receiver using the proposed estimator performs as good as one employing a pure MMSE estimator, and very closely to a receiver having perfect knowledge of the channel coefficients.**

I. Introduction

Orthogonal Frequency Division Multiplexing (OFDM) has become the selected transmission technique for several recent wireless standards, such as the IEEE standard for local and metropolitan area networks (better known as WiMAX) [1], or the 3GPP UTRA Long Term Evolution (LTE) [2]. Its ability to cope with time-dispersive channels while allowing for receivers with low complexity, its easy integration with multiple antenna techniques and its flexibility in terms of bandwidth usage and resource allocation are some of the advantages that have motivated its selection.

In OFDM, the transmission bandwidth is divided into multiple narrowband subcarriers. By the addition of a proper cyclic prefix (CP), these subcarriers become fully orthogonal and experience frequency flat fading conditions in time invariant channels [3]. This allows for simple equalization of the signal at the receiver, while keeping a high spectral efficiency due to the use of orthogonal overlapping subcarriers. In OFDM systems with frequency re-use, however, the signal transmitted from other cells may create co-channel interference which, if not correctly treated, can induce a severe degradation of the receiver performance, especially at the cell edge.

Much work has been done in interference cancellation techniques for OFDM, as in [4]–[6]. These methods, however, assume perfect knowledge of the channel at the receiver. In [7], a minimum mean-squared error interference rejection combiner (MMSE-IRC) for OFDM receivers with multiple antennas is proposed. The combiner parameters are estimated using a discrete-Fourier-transform-based robust MMSE instantaneous correlation estimator, which is therefore sensitive to the *leakage* effect [8] when the channel is not sample-spaced.

In this work, we propose a pilot-aided channel estimator for OFDM systems with severe synchronous co-channel interference in both the data and pilot subcarriers. The estimator is derived by applying the Kullback-Leibler (KL) divergence minimization (DM) approach, which was presented in [9] for multiuser detection in a code-division multiple access system. Our proposed scheme is able to estimate the desired user's and the interferer's channels based on just the signal received at pilot subcarriers. The estimates are then used in a MMSE-IRC combiner, effectively mitigating the effect of the interference. A similar problem was studied in [10]. The solution proposed there, however, requires a preamble in which no interference is present at the pilot subcarriers. Our estimator, on the contrary, can effectively separate and estimate both channels when the pilot signals of the desired user and the interferer overlap in frequency for every OFDM symbol.

The remainder of the paper is organized as follows. The signal model for our considered system is presented in Section II. In Section III, the DM framework is briefly introduced, and the channel estimator is derived. The performance of the estimator is assessed by means of Monte-Carlo simulations in Section IV. Finally, some concluding remarks are given in Section V.

The following notation will be used throughout the paper.

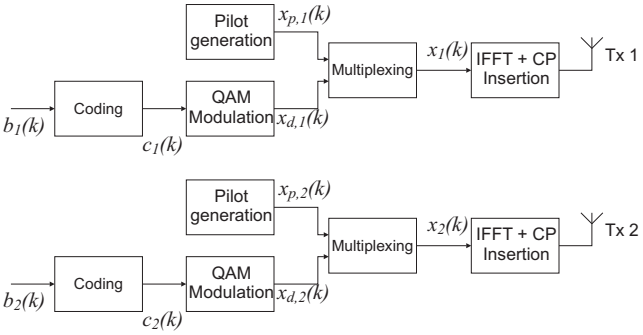

Fig. 1. Block diagram of the transmitters.

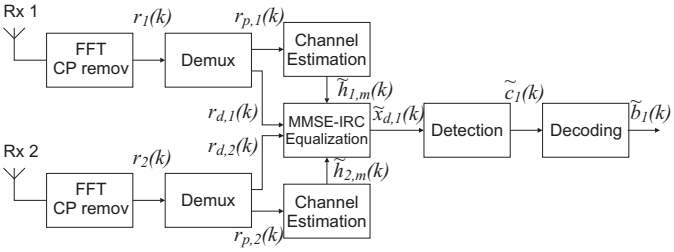

Fig. 2. Block diagram of the receiver

Vectors are represented by boldface lowercase letters, while matrices are denoted as boldface uppercase letters. $(\cdot)^T$ and $(\cdot)^H$ denote respectively the transpose and conjugate transpose of a vector. tr$\{\cdot\}$ denotes the trace operation, and $diag\{\mathbf{x}\}$ represents a diagonal matrix with the elements of vector $\mathbf{x}$. $x \propto y$ denotes direct proportionality, i.e., $x = \alpha y$, and $x \propto^e y$ denotes exponential proportionality, i.e., $\exp[x] = \exp[\beta + y]$, for arbitrary constants α and β. Finally, $\mathrm{E}_{q_x}\{f(\mathbf{x})\}$ represents the expectation of the function $f(\mathbf{x})$ with respect to the probability distribution $q_x(\mathbf{x})$ of $\mathbf{x}$.

II. Signal Model

We consider an OFDM system with single transmit antenna and one interferer, as depicted in Fig. 1. In the diagram, the first transmitter represents the user of interest, while the second transmitter represents a synchronized interferer transmitting in the same time-frequency resources. For each of them, the information bits $b_m(k)$, $m = 1, 2$, $k = 0, \ldots, N_b - 1$ are coded, yielding a stream of coded bits $c_m(k)$, $k = 0, \ldots, N_c - 1$. These are modulated onto a set of QAM symbols $x_{d,m}(k)$, $k = 0, \ldots, N_d - 1$ to be mapped onto an OFDM block. The number of subcarriers used for data transmission in an OFDM block is $N_d = N_c/M$, N_c is the number of coded bits transmitted in one OFDM block and M is the modulation order. The data symbols are then multiplexed with a sequence of pilot symbols $x_{p,m}(k)$, $k = 0, \ldots, N_p - 1$, N_p being the number of pilot subcarriers per block. We assume that pilot symbols are allocated to the same subcarriers at both transmitters. The resulting sequence of symbols $x_m(k)$, $k = 0, \ldots, N_u - 1$ is then mapped to the $N_u = N_d + N_p$ active subcarriers of the OFDM system, and transmitted through the wireless channel after insertion of a cyclic prefix (CP). We assume in this work that the CP is long enough to cope with the time dispersion in both the desired and interfering channels.

The structure of the receiver is shown in Fig. 2. We assume a receiver with two antenna ports. The extension to a higher number of antennas is straightforward. After FFT and CP removal, the received signal at the k^{th} subcarrier of the n^{th} antenna port is given by:

$$r_n(k) = x_1(k)h_{n1}(k) + x_2(k)h_{n2}(k) + w_n(k), \qquad (1)$$

where $w_n(k)$ is additive white Gaussian noise (AWGN) with variance σ_w^2 and $h_{nm}(k)$ represents the frequency-domain channel gain from transmitter m to receive antenna n at the k^{th} subcarrier. In (1), we assume that the channel response is static during one OFDM block. Hence, full orthogonality between subcarriers is achieved. The received signal at antenna port n for all subcarriers can be re-written in matrix-vector notation as

$$\mathbf{r}_n = \mathbf{X}_1\mathbf{h}_{n1} + \mathbf{X}_2\mathbf{h}_{n2} + \mathbf{w}_n \qquad (2)$$

with $\mathbf{r}_n = [r_n(0) \cdots r_n(N_u - 1)]^T$, $\mathbf{h}_{n,m} = [h_{nm}(0) \cdots h_{nm}(N_u - 1)]^T$, $\mathbf{w}_n = [w_n(0) \cdots w_n(N_u - 1)]^T$ and $\mathbf{X}_m = diag\{[x_m(0) \cdots x_m(N_u - 1)]\}$ is a diagonal matrix containing the transmitted symbols.

The demultiplexer following the FFT and CP removal block separates the signal received at pilot and data subcarriers. The pilot signals $\mathbf{r}_{p,n} = [r_{p,n}(0) \cdots r_{p,n}(N_p - 1)]^T$ are fed to the respective channel estimator blocks, while the data signals $\mathbf{r}_{d,n} = [r_{d,n}(0) \cdots r_{d,n}(N_d - 1)]^T$ are sent to the equalizer. Based on the signal received on the pilot subcarriers, the channel estimation block (which will be explained in detail in Section III) provides the equalizer with estimates $\tilde{\mathbf{h}}_{n,m}$ of the channel frequency responses of both the desired and interfering channels. Using these estimates and the signal received at data subcarriers, the equalizer performs MMSE-IRC filtering to recover the desired transmitted symbols as:

$$\tilde{x}_{d,1}(k) = \mathbf{h}_{d,1}^H(k) \left(\mathbf{H}_d^H(k)\mathbf{H}_d(k) + \sigma_w^2\mathbf{I}\right)^{-1} \mathbf{r}_d(k). \qquad (3)$$

In the above equation, $\mathbf{r}_d(k) = [r_{d,1}(k) r_{d,2}(k)]^T$, $\mathbf{H}_d(k) = [\mathbf{h}_{d,1}(k)\mathbf{h}_{d,2}(k)]$ and $\mathbf{h}_{d,m}(k) = [h_{d,1m}(k) h_{d,2m}(k)]^T$, with $h_{d,nm}(k)$ being the channel coefficient for the k^{th} data subcarrier from transmitter m to receive antenna n, and $\mathbf{I}$ denotes the 2x2 identity matrix. Finally, the coded bits of the user of interest $\tilde{c}_1(k)$ are recovered from the equalized symbols in the QAM detector, and are fed to the channel decoder which yields the estimates of the information bits $\tilde{b}_1(k)$.

III. Channel Estimator

In this section, two channel estimation approaches are presented. The first one is the linear MMSE estimator, which will be used as a benchmark for the performance evaluation of our estimator. Next, our proposed channel estimator, based on the DM framework, is introduced. The DM principle is briefly explained, along with the application to our specific scenario. More details about the DM framework and its relation to other known algorithms can be found in [9].

A. MMSE Channel Estimator

The linear MMSE channel estimator aims at minimizing the mean-squared error of the estimate. For the signal model presented, the MMSE estimate of the channel from transmit antenna 1 to receive antenna n reads:

$$\begin{aligned}\tilde{\mathbf{h}}_{\mathbf{1}} &= \arg\min_{\tilde{\mathbf{h}}_{n1}} \mathrm{E}\{(\mathbf{h}_{n1}-\tilde{\mathbf{h}}_{n1})^H(\mathbf{h}_{n1}-\tilde{\mathbf{h}}_{n1})\} \\ &= \boldsymbol{\Sigma}_{h_{n1}h_{p,n1}}\mathbf{X}_{p,1}^H(\mathbf{X}_{p,1}\boldsymbol{\Sigma}_{h_{p,n1}}\mathbf{X}_{p,1}^H \\ &+ \mathbf{X}_{p,2}\boldsymbol{\Sigma}_{h_{p,n2}}\mathbf{X}_{p,2}^H + \boldsymbol{\Sigma}_{w_p})^{-1}\mathbf{r}_{p,n} \end{aligned} \quad (4)$$

where $\boldsymbol{\Sigma}_{w_p} = \mathrm{E}\{\mathbf{w}_p\mathbf{w}_p^H\} = \sigma_w^2\mathbf{I}$, $\boldsymbol{\Sigma}_{h_{n1}h_{p,n1}} = \mathrm{E}\{\mathbf{h}_{n1}\mathbf{h}_{p,n1}^H\}$ and $\boldsymbol{\Sigma}_{h_{p,nm}} = \mathrm{E}\{\mathbf{h}_{p,nm}\mathbf{h}_{p,nm}^H\}$. The estimator requires the inversion of an $N_p \times N_p$ matrix every OFDM symbol, which is normally to complex to compute in a mobile receiver for a system with a large number of subcarriers. In the rest of the section, we present an iterative approach which avoids this matrix inversion.

B. Divergence minimization

Let $\boldsymbol{\Phi}$ denote a vector including as components all the unknown parameters to be estimated and $p(\boldsymbol{\Phi}|\mathbf{r})$ be the posterior probability density function (pdf) of $\boldsymbol{\Phi}$ given an observation $\mathbf{r}$. The DM framework approximates $p(\boldsymbol{\Phi}|\mathbf{r})$ by an auxiliary pdf $q(\boldsymbol{\Phi})$ minimizing the KL divergence [11]

$$D\Big(q(\boldsymbol{\Phi})\Big|\Big|p(\boldsymbol{\Phi}|\mathbf{r})\Big) \triangleq \int d\boldsymbol{\Phi} q(\boldsymbol{\Phi}) \log\frac{q(\boldsymbol{\Phi})}{p(\boldsymbol{\Phi}|\mathbf{r})} \quad (5)$$

In order to make the mathematical problem tractable, the auxiliary distribution function $q(\boldsymbol{\Phi})$ is assumed to factorize as shown below.

In our application, the parameters to estimate are the channel responses of the desired and interfering channels as well as the inverse of the noise covariance matrix, i.e., $\boldsymbol{\Phi} = \{\mathbf{h}_{p,n1}, \mathbf{h}_{p,n2}, \boldsymbol{\Sigma}_{w_{p,n}}^{-1}\}$, where $\boldsymbol{\Sigma}_{w_{p,n}} = \mathrm{E}\{\mathbf{w}_{p,n}\mathbf{w}_{p,n}^H\}$. The subindex p indicates that only pilot subcarriers are taken into account. The auxiliary pdf is assumed to factorize according to:

$$\begin{aligned} q(\boldsymbol{\Phi}) &= q(\mathbf{h}_{p,n1}, \mathbf{h}_{p,n2}, \boldsymbol{\Sigma}_{w_{p,n}}^{-1}) \\ &= q_{h_{p,n1}}(\mathbf{h}_{p,n1}) q_{h_{p,n2}}(\mathbf{h}_{p,n2}) q_{\Sigma_{w_{p,n}}^{-1}}(\boldsymbol{\Sigma}_{w_{p,n}}^{-1}). \end{aligned} \quad (6)$$

The observation is the received signal at the pilot subcarriers, i.e

$$\mathbf{r} = \mathbf{r}_{p,n} = \mathbf{X}_{p,1}\mathbf{h}_{p,n1} + \mathbf{X}_{p,2}\mathbf{h}_{p,n2} + \mathbf{w}_{p,n}. \quad (7)$$

The algorithm iteratively minimizes the KL divergence with respect to one of the factors in (7), while the other factors are kept fixed, resulting in an iterative scheme.

Note that the channel estimation process is done independently for each of the receive antennas. In the remainder of the section we therefore drop the receive antenna subindex n in order to simplify the notation (e.g. $\mathbf{h}_{p,1}$ denotes $\mathbf{h}_{p,n1}$). The algorithm is started with initial distributions $q_{h_{p,1}}^{[0]}(\mathbf{h}_{p,1})$, $q_{h_{p,2}}^{[0]}(\mathbf{h}_{p,2})$ and $q_{\Sigma_{wp}^{-1}}^{[0]}(\boldsymbol{\Sigma}_{w_p}^{-1})$, and these distributions are successively updated according to the updating steps detailed in the following two subsections.

C. Update of the channel vectors

In this subsection, the derivation of the updating step for $q_{h_{p,1}}(\mathbf{h}_{p,1})$ is detailed. Due to the symmetry of the problem, the update for $q_{h_{p,2}}(\mathbf{h}_{p,2})$ is analogous.

To update $q_{h_{p,1}}(\mathbf{h}_{p,1})$, the distributions $q_{h_{p,2}}^{[i]}(\mathbf{h}_{p,2})$ and $q_{\Sigma_{w_p}^{-1}}^{[i]}(\boldsymbol{\Sigma}_{w_p}^{-1})$ are kept fixed, and $q_{h_{p,1}}(\mathbf{h}_{p,1})$ is updated by solving the following problem:

$$\begin{aligned} \text{minimize} \quad & D\Big(q_{h_{p,1}}(\mathbf{h}_{p,1}) q_{h_{p,2}}^{[i]}(\mathbf{h}_{p,2}) \\ & \cdot q_{\Sigma_{w_p}^{-1}}^{[i]}(\boldsymbol{\Sigma}_{w_p}^{-1})\Big|\Big| p(\mathbf{h}_{p,1}, \mathbf{h}_{p,2}, \boldsymbol{\Sigma}_{w_p}^{-1}|\mathbf{r}_p)\Big) \\ \text{subject to} \quad & \int q_{h_{p,1}}(\mathbf{h}_{p,1}) d\mathbf{h}_{p,1} = 1 \\ & q_{h_{p,1}}(\mathbf{h}_{p,1}) \geq 0. \end{aligned} \quad (8)$$

The distribution $q_{h_{p,1}}^{[i+1]}(\mathbf{h}_{p,1})$ solving (8) is found to be

$$\begin{aligned} & q_{h_{p,1}}^{[i+1]}(\mathbf{h}_{p,1}) \propto p(\mathbf{h}_{p,1}) \\ & \cdot \exp\Big[\mathrm{E}_{q_{h_{p,2}}^{[i]}}\Big\{\mathrm{E}_{q_{\Sigma_{w_p}^{-1}}^{[i]}}\Big\{\log p(\mathbf{r}_p|\mathbf{h}_{p,1}, \mathbf{h}_{p,2}, \boldsymbol{\Sigma}_{w_p}^{-1})\Big\}\Big\}\Big] \end{aligned} \quad (9)$$

where $p(\mathbf{h}_{p,1})$ is the prior pdf of $\mathbf{h}_{p,1}$. The log-likelihood function in (9) reads

$$\begin{aligned} & \log p(\mathbf{r}_p|\mathbf{h}_{p,1}, \mathbf{h}_{p,2}, \boldsymbol{\Sigma}_{w_p}^{-1}) \\ & \quad \propto^e \log|\boldsymbol{\Sigma}_{w_p}^{-1}| - \mathrm{tr}\Big\{\boldsymbol{\Sigma}_{w_p}^{-1}(\mathbf{r}_p - \mathbf{X}_{p,1}\mathbf{h}_{p,1} - \mathbf{X}_{p,2}\mathbf{h}_{p,2}) \\ & \quad \cdot (\mathbf{r}_p - \mathbf{X}_{p,1}\mathbf{h}_{p,1} - \mathbf{X}_{p,2}\mathbf{h}_{p,2})^H\Big\}. \end{aligned} \quad (10)$$

The marginalization of (10) with respect to $q_{h_{p,2}}^{[i]}(\mathbf{h}_{p,2})$ and $q_{\Sigma_{w_p}^{-1}}^{[i]}(\boldsymbol{\Sigma}_{w_p}^{-1})$ yields

$$\begin{aligned} & \mathrm{E}_{q_{h_{p,2}}^{[i]}}\Big\{\mathrm{E}_{q_{\Sigma_{w_p}^{-1}}^{[i]}}\Big\{\log p(\mathbf{r}_p|\mathbf{h}_{p,1}, \mathbf{h}_{p,2}, \boldsymbol{\Sigma}_{w_p}^{-1})\Big\}\Big\} \\ & \quad \propto^e -\mathrm{tr}\Big\{(\boldsymbol{\Omega}_{w,p}^{-1})^{[i]}\mathbf{A}^{[i]}\Big\}, \end{aligned} \quad (11)$$

where $(\boldsymbol{\Omega}_{w,p}^{[i]})^{-1} \triangleq \mathrm{E}_{q_{\Sigma_{w_p}^{-1}}^{[i]}}\Big\{\boldsymbol{\Sigma}_{w_p}^{-1}\Big\}$ and

$$\begin{aligned} \mathbf{A}^{[i]} = & (\mathbf{r}_p - \mathbf{X}_{p,1}\mathbf{h}_{p,1} - \mathbf{X}_{p,2}\mathbf{h}_{p,2}^{[i]}) \\ & \cdot (\mathbf{r}_p - \mathbf{X}_{p,1}\mathbf{h}_{p,1} - \mathbf{X}_{p,2}\mathbf{h}_{p,2}^{[i]})^H + \mathbf{X}_{p,2}\boldsymbol{\Sigma}_{h_{p,2}}^{[i]}\mathbf{X}_{p,2}^H. \end{aligned} \quad (12)$$

Details on $(\boldsymbol{\Omega}_{w,p}^{[i]})^{-1}$ and $\boldsymbol{\Sigma}_{h_{p,2}}^{[i]}$ are given later on in this section. Note that terms independent of $\mathbf{h}_{p,1}$ have been neglected in the derivation as they do not affect $q_{h_{p,1}}^{[i+1]}(\mathbf{h}_{p,1})$.

For Rayleigh fading channels, the prior distribution of $\mathbf{h}_{p,1}$ is Gaussian with zero mean and covariance matrix $\boldsymbol{\Sigma}_{h_{p,1}} = \mathrm{E}\Big\{\mathbf{h}_{p,1}\mathbf{h}_{p,1}^H\Big\}$. Using this prior distribution and (11) in (9), we obtain an updated distribution, which is also Gaussian, with pdf:

$$\begin{aligned} & q_{h_{p,1}}^{[i+1]}(\mathbf{h}_{p,1}) \propto \\ & \quad \exp\Big[-(\mathbf{h}_{p,1} - \mathbf{h}_{p,1}^{[i+1]})^H \boldsymbol{\Sigma}_{h_{p,1}}^{[i+1]^{-1}}(\mathbf{h}_{p,1} - \mathbf{h}_{p,1}^{[i+1]})\Big] \end{aligned} \quad (13)$$

with mean vector

$$\mathbf{h}_{p,1}^{[i+1]} = \mathbf{\Sigma}_{h_{p,1}}\Big(\mathbf{\Sigma}_{h_{p,1}}\mathbf{X}_{p,1}^H\mathbf{X}_{p,1} + \mathbf{\Omega}_{w,p}^{[i]}\Big)^{-1}\mathbf{X}_{p,1}^H \cdot \Big(\mathbf{r}_p - \mathbf{X}_{p,2}\mathbf{h}_{p,2}^{[i]}\Big) \quad (14)$$

and covariance matrix

$$\mathbf{\Sigma}_{h_{p,1}}^{[i+1]} = \Big(\mathbf{\Sigma}_{h_{p,1}}^{-1} + (\mathbf{\Omega}_{w,p}^{[i]})^{-1}\mathbf{X}_{p,1}^H\mathbf{X}_{p,1}\Big)^{-1}. \quad (15)$$

By inspecting (14), it is seen that the channel response updating step has the form of an MMSE or Wiener filter [12], applied to the interference-cancelled received signal at pilot positions. As the interference cancellation is not ideal, the estimate of the noise covariance matrix $\mathbf{\Omega}_{w,p}^{[i]}$ takes into account both the noise and the residual interference power, in order to correctly smooth the channel response, as it is shown in the next subsection.

Note that the update of the channel coefficients in (14) does only provide estimates of the channel response at pilot subcarriers. Estimates of the full frequency response at all active subcarriers are obtained by using

$$\tilde{\mathbf{h}}_1 = \mathbf{\Sigma}_{h_1h_{p,1}}\Big(\mathbf{\Sigma}_{h_{p,1}}\mathbf{X}_{p,1}^H\mathbf{X}_{p,1} + \mathbf{\Omega}_{w,p}^{[i]}\Big)^{-1}\mathbf{X}_{p,1}^H \cdot \Big(\mathbf{r}_p - \mathbf{X}_{p,2}\mathbf{h}_{p,2}^{[i]}\Big) \quad (16)$$

instead of (14) in the last iteration of the algorithm with $\mathbf{\Sigma}_{h_1h_{p,1}} = \mathrm{E}\Big\{\mathbf{h}_1\mathbf{h}_{p,1}^H\Big\}$.

D. Update of the noise covariance matrix

When updating $q_{\Sigma_{w_p}^{-1}}(\mathbf{\Sigma}_{w_p}^{-1})$, the distributions $q_{h_{p,1}}^{[i]}(\mathbf{h}_{p,1})$ and $q_{h_{p,2}}^{[i]}(\mathbf{h}_{p,2})$ are kept fixed, and the optimization problem to solve is the following:

$$\begin{aligned} \text{minimize} \quad & D\Big(q_{h_{p,1}}^{[i]}(\mathbf{h}_{p,1})q_{h_{p,2}}^{[i]}(\mathbf{h}_{p,2}) \\ & \cdot q_{\Sigma_{w_p}^{-1}}(\mathbf{\Sigma}_{w_p}^{-1})\Big\|p(\mathbf{h}_{p,1},\mathbf{h}_{p,2},\mathbf{\Sigma}_{w_p}^{-1}|\mathbf{r}_p)\Big) \\ \text{subject to} \quad & \int q_{\Sigma_{w_p}^{-1}}(\mathbf{\Sigma}_{w_p}^{-1})d\mathbf{\Sigma}_{w_p}^{-1} = 1 \\ & q_{\Sigma_{w_p}^{-1}}(\mathbf{\Sigma}_{w_p}^{-1}) \geq 0. \end{aligned} \quad (17)$$

The solution reads

$$q_{\Sigma_{w_p}^{-1}}^{[i+1]}(\mathbf{\Sigma}_{w_p}^{-1}) \propto p(\mathbf{\Sigma}_{w_p}^{-1}) \cdot \exp\Big[\mathrm{E}_{q_{h_{p,1}}^{[i]}}\Big\{\mathrm{E}_{q_{h_{p,2}}^{[i]}}\Big\{\log p(\mathbf{r}_p|\mathbf{h}_{p,1},\mathbf{h}_{p,2},\mathbf{\Sigma}_{w_p}^{-1})\Big\}\Big\}\Big]. \quad (18)$$

The marginalization of (10) is taken with respect to $\mathbf{h}_{p,1}^{[i]}$ and $\mathbf{h}_{p,2}^{[i]}$, resulting in

$$\mathrm{E}_{q_{h_{p,1}}^{[i]}}\Big\{\mathrm{E}_{q_{h_{p,2}}}^{[i]}\Big\{\log p(\mathbf{r}_p|\mathbf{h}_{p,1},\mathbf{h}_{p,2},\mathbf{\Sigma}_{w_p}^{-1})\Big\}\Big\} \propto^e \log|\mathbf{\Sigma}_w^{-1}| - \mathrm{tr}\Big\{\mathbf{\Sigma}_{w,p}^{-1}\mathbf{B}^{[i]}\Big\}, \quad (19)$$

where

$$\mathbf{B}^{[i]} = (\mathbf{r}_p - \mathbf{X}_{p,1}\mathbf{h}_{p,1}^{[i]} - \mathbf{X}_{p,2}\mathbf{h}_{p,2}^{[i]}) \cdot (\mathbf{r}_p - \mathbf{X}_{p,1}\mathbf{h}_{p,1}^{[i]} - \mathbf{X}_{p,2}\mathbf{h}_{p,2}^{[i]})^H + \mathbf{X}_{p,1}\mathbf{\Sigma}_{h_{p,1}}^{[i]}\mathbf{X}_{p,1}^H + \mathbf{X}_{p,2}\mathbf{\Sigma}_{h_{p,2}}^{[i]}\mathbf{X}_{p,2}^H. \quad (20)$$

By choosing the prior pdf $\mathbf{\Sigma}_{w_p}^{-1}$ to be flat, (18) becomes

$$q_{\Sigma_{w_p}^{-1}}^{[i+1]}(\mathbf{\Sigma}_{w_p}^{-1}) \propto |\mathbf{\Sigma}_w^{-1}| \exp\Big[-\mathrm{tr}\Big\{\mathbf{\Sigma}_{w,p}^{-1}\mathbf{B}^{[i]}\Big\}\Big], \quad (21)$$

which has the form of a Wishart distribution [13] as $\mathbf{\Sigma}_{w,p}^{-1} \sim W_{N_p}\Big(N_p+2, \big(\mathbf{B}^{[i]}\big)^{-1}\Big)$. The mean of $\mathbf{\Sigma}_{w_p}^{-1}$ is therefore

$$(\mathbf{\Omega}_{w,p}^{[i+1]})^{-1} \triangleq \mathrm{E}_{q_{\Sigma_{w_p}^{-1}}^{[i+1]}}\Big\{\mathbf{\Sigma}_{w_p}^{-1}\Big\} = \left(\frac{\mathbf{B}^{[i]}}{N_p+2}\right)^{-1}. \quad (22)$$

In order to simplify the algorithm, it is assumed that $\mathbf{\Sigma}_{w_p}$ represents the covariance matrix of a white Gaussian noise vector with $\mathbf{\Sigma}_{w_p}^{-1} = \mathrm{diag}\{\sigma_{w_p}^{-2},\ldots,\sigma_{w_p}^{-2}\}$. In this case, the updated pdf is given by

$$q_{\sigma_{w_p}^{-2}}(\sigma_{w_p}^{-2}) \propto (\sigma_{w_p}^{-2})^{N_p}\exp\Big[-\sigma_{w_p}^{-2}\mathrm{tr}\Big\{\mathbf{B}^{[i]}\Big\}\Big] \quad (23)$$

which is a chi-square distribution [13]. Specifically $\sigma_{w_p}^{-2} \sim \chi_{N_p+2}^2$, and the expectation of $\sigma_{w_p}^{-2}$ is

$$(\sigma_{w_p}^{-2})^{[i+1]} = \mathrm{E}_{q_{\sigma_{w_p}^{-2}}^{[i+1]}}\Big\{\sigma_{w_p}^{-2}\Big\} = \left(\frac{\mathrm{tr}\Big\{\mathbf{B}^{[i]}\Big\}}{N_p+2}\right)^{-1}. \quad (24)$$

E. Implementation Issues

1) Matrix inverse in the update of the channel vectors: As it can be observed in (14), the inversion of a matrix of dimensions $N_p \times N_p$ is still required for the update of the channel coefficients vector. To avoid the matrix inversion, (14) can be rewritten as:

$$\mathbf{h}_{p,1}^{[i+1]} = \mathbf{U}\mathbf{S}\Big(\mathbf{S} + (\sigma_{w_p}^{-2})^{[i]}\mathbf{I}_{N_p}\Big)^{-1}\mathbf{U}^H\mathbf{X}_{p,1}^H \cdot \Big(\mathbf{r}_p - \mathbf{X}_{p,2}\mathbf{h}_{p,2}^{[i]}\Big) \quad (25)$$

where $\mathbf{\Sigma}_{h_{p,1}} = \mathbf{U}\mathbf{S}\mathbf{U}^H$ is the singular value decomposition (SVD) of the channel covariance matrix. We have also made use of the fact that $\mathbf{X}_{p,1}^H\mathbf{X}_{p,1} = \mathbf{I}_{N_p}$ for constant unit-power pilots, and the simplification of the noise covariance matrix introduced in (23) and (24). Note that the matrix to invert is now a diagonal matrix, which can be inverted with just N_p complex operations. Also, in a wide-sense stationary channel, the prior covariance matrices of the channels will not change over time, and therefore the SVDs need to be computed only once for each channel.

2) Initialization: Previously in this section, details on how to update each of the pdfs have been given. An initialization of them for the first iteration of the algorithm, however, is needed. In our proposed implementation, the channel responses are initialized to null vectors, i.e., $\mathbf{h}_{p,m}^{[0]} = [0,\ldots,0]^T$, and their covariance matrices are initialized to the prior covariance matrices of the channel, $\mathbf{\Sigma}_{h_{p,m}}^{[0]} = \mathbf{\Sigma}_{h_{p,m}}$. As for the noise variance, it is initialized to the AWGN variance, i.e., $(\sigma_{w_p}^{-2})^{[0]} = \sigma_w^{-2}$. In subsequent iterations, this initialization is updated with the residual interference after the interference cancellation performed in the updates of the channel response vectors.

3) Updating schedule: Another important aspect having an impact on the performance of the algorithm is the order in which the pdfs are updated. So far, no analytical way of determining the optimal updating order has been found. In this article, we evaluate the following updating scheme:

1) Update $q_{h_{p,1}}(\mathbf{h}_{p,1})$
2) Update $q_{h_{p,2}}(\mathbf{h}_{p,2})$
3) Update $q_{\sigma_{w_p}^{-2}}(\sigma_{w_p}^{-2})$

Intuitively, the desired user channel should be as strong or stronger than the interfering channel, thus it is selected to be estimated first. Once a first estimate of the desired channel is available, the interfering channel can be estimated more accurately. Finally an estimate of the residual noise plus interference is obtained to improve the channel estimates in subsequent iterations. Simulation results (which have not been included here due to lack of space) showed no relevant gain by updating the reciprocal of the noise variance between the estimates of the desired and interfering channel. Therefore, this step is not included in the algorithm, yielding a less complex scheme with no appreciable loss in performance.

IV. Performance Evaluation

In this section, we evaluate the performance of the proposed channel estimator by means of Monte-Carlo simulations. In order to do so, we define an OFDM system with parameters inspired by the 3GPP Long Term Evolution (LTE) 5 MHz downlink physical layer parameters [2]. The system operates with an FFT size of 512, with 300 active subcarriers, and a frequency spacing of 15 KHz between them. Pilot subcarriers are transmitted in every OFDM symbol, with a frequency spacing of 6 subcarriers (i.e. 300 KHz) between them. Both the desired and interfering signals have their pilots in the same subcarriers, and perfect synchronization between the transmitters is assumed. Hence, pilots of both transmitted signals overlap in frequency. The pilot sequences are made of random independent and uniformly distributed QPSK symbols. The power of the interfering signal is equal to that of the desired signal, and 16QAM modulation is employed for the data symbols. A convolutional code is used for channel coding, with BCJR [14] decoding at the receiver.

Two different channel models are considered, namely the ITU Indoor Office A channel [15] and the COST 259 Typical Urban channel [16]. The former channel exhibits a low frequency selectivity, with a coherence bandwidth of about 3.2 MHz, while the latter has a much narrower coherence bandwidth of around 467 KHz. Block fading is assumed, with a static channel response over the duration of an OFDM symbol and independent realizations between consecutive OFDM symbols. The same channel profile is assumed for all wireless links (desired and interfering).

In Fig. 3, the Mean-Squared Error (MSE) of the channel estimates of the desired and interfering channel versus the number of iterations of the estimator are shown for the two considered channels. The MSE of the MMSE estimator is also depicted for comparison's sake. The signal-to-noise ratio (SNR), which is calculated as the ratio between the desired signal power and the noise power for each antenna branch, is fixed to 25 dB. It is observed that the iterative process improves greatly the quality of the estimates, due to the effectiveness of the interference cancellation and the updating of the noise covariance matrix, which accounts for both the AWGN and the residual interference. A lower MSE (about a 7 dB difference) is achieved in the Indoor A channel. This is a consequence of the lower frequency selectivity, a well-known result from MMSE channel estimation. It is also noted that the convergence rate of the algorithm depends on the frequency selectivity of the channel as well: while 5 iterations are enough to achieve convergence in the Indoor channel, around 10 iterations are needed in the Typical Urban channel. As the results show, the DM channel estimator performance converges to the MMSE estimator with sufficient number of iterations, and the number of iterations required for convergence depends on the frequency selectivity of the channel.

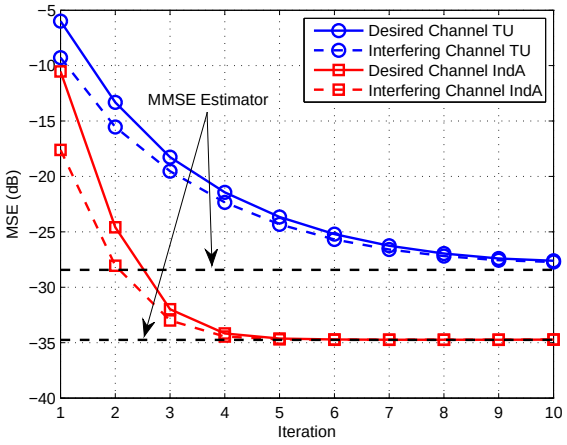

Fig. 3. MSE of the channel estimates versus the number of iterations of the channel estimator at a fixed SNR of 25 dB.

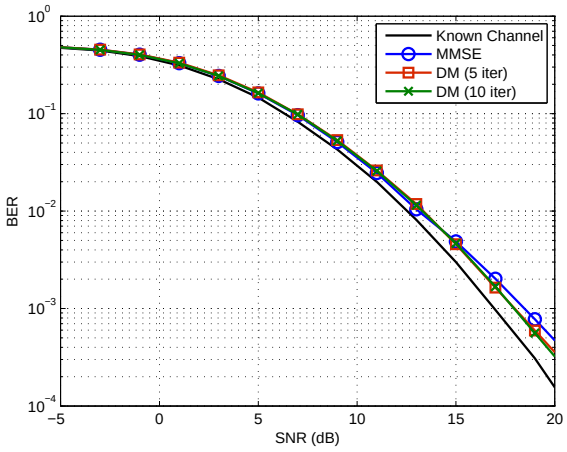

Fig. 4. BER performance for an Indoor A Channel.

The receiver's performance is evaluated in terms of bit-error-rate (BER) in Fig. 4 for the Indoor Office A channel

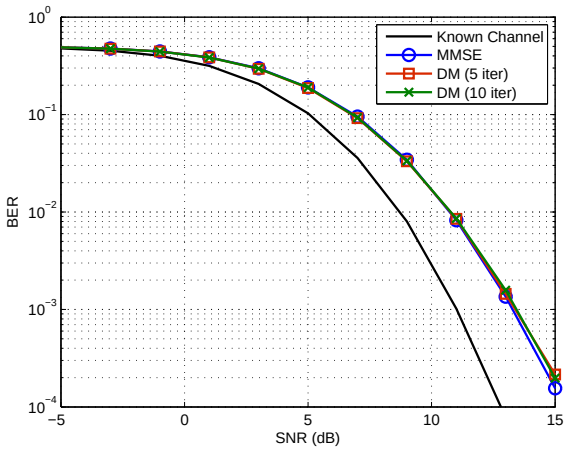

Fig. 5. BER performance for a Typical Urban Channel.

and in Fig. 5 for the Typical Urban channel. Results are shown when the estimators use 5 and 10 iterations. As a reference, the BER of the receiver with perfect knowledge of the channel is also depicted, as well as the BER of a receiver using the MMSE estimator. In the Indoor Channel, the performance of the DM and MMSE estimators is equivalent. When compared with a receiver with perfect knowledge of the channel, a very small degradation in the range of 1 dB is observed in the high SNR range. Furthermore, as commented above, the performance of the estimator does not significantly improve after 5 iterations, with only a very marginal gain after 10 iterations. In the Typical Urban channel, a larger deviation from the perfect channel knowledge results is observed. The degradation ranges from 1.7 dB to 2.4 dB at BER of 10% and 0.1% respectively. However, the degradation in the high SNR range is relatively small when considering a scenario with such a severe interference. Again, the performance of the DM estimator is very close to the MMSE estimator, and only a very slight gain is observed when increasing the number of iterations of the algorithm from 5 to 10.

V. Conclusion

In this paper, we have presented a novel approach for channel estimation in OFDM systems with synchronized co-channel interferers and overlapped pilot symbols. Based on the KL-divergence minimization principle, an iterative algorithm for estimation of the channel gains based on the signal observed at pilot locations has been derived. The resulting algorithm combines MMSE channel estimation with successive interference cancellation and estimation of the noise and residual interference power. The effectiveness of the proposed estimator is assessed by Monte-Carlo simulations. The results show that our algorithm performs as good as the MMSE channel estimator, with the advantage of avoiding the cumbersome matrix inversion in the latter. An overall receiver performance very close to that of a receiver with perfect knowledge of the channel coefficients is attained, especially in channels with low frequency selectivity.

To conclude, it is worth remarking that although the estimator has been presented and evaluated for an OFDM system with synchronized co-channel interference, application to other scenarios could be very advantageous. For instance, our estimator would allow to reduce the pilot overhead in a MIMO-OFDM system by placing the pilot sequences of all transmit antennas in the same time-frequency locations, instead of having specific locations reserved for each of the antennas as it is common in current wireless standards, e.g. LTE.

Acknowledgment

This work has been partly funded by the FP7-ICT Network of Excellence in Wireless Communications, NEWCOM++ (Contract No. 216715). The authors would also like to thank Infineon Technologies Denmark A/S for the financial support which made this work possible.

References

[1] *IEEE Standard for Local and metropolitan area networks Part 16: Air Interface for Fixed and Mobile Broadband Wireless Access Systems Amendment 2: Physical and Medium Access Control Layers for Combined Fixed and Mobile Operation in Licensed Bands and Corrigendum 1*, IEEE Std. 802.16e-2005, 2006.

[2] "Evolved Universal Terrestrial Radio Access (E-UTRA); LTE Physical Layer - General Description (release 8)," 3rd Generation Partnership Project, Tech. Rep. TS 36.211, V8.1.0, Nov. 2007.

[3] L. Hanzo, M. Munster, B. J. Choi, and T. Keller, *OFDM and MC-CDMA for Broadband Multi-User Communications, WLANs and Broadcasting*. West Sussex, England: John Wiley & Sons, 2003.

[4] M. Munster, T. Keller, and L. Hanzo, "Co-channel interference suppression assisted adaptive OFDM in interference limited environments," *Vehicular Technology Conference, 1999. VTC 1999 - Fall. IEEE VTS 50th*, vol. 1, pp. 284–288 vol.1, 1999.

[5] J. Li, K. Ben Letaief, and Z. Cao, "Co-channel interference cancellation for space-time coded OFDM systems," *Wireless Communications, IEEE Transactions on*, vol. 2, no. 1, pp. 41–49, Jan. 2003.

[6] C.-S. Ni and K.-C. Chen, "Cochannel interference suppression for coded OFDM systems over frequency-selective slowly fading channels," *Vehicular Technology Conference, 2004. VTC2004-Fall. 2004 IEEE 60th*, vol. 1, pp. 679–683 Vol. 1, Sept. 2004.

[7] Y. Li and N. Sollenberger, "Adaptive antenna arrays for OFDM systems with cochannel interference," *Communications, IEEE Transactions on*, vol. 47, no. 2, pp. 217–229, Feb 1999.

[8] J.-J. van de Beek, O. Edfors, M. Sandell, S. Wilson, and P. Borjesson, "On channel estimation in ofdm systems," *Vehicular Technology Conference, 1995 IEEE 45th*, vol. 2, pp. 815–819 vol.2, Jul 1995.

[9] B. Hu, I. Land, L. Rasmussen, R. Piton, and B. Fleury, "A divergence minimization approach to joint multiuser decoding for coded CDMA," *Selected Areas in Communications, IEEE Journal on*, vol. 26, no. 3, pp. 432–445, April 2008.

[10] M. Raghavendra, S. Bhashyam, and K. Giridhar, "Parametric channel estimation in reuse-1 OFDM systems," *Communications, 2007. ICC '07. IEEE International Conference on*, pp. 2999–3004, June 2007.

[11] T. Cover and J. Thomas, *Elements of information theory*. John Wiley & Sons, 1991.

[12] P. Hoeher, S. Kaiser, and P. Robertson, "Two-dimensional pilot-symbol-aided channel estimation by Wiener filtering," *Acoustics, Speech, and Signal Processing, 1997. ICASSP-97., 1997 IEEE International Conference on*, vol. 3, pp. 1845–1848 vol.3, Apr 1997.

[13] A. Gupta and D. Nagar, *Matrix Variate Distributions*. Chapman & Hall/CRC, 2000.

[14] L. Bahl, J. Cocke, F. Jelinek, and J. Raviv, "Optimal decoding of linear codes for minimizing symbol error rate," *Information Theory, IEEE Transactions on*, vol. 20, no. 2, pp. 284–287, Mar 1974.

[15] "Guidelines for evaluation of radio transmission technologies for IMT-2000," ITU, Tech. Rep. Recommendation ITU-R M.1225, 1997.

[16] "Deployment aspects," 3rd Generation Partnership Project, Tech. Rep. TS 25.943, Jun. 2002.

Paper H

Application of Bayesian Hierarchical Prior Modeling to Sparse Channel Estimation

Niels L. Pedersen, Dimitriy Shutin, Carles Navarro Manchón and Bernard H. Fleury

Submitted to the IEEE International Conference on Communications, ICC 2012.

H. APPLICATION OF BAYESIAN HIERARCHICAL PRIOR MODELING TO SPARSE CHANNEL ESTIMATION

Application of Bayesian Hierarchical Prior Modeling to Sparse Channel Estimation

Niels Lovmand Pedersen*, Carles Navarro Manchón*, Dmitriy Shutin† and Bernard Henri Fleury*
*Department of Electronic Systems, Aalborg University
Niels Jernes Vej 12, DK-9220 Aalborg, Denmark, Email: {nlp,cnm,bfl}@es.aau.dk
†Institute of Communications and Navigation, German Aerospace Center
Oberpfaffenhofen, D-82234 Wessling, Germany, Email: dmitriy.shutin@dlr.de

***Abstract*—In the literature efficient methods have been proposed for sparse channel estimation with a solution typically obtained through ℓ_1-norm penalization of the parameter of interest. However, other penalization terms than the ℓ_1-norm have proven to have strong sparsity-inducing properties. In this work, we propose a sparse Bayesian learning channel estimator based on hierarchical Bayesian prior modeling and variational message passing (VMP). Using the developed prior model, the VMP algorithm is able to realize various sparsity-inducing constraints to the channel estimation task. The numerical results show superior performance of our channel estimator as compared to traditional and state-of-the-art sparse methods.**

I. Introduction

During the last few years the research on compressive sensing techniques and sparse signal representations [1], [2] applied to channel estimation has received considerable attention, see e.g., [3]–[7]. The reason is that, typically, the impulse response of the wireless channel has a few dominant multipath components. A channel exhibiting this property is said to be sparse [3].

The general goal of sparse signal representations from overcomplete dictionaries is to estimate the sparse vector $\boldsymbol{\alpha}$ of the following system model:

$$\boldsymbol{y} = \boldsymbol{\Phi}\boldsymbol{\alpha} + \boldsymbol{w}. \tag{1}$$

In this expression $\boldsymbol{y} \in \mathbb{C}^M$ is the vector of measurement samples and $\boldsymbol{w} \in \mathbb{C}^M$ is the additive white Gaussian random noise with covariance matrix $\lambda^{-1}\boldsymbol{I}$ and noise precision parameter $\lambda > 0$. The matrix $\boldsymbol{\Phi} = [\boldsymbol{\phi}_1, \ldots, \boldsymbol{\phi}_L] \in \mathbb{C}^{M\times L}$ is the overcomplete dictionary with more columns than rows ($L > M$) and $\boldsymbol{\alpha} \in \mathbb{C}^L$ is an unknown sparse vector with few non-zero elements at unknown locations.

Often, a sparse channel estimator is constructed by solving the ℓ_1-norm constrained quadratic optimization problem, see among others [4]–[6]:

$$\widehat{\boldsymbol{\alpha}} = \underset{\boldsymbol{\alpha}}{\operatorname{argmin}} \left\{ \|\boldsymbol{y} - \boldsymbol{\Phi}\boldsymbol{\alpha}\|_2^2 + \kappa\|\boldsymbol{\alpha}\|_1 \right\} \tag{2}$$

with $\kappa > 0$ being some regularization constant and $\|\cdot\|_p$ denotes the ℓ_p vector norm. This method is also known as Least Absolute Shrinkage and Selection Operator (LASSO) regression [8] or Basis Pursuit Denoising [9]. The popularity of the LASSO regression is mainly attributed to the convexity of the cost function, as well as to its provable sparsity-inducing properties (see [2]). In [4]–[6] LASSO regression is applied to *orthogonal frequency-division multiplexing* (OFDM) pilot-aided channel estimation. Various convex optimization based channel estimation algorithms that minimize the LASSO cost function are compared in [6].

Another approach to sparse channel estimation is sparse Bayesian learning (SBL) [7], [10]–[12]. Specifically, SBL aims at finding a sparse *maximum a posteriori* (MAP) estimate of $\boldsymbol{\alpha}$

$$\widehat{\boldsymbol{\alpha}} = \underset{\boldsymbol{\alpha}}{\operatorname{argmin}} \left\{ \|\boldsymbol{y} - \boldsymbol{\Phi}\boldsymbol{\alpha}\|_2^2 + \lambda^{-1}Q(\boldsymbol{\alpha}) \right\} \tag{3}$$

by specifying a prior $p(\boldsymbol{\alpha})$ such that the penalty term $Q(\boldsymbol{\alpha}) \propto^e -\log p(\boldsymbol{\alpha})$ induces a sparse estimate $\widehat{\boldsymbol{\alpha}}$.[1]

Obviously, by comparing (2) and (3) the SBL framework realizes the LASSO cost function by choosing the ℓ_1-prior $p(\boldsymbol{\alpha}) \propto \exp(-a\|\boldsymbol{\alpha}\|_1)$ with $\kappa = \lambda^{-1}a$.[2] However, instead of working directly with the prior $p(\boldsymbol{\alpha})$, SBL models this using a two-layer (2-L) hierarchical structure. This involves specifying a conditional prior $p(\boldsymbol{\alpha}|\boldsymbol{\gamma})$ and a hyperprior $p(\boldsymbol{\gamma})$ such that $p(\boldsymbol{\alpha}) = \int p(\boldsymbol{\alpha}|\boldsymbol{\gamma})p(\boldsymbol{\gamma})\mathrm{d}\boldsymbol{\gamma}$ has a sparsity-inducing nature. The hierarchical approach to the representation of $p(\boldsymbol{\alpha})$ has several important advantages. First of all, one is free to choose simple and analytically tractable prior pdfs. Second, when carefully chosen, the resulting hierarchical structure then allows for the construction of efficient inference algorithms with analytical derivation of the inference expressions.

In [13] we propose a 2-L and a three-layer (3-L) prior model for $\boldsymbol{\alpha}$. The introduced hierarchical prior models lead to novel sparse inducing priors that as a special case result in the ℓ_1-prior for complex variables. We also propose a variational message passing (VMP) algorithm for estimating $\boldsymbol{\alpha}$ that effectively exploits the hierarchical structure of the prior model. This paper adapts the Bayesian probabilistic framework introduced in [13] to OFDM pilot-aided sparse channel estimation. This approach leads to a novel channel estimation algorithm that makes use of various priors with strong sparsity-inducing properties. The numerical results re-

[1]Here $x \propto^e y$ denotes $\exp(x) = \exp(v)\exp(y)$, and thus $x = v + y$, for some arbitrary constant v. We will also make use of $x \propto y$ which denotes $x = vy$ for some positive constant v.

[2]In the case $\boldsymbol{\alpha} \in \mathbb{R}^L$, $p(\boldsymbol{\alpha}) \propto \exp(-a\|\boldsymbol{\alpha}\|_1)$ is the product of Laplace pdfs. To the best of our knowledge the Laplace pdf has not yet been defined for complex variables. We therefore refer to it as the ℓ_1-prior.

veal the promising potential of our estimator with improved performance as compared to state-of-the-art methods. In particular the estimator outperforms LASSO.

Throughout the paper we shall make use of the following notation: $(\cdot)^T$ and $(\cdot)^H$ denote respectively the transpose and the Hermitian transpose; the expression $\langle f(\boldsymbol{x})\rangle_{q(\boldsymbol{x})}$ denotes the expectation of the function $f(\boldsymbol{x})$ with respect to the density $q(\boldsymbol{x})$; $\mathrm{CN}(\boldsymbol{x}|\boldsymbol{a},\boldsymbol{B})$ denotes a multivariate complex Gaussian pdf with mean $\boldsymbol{a}$ and covariance matrix $\boldsymbol{B}$; similarly, $\mathrm{Ga}(x|a,b) = \frac{b^a}{\Gamma(a)}x^{a-1}\exp(-bx)$ denotes a Gamma pdf with shape parameter a and rate parameter b.

II. Signal Model

We consider a single-input single-output OFDM system with N subcarriers. A cyclic prefix (CP) is added to preserve orthogonality between subcarriers and to eliminate inter-symbol interference between consecutive OFDM symbols. The channel is assumed static during the transmission of each OFDM symbol. In baseband representation the received OFDM signal $\boldsymbol{r} \in \mathbb{C}^N$ reads in matrix-vector notation

$$\boldsymbol{r} = \boldsymbol{X}\boldsymbol{h} + \boldsymbol{n}. \tag{4}$$

The diagonal matrix $\boldsymbol{X} = \mathrm{diag}\{x_1, x_2, \ldots, x_N\}$ contains the transmitted symbols. The components of the vector $\boldsymbol{h} \in \mathbb{C}^N$ are the samples of the channel frequency response at the N subcarriers. Finally, $\boldsymbol{n} \in \mathbb{C}^N$ is a zero-mean complex symmetric Gaussian random vector with independent components with variance λ^{-1}.

To estimate the vector $\boldsymbol{h}$ in (4), a total of M pilot symbols are transmitted at selected subcarriers. The pilot pattern $\mathcal{P}$ denotes the set of indices of the pilot subcarriers. The received signals observed at the pilot positions $\boldsymbol{r}_\mathcal{P}$ are then divided by the corresponding pilot symbols $\boldsymbol{X}_\mathcal{P}$ to produce the observations used to estimate the channel vector $\boldsymbol{h}$:

$$\boldsymbol{y} \triangleq (\boldsymbol{X}_\mathcal{P})^{-1}\boldsymbol{r}_\mathcal{P} = \boldsymbol{h}_\mathcal{P} + (\boldsymbol{X}_\mathcal{P})^{-1}\boldsymbol{n}_\mathcal{P}. \tag{5}$$

We assume that all pilot symbols hold unit power such that the statistics of the noise term $(\boldsymbol{X}_\mathcal{P})^{-1}\boldsymbol{n}_\mathcal{P}$ remain unchanged, i.e., $\boldsymbol{y} \in \mathbb{C}^M$ yields the samples of the true channel frequency response (at the pilot subcarriers) corrupted by additive complex circularly symmetric white Gaussian noise with component variance λ^{-1}.

In this work, we consider a frequency-selective wireless channel that remains constant during the transmission of each OFDM symbol. The maximum relative delay $\tau_{\max}$ is assumed to be large compared to the sampling time T_s, i.e., $\tau_{\max}/T_\mathrm{s} \gg 1$ [3]. The impulse response of the wireless channel is modeled as a sum of multipath components:

$$g(\tau) = \sum_{k=1}^{K} \beta_k \delta(\tau - \tau_k). \tag{6}$$

In this expression, β_k and τ_k are respectively the complex weight and the continuous delay of the kth multipath component, and $\delta(\cdot)$ is the Dirac delta function. The parameter K is the total number of multipath components. The channel parameters β_k, τ_k, and K are random variables. Specifically, the weights $\{\beta_k\}$ are mutually uncorrelated zero-mean with the sum of their variances normalized to one. Additional details regarding the assumptions on the model (6) are provided in Section VI.

III. The Dictionary Matrix

Our goal is to estimate $\boldsymbol{h}$ in (4) by applying the general optimization problem (3) to the observation model (5). For doing so, we must define a proper dictionary matrix $\boldsymbol{\Phi}$. In this section we give an example of such a matrix. As a starting point, we invoke the parametric model (6) of the channel. Making use of this model, (5) can be written as

$$\boldsymbol{y} = \boldsymbol{T}(\boldsymbol{\tau})\boldsymbol{\beta} + \boldsymbol{w} \tag{7}$$

with $\boldsymbol{h}_\mathcal{P} = \boldsymbol{T}(\boldsymbol{\tau})\boldsymbol{\beta}$, $\boldsymbol{w} = (\boldsymbol{X}_\mathcal{P})^{-1}\boldsymbol{n}_\mathcal{P}$, $\boldsymbol{\beta} = [\beta_1, \ldots, \beta_K]^T$, $\boldsymbol{\tau} = [\tau_1, \ldots, \tau_K]^T$, and $\boldsymbol{T}(\boldsymbol{\tau}) \in \mathbb{C}^{M\times K}$ depending on the pilot pattern $\mathcal{P}$ as well as the unknown delays in $\boldsymbol{\tau}$. Specifically, the (m,k)th entry of $\boldsymbol{T}(\boldsymbol{\tau})$ reads

$$\boldsymbol{T}(\boldsymbol{\tau})_{m,k} \triangleq \exp\left(-j2\pi f_m \tau_k\right), \quad \begin{matrix} m = 1,2,\ldots,M \\ k = 1,2,\ldots,K \end{matrix} \tag{8}$$

with f_m denoting the frequency of the mth pilot subcarrier. In the general optimization problem (3) the columns of $\boldsymbol{\Phi}$ is known. However, the columns of $\boldsymbol{T}(\boldsymbol{\tau})$ in (7) depends on the unknown delays in $\boldsymbol{\tau}$. To circumvent this discrepancy we follow the same approach as in [5] and consider a grid of uniformly spaced delay samples in the interval $[0, \tau_{\max}]$:

$$\boldsymbol{\tau}_d = \left[0, \frac{T_\mathrm{s}}{\zeta}, \frac{2T_\mathrm{s}}{\zeta}, \ldots, \tau_{\max}\right]^T \tag{9}$$

with ζ being some positive constant. We now define the dictionary $\boldsymbol{\Phi} \in \mathbb{C}^{M\times L}$ as $\boldsymbol{\Phi} = \boldsymbol{T}(\boldsymbol{\tau}_d)$. Thus, the entries of $\boldsymbol{\Phi}$ are of the form (8) with delay vector $\boldsymbol{\tau}_d$. The number of columns $L = \zeta\tau_{\max}/T_\mathrm{s} + 1$ in $\boldsymbol{\Phi}$ is thereby inversely proportional to the selected delay resolution T_s/ζ.

It is important to notice that the system model (1) with $\boldsymbol{\Phi}$ defined using discretized delay components is an approximation of the true system model (7). This approximation model is introduced so that (3) can be applied to solve the channel estimation task. The estimate of the channel vector at the pilot subcarriers is then $\widehat{\boldsymbol{h}}_\mathcal{P} = \boldsymbol{\Phi}\widehat{\boldsymbol{\alpha}}$. In order to estimate the channel $\boldsymbol{h}$ in (4) the dictionary $\boldsymbol{\Phi}$ is appropriately expanded (row-wise) to include all N subcarrier frequencies.

IV. Bayesian Prior Modeling

In this section we specify the two types of hierarchical prior models for $\boldsymbol{\alpha}$: the 2-L and the 3-L hierarchical prior model. We begin by specifying the joint pdf of the system model (1) for respectively the 2-L and the 3-L hierarchical prior model. Specifically, in case of the 2-L prior model, the joint pdf of the system model (1) reads

$$p(\boldsymbol{y}, \boldsymbol{\alpha}, \boldsymbol{\gamma}, \lambda) = p(\boldsymbol{y}|\boldsymbol{\alpha}, \lambda)p(\lambda)p(\boldsymbol{\alpha}|\boldsymbol{\gamma})p(\boldsymbol{\gamma}; \boldsymbol{\eta}). \tag{10}$$

For the 3-L prior model, the parameter $\boldsymbol{\eta}$ specifying the prior of $\boldsymbol{\gamma}$ in (10) is assumed random. The joint pdf is then of the

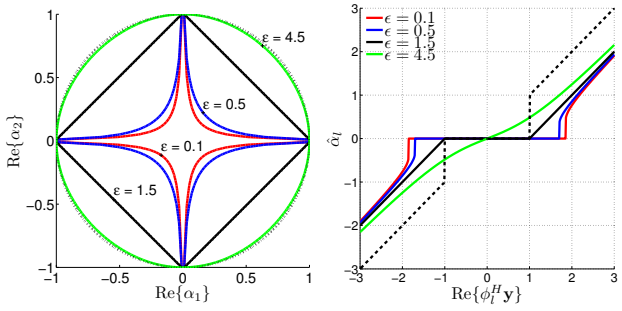

(a) (b)

Fig. 1. 2-L hierarchical prior pdf for $\boldsymbol{\alpha} \in \mathbb{C}^2$: (a) Contour plot of the restriction to the $\mathrm{Im}\{\alpha_1\} = \mathrm{Im}\{\alpha_2\} = 0$ – plane of the penalty term $Q(\alpha_1, \alpha_2; \epsilon, \eta) \propto^e -\log(p(\alpha_1; \epsilon, \eta)p(\alpha_2; \epsilon, \eta))$. (b) Restriction to $\mathrm{Im}\{\boldsymbol{h}_l^H \boldsymbol{y}\} = 0$ of the resulting MAP estimation rule (3) with ϵ as a parameter in the case when $\boldsymbol{\Phi}$ is orthonormal. The black dashed line indicates the hard-threshold rule and the black solid line the soft-threshold rule (obtained with $\epsilon = 3/2$). The black dashed line indicates the penalty term resulting when the prior pdf is a circular symmetric Gaussian pdf.

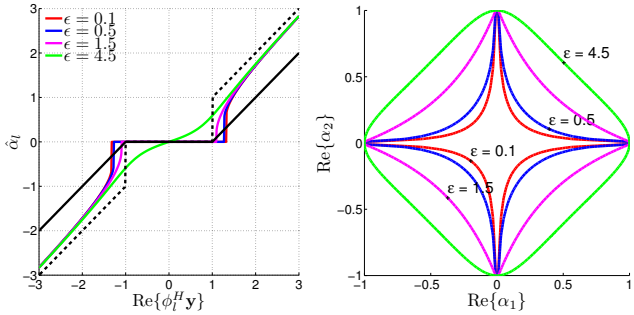

(a) (b)

Fig. 2. Three-layer hierarchical prior pdf for $\boldsymbol{\alpha} \in \mathbb{C}^2$ with the setting $a = 1$, $b = 0.1$: (a) Restriction to $\mathrm{Im}\{\boldsymbol{h}_l^H \boldsymbol{y}\} = 0$ of the resulting MAP estimation rule (3) with ϵ as a parameter in the case when $\boldsymbol{\Phi}$ is orthonormal. The black dashed line indicates the hard-threshold rule and the black solid line the soft-threshold rule. (b) Contour plot of the restriction to the $\mathrm{Im}\{\alpha_1\} = \mathrm{Im}\{\alpha_2\} = 0$ – plane of the penalty term $Q(\alpha_1, \alpha_2; \epsilon, a, b) \propto^e -\log(p(\alpha_1; \epsilon, a, b)p(\alpha_2; \epsilon, a, b))$.

form:

$$p(\boldsymbol{y}, \boldsymbol{\alpha}, \boldsymbol{\gamma}, \boldsymbol{\eta}, \lambda) = p(\boldsymbol{y}|\boldsymbol{\alpha}, \lambda)p(\lambda)p(\boldsymbol{\alpha}|\boldsymbol{\gamma})p(\boldsymbol{\gamma}|\boldsymbol{\eta})p(\boldsymbol{\eta}). \quad (11)$$

In (10) and (11) we have $p(\boldsymbol{y}|\boldsymbol{\alpha}, \lambda) = \mathrm{CN}(\boldsymbol{y}|\boldsymbol{\Phi}\boldsymbol{\alpha}, \lambda^{-1}\boldsymbol{I})$ due to (1). Furthermore, we let $p(\lambda) = p(\lambda; c, d) \triangleq \mathrm{Ga}(\lambda|c, d)$. This choice is motivated by the fact that the gamma distribution is a conjugate prior for the precision of a Gaussian likelihood function. In addition, setting $c = d = 0$ makes $p(\lambda)$ non-informative. Finally, we select $p(\boldsymbol{\alpha}|\boldsymbol{\gamma}) = \prod_{l=1}^{L} p(\alpha_l|\gamma_l)$ with $p(\alpha_l|\gamma_l) \triangleq \mathrm{CN}(\alpha_l|0, \gamma_l)$. In the following we show the main results and properties of these prior models. We refer to [13] for a more detailed analysis.

A. Two-Layer Hierarchical Prior Model

The 2-L prior model assumes that $p(\boldsymbol{\gamma}) = \prod_{l=1}^{L} p(\gamma_l)$ with $p(\gamma_l) = p(\gamma_l; \epsilon, \eta_l) \triangleq \mathrm{Ga}(\gamma_l|\epsilon, \eta_l)$. We compute the prior of $\boldsymbol{\alpha}$ to be

$$p(\boldsymbol{\alpha}; \epsilon, \boldsymbol{\eta}) = \int_0^\infty p(\boldsymbol{\alpha}|\boldsymbol{\gamma})p(\boldsymbol{\gamma}; \epsilon, \boldsymbol{\eta})\mathrm{d}\boldsymbol{\gamma} = \prod_{l=1}^{L} p(\alpha_l; \epsilon, \eta_l) \quad (12)$$

with

$$p(\alpha_l; \epsilon, \eta_l) = \frac{2}{\pi\Gamma(\epsilon)} \eta_l^{\frac{(\epsilon+1)}{2}} |\alpha_l|^{\epsilon-1} K_{\epsilon-1}(2\sqrt{\eta_l}|\alpha_l|). \quad (13)$$

In this expression, $K_\nu(\cdot)$ is the modified Bessel function of the second kind with order $\nu \in \mathbb{R}$. Thus, the prior (13) leads to the general optimization problem (3) with penalty term

$$Q(\boldsymbol{\alpha}; \epsilon, \boldsymbol{\eta}) = \sum_{l=1}^{L} \log\left(|\alpha_l|^{\epsilon-1} K_{\epsilon-1}\left(2\sqrt{\eta_l}|\alpha_l|\right)\right). \quad (14)$$

We show now that the 2-L prior model induces the ℓ_1-norm penalty term and thereby the LASSO cost function as a special case. Selecting $\epsilon = 3/2$ and using the identity $K_{\frac{1}{2}}(z) = \sqrt{\frac{\pi}{2z}}\exp(-z)$ [14], (13) yields the prior

$$p(\alpha_l; \epsilon = 3/2, \eta_l) = \frac{2\eta_l}{\pi} \exp(-2\sqrt{\eta_l}|\alpha_l|). \quad (15)$$

It clearly leads to the ℓ_1-norm of penalty term $Q(\boldsymbol{\alpha}; \eta) = 2\sqrt{\eta}\|\boldsymbol{\alpha}\|_1$ with the selection $\eta_l = \eta$, $l = 1, \ldots, L$.

The prior pdf (13) is specified for each choice of ϵ and of the regularization parameter $\boldsymbol{\eta}$. In order to get insight into the impact of ϵ on the properties of this prior pdf we consider the case $\boldsymbol{\alpha} \in \mathbb{C}^2$. In Fig. 1(a) the contour lines of the restriction to $\mathbb{R}$ of $Q(\alpha_1, \alpha_2; \epsilon, \eta) \propto^e -\log(p(\alpha_1; \epsilon, \eta)p(\alpha_2; \epsilon, \eta))$ are visualized;[3] each contour line is computed for a specific choice of ϵ. Notice that as ϵ decreases towards 0 more probability mass accumulates along the $\boldsymbol{\alpha}$-axes; as a consequence, the mode of the resulting posterior is more likely to be found close to the axes, thus promoting a sparse solution. The behavior of the classical ℓ_1 penalty term obtained for $\epsilon = 3/2$ can also be clearly recognized. In Fig. 1(b) we consider the case when $\boldsymbol{\Phi}$ is orthonormal and compute the MAP estimator (3) with penalty term (14) for different values of ϵ. Note the typical soft-threshold-like behavior (see e.g., [15]) of the estimators. As $\epsilon \to 0$, more components of $\widehat{\boldsymbol{\alpha}}$ are pulled towards zero since the threshold value increases, thus encouraging a sparser solution.

B. Three-Layer Hierarchical Prior Model

We now turn to the SBL problem with a 3-L prior model for $\boldsymbol{\alpha}$ represented by the joint pdf in (11). Specifically, the goal is to incorporate the regularization parameter $\boldsymbol{\eta}$ into the inference framework, such that it can be automatically set by the algorithm. We assume that $p(\boldsymbol{\eta}) = \prod_l^L p(\eta_l)$ with $p(\eta_l) = p(\eta_l; a_l, b_l) \triangleq \mathrm{Ga}(\eta_l|a_l, b_l)$. Let us now compute the prior $p(\boldsymbol{\alpha})$ that corresponds to the 3-L prior model. Defining $\boldsymbol{a} \triangleq [a_1, \ldots, a_l]^T$ and $\boldsymbol{b} \triangleq [b_1, \ldots, b_L]^T$ we obtain $p(\boldsymbol{\alpha}; \epsilon, \boldsymbol{a}, \boldsymbol{b}) =$

[3]Let f denote a function defined on a set A. The restriction of f to a subset $B \subset A$ is the function defined on B that coincides with f on this subset.

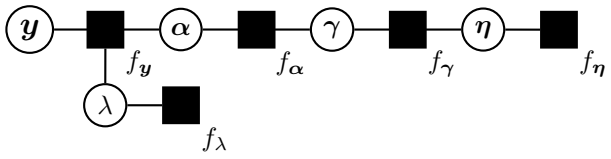

Fig. 3. A factor graph that represents the joint pdf (11). In this figure $f_{\boldsymbol{y}} \equiv p(\boldsymbol{y}|\boldsymbol{\alpha},\lambda)$, $f_{\boldsymbol{\alpha}} \equiv p(\boldsymbol{\alpha}|\boldsymbol{\gamma})$, $f_{\boldsymbol{\gamma}} \equiv p(\boldsymbol{\gamma}|\boldsymbol{\eta})$, $f_{\boldsymbol{\eta}} \equiv p(\boldsymbol{\eta})$, and $f_\lambda \equiv p(\lambda)$.

$\prod_l^L p(\alpha_l;\epsilon,a_l,b_l)$ with

$$p(\alpha_l;\epsilon,a_l,b_l) = \int_0^\infty p(\alpha_l|\gamma_l)p(\gamma_l)\mathrm{d}\gamma_l = \frac{\Gamma(\epsilon+a_l)\Gamma(a_l+1)}{\pi b_l \Gamma(\epsilon)\Gamma(a_l)}\left(\frac{|\alpha_l|^2}{b_l}\right)^{\epsilon-1} U\left(\epsilon+a_l;\epsilon;\frac{|\alpha_l|^2}{b_l}\right). \quad (16)$$

In this expression, $U(\cdot;\cdot;\cdot)$ is the confluent hypergeometric function [14]. In Fig. 2(a) we show the estimation rules produced by the MAP solver for different values of ϵ and fixed parameters a_l and b_l when $\boldsymbol{\Phi}$ is orthonormal. It can be seen that the estimation rules obtained with the 3-L prior model approximate the hard-thresholding rule. In Fig. 2(b), we depict the contour of the penalty term $Q(\alpha_1,\alpha_2;\epsilon,a,b) \propto^e -\log(p(\alpha_1;\epsilon,a,b)p(\alpha_2;\epsilon,a,b))$. Observe that although the contours behave qualitatively similarly to those shown in Fig. 1(a) for the 2-L prior model, the corresponding estimation rules in Fig. 2(a) and Fig. 1(b) are different.

Naturally, the 3-L prior model has three free parameters to be set, ϵ, $\boldsymbol{a}$, and $\boldsymbol{b}$. In [13], it is shown that the choice $\epsilon = 0$ and b_l small (practically we let $b_l = 10^{-6}$, $l = 1,\ldots,L$) induces a weighted log-sum penalization term. This type of penalty is known to strongly promote a sparse estimate [10], [11]. Later in the text we will also adopt this parameter choice.

V. Variational Message Passing

In this section we present a VMP algorithm for estimating $\boldsymbol{h}$ in (4) given the observation $\boldsymbol{y}$ in (5). Let $\boldsymbol{\Theta} = \{\boldsymbol{\alpha},\boldsymbol{\gamma},\boldsymbol{\eta},\lambda\}$ be the set of unknown parameters and $p(\boldsymbol{y},\boldsymbol{\Theta})$ be the joint pdf specified in (11). The factor graph [16] that encodes the factorization of $p(\boldsymbol{y},\boldsymbol{\Theta})$ is shown in Fig. 3. Consider an auxiliary pdf $q(\boldsymbol{\Theta})$ for the unknown parameters that factorizes according to $q(\boldsymbol{\Theta}) = q(\boldsymbol{\alpha})q(\boldsymbol{\gamma})q(\boldsymbol{\eta})q(\lambda)$. The VMP algorithm is an iterative scheme that attempts to compute the auxiliary pdf that minimizes the Kullback-Leibler (KL) divergence $\mathrm{KL}(q(\boldsymbol{\Theta})\|p(\boldsymbol{\Theta}|\boldsymbol{y}))$. In the following we summarize the key steps of the algorithm; the reader is referred to [17] for more information on VMP.

From [17] the auxiliary function $q(\boldsymbol{\theta}_i)$, $\boldsymbol{\theta}_i \in \boldsymbol{\Theta}$ is updated as the product of incoming messages from the neighboring factor nodes f_n to the variable node $\boldsymbol{\theta}_i$:

$$q(\boldsymbol{\theta}_i) \propto \prod_{f_n \in \mathcal{N}_{\boldsymbol{\theta}_i}} m_{f_n \to \boldsymbol{\theta}_i}. \quad (17)$$

In (17) $\mathcal{N}_{\boldsymbol{\theta}_i}$ is the set of factor nodes neighboring the variable node $\boldsymbol{\theta}_i$ and $m_{f_n\to\boldsymbol{\theta}_i}$ denotes the message from factor node f_n to variable node $\boldsymbol{\theta}_i$. This message is computed as

$$m_{f_n\to\boldsymbol{\theta}_i} = \exp\left(\langle \ln f_n\rangle_{\prod_j q(\boldsymbol{\theta}_j),\, \boldsymbol{\theta}_j\in\mathcal{N}_{f_n}\setminus\{\boldsymbol{\theta}_i\}}\right), \quad (18)$$

where $\mathcal{N}_{f_n}$ is the set of variable nodes neighboring the factor node f_n. After an initialization procedure, the individual factors of $q(\boldsymbol{\Theta})$ are then updated iteratively in a round-robin fashion using (17) and (18).

We provide two versions of the VMP algorithm: one applied to the 2-L prior model (referred to as VMP-2L), and another one applied to the 3-L model (VMP-3L). The messages corresponding to VMP-2L are easily obtained as a special case of the messages computed for VMP-3L by assuming $q(\eta_l) = \delta(\eta_l - \hat{\eta}_l)$, where $\hat{\eta}_l$ is some fixed real number.

1) Update of $q(\boldsymbol{\alpha})$: According to (17) and Fig. 3 the computation of the update of $q(\boldsymbol{\alpha})$ requires evaluating the product of messages $m_{f_{\boldsymbol{y}}\to\boldsymbol{\alpha}}$ and $m_{f_{\boldsymbol{\alpha}}\to\boldsymbol{\alpha}}$. Multiplying these two messages yields the Gaussian auxiliary pdf $q(\boldsymbol{\alpha}) = \mathrm{CN}\left(\boldsymbol{\alpha}|\hat{\boldsymbol{\alpha}},\hat{\boldsymbol{\Sigma}}_{\boldsymbol{\alpha}}\right)$ with corresponding mean and covariance given by

$$\hat{\boldsymbol{\Sigma}}_{\boldsymbol{\alpha}} = (\langle\lambda\rangle_{q(\lambda)}\boldsymbol{\Phi}^H\boldsymbol{\Phi} + \boldsymbol{V}(\boldsymbol{\gamma}))^{-1}, \quad (19)$$

$$\hat{\boldsymbol{\alpha}} = \langle\boldsymbol{\alpha}\rangle_{q(\boldsymbol{\alpha})} = \langle\lambda\rangle_{q(\lambda)}\hat{\boldsymbol{\Sigma}}_{\boldsymbol{\alpha}}\boldsymbol{\Phi}^H\boldsymbol{y}. \quad (20)$$

In the above expression we have defined $\boldsymbol{V}(\boldsymbol{\gamma}) = \mathrm{diag}\{\langle\gamma_1^{-1}\rangle_{q(\boldsymbol{\gamma})},\ldots,\langle\gamma_L^{-1}\rangle_{q(\boldsymbol{\gamma})}\}$.

2) Update of $q(\boldsymbol{\gamma})$: The update of $q(\boldsymbol{\gamma})$ is proportional to the product of the messages $m_{f_{\boldsymbol{\alpha}}\to\boldsymbol{\gamma}}$ and $m_{f_{\boldsymbol{\gamma}}\to\boldsymbol{\gamma}}$:

$$q(\boldsymbol{\gamma}) \propto \prod_{l=1}^L \gamma_l^{\epsilon-2}\exp\left(-\gamma_l^{-1}\langle|\alpha_l|^2\rangle_{q(\boldsymbol{\alpha})} - \gamma_l\langle\eta_l\rangle_{q(\boldsymbol{\eta})}\right). \quad (21)$$

The right-hand side expression in (21) is recognized as the product of Generalized Inverse Gaussian (GIG) pdfs [18] with order $p = \epsilon - 1$. Observe that the computation of $\boldsymbol{V}(\boldsymbol{\gamma})$ in (19) requires evaluating $\langle\gamma_l^{-1}\rangle_{q(\boldsymbol{\gamma})}$ for all $l = 1,\ldots,L$. Luckily, the moments of the GIG distribution are given in closed form for any $n \in \mathbb{R}$ [18]:

$$\langle\gamma_l^n\rangle_{q(\boldsymbol{\gamma})} = \left(\frac{\langle|\alpha_l|^2\rangle_{q(\boldsymbol{\alpha})}}{\langle\eta_l\rangle_{q(\boldsymbol{\eta})}}\right)^{\frac{n}{2}} \frac{K_{p+n}\left(2\sqrt{\langle\eta_l\rangle_{q(\boldsymbol{\eta})}\langle|\alpha_l|^2\rangle_{q(\boldsymbol{\alpha})}}\right)}{K_p\left(2\sqrt{\langle\eta_l\rangle_{q(\boldsymbol{\eta})}\langle|\alpha_l|^2\rangle_{q(\boldsymbol{\alpha})}}\right)}. \quad (22)$$

3) Update of $q(\boldsymbol{\eta})$: The update of $q(\boldsymbol{\eta})$ is proportional to the product of messages $m_{f_{\boldsymbol{\eta}}\to\boldsymbol{\eta}}$ and $m_{f_{\boldsymbol{\gamma}}\to\boldsymbol{\eta}}$:

$$q(\boldsymbol{\eta}) \propto \prod_{l=1}^L \eta_l^{\epsilon+a_l-1}\exp\left(-(\langle\gamma_l\rangle_{q(\boldsymbol{\gamma})} + b_l)\eta_l\right), \quad (23)$$

which is identified as a gamma pdf. The first moment of η_l used in (22) is easily computed as

$$\langle\eta_l\rangle_{q(\boldsymbol{\eta})} = \frac{\epsilon + a_l}{\langle\gamma_l\rangle_{q(\boldsymbol{\gamma})} + b_l}. \quad (24)$$

Naturally, $q(\boldsymbol{\eta})$ is only computed for VMP-3L.

4) Update of $q(\lambda)$: The update of $q(\lambda)$ can be shown to be $q(\lambda) = \mathrm{Ga}(\lambda|M+c, \langle\|\boldsymbol{y}-\boldsymbol{\Phi}\boldsymbol{\alpha}\|_2^2\rangle_{q(\boldsymbol{\alpha})} + d)$. The first moment

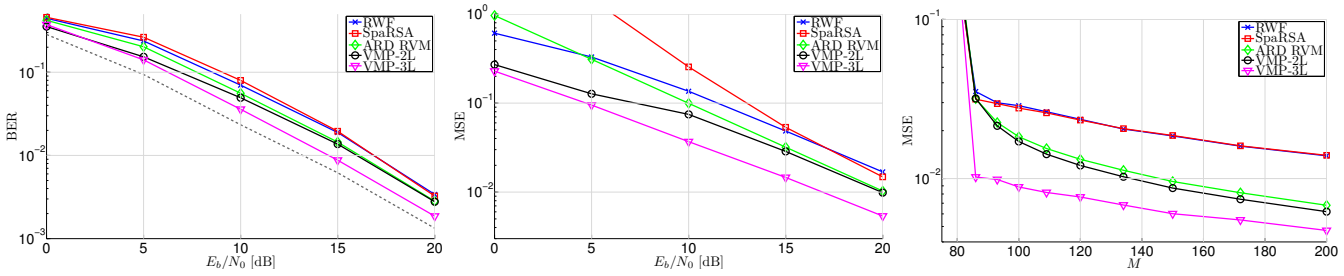

(a) (b) (c)

Fig. 4. Comparison of the performance of the VMP-2L, VMP-3L, RWF, ARD RVM, and SparseRSA algorithms: (a) BER versus E_b/N_0, (b) MSE versus E_b/N_0, (c) MSE versus number of available pilots M with fixed $L = 200$ and the ratio between received symbol power and noise variance set to 15 dB. In (a,b) we have $M = 100$ and $L = 200$. In (a) the dashed line shows the BER performance when the true channel vector $\boldsymbol{h}$ in (4) is known.

of λ used in (19) and (20) is therefore

$$\langle \lambda \rangle_{q(\lambda)} = \frac{M + c}{\langle \|\boldsymbol{y} - \boldsymbol{\Phi}\boldsymbol{\alpha}\|_2^2 \rangle_{q(\boldsymbol{\alpha})} + d}. \tag{25}$$

VI. Numerical Results

We perform Monte Carlo simulations to evaluate the performance of the two versions of the derived VMP algorithm in Section V. We consider a 3GPP LTE alike scenario [21] with the settings specified in Table I. The multipath channel (6) is inspired by [22] where for each realization of the channel, the total number of multipath components K is Poisson distributed with a mean of $\langle K \rangle_{p(K)} = 10$ and the delays τ_k, $k = 1, \ldots, K$, are independent and uniformly distributed random variables drawn from the continuous interval [0, 144 T_s] (the CP length). The kth non-zero component β_k conditioned on the delay τ_k has a zero-mean complex circular symmetric Gaussian distribution with variance $\sigma^2(\tau_k) = \langle |\beta_k|^2 \rangle_{p(\beta_k|\tau_k)} = u \exp(-\tau_k/v)$ and parameters $u, v > 0$.[4]

To initialize the VMP algorithm we set $\langle \lambda \rangle_{q(\lambda)}$ equal to the inverse of the sample variance of $\boldsymbol{y}$ and $\langle \gamma_l^{-1} \rangle_{q(\boldsymbol{\gamma})}$ is set equal to the inverse number of columns L. Furthermore, we let $c = d = 0$ in (25), which corresponds to a non-informative prior for λ. Once the initialization is completed, the algorithm sequentially updates the auxiliary pdfs $q(\boldsymbol{\alpha})$, $q(\boldsymbol{\gamma})$, $q(\boldsymbol{\eta})$, and $q(\lambda)$ until convergence is achieved. Naturally, $q(\boldsymbol{\eta})$ is only updated for VMP-3L, whereas for VMP-2L the entries in $\boldsymbol{\eta}$ are set to M. For both versions we select $\epsilon = 0$ and for VMP-3L we set $a_l = 1$ and $b_l = 10^{-6}$, $l = 1, \ldots, L$. Finally, the dictionary $\boldsymbol{\Phi}$ is specified by M pilot subcarriers and a total of $L = 200$ columns (corresponding to the choice $\tau_{\max} = 144$ T_s and $\zeta \approx 1.4$ in (9)).

The VMP is compared to a classical channel estimator and two state-of-the-art sparse estimation schemes. Specifically, we use as benchmark the robustly designed Wiener Filter (RWF) [23], the automatic relevance determination (ARD) formulation of the relevance vector machine (RVM) [10], [11], and the *sparse reconstruction by separable approximation* (SpaRSA) algorithm [24].[5] The ARD RVM solves the optimization problem (3) with the log-sum penalization term $Q(\boldsymbol{\alpha}) = 2\sum_{l=1}^{L} \log|\alpha_l|$, whereas SpaRSA is a proximal gradient method for solving (2). In case of the SpaRSA algorithm the regularization parameter κ needs to be set. In all simulations, we let $\kappa = 1/2$ which leads to good performance in high signal-to-noise ratio (SNR) regime.

The performance is compared with respect to the resulting bit-error-rate (BER) and mean-squared error (MSE) of the estimate $\widehat{\boldsymbol{h}}$ versus the SNR (E_b/N_0). In addition, in order to quantify the algorithms' ability to reduce the pilot overhead, we evaluate the MSE versus the number of available pilots M. Hence, in this setup M is no longer fixed as in Table I.

In Fig. 4(a) we compare the BER performance of the different schemes. We see that VMP-3L outperforms the other schemes across all the SNR range considered. Specifically, at 1 % BER the gain is approximately 2 dB compared to VMP-2L and ARD RVM and 3 dB compared to SpaRSA and RWF. Also VMP-2L achieves lower BER in the SNR range 0 - 12 dB as compared to ARD RVM and across the whole SNR range compared to SpaRSA and RWF.

The superior BER performance of the VMP algorithm is well reflected in the MSE performance shown in Fig. 4(b). Again VMP-3L is a clear winner followed by VMP-2L. The bad MSE performance of the SpaRSA for low SNR is due

[4] By specifying $\langle K \rangle_{p(K)} = 10$, $\tau_{\max} = 144$ T_s, and a decay rate $v = 20$ T_s then u is computed such that $\langle \sum_{k=1}^{K} |\beta_k(t)|^2 \rangle_{p(\boldsymbol{\beta},\boldsymbol{\tau},K)} = 1$.

TABLE I
Parameter settings for the simulations. The convolutional code and decoder has been implemented using [19].

Sampling time, T_s	32.55 ns
CP length	4.69 μs / 144 T_s
Subcarrier spacing	15 kHz
Pilot pattern	Equally spaced, QPSK
Modulation	QPSK
Subcarriers, N	1200
Pilots, M	100
OFDM symbols	1
Information bits	727
Channel interleaver	Random
Convolutional code	$(133, 171, 165)_8$
Decoder	BCJR algorithm [20]

[5] The software is available on-line at http://www.lx.it.pt/~mtf/SpaRSA/

to the difficulty in specifying the regularization parameter κ across a large SNR range.

We next fix the ratio between received symbol power and noise variance to 15 dB and evaluate the MSE versus number of available pilots M. The results are depicted in Fig. 4(c). Observe a noticeable performance gain obtained with VMP-3L. In particular, VMP-3L exhibits the same MSE performance as VMP-2L and ARD RVM using only approximately 85 pilots, roughly half as many as VMP-2L and ARD RVM. Furthermore, VMP-3L achieves a significant improvement using this number of pilots as compared to SpaRSA and RWF where all 200 pilots are available.

VII. Conclusion

In this paper, we proposed a sparse Bayesian learning based channel estimation algorithm. The channel estimator relies on Bayesian hierarchical prior modeling and variational message passing (VMP). The VMP algorithm effectively exploits the probabilistic structure of the hierarchical prior model and thereby applies various priors with strong sparsity-inducing properties. It was shown that we obtain an estimator with better performance than the typically applied ℓ_1-norm constrained based estimator. Our numerical results show that the proposed channel estimator yields superior performance in terms of bit-error-rate and mean-squared error. It also allows for a significant reduction of the amount of pilot subcarriers needed for estimating the channel as compared to other existing estimators.

Acknowledgment

This work was supported in part by the 4GMCT cooperative research project funded by Intel Mobile Communications, Agilent Technologies, Aalborg University and the Danish National Advanced Technology Foundation. This research was also supported in part by the project ICT- 248894 Wireless Hybrid Enhanced Mobile Radio Estimators (WHERE2).

References

[1] R. Baraniuk, "Compressive sensing," *IEEE Signal Processing Magazine*, vol. 24, no. 4, pp. 118–121, July 2007.

[2] E. J. Candes and M. B. Wakin, "An introduction to compressive sampling," *IEEE Signal Process. Mag.*, vol. 25, no. 2, pp. 21–30, Mar. 2008.

[3] W. Bajwa, J. Haupt, A. Sayeed, and R. Nowak, "Compressed channel sensing: A new approach to estimating sparse multipath channels," *Proceedings of the IEEE*, vol. 98, no. 6, pp. 1058–1076, Jun. 2010.

[4] G. Taubock and F. Hlawatsch, "A compressed sensing technique for OFDM channel estimation in mobile environments: Exploiting channel sparsity for reducing pilots," in *Proc. IEEE Int. Conf. Acoustics, Speech and Signal Processing ICASSP 2008*, 2008, pp. 2885–2888.

[5] C. R. Berger, S. Zhou, J. C. Preisig, and P. Willett, "Sparse channel estimation for multicarrier underwater acoustic communication: From subspace methods to compressed sensing," *IEEE Trans. on Sig. Proc.*, vol. 58, no. 3, pp. 1708–1721, 2010.

[6] J. Huang, C. R. Berger, S. Zhou, and J. Huang, "Comparison of basis pursuit algorithms for sparse channel estimation in underwater acoustic OFDM," in *Proc. OCEANS 2010 IEEE - Sydney*, 2010, pp. 1–6.

[7] D. Shutin and B. H. Fleury, "Sparse variational Bayesian SAGE algorithm with application to the estimation of multipath wireless channels," *IEEE Trans. on Sig. Proc.*, vol. 59, pp. 3609–3623, 2011.

[8] R. Tibshirani, "Regression shrinkage and selection via the LASSO," *J. R. Statist. Soc.*, vol. 58, pp. 267–288, 1994.

[9] S. S. Chen, D. L. Donoho, Michael, and A. Saunders, "Atomic decomposition by basis pursuit," *SIAM Journal on Scientific Computing*, vol. 20, pp. 33–61, 1998.

[10] M. Tipping, "Sparse Bayesian learning and the relevance vector machine," *J. of Machine Learning Res.*, vol. 1, pp. 211–244, June 2001.

[11] D. Wipf and B. Rao, "Sparse Bayesian learning for basis selection," *IEEE Trans. on Sig. Proc.*, vol. 52, no. 8, pp. 2153 – 2164, aug. 2004.

[12] D. G. Tzikas, A. C. Likas, and N. P. Galatsanos, "The variational approximation for Bayesian inference," *IEEE Signal Process. Mag.*, vol. 25, no. 6, pp. 131–146, November 2008.

[13] N. L. Pedersen, D. Shutin, C. N. Manchón, and B. H. Fleury, "Sparse estimation using Bayesian hierarchical prior modeling for real and complex models," *submitted to IEEE Trans. on Sig. Proc.*, 2011.

[14] M. Abramowitz and I. A. Stegun, *Handbook of Mathematical Functions with Formulas, Graphs, and Mathematical Tables*. Dover, 1972.

[15] P. Moulin and J. Liu, "Analysis of multiresolution image denoising schemes using generalized Gaussian and complexity priors," *IEEE Trans. on Information Theory*, vol. 45, no. 3, pp. 909–919, 1999.

[16] F. R. Kschischang, B. J. Frey, and H. A. Loeliger, "Factor graphs and the sum-product algorithm," *IEEE Trans. on Information Theory*, vol. 47, no. 2, pp. 498–519, Feb 2001.

[17] J. Winn and C. M. Bishop, "Variational message passing," *J. Mach. Learn. Res.*, vol. 6, pp. 661–694, 2005.

[18] B. Jorgensen, *Statistical Properties of the Generalized Inverse Gaussian Distribution (Lecture Notes in Statistics 9)*. Springer-Verlag New York Inc, 1982.

[19] The iterative solutions coded modulation library. [Online]. Available: http://www.iterativesolutions.com

[20] L. Bahl, J. Cocke, F. Jelinek, and J. Raviv, "Optimal decoding of linear codes for minimizing symbol error rate," *IEEE Trans. on Inform. Theory*, vol. 20, no. 2, pp. 284–287, 1974.

[21] 3rd Generation Partnership Project (3GPP) Technical Specification, "Evolved universal terrestrial radio access (e-utra); base station (bs) radio transmission and reception," TS 36.104 V8.4.0, Tech. Rep., 2008.

[22] M. L. Jakobsen, K. Laugesen, C. Navarro Manchón, G. E. Kirkelund, C. Rom, and B. Fleury, "Parametric modeling and pilot-aided estimation of the wireless multipath channel in OFDM systems," in *Proc. IEEE Int Communications (ICC) Conf*, 2010, pp. 1–6.

[23] O. Edfors, M. Sandell, J.-J. van de Beek, S. K. Wilson, and P. O. Börjesson, "OFDM channel estimation by singular value decomposition," *IEEE Trans. on Communications*, vol. 46, no. 7, pp. 931–939, 1998.

[24] S. J. Wright, R. D. Nowak, and M. A. T. Figueiredo, "Sparse reconstruction by separable approximation," *IEEE Trans. on Sig. Proc.*, vol. 57, no. 7, pp. 2479–2493, 2009.

Paper I

On the Design of a MIMO-SIC Receiver for LTE Downlink

Carles Navarro Manchón, Luc Deneire, Preben Mogensen and Troels B. Sørensen

IEEE 68th Vehicular Technology Conference, VTC Fall-2008. Calgary, September 2008.

I. ON THE DESIGN OF A MIMO-SIC RECEIVER FOR LTE DOWNLINK

On the Design of a MIMO-SIC Receiver for LTE Downlink

Carles Navarro Manchón*, Luc Deneire*†‡, Preben Mogensen* and Troels B. Sørensen*
*Department of Electronic Systems
Aalborg University, Niels Jernes Vej 12, 9220 Aalborg East
Email: cnm@es.aau.dk
†Université de Nice, Sophia Antipolis
‡Centre National de la Recherche Scientifique
I3S, UMR 6070, France

***Abstract*—In this paper, we investigate different multiple-input multiple-output (MIMO) receiver structures based on MMSE filtering and sequential interference cancellation (SIC) for the downlink of the 3GPP long term evolution (LTE) system. We divide them into two approaches: symbol-SIC receivers, in which the detection and interference cancellation is done independently for each subcarrier, and codeword-SIC structures, in which the processing is carried out for each independently-coded stream by including the turbo-decoder inside the feedback loop. The results show that symbol-SIC receivers need to take into account the propagation of errors in the interference cancellation to provide the turbo decoder with reliable soft bit values. However, these are clearly outperformed by codeword-SIC schemes, due to the error correction capabilities of the turbo-decoder inside the feedback loop. We show that the best tradeoff between computational complexity and receiver performance is achieved by only cancelling the interference of a codeword when this has been successfully decoded.**

I. Introduction

The 3rd Generation Partnership Project (3GPP) is currently finalizing the standardization of UTRA long term evolution (LTE). This new system aims at peak data rates of 100 Mbps in 20 MHz bandwidth in the downlink [1]. To achieve the required spectral efficiency, a physical-layer air interface based on the combination of orthogonal frequency-division multiplexing (OFDM) and multiple-input multiple-output (MIMO) has been defined [2]. OFDM divides the available bandwidth into narrow orthogonal subcarriers. With the addition of a cyclic prefix (CP), the subcarriers become flat-fading, allowing simple equalization of the channel, and easing the integration with MIMO techniques [3].

MIMO techniques have promised a linear increase of the capacity of wireless links with the number of antennas used at the receiver and the transmitter [4]. An efficient way of achieving most of this capacity increase is the combination of space-division multiplexing (SDM) with sequential interference cancellation (SIC) at the receiver. Since this approach was presented in [5], many different receiver algorithms have been proposed ([6]–[9]) and, for a practical system, it is unclear which the optimal choice in terms of performance and complexity is.

In this paper, we review different approaches suggested in literature. We divide them into symbol-SIC, in which the interference cancellation is done at modulated-symbol level, and codeword-SIC, where the interference is cancelled in a per-codeword fashion. Furthermore, we propose two modifications of the codeword-SIC receiver, one avoiding error propagation, and the other compensating for the error introduced in the interference cancellation step. All the different schemes are evaluated under LTE parameters by means of link-level simulations, showing the superiority of the proposed structures.

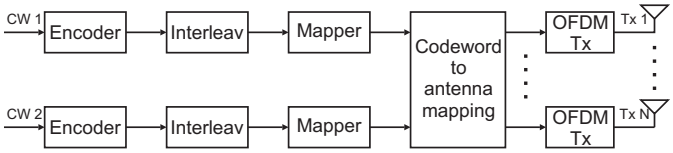

Fig. 1. Block diagram of the transmitter

The remainder of the paper is organized as follows. Section II describes the system considered. In Section III, the different SIC algorithms are presented, and a performance evaluation is done in Section IV. Finally, Section V concludes the work.

II. System Description

In the following, the considered MIMO-OFDM system will be described. A block diagram of a transmitter with N antennas is shown in Fig. 1. As it is shown, the information bits are split into two codewords, which are independently encoded and interleaved before being mapped to complex modulated symbols. The complex symbols are then mapped to the antennas depending on the MIMO order of the system: for a 2×2 system, each codeword is transmitted through one antenna; for a 4×4 system, codeword 1 is mapped to transmit antennas 1 and 2, and codeword 2 is mapped to transmit antennas 3 and 4. Finally, the bits are OFDM modulated by applying an inverse fast Fourier transform (IFFT) and adding a CP.

Assuming that the channel response is static over the duration of an OFDM symbol and the cyclic prefix is long enough to cope with the multipath delays of the channel, the signal seen from the M antennas at the receiver after CP removal and fast Fourier transform (FFT) can be expressed

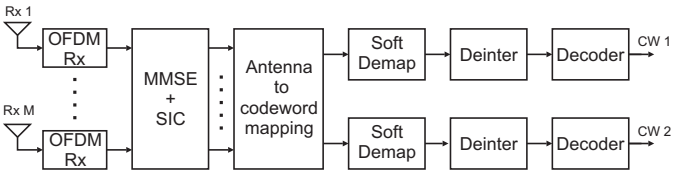

Fig. 2. Block diagram of a symbol-SIC MIMO-OFDM receiver

as:

$$\mathbf{y}[k] = \mathbf{H}[k]\mathbf{x}[k] + \mathbf{w}[k] \tag{1}$$

where $\mathbf{x}[k] = [x_1(k)x_2(k)\cdots x_N(k)]^T$ represents the complex transmitted symbols at subcarrier k from the N transmitting antennas, $\mathbf{w}[k] = [w_1(k)w_2(k)\cdots w_M(k)]^T$ is the i.i.d. complex additive white Gaussian noise (AWGN) vector and

$$\mathbf{H}[k] = \begin{bmatrix} h_{11}(k) & \cdots & h_{1N}(k) \\ \vdots & \ddots & \vdots \\ h_{M1}(k) & \cdots & h_{MN}(k) \end{bmatrix} \tag{2}$$

is the channel transfer function matrix at the kth subcarrier frequency. The coefficients $h_{ij}(k)$ in (2) describe the complex channel gain from the transmit antenna j to the receive antenna i. Since no channel state information (CSI) is assumed at the transmitter, the transmitted power is equally distributed among the transmit antennas, leading to a variance of the transmitted symbols $\sigma_x^2 = \mathrm{E}[x_i(k)x_i(k)^*] = \frac{P}{N}$, where P is the total power transmitted at each subcarrier, and $\mathrm{E}[\cdot]$ and $(\cdot)^*$ represent the expected value and conjugate operations respectively. The AWGN terms $w_i(k)$ have variance σ_w^2.

III. MIMO SIC Receivers

In this section, we describe the different receiver structures evaluated. We classify them in two types: symbol SIC and codeword SIC. In symbol-SIC, the interference cancellation is done independently at each subcarrier on modulated-symbol level, whereas in codeword-SIC the detection is done on codeword level and the interference contribution is subtracted after decoding and re-encoding of the codeword.

A. Symbol-SIC Receivers

The structure of a symbol-SIC receiver is shown in Fig. 2. MMSE processing and sequential interference cancellation are performed independently at each subcarrier. Next, the structure of the codewords is re-built and, after soft demodulation and deinterleaving, the decoder yields hard decisions on the information bits. To simplify the notation, we will assume here that $\mathbf{H}[k]$ and $\mathbf{x}[k]$ have been reordered at each subcarrier k according to the optimal detection order proposed in [5], i.e., symbols with transmit antenna subindex 1 will be detected first, whilst the ones with subindex N will be detected last.

1) Conventional Symbol-SIC: We consider here the conventional symbol-SIC (S-SIC) approach described in [5], with the difference that we employ a linear MMSE filter instead of the zero-forcing approach. The MMSE estimate of the symbol transmitted from the ith antenna after detection and interference cancellation of the previous $i-1$ symbols is:

$$\tilde{x}_i(k) = \mathbf{g}_i[k]\mathbf{y}_{i-1}[k]. \tag{3}$$

Here, $\mathbf{g}_i[k]$ denotes the ith row of the MMSE matrix:

$$\mathbf{G}_i[k] = \left(\mathbf{H}_{i:N}^H[k]\mathbf{H}_{i:N}[k] + \frac{\sigma_w^2}{\sigma_x^2}\mathbf{I}_{N-i+1}\right)^{-1}\mathbf{H}_{i:N}^H[k] \tag{4}$$

where $\mathbf{H}_{i:N}[k]$ is the matrix formed by removing the $i-1$ first columns of $\mathbf{H}[k]$. The vector $\mathbf{y}_{i-1}[k]$ in (3) is the received signal in subcarrier k after cancelling the interference contribution from the first $i-1$ transmit antennas:

$$\mathbf{y}_{i-1}[k] = \mathbf{y}[k] - \mathbf{H}_{1:i-1}[k]\hat{\mathbf{x}}_{1:i-1}[k] \tag{5}$$

where $\mathbf{H}_{1:i-1}[k]$ and $\hat{\mathbf{x}}_{1:i-1}[k]$ represent the $i-1$ first columns and elements of $\mathbf{H}[k]$ and $\hat{\mathbf{x}}[k]$ respectively. The elements $\hat{x}_i(k)$ are calculated by taking hard decisions of the MMSE estimates in (3). Subsequently, the interference from the ith detected symbol is cancelled from the received signal, giving:

$$\mathbf{y}_i[k] = \mathbf{y}_{i-1}[k] - \mathbf{h}_i[k]\hat{x}_i(k) = \mathbf{y}[k] - \mathbf{H}_{1:i}[k]\hat{\mathbf{x}}_{1:i}[k] \tag{6}$$

with $\mathbf{h}_i[k]$ denoting the ith column of $\mathbf{H}[k]$.

The MMSE estimates $\tilde{x}_i(k)$ are then fed to a soft-demapper which calculates log-likelihood ratios (LLRs) of the coded bits. To do so, the estimates are approximated to a Gaussian process described by:

$$\tilde{x}_i(k) = \mu x_i(k) + \eta \tag{7}$$

where $\mu = \mathbf{g}_i[k]\mathbf{h}_i[k]$ and η is normally distributed with zero mean and variance $\sigma_\eta^2 = \sigma_x^2(\mu - \mu^2)$ [10].

2) Symbol-SIC with Error Compensation: A drawback of the previous scheme is that it doesn't take into account the error introduced in the interference cancellation step when a wrong hard-decision $\hat{x}_i(k)$ is taken. To show the effect of these errors, (5) can be re-written as:

$$\mathbf{y}_{i-1}[k] = \mathbf{H}_{i:N}[k]\mathbf{x}_{i:N}[k] + \mathbf{H}_{1:i-1}[k]\hat{\mathbf{e}}_{1:i-1}[k] + \mathbf{w}[k] \tag{8}$$

where the vector $\hat{\mathbf{e}}_{1:i-1}[k] = \mathbf{x}_{1:i-1}[k] - \hat{\mathbf{x}}_{1:i-1}[k]$ represents the error introduced by wrong symbol-decisions. In order to compensate for these errors, Lee *et al.* proposed the use of an improved MMSE matrix taking error propagation into account [6]. In this receiver, which we refer to as symbol-SIC with error compensation (S-SIC EC), (4) is replaced by:

$$\begin{aligned}\mathbf{G}_i[k] &= \mathbf{H}_{i:N}^H[k]\left(\mathbf{H}_{i:N}[k]\mathbf{H}_{i:N}^H[k] + \frac{\sigma_w^2}{\sigma_x^2}\mathbf{I}_{N-i+1}\right. \\ &+ \left.\frac{1}{\sigma_x^2}\mathbf{H}_{1:i-1}[k]\mathbf{Q}_{\hat{\mathbf{e}}_{1:i-1}[k]}\mathbf{H}_{1:i-1}^H[k]\right)^{-1}\end{aligned} \tag{9}$$

where $\mathbf{Q}_{\hat{\mathbf{e}}_{1:i-1}[k]}$ is the covariance matrix of the decision errors in the $i-1$ previously detected symbols, whose elements are given by $q_{p,r}(k) = \mathrm{E}\{\hat{e}_p(k)\hat{e}_r^*(k)|\hat{x}_p(k), \hat{x}_r(k)\}$, i.e. the expected value of the errors product given the hard decisions on the symbols. The off-diagonal elements can be neglected by assuming uncorrelated symbol errors. For the diagonal elements, the authors in [6] propose to calculate

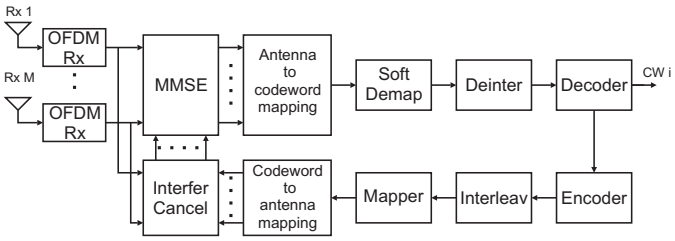

Fig. 3. Block diagram of a Codeword-SIC MIMO-OFDM receiver

the elements of the matrix from an approximation of the probability of error given the modulation constellation and the noise variance in (7). We adopt however a different approach: by assuming that the LLRs of the bits corresponding to $x_i(k)$ are available, the probability of each symbol s in the constellation $\mathrm{P}\big(x_i(k) = s|\tilde{x}_i(k)\big)$ can be obtained. Hence, diagonal elements of $\mathbf{Q}_{\hat{\mathbf{e}}_{1:i-1}[k]}$ can be obtained by:

$$\begin{aligned} q_{p,p}(k) &= \mathrm{E}\{|\hat{e}_p(k)|^2 \big| \hat{x}_p(k)\} \\ &= \sum_{s\in\mathcal{S}} |\hat{x}_p(k) - s|^2 \mathrm{P}\big(x_p(k) = s|\tilde{x}_p(k)\big) \quad (10) \end{aligned}$$

where $\mathcal{S}$ is a set with all the possible points of the constellation used. The detection and interference cancellation process is the same as in the conventional symbol-SIC, but using (9) instead of (4).

B. Codeword-SIC

In the following, three codeword-SIC algorithms are described. In a codeword-SIC receiver, the detection and decoding process is done sequentially for each of the codewords. We will assume here that the codewords are ordered according to the optimal detection and decoding sequence. A detailed analysis on how to select the detection order can be found in [8].

1) Conventional Codeword-SIC: The conventional codeword-SIC (C-SIC) is analogous to the symbol-SIC receiver. However, the ordering, detection, decoding and interference cancellation are done in a per-codeword fashion, as shown in Fig. 3, rather than independently for individual subcarriers. In the first stage, the MMSE estimates of the symbols transmitted by the antennas corresponding to the selected codeword, $\tilde{\mathbf{x}}_{cw1}[k]$, are obtained for all subcarriers by using the $M \times N$ MMSE matrix:

$$\mathbf{G}[k] = \left(\mathbf{H}^H[k]\mathbf{H}[k] + \frac{\sigma_w^2}{\sigma_x^2}\mathbf{I}_N\right)^{-1} \mathbf{H}^H[k]. \quad (11)$$

Note that in the case of 4 transmit antennas, the symbols transmitted through two antennas (the ones corresponding to the selected codeword) will be detected. Subsequently, the symbols are soft demapped, providing the decoder with soft values on the coded bits. After decoding, the hard decisions on the information bits are re-encoded and mapped to the complex symbol constellation in order to re-build the transmitted signal. Then, the interference term created by the selected codeword is cancelled from the received signal at all subcarriers by:

$$\mathbf{y}'[k] = \mathbf{y}[k] - \mathbf{H}_{cw1}[k]\hat{\mathbf{x}}_{cw1}[k] \quad (12)$$

where $\mathbf{H}_{cw1}[k]$ denotes the columns of $\mathbf{H}[k]$ corresponding to the antennas on which the selected codeword has been mapped, and $\hat{\mathbf{x}}_{cw1}[k]$ are the reconstructed symbols transmitted over those antennas, obtained from the re-encoded bit decisions. In the second stage, the MMSE estimates of the symbols corresponding to the the remaining codeword are obtained with the matrix:

$$\mathbf{G}'[k] = \left(\mathbf{H}_{cw2}^H[k]\mathbf{H}_{cw2}[k] + \frac{\sigma_w^2}{\sigma_x^2}\mathbf{I}_{N/2}\right)^{-1} \mathbf{H}_{cw2}^H[k] \quad (13)$$

where the matrix $\mathbf{H}_{cw2}[k]$ denotes the columns of $\mathbf{H}[k]$ corresponding to the antennas where the undetected codeword is mapped.

2) Codeword-SIC with Verified Feedback: Coded packet-based systems usually have some error-detection capabilities, so that the receiver can check whether the packet has been correctly received or a retransmission is required. A common way of achieving this (and the one used in LTE) is to append a cyclic redundancy code (CRC) to the information bits of the packet. After decoding of the packet, the receiver can, by checking the CRC, know if the detection process has been successful. We propose here to make use of this error detection capability in our codeword-SIC structure, in a scheme we call codeword-SIC with verified feedback (C-SIC VF). The detection and decoding of the first codeword selected is equivalent to the C-SIC scheme. After decoding, the CRC of the decoded codeword is checked. If the CRC is correct, re-encoding and re-mapping of the codeword is done, and interference cancellation and decoding of the remaining codeword is performed according to (12) and (13), as in the C-SIC approach. Otherwise, no feedback is performed and the remaining codeword is detected with a plain MMSE as in (11). This avoids the introduction of errors in the interference cancellation, as well as reducing the processing involved in the case in which the first codeword is not successfully decoded.

3) Codeword-SIC with Error Compensation: We introduce here a new modification to the Codeword-SIC scheme which makes use of both the error detection and the error correction properties of the channel decoder. To do so, we make use of a soft-input soft-output decoder, which yields soft decisions on both the information and the coded bits in the form of LLRs. These soft values will have better quality than the ones generated at the soft demapper, as they benefit from the decoding process. In the first stage of the receiver, the codeword selected to be decoded first is detected through MMSE (11), exactly as in the other two schemes. Then, soft decoding of the codeword is performed, and hard decisions on the information bits are taken. If the CRC is correct, the soft values of the coded bits can be fully trusted; thus, hard-decision on the coded bits is taken, and the interfering signal is reconstructed by complex modulation of the bits. Then, interference cancellation and detection can be performed on the second codeword as in (12) and (13), having the certainty

that no errors are being fed back. When the CRC is not correct, there are errors among the soft coded bits delivered by the soft decoder. Nevertheless, the coded bits are also sliced to hard values, complex modulated, and the interference on the second codeword is cancelled by (12). In the MMSE fiter, however, we compensate for the errors introduced, analogously to the S-SIC EC, by using the following MMSE matrix:

$$\mathbf{G}'[k] = \mathbf{H}_{cw2}^H[k]\left(\mathbf{H}_{cw2}[k]\mathbf{H}_{cw2}^H[k] + \frac{\sigma_w^2}{\sigma_x^2}\mathbf{I}_{N/2} + \frac{1}{\sigma_x^2}\mathbf{H}_{cw1}[k]\mathbf{Q}_{\hat{\mathbf{e}}_{cw1}[k]}\mathbf{H}_{cw1}^H[k]\right)^{-1} \quad (14)$$

where $\mathbf{Q}_{\hat{\mathbf{e}}_{cw1}[k]}$ denotes the covariance matrix of the error of the remodulated symbols $\hat{\mathbf{e}}_{cw1} = \mathbf{x}_{cw1} - \hat{\mathbf{x}}_{cw1}$. Again, the off-diagonal elements of $\mathbf{Q}_{\hat{\mathbf{e}}_{cw1}[k]}$ can be neglected, and the diagonal elements can be calculated as in (10). In this case, however, the probabilities of each symbol of the constellation will be obtained from the LLRs provided by the soft-output decoder, thus taking advantage of the coding gain.

IV. Performance Evaluation

In this section, the simulation results of the described SIC schemes are presented. The performance of a linear receiver using conventional MMSE detection is also shown for comparison's sake. A turbo-coded OFDM system with LTE parameters is considered. The 5MHz transmission bandwidth configuration is selected [2], [11], which corresponds to 300 subcarriers, and the antenna configurations evaluated are 2×2 and 4×4. In both configurations, two codewords are independently encoded, rate-matched and interleaved following 3GPP specifications in [12]. The channel model used is the 20 taps Typical Urban channel in [13], where we assume no correlation between spatial channels and uncorrelated block fading, i.e., the channel is constant over the duration of one transmission time interval (TTI). No hybrid automatic repeat request (HARQ) retransmissions are used.

In Fig. 4, the packet error rate (PER) obtained with all the considered schemes is depicted for the 2×2 system with 16QAM modulation and coding rate $1/2$. The conventional S-SIC receiver shows a very poor performance, being considerably worse than the linear MMSE receiver. This is due to error propagation in the interference cancellation and the soft-values calculation. As this scheme assumes that the interference of each symbol has been perfectly removed, the channel decoder is unable to compensate for errors in the detection process. On the other hand, when information on the reliability of previously detected symbols is incorporated into the MMSE filtering and the soft-values calculation, as in the S-SIC EC scheme, the decoder has precise information about the quality of the detected bits, thus being able to decode the codewords with much better accuracy. For the configuration shown, the S-SIC EC receiver outperforms the linear MMSE receiver, obtaining an SNR gain of about 0.8 dB at 1% PER. Larger gains can be achieved when a codeword-SIC scheme is used. These schemes perform better than the linear receiver by between 1.9 and 2.2 dB. The best

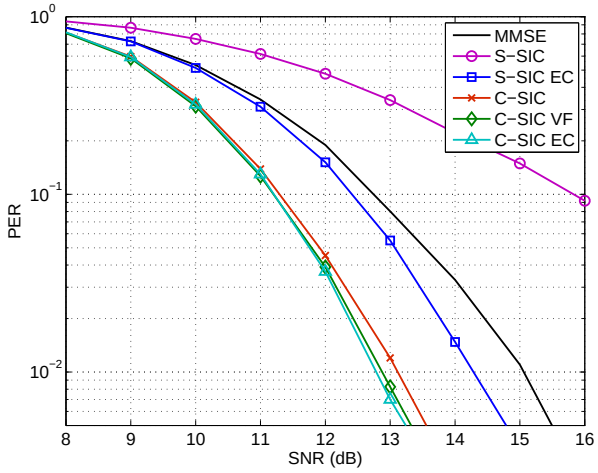

Fig. 4. PER for a 2×2 antenna system with 16QAM and coding rate $1/2$

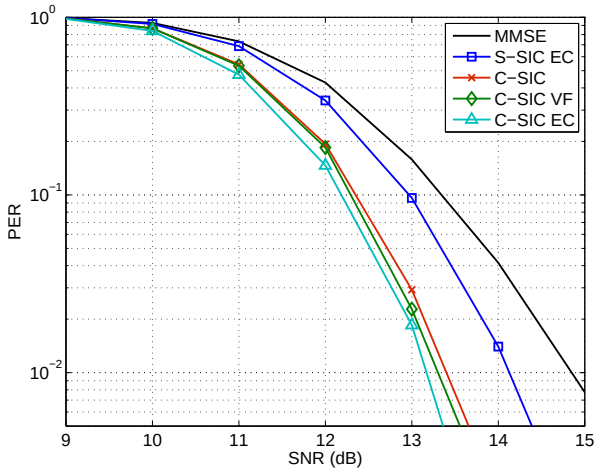

Fig. 5. PER for a 4×4 antenna system with 16QAM and coding rate $1/2$

performance corresponds to the C-SIC EC receiver, although it only achieves a marginal gain over the C-SIC VF. These two schemes slightly outperform the conventional C-SIC; the reason is that, in C-SIC, error propagation takes place when the first codeword is not correctly decoded. This drawback is avoided by not cancelling the interference in the case of C-SIC VF, or by making use of the soft information at the output of the decoder in the case of the C-SIC EC.

The PER performance of the studied receivers for the 4×4 antenna configuration case is shown in Fig. 5, where again 16QAM modulation and coding rate of 1/2 have been employed. Note that the conventional S-SIC scheme has not been plotted as its poor performance was already stated above. As it can be observed, the trends are similar to the 2×2 configuration. Again, codeword-SIC schemes perform best, while the achievable gain of the S-SIC EC with respect to MMSE does not exceed 1 dB at 1% PER. For this antenna configuration, the gain obtained by considering error com-

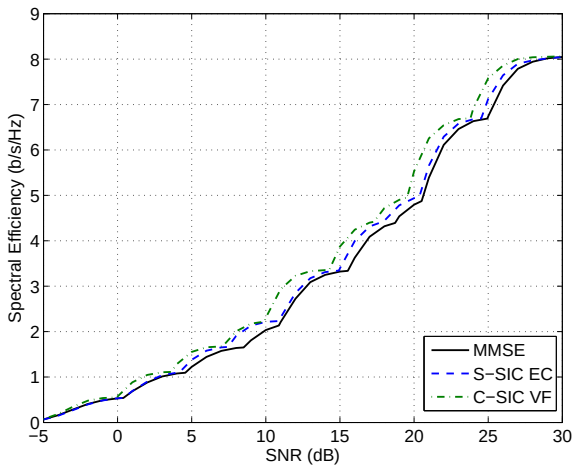

Fig. 6. Spectral efficiency curve for a 2×2 antenna system

TABLE I
MCS USED FOR SPECTRAL EFFICIENCY CURVE

Modulation	Coding Rates
QPSK	$1/6$, $1/3$, $1/2$, $2/3$
16QAM	$1/2$, $2/3$, $3/4$
64QAM	$2/3$, $4/5$

pensation in the codeword-SIC scheme is more noticeable, but still inside 0.2 to 0.3 dB with respect to C-SIC VF. The conventional C-SIC receiver, again, is the one obtaining worst results due to error propagation. From the results obtained, it is observed that when the first codeword decoding is erroneous, not performing interference cancellation is better than doing it without compensating for the errors introduced. When compensation is done, slightly better results can be obtained at the expense of a significant complexity increase.

In order to evaluate the performance of the proposed schemes in the whole SNR range, a spectral efficiency curve obtained with MMSE, S-SIC EC and C-SIC VF schemes is presented in Fig 6. This curve has been generated by selecting the modulation and coding schemes (MCS) from Table I which provide the highest spectral efficiency for a given SNR. The curves show how the C-SIC VF scheme outperforms both S-SIC EC and MMSE over the whole SNR range and for every MCS. For SNR larger than 5 dB, the codeword SIC scheme is between 1.5 and 2 dB better than a conventional MMSE receiver. The S-SIC EC receiver, on the other hand, exhibits different performance gains depending on the modulation and coding rate. For a given modulation, the performance is increased at higher coding rates. The explanation is that this high coding rates are used at higher SNR and, as a consequence, the probability of errors in the detected symbols is lower, which benefits the interference cancellation process. A codeword SIC can still benefit from the interference cancellation at low SNR by making use of the strong error correction capabilities of the low code rates employed.

V. Conclusion

In this paper, we have addressed the design of a MIMO SIC receiver for 3GPP LTE. The studied receivers have been split into two categories: symbol-SIC receivers, where detection and interference cancellation is done independently for each subcarrier, and codeword-SIC receivers, in which the detection is done on a per-codeword basis, and the channel turbo-decoder is included in the interference cancellation loop. Our results show that the codeword schemes outperform the symbol-based significantly over the whole SNR range and for every MCS. Furthermore, the best tradeoff between complexity and performance corresponds to the C-SIC VF scheme, in which the interference from any codeword is only cancelled when this has been correctly decoded. By doing so, SNR gains of up to 2 dB with respect to a conventional MMSE receiver can be obtained, whilst the complexity is kept low by avoiding the feedback loop when decoding errors are detected.

Acknowledgement

The authors would like to thank Infineon Technologies Denmark A/S for its financial support, and Christian Rom and Luis Ángel Maestro for their useful comments.

References

[1] "Requirements for Evolved UTRA (E-UTRA) and Evolved UTRAN (E-UTRAN)," 3rd Generation Partnership Project, Tech. Rep. TS 25.913, V7.3.0, 2006.

[2] "Evolved Universal Terrestrial Radio Access (E-UTRA); LTE Physical Layer - General Description (release 8)," 3rd Generation Partnership Project, Tech. Rep. TS 36.211, V8.1.0, Nov. 2007.

[3] L. Hanzo, M. Mnster, B. J. Choi, and T. Keller, *OFDM and MC-CDMA for Broadband Multi-User Communications, WLANs and Broadcasting*. West Sussex, England: John Wiley & Sons, 2003.

[4] E. Telatar, "Capacity of multi-antenna gaussian channels," *European Transactions on Telecommunications*, vol. 10, pp. 585–595, 1999.

[5] P. Wolniansky, G. Foschini, G. Golden, and R. Valenzuela, "V-BLAST: an architecture for realizing very high data rates over the rich-scattering wireless channel," *Signals, Systems, and Electronics, 1998. ISSSE 98. 1998 URSI International Symposium on*, pp. 295–300, 29 Sep-2 Oct 1998.

[6] H. Lee, B. Lee, and I. Lee, "Iterative detection and decoding with an improved V-BLAST for MIMO-OFDM systems," *Selected Areas in Communications, IEEE Journal on*, vol. 24, no. 3, pp. 504–513, March 2006.

[7] A. van Zelst, "Per-antenna-coded schemes for MIMO OFDM," *Communications, 2003. ICC '03. IEEE International Conference on*, vol. 4, pp. 2832–2836 vol.4, 11-15 May 2003.

[8] D. Wubben and K.-D. Kammeyer, "Low complexity successive interference cancellation for per-antenna-coded MIMO-OFDM schemes by applying parallel-SQRD," *Vehicular Technology Conference, 2006. VTC 2006-Spring. IEEE 63rd*, vol. 5, pp. 2183–2187, 7-10 May 2006.

[9] X. Li, H. Huang, G. Foschini, and R. Valenzuela, "Effects of iterative detection and decoding on the performance of BLAST," *Global Telecommunications Conference, 2000. GLOBECOM '00. IEEE*, vol. 2, pp. 1061–1066 vol.2, 2000.

[10] X. Wang and H. Poor, "Iterative (turbo) soft interference cancellation and decoding for coded CDMA," *Communications, IEEE Transactions on*, vol. 47, no. 7, pp. 1046–1061, Jul 1999.

[11] "Evolved Universal Terrestrial Radio Access (E-UTRA); LTE Physical Layer - base station (BS) radion transmission and reception (release 8)," 3rd Generation Partnership Project, Tech. Rep. TS 36.104, V8.0.0, Dec. 2007.

[12] "Multiplexing and channel coding (FDD) (release 7)," 3rd Generation Partnership Project, Tech. Rep. TS 25.212, V7.7.0, Nov. 2007.

[13] "Deployment aspects (release 7)," 3rd Generation Partnership Project, Tech. Rep. TS 25.943, V7.0.0, Jun. 2007.

Paper J

Turbo-Receivers for Single User MIMO LTE-A Uplink

Gilberto Berardinelli, Carles Navarro Manchón, Luc Deneire, Troels B. Sørensen, Preben Mogensen and Kari Pajukoski

IEEE 69th Vehicular Technology Conference, VTC Spring 2009. Barcelona, April 2009.

Turbo Receivers for Single User MIMO LTE-A Uplink

Gilberto Berardinelli [(1)], Carles Navarro Manchón [(1)], Luc Deneire [(1)(2)(3)], Troels B.Sørensen [(1)], Preben Mogensen [(1)], Kari Pajukoski [(4)]

[(1)] Department of Electronic Systems, Aalborg University, Denmark
Email: gb@es.aau.dk
[(2)] Université de Nice, Sophia Antipolis
[(3)] Centre National de la Recherche Scientifique
I3S,UMR 6070, France
[(4)] Nokia-Siemens Networks, Oulu, Finland

***Abstract*—The paper deals with turbo detection techniques for Single User Multiple-Input-Multiple-Output (SU MIMO) antenna schemes. The context is on the uplink of the upcoming Long Term Evolution - Advanced (LTE-A) systems. Iterative approaches based on Parallel Interference Cancellation (PIC) and Successive Interference Cancellation (SIC) are investigated, and a low-complexity solution allowing to combine interstream interference cancellation and noise enhancement reduction is proposed. Performance is evaluated for Orthogonal Frequency Division Multiplexing (OFDM) and Single Carrier Frequency Division Multiplexing (SC-FDM) as candidate uplink modulation schemes for LTE-A. Simulation results show that, in a 2x2 antenna configuration, the turbo processing allows a consistent improvement of the link performance, being SC-FDM the one having higher relative gain with respect to linear detection. The turbo receiver's impact is however much reduced for both modulation schemes in a 2x4 configuration, due to the higher diversity gain provided by the additional receive antennas.**

***Index Terms*—LTE-A, MIMO, OFDM, SC-FDM, turbo receiver, PIC, SIC**

I. Introduction

The 3rd Generation Partnership Project (3GPP) is currently specifying the system requirements for the upcoming Long Term Evolution - Advanced (LTE-A) systems, aiming at target peak data rates of 1 Gbits/s in local areas and 100 Mbit/s in wide areas. While in the previous Release 8 [1] only single transmit antenna schemes have been standardized for the uplink, multiple-input-multiple-output (MIMO) techniques are expected to be deployed to meet these ambitious requirements. Orthogonal Frequency Division Multiplexing (OFDM) has been selected in the Release 8 for the downlink due to its high robustness to multipath as well as its flexibility, allowing to easily share resources among users while keeping full intra-cell orthogonality [2]. In this scheme, the modulated symbols are split over narrowband subcarriers and transmitted in parallel over the wireless channel; a cyclic prefix (CP) is inserted to mitigate the intersymbol interference (ISI) and the intercarrier interference (ICI), allowing simple equalization in the receiver. Despite its advantages, OFDM suffers from high Peak to Average Power Ratio (PAPR) of the transmitted signals, which requires higher power backoff in the transmitter to avoid distortions, and hence leading to lower power efficiency. This is particularly critical in uplink because of the power consumption constraint in the User Equipment (UE). Therefore, Single Carrier Frequency Division Multiplexing (SC-FDM) has been selected for the uplink in LTE [1]. This modulation scheme exploits the same benefits in terms of multipath mitigation and flexibility as OFDM. However, data symbols are transmitted serially in the time domain, leading to a consistent reduction of the PAPR [3]. Nevertheless, the choice of the uplink modulation scheme for LTE-A has not yet been finalized. It has been shown that OFDM generally outperforms SC-FDM in terms of spectral efficiency when linear receivers are used [4]; this is because SC-FDM systems suffer from an effect called "noise enhancement", which degrades the estimation of the data symbols. In a previous study [5], we implemented an iterative receiver for a single-input-multiple-output (SIMO) SC-FDM system, showing that the noise enhancement can be overcome by the non-linear detection. That makes the performance of SC-FDM similar to OFDM.

In this paper, we extend the previous work to a double stream Single User MIMO scheme for the upcoming LTE-A systems. Iterative approaches based on parallel and successive interference cancellation are investigated, and a new turbo processing solution allowing to reduce the computational complexity is proposed. Both parallel and successive interference cancellation have been widely treated in literature, for CDMA as well as OFDM systems (e.g.,[6],[7] and [8]). Their aim is basically a progressive reduction of the interstream interference by including in the detection process a previous estimate of the transmitted data sequences. Here, since our main scope is leveraging SC-FDM performance, we combine in the iterative processing (even called *turbo* processing) both the traditional interstream interference removal provided by the aforementioned techniques and the noise enhancement reduction.

The remainder of the paper is structured as follows. In

978-1-4244-2517-4/09/$20.00 ©2009 IEEE

Section I, the MIMO LTE-A system is presented. Section II describes the principles of the iterative detection, focusing on Parallel and Successive Interference Cancellation. Section III shows our proposed turbo processing strategy with limited complexity. In Section IV, simulation results are presented and discussed. Finally, Section V summarizes the conclusions.

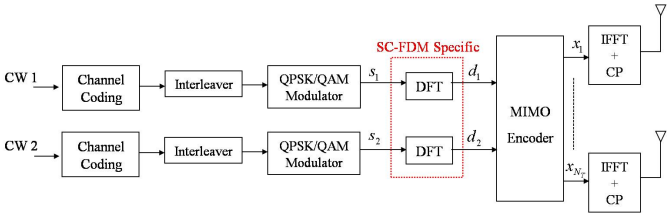

Fig. 1. MIMO transmitter with 2 codewords.

II. System Model

A simplified baseband model of a MIMO OFDM/SC-FDM transmitter with 2 codewords (CWs) and N_T transmit antennas is depicted in Fig.1. For each CW, the information bits are independently encoded, interleaved, and finally mapped to QPSK/M-QAM symbols, yielding the vectors $\mathbf{s_i}$, i=1,2. Then, a Discrete Fourier Transform (DFT) is performed in the case of SC-FDM, spreading each data symbol over all the subcarriers, obtaining the vectors $\mathbf{d_i}$. For OFDM instead, each data symbol is mapped over one subcarrier, i.e. $\mathbf{d_i} = \mathbf{s_i}$. Symbols $\mathbf{d_i}$ are then mapped over the transmit antennas by the MIMO encoder block. Finally, an Inverse Fast Fourier Transform (IFFT) is applied and a CP is appended. Assuming that the channel response is static over the duration of an OFDM symbol, and the CP is long enough to cope with the delay spread of the channel, the received signal after CP removal and fast Fourier transform (FFT) can be written as follows:

$$\mathbf{y}[k] = \mathbf{H}[k]\mathbf{x}[k] + \mathbf{w}[k] \tag{1}$$

where $\mathbf{x}[k] = [x_1(k), x_2(k), \ldots, x_{N_T}(k)]^T$ is a vector containing the encoded complex transmitted MIMO symbols at subcarrier k from the N_T transmit antennas, $\mathbf{w}[k] = [w_1(k), w_2(k), \ldots, w_{N_R}(k)]^T$ is the additive white Gaussian noise vector with $E[w_i(k)w_i(k)^*] = \sigma_w^2$ and

$$\mathbf{H}[k] = \begin{bmatrix} h_{11}(k) & \ldots & h_{1N_T}(k) \\ \vdots & \ddots & \vdots \\ h_{N_R1}(k) & \ldots & h_{N_RN_T}(k) \end{bmatrix} \tag{2}$$

is the channel transfer function matrix at subcarrier k. $h_{ij}(k)$ denotes the complex channel gain from the transmit antenna j to the receive antenna i. In this study, it is assumed that $E[s_i(k)s_i(k)^*] = 1$ and that the transmitted power is equally distributed among the transmit antennas.

III. Iterative detection

The structure of the considered turbo receiver is shown in Fig.2. The equalizer and the turbo decoder are joint in a loop, benefiting from the mutual information exchange. The aim is improving the performance with respect to the linear receiver by iteratively enhancing the reliability of the data estimates for each CW. The turbo decoder provides an estimate of all the coded bits in the form of likelihood ratios, that are subsequentely interleaved and modulated as done in [5] to get a *soft* estimate of the transmitted symbols. These soft estimates are then fed back to an interference canceller, allowing to progressively remove the mutual interference contribution. In SC-FDM systems, the inverse discrete Fourier transform (IDFT) performed at the receiver spreads the noise contribution from faded subcarriers over all the data symbols. Iterative processing aims even at reducing this noise enhancement. In the following, we present the principles of two widely adopted iterative detection techniques: Parallel Interference Cancellation and Successive Interference Cancellation.

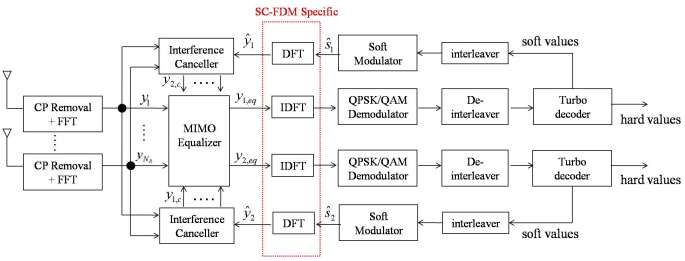

Fig. 2. MIMO Turbo Receiver.

A. Parallel Interference Cancellation (PIC)

In the PIC technique, all the CWs are detected in parallel, interleaved, re-modulated and sent back to the interference canceller, whose output for the *m*-th CW in the subcarrier *k* at *n*-th iteration can be written as follows:

$$\mathbf{y}_{m,c}^n[k] = \mathbf{y}[k] - \mathbf{H}_{Z-\{m\}}[k]\widehat{\mathbf{d}}_{Z-\{m\}}^{n-1}[k] \tag{3}$$

where $Z = \{1, 2\}$ is the set of the CWs'indexes, $\mathbf{H}_{Z-\{m\}}$ denotes the column of $\mathbf{H}$ corresponding to the antennas on which the $(Z - \{m\})$-th CW has been mapped, and $\widehat{\mathbf{d}}_{\mathbf{Z-\{m\}}}^{\mathbf{n-1}}$ is the frequency domain soft estimate of the $(Z - \{m\})$-th CW, obtained in the previous iteration. Note that for SC-FDM, $\widehat{\mathbf{d}}_{\mathbf{Z-\{m\}}}^{\mathbf{n-1}}$ is obtained through a DFT operation over the soft modulated symbols $\widehat{\mathbf{s}}_{\mathbf{Z-\{m\}}}^{\mathbf{n-1}}$ (for OFDM, $\widehat{\mathbf{d}}_{\mathbf{Z-\{m\}}}^{\mathbf{n-1}} = \widehat{\mathbf{s}}_{\mathbf{Z-\{m\}}}^{\mathbf{n-1}}$). The residual error after the interference cancellation should be taken into account in the equalization. The frequency domain equalization for the *m*-th CW in subcarrier *k* can be carried out as follows [8]:

$$\mathbf{y}_{m,eq}^n[k] = \mathbf{H}_m^H[k]\left[\mathbf{H}[k]\mathbf{Q}_n\mathbf{H}^H[k] + N_T\sigma_w^2\mathbf{I}_{N_R}\right]^{-1}\mathbf{y}_{m,c}^n[k] \tag{4}$$

where $(\cdot)^H$ denotes the hermitian operator, $\mathbf{I_{N_R}}$ is the $N_R \times N_R$ identity matrix, and $\mathbf{Q_n} = \mathbf{diag}\left[\mathbf{q_1}, \cdots, \mathbf{q_{N_T}}\right]$ is the $N_T \times N_T$ diagonal matrix of the residual interference powers, whose *j*-th element can be expressed as:

$$q_j = \begin{cases} 1, & \text{if } j = m \\ 1 - \widehat{\sigma}_{Z-\{m\},n-1}^2 & \text{if } j \neq m \end{cases} \tag{5}$$

where $\widehat{\sigma}^2_{Z-\{m\},n-1}$ is the variance of the soft modulated symbols of the $(Z-\{m\})$-th CW at *(n-1)*-th iteration. It can be computed as follows:

$$\widehat{\sigma}^2_{Z-\{m\},n-1} = \frac{1}{N_{sub}} \sum_{k=1}^{N_{sub}} \left| \widehat{s}^{n-1}_{Z-\{m\}}[k] \right|^2 \quad (6)$$

where N_{sub} is the number of subcarriers. Note that at the beginning, when no apriori information is available, $\widehat{\sigma}^2 = 0$ and Eq.(4) acts as a traditional Minimum Mean Square Error (MMSE) equalizer. The receiver performs the tasks described above for a number of iterations; after that, the turbo decoder takes hard decisions about the transmitted bits.

B. Successive Interference Cancellation (SIC)

In the SIC technique the CWs are first ordered depending on some criterion, and the detection and the decoding processes are performed sequentially. The CWs are usually ordered according to their equivalent channel gain, so that the CW with highest equivalent channel gain is detected first. The equivalent channel gain of the *m*-th CW at the *n*-th iteration can be expressed as follows:

$$\tilde{H}^n_m = \frac{1}{N_{sub}} \sum_{k=1}^{N_{sub}} \mathbf{H}^H_m[k] \left[\mathbf{H}[k] \mathbf{Q_n} \mathbf{H}^H[k] + N_T \sigma^2_w \mathbf{I}_{N_R} \right]^{-1} \mathbf{H}_m[k] \quad (7)$$

The selected CW is detected, soft modulated and fed back to the interference canceller, whose output can be written as follows:

$$\begin{aligned} \mathbf{y}^n_{m,c}[k] = \mathbf{y}[k] - \mathbf{H}_{Z-\{m\}}[k] \widehat{\mathbf{d}}^p_{Z-\{m\}}[k], \; where \\ p = n \text{ if } Z-\{m\} = argmax_{i=1,2} \tilde{H}^n_i \\ p = n-1 \text{ if } Z-\{m\} \neq argmax_{i=1,2} \tilde{H}^n_i \end{aligned} \quad (8)$$

The equalizer's output for the *m*-th CW in subcarrier *k* is given by:

$$\mathbf{y}^n_{m,eq}[k] = \mathbf{H}^H_m[k] \left[\mathbf{H}[k] \tilde{\mathbf{Q}}_n \mathbf{H}^H[k] + N_T \sigma^2_w \mathbf{I}_{N_R} \right]^{-1} \mathbf{y}^n_{m,c}[k] \quad (9)$$

where $\tilde{\mathbf{Q}}_n = diag\left[\tilde{q}_1, \cdots, \tilde{q}_{N_T}\right]$, whose generic *j*-th element can be written as:

$$\tilde{q}_j = \begin{cases} 1, & \text{if } \; j = m \\ 1 - \widehat{\sigma}^2_{Z-\{m\},n} & \text{if } \; j \neq m, j = argmax_{i=1,2} \tilde{H}^n_i \\ 1 - \widehat{\sigma}^2_{Z-\{m\},n-1} & \text{if } \; j \neq m, j \neq argmax_{i=1,2} \tilde{H}^n_i \end{cases} \quad (10)$$

IV. Turbo processing with limited complexity

An obvious drawback of the iterative detection techniques is their computational complexity, increasing with the number of iterations. However, since an estimate of the transmitted CWs is available at each iteration, the turbo processing presented above is redundant once at least one of them has been correctly detected. In LTE, a cyclic redundancy code (CRC) is appended to the information bits of the CW to check if the detection process has been successful. Here, we propose to use this error-detection capability to reduce the turbo processing complexity. In fact, checking the CRC allows to stop the iterative process once CWs are correctly decoded. Furthermore, we combine in the same process both the interstream interference removal and the noise enhancement reduction for SC-FDM. For simplicity, in the following we will refer to a double transmit antenna system.

Let us suppose to perform the generic *n*-th iteration of the PIC or SIC algorithm. After both CWs have been detected, their CRC is checked by taking hard decisions on the soft bits. The possible options and the subsequent behaviour to be adopted are the followings:

- Both CWs are not successfully detected. Continue performing PIC or SIC in the *(n+1)*-th iteration.
- Only one CW is successfully detected. In this case, the interstream interference can be fully removed from the wrong CW. Therefore, the MIMO system is virtually reduced to a single-input-multiple-output one, and the noise enhancement reduction strategy for SC-FDM presented in [5] can be adopted. To sum up, the following steps have to be performed:
  - *(n+1)*-th iteration: feed back only the correct CW for interstream interference removal and equalization;
  - from *(n+2)*-th iteration: re-modulate the wrong CW obtaining $\widehat{\mathbf{d}}^{\mathbf{n+1}}_{\mathbf{wr}}$ and use the equalizer coefficients defined in [5], that have been shown to reduce the noise enhancement of SC-FDM in a SIMO system. We distinguish between forward coefficients, which aim at increasing the Signal-to-Noise Ratio (SNR), and feedback coefficients, designed at the purpose of reducing the noise contribution in the estimated sequence. The forward coefficient at the *q*-th receive antenna in subcarrier *k* can be defined as follows:

$$C_{ff,q}(k) = \frac{1}{1+\beta\widehat{\sigma}^2_{wr,n+1}} \frac{h^*_{q,wr}(k)}{\left(1-\widehat{\sigma}^2_{wr,n+1}\right) \sum_{q=1}^{N_R} \left|h_{q,wr}(k)\right|^2 + \sigma^2_w} \quad (11)$$

where

$$\beta = \frac{1}{N_{sub}} \sum_{k=1}^{N_{sub}} \frac{\sum_{q=1}^{N_R} \left|h_{q,wr}(k)\right|^2}{\left(1-\widehat{\sigma}^2_{wr,n+1}\right) \sum_{q=1}^{N_R} \left|h_{q,wr}(k)\right|^2 + \sigma^2_w} \quad (12)$$

The feedback coefficient in subcarrier *k* can be expressed as:

$$C_{fb}(k) = \sum_{q=1}^{N_R} h_{q,wr}(k) C_{ff,q}(k) - 1 \quad (13)$$

Therefore the resultant output of the equalizer is given by:

$$y^{n+2}_{wr,eq}[k] = \underline{\mathbf{C_{ff}}}[k] \mathbf{y}^{n+1}_{wr,c}[k] - C_{fb}(k) \widehat{\mathbf{d}}^{n+1}_{wr}[k] \quad (14)$$

where $\underline{\mathbf{C_{ff}}}[\mathbf{k}] = [\mathbf{C_{ff,1}}(\mathbf{k}), \cdots, \mathbf{C_{ff,N_R}}(\mathbf{k})]$. For further details, we refer to [5].
- Both CWs are successfully detected: jump to the detection of the next data frame.

TABLE I
SIMULATION PARAMETERS

Carrier frequency	2 GHz
Sampling frequency	15.36 MHz
Subcarrier spacing	15 KHz
FFT size	1024
Used subcarriers	600
CP length	$5.2^a/4.68^b$ μs
Slot duration	0.5 ms
Symbols per slot	7
MIMO schemes	(2x2, 2x4) SM
User speed	3 kmph
MCS settings	QPSK: 1/6, 1/3, 1/2, 2/3 16QAM: 1/2, 2/3, 3/4 64QAM: 2/3, 4/5
Channel code	3GPP Rel.8 compliant Turbo code with basic rate 1/3
Turbo decoder iterations	8
Receiver scheme	MMSE, PIC, SIC

[a]First OFDM/SC-FDM symbol in a slot.
[b]$2^{th} - 7^{th}$ OFDM/SC-FDM symbol in a slot.

V. PERFORMANCE EVALUATION

The performance of the turbo receiver is evaluated by Monte Carlo simulations. We use as a reference 10 MHz LTE configuration parameters [1]. The main simulation parameters are gathered in Table I. An urban micro channel model (SCM-D) [9] is used in the simulations, and perfect channel knowledge is assumed. In the following, we will assume that an iteration of both PIC and SIC is completed once an estimate of both CWs is available by exploiting the feedback information. The linear MMSE equalization can instead be considered as the 0-*th* iteration of the PIC scheme.

Fig.3 shows the performance of PIC and SIC for a 2x2 SC-FDM system in terms of Block Error Rate (BLER), assuming 16QAM 2/3. Linear MMSE performance is also included. Both iterative techniques lead to a consistent gain over linear detection, up to 5 dB with 6 iterations. Most of the gain is already obtained after the first iteration. Note that at the first iteration PIC performs better than SIC because in the latter the soft interference is removed only from one CW. However, for higher number of iterations both techniques tend to perform similarly. It can be seen (Fig.4) that SIC converges slightly faster than PIC. This is because in SIC one of the soft estimates used in the interference cancellation is obtained in the current iteration, while in PIC both are obtained in the previous iteration.

Fig.5 depicts a comparison between OFDM and SC-FDM for SIC receivers. As it can be observed, OFDM clearly outperforms SC-FDM when linear receivers are used. This is due to the noise enhancement in SC-FDM systems. OFDM performance can be further improved by the iterative detection. However, for OFDM the gain of SIC with respect to MMSE is limited to 3.5 dB. This allows reducing the performance

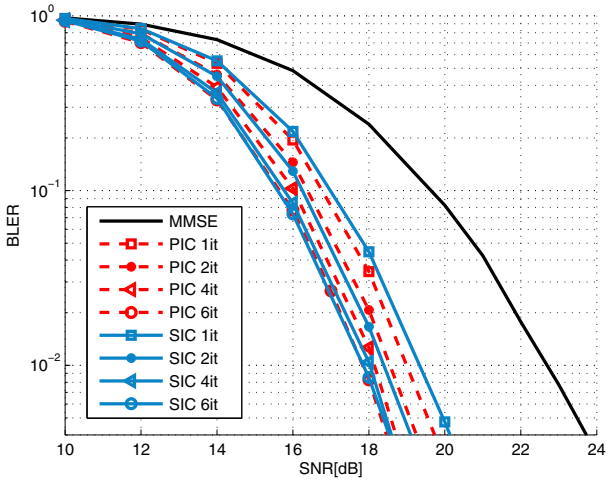

Fig. 3. BLER performance of SC-FDM in a 2x2 antenna system, with 16QAM 2/3.

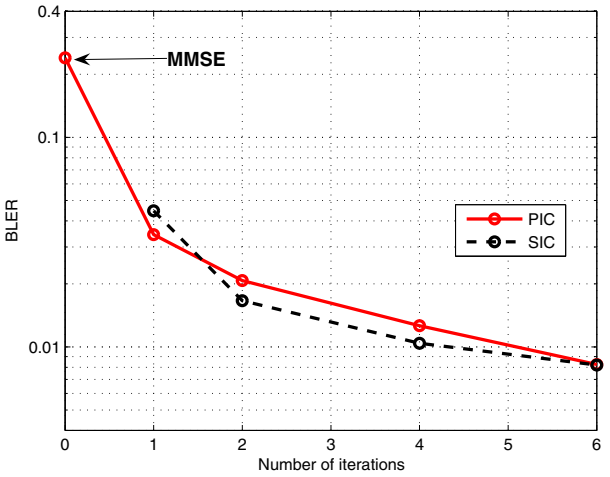

Fig. 4. SC-FDM PIC vs. SIC, SNR=18dB.

gap between OFDM and SC-FDM, to within 1 dB. The higher relative gain of SC-FDM compared to MMSE is due to the reduction of the noise enhancement provided by the turbo processing. Furthermore, comparing Fig.3 and Fig.5, it can also be noticed that the relative gain between different iterations is slightly higher for SC-FDM.

The gap between the modulation schemes with MMSE is quite reduced with a 2x4 antenna configuration, as presented in Fig.6. This is due to the increase of diversity, which averages the channel seen at the receiver. In this way, the deep fades of the channel are smoothed, and therefore the noise enhancement of SC-FDM is reduced. Here, the iterative processing only leads to a gain up to 2 dB for SC-FDM and 1.5 dB for OFDM, thus further reducing their performance gap.

The performance result on the whole SNR range, when link adaptation is used, is shown in Fig.7. The link adaptation is done based on average SNR and the corresponding curve

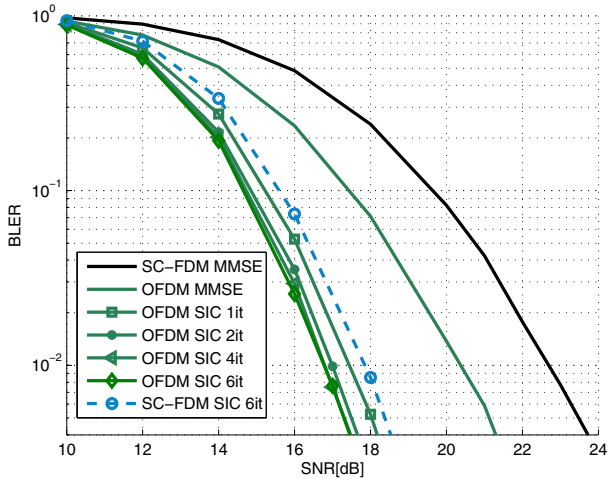

Fig. 5. Performance comparison between OFDM and SC-FDM in a 2x2 antenna system, with 16QAM 2/3.

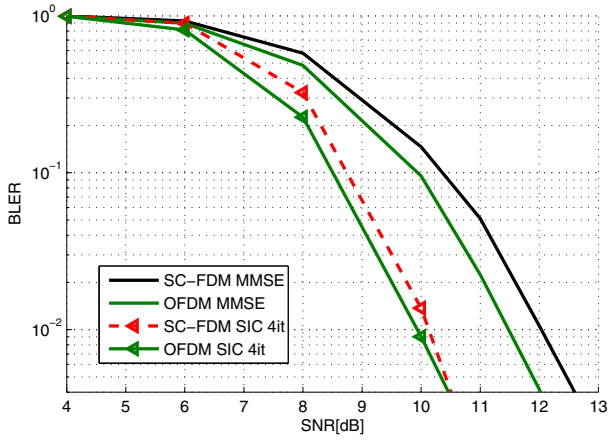

Fig. 6. Performance comparison between OFDM and SC-FDM in a 2x4 antenna system, with 16QAM 2/3.

results from the envelope of the spectral efficiency curves for several Modulation and Coding Schemes (MCSs). For low SNRs, OFDM performs as good as SC-FDM for both linear and iterative detection. The performance gap is relevant for high order MCSs, where the higher relative gain of the turbo receiver for SC-FDM is evident. OFDM and SC-FDM tend perform similarly in a 2x4 antenna system, as suggested by the previous results.

VI. Conclusions

In this paper, iterative detection techniques are presented and investigated in a Single User MIMO context for the uplink of the upcoming LTE-A standard, and a limited complexity solution combining interstream interference removal and noise enhancement reduction is proposed. Performance is evaluated for both OFDM and SC-FDM as candidate modulation schemes for the uplink of LTE-A. Simulation results show that the proposed solution leads to a gain in terms of BLER

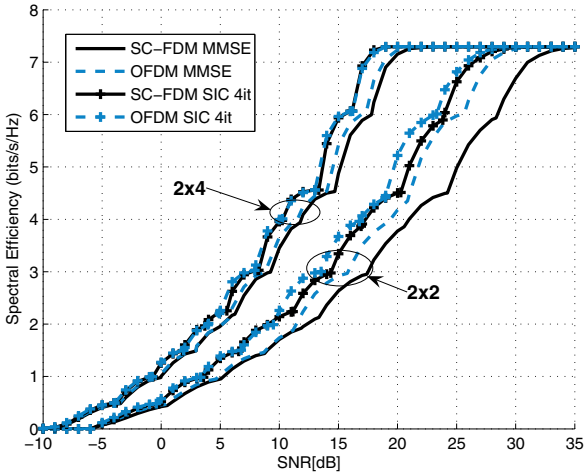

Fig. 7. Link adaptation curves for 2x2 and 2x4 antenna configurations.

up to 5 dB over linear detection for a SC-FDM 2x2 antenna configuration, thus outperforming OFDM with linear MMSE receiver. For OFDM, the gain of the turbo processing over linear detection is limited to 3.5 dB. The diversity gain obtained by adding antennas at the receiver reduces the impact of the turbo processing: in fact, link adaptation based on average SNR shows no relevant difference in performance when the antenna configuration is increased to a 2x4 system.

Acknowledgment

The authors would like to thank Nokia-Siemens Networks for sponsoring the work, and Luis Ángel Maestro Ruiz de Temiño for the helpful comments and fruitful discussions.

References

[1] "LTE Physical Layer - General Description (Release 8)," 3rd Generation Partnership Project, Tech. Rep. TS 36201, V8.1.0, Nov. 2007.

[2] L. Hanzo, M. Munster, B. Choi, and T. Keller, *OFDM and MC-CDMA for Broadband MultiUser Communications, WLANs and Broadcasting*. John Wiley - IEEE Press, 2003.

[3] H. Myung, J. Lim, and D. Goodman, "Single carrier FDMA for uplink wireless transmission," *Vehicular Technology Magazine, IEEE*, vol. 2, no. 3, pp. 30–38, September 2006.

[4] B. Priyanto, H. Codina, S. Rene, T. Sorensen, and P. Mogensen, "Initial performance evaluation of DFT-spread OFDM based SC-FDMA for UTRA LTE uplink," *IEEE 65th Vehicular Technology Conference, VTC2007-Spring*, pp. 3175–3179, April 2007.

[5] G. Berardinelli, B. E. Priyanto, T. B. Sørensen, and P. Mogensen, "Improving SC-FDMA performance by turbo equalization in UTRA LTE uplink," *IEEE Vehicular Technology Conference*, pp. 2557–2561, May 2008.

[6] N. Benvenuto and P. Bisaglia, "Parallel and successive interference cancellation for MC-CDMA and their near-far resistance," *Vehicular Technology Conference*, vol. 2, pp. 1045–1049, October 2003.

[7] H. Lee, , B. Lee, and I. Lee, "Iterative detection and decoding with an improved V-BLAST for MIMO-OFDM systems," *IEEE Journal on Selected Areas in Communications*.

[8] A. Nakajima and F. Adachi, "Iterative joint PIC and 2D MMSE-FDE for Turbo-coded HARQ with SC-MIMO Multiplexing," *Vehicular Technology Conference*, vol. 5, pp. 2503 – 2507, May 2006.

[9] "Physical layer aspects for evolved Universal Terrestrial Radio Access (UTRA)," 3rd Generation Partnership Project, Tech. Rep. TR 25.814, V7.1.0, 2006.

Paper K

Parametric Modeling and Pilot-Aided Estimation of the Wireless Multipath Channel in OFDM Systems

Morten L. Jakobsen, Kim Laugesen, Carles Navarro Manchón, Gunvor E. Kirkelund, Christian Rom and Bernard H. Fleury

IEEE International Conference on Communications, ICC 2010. Cape Town, May 2010.

This full text paper was peer reviewed at the direction of IEEE Communications Society subject matter experts for publication in the IEEE ICC 2010 proceedings

Parametric Modeling and Pilot-Aided Estimation of the Wireless Multipath Channel in OFDM Systems

Morten Lomholt Jakobsen*, Kim Laugesen*, Carles Navarro Manchón*
Gunvor E. Kirkelund*, Christian Rom† and Bernard Fleury*‡
*Department of Electronic Systems, Aalborg University
Niels Jernes Vej 12, DK-9220 Aalborg East, Denmark
†Infineon Technologies Denmark A/S
Alfred Nobels Vej 25, DK-9220 Aalborg, Denmark
‡Forschungszentrum Telekommunikation Wien (FTW), Vienna, Austria

***Abstract*—In this paper we present a refined model of the wireless multipath channel along with a thorough analysis on the impact of spatial smoothing techniques when used for improved channel estimation. The state-of-the-art channel estimation algorithm for pilot-aided OFDM systems is robustly designed and operates without knowledge of the time-varying multipath propagation delays in the wireless channel. However, algorithms exploiting knowledge of these time-varying delay parameters can outperform the state-of-the-art solution. We demonstrate from simulations how the Unitary ESPRIT algorithm together with spatial smoothing techniques exhibit a promising potential for multipath propagation delay estimation. Furthermore, we show that the optimum smoothing parameters depend notably on the channel model assumed, specifically in terms of the dynamical behavior of the multipath delays.**

I. Introduction

During the last decade, the technique of *orthogonal frequency-division multiplexing* (OFDM) has entered and settled within several wireless standards, e.g. European digital audio broadcasting, IEEE 802.11a wireless local area networking and 3GPP *long term evolution* (LTE). The reasons for OFDM being widely selected are manifold. A few motivations include the flexibility in spectrum occupancy, robustness against inter-symbol-interference and easy integration with multiple antenna techniques.

Today, even higher data rates are demanded - calling for larger digital constellation sizes and coherent detection. Channel estimation is therefore required and commonly achieved using pilot symbol transmissions. In principle, the channel estimation may be conducted in a completely non-parametric manner. However, this approach conflicts with the requirement of high data rates due to the dimensionality of the estimation problem and also due to the time-varying behavior of the wireless channel (expensive time-frequency overhead of pilot symbols). With the aim of lowering the dimension of the estimation task and the amount of pilot symbols needed, a parametric structure of the wireless multipath channel is typically imposed [1]–[4]. Yet, the parametric channel model assumed in scientific literature and wireless standards [5] does not adequately reflect dynamic environments, e.g. with a mobile receiver. For instance, the multipath propagation delays, the inter-delay gaps and the overall number of delays are often modeled as persistently fixed - even though the receiver is assumed to be moving. Furthermore, it is common to include modeling of the Doppler frequency shifts experienced by the receiver [2], [4] - despite the fact that Doppler shifts and delay fluctuations are indisputably related. Hence, the default and widely used modeling of the wireless channel is counterintuitive and inadequate.

When employing the state-of-the-art channel estimator [1] (robust design), the fluctuating behavior of the multipath delays are of no importance since a continuum of equally powered channel components is assumed. However, this robust design yields an irreducible performance degradation which is avoidable if instead a channel estimator presupposing knowledge of the time-varying delays is used. Hence, if sufficiently accurate delay estimates can be obtained, the robust state-of-the-art channel estimator [1] can be outperformed. Yet, for this opposing solution to earn practical attention it requires a sufficiently accurate/realistic model of the wireless multipath channel.

In recent literature [2] the ESPRIT algorithm [6] has been proposed to serve as initial multipath delay acquisition tool for pilot-aided OFDM systems. The ESPRIT algorithm is an eigenvalue decomposition based method which exhibits satisfactory estimation performance when the multipath propagation delays in the channel model stay persistently fixed. However, in more realistic scenarios the propagation delays will fluctuate over time, the overall number of delays will change and also the inter-delay gaps will vary. Thus, depending on the individual realizations of the channel the delays will sometimes tend to cluster while other times tend to be more dispersed. Such effects are typically not captured by the channel models in use. Accordingly, promising simulation-based algorithm performance may implicitly give rise to erroneous comprehension - directly inherited from the inappropriate channel modeling.

In this paper we present an advanced multipath channel model which manages to mimic an increased amount of real-world channel effects. Compared to the default state-of-the-art channel model, this advanced model is of supplementary dynamic nature and therefore allows for interesting simulation-based comparisons. In terms of channel estimation perfor-

978-1-4244-6404-3/10/$26.00 ©2010 IEEE

mance we compare the state-of-the-art algorithm [1] with the *linear minimum mean squared error* (LMMSE) estimator [2] using Unitary ESPRIT [7] as multipath delay estimation tool. Additionally, a key contribution of this paper is a thorough analysis of the performance gain obtained when applying a spatial smoothing scheme for improved delay estimation accuracy. The smoothing scheme is also employed in [2], yet no analysis of its impact is provided and no justification for the smoothing parameters are given. We investigate how to optimize the smoothing parameters depending on the dynamical behavior of the wireless multipath channel model assumed.

The remaining parts of this paper are organized as follows. In Section II a scenario involving an OFDM system is described and the signal model is presented. The channel models considered are introduced and discussed in Section III. In Section IV we briefly describe the main principles of the ESPRIT algorithm. Performance evaluations are conducted and compared in terms of Monte-Carlo simulations in Section V. Concluding remarks are provided in Section VI.

II. OFDM Signal Model

We consider a single-input single-output OFDM system designed with a total of N subcarriers. The effective spectrum occupied by the system is often adjusted by forcing certain subcarriers inactive, for instance at each edge of the overall bandwidth. Accordingly, only $N_u \leq N$ subcarriers are used for actual transmissions.

The OFDM signal is generated as follows. Initially, a stream of raw information bits are modulated onto a set of PSK/QAM symbols which are then multiplexed with a sequence of M pilot symbols. After multiplexing the sequence consists of exactly N_u symbols $x_1, x_2, \ldots, x_{N_u}$, and these are intended for transmission. Finally, OFDM modulation by means of an IFFT is performed and a cyclic prefix is inserted.

The received signal is OFDM demodulated by discarding the samples corresponding to the cyclic prefix and the N time-domain samples left are exposed to a FFT. We assume that the channel remains static during transmission of each OFDM symbol and furthermore that the duration of the cyclic prefix exceeds the maximum excess delay of the channel. The OFDM demodulated signal at the receiver is then given as

$$\boldsymbol{r} = \big[r_1, r_2, \ldots, r_{N_u}\big]^\top = \mathbf{X}\boldsymbol{h} + \boldsymbol{w}, \tag{1}$$

where $\mathbf{X} = \operatorname{diag}\big\{x_1, x_2, \ldots, x_{N_u}\big\}$ is a diagonal matrix built from the transmitted symbols and $\boldsymbol{h} = [h_1, h_2, \ldots, h_{N_u}]^\top$ contains as components the channel frequency responses at the N_u active subcarriers. Circular symmetric additive white Gaussian noise contributions with variance σ^2 are contained in the vector $\boldsymbol{w} = [w_1, w_2, \ldots, w_{N_u}]^\top$.

A. Pilot Symbol Observations

The received pilot symbol observations are used to estimate the channel frequency response at all subchannels carrying non-redundant data symbols. Conveniently, we define the following subset of indices

$$\mathcal{P} := \big\{p(1), p(2), \ldots, p(M)\big\} \subset \big\{1, 2, \ldots, N_u\big\},$$

which identifies the M subcarriers used for pilot symbol transmissions. We extract the M equations from (1) corresponding to the indices contained in $\mathcal{P}$ and define

$$y_m := \frac{r_{p(m)}}{x_{p(m)}}, \qquad m = 1, 2, \ldots, M,$$

which we can appropriately and compactly formulate as

$$\boldsymbol{y} := \big(\mathbf{X}_\mathcal{P}\big)^{-1}\boldsymbol{r}_\mathcal{P} = \boldsymbol{h}_\mathcal{P} + \big(\mathbf{X}_\mathcal{P}\big)^{-1}\boldsymbol{w}_\mathcal{P}, \tag{2}$$

meanwhile the subscript notation should be obvious to interpret. We assume that all pilot symbols hold unit power, whereby the statistics of the noise term $\big(\mathbf{X}_\mathcal{P}\big)^{-1}\boldsymbol{w}_\mathcal{P}$ remains unchanged. Hence, the observations available in (2) are known to the receiver due to the pilot symbol data and $\boldsymbol{y}$ yields the true channel frequency responses (at the pilot subcarriers) embedded in zero-mean complex Gaussian noise. To properly estimate the channel frequency responses at *all* active subcarriers, i.e. the vector $\boldsymbol{h}$ in (1), a parametric model of the wireless channel is invoked. In this way the dimension is notably reduced since the task is now altered to estimate only a relatively small number of channel model parameters.

III. Multipath Channel Models

Two different multipath channels are presented in this section. The overall model for these two channels is the same and the first configuration described is simpler but unrealistic with respect to certain physical interpretations. The second configuration described is more dynamic and sophisticated while easier to accept from a physical point of view. In the entire paper we assume a non-line-of-sight, far-field scenario where *only* the receiver is moving.

The model commonly used to describe a time-varying multipath channel impulse response is given by

$$g(t, \tau) = \sum_{\ell=1}^{L(t)} \alpha_\ell(t)\delta\big(\tau - \tau_\ell(t)\big), \tag{3}$$

where δ is the Dirac delta. Each complex-valued amplitude α_ℓ, $\ell = 1, 2, \ldots, L(t)$, is typically modeled as a wide-sense stationary, zero-mean complex Gaussian process [1]–[4]. The processes $\{\alpha_\ell\}$ are furthermore assumed to be mutually uncorrelated, i.e. the channel described by (3) is a so-called *wide-sense stationary* and *uncorrelated scattering* [8] (WSSUS) Rayleigh fading channel.

A. Static Reference Channel

The simpler and static channel model is described according to a relaxed version of (3) reading

$$g(t, \tau) = \sum_{\ell=1}^{L} \alpha_\ell(t)\delta(\tau - \tau_\ell). \tag{4}$$

The overall number L of echoes in the channel is fixed and also the delay parameters $\{\tau_\ell\}$ are persistently static. All amplitude processes $\{\alpha_\ell\}$ are assumed to share the same normalized autocorrelation function, given in terms of the zeroth-order Bessel function of the first kind. Accordingly, the normalized

Doppler power spectrum associated with each echo is bathtub-shaped and usually referred to in terms of Clarke or Jakes, see [9, Sec. 3.2] and the references therein. Such modeling is based on the assumption of a *uniform scattering environment*, a scenario which is difficult to accept by physical means. Specifically, it is hard to imagine a propagation environment such that the transmitted signal is scattered into plenty reflections arriving uniformly from every direction, all equally delayed, and thereby combining into one of the L dominant echoes in the channel. Nonetheless, such a channel model is usually assumed, e.g. by 3GPP in [5].

B. Dynamic Channel

A more realistic model would allow for the delay parameters to fluctuate over time as a result of receiver mobility. Also, the overall number of echoes in the channel may change from time to time due to blocking obstacles in the environment. Hence, a channel impulse response as described by (3) is appropriate and notably more realistic than the model in (4). Initially, for $\ell = 1, 2, \ldots, L(t)$, the channel echoes are modeled as

$$\alpha_\ell(t) = \sqrt{\frac{Q_\ell}{R}} \sum_{r=1}^{R} \exp\big(j2\pi f_{D} \cos(\theta_{\ell,r})\, t + j\varphi_{\ell,r}\big), \qquad (5)$$

where Q_ℓ is the average power of the ℓ'th echo, f_{D} denotes the maximum Doppler frequency and $\{\varphi_{\ell,r}\}$ are i.i.d. uniform initial phases. In contrast to the uniform scattering environment, each channel echo α_ℓ in (5), is (heuristically) modeled from R azimuth excited subcomponents centered around a nominal angle of arrival $\bar{\theta}_\ell$. Specifically, the modeling reads

$$\bar{\theta}_\ell \overset{\text{i.i.d.}}{\sim} \mathcal{U}(-\pi, \pi) \qquad \text{and} \qquad \theta_{\ell,r} \big| \bar{\theta}_\ell \overset{\text{i.i.d.}}{\sim} \text{vM}\big(\bar{\theta}_\ell, \kappa\big),$$

where the notation $\text{vM}\big(\bar{\theta}_\ell, \kappa\big)$ refers to the *von Mises* distribution with location parameter $\bar{\theta}_\ell$ and concentration parameter $\kappa \geq 0$, see [10] for details. In this setup the channel echoes do *not* share the same normalized autocorrelation function and the Doppler power spectra are therefore individual too.

Following the modeling suggestion in [11], it is convenient to let transitions of arising channel echoes occur according to a homogeneous Poisson process with rate λ_{A}. Assigning i.i.d. exponential lifetimes with mean $1/\lambda_{B}$ to the echoes then results in $L(t)$ being a Poisson distributed random variable with $\mathbb{E}\big[L(t)\big] = \lambda_{A}/\lambda_{B}$. For simplicity and due to our receiver mobility assumption, it is furthermore convenient to model the delay fluctuations from straight line advancements, i.e.

$$\tau_\ell(t) = \tau_{\ell,0} + \frac{f_{D} \cos(\bar{\theta}_\ell)}{f_{c}} (t - t_{\ell,0}), \qquad t \geq t_{\ell,0},$$

where f_{c} denotes the carrier frequency of the communication system and $t_{\ell,0}$ is the birth time of the ℓ'th echo. The distribution of the initial delays $\{\tau_{\ell,0}\}$ can be specified as desired - a simple choice is to select the uniform distribution on an appropriate interval. The average power terms $\{Q_\ell\}$ may then be assigned according to an exponentially decaying function (i.e. the power delay profile is specified). The straight line advancements of the multipath delays are illustrated in Fig. 1 which reports a ten seconds realization of the dynamic channel with $\mathbb{E}\big[L(t)\big] = 15$ delays on average. As can be seen from the figure the channel exhibits a reasonable amount of dynamical behavior, e.g. the overall number of delays is changing over time and also the straight line patterns of the delays are quite apparent.

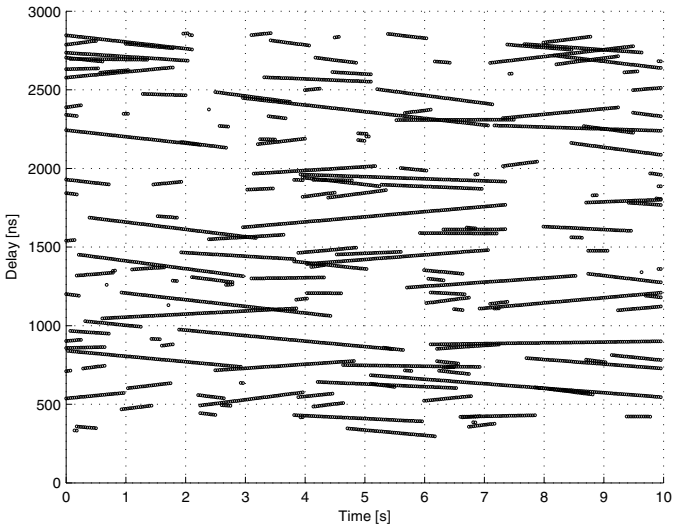

Figure 1. Contiguous realization of the dynamic channel with maximum Doppler frequency $f_{D} = 100$Hz and carrier frequency $f_{c} = 2$GHz.

The simpler and more static channel model described comprises the state-of-the-art reference. The intention with the more realistic and dynamic channel model described is to mimic a time-varying and fluctuating behavior of $L(t)$, $\big\{\tau_\ell(t)\big\}$ and $\big\{|\tau_\ell(t) - \tau_{k}(t)|\big\}$. Our goal is to investigate how incorporation of such dynamics affects the pilot-aided channel estimation performance.

IV. Propagation Delay Estimation

Assuming the reference channel model (4) as described in Section III-A, we reformulate the observation model (2) as

$$\boldsymbol{y} = \mathbf{T}(\boldsymbol{\tau})\boldsymbol{\alpha} + \boldsymbol{n}, \qquad (6)$$

where we have introduced a $M \times L$ matrix $\mathbf{T}(\boldsymbol{\tau})$, the vector $\boldsymbol{\alpha} = [\alpha_1, \alpha_2, \ldots, \alpha_{L}]^{\top}$ and the additive noise vector $\boldsymbol{n}$. The matrix $\mathbf{T}(\boldsymbol{\tau})$ depends on the delay parameters and the pilot symbol positions in such a way that its (m, ℓ)'th entry reads

$$\mathbf{T}_{m,\ell} = \exp\Big(-j2\pi \tfrac{p(m)}{N} \tfrac{\tau_\ell}{T_{\text{s}}}\Big), \qquad \begin{matrix} m = 1, 2, \ldots, M, \\ \ell = 1, 2, \ldots, L, \end{matrix}$$

where T_{s} denotes the sampling time of the communication system. Notice that the L columns building up the matrix $\mathbf{T}(\boldsymbol{\tau})$ are of identical structure and by system design the parameters N, T_{s} and $\mathcal{P}$ are known - only the delays $\{\tau_\ell\}$ are unknown. The theoretical covariance matrix associated with $\boldsymbol{y}$ reads

$$\mathbf{R} := \mathbb{E}\Big[\boldsymbol{y}\boldsymbol{y}^{H}\Big] = \mathbf{T}(\boldsymbol{\tau})\mathbf{A}\mathbf{T}^{H}(\boldsymbol{\tau}) + \sigma^2 \mathbf{I}_{M}, \qquad (7)$$

where we have implicitly assumed that any component of $\boldsymbol{\alpha}$ is statistically independent of any component of $\boldsymbol{n}$. Furthermore,

$\mathbf{A} := \mathbb{E}\big[\boldsymbol{\alpha}\boldsymbol{\alpha}^H\big]$ is a $L \times L$ diagonal matrix due to the uncorrelated scattering assumption. Notice in (7), that since the delay parameters are assumed static the covariance matrix $\mathbf{R}$ does not change over time.

Now, any vector in the null space of $\mathbf{T}^H(\boldsymbol{\tau})$ is an eigenvector of $\mathbf{R}$ with associated eigenvalue σ^2. Therefore, the particular eigenvectors of $\mathbf{R}$ not belonging to the null space of $\mathbf{T}^H(\boldsymbol{\tau})$ are all associated with eigenvalues strictly greater than σ^2. This key fact provides insight on how the signal subspace and the noise subspace can be separated according to the individual magnitudes of the eigenvalues. From a proper design of the set $\mathcal{P}$, the structure inherited by the matrix $\mathbf{T}(\boldsymbol{\tau})$ allows for two specific submatrices to be related by a simple rotational (i.e. unitary) transform. Estimation of this unitary transform is essentially how the ESPRIT algorithm is used to estimate the unknown delay parameters, see [2].

Obviously, the theoretical covariance matrix $\mathbf{R}$ is not available. Instead the ESPRIT algorithm is applied to some 'prudent' estimate of the matrix. Observations which we denote by $\{\boldsymbol{y}_k\}$ are collected temporally, and in a generic manner we arrange K of such vectors in the $M \times K$ matrix

$$\mathbf{Y} := \begin{bmatrix} | & | & & | \\ \boldsymbol{y}_1 & \boldsymbol{y}_2 & \cdots & \boldsymbol{y}_K \\ | & | & & | \end{bmatrix}. \tag{8}$$

The estimate used could then be the sample covariance matrix

$$\widehat{\mathbf{R}} := \frac{1}{K}\mathbf{Y}\mathbf{Y}^H \qquad \text{or} \qquad \widetilde{\mathbf{R}} := \frac{1}{2}\Big(\widehat{\mathbf{R}} + \mathbf{J}\widehat{\mathbf{R}}^\top\mathbf{J}\Big),$$

where $\widetilde{\mathbf{R}}$ is the centrosymmetric equivalent[1] of $\widehat{\mathbf{R}}$. Here $\mathbf{J}$ denotes the $M \times M$ reversal matrix with 1's in its entire anti-diagonal and 0's elsewhere, see [12, Sec. 4.8, 6.5.8].

If instead we assume the more realistic and dynamic channel model (3) as described in Section III-B, the entire situation is crucially altered. In (6), the delay parameter $\boldsymbol{\tau} = \boldsymbol{\tau}(t)$ is now time-variant and the basis of the underlying signal subspace is therefore changing over time (potentially, the dimension changes too, e.g. while gathering data for the matrix $\mathbf{Y}$). Essentially, the rotational transform to be estimated is time-variant since the delay parameters no longer stay fixed and hence, the basic assumptions for ESPRIT are not satisfied. Yet, by considering only time frames of sufficiently short duration, the delay fluctuations can be considered negligible. Finally, to achieve improved estimation accuracy and reduced complexity we employ Unitary ESPRIT [7], not standard ESPRIT.

A. Spatial Smoothing

To decrease any disturbing impact from the time-varying delay parameters it seem obvious to use an observation matrix $\mathbf{Y}$ where K is as small as possible. With K small, only a few observations are collected in the time direction and this fact complies well with the rigorous latency requirements of today's communication systems. If the number of pilot symbols M is relatively large and if the set $\mathcal{P}$ is designed appropriately, we can apply a so-called spatial smoothing technique. By doing so we artificially build up more time-direction observations by suffering on overall dimension (aperture) in the frequency direction. By applying a vertical sliding window of size $M_1 \leq M$ to the $M \times K$ matrix in (8) we obtain a new observation array of size

$$M_1 \times K(M - M_1 + 1).$$

Notice how the attribute of wide-sense stationarity in the frequency domain (inherited from the uncorrelated scattering assumption in the delay domain) is paramount when applying the smoothing window. Obviously, the number M_1 should be chosen according to a trade-off between aperture and estimation accuracy. Choosing M_1 smaller generates more snapshots while is (simultaneously) penalized by poorer ability to resolve closely displaced delay parameters. Notice that with $K = 1$ the data matrix $\mathbf{Y}$ in (8) has unit rank and consequently $\widehat{\mathbf{R}}$ only holds a single nonzero eigenvalue. In this case we should indeed make sure that $M - M_1 + 1$ exceeds the total number of delays in the channel - otherwise there are not enough nonzero eigenvalues for ESPRIT to process. Spatial smoothing techniques are commonly employed to decorrelate coherent signal sources, see e.g. [13] and the references therein.

V. Performance Evaluation

In this section we evaluate the pilot-assisted channel estimation performance of the LMMSE estimator from [2] using Unitary ESPRIT as delay estimation tool. For all configurations considered we evaluate uncoded *bit-error-rate* (BER) performance of the OFDM system. We investigate the impact of spatial smoothing as a function of the window size M_1 and the two different channel models are treated separately. We consider a 3GPP LTE alike scenario with system parameters:

$$N = 2048,\ N_u = 1200,\ T_s = 32.55\text{ns},\ M = 200.$$

The duration of the cyclic prefix is 4.69μs, corresponding to 144 T_s-samples. A total of 14 OFDM symbols are transmitted every millisecond and four of these carry $M = 200$ pilots each. We assume the pilot symbols to be evenly positioned along the $N_u = 1200$ active subchannels with a fixed spacing of six subcarriers, i.e.

$$\mathcal{P} = \big\{3, 9, 15, \ldots, 597, 603, \ldots, 1185, 1191, 1197\big\}. \tag{9}$$

The set of pilot symbol positions $\mathcal{P}$ in (9) represents a uniform linear array of sensors with maximum overlap. The carrier frequency of the system is assumed to be $f_c = 2$GHz and we consider a receiver traveling at walking speed, i.e. the maximum Doppler frequency is assumed to be $f_D = 10$Hz. The digital modulation scheme used is QPSK (gray coded), both for data symbols and pilot symbols.

A. Performance in Static Reference Channel

As the static reference channel we employ the 3GPP EVA-profile from [5, Annex B.2] which constantly holds $L = 9$ multipath echoes with fixed delays and its maximum excess

[1] The theoretical covariance matrix in (7) is Toeplitz when the subcarrier spacings between adjacent pilots are all identical.

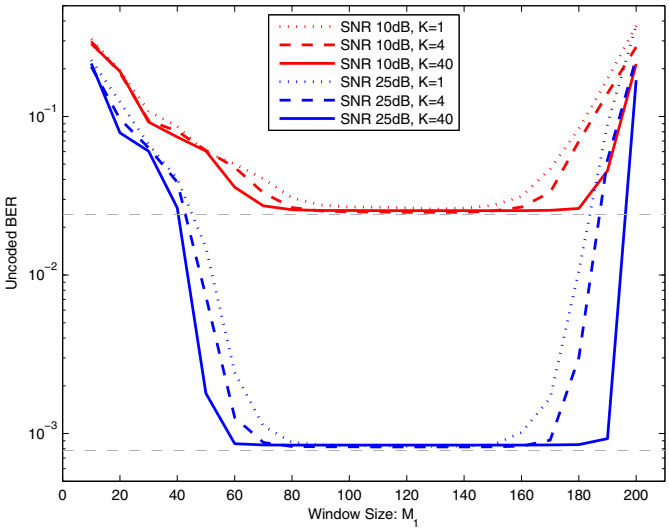

Figure 2. BER performance as a function of M_1. The two grey-dashed lines indicate the BER performance at 10dB and 25dB of *signal-to-noise ratio* (SNR) using true/known channel frequency responses.

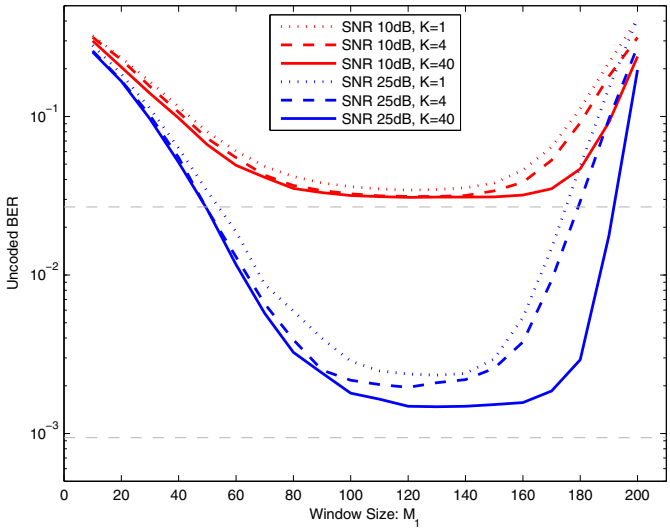

Figure 3. BER performance as a function of M_1. The two grey-dashed lines indicate the BER performance at 10dB and 25dB of SNR using true/known channel frequency responses.

delay is approximately half the duration of the cyclic prefix. To visualize how the window size M_1 impacts the overall system performance, we consider a span from $M_1 = 200$ towards $M_1 = 10$, corresponding to no smoothing and full-scale smoothing, respectively. Figure 2 reports the uncoded BER-performance of the OFDM system as a function of the window size M_1. We always feed the true number of delays (i.e. $L = 9$) directly to Unitary ESPRIT, since estimation of the number of channel echoes is not an objective in this paper. In Fig. 2, it is interesting to note that a rather wide range of window sizes are leading to the same degree of performance (near to that of using known channel coefficients). Even with $K = 1$ we realize that near-optimal performance is achievable. However, additional smoothing is required and the range of window sizes inheriting splendid performance is more tight when K is smaller. Notice also the immediate and steep performance gains obtained when M_1 decreases from its maximum value $M = 200$. This behavior partly reflects the fact that rank is building up in the covariance matrix estimate, cf. the discussion at the end of Section IV. Finally, recall that the inter-delay gaps are persistently fixed in this scenario and hence, the resolvability issues for Unitary ESPRIT to deal with are identical/constant for *all* individual channel realizations.

B. Performance in Dynamic Multipath Channel

With a channel inheriting additional dynamical behavior we now repeat the same simulation study as just described in the previous section. Hence, we wish to visualize the impact of the window size M_1 in a scenario where the delay resolvability issue is non-constant across the individual realizations of the channel. For simulation technical reasons the dynamic channel holds fifteen echoes on average[2], i.e. $L(t)$ is Poisson distributed with mean parameter equal to 15. The maximum excess delay is the same as for the static reference channel and also the power delay profile is similar to that of the static reference channel. Since $\mathbb{E}\big[L(t)\big] = 15$, then roughly anything from five to twenty-five echoes can be observed in the instantaneous realizations of the channel. In some realizations the delays will tend to cluster while in others tend to be more dispersed. As before, we feed the true number of delays to Unitary ESPRIT such that it always seeks for the instantaneous amount of channel echoes. Figure 3 illustrates how the window size M_1 affects the system performance in this case.

As can be readily seen from Fig. 3, the wide range of window sizes leading to the same degree of performance is not present anymore. The curves are still bathtub shaped, however, notably less steep and edged compared to Fig. 2. Also, none of the curves appear tight along the known channel bound as in the first case considered. This is jointly caused by the fact that more delays have to be estimated on average and since the instantaneous realizations of the channel sometimes trigger the delays more clustered. If for system design purposes we were to select and fix a single value of M_1, then based on Fig. 2, anything in the range from 90 to 150 would seem appropriate. Based on Fig. 3, however, the optimum value of M_1 seems to appear tightly around 120.

C. State-of-the-art Comparison

To get a full picture of the BER performance across a wide SNR-range we have fixed $M_1 = 120$ and conducted another simulation study. We now compare the LMMSE estimator from [2] using Unitary ESPRIT against the robustly designed state-of-the-art channel estimator from [1]. Our comparison is carried out using the dynamical channel with parameters as in the previous section. Figure 4 reports the outcome, where two selected values for K are shown, namely $K = 1$ and $K = 40$.

[2]Basically, we require $P\big(L(t) = 0\big)$ to be negligible.

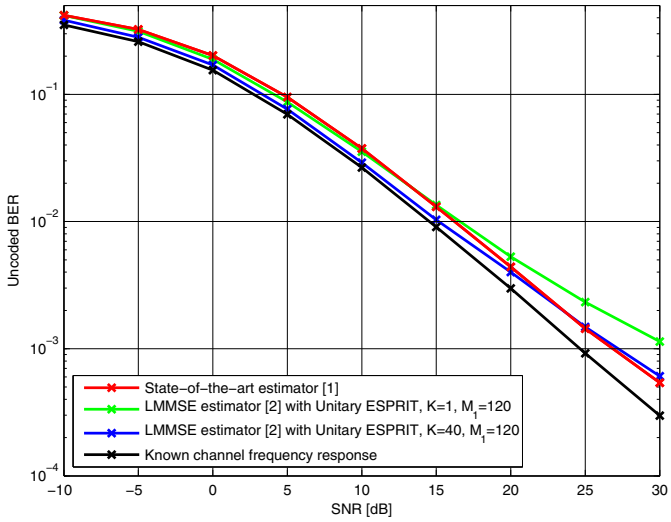

Figure 4. BER-performance as a function of average SNR.

In the SNR-range from -10dB to 15dB the state-of-the-art solution is marginally outperformed with $K = 1$. However, when using $K = 40$ the state-of-the-art solution is more notably outperformed and in a slightly wider SNR-range. That is, better or similar performance can be achieved using the LMMSE estimator from [2] together with Unitary ESPRIT. Yet, the state-of-the-art solution operates on lower computational complexity and this fact directly implies a need for complexity reductions in order to comparably gain the performance enhancements suggested in Fig. 4.

Notice from Fig. 2, where the static channel model was assumed, that a similar study as reported in Fig. 4 would conclude that the state-of-the-art solution could be notably outperformed in the entire SNR-range considered, even with $K = 1$. This follows since the BER performance in Fig. 2 with $K = 1$ and $M_1 = 120$ is almost as good as using known channel frequency responses, both at 10dB and 25dB of SNR. The point here is that the channel model selection can importantly affect the results obtained. In general, validity of the evaluated algorithm performance is achieved through adequate and comprehensive modeling.

VI. Conclusion

In this paper we have considered channel estimation techniques for pilot-aided OFDM systems, where the estimation is grounded on a parametric model of the wireless channel. The multipath delay parameters in the channel model have been estimated via the Unitary ESPRIT algorithm and spatial smoothing techniques have been applied to improve the estimation accuracy. Incorporation of the delay estimates in a LMMSE estimator allows for improved performance compared to the robustly designed state-of-the-art solution. That is, the state-of-the-art channel estimator can be outperformed over a wide SNR-range. Yet, computational complexity and estimation of the instantaneous number of channel echoes remain critical issues for the opposing channel estimator investigated.

In order to provide a rigorous performance assessment of the opposing channel estimation solution, we have compared state-of-the-art channel modeling against a refined channel model of additional dynamical nature. The main additional features comprise a time-varying number of channel echoes together with fluctuating delay positions, i.e. non-constant inter-delay gaps. From simulations we have analyzed the impact of spatial smoothing techniques when used to improve the multipath delay estimation accuracy. Our results indicate that both estimation accuracy and the optimum smoothing parameters are notably affected with increased dynamical behavior of the channel model assumed.

To conclude, our work shows that the selection of appropriate channel models is crucial when assessing the performance of receiver algorithms. Choosing inadequate models may imply misleading comprehension and could therefore yield improper algorithm selection for practical applications.

Acknowledgment

The authors would like to thank Infineon Technologies Denmark A/S and Nokia Denmark for the financial support which made this work possible. This work has been funded in part by the European Commission within the ICT-216715 FP7 Network of Excellence in Wireless Communications (NEWCOM++) and by the project ICT-217033 Wireless Hybrid Enhanced Mobile Radio Estimators (WHERE).

References

[1] O. Edfors, M. Sandell, J.-J. van de Beek, S. K. Wilson and P. O. Börjesson, "OFDM Channel Estimation by Singular Value Decomposition", *IEEE Transactions on Communications*, Vol. 46, No. 7, 1998.

[2] B. Yang, K. B. Letaief, R. S. Cheng and Z. Cao, "Channel Estimation for OFDM Transmission in Multipath Fading Channels Based on Parametric Channel Modeling", *IEEE Transactions on Communications*, 2001.

[3] J.-J. van de Beek, O. Edfors, M. Sandell, S. K. Wilson and P. O. Börjesson, "On Channel Estimation in OFDM Systems", *In Proceedings of the IEEE Vehicular Technology Conference*, Vol. 2, 1995.

[4] Y. Li, L. J. Cimini Jr. and N. R. Sollenberger, "Robust Channel Estimation for OFDM Systems with Rapid Dispersive Fading Channels", *IEEE Transactions on Communications*, Vol. 46, No. 7, 1998.

[5] "Evolved Universal Terrestrial Radio Access; Base Station Radio Transmission and Reception", *3rd Generation Partnership Project (3GPP) Technical Specification*, TS 36.104 V8.4.0, December 2008.

[6] R. Roy and T. Kailath, "ESPRIT - Estimation of Signal Parameters Via Rotational Invariance Techniques", *IEEE Transactions on Acoustics, Speech and Signal Processing*, Vol. 37, No. 7, 1989.

[7] M. Haardt and J. A. Nossek, "Unitary ESPRIT: How to Obtain Increased Estimation Accuracy with a Reduced Computational Burden", *IEEE Transactions on Signal Processing*, Vol. 43, No. 5, 1995.

[8] P. A. Bello, "Characterization of Randomly Time-Variant Linear Channels", *IEEE Transactions on Communications Systems*, 1963.

[9] A. Goldsmith, "Wireless Communications", *Cambridge University Press*, 2005.

[10] A. Abdi, J. A. Barger and M. Kaveh, "A Parametric Model for the Distribution of the Angle of Arrival and the Associated Correlation Function and Power Spectrum at the Mobile Station", *IEEE Transactions on Vehicular Technonlgy*, Vol. 51, No. 3, 2002.

[11] R. Heddergott, U. P. Bernhard and B. H. Fleury, "Stochastic Radio Channel Model For Advanced Indoor Mobile Communication Systems", *Proceedings of the 8th IEEE International Symposium on Personal, Indoor and Mobile Radio Communications*, Vol. 1, 1997.

[12] P. Stoica and R. Moses, "Spectral Analysis of Signals", *Pearson Prentice Hall*, 2005.

[13] H. Krim and M. Viberg, "Two Decades of Array Signal Processing Research: The Parametric Approach", *IEEE Signal Processing Magazine*, Vol. 13, No. 4, 1996.

Paper L

Iterative Channel Estimation with Robust Wiener Filtering in LTE Downlink

Luis A. Maestro Ruiz de Temiño, Carles Navarro Manchón, Christian Rom, Troels B. Sørensen and Preben Mogensen

IEEE 68th Vehicular Technology Conference, VTC Fall-2008. Calgary, September 2008.

L. ITERATIVE CHANNEL ESTIMATION WITH ROBUST WIENER FILTERING IN LTE DOWNLINK

Iterative Channel Estimation with Robust Wiener Filtering in LTE Downlink

Luis Ángel Maestro Ruiz de Temiño*, Carles Navarro i Manchón*, Christian Rom†,
Troels B. Sørensen* and Preben Mogensen*
*Department of Electronic Systems, Aalborg University
Niels Jernes Vej 12, 9220 Aalborg, Denmark
Email: {lam, cnm, tbs, pm}@es.aau.dk
†Infineon Technologies
Alfred Nobels Vej 25, 9220 Aalborg, Denmark
Email: christian.rom@infineon.com

***Abstract*—In this paper, an iterative enhancement of the robust Wiener filter (RWF) estimator is presented for a turbo-coded orthogonal frequency division multiplexing (OFDM) system under the umbrella of the 3GPP Long Term Evolution. The proposed scheme can operate with uncoded or coded feedback, and outperforms the conventional linear RWF in the whole signal-to-noise ratio (SNR) range with both approaches. Results show that most of the gain is obtained in the first iteration of the algorithm, and better performance is achieved with the coded feedback scheme. A good tradeoff between accuracy and complexity is achieved by selecting a low number of turbo coding iterations (TCI) in the iterative loop and concentrating most of them at the final decoding stage. Following this design, cell spectral efficiency gains of around $2.7\ \%$ and $6.5\ \%$ can be obtained with respect to linear RWF for micro- and macro-cell scenarios respectively.**

I. Introduction

Over the recent years, an increasing demand for higher data rates in wireless communications systems has arisen in order to support broadband services. To achieve such high data rates, wideband transmission over the dispersive mobile channel is required. A highly efficient way to cope with the frequency selectivity of wideband channels is orthogonal frequency division multiplexing (OFDM). In OFDM, the transmission bandwidth is divided into lower-rate narrowband orthogonal subcarriers. This, together with the employment of a proper cyclic prefix (CP), allows simple equalization of the multipath channel [1]. The ability to easily cope with multipath distortion and the high spectral efficiency has motivated the election of OFDM in upcoming wireless standards, such as the 3GPP Long Term Evolution (LTE) [2] or the IEEE 802.16e-2005 standard (WiMAX) [3]. In both standards, pilot-assisted channel estimation (PACE) is defined in order to allow coherent detection at the receiver.

When PACE is employed, pilot symbols, known by both the transmitter and the receiver, are sent in pre-defined subcarrier locations. By processing the received signal at these positions, the receiver can estimate the whole channel response for each OFDM symbol. Minimum mean-squared-error (MMSE) interpolation of the channel response has been proposed as a solution [4], known as Wiener filtering interpolation. Although it exhibits the best performance among the existing linear algorithms in literature, it requires accurate knowledge of second order channel statistics, which is not always feasible at a mobile receiver. To overcome this, a robust design of the filter can be used [5], which eases the practical implementation while still keeping an acceptable performance. To further improve the accuracy of the estimator, iterative channel estimators can be employed. In these schemes, the estimates are improved by feeding back data decisions to the channel estimation block in an iterative fashion, as done for instance in [6], [7]. However, these schemes usually suffer from a prohibitive computational complexity.

In this paper, we propose an iterative enhancement of the robust Wiener filter (RWF) in a turbo-coded OFDM system. The complexity of the scheme can be tuned by varying the number of channel estimation iterations as well as the number of iterations inside the turbo decoder. The performance of the estimator is evaluated for LTE parameters, showing that improved accuracy can be achieved while keeping the computational complexity at a reasonable level, making it suitable for practical implementation in a mobile receiver.

The remainder of the paper is organized as follows: in Section II, the considered OFDM system is described. The proposed iterative scheme is presented in Section III, and its performance is analyzed in Section IV. Finally, Section V concludes the work.

II. System Description

A simplified block diagram of the considered OFDM system, with classical linear reception, is depicted in Fig. 1. On the transmitter side, the bit stream $\mathbf{b}$ is fed to the turbo encoder block, which follows 3GPP Release 7 specifications [8]. This block contains a rate 1/3 turbo encoder, a rate matching module that performs repetition or puncturing of the coded bits depending on the selected coding rate, and a bit interleaver. The coded bits, denoted by the vector $\mathbf{c}$, are then modulated onto a QPSK, 16QAM or 64QAM constellation and pilot symbols are inserted in the data stream. These modulated symbols, both data and pilots, are mapped onto the N_u central subcarriers of the system, and an inverse fast Fourier transform (IFFT) of size N_{fft} is performed to obtain the time-domain

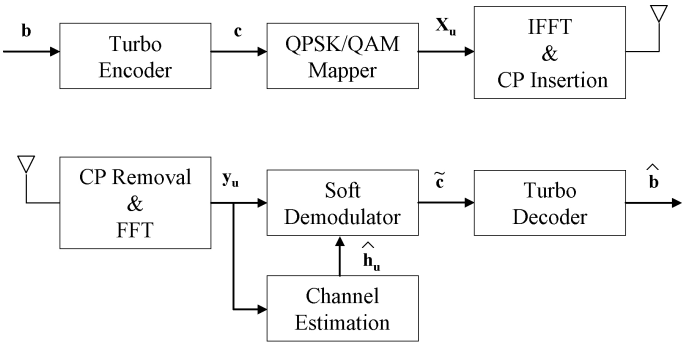

Fig. 1. Block diagram of the considered system with classical linear reception

OFDM signal. After the addition of the CP, the signal is transmitted over a wireless multipath channel characterized by its channel impulse response:

$$g(\tau,t) = \sum_{i=0}^{N_t-1} \alpha_i(t)\delta(\tau-\tau_i) \tag{1}$$

where $\alpha_i(t)$ are wide sense stationary, uncorrelated complex Gaussian random path gains at time instant *t*, with their respective delays τ_i. N_t denotes the total number of paths.

At the receiver, the CP is first discarded, and a fast Fourier transform (FFT) is performed to recover the frequency-domain signal. Assuming that the channel is static over the duration of one OFDM symbol and that the CP is longer than the maximum excess delay of the channel τ_{N_t-1}, the signal $\mathbf{y_u} \in \mathbb{C}^{N_u}$ can be described as:

$$\mathbf{y}_u = \mathbf{X}_u\mathbf{h}_u + \mathbf{w}_u \tag{2}$$

Note that the subindex u indicates that only the N_u subcarriers filled with symbols are considered. In (2), $\mathbf{X}_u \in \mathbb{C}^{N_u\times N_u}$ is a diagonal matrix containing the transmitted symbols and $\mathbf{h}_u \in \mathbb{C}^{N_u}$ is a vector with the channel transfer function (CTF) coefficients at each subcarrier:

$$\mathbf{h}_u[k] = \sum_{i=0}^{N_t-1} \alpha_i e^{\frac{-j2\pi k\tau_i}{T_0 N_{fft}}} \tag{3}$$

where k denotes the subcarrier index and T_0 denotes the sampling period. Finally, $\mathbf{w_u} \in \mathbb{C}_u^N$ is an additive white Gaussian noise vector with variance σ_w^2.

In order to recover the transmitted bits, the channel estimator block needs to obtain an estimate of $\mathbf{h}_u$, which is used by the soft demodulator to derive the soft estimates $\tilde{\mathbf{c}}$ of the coded bits. To this end, N_p pilot symbols are transmitted in some predefined subcarrier positions. The received signal in these locations can be written as:

$$\mathbf{y}_p = \mathbf{X}_p\mathbf{h}_p + \mathbf{w}_p \tag{4}$$

with $\mathbf{X}_p \in \mathbb{C}^{N_p\times N_p}$ and $(\mathbf{w}_p, \mathbf{h}_p) \in \mathbb{C}^{N_p}$ being subsets of the corresponding matrices defined in (2). Finally, the soft estimates of the coded bits pass through an iterative turbo decoder, which is based on the max-log maximum a-posteriori algorithm [9], [10], obtaining as output the hard decisions on the information bits $\hat{\mathbf{b}}$.

III. Iterative Robust Wiener Filter

In this section, we present an iterative enhancement of the RWF in which the demodulated data symbols are re-used, as if they were known, in order to improve the estimates' accuracy. The operation of the algorithm is depicted in Fig.2. In the first stage, only the pilot symbols are used to obtain the estimate of the CTF which can be expressed as:

$$\hat{\mathbf{h}}_{RWF}^{(0)} = \bar{\mathbf{R}}_{\mathbf{h}_u\mathbf{h}_p}(\bar{\mathbf{R}}_{\mathbf{h}_p\mathbf{h}_p} + \beta\cdot\sigma_w^2\cdot\mathbf{I}_p)^{-1}\hat{\mathbf{h}}_{LS,p} \tag{5}$$

where $\hat{\mathbf{h}}_{LS,p} = \mathbf{X}_p^{-1}\mathbf{y}_p \in \mathbb{C}^{N_p}$ is the least squares channel estimate in frequency-domain at pilot positions, $\beta \in \mathbb{R}$ is a constant that depends on the modulation, $\mathbf{I}_p \in \mathbb{N}^{N_p\times N_p}$ is the identity matrix and ($\bar{\mathbf{R}}_{\mathbf{h}_u\mathbf{h}_p} \in \mathbb{C}^{N_u\times N_p}, \bar{\mathbf{R}}_{\mathbf{h}_p\mathbf{h}_p} \in \mathbb{C}^{N_p\times N_p}$) are subsets of the covariance matrix $\bar{\mathbf{R}}_{\mathbf{hh}} \in \mathbb{C}^{N_{fft}\times N_{fft}}$. The latter is defined assuming a uniform power delay profile (PDP) with paths' delays uniformly distributed between 0 and τ_{N_t-1} as [5]:

$$\bar{\mathbf{R}}_{\mathbf{hh}}[k,n] = \frac{1-e^{-2\pi j\frac{\tau_{N_t-1}}{T_0}(k-n)/N_{fft}}}{2\pi j\frac{\tau_{N_t-1}}{T_0}\frac{k-n}{N_{fft}}} \tag{6}$$

The estimate of the CTF in the used subcarriers $\hat{\mathbf{h}}_{RWF}^{(0)}$ is then employed, together with the received signal, in the soft demodulator block to obtain an estimate of the transmit coded bits $\tilde{\mathbf{c}}$. Note that in this block, the pilot symbols have been removed from the information stream. If the maximum number of iterations has not been reached, the vector $\tilde{\mathbf{c}}$ is decoded using an iterative turbo decoder, with *M* turbo coding iterations (TCI), thus obtaining a hard estimate of the uncoded transmit bits $\hat{\mathbf{b}}$. Finally, the vector $\hat{\mathbf{b}}$ is re-encoded and posteriorly re-modulated to QPSK/QAM symbols in the mapper block. It is important to highlight here that this block is also responsible to re-multiplex the pilots with the data symbols in order to keep the same structure as in the received signal. This point is the end of the first stage, which is related to $i = 0$ with *i* denoting the iteration index. From this point on $(i > 0)$, all demodulated transmit symbols, both data and pilots, are used in the estimation process. Hence, it is appropriate to rewrite the estimate of the CTF for $i > 0$ as:

$$\hat{\mathbf{h}}_{RWF}^{(i)} = \bar{\mathbf{R}}_{\mathbf{h}_u\mathbf{h}_u}(\bar{\mathbf{R}}_{\mathbf{h}_u\mathbf{h}_u} + \beta\cdot\sigma_w^2\cdot\mathbf{I}_u)^{-1}(\hat{\mathbf{X}}_u)^{-1}\mathbf{y}_u \tag{7}$$

where $\hat{\mathbf{X}}_u \in \mathbb{C}^{N_u\times N_u}$ is a diagonal matrix whose elements are the estimated transmit symbols (both data and pilots).

This iterative process is repeated until the maximum number of iterations I_{max} is achieved. Then, the vector $\tilde{\mathbf{c}}$ is decoded with *N* TCI, obtaining the output bit vector $\hat{\mathbf{b}}$. It is worth mentioning the employment of a different number of TCI inside and outside the estimation loop since it will be demonstrated later that it plays an important role on the system performance.

IV. Performance Evaluation

In the following, the performance of the iterative estimator proposed in Section III will be evaluated by means of Monte Carlo simulations. To this end, a single-input single-output (SISO) downlink OFDM system based on the 10 MHz LTE physical layer parameters [11] will be considered. These

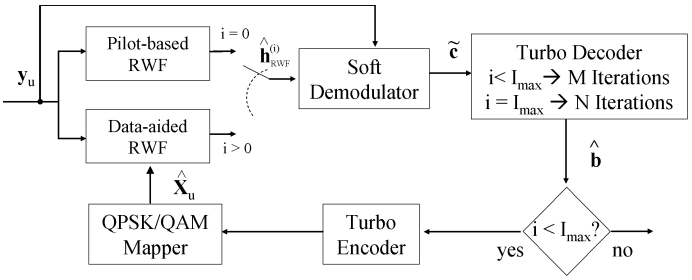

Fig. 2. Iterative RWF Block Diagram

TABLE I
SIMULATION PARAMETERS

Sampling frequency	15.36 MHz
Subcarrier spacing	15 KHz
N_{fft}	1024
N_u	600
CP length	5.2^a/4.68^b μs
Pilot spacing	6
Pilot overhead	4.76%
Slot duration	0.5 ms
OFDM symbols per slot	7
Antenna scheme	SISO
User speed	3 kmph
MCS settings	QPSK: 1/6, 1/3, 1/2, 2/3 16QAM: 1/2, 2/3, 3/4 64QAM: 1/2, 2/3, 3/4, 4/5

[a]First OFDM symbol in a slot.
[b]$2^{th} - 7^{th}$ OFDM symbol in a slot.

parameters are gathered in Table I as well as the modulation and coding set (MCS) formats employed. QPSK modulation has been considered for pilot symbols, which are transmitted in the first and fifth OFDM symbol within a slot with an even frequency-domain spacing of 6. Furthermore, Typical Urban 20 taps channel model [12] is employed in the simulations and low user speed is considered. Results are presented in terms of packet error rate (PER), spectral efficiency (bits/s/Hz) and mean squared error (MSE) of the CTF as a function of the signal-to-noise ratio (SNR).

A. Turbo Coding Iterations Evaluation

The goal of this subsection is to provide the optimum distribution of TCI inside and outside the estimation loop. Furthermore, in order not to increase the complexity at the receiver, while compared with the linear RWF, the maximum number of TCI is fixed to be $M + N = 8$. In the rest of the document, only one iteration of the algorithm has been considered since it has been observed that most of the gain is obtained in this first stage. Fig.3 depicts the average MSE in dB for the proposed iterative estimator at the end of the first iteration using QPSK $1/2$. The number of TCI inside the estimation loop (*M*) varies from 0 (uncoded feedback) to 8. For the sake of comparison, the MSE of the linear RWF

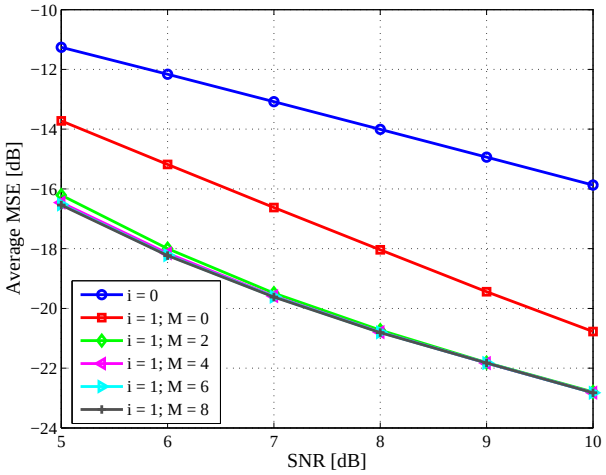

Fig. 3. Average MSE for RWF with QPSK 1/2

TABLE II
RELATIVE SPECTRAL EFFICIENCY GAINS (%)

Configuration	M=2, N=6	M=1, N=7	M=3, N=5	M=4, N=4
Relative gain	4.4	3.3	1.6	0.5

$(i = 0)$ has also been plotted. First of all, the employment of the iterative RWF allows for a reduced MSE compared to the linear algorithm. Besides, it can be observed that the estimates' accuracy is highly improved with $M = 2$ TCI since the MSE is significantly lowered. There is not appreciative gain by increasing *M* further than 2. From the results, we can conclude that it is worth employing a low number of TCI (*M*) in the inner decoding while concentrating most of them (*N*) in the last one to correct as many errors as possible.

Table II gathers the relative gains in spectral efficiency of the iterative RWF at $i = 1$ with respect to the linear estimator with different combinations of *M* and *N*. In this case, 16QAM $2/3$ has been considered as well as an operating point at $SNR = 15\ dB$. The results confirm the statement above mentioned since the configuration with $M = 2$ and $N = 6$ provides the highest gain $\sim 4.4\,\%$.

Finally, Fig. 4 depicts PER vs SNR curves for the $M = 2$, $N = 6$ configuration for two selected MCS, namely QPSK 1/2 and 16QAM 2/3. Results show that in both cases, this configuration performs slightly better than uncoded feedback ($i = 1$, $M = 0$, $N = 8$), obtaining a gain around $\sim 0.3\,dB$ at $PER = 10^{-2}$ with respect to the linear estimator ($i = 0$).

B. Spectral Efficiency Results

In this section, we extend the previous results and build the link adaptation (LA) curves for the iterative RWF. Fig. 5 presents the spectral efficiency results for: uncoded feedback, coded feedback with $M = 2$, $N = 6$ and linear RWF. The latter has been represented for comparison purposes. Results show that coded feedback with $M = 2$, $N = 6$ obtains the highest gains with respect to the linear algorithm. At

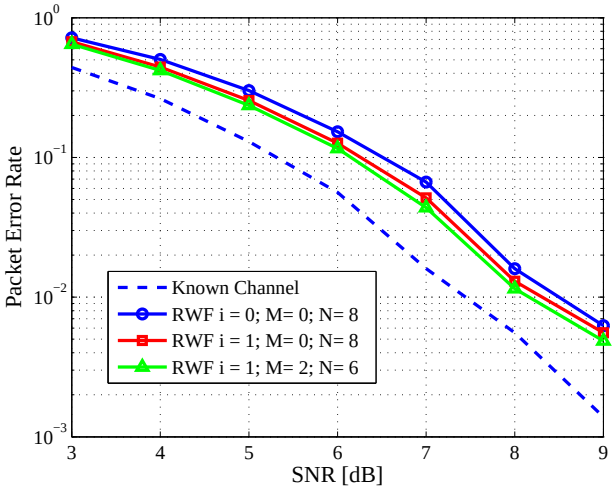

(a)

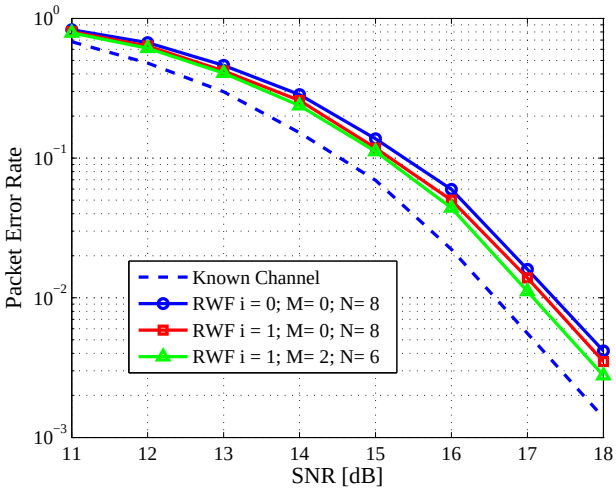

(b)

Fig. 4. Packet error rate for: (a) QPSK 1/2; and (b) 16QAM 2/3

$SNR = -2\,dB$, which corresponds to QPSK 1/6, a relative gain of $36\,\%$ in spectral efficiency is achieved. At medium SNR, e.g., $SNR = 15\,dB$ (16QAM 2/3), the gain is reduced to $4.4\,\%$ whereas at $SNR = 25\,dB$ (64QAM 4/5) it is only $1.3\,\%$. These gains are further reduced in the case of uncoded feedback, being almost negligible at low SNR. This is due to the fact that at this SNR range many errors committed in the symbols' detection are fed back to the channel estimator, which will use this wrong information as correct symbol decisions. However, we must highlight that no degradation in performance is observed, i.e., the iterative algorithm is always better than the linear one even at low SNR and considering uncoded feedback.

Finally, the LA curves are mapped to cell spectral efficiency by means of SNR distributions for macro- and micro-cell environments [13]. The relative spectral efficiency gains obtained with the iterative estimator compared to the linear one are

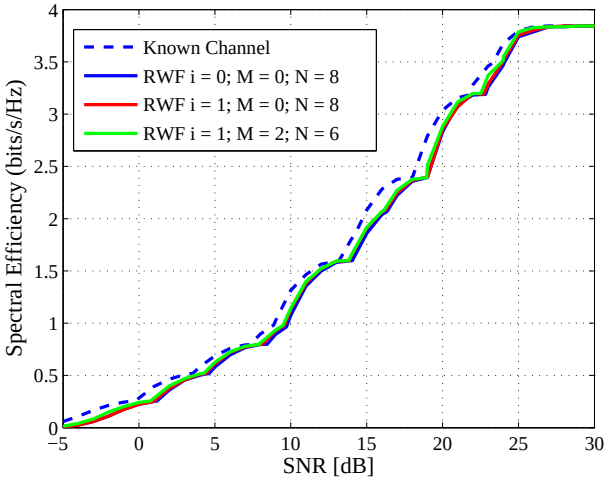

Fig. 5. Spectral efficiency curves for RWF

TABLE III
RELATIVE CELL EFFICIENCY GAINS (%)

Cell environment	M=0, N=8	M=2, N=6	M=2, N=8
Micro	0.8	2	2.7
Macro	2.2	5	6.5

presented in Table III, which also includes results for a new configuration with $M = 2$ and $N = 8$ TCI. As expected, the gains are higher for coded feedback and for macro-cell environment, since lower values of SNR are more likely to happen in this scenario and, as shown before, the iterative estimation is better exploited for medium-low SNR. Note that the $M = 2$, $N = 8$ configuration obtains the highest gains up to $6.5\,\%$ and $2.7\,\%$ in macro- and micro-cell scenarios, respectively.

C. Complexity

Regarding the complexity of the iterative approach, it has to be mentioned that each iteration of the algorithm has a complexity of the same order as the one of linear RWF. For this estimator, the main contribution to the complexity comes from the term $(\bar{\mathbf{R}}_{\mathbf{h}_u\mathbf{h}_u} + \beta \cdot \sigma_w^2 \cdot \mathbf{I}_u)^{-1}$. This matrix can be pre-calculated and stored for several scenarios, thus only one run-time matrix multiplication is required (N_u^2 complex multiplications). However, this complexity can be significantly lowered by using a low-rank reduction based on the singular value decomposition (SVD) of the channel autocovariance matrix $\bar{\mathbf{R}}_{\mathbf{h}_u\mathbf{h}_u}$ [5]. This low-rank estimator only requires $2pN_u$ multiplications where *p* is the index of the first singular value approximately equal to zero. Fig. 6 depicts the amplitude of the singular values of $\bar{\mathbf{R}}_{\mathbf{h}_u\mathbf{h}_u}$ for different channel profiles. Note that in scenarios with long maximum path delay, such as the exponential decaying profile (EDP) with $\tau_{N_t-1} = 17\ \mu s$, the number of singular values with significant amplitude becomes larger; therefore, the number of required multiplications (complexity) increases. Table IV

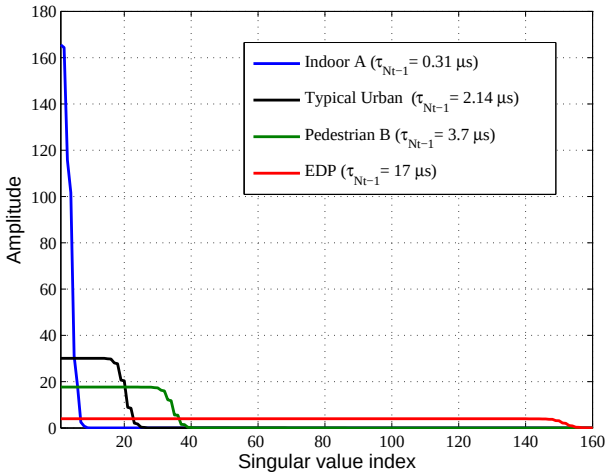

Fig. 6. SVD of $\bar{\mathbf{R}}_{\mathbf{h}_u\mathbf{h}_u}$ in 10 MHz

TABLE IV
COMPLEXITY REDUCTION (%)

Channel profile	Selected p	Complexity reduction
Indoor A	10	97
Typical Urban	28	91
Pedestrian B	40	87
EDP	160	47

summarizes the complexity reduction achieved by means of the low-rank estimator with respect to the full-rank RWF. This reduction is strictly dependant on the length of the channel considered, being up to $97\,\%$ for Indoor A profile.

V. CONCLUSION

In this work, we have proposed an iterative enhancement of the RWF estimator with relatively low complexity. It has been seen that most of the gain is obtained in the first iteration for both uncoded and coded feedback. Even though the latter is shown to provide the best results, both approaches improve the performance with respect to the linear estimator for all the SNR range. The optimal combination of TCI among the inner and outer turbo decoding has been investigated fixing a total number of $M + N = 8$ for complexity constraints. Results show that selecting $M = 2$ and $N = 6$, relative spectral efficiency gains up to $36\,\%$ can be obtained compared to the linear RWF. Furthermore, by slightly increasing the number of TCI in the last decoding to $N = 8$, cell spectral efficiency gains of $2.7\,\%$ and $6.5\,\%$ are achievable over linear RWF for micro- and macro-cell environments, respectively. Finally, using a low-rank estimator based on the SVD decomposition of the channel autocovariance matrix, the complexity can be significantly reduced, especially for channels with short maximum excess delay.

REFERENCES

[1] L. Hanzo, M. Munster, B. Choi, and T. Keller, *OFDM and MC-CDMA for Broadband MultiUser Communications, WLANs and Broadcasting*. John Wiley - IEEE Press, 2003.

[2] "Evolved Universal Terrestrial Radio Access (E-UTRA); LTE Physical Layer - General Description," 3rd Generation Partnership Project, Tech. Rep. TS 36.201, V8.1.0, Nov. 2007.

[3] *IEEE Standard for Local and metropolitan area networks Part 16: Air Interface for Fixed and Mobile Broadband Wireless Access Systems Amendment 2: Physical and Medium Access Control Layers for Combined Fixed and Mobile Operation in Licensed Bands and Corrigendum 1*, IEEE Std. 802.16e-2005, 2006.

[4] P. Hoeher, S. Kaiser, and P. Robertson, "Two-dimensional pilot-symbol-aided channel estimation by wiener filtering," *Acoustics, Speech, and Signal Processing, 1997. ICASSP-97., 1997 IEEE International Conference on*, vol. 3, pp. 1845–1848 vol.3, 21-24 Apr 1997.

[5] O. Edfors, M. Sandell, J. van de Beek, and S. Wilson, "OFDM channel estimation by singular value decomposition," *IEEE Transactions on Communications*, vol. 46, no. 7, pp. 931–939, July 1998.

[6] S. ten Brink, F. Sanzi, and J. Speidel, "Two-dimensional iterative APP channel estimation and decoding for OFDM systems," *Global Telecommunications Conference, 2000. GLOBECOM '00. IEEE*, vol. 2, pp. 741–745 vol.2, 2000.

[7] S. Y. Park, Y. G. Kim, and C. G. Kang, "Iterative receiver for joint detection and channel estimation in OFDM systems under mobile radio channels," *Vehicular Technology, IEEE Transactions on*, vol. 53, no. 2, pp. 450–460, March 2004.

[8] "Evolved Universal Terrestrial Radio Access (E-UTRA); Multiplexing and channel coding (FDD)," 3rd Generation Partnership Project, Tech. Rep. TS 25.212, V7.6.0, Sep. 2007.

[9] W. Koch and A. Baier, "Optimum and sub-optimum detection of coded data disturbed by time-varying inter-symbol interference," *IEEE Globecom*, pp. 1679–1684, Dec. 1990.

[10] A. Erfanian, S. Pasupathy, and G. Gulak, "Reduced complexity symbol detectors with parallel structures for ISI channels," *IEEE Transactions on Communications*, vol. 42, no. 4, pp. 1661–1671, April 1994.

[11] "Evolved Universal Terrestrial Radio Access (E-UTRA); Physical Channels and Modulation," 3rd Generation Partnership Project, Tech. Rep. TS 36.211, V8.1.0, Nov. 2007.

[12] "Technical Specification Group Radio Access Networks; deployment aspects," 3rd Generation Partnership Project, Tech. Rep. TR 25.943, V7.0.0, Jun. 2007.

[13] I. Z. Kovacs, K. I. Pedersen, J. Wigard, F. Frederiksen, and T. E. Kolding, "HSDPA performance in mixed outdoor-indoor micro cell scenarios," *IEEE International Symposium on Personal, Indoor and Mobile Radio Communications*, pp. 1–5, Sept. 2006.

Paper M

Unification of Frequency Direction Pilot-Symbol Aided Channel Estimation (PACE) for OFDM

Christian Rom, Carles Navarro Manchón, Luc Deneire, Troels B. Sørensen and Preben Mogensen

10th International Symposium on Wireless Personal Multimedia Communications, WPMC 2007. Jaiupur, December 2007.

M. UNIFICATION OF FREQUENCY DIRECTION PILOT-SYMBOL AIDED CHANNEL ESTIMATION (PACE) FOR OFDM

Unification of Frequency Direction PACE Algorithms for OFDM

Christian Rom*, Carles Navarro Manchón*, Luc Deneire*,+,
Troels Bundgaard Sørensen*, Preben Mogensen*
∗ department of Electronic Systems, Aalborg University, Aalborg, Denmark
+ I3S, Université de Nice Sophia-Antipolis, CNRS, Sophia-Antipolis, France

***Abstract*— Frequency direction Pilot-symbol Aided Channel Estimation (PACE) for Orthogonal Frequency Division Multiplexing (OFDM) is crucial in high-rate wireless systems. The choice of an estimator for upcoming standards, such as the Long Term Evolution (LTE) of UTRA, has to take into account their specificities, namely the presence of virtual subcarriers and non-sample-spaced channels. To ease this choice, we propose a unified presentation of estimators encompassing most of the algorithms that can be found in literature, which only differ by the assumptions made on the channel. This unification leads to common Mean Squared Error (MSE) expression, both for sample-spaced and non sample-spaced channels, and enables easy, yet comprehensive comparisons between the estimators.**

I. Introduction

In the frame of OFDM for upcoming wireless systems, much attention has been given to pilot-based channel estimators (PACE) showing that the performance tradeoff of the algorithms depends on the relationship between the Power Delay Profile (PDP) properties and the frequency-domain pilot spacing. Deterministic approaches have, so far, been separated into time- and frequency-domain solutions. Deterministic time-domain solutions are: the Time-Domain Least Squares (TDLS) [3], [4], the Maximum Likelihood (ML) approach [5], [6] and the Noise Reduction Algorithm (NRA) [7]. Deterministic frequency-domain methods are Spline, Gaussian or Lagrange interpolation, and require higher pilot overhead to achieve an acceptable performance [8]. Bayesian approaches such as the Minimum Mean Squared Error (MMSE) estimator in time domain and/or frequency domain have been proposed in [2], [3], with complexity reduction by Singular Value Decomposition (SVD) suggested in [9].

The major contribution of this paper is to provide a framework for the choice of a channel estimation algorithm for the upcoming PACE OFDM-based standards. In this study we derive a uniform algorithm and Mean Squared Error (MSE) formulation, covering all studied algorithms and thereby facilitating a generic performance comparison. Three main effects will be studied: the impact of a priori knowledge in a full bandwidth system with a SS channel, the effect of virtual subcarriers and the effect of a NSS channel. Performance simulations are conducted in a LTE context and will show the importance of knowing the exact tap delays, for the studied algorithms, at the receiver in order to avoid the leakage effect due to NSS channel.

II. Analytical Model

A. Multipath Channel Model

The OFDM signal is transmitted over a block fading normalized multipath Rayleigh channel with a Channel Impulse Response (CIR) given by:

$$g(\tau) = \sum_{i=0}^{N-1} a_i \delta(\tau - \tau_i) \text{ with } \sum_{i=0}^{N-1} \mathrm{E}\{|a_i|^2\} = 1 \quad (1)$$

where a_i are the different wide sense stationary, uncorrelated complex Gaussian random path gains with their corresponding time delays τ_i, N is the number of paths and τ_{N-1} is assumed to be smaller than the cyclic prefix.

B. Baseband Model

Due to spectral constraints, many multicarrier systems make use of only a subset of $N_u < N_{fft}$ subcarriers, leaving unused the $N_{fft} - N_u$ remaining ones, usually placed at the edges of the transmission bandwidth. The latter are the so-called virtual subcarriers, and this scenario will be referred to as Partial Bandwidth, where N_{fft} is the FFT size. In such a context, the received signal at the used subcarriers can be described by:

$$\mathbf{y}_u = \mathbf{D}_u \mathbf{h}_u + \mathbf{w}_u = \mathbf{D}_u \mathbf{F}_u \mathbf{g} + \mathbf{w}_u \quad (2)$$

where the (frequency) Channel Transfer Function (CTF) at the used subcarrier positions $\mathbf{h}_u \in \mathbb{C}^{N_u}$ is:

$$\mathbf{h}_u = \mathbf{F}_u \mathbf{g} \quad (3)$$

$\mathbf{D}_u \in \mathbb{C}^{N_u \times N_u}$ is a diagonal matrix with the transmitted symbols at the used subcarriers, $\mathbf{w}_u \in \mathbb{C}^{N_u}$ is the AWGN vector corresponding to the used subcarriers, and $\mathbf{F}_u \in \mathbb{C}^{N_u \times N_{fft}}$ is a subset of the Fourier matrix $\mathbf{F}$ with $\mathbf{F}_u[k,n] = \mathbf{F}[k,n] = e^{-j2\pi \frac{nk}{N_{fft}}}$ for $\frac{-N_u}{2} \leq k \leq \frac{N_u}{2} - 1$.

C. Received Signal at Pilot Subcarriers

N_p pilot symbols are transmitted in positions $\{p_m,\ 0 \leq m \leq N_p - 1\}$. The received signal in these pilot subcarriers can be then written as:

$$\mathbf{y}_p = \mathbf{D}_p \mathbf{h}_p + \mathbf{w}_p = \mathbf{D}_p \mathbf{F}_p \mathbf{g} + \mathbf{w}_p \quad (4)$$

$\mathbf{D}_p \in \mathbb{C}^{N_p \times N_p}$, $\mathbf{h}_p \in \mathbb{C}^{N_p}$, $\mathbf{F}_p \in \mathbb{C}^{N_p \times N_{fft}}$ and $\mathbf{w}_p \in \mathbb{C}^{N_p}$ with $\mathbf{D}_p[m,m] = \mathbf{D}_u[p_m, p_m]$, $\mathbf{h}_p[m] = \mathbf{h}_u[p_m]$, $\mathbf{F}_p[m,n] = \mathbf{F}_u[p_m, n]$ and $\mathbf{w}_p[m] = \mathbf{w}_u[p_m]$.

III. Channel Estimation Algorithms

The initial Least Squares (LS) estimate at the pilots is :

$$\mathbf{h}_{ls} = \mathbf{D}_p{}^{-1}\mathbf{y}_p = \mathbf{h}_p + \mathbf{D}_p{}^{-1}\mathbf{w}_p \quad (5)$$

The pilot symbols are M-PSK modulated with unit power and the number of pilot symbols used N_p is assumed to be larger than the normalized maximum delay of the channel.In the following, at sampling rate τ_s, two scenarios are considered:

Case 1 A SS-CIR scenario, where it is assumed that the delays τ_i are sample spaced on the same grid as the receiver and all $\frac{\tau_i}{\tau_s}$ are integer values.

Case 2 A NSS-CIR scenario, where it is assumed that the delays τ_i are not sample spaced on the same grid as the receiver and some $\frac{\tau_i}{\tau_s}$ are not integer values.

A. Sample-Spaced Channel

The different studied algorithms can be written in the following generic formula:

$$\mathbf{h}_{est} = \mathbf{F}_{ux}\mathbf{g}_{est} = \mathbf{F}_{ux}\mathbf{M}_{est}\mathbf{h}_{ls} \quad (6)$$

which will be specified for each estimator.

1) Time-Domain Least Squares: This estimator [3], [4] assumes no a priori knowledge of the channel, and estimates $N_x = N_p$ samples of $\mathbf{g}$, corresponding to $\mathbf{g}_p[n] = \mathbf{g}[n]$ for $0 \leq n \leq N_p - 1$. The formulation of TDLS is:

$$\mathbf{h}_{tdls} = \mathbf{F}_{up}\mathbf{g}_{tdls} = \mathbf{F}_{up}\mathbf{F}_{pp}^{-1}\mathbf{h}_{ls} \quad (7)$$

where $\mathbf{F}_{pp} \in \mathbb{C}^{\mathbf{N}_p \times \mathbf{N}_p}$ and $\mathbf{F}_{up} \in \mathbb{C}^{\mathbf{N}_u \times \mathbf{N}_p}$ correspond, respectively, to $\mathbf{F}_{pp}[m,n] = \mathbf{F}_p[m,n]$ and $\mathbf{F}_{up}[k,n] = \mathbf{F}_u[k,n]$ for $0 \leq n \leq N_p - 1$. For the TDLS estimator, then, $\mathbf{M}_{est} = \mathbf{F}_{pp}^{-1}$. Note that $\mathbf{F}_{pp}$ is always invertible due to the Vandermonde structure of the DFT matrix [4]; however, in a Partial Bandwidth scenario, this matrix can become ill-conditioned depending on the number of virtual subcarriers.

2) Maximum Likelihood: The ML estimator [5], [6], assumes that the receiver knows the CIR length, i.e, the last channel path's delay τ_{N-1}, and only estimates the $N_x = N_s = \frac{\tau_{N-1}}{\tau_s} + 1$ first samples of the SS-CIR, corresponding to $\mathbf{g}_s[n] = \mathbf{g}[n]$ for $0 \leq n \leq N_s - 1$. The ML estimator is expressed as:

$$\mathbf{h}_{ml} = \mathbf{F}_{us}\mathbf{g}_{ml} = \mathbf{F}_{us}(\mathbf{F}_{ps}^H\mathbf{F}_{ps})^{-1}\mathbf{F}_{ps}^H\mathbf{h}_{ls} \quad (8)$$

where $\mathbf{F}_{ps} \in \mathbb{C}^{\mathbf{N}_p \times \mathbf{N}_s}$ and $\mathbf{F}_{us} \in \mathbb{C}^{\mathbf{N}_u \times \mathbf{N}_s}$ correspond, respectively, to $\mathbf{F}_{ps}[m,n] = \mathbf{F}_p[m,n]$ and $\mathbf{F}_{us}[k,n] = \mathbf{F}_u[k,n]$ for $0 \leq n \leq N_s - 1$. In this case, $\mathbf{M}_{est} = (\mathbf{F}_{ps}^H\mathbf{F}_{ps})^{-1}\mathbf{F}_{ps}^H$. Similarly to the case of the TDLS estimator, the matrix $\mathbf{F}_{ps}$ is always of full column rank (for $N_p \geq N_s$), implying that $\mathbf{F}_{ps}^H\mathbf{F}_{ps}$ is of full rank. However, in the presence of virtual subcarriers this matrix can become ill-conditioned, as for the TDLS estimator.

3) Noise Reduction Algorithm : As a solution to the ill-conditioning problems [11] of the previous estimators, a small value can be added to the diagonal of the matrix to be inverted [7], thus avoiding numerical instability :

$$\mathbf{h}_{nra} = \mathbf{F}_{us}\mathbf{g}_{nra} = \mathbf{F}_{us}(\mathbf{F}_{ps}^H\mathbf{F}_{ps} + \gamma_{nra}\mathbf{I}_s)^{-1}\mathbf{F}_{ps}^H\mathbf{h}_{ls} \quad (9)$$

where $\mathbf{I}_s$ is the identity matrix of size N_s, and γ_{nra} is a positive scalar value. From (9), it follows that $\mathbf{M}_{est} = (\mathbf{F}_{ps}^H\mathbf{F}_{ps} + \gamma_{nra}\mathbf{I}_s)^{-1}\mathbf{F}_{ps}^H$. In a Full Bandwidth scenario with evenly spaced pilot subcarriers, it can be shown that the optimum value is $\gamma_{nra} = N_s\sigma_w^2$.

4) Enhanced Noise Reduction Algorithm : The Enhanced Noise Reduction Algorithm (ENRA) differs from the NRA by only estimating the $N_x = N_t$ samples of $\mathbf{g}$ which are not null, i.e., $\mathbf{g}_t[n] = \mathbf{g}[\tau_n/\tau_s]$ for $0 \leq n \leq N_t - 1$. Therefore, the knowledge of the number of paths and their corresponding delays is required. The estimator is given by:

$$\mathbf{h}_{enra} = \mathbf{F}_{ut}\mathbf{g}_{enra} = \mathbf{F}_{ut}(\mathbf{F}_{pt}^H\mathbf{F}_{pt} + \gamma_{enra}\mathbf{I}_t)^{-1}\mathbf{F}_{pt}^H\mathbf{h}_{ls} \quad (10)$$

where $\mathbf{F}_{pt} \in \mathbb{C}^{\mathbf{N}_p \times \mathbf{N}_t}$ and $\mathbf{F}_{us} \in \mathbb{C}^{\mathbf{N}_u \times \mathbf{N}_t}$ correspond, respectively, to $\mathbf{F}_{pt}[m,n] = \mathbf{F}_p[m,\tau_n/\tau_s]$ and $\mathbf{F}_{ut}[k,n] = \mathbf{F}_u[k,\tau_n/\tau_s]$ for $0 \leq n \leq N_t - 1$. $\mathbf{I}_t$ denotes the identity matrix of size N_T. Hence, for the ENRA $\mathbf{M}_{est} = (\mathbf{F}_{pt}^H\mathbf{F}_{pt} + \gamma_{enra}\mathbf{I}_t)^{-1}\mathbf{F}_{pt}^H$. Analogously to the NRA, the value $\gamma_{enra} = N_t\sigma_w^2$ is optimum in a Full Bandwidth with equally spaced pilots scenario.

5) Wiener Filter: The Wiener filter (WF) estimator minimizes the MSE of the estimate by making use of channel and noise correlation properties, and has been broadly treated in literature [2], [9], [10], [12]. It is classically formulated as:

$$\mathbf{h}_{wf} = \mathbf{R}_{\mathbf{h}_u\mathbf{h}_p}(\mathbf{R}_{\mathbf{h}_p\mathbf{h}_p} + \sigma_w^2\mathbf{I}_p)^{-1}\mathbf{h}_{ls} \quad (11)$$

where $\mathbf{R}_{\mathbf{h}_u\mathbf{h}_p} = \mathrm{E}\{\mathbf{h}_u\mathbf{h}_p^H\}$ is the correlation matrix of $\mathbf{h}_u$ and $\mathbf{h}_p$, $\mathbf{R}_{\mathbf{h}_p\mathbf{h}_p} = \mathrm{E}\{\mathbf{h}_p\mathbf{h}_p^H\}$ is the autocorrelation matrix of $\mathbf{h}_p$, and $\mathbf{I}_p$ is the identity matrix of size N_p. In the sample spaced case, it leads to:

$$\mathbf{h}_{wf} = \mathbf{F}_{ut}\mathbf{g}_{wf} = \mathbf{F}_{ut}(\mathbf{F}_{pt}^H\mathbf{F}_{pt} + \sigma_w^2\mathbf{R}_{\mathbf{g}_t\mathbf{g}_t}^{-1})^{-1}\mathbf{F}_{pt}^H\mathbf{h}_{ls} \quad (12)$$

For WF, $\mathbf{M}_{est} = (\mathbf{F}_{pt}^H\mathbf{F}_{pt} + \sigma_w^2\mathbf{R}_{\mathbf{g}_t\mathbf{g}_t}^{-1})^{-1}\mathbf{F}_{pt}^H$.

Note that when no information about the channel correlation is available, a robust design of the filter is proposed, and consists of assuming a sample-spaced PDP with N_s samples and equal mean power in all taps. In such conditions $\mathbf{F}_{ut} = \mathbf{F}_{us}$, $\mathbf{F}_{pt} = \mathbf{F}_{ps}$ and $\mathbf{R}_{\mathbf{g}_t\mathbf{g}_t} = \frac{1}{N_s}\mathbf{I}_s$, showing that this robust WF implementation is equivalent to the NRA given in (9).

6) Generic Formulation: When observing the expressions of the studied algorithms, a general formulation that covers all the cases can be given by:

$$\mathbf{h}_{est} = \mathbf{F}_{ux}\mathbf{g}_{est} = \mathbf{F}_{ux}(\mathbf{F}_{px}^H\mathbf{F}_{px} + \gamma_{est}\mathbf{C}_{\mathbf{est}})^{-1}\mathbf{F}_{px}^H\mathbf{h}_{ls} \quad (13)$$

An overview over the specific values taken by each element of (13) is given in Table 1.

Table 1: Generalization of the algorithms

Estimator	$\mathbf{F}_{ux}$	$\mathbf{F}_{px}$	γ_{est}	$\mathbf{C}_{\mathbf{est}}$	$\mathbf{g}_x$	N_{est}
TDLS	$\mathbf{F}_{up}$	$\mathbf{F}_{pp}$	0	0	$\mathbf{g}_p$	N_p
ML	$\mathbf{F}_{us}$	$\mathbf{F}_{ps}$	0	0	$\mathbf{g}_s$	N_s
NRA	$\mathbf{F}_{us}$	$\mathbf{F}_{ps}$	$N_s\sigma_w^2$	$\mathbf{I}_s$	$\mathbf{g}_s$	N_s
ENRA	$\mathbf{F}_{ut}$	$\mathbf{F}_{pt}$	$N_t\sigma_w^2$	$\mathbf{I}_t$	$\mathbf{g}_t$	N_t
WF	$\mathbf{F}_{ut}$	$\mathbf{F}_{pt}$	σ_w^2	$\mathbf{R}_{\mathbf{g}_t\mathbf{g}_t}^{-1}$	$\mathbf{g}_t$	N_t

7) MSE of the Estimators: The different studied estimators are all described by (6). It is then possible to evaluate their respective performance by using one single generic MSE expression. The MSE is calculated as:

$$\mathbf{MSE}\{\mathbf{h}_{est}[k]\} = \mathrm{E}\{|\mathbf{h}_u[k] - \mathbf{h}_{est}[k]|^2\} \tag{14}$$

Using (6), the MSE for the k^{th} subcarrier becomes:

$$\mathbf{MSE}\{\mathbf{h}_{est}[k]\} = \mathbf{Q}[k,k] \tag{15}$$

where

$$\begin{aligned}\mathbf{Q} &= \mathbf{F}_{ux}[(\mathbf{I} - \mathbf{M}_{est}\mathbf{F}_{px})\mathbf{R}_{\mathbf{g}_x\mathbf{g}_x}(\mathbf{I} - \mathbf{F}_{px}^H\mathbf{M}_{est}^H) \\ &+ \sigma_w^2\mathbf{M}_{est}\mathbf{M}_{est}^H]\mathbf{F}_{ux}^H\end{aligned} \tag{16}$$

Note that $\mathbf{R}_{\mathbf{g}_x\mathbf{g}_x} = \mathrm{E}\{\mathbf{g}_x\mathbf{g}_x^H\}$ depends on the a priori assumptions made by each estimator. The average MSE of the estimator can consequently be defined as:

$$\overline{\mathbf{MSE}}\{\mathbf{h}_{est}\} = \frac{1}{\mathrm{N}_u}\mathrm{tr}\{\mathbf{Q}\} \tag{17}$$

In a Full Bandwidth ($N_u = N_{fft}$) scenario with a constant pilot spacing $\Delta_p = \frac{N_{fft}}{N_p}$, the products between the DFT-based matrices become diagonal matrices, and it is easy to simplify (16). Under such conditions, the MSE of the estimate becomes independent on the subcarrier index k. For the estimators which do not assume any knowledge of the mean power of the paths (TDLS, ML, NRA and ENRA), the MSE reduces to the generic expression:

$$\overline{\mathbf{MSE}}\{\mathbf{h}_{est,full}\} = \frac{\gamma_{est}^2 + N_xN_p\sigma_w^2}{(N_p + \gamma_{est})^2}. \tag{18}$$

B. Non-Sample-Spaced Channel

In an NSS scenario, there is at least one path of the channel with a delay τ_i which is not an integer multiple of the sampling period τ_s. In this situation, the i^{th} column of the leakage matrix $\mathbf{L}$ [1] will have non zero values for every element, i.e., $\mathbf{L}[n,i] \neq 0\ \forall n$. $\mathbf{a}$ is the vector of size N_t containing only the channel taps. As a consequence, the complex gain of the i^{th} path will have a contribution on all the samples of the equivalent SS-CIR. Fig. 1 illustrates how NSS paths are mapped to the equivalent SS-CIR for a simple example where $N_{fft} = 64$ and the channel is $g(\tau) = 0.8\delta(\tau - 0.5\tau_s) + 0.5\delta(\tau - 3.5\tau_s) + 0.3\delta(\tau - 7.5\tau_s)$. As can be seen, most of the power of each path is mapped to the surrounding samples in the SS-CIR. It is especially interesting how the last samples have significant amplitude, due to the leakage of the first channel paths.

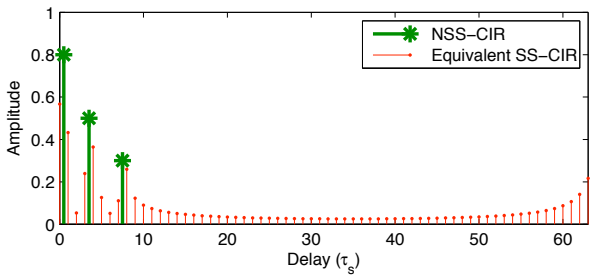

Fig. 1. Leakage of the NSS-CIR paths to the equivalent SS-CIR

The estimators studied in the sample-spaced case rely on the fact that most of the samples of $\mathbf{g}$ are zero, and thus they can be canceled in the estimation problem. Obviously, this assumption does not hold any more in the NSS scenario, and the estimators must be modified accordingly. Due to the ill-condition problems of the TDLS and ML estimators, only NRA, ENRA and WF will be considered in the following.

1) Modified NRA: The NRA algorithm for SS channel is based on the knowledge of the CIR length, i.e., the maximum excess delay of the channel, so that every sample of $\mathbf{g}$ beyond this value is assumed to be zero. For the NSS scenario, however, the length of the SS-CIR is N_{fft} due to the leakage effect, which will cause a performance degradation if $N_p < N_{fft}$. Since the actual path delays are considered unknown, the selection of the samples to estimate can only be approximated: it is expected that they will be concentrated at the beginning and at the end of the SS-CIR. Therefore, a suboptimal solution to the problem, provided that no knowledge of the actual channel paths is available, is given by the Modified NRA, (MNRA), which is formulated as:

$$\begin{aligned}\mathbf{h}_{mnra} &= \mathbf{F}_{um}\mathbf{g}_{mnra} \\ &= \mathbf{F}_{um}(\mathbf{F}_{pm}^H\mathbf{F}_{pm} + \gamma_{mnra}\mathbf{I}_m)^{-1}\mathbf{F}_{pm}^H\mathbf{h}_{ls}\end{aligned} \tag{19}$$

where the matrix $\mathbf{F}_{um} \in \mathbb{C}^{N_u \times N_m}$ is defined as:

$$\mathbf{F}_{um}[k,n] = \begin{cases} \mathbf{F}_u[k,n], & 0 \leq n \leq \lceil N_m(1-\alpha)\rceil - 1 \\ \mathbf{F}_u[k, N_{fft} - N_m + n], & \lceil N_m(1-\alpha)\rceil \leq n \leq N_m - 1 \end{cases} \tag{20}$$

and $\mathbf{F}_{pm} \in \mathbb{C}^{N_p \times N_u}$ is defined analogously with respect to $\mathbf{F}_p$. $\mathbf{I}_m$ is the identity matrix of size N_m. Furthermore, the parameter γ_{mnra} is selected to be $\gamma_{mnra} = N_m\sigma_w^2$, analogously to the sample-spaced case.

Two parameters shall be adapted depending on the PDP and σ_w^2: N_m representing the number of samples of the equivalent SS-CIR to estimate, and α representing the proportion of the estimated samples in the final part of the SS-CIR.

2) ENRA and Wiener Filter: When using the ENRA or the Wiener Filter estimator, it is assumed that the delays of the channel are perfectly known, so that there is no need to estimate the equivalent SS-CIR. Instead, the parameters

[1] The relationship between $\mathbf{g}$ and $\mathbf{a}$ can be found to be: $\mathbf{g} = \frac{1}{N_{fft}}\mathbf{F}^H\mathbf{T}\mathbf{a} = \mathbf{L}\mathbf{a}$ where $\mathbf{T}[k,i] = e^{-j2\pi\frac{k}{N_{fft}}\frac{\tau_i}{\tau_s}}$ and $\mathbf{L}[n,i] = \frac{1}{N_{fft}}\frac{sin(\pi\frac{\tau_i}{\tau_s})}{sin(\frac{-\pi}{N_{fft}}(n-\frac{\tau_i}{\tau_s}))}e^{-j\frac{\pi}{N_{fft}}((N_{fft}-1)\frac{\tau_i}{\tau_s}+n)}$, $\mathbf{L} \in \mathbb{C}^{N_{fft}\times N}$ is the *leakage* matrix, and represents how the complex gain a_i of each channel path is mapped to the SS-CIR.

to estimate are the complex gains a_i of each of the paths, represented by the vector $\mathbf{a}$. The estimators can be rewritten for the NSS scenario as:

$$\mathbf{h}_{enra} = \mathbf{T}_u \mathbf{a}_{enra} = \mathbf{T}_u (\mathbf{T}_p^H \mathbf{T}_p + \gamma_{enra} \mathbf{I}_t)^{-1} \mathbf{T}_p^H \mathbf{h}_{ls} \quad (21)$$

$$\mathbf{h}_{wf} = \mathbf{T}_u \mathbf{a}_{wf} = \mathbf{T}_u (\mathbf{T}_p^H \mathbf{T}_p + \sigma_w^2 \mathbf{R}_{aa}^{-1}) \mathbf{T}_p^H \mathbf{h}_{ls} \quad (22)$$

where the matrices $\mathbf{T}_u \in \mathbb{C}^{N_u \times N_t}$ and $\mathbf{T}_p \in \mathbb{C}^{N_p \times N_t}$ are defined with respect to $\mathbf{T}$ in the same way as $\mathbf{F}_u$ and $\mathbf{F}_p$ with respect to $\mathbf{F}$. As in the SS case, $\gamma_{enra} = \sigma_w^2 N_t$, and $\mathbf{R}_{aa} \in \mathbb{C}^{N_t \times N_t}$ is the correlation matrix of the channel gains, i.e, $\mathbf{R}_{aa} = \text{diag}\{\text{E}\{|a_0|^2\}, \ldots, \text{E}\{|a_{N_t-1}|^2\}\}$ as we assume i.i.d. channel taps. It can be seen that these definitions of the ENRA and WF estimator are equivalent to (10) and (12) when the channel is restricted to be sample-spaced.

3) MSE of the Estimators: Unlike the SS scenario, it is difficult to find a general expression that includes all the studied algorithms for an NSS channel. For this reason, we will study the performance of a generic estimator such as:

$$\mathbf{h}_{est} = \mathbf{M}_{est} \mathbf{h}_{ls} \quad (23)$$

which includes any linear estimator that can be expressed in matrix form. With this formulation, the MSE over an NSS channel is:

$$\begin{aligned} \overline{\mathbf{MSE}}\{\mathbf{h}_{est}\} = \tfrac{1}{\mathbf{N}_u} \text{tr} \Big\{ & \mathbf{T}_u \mathbf{R}_{aa} \mathbf{T}_u^H \\ & - \mathbf{T}_u \mathbf{R}_{aa} \mathbf{T}_p^H \mathbf{M}_{est}^H - \mathbf{M}_{est} \mathbf{T}_p \mathbf{R}_{aa} \mathbf{T}_u^H \\ & + \mathbf{M}_{est} \mathbf{T}_p \mathbf{R}_{aa} \mathbf{T}_p^H \mathbf{M}_{est}^H + \sigma_w^2 \mathbf{M}_{est} \mathbf{M}_{est}^H \Big\} \end{aligned} \quad (24)$$

and the specific values of $\mathbf{M}_{est}$ for each studied algorithm are:

$$\mathbf{M}_{est} = \begin{cases} \mathbf{F}_{um} (\mathbf{F}_{pm}^H \mathbf{F}_{pm} + \gamma_{mnra} \mathbf{I}_m)^{-1} \mathbf{F}_{pm}^H, & \text{MNRA} \\ \mathbf{T}_u (\mathbf{T}_p^H \mathbf{T}_p + \gamma_{enra} \mathbf{I}_t)^{-1} \mathbf{T}_p^H, & \text{ENRA} \\ \mathbf{T}_u (\mathbf{T}_p^H \mathbf{T}_p + \sigma_w^2 \mathbf{R}_{aa}^{-1}) \mathbf{T}_p^H, & \text{WF} \end{cases} \quad (25)$$

IV. Performance Evaluation

In the following, the performance of the estimators discussed in section III will be studied via Monte Carlo simulations. A single-input single-output OFDM system with physical layer parameters proposed for the downlink of UTRA LTE will be used [1]. QPSK modulation is used for both pilot and data symbols. Evenly spaced pilot symbols with a spacing of $\Delta_p = 6$ subcarriers are transmitted in every OFDM block.

Two channel power delay profiles, with 20 equispaced taps and a decay of 1dB per tap leading to an overall loss of 19dB, are used for this simulation study. The "long SS" profile is sample spaced of length 3.711 μs and the "long NSS" profile is not sample spaced differing by 0.5 T_s added to all delays of the "long SS" profile.

Results for Bit Error Rate (BER) using the studied estimators as a function of the Signal-to-Noise Ratio (SNR) will be given.

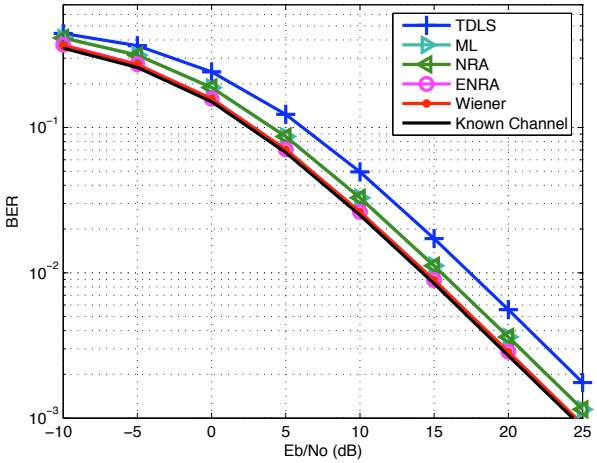

Fig. 2. Performance of the different estimators in a Full Bandwidth OFDM system ($Nu = N_{fft} = 2048$) and a pilot spacing of 6 for the "long SS" channel.

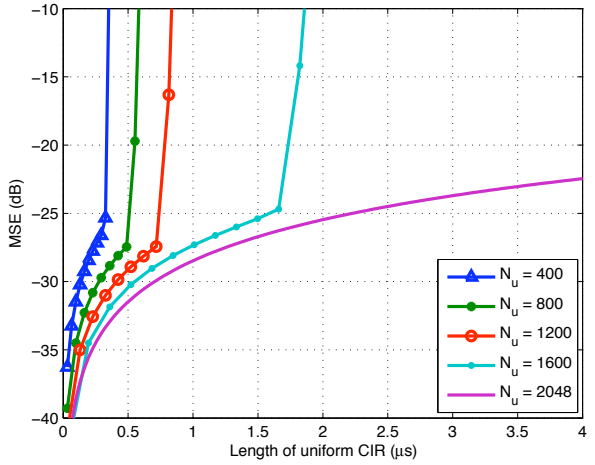

Fig. 3. MSE of the ML estimator for varying assumed CIR length and different N_u, $N_{fft} = 2048$ and $Eb/No = 15$ dB

A. Sample-Spaced Scenario

The performance of the different studied algorithms in a Full Bandwidth system using the "long SS" channel profile is depicted in Fig. 2. From the BER results shown in IV-A, we see that the TDLS curve lies 3.5 dB from the known channel performance at $\frac{E_b}{N_0}$ =10 dB, whereas this distance is reduced to 0.25 dB for the ENRA and WF estimators.

In the case of partial bandwidth the TDLS totally fails, due to bad conditioning. The ML fails as seen on Fig. 3, leading to ill-conditionning of the matrix to be inverted, when the size of the CIR is large for a given N_u.

B. Non-Sample-Spaced Scenario

The effect of having an NSS PDP on the classical algorithms is studied. The BER results are given in Fig. 4 for the NRA, MNRA, ENRA and WF using the "long NSS" channel profile. It is noted that the ENRA and WF have the same performance

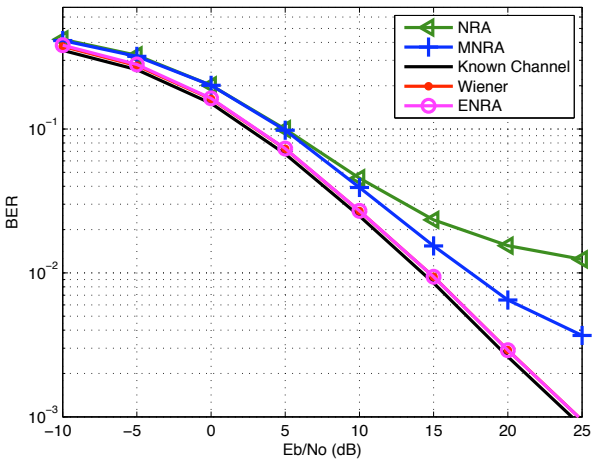

Fig. 4. Effect of leakage on the classical algorithms in an LTE scenario with $Nu = 1200$, $N_{fft} = 2048$ and a pilot spacing of 6 for the "long" NSS channel.

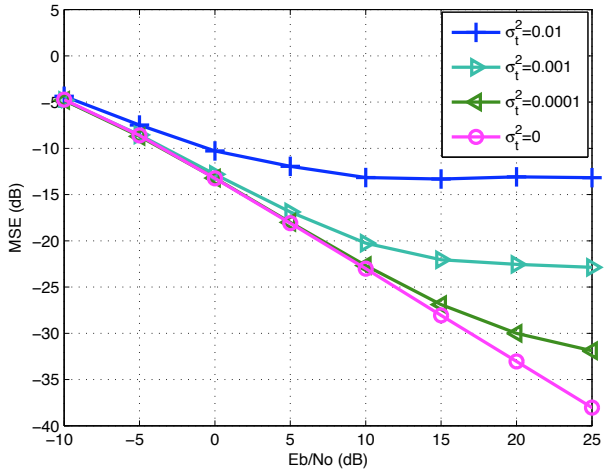

Fig. 5. MSE of the ENRA with different delay estimation errors in an LTE scenario with $Nu = 1200$, $N_{fft} = 2048$ and a pilot spacing of 6 for the "long" NSS channel.

as when employing the "long SS" PDP. The NRA, on the other hand, suffers from significant degradation for $\frac{E_b}{N_0} \geq$10 dB in both MSE and BER. From these results it can be observed that the knowledge of the tap delays of the PDP is of crucial importance to avoid the leakage effect.

In Fig. 5 the robustness of the ENRA against delay estimation errors is studied. A random zero-mean Gaussian error with variance σ_τ^2 has been added to the delay's values to simulate imperfect delay estimates, and the MSE of the estimates has been represented. The results show that even with small errors the ENRA suffers from severe degradation as the SNR increases. Very high accuracy in the tap delay estimates is therefore needed in order to avoid leakage.

V. Conclusion

In this paper, we have propose a unification of linear PACE OFDM algorithms. Analysis and simulation results are first given for a sample-spaced channel and Full Bandwidth. The effects of introducing virtual subcarriers as well as a non-sample-spaced channel are studied.

When Partial Bandwidth is used, the TDLS and ML algorithms suffer from severe ill-conditioned matrices an cannot be used as such if the number of virtual subcarriers is too large.

When the channel is non-sample-spaced, exact knowledge of the tap delays is necessary to avoid leakage, with the studied algorithms, but even small errors of tap delay estimates lead to significant performance degradation. This means that without an accurate tap delay estimator the target peak data rates at high SNR in LTE might be compromised.

A modified DFT based robust Wiener seems to be a good candidate for low and middle range SNR (up to 15 dB). However at higher SNR this solution is not recommended and other solutions should be used. These could be based on accurate tap delay estimation or iterative data aided estimation.

References

[1] 3GPP TR 25.814 V7.1.0 (2006), "Physical Layer Aspects for Evolved Universal Terrestrial Radio Access (UTRA)."

[2] P. Hoeher,S. Kaiser and I. Robertson, "Two-dimensional pilot-symbol-aided channel estimation by Wiener filtering," in *Proc. Int. Conf. Acoustics Speech and Signal Processing (ICASSP)*, pp. 1845-1848, 1997.

[3] J.-J. van de Beek,O. Edfors, M. Sandell, S. K. Wilson and P.O. Borjesson, "On channel estimation in OFDM systems," in *Proc. IEEE VTC'96*, pp. 815-819, Nov. 1996.

[4] R. Negi and J. Cioffi, "Pilot tone selection for channel estimation in a mobile OFDM system," in *IEEE Trans. Consumer Electron.*, vol. 44, pp. 1122-1128, Aug. 1998.

[5] L. Deneire, P. Vandenameele, L. van der Pierre, B. Gyselinckx and M. Engels, "A low complexity ML channel estimator for OFDM," in *IEEE Trans. Commun*, vol. 51, no.2, pp. 135-140, Feb. 2003.

[6] M. Morelli and U. Mengali, "A comparison of pilot-aided channel estimation methods for OFDM systems," in *IEEE Trans. Signal Proc.*, vol. 49, pp. 3065-3073, December 2001.

[7] H. Schmidt, V. Kuhn, K.D. Kammeyer, R. Rueckriem and S. Fechtel, "Channel tracking in wireless OFDM systems," in *SCI 2001*, Orlando, Florida, USA, 22-25 July 2001.

[8] M.H. Hsieh and C.H. Wei, "Channel estimation for OFDM systems based on comb-type pilot arrangement in frequency selective fading channels," *IEEE Trans. Consumer Electronics*, vol.44, pp. 217-225, Feb. 1998.

[9] O. Edfors, M. Sandell, J. van de Beek, S.K. Wilson and P.O. Borjesson, "OFDM channel estimation by singular value decomposition," in *IEEE Trans. Commun.*, vol. 46, pp. 931-939, July 1998.

[10] B. Yang, K.B. Letaief, R.S. Cheng and Z. Cao, "Channel estimation for OFDM transmission in multipath fading channels based on parameteric channel modelling," in *IEEE Trans. Commun.*, vol. 49, pp. 467-479, March 2001.

[11] A. Tikhonov and V. Arsenin, *Solutions of Ill-Posed Problems*. Washington: Winston, 1977.

[12] Y. Li, L.J. Cimini, and N.R. Sollenberger, "Robust channel estimation for OFDM systems with rapid dispersive fading," in *IEEE Trans. Commun.*, vol. 46, pp. 902-915, July 1998.

[13] S.R. Searle, *Matrix Algebra Useful for Statistics*. New York: Wiley, 1982.

[14] J.G. Proakis, *Digital Communications*, 4th ed. New York: McGraw-Hill, 2001.

Paper N

Analysis of Time and Frequency Domain PACE Algorithms for OFDM with Virtual Subcarriers

Christian Rom, Carles Navarro Manchón, Troels B. Sørensen, Preben Mogensen and Luc Deneire

IEEE 18th International Symposium on Personal, Indoor and Mobile Radio Communications, PIMRC 2007. Athens, September 2007.

N. ANALYSIS OF TIME AND FREQUENCY DOMAIN PACE ALGORITHMS FOR OFDM WITH VIRTUAL SUBCARRIERS

The 18th Annual IEEE International Symposium on Personal, Indoor and Mobile Radio Communications (PIMRC'07)

ANALYSIS OF TIME AND FREQUENCY DOMAIN PACE ALGORITHMS FOR OFDM WITH VIRTUAL SUBCARRIERS

Christian Rom, Carles Navarro Manchón,
Troels Bundgaard Sørensen and Preben Mogensen
Department of Electronic Systems, Aalborg University
Niels Jernes Vej 12, Aalborg East, Denmark
E-mail: {chr, cnm, tbs, pm}@es.aau.dk

Luc Deneire[1,2]
(1) Université de Nice, Sophia Antipolis
(2) Centre National de la Recherche Scientifique
I3S, UMR 6070, France
Email: deneire@i3s.unice.fr

ABSTRACT

This paper studies common linear frequency direction pilot-symbol aided channel estimation algorithms for orthogonal frequency division multiplexing in a UTRA long term evolution context. Three deterministic algorithms are analyzed: the maximum likelihood (ML) approach, the noise reduction algorithm (NRA) and the robust Wiener (RW) filter. A closed form mean squared error is provided for these three algorithms. Analytical and simulation results show that, in the presence of virtual subcarriers, the ML can suffer large performance degradation due to ill-conditioned matrix issues. A solution to this problem is to use the Tikhonov regularization method giving the NRA. The equivalence between the NRA and the RW is proved analytically. A practical implementation of the NRA and RW is proposed based on partial-input partial-output FFT, leading to 6 to 8 times lower complexity than the reference implementation.

I. INTRODUCTION

Over the last years Orthogonal Frequency Division Multiplexing (OFDM) has been adopted in high data-rates communication systems. By using a Cyclic Prefix (CP) the subcarrier orthogonality is preserved over the dispersive multipath channel. OFDM is used in upcoming standards such as IEEE 802.16 and UTRA Long Term Evolution (LTE) [1]. Both standards use coherent detection through Pilot-symbol Aided Channel Estimation (PACE) with virtual subcarriers.

Peter Hoeher showed in [2] that the two dimensional interpolation problem of PACE could be solved by using 2 cascaded orthogonal 1-D filters, giving virtually no performance loss compared to the 2-D filter. The latency requirements of standards such as LTE or IEEE 802.16e limit the pilot span available for channel estimation in time direction to a low amount of samples. This increases the importance of the frequency direction interpolation which is the focus of this paper.

Much attention has been given to this topic showing that the performance tradeoff of the algorithms depends on the relationship between the Power Delay Profile (PDP) length and the frequency domain pilot spacing. Deterministic approaches can be separated into time and frequency domain solutions. Deterministic time domain solutions are: the Time Domain Least Squares (TDLS) [3] and [4], The Maximum Likelihood approach (ML) [5], [6] and The Noise Reduction Algorithm (NRA) [7]. Deterministic frequency domain methods are Spline, Gaussian or Lagrange interpolation, and require higher pilot overhead to achieve an acceptable performance [8]. Bayesian approaches such as the Minimum Mean Squared Error (MMSE) in time domain or frequency domain have been proposed in [2], [3], with complexity reduction by Singular Value Decomposition (SVD) suggested in [9]. However, Bayesian approaches cannot directly be used as they need large channel dependent matrix inversions and require accurate knowledge of channel correlation properties. To reduce their complexity, different solutions have been proposed by, for example assuming a uniform PDP [9], [10].

We propose to study three algorithms: ML, NRA and RW. When introducing virtual subcarriers in the OFDM symbol, unequal MSE distribution at different carriers appears, in particular, MSE increases at band edges [6]. This MSE increase at the band-edges is analyzed, and solutions to alleviate the problem are suggested. The ML approach shows not to be suitable when introducing too many virtual subcarriers, or having channel profiles with large delays. A more convenient approach is to use the NRA by introducing a diagonal matrix in the calculation of the pseudo-inverse of the ML, known as the Tikhonov regularization. The authors prove that the NRA is equivalent to the Robust Wiener (RW) approach when assuming identical channel statistics knowledge at the receiver and a sample spaced PDP. Performance is then evaluated for LTE parameters, and implementation strategies are analyzed focusing on the computational complexity.

The remainder of this paper is structured as follows: the OFDM baseband received signal model is given in section II. An algorithm study is presented in section III, followed by a performance analysis in section IV. The complexity study and implementation strategy are then given in section V. Finally section VI concludes the work.

II. OFDM BASEBAND RECEIVED SIGNAL

A. Notations

The notations used throughout this paper are:

$\forall$	:	for all
$\in$	:	membership
$(\cdot)^H$	:	hermitian transpose of a matrix or vector
$\lvert\cdot\rvert$	:	absolute value
$\mathrm{tr}\{\cdot\}$	:	trace operator
$\mathrm{E}\{\cdot\}$	:	expectation operator
$\mathbf{X}[n,k]$	:	the n^{th} row and k^{th} column element of a matrix $\mathbf{X}$

1-4244-1144-0/07/$25.00©2007 IEEE

Bold upper-case letters are used for matrices and bold lower-case letters are used for vectors.

B. Received Signal

In the following an analytical model is derived with the purpose of studying some specific frequency direction channel estimation algorithms. In order to simplify the mathematical expressions of this model, we will assume that the maximum excess delay of the channel is shorter than the CP and accordingly, assume no Inter-Symbol Interference (ISI) between consecutive OFDM symbols. The channel variations are considered negligible over the duration of 1 OFDM symbol giving Inter-Carrier Interference (ICI) free signal reception. Furthermore, we will consider that the receiver is ideally synchronized with the arrival of the first physical path of the channel. Depending on the initial assumptions different matrix vector models can be derived. Starting with a very general case with all subcarriers used for data transmission, the received signal before channel equalization is:

$$\mathbf{y} = \mathbf{XFg} + \mathbf{w} = \mathbf{Xh} + \mathbf{w} \tag{1}$$

$\mathbf{X}$: data symbol diagonal (N_{fft}·N_{fft})
$\mathbf{F}$: DFT (N_{fft}·N_{fft})
$\mathbf{g}$: Channel Impulse Response (CIR) (N_{fft}·1)
$\mathbf{h}$: Channel Transfer Function (CTF) (N_{fft}·1)
$\mathbf{w}$: Additive White Gaussian Noise (AWGN) (N_{fft}·1)
with $\forall\{n,k\} \in [0, \mathrm{N}_{fft}-1]^2$, $\mathbf{F}[n,k] = e^{\frac{-j2\pi nk}{\mathrm{N}_{fft}}}$.
When virtual subcarriers are introduced, data and pilot symbols are only partially using the bandwidth. It is then possible to reorder the rows of $\mathbf{y}$ to have a clear notation that separates virtual subcarriers from the used subcarriers. The perceived CIR is assumed to have a finite length and to be sample spaced. The received vector may be written as:

$$\mathbf{y} = \begin{bmatrix} \mathbf{X}_u & 0 \\ 0 & 0 \end{bmatrix} \begin{bmatrix} \mathbf{F}_{us} & \mathbf{F}_{un} \\ \mathbf{F}_{vs} & \mathbf{F}_{vn} \end{bmatrix} \begin{bmatrix} \mathbf{g}_s \\ 0 \end{bmatrix} + \mathbf{w}. \tag{2}$$

$\mathbf{X}_u$: data and pilot symbol diagonal matrix (N_u·N_u)
$\mathbf{F}_{us}$: subDFT of used subcarriers and CIR (N_u·N_s)
$\mathbf{F}_{un}$: subDFT of used subcarriers and noise (N_u·($\mathrm{N}_{fft}-\mathrm{N}_s$))
$\mathbf{F}_{vs}$: subDFT of virtual subcarriers and CIR (($\mathrm{N}_{fft}-\mathrm{N}_u$)·$\mathrm{N}_s$)
$\mathbf{F}_{vn}$: subDFT of virtual subcarriers and noise (($\mathrm{N}_{fft}-\mathrm{N}_u$) · ($\mathrm{N}_{fft}-\mathrm{N}_s$))
$\mathbf{g}_s$: CIR vector of length of the maximum excess delay (N_s·1)
N_{fft}: FFT size
N_u: number of used subcarriers for data and pilots
N_p: number of pilot subcarries in one OFDM symbol
N_s: number of CIR samples with energy
Only the subset of pilot-carrying subcarriers are available for channel estimation leading to:

$$\mathbf{y}_p = \mathbf{X}_p\mathbf{F}_{ps}\mathbf{g}_s + \mathbf{w}_p = \mathbf{X}_p\mathbf{h}_p + \mathbf{w}_p \tag{3}$$

where $\mathbf{X}_p$ is a diagonal subset matrix of $\mathbf{X}_u$ and $\mathbf{F}_{ps}$ is a subset matrix of $\mathbf{F}_{us}$ where only the elements affecting the pilot subcarriers are considered.

III. Algorithm Study

Different classical algorithms are presented in this section. However they are studied in the case of OFDM containing virtual subcarriers which will affect their notation and performance. They are all based on an initial least-squares estimate at the pilot positions. It is noted that the pilots are all transmitted with a M-PSK constellation leading to a constant pilot power. Without loss of generality we assume that this power is set to unity. The initial least-squares estimate at the pilots is given by:

$$\mathbf{h}_{ls} = {\mathbf{X}_p}^{-1}\mathbf{y}_p. \tag{4}$$

A. Maximum Likelihood

Assuming that the maximum CIR length is known at the receiver, the ML estimate of the channel response is expressed as [5]:

$$\mathbf{h}_{ml} = \mathbf{F}_{us}\mathbf{g}_{ml} = \mathbf{F}_{us}(\mathbf{F}_{ps}^H\mathbf{F}_{ps})^{-1}\mathbf{F}_{ps}^H\mathbf{h}_{ls}. \tag{5}$$

However, when virtual subcarriers are present, the matrix:

$$\mathbf{T} = \mathbf{F}_{ps}^H\mathbf{F}_{ps} \tag{6}$$

can become ill-conditioned, leading to high MSE, as it will be shown in Section IV.

B. Noise Reduction Algorithm

A simple solution to alleviate the ill-conditioning problem is to add a small value γ to the diagonal of the matrix $\mathbf{T}$, also known as the Tikhonov regularization method. This is suggested in [7], giving the NRA algorithm:

$$\mathbf{h}_{nra} = \mathbf{F}_{us}\mathbf{g}_{nra} = \mathbf{F}_{us}(\mathbf{F}_{ps}^H\mathbf{F}_{ps} + \gamma\mathbf{I})^{-1}\mathbf{F}_{ps}^H\mathbf{h}_{ls}. \tag{7}$$

Assuming that $\mathbf{F}_{ps} = \mathbf{U}\Delta\mathbf{V}^H$ by SVD, with λ_i being the i^{th} singular value of $\mathbf{F}_{ps}$, (7) can be rewritten as:

$$\mathbf{h}_{nra} = \mathbf{F}_{us}\mathbf{V}\Delta_{nra}\mathbf{U}^H\mathbf{h}_{ls} \tag{8}$$

where $\Delta_{nra}[i,j] = \frac{\lambda_i}{\lambda_i^2+\gamma}$ for $(i=j)$, and $\Delta_{nra}[i,j] = 0$ for $i \neq j$.

C. Wiener and Robust Wiener

In his work, Hoeher showed that the optimum linear estimator, in the MSE sense, in PACE OFDM is the Wiener filter, which is given by [2]:

$$\mathbf{h}_w = \mathbf{R}_{\mathbf{hh}_p}(\mathbf{R}_{\mathbf{h}_p\mathbf{h}_p} + \sigma_w^2\mathbf{I}_{N_p})^{-1}\mathbf{h}_{ls} \tag{9}$$

where $\mathbf{R}_{\mathbf{hh}_p}$ is the cross-correlation matrix of $\mathbf{h}$ and $\mathbf{h}_p$, $\mathbf{R}_{\mathbf{h}_p\mathbf{h}_p}$ is the autocorrelation matrix of $\mathbf{h}_p$ and σ_w^2 is the power of the gaussian noise. Generally, the frequency correlation properties are not known at the receiver, and furthermore they can vary over time. For this reason, a robust design based on the assumption of a uniform PDP with sample-spaced equally-powered taps and the same length of the CIR is proposed. The resulting constant correlation matrices can be

then expressed as:

$$\mathbf{R}_{\mathbf{hh}_p} = \mathrm{E}\{\mathbf{h}\mathbf{h}_p^H\} = \frac{1}{N_s}\mathbf{F}_{us}\mathbf{I}_{N_s}\mathbf{F}_{ps}^H \quad (10)$$

and

$$\mathbf{R}_{\mathbf{h}_p\mathbf{h}_p} = \mathrm{E}\{\mathbf{h}_p\mathbf{h}_p^H\} = \frac{1}{N_s}\mathbf{F}_{ps}\mathbf{I}_{N_s}\mathbf{F}_{ps}^H. \quad (11)$$

Using this formulation, (9) can be rewritten as:

$$\mathbf{h}_{rw} = \mathbf{F}_{us}\mathbf{F}_{ps}^H(\mathbf{F}_{ps}\mathbf{F}_{ps}^H + \sigma_w^2\mathbf{I}_{N_p})^{-1}\mathbf{h}_{ls}. \quad (12)$$

We refer to this estimator as RW.

D. Equivalence Between NRA and RW

Comparing (7) and (12), a strong similarity can be observed. By using the SVD of the matrix $\mathbf{F}_{ps}$, the RW estimator can be expressed as:

$$\mathbf{h}_{rw} = \mathbf{F}_{us}\mathbf{V}\Delta_{rw}\mathbf{U}^H\mathbf{h}_{ls} \quad (13)$$

where $\Delta_{rw}[i,j] = \frac{\lambda_i}{\lambda_i^2 + N_s\sigma_w^2}$ for $i = j$, and $\Delta_{rw}[i,j] = 0$ for $i \neq j$.

From inspection of (8) and (13), it is straightforward to see that $\mathbf{h}_{nra} = \mathbf{h}_{rw}$ when $\gamma = N_s\sigma_w^2$. Moreover, it can be shown that this value minimizes the MSE of the estimator when no virtual subcarriers are present and regularly-spaced pilots are used, and it will be assumed for the NRA algorithm in the reminder of this paper. Therefore the full equivalence between the time-domain NRA algorithm and the frequency domain RW algorithm has been proven, assuming the same a priori knowledge available at the receiver.

E. MSE of the Estimators

The different proposed practical solutions are all covered by (7). It is therefore possible to study their respective performance by using one single closed form MSE expression. The MSE is calculated as:

$$\mathbf{MSE}\{\mathbf{h}_{nra}[n]\} = \mathrm{E}\{|\mathbf{h}[n] - \mathbf{h}_{nra}[n]|^2\}. \quad (14)$$

Using (7), the MSE for the n^{th} subcarrier becomes:

$$\mathbf{MSE}\{\mathbf{h}_{nra}[n]\} = \mathbf{M}[n,n] \quad (15)$$

where

$$\mathbf{M} = \mathbf{F}_{us}[(\mathbf{I} - \mathbf{A})\mathbf{R}_{\mathbf{g}_s\mathbf{g}_s}(\mathbf{I} - \mathbf{A}) + \sigma_w^2\mathbf{A}^2\mathbf{T}^{-1}]\mathbf{F}_{\mathbf{us}}^{\mathbf{H}}. \quad (16)$$

In the previous equation, $\mathbf{A} = (\mathbf{T} + \gamma\mathbf{I})^{-1}\mathbf{T}$, where $\mathbf{T}$ is defined in (6), and $\mathbf{R}_{\mathbf{g}_s\mathbf{g}_s}$ is the autocorrelation matrix of $\mathbf{g}_s$. The average MSE of the estimator can consequently be defined as:

$$\overline{\mathbf{MSE}}\{\mathbf{h}_{nra}[n]\} = \frac{1}{\mathbf{N}_u}\mathrm{tr}\{\mathbf{M}\}. \quad (17)$$

Note that the MSE of the ML estimator is obtained by setting $\gamma = 0$ and the MSE of the RW estimator is obtained by setting $\gamma = N_s\sigma_w^2$.

IV. Performance Analysis

In the following, the performance of the estimators discussed in section III will be studied. A single input single output OFDM system with the physical layer parameters proposed for the downlink of UTRA LTE will be used [1]. The system is based on a constant subcarrier spacing of 15 KHz, with different bandwidth configurations ranging from 1,25 to 20 MHz, as shown in Table 1. The CP is assumed to be always longer than the maximum delay of the channel, and QPSK modulation is used for both pilot and data symbols. Evenly spaced pilot symbols with a spacing of 6 subcarriers are transmitted in every OFDM block.

Table 1: OFDM parameters for LTE

Signal Bandwidth	Nfft	Nu	Sampling frequency
1.25 MHz	128	75	1.92 MHz
2.5 MHz	256	150	3.84 MHz
5 MHz	512	300	7.68 MHz
10 MHz	1024	600	15.36 MHz
20 MHz	2048	1200	30.72 MHz

In Fig. 1, the MSE of the ML estimator depending on the maximum delay of the channel is analyzed using (17), where a sample-spaced uniform PDP and an OFDM system with an FFT size of 2048 and different number of used subcarriers have been used. The Signal-to-Noise Ratio (SNR) is set to 15 dB and the sampling rate is the one corresponding to the LTE 20 MHz configuration. When all the subcarriers are used, the error of the estimate grows linearly with the channel length. When virtual subcarriers are used, however, the matrix $\mathbf{T}$ to be inverted becomes ill-conditioned after a certain channel length, yielding a large degradation of the MSE that makes the estimator unusable. The maximum channel length before the estimator becomes unstable decreases as the number of used subcarriers is reduced.

Fig. 2 depicts the same analysis for the different LTE configurations shown in Table 1, which all have the same ratio between used and virtual subcarriers. The results show that the larger the bandwidth, the smaller is the maximum length of the channel that can be estimated without suffering from the ill-conditioning effect. In the extreme case of 20 MHz bandwidth, only channels with a maximum delay lower than 800 ns can be estimated accurately, showing that ML is not a good option for systems with large FFT sizes and virtual subcarriers.

By adding a diagonal of small values to the matrix $\mathbf{T}$, the ill-conditioning of the matrix to be inverted is avoided . This is illustrated in Fig. 3, where the MSE corresponding to each subcarrier has been represented for the ML and the NRA estimators in a LTE 2,5 MHz configuration. Only half of the bandwidth has been represented, where subcarrier 0 indicates the central subcarrier. The channel profile used is a sample spaced modified ITU Pedestrian B profile, which has a maximum excess delay of 3.7 μs, and the SNR has been set to 15 dB. As can be seen, ML suffers severe degradation in the edge of the bandwidth, due to the use of virtual subcarriers. NRA significantly alleviates this problem and also achieves a better performance

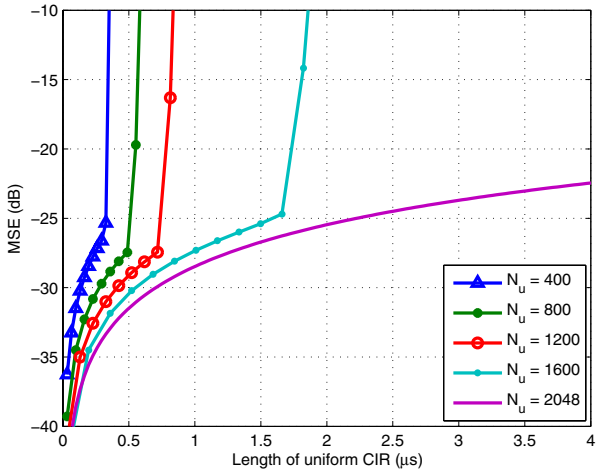

Figure 1: MSE for varying CIR length, different used bandwidths sizes, ML algorithm, $N_{fft} = 2048$ at Eb/No = 15dB

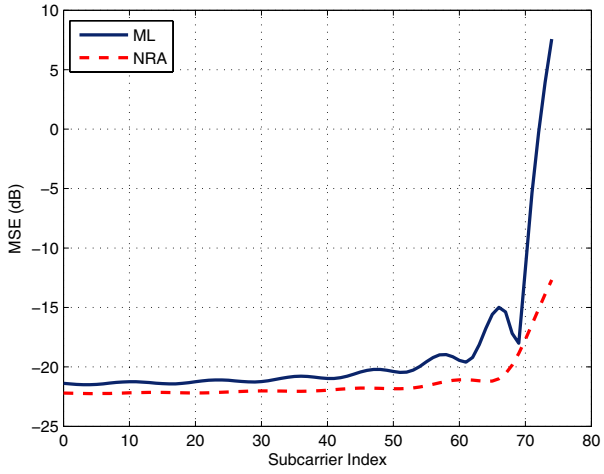

Figure 3: MSE per subcarrier for 2.5Mhz LTE settings, PedB channel, at Eb/No = 15dB

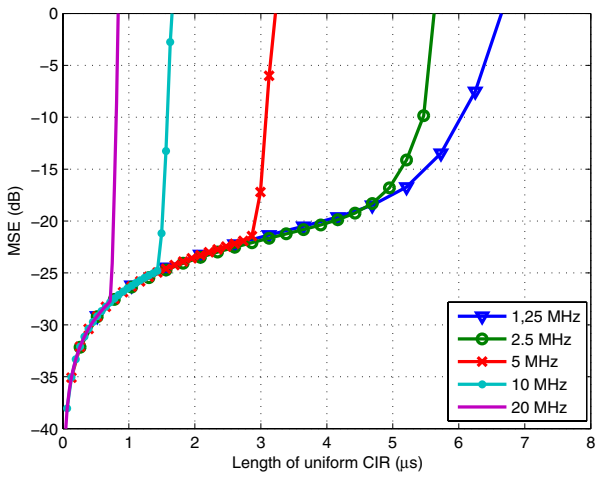

Figure 2: MSE for different bandwidths of the LTE standard and a varying uniform channel profile length, at Eb/No = 15dB. The ratio $\frac{N_u}{N_{fft}}$ is fixed to 0.586

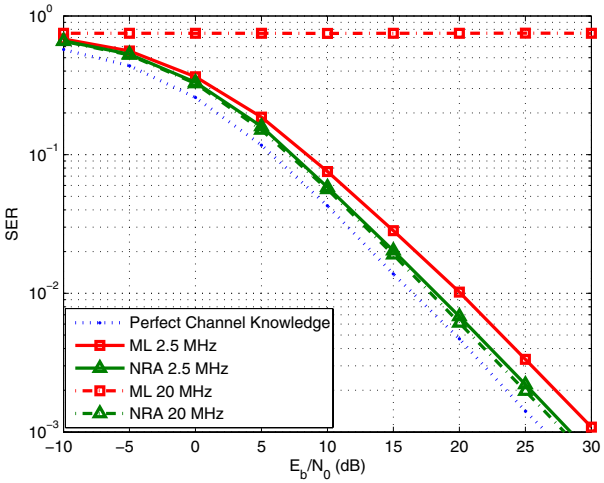

Figure 4: SER as a function of SNR for Pedestrian B channel profile, for 2,5 MHz and 20 MHz

over all the bandwidth, as it makes use of the noise variance knowledge.

Finally, the Symbol Error Rate (SER) performance of ML and NRA is shown in Fig. 4, where again a sample spaced modified Pedestrian B channel profile has been used. The curves for 20 and 2.5 MHz configurations are depicted. The results for ML show an acceptable performance for the 2.5 MHz settings, with a degradation of around 3.5 dB at 1% SER with respect to perfect channel estimation. For 20 MHz, however, ML is unable to estimate the channel, as the estimator becomes numerically unstable due to the matrix inversion. NRA, on the other hand, performs better than ML in both scenarios, with a distance of 1.5 dB to the known channel curve. Furthermore, it exhibits total robustness to the FFT size and number of subcarriers used, turning out to be a more suitable estimator for OFDM systems in both large and small bandwidth scenarios.

V. Complexity and Implementation Strategy

The optimal linear Wiener filter is discarded as it requires computation of a matrix inverse that depends on the channel statistics and is therefore computationally prohibitive for large bandwidths. Due to the high MSE's experienced by the ML algorithm, only different approaches of computing the RW or NRA algorithm are studied.

Three main implementation proposals are considered and discussed for different parameter settings. They are given as follows:

I) A precalculated RW filter, where the filter coefficients are calculated in advance and pre-stored in memory.

II) SVD of RW where the coefficients are also pre-stored in memory.

III) FFT based NRA, where $\mathbf{F}_{us}$ is computed by a partial input partial output FFT, as suggested in [11]. It is noted that a general analytical expression of the complexity is nontrivial in this case. For this reason the complexity of a full FFT is considered as an upper bound.

Table 2: Complexity of the Estimator

Proposal	Complexity
I	$O(N_u N_p)$
II	$O(N_s N_u + N_s + N_p^2)$
III	$O(N_{fft} log_2(N_{fft}) + N_s N_p)$

The orders of complexity of the different proposals are given in Table II. Practical Complex Multiply Accumulate (CMAC) operations per estimated CTF are used as complexity unit. Parameters are chosen according to the LTE settings given in Table I for the 2,5MHz and the 20MHz bandwidths. The complexity results are then shown in Fig. 5. The main complexity factor is the FFT size allowing an increased data rate. However, for the chosen solutions, the length of the CIR is critical in determining the solution with lowest complexity. When considering a small FFT size of 256, the SVD of RW has the lowest complexity if the CIR length is below 3,5 μs. On the other hand, for an FFT size of 2048, the FFT based solution has the lowest complexity for CIR lengths above 1,7 μs. As the interest of complexity reduction lies in the worst case scenarios, the most promising algorithm implementation would be the one based on partial-input, partial-output FFT, where III is an upper complexity bound. As the input is of size N_u and the output of size N_s the complexity of III could be further reduced by an approximate factor of 1,5 to 2. From Fig. 5 solution III is up to 4 times less complex than solution I and II, and with an optimized implementation [11] this could be further enhanced leading to a factor 6 to 8 times lower complexity.

VI. Conclusion

Frequency direction PACE is studied for OFDM in an LTE context. In this paper we show that when virtual subcarriers are introduced, the ML time domain algorithm suffers from high MSE due to ill-conditioned matrices. The FFT size and the number of used subcarriers will determine the length of supported CIR for an ML with acceptable performance. A solution to this problem is to introduce a small value to the diagonal of the matrix to be inverted giving the NRA. We prove that there is a full equivalence between the time domain NRA and the frequency domain RW algorithm. This proof helps us to define a low complex FFT based implementation of the RW solution. Complexity evaluations show that this solution has significantly lower complexity than the classical implementations by SVD in the case of large FFT sizes.

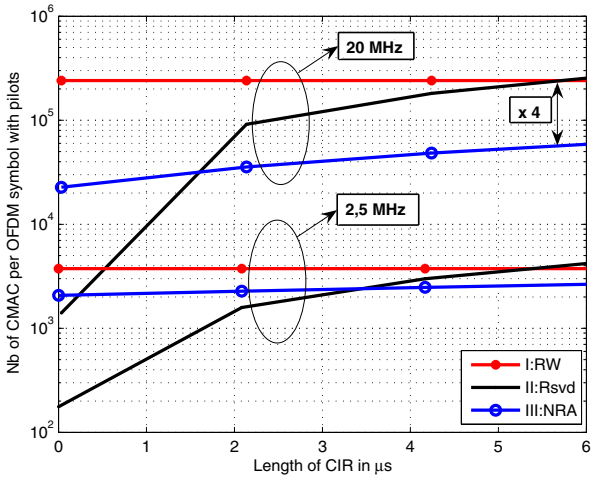

Figure 5: Complexity in CMAC of different implementations for LTE settings in both 2,5 MHz and 20 MHz

Acknowledgment

The authors would like to thank Infineon Technologies Denmark and Benny Vejlgaard for their advice and financial support, thanks to whom this work was possible.

References

[1] 3GPP TR 25.814 V7.1.0 (2006), "Physical Layer Aspects for Evolved Universal Terrestrial Radio Access (UTRA)"

[2] P. Hoeher,S. Kaiser and I. Robertson, "Two-dimensional pilot-symbol-aided channel estimation by Wiener filtering," in *Proc. Int. Conf. Acoustics Speech and Signal Processing (ICASSP)*, pp. 1845-1848, 1997.

[3] J.-J. van de Beek,O. Edfors, M. Sandell, S. K. Wilson and P.O. Borjesson, "On channel estimation in OFDM systems," in *Proc. IEEE VTC'96*, pp. 815-819, Nov. 1996.

[4] R. Negi and J. Cioffi, "Pilot tone selection for channel estimation in a mobile OFDM system," in *IEEE Trans. Consumer Electron.*, vol. 44, pp. 1122-1128, Aug. 1998.

[5] L. Deneire, P. Vandenameele, L. van der Pierre, B. Gyselinckx and M. Engels, "A low complexity ML channel estimator for OFDM," in *IEEE Trans. Commun*, vol. 51, no.2, pp. 135-140, Feb. 2003.

[6] M. Morelli and U. Mengali, "A comparison of pilot-aided channel estimation methods for OFDM systems," in *IEEE Trans. Signal Proc.*, vol. 49, pp. 3065-3073, December 2001.

[7] H. Schmidt, V. Kuhn, K.D. Kammeyer, R. Rueckriem and S. Fechtel, "Channel tracking in wireless OFDM systems," in *SCI 2001*, Orlando, Florida, USA, 22-25 July 2001.

[8] M.H. Hsieh and C.H. Wei, "Channel estimation for OFDM systems based on comb-type pilot arrangement in frequency selective fading channels," *IEEE Trans. Consumer Electronics*, vol.44, pp. 217-225, Feb. 1998.

[9] O. Edfors, M. Sandell, J. van de Beek, S.K. Wilson and P.O. Borjesson, "OFDM channel estimation by singular value decomposition," in *IEEE Trans. Commun.*, vol. 46, pp. 931-939, July 1998.

[10] Y. Li, L.J. Cimini, and N.R. Sollenberger, "Robust channel estimation for OFDM systems with rapid dispersive fading," in *IEEE Trans. Commun.*, vol. 46, pp. 902-915, July 1998.

[11] T.V. Sreenivas and P.V.S. Rao, "High-resolution narrow-band spectra by FFT prunning," in *IEEE Trans. on Acoustics Speech and Signal Processing*, vol. assp-28, pp. 254-257, No.2, Apr. 1980.

Paper O

Effect of Phase Noise on Spectral Efficiency for UTRA Long Term Evolution

Basuki E. Priyanto, Christian Rom, Carles Navarro Manchón, Troels B. Sørensen, Preben Mogensen and Ole Kiel Jensen

IEEE 17th International Symposium on Personal, Indoor and Mobile Radio Communications, PIMRC 2006. Helsinki, September 2006.

O. EFFECT OF PHASE NOISE ON SPECTRAL EFFICIENCY FOR UTRA LONG TERM EVOLUTION

The 17th Annual IEEE International Symposium on Personal, Indoor and Mobile Radio Communications (PIMRC'06)

EFFECT OF PHASE NOISE ON SPECTRAL EFFICIENCY FOR UTRA LONG TERM EVOLUTION

Basuki E. Priyanto, Christian Rom, Carles Navarro, Troels B. Sørensen, Preben Mogensen, Ole Kiel Jensen
Department of Communication Technology, Aalborg University
Niels Jernes Vej 12, Aalborg East
Denmark
E-mail: {bep,chr,krlsnav,tbs,pm,okj}@kom.aau.dk

ABSTRACT

In this paper, the effects of phase noise on the spectral efficiency of the next generation of OFDM based mobile systems with channel estimation is investigated. The simulation context and parameter settings are taken from the 3GPP Evolved UTRA (E-UTRA) study item, focusing on an OFDM downlink single antenna system in 20 MHz bandwidth. Phase noise is modeled as a Wiener-Lévy process and several phase noise powers are evaluated. The OFDM coherent detection method is based on Pilot Assisted Channel Estimation (PACE) with Wiener based frequency domain interpolation and second order gaussian interpolation for the time domain interpolation. The cell level spectral efficiency is also evaluated for micro and macro-cell scenarios. The simulation results indicate that the phase noise effect in E-UTRA downlink can be reduced by using high performance local oscillator or by placing pilots in every OFDM symbols.

I. INTRODUCTION

The work presented in this paper investigates the phase noise effects in a downlink E-UTRA system including channel estimation. 3GPP has initiated a study item looking into long term evolution of the existing 3G radio technology known as the Evolved UTRA (E-UTRA) [1]. OFDM has been proposed as the modulation scheme for downlink and will use coherent detection based on *Pilot Assisted Channel Estimation* (PACE).

One of the OFDM system drawbacks is its sensitivity to phase noise [3], [4], [5]. Phase noise is a characteristic of the local oscillator in the transmitter and receiver and it can be modeled as a Wiener-Lévy process [3]. This model is quite accurate and appropriate for quantitative studies of system performance degradation due to phase noise [3]. The phase noise parameters suitable for beyond 3G system are given in [11], [12].

Channel estimation in OFDM is also sensitive to phase noise [3]. Large attention has been given to research on channel estimation algorithms in such a context. The phase noise effects in the OFDM system with channel estimation for Wireless LAN 802.11a have previously been investigated in [9]. The Optimum linear solution, in a *Minimum Mean Square Error* (MMSE) sense is achieved with Wiener filtering [2] which, requires knowledge of channel statistics (such as the *Power Delay Profile* (PDP)) and noise variance. This algorithm will be chosen throughout this paper due to its high performance.

In this paper , an analytical study is conducted and the performance loss is divided into pilot overhead, channel estimate inaccuracy, and phase noise. The phase noise effect on spectral efficiency for an E-UTRA downlink with channel estimation is evaluated. Moreover, the link level throughput is mapped to corresponding cell-level spectral efficiency using available Geometry[1] (G-factor) distributions for macro and micro-cell scenarios.

This paper is organized as follows: Section II gives a brief description of the E-UTRA simulator and the used parameter set, the analytical model and performance loss analysis is presented in section III. The phase noise model and channel estimation algorithm are explained in section IV and V. The simulation results are shown in section VI and, finally, in section VII conclusions are drawn.

II. SIMULATOR AND SYSTEM PARAMETERS

Throughout this paper results will be given through Monte Carlo simulations from a developed Link Simulator, using the proposed parameter values of Table 1. The study will be done using a SISO, downlink OFDM based transmission. The downlink bandwidth occupied in this system is scalable into 1.25 MHz, 2.5 MHz, 5 MHz, 10 MHz, 15 MHz and 20 MHz. However in this study, we will only deal with a fixed bandwidth of 20 MHz. Different *modulation and coding sets* (MCS) are chosen according to the spectral efficiency they can achieve. All pilot and data symbols will have equal power in this study. Turbo decoding and interleaving following the UTRA specifications release 6 are used throughout the simulations.

III. ANALYTICAL MODEL

A. Assumptions

In order to simplify the mathematical expressions of this model, we will assume that the maximum excess delay of the channel is shorter than the cyclic prefix and, therefore, there is no *inter-symbol interference* (ISI) between consecutive OFDM symbols. Furthermore, we will consider that the receiver is ideally synchronized with the arrival of the first physical path of the channel.

B. Transmitted Signal

The m^{th} transmitted symbol in an OFDM system can be expressed as a vector of length N_{gs} samples, defined by:

[1]The G-factor is the ratio of total received wideband BS power and other-cell/noise interference at the MS. It is averaged over short-term fading but not shadowing.

Table 1: E-UTRA parameters for simulation.

Parameter	Value
Carrier Frequency	2 GHz
Transmission BW	20 MHz
Sub-frame duration	0.5 ms
Sub-carrier spacing	15 kHz
OFDM symbols per sub-frame	7
CP length	4.7 μs
FFT size	2048
Useful subcarriers	1200
MCS settings	QPSK: 1/6, 1/3, 1/2, 2/3 16QAM: 1/2, 2/3, 3/4 64QAM: 1/2, 2/3, 3/4, 4/5
Channel model	Typical Urban 20 paths [10]

$$\mathbf{s_m} = \mathbf{\Psi_m}.\mathbf{d_m} \tag{1}$$

where $\mathbf{d_m}$ is a vector with N_s QAM or PSK modulated symbols, and $\mathbf{\Psi_m}$ (2) is a matrix which performs both an *Inverse Discrete Fourier Transform* (IDFT) operation and ads a redundant *Cyclic Prefix* (CP) of N_g samples. The elements of $\mathbf{\Psi_m}$ are defined by:

$$\Psi_{m,k}[n] = \frac{1}{\sqrt{N_s}}.e^{j2\pi k\left(\frac{n-N_g}{N_s}\right)} \tag{3}$$

where k is the sub-carriers index and n is the time sample. Furthermore, $N_{gs} = N_g + N_s$ is the total length in samples of the OFDM symbol and N_s is the number of subcarriers (size of the IDFT).

C. Received Signal

After the convolution with the channel, the signal that reaches the receiver can be written as:

$$\mathbf{r_m} = \mathbf{P_m}.\mathbf{H_m}.\mathbf{s_m} + \mathbf{w_m} \tag{4}$$

$\mathbf{H_m}$ is the $N_{gs} \times N_{gs}$ channel matrix for the m^{th} OFDM symbol, defined in (5).

In (5) $a_{m,p}[n]$ represents the p^{th} complex tap coefficient of the channel impulse response in the n^{th} time sample of the m^{th} OFDM symbol. $\mathbf{P_m}$ is a $N_{gs} \times N_{gs}$ diagonal matrix that models the effects of phase noise at the receiver. The elements of its diagonal are:

$$\mathbf{P_m}[\mathrm{n},\mathrm{n}] = \mathrm{e}^{\Phi_m[\mathrm{n}]} \tag{6}$$

When $\Phi_m[n]$ is small compared to 1, the elements in the diagonal can be approximated by $e^{j\Phi_m[n]} \approx 1 + j\Phi_m[n]$, and therefore:

$$\mathbf{P_m} = \mathbf{I} + \mathrm{j}\mathbf{\Phi_m} \tag{7}$$

where $\mathbf{\Phi_m}$ is a diagonal matrix with the values of $\Phi_m[n]$ in its diagonal, and $\mathbf{I}$ is the identity matrix. Finally, $\mathbf{w_m}$ is an N_{gs} long vector with *additive white Gaussian noise* (AWGN). Using (7), we can re-write the received signal as:

$$\mathbf{r_m} = (\mathbf{I} + \mathrm{j}\mathbf{\Phi_m}).\mathbf{H_m}.\mathbf{s_m} + \mathbf{w_m} \tag{8}$$

D. Signal After Receiver DFT

Once the signal reaches the receiver, the CP is removed, and a *Discrete Fourier Transform* (DFT) is performed. Both operations are modeled by the matrix $\widetilde{\mathbf{\Psi}}^{\mathbf{H}}_{\mathbf{m}}$, which is a matrix equal to $\mathbf{\Psi}^{\mathbf{H}}_{\mathbf{m}}$ but with zeros in the first N_g columns. The received signal after the DFT can be written as:

$$\mathbf{z_m} = \widetilde{\mathbf{\Psi}}^{\mathbf{H}}_{\mathbf{m}}\mathbf{r_m} = (\mathbf{CO_m} + \mathbf{C_{PN,m}})\,\mathbf{d_m} + \mathbf{w_m} \tag{9}$$

where, $\mathbf{CO_m} = \widetilde{\mathbf{\Psi}}^{\mathbf{H}}_{\mathbf{m}}\mathbf{H_m}\mathbf{\Psi_m}$, and $\mathbf{C_{PN,m}} = \widetilde{\mathbf{\Psi}}^{\mathbf{H}}_{\mathbf{m}}(\mathrm{j}\mathbf{\Phi_m}\mathbf{H_m})\,\mathbf{\Psi_m}$.

E. Channel Equalization

After the DFT at the receiver, a 1 tap equalizer is applied. The elements of $\mathbf{z_m}$ are divided by an estimate of the channel transfer function in the corresponding subcarrier to obtain an estimate of the transmitted symbol:

$$\mathbf{y_m}[\mathrm{k}] = \frac{\mathbf{z_m}[\mathrm{k}]}{\widetilde{\mathbf{h}}_{\mathbf{m}}[\mathrm{k}]} \tag{10}$$

$\widetilde{\mathbf{h}}_{\mathbf{m}}$ is an estimate of the diagonal of $\mathbf{CO_m} + \mathbf{C_{PN,m}}$, obtained by the use of PACE and a given channel estimation algorithm.

F. Degradation Mechanisms

From the analysis above, it comes out that there are three main mechanisms that will cause a loss in the system performance:

$$Total\ loss = L_{ALGO} + L_{PILOT} + L_{PN} \tag{11}$$

L_{ALGO} represents the loss due to the inaccuracy of the channel transfer function estimate, $\widetilde{\mathbf{h}}_{\mathbf{m}}$, and it depends on the algorithm used. L_{PILOT} is the loss due to the use of pilot symbols to estimate the channel, which will decrease the amount of useful information, and is dependent on the pilot density. L_{PN} is the loss due to the phase noise effect and the error is caused by a common phase rotation and *inter-carrier interference* (ICI) [3]. It should be noted that the three degradation mechanisms are coupled and therefore, there are not independent of one another.

IV. Phase Noise Model

Phase noise in the local oscillator can be seen as a multiplication of the transmitted signal with a noisy carrier $e^{j\Phi(t)}$. The random phase of this carrier is modeled by a Wiener-L*é*vy process as follows [5]:

$$\Phi(t) = 2\pi\int_0^t \mu(\tau)\,d\tau \tag{12}$$

In (12), $\mu(t)$ is a zero-mean white Gaussian process with power spectral density N_0 . The *single-sideband* (SSB) phase noise power is a Lorentzian spectrum [7]:

$$L(f) = \frac{2}{\pi\Delta f_{3dB}}.\frac{1}{1+\left(\frac{2f}{\Delta f_{3dB}}\right)^2} \tag{13}$$

$$\mathbf{\Psi_m} = \begin{pmatrix} \Psi_{m,0}[0] & \cdots & \Psi_{m,N_s-1}[0] \\ & \ddots & \\ \vdots & \Psi_{m,k}[n] & \vdots \\ & & \ddots \\ \Psi_{m,0}[N_{gs}-1] & \cdots & \Psi_{m,N_s-1}[N_{gs}-1] \end{pmatrix} \tag{2}$$

$$\mathbf{H_m} = \begin{pmatrix} a_{m,0}[0] & 0 & & & \cdots & & 0 \\ a_{m,0}[0] & a_{m,0}[1] & 0 & & & & \\ \vdots & a_{m,1}[1] & \ddots & & & & \\ a_{m,N_g-1}[0] & \vdots & \ddots & a_{m,0}[n] & 0 & & \vdots \\ 0 & a_{m,N_g-1}[1] & & & \ddots & & \\ \vdots & \ddots & & & \ddots & \ddots & 0 \\ 0 & \cdots & 0 & a_{m,N_g-1}[N_s] & \cdots & a_{m,1}[N_{gs}-2] & a_{m,0}[N_{gs}-1] \end{pmatrix} \tag{5}$$

In (13), $\Delta f_{3dB} = 2\pi N_0$ is the two-sided 3 dB bandwidth of phase noise. The power spectrum in (13) is an approximation to practical oscillator spectra, which enables analytical treatment.

In discrete time, phase noise can be modeled as a Markov process [3]. The random phase value of the disturbed subcarrier at the n^{th} sample of the m^{th} OFDM symbol can be written as:

$$\Phi_m[n] = \Phi_{m-1}[N_{gs}-1] + \sum_{i=0}^{n} u[mN_{gs}+i] \tag{14}$$

where $u[i]$ is a white Gaussian random process with zero mean and variance $\sigma_u = 2\pi\Delta f_{3dB}\frac{T}{N_s}$, T denotes the OFDM symbol period.

V. Channel Estimation Algorithm

The channel estimation problem is solved by using Wiener based frequency domain interpolation and second order gaussian interpolation for the time domain interpolation. Pilot symbols are used to estimate the *channel transfer function* (CTF). For the simplicity of derivation of the channel estimation algorithm, the channel impulse response is considered constant over the duration of an OFDM symbol, and phase noise will not be included in the derivation of the estimation algorithm.

First, an estimate of the CTF at the pilot subcarriers is obtained. Then, the full CTF is calculated using the following interpolation method.

1) Estimate at Pilot Position: Let $p_i, i = 0, 1, ..., N_p - 1$ be a set of indexes containing the subcarrier indexes that carry pilot symbols, where N_p is the number of pilot symbols in an OFDM symbol. A *Least-Squares* (LS) estimate of the channel transfer function at these pilot positions can be calculated as:

$$\widetilde{\mathbf{h}}_{\mathbf{p}}[\mathrm{i}] = \frac{\mathbf{z}[\mathrm{p_i}]}{\mathbf{d}[\mathrm{p_i}]} \tag{15}$$

$\mathbf{z}[\mathrm{p_i}]$and $\mathbf{d}[\mathrm{p_i}]$ are respectively the received symbol after the FFT and the transmitted symbol in the i^{th} pilot subcarrier.

2) Wiener filtering Interpolation: Wiener filtering is the optimum interpolation method in terms of mean square error. Using the statistics of the channel and noise, it performs a MMSE interpolation of the estimates at pilot sub-carriers, optimally reducing the effects of noise and channel distortion. In the presence of additive white Gaussian noise,The full CTF estimate is obtained by:

$$\widetilde{\mathbf{h}} = \mathbf{R_{hh_p}} \cdot \left(\mathbf{R_{h_ph_p}} + \sigma_{\mathbf{w}}^{\mathbf{2}}\mathbf{I_{N_p}}\right)^{-1}\widetilde{\mathbf{h}}_{\mathbf{p}} \tag{16}$$

where $\mathbf{R_{hh_p}}$ is the cross correlation matrix of the true channel transfer function and the true channel transfer function $\mathbf{h}$ at pilot subcarriers $\mathbf{h_p}$, $\mathbf{R_{h_ph_p}}$ is the autocorrelation matrix of the true channel transfer function at pilot subcarriers, σ_w^2 is the noise power and $\mathbf{I_{N_p}}$ is the $N_p \times N_p$ identity matrix. Note that the channel transfer function coefficients are assumed to be uncorrelated to the noise process.

3) Second Order Interpolation: The frequency response of the channel changes through time. Thus, the channel estimates require to be updated. Second order interpolation has been chosen as the performance degradation is neglegible for the proposed pilot schemes. The expression of the interpolated estimates for evenly spaced pilots is [8]:

$$\begin{aligned} \widetilde{\mathbf{h}}_{\mathrm{m}} = \mathrm{C_{p,i-1}(m)}\widetilde{\mathbf{h}}_{\mathrm{p,m_{i-1}}} + \mathrm{C_{p,i}(m)}\widetilde{\mathbf{h}}_{\mathrm{p,m_i}} .. \\ + C_{p,i+1}(m)\widetilde{\mathbf{h}}_{\mathrm{p,m_{i+1}}}, \mathrm{m_{p,i}} \leq \mathrm{m} < \mathrm{m_{p,i+1}} \end{aligned} \tag{17}$$

where $m_{p,i}, ..., m_{p,i+1}$ represent the OFDM symbols index of the symbols carrying pilots, Δp_t is the spacing between OFDM symbols carrying pilots, and the interpolation coefficients are:

$$\begin{aligned} C_{p,i-1}(m) &= \frac{1}{2}\left\{\left(\frac{m-m_{p,i}}{\Delta p_t}\right)^2 - \frac{m-m_{p,i}}{\Delta p_t}\right\} \\ C_{p,i}(m) &= 1 - \left(\frac{m-m_{p,i}}{\Delta p_t}\right)^2 \\ C_{p,i+1}(m) &= \frac{1}{2}\left\{\left(\frac{m-m_{p,i}}{\Delta p_t}\right)^2 + \frac{m-m_{p,i}}{\Delta p_t}\right\} \end{aligned} \tag{18}$$

Table 2: Phase Noise Characteristics.

SSB Power at 1 MHz offset	Bandwidth Δf_{3dB}	Ratio ρ_{PN}
-100 dBc/Hz	625 Hz	4.17%
-110 dBc/Hz	62 Hz	0.41%
-115 dBc/Hz	20 Hz	0.13%
-120 dBc/Hz	6 Hz	0.04%

VI. Simulation Results

The main parameters for the simulation are shown in Table 1. A low velocity environment is considered $(3\ \mathrm{kmph})$. Two pilot patterns are used to investigate the impact of using dense/sparse pilot symbols in time domain. The 1^{st} pilot scheme (P_1) is a comb type with pilot in all OFDM symbols. The 2^{nd} pilot scheme (P_2) is a rectangular type with pilots in the 3^{rd} and 7^{th}OFDM symbols of each sub-frame. One sub-frame contains 7 OFDM symbols. Both pilot schemes have a equally frequency spacing of 8. P_1 and P_2 introduce a total pilot overhead of 12.5% and 3.6%, respectively.

Several phase noise powers are considered based on the SSB phase noise power at 1 MHz frequency offset from the carrier. It is indicated in [11] that good quality phase noise oscillators achieve -120 dBc/Hz at 1 MHz offset and medium quality -100 dBc/Hz. These phase noise powers can be related with the phase noise bandwidth using (13). The phase noise characteristics for this simulation are summarized in Table 2. It may be useful to characterize the quality of an OFDM oscillator by the relation between its phase noise bandwidth and the subcarrier spacing of the OFDM signal (Δf_{sc}):

$$\rho_{PN} = \frac{\Delta f_{3dB}}{\Delta f_{sc}} \tag{19}$$

The link performance evaluation is conducted from very low G-factor (-10 dB) to very high G-factor (40 dB). In practice, the maximum G-factor is around 30 dB, due to the RF impairments such as non-linearity in amplifier. In this study, the investigation is still conducted up to 40 dB in order to investigate the performance of the higher-order MCS schemes.

Fig. 1 shows *link adaptation* (LA) curves with various MCS schemes for the case with and without phase noise of -115 dBc/Hz. The spectral efficiency for individual MCS schemes versus G-factor is also plotted. The LA curve without phase noise represents the achievable performance with the given pilot pattern. At low speed, the degradation due to the estimation error is negligible and therefore, the main loss is due to the pilot overhead. Phase noise does not affect the spectral efficiency of lower order MCS schemes.

Fig. 2 shows the LA curves when the pilot schemes P_1 is used. The link performance using various phase noise powers is illustrated. The maximum achievable spectral efficiency for this pilot schemes is 3.5 b/s/Hz. Phase noise of -120 dBc/Hz gives no noticeable degradation. A significant degradation is shown for the phase noise of -100 dBc/Hz.

The LA curves for the pilot schemes P_2 is shown in Fig. 3. The maximum achievable spectral efficiency is close to

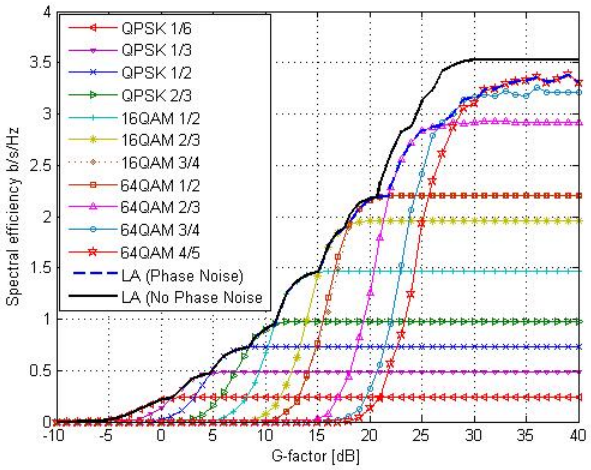

Figure 1: Spectral efficiency of PN= -115 dBc/Hz & pilot scheme P_1 with different MCS schemes.

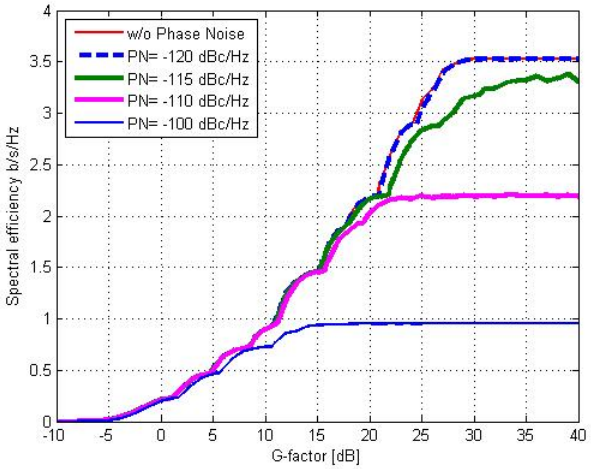

Figure 2: LA curves for pilot scheme P_1.

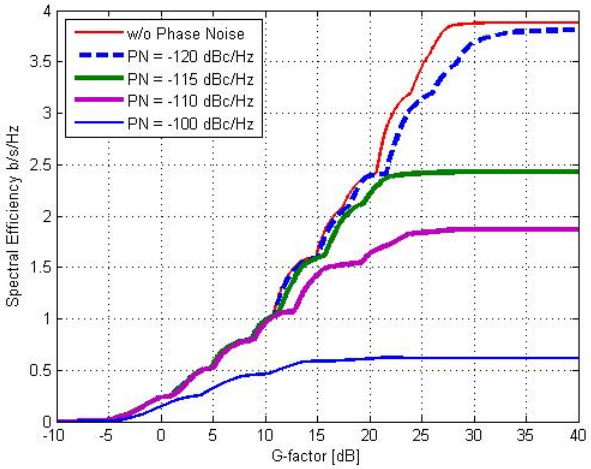

Figure 3: LA curves for pilot scheme P_2.

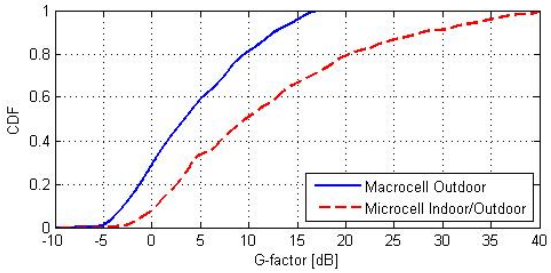

Figure 4: CDF of G-factor in macro & micro-cell scenarios.

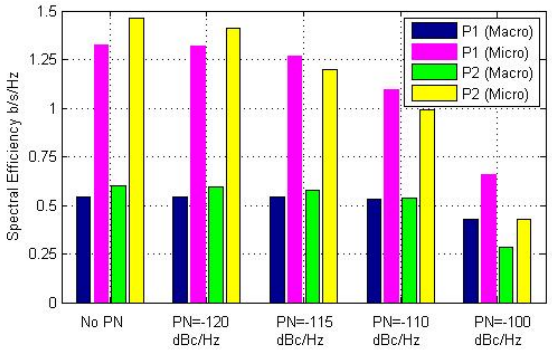

Figure 5: Cell throughput for different phase noise powers.

4 b/s/Hz. Phase noise of -120 dBc/Hz gives degradation in higher order MCS schemes. The spectral efficiency is getting worse for phase noise of -115 dBc/Hz, -110 dBc/Hz, and -100 dBc/Hz, respectively.

From Fig. 2 and Fig. 3, it is shown that P_1 can reduce the phase noise effect with the cost of pilot overhead. P_2 can achieve higher spectral efficiency compared to P_1 when high performance oscillator (phase noise $\leq$ -120 dBc/Hz) is used. P_1 outperform compared to P_2 by using oscillator with phase noise $\geq$ -115 dBc/Hz. The reason is that P_1 has pilots in every OFDM symbols. Thus, it can track the common phase error introduced by the phase noise. The results in Fig. 2 and Fig. 3 also indicate that low ρ_{PN} ratio factor (Table 2) results in higher performance.

The study in the cell level requires G-factor distributions used for the macro-cell outdoor and the micro-cell indoor/outdoor scenarios, which are shown in Fig. 4 [13]. The spectral efficiency at cell level is evaluated by conditioning the G-factor dependent throughput with the probability of obtaining a given G-factor and integrating over the whole G-factor range. The results are shown in Fig. 5 where the bar plot of the cell level spectral efficiency obtained for both pilot schemes and several phase noise powers are presented. For the P_1 case in the macro-cell scenario, phase noise does not give significant degradation except for a phase noise of -100 dBc/Hz that leads to a spectral efficiency degradation of around 21%. In the microcell scenario, significant degradations of 17% and 50% are shown for phase noise of -110 dBc/Hz and -100 dBc/Hz, respectively. Overall, the P_2 case has similar trend as the P_1. In the macro-cell scenario, a significant degradation of 53% is caused by phase noise of -100 dBc/Hz. In the micro-cell scenario, a phase noise of -110 dBc/Hz and -100 dBc/Hz give degradation of 32% and 71%, respectively.

VII. Conclusion

The goal of this paper has been to give an estimate of the performance degradation due to phase noise in a downlink E-UTRA SISO scenario with channel estimation. An analytical model of the received signal has been derived to give an expression for the performance loss, including loss due to phase noise. The phase noise is modeled as a Wiener-Lévy process. It is concluded that the higher order modulation schemes suffered most in spectral efficiency degradation. The throughput obtained at link-level was mapped to a cell level spectral efficiency using available Geometry (G-factor) distributions for the macro and micro-cell scenarios. In the macro-cell scenarios, significant spectral efficiency degradation appears at a phase noise level of -100 dBc/Hz, while in the micro-cell scenarios, it already appears at a phase noise level of -110 dBc/Hz. The phase noise effect in E-UTRA downlink can be reduced by using high performance local oscillator or by placing pilots in every OFDM symbols. In future work, an advanced receiver can be considered to minimize ICI due to the phase noise.

References

[1] 3GPP TR 25.814 V1.0.1 (2005-2006), "Physical Layer Aspects for Evolved UTRA".

[2] P. Hoeher, S. Kaiser and P. Robertson, "Two-Dimensional Pilot-Symbol-aided channel estimation by wiener filtering," *in Proc. ICASSP'97*, vol.3 pp.1845, 1997.

[3] W. Songping, Y. Bar-Ness, "OFDM Systems in the Presence of Phase Noise: Consequences and Solutions," *Communications, IEEE Transactions on* , vol.52, no.5 pp.855- 855, May 2004.

[4] A. Garcia Armada, "Understanding the effects of phase noise in orthogonal frequency division multiplexing (OFDM)," *Broadcasting, IEEE Transactions on* , vol.47, no.2 pp.153-159, Jun 2001.

[5] E. Costa, S. Pupolin, "M-QAM-OFDM system performance in the presence of a nonlinear amplifier and phase noise," *Communications, IEEE Transactions on* , vol.50, no.3 pp.462-472, Mar 2002.

[6] L. Tomba, "On the effect of Wiener phase noise in OFDM systems," *Communications, IEEE Transactions on* , vol.46, no.5 pp.580-583, May 1998.

[7] A. Demir, A. Mehrotra, J. Roychowdhury, "Phase noise in oscillators: a unifying theory and numerical methods for characterization," *Circuits and Systems, IEEE Transactions on*, vol.47, no.5 pp.655-674, May 2000.

[8] S. Sampei, T. Sunaga, "Rayleigh fading compensation for QAM in land mobile radio communications," *Vehicular Technology, IEEE Transactions on* , vol.42, no.2 pp.137-147, May 1993.

[9] C. Ji-Woong, L. Yong-Hwan, "Design of the Optimum Pilot Pattern for Channel Estimation in OFDM Systems," *in Proc. Globecom'2004*, pp. 3661-3665, Dec. 2004.

[10] 3GPP TR 25.943, "Deployment aspects".

[11] L. Maret, M. Des Noes, D. Morche, J. Barletta, "Sensitivity of a MC-CDMA Beyond 3G System to RF Impairments," *in Proc 14th IST Mobile Wireless Comms*, Dresden, Germany, 2005.

[12] IST-2003-507581 WINNER,"Feasibility of Multi-bandwidth Transmissions," D2.2 v1.0, Oct 2004.

[13] I. Z. Kovacs, K. I. Pedersen, J. Wigard, F. Frederiksen, T. E. Kolding, "HSDPA Performance in mixed outdoor-indoor micro cell scenarios," *The 17th Annual IEEE Intl Symposium on PIMRC*, Helsinki, Sep. 2006.